GEOCHEMISTRY OF PRECAMBRIAN IGNEOUS ROCKS IN THE LOWER ORANGE RIVER REGION

DAVID LOUIS REID

Thesis submitted for the degree of
Ph.D. in the Faculty of Science
University of Cape Town

Department of Geochemistry
University of Cape Town

September, 1977

The copyright of this thesis vests in the author. No quotation from it or information derived from it is to be published without full acknowledgement of the source. The thesis is to be used for private study or non-commercial research purposes only.

Published by the University of Cape Town (UCT) in terms of the non-exclusive license granted to UCT by the author.

University of Cape Town

ABSTRACT

Precambrian igneous rocks underlie the mountainous tract that straddles the lower Orange River between Vioolsdrif and Henkries. The oldest rocks are lavas and related fragmental rock types of the Haib Volcanic Group (HVG). Total rock Rb-Sr, Th-Pb and Pb-Pb ages indicate that the HVG was formed about 2000 Ma ago. The base of the volcanic succession is cut by later intrusives and the top has been removed by erosion. The exposed section through the succession is at least 8000 m thick.

The earliest volcanics were predominantly andesitic-rhyolitic, being made up of two distinct components : (1) non-porphyritic rhyolites (ignimbrites?) and related pumice sheets and bedded tuffs; (2) a differentiated suite of porphyritic lavas ranging in composition from andesite to rhyolite, with andesite being the most abundant. Later extrusive activity was characterised by an increased proportion of basaltic-andesitic and andesitic material, in the form of porphyritic lavas, pyroclastic beds and volcanogenic sediments.

The primary igneous mineralogy of the volcanic rocks has been replaced by a metamorphic assemblage appropriate to upper greenschist facies. Basaltic andesite metalavas are characterised by the presence of a complex intergrowth of two metamorphic amphiboles - actinolite and blue green hornblende, together with the assemblage albite-epidote-chlorite-quartz-biotite. Field relationships suggest that the pervasive metamorphic reconstitution experienced by the HVG was caused by the regional emplacement of later plutonic rocks in the Vioolsdrif batholith. The intrusive rocks are essentially unmetamorphosed and the metamorphism of the volcanics is interpreted as a regional contact phenomenon.

The differentiated suite of porphyritic lavas follows a calc-alkaline trend, ranging in composition from basaltic andesite, through andesite and dacite, to rhyolite. Andesite is the most abundant rock type. Major and trace element modelling suggest that this suite could have been produced by fractional crystallisation of a basaltic andesite parent. The most basic lava (basaltic andesite) is probably not a primary magma and a more basic

precursor is preferred. The early non-porphyritic rhyolites do not appear to be related to the porphyritic lava suite through fractional crystallisation and may represent a separate, crustal derived, primary magma. This suggests that a significant proportion of the volcanic pile (about 40%) represents remobilised continental crust, while the remaining 60% may be juvenile addition from the upper mantle. Strong evidence for such a contribution from the upper mantle is the basic nature of the presumed parental magma and the low initial Sr^{87}/Sr^{86} ratio (.7034) of the porphyritic lava suite.

Sustained intrusion of magma into volcanic pile resulted in the development of a composite batholith - the Vioolsdrif Intrusive Suite (VIS). The compositional variation exhibited by the VIS broadly parallels that of its volcanic envelope, but certain chemical features argue against the two suites being entirely comagmatic. The earliest rocks of the batholith are differentiated basic-ultrabasic complexes exhibiting tholeiitic affinities and compositions which are more basic than those displayed by the lavas. Intrusion of granitic rocks that form 95% of the batholith resulted in the fragmentation of the early basic-ultrabasic complexes, such that they now appear as scattered relicts, and metamorphosed to the same grade as the volcanic country rock. The radiometric age pattern exhibited by the intrusive rocks suggests an emplacement period of about 200 Ma, starting soon after eruption of the volcanic pile ($\pm$ 2000 Ma) and ending at about 1800 Ma. Field relationships suggest that emplacement involved the intrusion of progressively more differentiated magma, such that the suite diorite - tonalite - granodiorite - adamellite - leucogranite also represents a temporal sequence.

Major and trace element modelling of the intrusive suite suggest that the tonalite and granodiorite could have been produced by fractional crystallisation of a dioritic parent. The adamellite and leucogranite could have been produced by stepwise fractionation of a tonalitic parent. Such a fractionation scheme is corroborated by Sr isotopes, at least for the more basic intrusives (diorite, tonalite, granodiorite). In order for the adamellite to be a derivative of the tonalite, enrichment in radiogenic Sr^{87} must have occurred, because the adamellite has a significantly higher Sr^{87}/Sr^{86}

ratio (.7065 ± 10) than the tonalite (.7030 ± 3). The required increase in Sr^{87}/Sr^{86} could have been achieved in the time between intrusion of the tonalite (about 1940 Ma) and the adamellite (about 1800 Ma), provided the latter formed as a magma by fractional crystallisation at 1940 Ma.

The initial Sr isotopic composition of the diorite is the same as that for the basaltic andesite, suggesting that the two suites could have been produced from a common, mantle derived parent. The contrasting major and trace element compositions of the more basic members of the two suites can be explained by the effect of P_{H_2O} on the crystallisation behaviour of a basaltic magma. The suppression of plagioclase at high P_{H_2O} could have been responsible for the production of the high Al diorites and tonalites. Fractionation of the same parental magma at lower P_{H_2O} may result in increased importance of plagioclase as a crystallising phase, with the result that derivative magmas (such as the lava suite) will not be as high in Al as those produced at higher P_{H_2O}.

In contrast with the volcanics, the more acid members of the intrusive suite have major and trace element compositions which are consistent with extreme fractional crystallisation of a more basic parent. Furthermore, the adamellites and leucogranites do not display the same disproportionate development as that observed for the non-porphyritic rhyolites and related fragmental rock types. If the Rb-Sr aging mechanism to explain the Sr isotopes is accepted, then the entire batholith represents juvenile addition from the upper mantle.

The rocks of the HVG and VIS constitute distinctive lithologic units, which exhibit a structural style, metamorphic history and radiometric age pattern quite different from that observed in the neighbouring Namaqua and Gariep tectonic provinces. It is concluded that the basement rocks in the Vioolsdrif - Haib region fulfil the requirements necessary to justify the use of the term "Precambrian tectonic province". However, to be consistent with the geographic connotation, the term "Vioolsdrif Province" should be used to describe basement rocks that display a distinctive structural - geo chemical - radiometric pattern, indicative of a fundamental pre-1000 Ma crust-producing event in the Precambrian history of the lower Orange River region.

TABLE OF CONTENTS

I

INTRODUCTION

1.1 Location

Precambrian volcanic and associated intrusive rocks crop out in the mountainous tract straddling the Orange River from Vioolsdrif to Henkries (Fig. 1). These rocks may also be present further east, but the complicated metamorphic and deformational history of this area does not allow ready identification and so this area was not covered in the investigation. The relief lessens to the north and south and as a result the amount of exposure decreases until the barren, featureless deserts of the Namib and Bushmanland are reached. To the west, the younger Nama strata cover the earlier Precambrian basement. The total area investigated is about 2000 square kilometres (780 square miles). Apart from the national highway from Cape Town to Windhoek, which crosses the Orange River at Vioolsdrif, roads in the region are few and access is only possible by means of a four-wheel drive vehicle along dry river beds.

1.2 Previous Investigations

The region has long been known for its mineral wealth, with the most important being rare element minerals in pegmatites (Gevers *et al.*, 1937; Schutte, 1972) and low grade Cu mineralisation (Von Backström and De Villiers, 1972). Geological maps of some of the region have been prepared by Gevers *et al.*, (1937), Von Backström and De Villiers (1972) and several exploration companies. The most recent mapping efforts have been Ward (1974) and Blignault (1975). The general geology of the region is displayed in the maps included with this work (Fig. 25 and Appendix 1) and is based on Blignault (1975), Von Backström and De Villiers (1972), plus some additions and modifications by the author.

All previous work has been of a reconnaissance nature, with emphasis on determining the distribution of major rock types, regional stratigraphy and

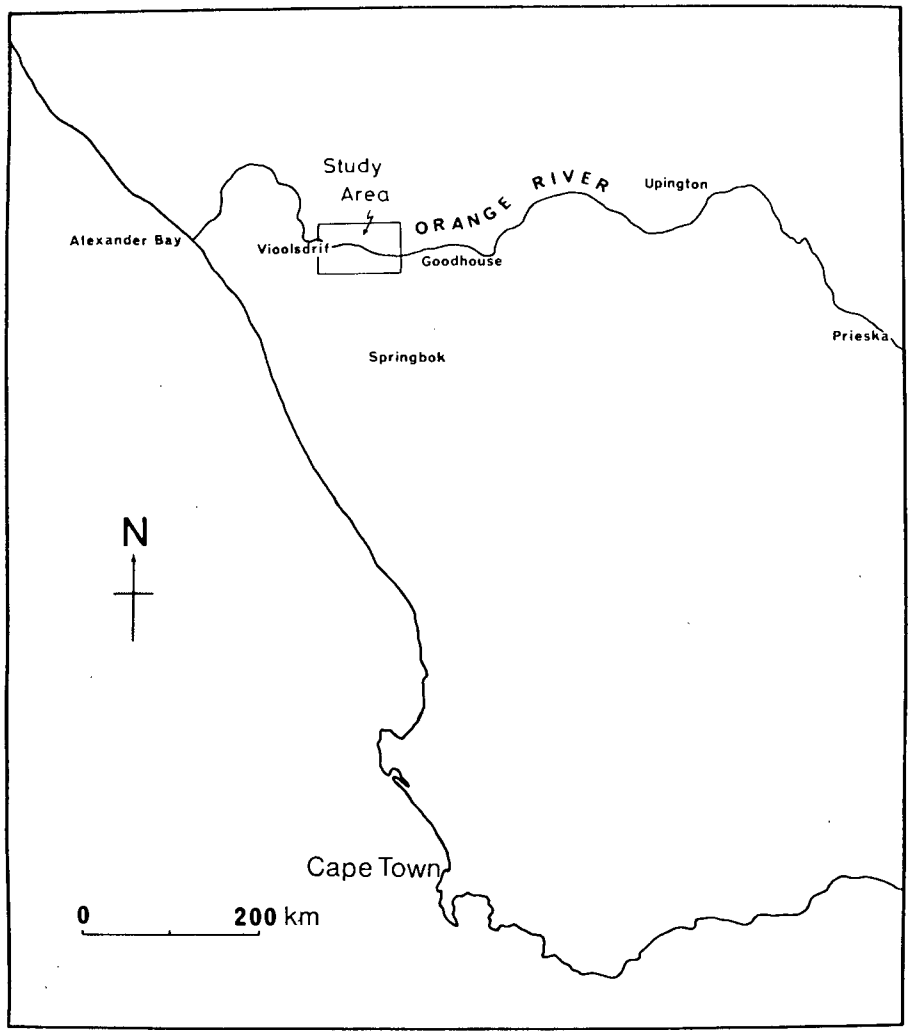

Fig. 1. Location of the present study area

structure. Little detailed petrographic or geochemical work, apart from brief supplements to the reconnaissance mapping, had been carried out before this study. Detailed petrographic work has been carried out on rocks in the neighbouring region of the south-eastern Richtersveld (Middlemost, 1964), which is underlain by probable correlatives with the igneous rocks in the Vioolsdrif region.

1.3 Scope of present study

The present study is complementary to current reconnaissance mapping and structural analysis carried out by the Precambrian Research Unit (PRU) in and beyond the area shown in Fig. 1. The areal extent of the volcanics and associated intrusives has been established on maps prepared by the PRU and the Geological Survey of South Africa.

The main aims of the study include:

(i) *To establish the extent of compositional variation within the volcanics and associated intrusives and to assess the effects of alteration and metamorphism.*

Of the several hundred samples collected about 160 were chosen for analysis of major elements and 15 trace elements. The effects of alteration were initially assessed by visual screening, which involved inspection of hand specimens and thin sections. Further screening involved the evaluation of various chemical criteria for alteration. Since the volcanics have been extensively reconstituted, the compositions of secondary minerals have been determined in order to establish the grade of metamorphism.

(ii) *To evaluate possible petrogenetic models to explain the observed petrographic and geochemical variation within both the extrusive and intrusive suites and to establish any genetic relationship between the two suites.*

Because of extensive metamorphic reconstitution, petrogenetic modelling

of the lava suite has involved assumptions as to the nature of the original phenocryst mineralogy. The predictions of various models have been compared with the observed major and trace element behaviour.

The major minerals in the intrusive rocks have been analysed to provide data for the evaluation of petrogenetic models involving fractional crystallisation and crystal accumulation. Further evaluation of these models has been carried out using trace elements and by applying recently developed ideas of trace element distribution (e.g. Gast, 1968; Allegre *et al.*, 1977).

An attempt has been made to estimate the composition of parental and primary magmas responsible for the lava suite and associated intrusives. Source region characteristics have been discussed in the light of estimated primary magma compositions.

(iii) *To augment trace element data with Sr and Pb isotopic analyses in order to establish radiometric age patterns and to provide constraints on the possible range of petrogenetic models.*

(iv) *To evaluate the role of these rocks in terms of crustal development in this area.*

The chemical characteristics of possible parental magmas have been discussed in terms of their alleged dependence on the prevailing geotectonic environment (e.g. Pearce and Cann, 1973; Jakes and White, 1972a). The status of the so-called Richtersveld Province (Kröner and Blignault, 1977) has been assessed in the light of the results from the present study.

1.4 Acknowledgements

I am sincerely grateful to Professor L. H. Ahrens for the opportunity to use the vast facilities of the Department of Geochemistry and for continued support throughout the study. The project was devised after an introductory field trip made possible by the Precambrian Research Unit, U.C.T., in collaboration with Professor J. De Villiers and Drs. P. Joubert and A. Kröner. The

Financial support was received from the C.S.I.R., University of Cape Town and Rio Tinto (Pty) Ltd. The latter also provided accomodation and assistence from time to time during the field work. In particular, I would like to thank Messrs. R.B. Cooke and J.J. Haumann of Rio Tinto for their continued support and for providing samples of drill core for analysis.

Finally, I would like to thank Ms. J. MacDonald and Ms. J. Elliott for typing the text and tables and especially Wendy Gledhill for the many, many hours she spent in performing the essential task of proof-reading.

THIS STUDY		AGE	Earlier Scheme
RIVER GRAVELS CALCRETE	Superficial Deposits	Cretaceous - Recent	Stratigraphy of Younger Rocks Unchanged
BASIC SHEETS DIKES	Karroo Dolerites	Jurassic	
intrusive			
DWYKA GROUP	Karroo Supergroup	Permo-Carboniferous	
disconformity			
SCHWARZKALK FORMATION	NAMA GROUP	Cambrian to Late Precambrian	
KUIBIS FORMATION			
unconformity			
BASIC DIKES	Gannakouriep Dike Swarm	Age Unknown	
intrusive contact			
ALKALINE DIKES	Richtersveld Dike Swarm	Age Unknown	
intrusive contact			
PEGMATITE APLITE QUARTZ VEINS	Namaqualand Pegmatite Swarm	900-1000 Ma	After DeVilliers & Söhnge
intrusive contact			
Leucogranite	VIOOLSDRIF INTRUSIVE SUITE	1800 - 2000 Ma	Richtersveld Granite
intrusive			
Adamellite			Vioolsdrif Granite
intrusive			
Granodiorite			Contaminated Vioolsdrif Granite or Granitised Metavolcanics
intrusive			
Tonalite			
intrusive			
Diorite			
intrusive			
Basic - Ultrabasics			Undifferentiated Ultramafic Intrusives
intrusive contact			
NOUS FORMATION	HAIB VOLCANIC GROUP	2000 Ma	Wilgenhoutdrif Series
conformable contact			
TSAMS FORMATION			
base not exposed			
NOT REPRESENTED	Rosyntjieberg Group	Age Unknown	Kaaien Series
	De Hoop Group	Age Unknown	Marydale Series

Table 1. Stratigraphy of the lower Orange River region.

correlatives of the Wilgenhoutsdrif Series eastwards from the Richtersveld into the Vioolsdrif region and it is upon these observations that the stratigraphic correlation of Von Backström and De Villiers (1972) was based. The implication is therefore that metasediments and volcanics may underlie the HVG in the Haib-Vioolsdrif region, but, as previously mentioned, such earlier rocks have not been recognised.

The so-called "grey gneissic granite" of De Villiers and Söhnge (1959) was subsequently re-defined as "Vioolsdrif Granite" by De Villiers and Burger (1967). The present study has identified the type Viooldsdrif Granite as an adamellite in the VIS (see Table I). Von Backström and De Villiers (1972) considered that the variation in composition of the Vioolsdrif Granite to be due to contamination, thereby implying the existence of only one magma type of granitic composition. However, the discovery of discrete plutons of different rock types, each showing distinct intrusive relations, suggests that more than one magma type was involved in the emplacement of the VIS. Strong evidence in favour of such an idea, is that the variation in composition of the intrusive rocks correlates with their relative age of emplacement; field relationships suggest that plutons containing more basic rocks (diorites and tonalites) are older than those containing felsic rock types (granodiorite, adamellite).

Von Backström and De Villiers recognised a pink, leucocratic granite in the Vioolsdrif region, which was demonstrably younger than their Vioolsdrif Granite and its assimilation products. The pink granite was correlated with the Richtersveld Granite, a great mass of younger granitic rocks (c. 850 Ma, Köstlin, 1971) occurring in the adjacent region to the west. Their correlation is not supported by radiometric data, which show that the pink granite is a component of the VIS.

indicated that for data arrays to be regarded as isochrons, a maximum allowable MSUM of 2.5 could be applied to Rb-Sr plots with as few as 5-6 points. Less duplicate data were available for the U-Th-Pb study so more data points were used in an attempt to define isochrons.

In view of the suspected Precambrian age for the HVIP, and the complex geological history experienced by these igneous rocks, the results reported below are very encouraging. It is inevitable in a study of this kind, that several analysed samples do not fall on the lines of best fit through the data points. The number of aberrant points are surprisingly few and inspection of Table 2 reveals that evaluation of possible reasons for such aberrancy is only necessary in a small number of cases. It was not possible to repeat mass spectrometric analyses of aberrant samples. Finally, it must be stressed that the data discussed should be viewed in the light of the comments expressed above.

This chapter presents all the isotopic data in order of individual rock types and a summary of ages and initial isotopic ratios is given towards the end of the chapter.

The following decay constants have been used (based on Stacey and Stearns, 1973):

$$Rb^{87} = 1.39 \times 10^{-11}\ y^{-1}$$
$$U^{235} = 9.85 \times 10^{-10}\ y^{-1}$$
$$U^{238} = 1.55 \times 10^{-10}\ y^{-1}$$
$$Th^{232} = 4.95 \times 10^{-11}\ y^{-1}$$

A separate section reports data on zircon separates, analysed during the present study, together with data on zircons from samples of the HVIP collected by other workers. Ages defined by scatter of the data on the conventional concordia-discordia diagram are reported and discussed.

3.2. Total rock Rb-Sr

3.2.1. Nous Formation

13 samples of porphyritic basaltic andesite and andesite lava, collected from the Nous Formation throughout the present study area, have been analysed. The resulting data are listed in Table 3 and plotted in Fig. 2. Apart from three analyses, which are considered to be aberrant, the data points define a reasonably good isochron (MSUM = 2.5) which yields an age of 1970 ± 70 Ma and an initial Sr^{87}/Sr^{86} ratio of .7035 ± 4. Errors quoted here and in subsequent sections are single standard deviations (one sigma). The uncertainty in the initial isotopic ratio is that for the last significant figure(s).

There are no obvious petrographic or chemical features that would explain the seemingly aberrant nature of samples 67, 125 and 126. Field relationships show that the aberrant samples were collected from flows within the volcanic succession and therefore could not represent rocks with a significantly different age. It is shown in Chapter 15 that the basaltic andesites and andesites may be related by fractional crystallisation, thereby implying that the aberrant samples could not have had a different initial Sr^{87}/Sr^{86} ratio. It is most likely that the aberrancy has been caused by Rb and/or Sr migration at some time after eruption. Samples 125 and 126 do not have significantly different total Rb and/or Sr contents from the concordant samples, but sample 67 has the highest Sr content of all analysed basaltic andesites, including those not used in the isotopic study. It is possible therefore, that sample 67 may have suffered Sr contamination. However, the fact that the other 10 data points appear to define a good isochron is considered to be of sufficient importance to temporarily disregard the three seemingly aberrant samples.

3.2.2. Tsams Formation

All analysed samples from the Tsams Formation have been collected over

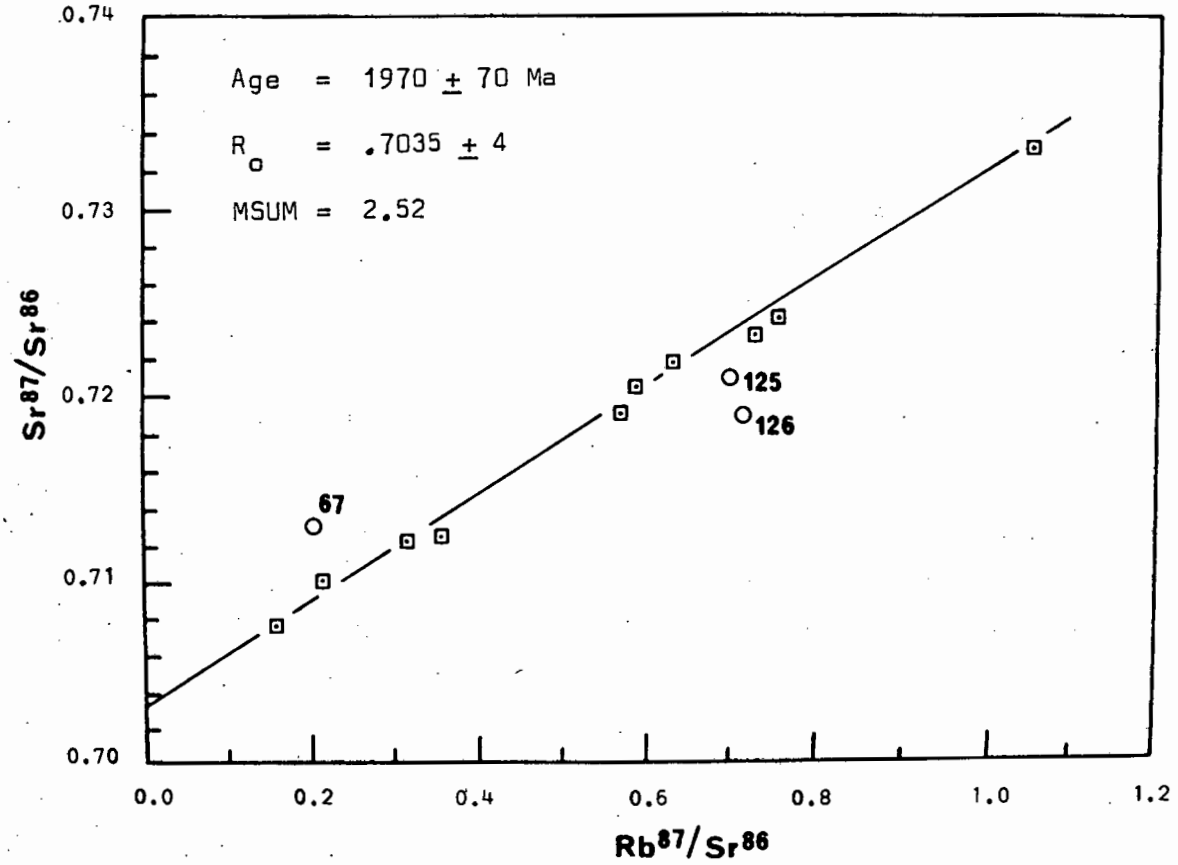

Fig. 2. Rb-Sr isochron for basaltic andesites and andesites from the Nous Formation. Data points not included in the regression are shown as circles. This convention is followed in all subsequent Rb-Sr diagrams.

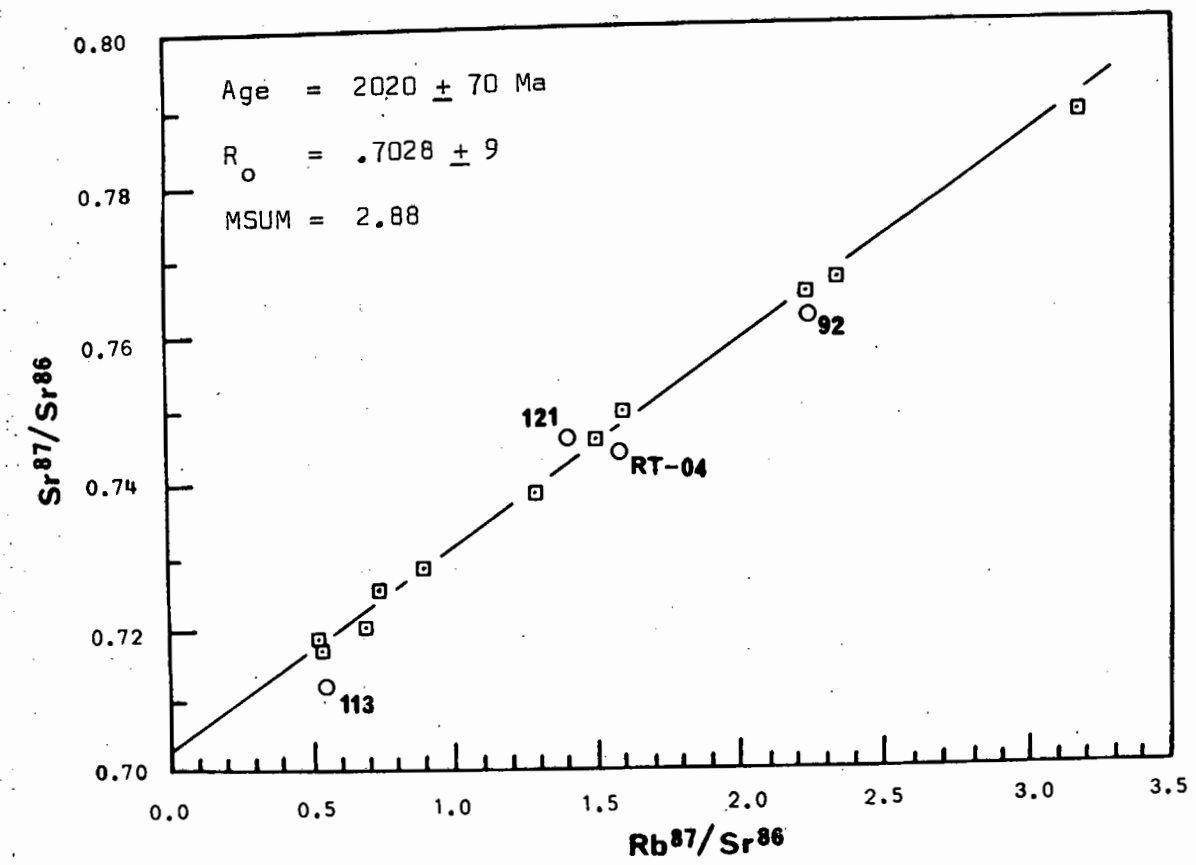

Fig. 3. Rb-Sr isochron for andesites, dacites and porphyritic rhyolites from the Tsams Formation.

after the consolidation of the lava pile is probably the most likely reason, but is difficult to evaluate. For the purposes of this study, the age and the initial Sr^{87}/Sr^{86} ratio obtained from the regression of 11 data points will be adopted and used in the later discussions.

3.2.3. Combined HVG

Since the Rb-Sr isochron data for the Nous Formation overlaps with those estimated for the Tsams Formation, a combined isochron may give the best estimate of the Rb-Sr age for the HVG. The combined isochron age is based on a regression of 21 data points (i.e. all concordant analyses listed in Table 2) and is 1980 ± 40 Ma. The initial Sr^{87}/Sr^{86} ratio for the combined samples is .7034 ± 3. The MSUM of 2.5 is sufficiently low as to enable these values for the age and initial ration to be adopted for the HVG.

3.2.4. Non-porphyritic rhyolites (?ignimbrites) of the Tsams Formation

Non-porphyritic rhyolites which occur in the Tsams Formation have been tentatively regarded as ignimbrite sheets. A particularly well exposed sheet in the Noujaseep River has been sampled in detail and four specimens have been analysed for Sr isotopes (see Table 3). Fig. 4 shows that there is only a rough correlation between Rb^{87}/Sr^{86} and Sr^{87}/Sr^{86}, with the line of best fit suggesting a slope age of 1550 ± 150 Ma and an intercept of .716 ± 11. The wide scatter renders the age and initial Sr^{87}/Sr^{86} ratio of dubious significance.

Field relationships indicate that the non-porphyritic rhyolites are definitely part of the Haib volcanic sequence and that the Noujaseep River exposures represent the top of the Tsams Formation in this area. The Rb-Sr ages reported for the porphyritic lavas are reasonably well defined and the "errorchron" age (Brooks et al., 1972) is probably a function of Rb and/or

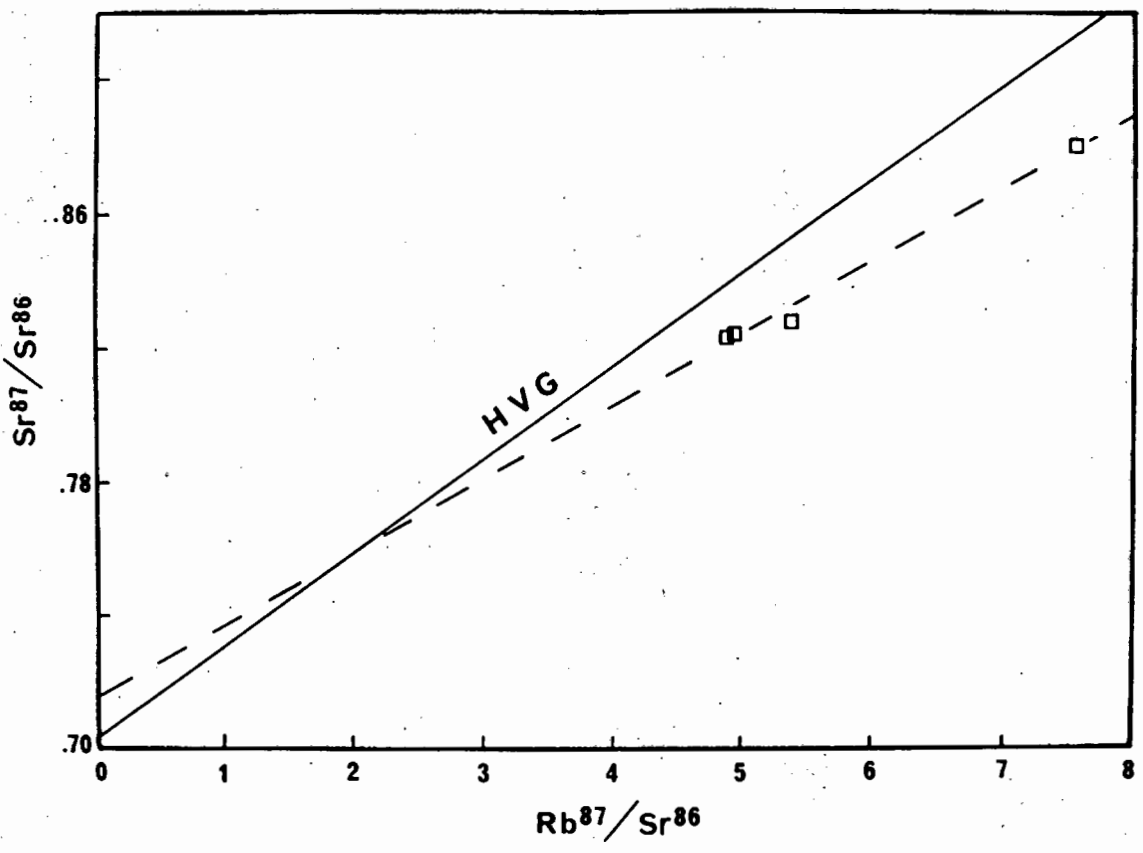

Fig. 4. Rb-Sr diagram containing data for non-porphyritic rhyolites from the Tsams Formation. The solid line represents the Rb-Sr isochron for the combined HVG.

Sr migration some time after eruption. It is also possible that these acid lavas and associated pyroclastics may not be related to the porphyritic lavas by fractional crystallisation (see Chapter 15) and may therefore have had a different initial Sr isotopic composition.

The non-porphyritic rhyolites have the lowest Sr contents (90-150 ppm) and CaO contents (0.5-0.9 percent) of all the lavas in the HVG. These chemical features are reflected in the very low modal plagioclase content and suggest that migration of radiogenic Sr may have been facilitated by the

Sample	Rb	Sr	Rb/Sr	Rb^{87}/Sr^{86}	Sr^{87}/Sr^{86}
			ADAMELLITE		
DRV-01	202	245	0.824	2.395	0.7675(4)
DRV-02	223	292	0.763	2.219	0.7608(6)
DRV-03	166	315	0.527	1.521	0.7464(7)
DRV-05	165	264	0.626	1.813	0.7529(7)
DRV-06	255	201	1.270	3.692	0.79122(2)
DRV-15B	204	312	0.655	1.902	0.7544(2)
DRV-51	147	351	0.418	1.212	0.7375(1)
DRV-70	230	274	1.028	2.978	0.78315(5)
DRV-72	237	285	0.831	2.413	0.7680(7)
DRV-21	211	359	0.587	1.710	0.7495(3)
			LEUCOGRANITE		
DRV-12	209	159	1.312	3.831	0.8035(8)
DRV-12A	324	45.4	7.130	21.381	1.0800(4)
DRV-12B	245	162	1.514	4.430	0.8211(3)
DRV-12C	153	241	1.575	4.609	0.8241(3)
DRV-12D	149	242	1.624	4.753	0.8250(2)
DRV-12E	292	178	1.640	4.800	0.8286(2)
DRV-11	196	78.5	2.492	7.335	0.8855(5)
DRV-16	337	42.2	7.981	24.037	1.12573(6)
DRH-06	279	181	1.544	4.512	0.81300(7)
DRV-22	161	187	0.860	2.504	0.7689(5)
DRV-34	288	41.6	6.931	21.053	1.2174(1)
DRV-35	146	56.7	2.572	7.561	0.8720(3)
DRV-58	225	46.4	4.838	14.520	1.0893(8)
DRV-59	255	55.1	4.621	13.800	1.0373(1)
DRV-60	184	71.4	2.578	7.600	0.89938(3)

Table 4. Continued

Sample	Rb	Sr	Rb/Sr	Rb^{87}/Sr^{86}	Sr^{87}/Sr^{86}
			HAIB PORPHYRY		
RT-01	153	405	.378	1.096	.73464(4)
RT-02	172	291	.591	1.718	.74558(4)
RT-03	148	390	.379	1.101	.73614(3)
DRP-01	136	385	.353	1.015	.73406(4)
DRP-01A	119	460	.259	.743	.7230(5)
DRP-02	197	379	.520	1.502	.7464(6)
DRP-03	166	392	.423	1.207	.74484
			XENOLITH IN XENOLITH		
DRV-33(X II)	178	462	.385	1.115	.73434(2)
DRV-33A(Host)	236	200	1.180	3.435	.78852(5)
DRV-33B(X I)	294	225	1.307	3.810	.80310(2)

Table 4. Continued

absence of any Sr "sinks" (Faure and Powell, 1972). The possibility of Sr migration in these rocks was anticipated and very large samples (10-15 kg) were collected. The results suggest that migration occurred over distances greater than 1-2 metres, a feature not observed in rocks with higher Sr (and higher modal plagioclase contents).

3.2.5. Swartkop basic-ultrabasic complex

Seven basic-ultrabasic samples from the Swartkop complex have been analysed for their Sr isotopic compositions; the data are shown in Table 4 and plotted in Fig. 5. Regression of 5 data points yields an age of 1900 ± 130 Ma and an initial Sr^{87}/Sr^{86} ratio of .7012 ± 6. The regression has an MSUM of 3.4, but if the peridotite sample (20) is excluded, regression of the four remaining data points has an MSUM of 1.7 and yields an age of 1840 ± 65 Ma and an initial Sr^{87}/Sr^{86} ratio of .7019 ± 4. The two results are indistinguishable at the one sigma level, but the second may be considered more reliable since the MSUM is below the upper limit of 2.5. However, the first regression may provide more realistic results because it uses one more data point.

Another peridotite (11) and a troctolite (18) fall far above the line of best fit and if a two point isochron is calculated, an impossibly high age of 9 Ga is obtained. Sample 11 is petrographically indistinguishable from 20 and it is difficult to believe that they are not cogenetic. The same can be said for the troctolite, since it occurs in the same complex and has mineralogical affinities with both the peridotites and gabbros. The aberrant nature of these two samples is not considered to be due to their having different initial Sr^{87}/Sr^{86} ratios from the other samples which lie in the isochron. Sample 11 has a similar Rb and Sr content and Rb/Sr ratio to sample 20, so the higher Sr^{87}/Sr^{86} ratio is probably a function of Sr contamination rather than Rb migration. The suspected altered nature of sample 11 is indicated by the presence of normative corundum, a feature which is incompatible with the presence of modal clinopyroxene. Small amounts

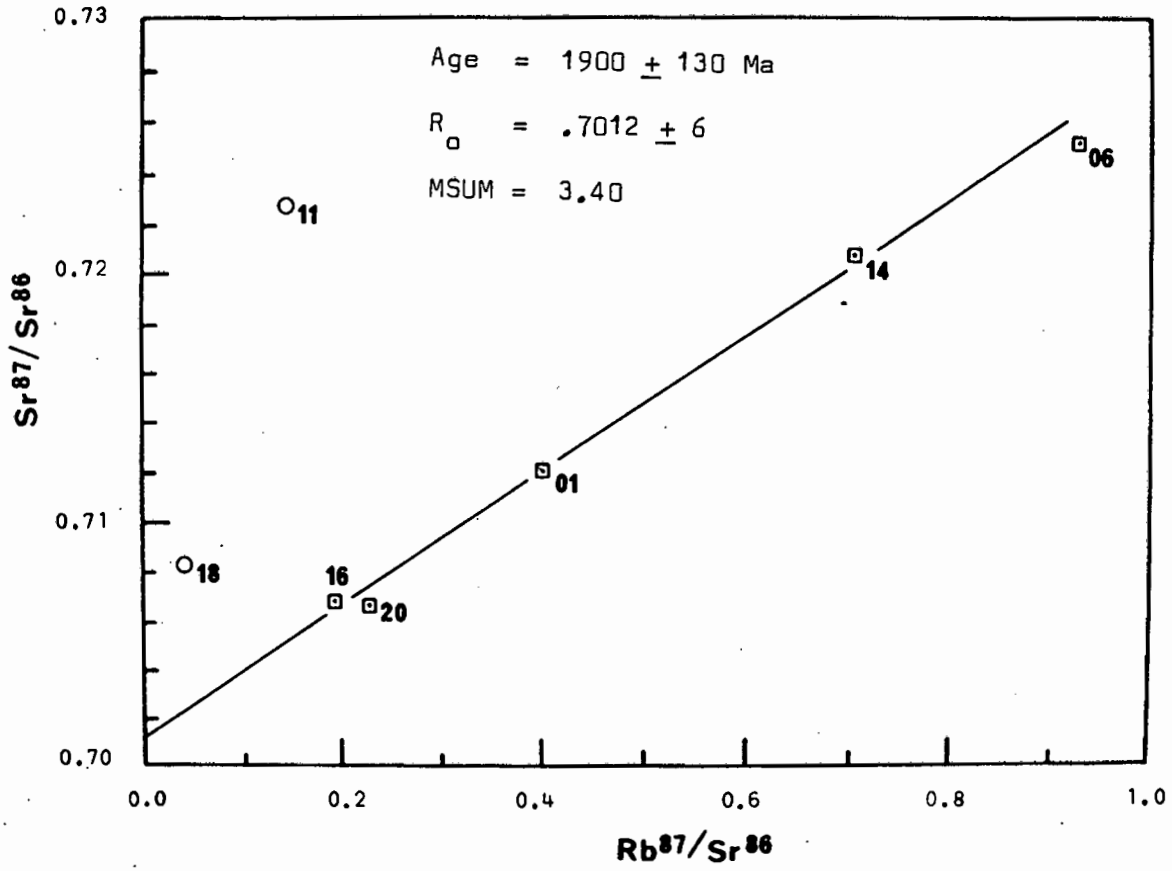

Fig. 5. Rb-Sr isochron for basic-ultrabasic rocks of the Swartkop complex.

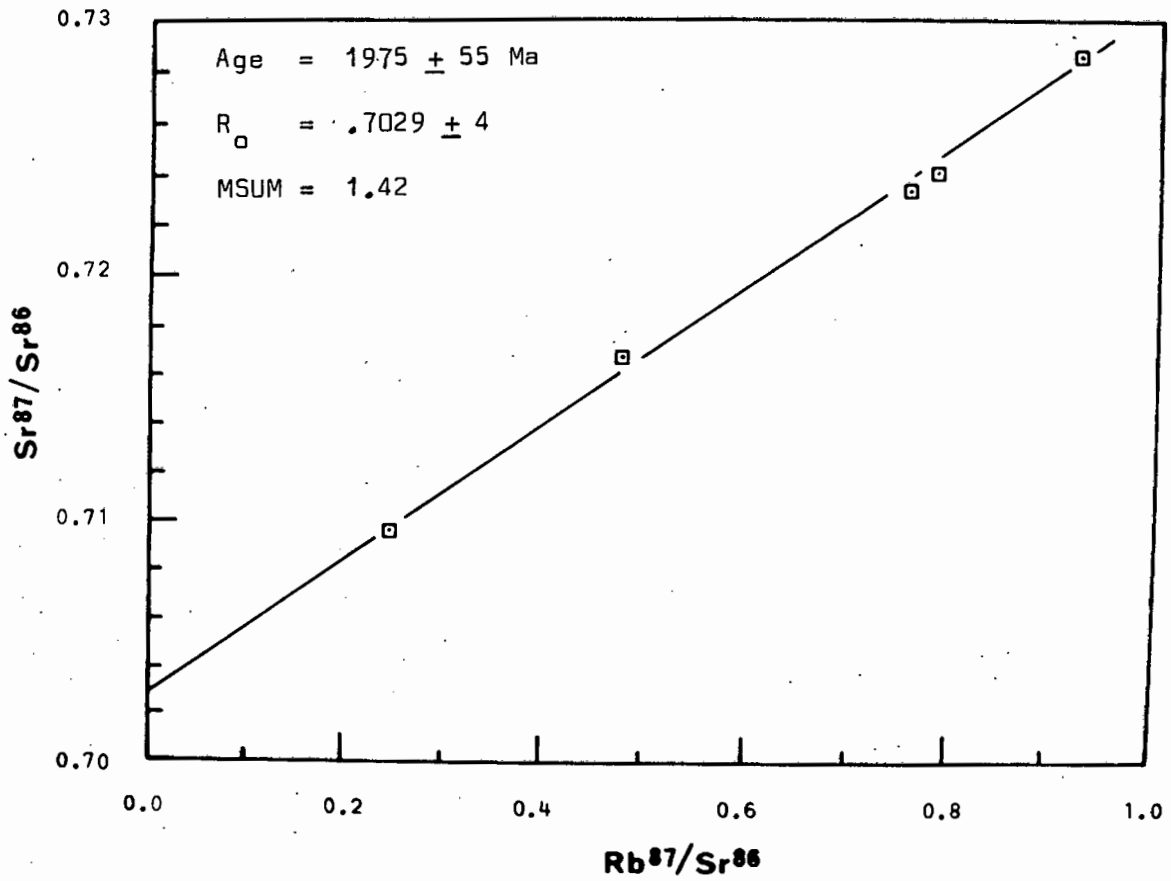

Fig. 6. Rb-Sr isochron for the Vioolsdrif diorite.

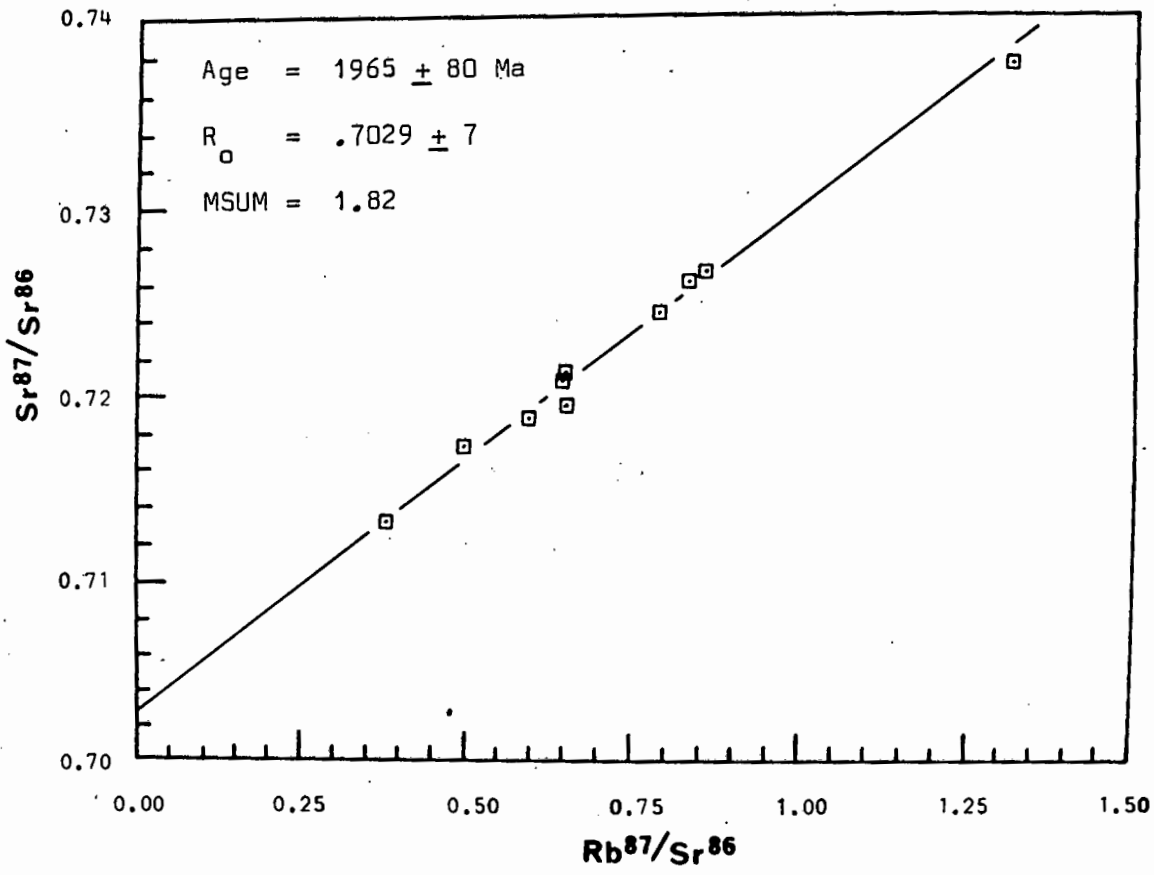

Fig. 7. Rb-Sr isochron for the Vioolsdrif tonalite.

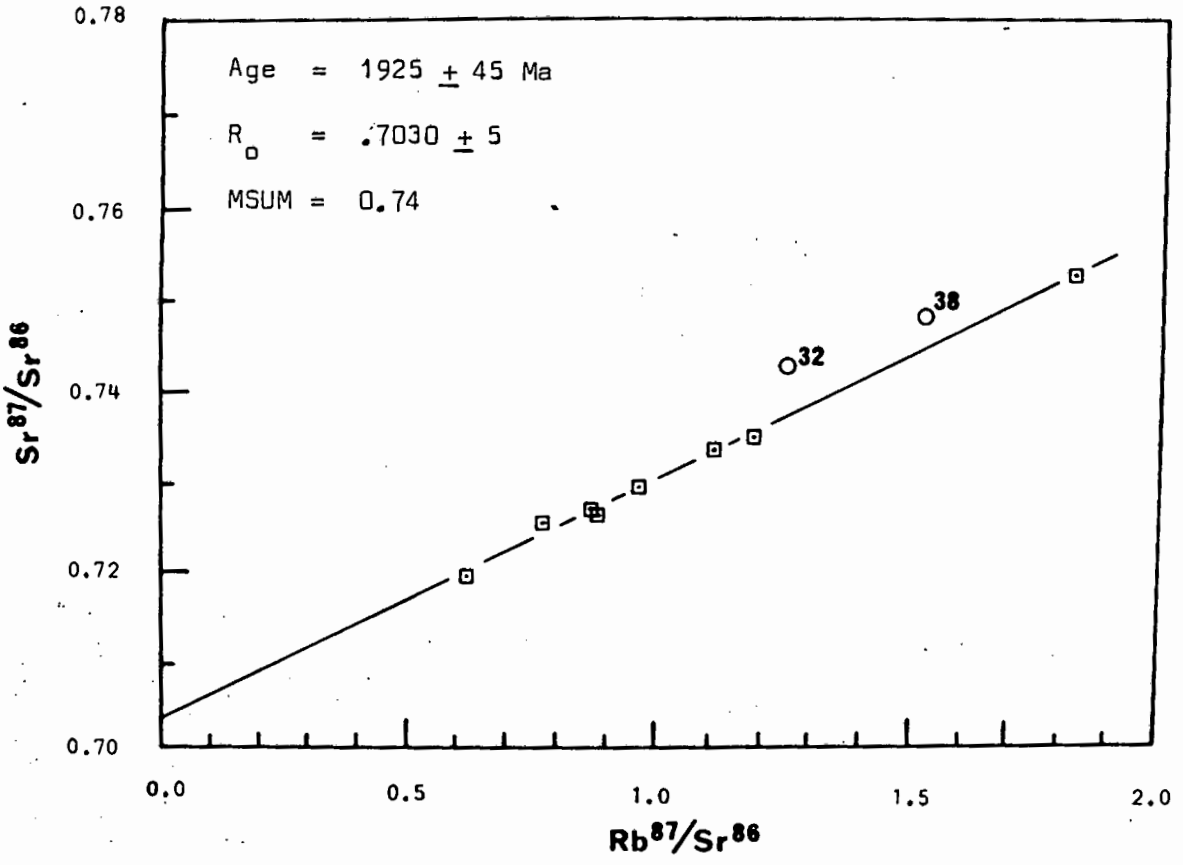

Fig. 8. Rb-Sr isochron for the Vioolsdrif granodiorite.

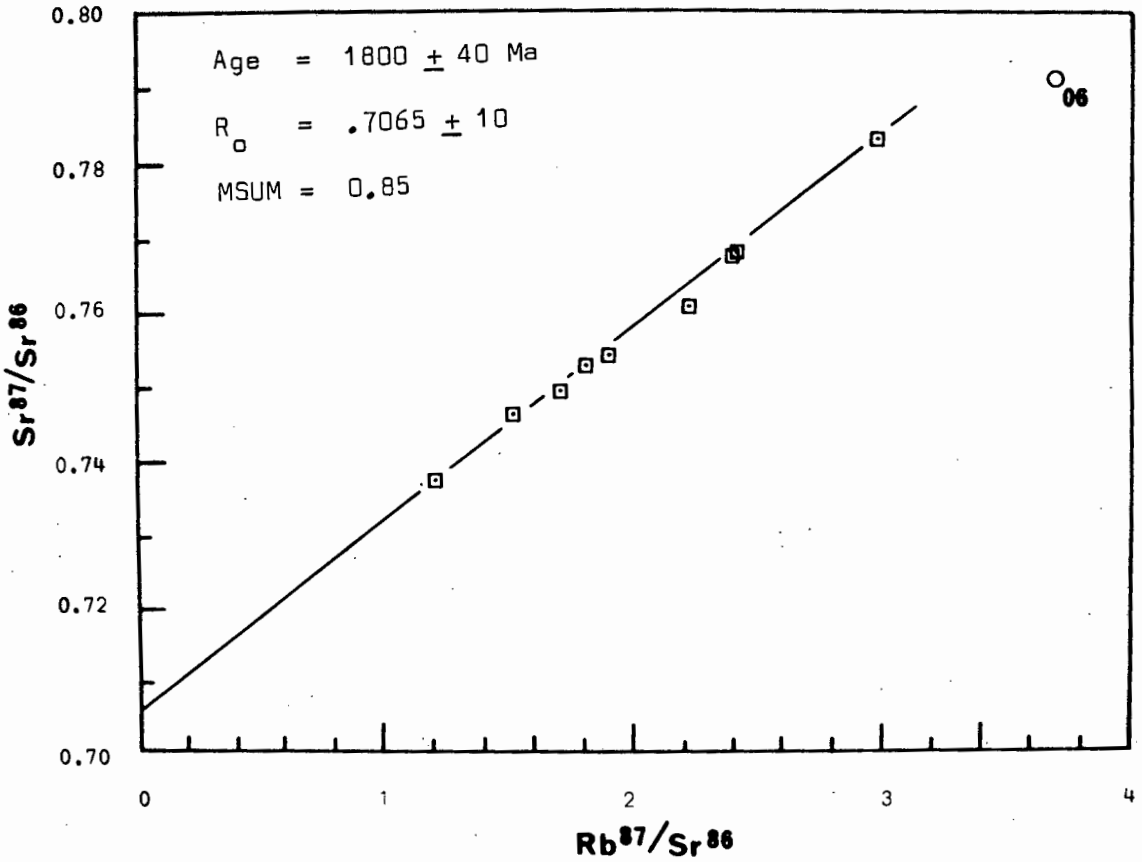

Fig. 9. Rb-Sr isochron for the Vioolsdrif adamellite.

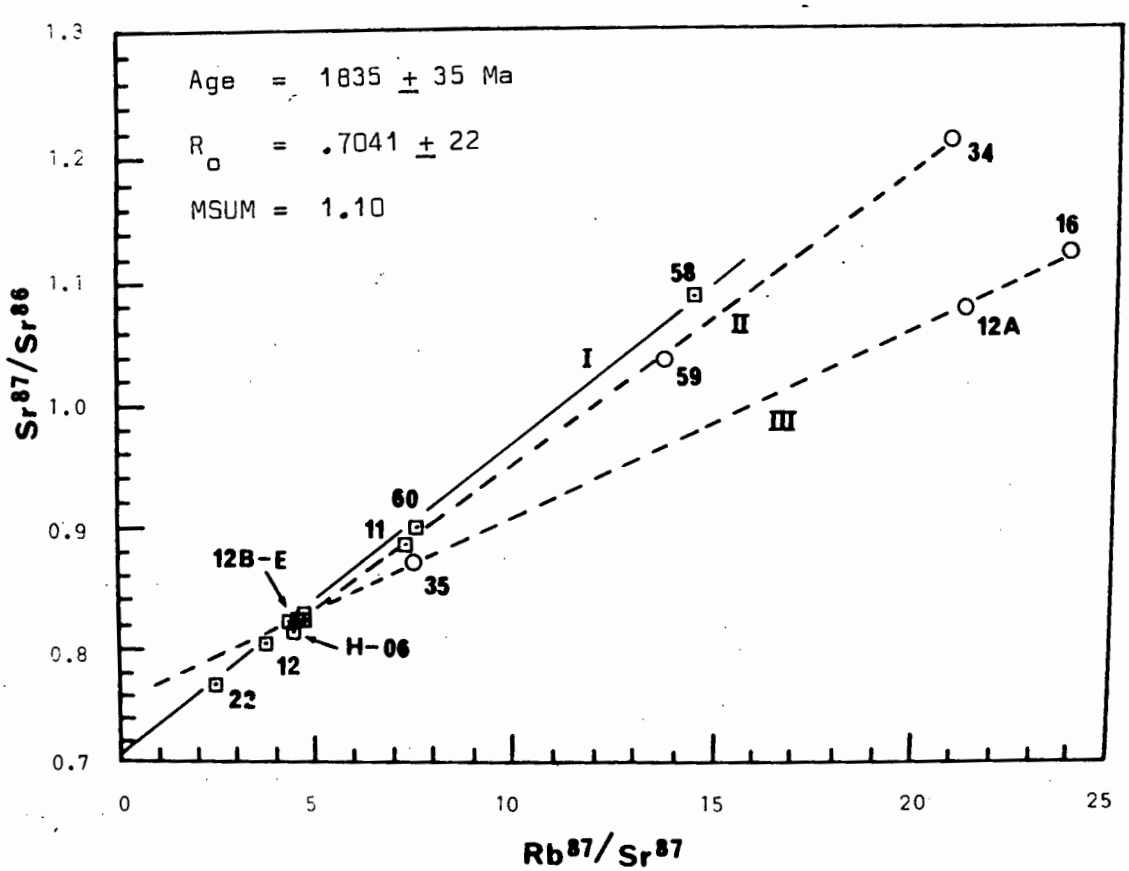

Fig. 10. Rb-Sr diagram for the Vioolsdrif leucogranite. The preferred age for the leucogranite is that defined by regression line (I).

ratio. A tenth point (sample 06) falls significantly below the line of best fit and was excluded from the regression analysis.

3.2.10. Leucogranite

The wide scatter of points on the Rb-Sr diagram (Fig. 10) makes it possible for more than one regression line to be constructed. The results of three separate regressions are as follows:

Regression	No. of points	Age (Ma)	$(Sr^{87}/Sr^{86})_o$	MSUM
I	9	1835 ± 35	.7041 ± 22	1.10
II	10	1740 ± 30	.7095 ± 18	1.14
III	7	1120 ± 20	.7520 ± 14	.70

None of the regressions may be rejected on the grounds of inferior precision since their respective MSUM values are all less than 2.5. The slope ages and initial Sr^{87}/Sr^{86} ratios defined in the three regressions are significantly different at the one sigma level. In the subsequent discussion, the results of the three regressions will be referred to as "I", "II" and "III" respectively.

A noteworthy feature is that the slopes of the three lines depend almost entirely on samples with the highest Rb/Sr ratios. The difference between I and II depends on three samples: 34, 58 and 59. All three are from the same pluton which does not display any evidence for being a multiple intrusion. In addition, the samples are very similar petrographically and chemically, so there seems to be no valid reason to justify two different ages of leucogranite intrusion. The slope of III is dependent on samples 16 and 12A and to a lesser extent on 35. Those samples with lower Rb/Sr ratios are common to all regressions. Sample 12A comes from the same pluton as 12, 12B to E and 60. The cluster of samples 12B to E are ambiguous and are of little help. Sample 12 has a slightly lower Rb/Sr ratio than

those of samples 12B to E, but although it falls closer to I and II, its departure from the extension of III is not very great. However, 60 is definitely aberrant with respect to III, but falls on I and II. The validity of III therefore depends on the relative importance of 60 and 12A. The latter sample was taken about 10 m from the western contact of the leucogranite pluton, while the former comes from 2 km further to the south-east, near the centre of the body. The weathered nature of the contact outcrops make it very difficult to secure fresh samples. In view of the effect that surface weathering has on Rb/Sr ratios (Bottino and Fullager, 1968), the position of 12A relative to I or II is consistent with surface weathering, which usually results in raising the Rb/Sr ratio. Sample 60 was taken from fresh, clean outcrops in a river channel, where it was easy to avoid weathered material. Some doubt is cast on the importance of surface weathering, however, by the fact that 16 was also collected from a clean river channel outcrop and their validity must therefore be given equal weight. An alternative mechanism to produce the aberrant points seems to be required.

Since the leucogranite intrudes the adamellite, which has a Rb-Sr age of about 1800 Ma, the maximum age of the leucogranite is probably around 1800 Ma. The oldest igneous rocks that cut the leucogranite are the Namaqualand Pegmatite Swarm at about 1000 Ma. The slope age of III is 1120 Ma, hence this regression cannot be rejected on the grounds that it falls outside the limits imposed above.

Leucogranites such as 12A and 16 have very low Sr contents (40-45 ppm) and extremely high Sr^{87}/Sr^{86} ratios (<1.0). Small amounts of Sr rich secondary minerals (epidote, calcite) could produce a drastic change in Sr^{87}/Sr^{86} ratios. Assuming that 12A has an age appropriate to I, and if the Rb^{87}/Sr^{86} ratio is kept constant, the predicted Sr^{87}/Sr^{86} would be 1.2565. The observed Sr^{87}/Sr^{86} is 1.0800 (see Table 4), which implies a decrease of 14 percent. If the Sr content of the contaminant is 500 ppm (average calcite value as estimated by Brookins et al., 1969) and a Sr^{87}/Sr^{86} of 0.72 (maximum known for calcite and hydrothermal fluids,

Faure and Powell, 1972), then the weight fraction necessary to bring about the 14 percent decrease in Sr^{87}/Sr^{86} is 0.042, i.e. 4.2 percent. This is a relatively high degree of contamination, and there is no petrographic evidence for such quantities of secondary material in 12A.

The leucogranites are composed predominantly of alkali feldspar and quartz, with subordinate amounts of biotite, sodic plagioclase and muscovite. Because of its abundance relative to micas and plagioclase, most of the Rb and Sr is probably contained in alkali feldspar. Experiments by Badsgaard and Van Breemen (1970) have shown that prolonged heating has no effect on the Sr^{87}/Sr^{86} ratio in alkali feldspar, so the low values exhibited by 12A and 16 are probably not the result of Sr^{87} migration during a later thermal episode.

A final possibility is partial or complete re-equilibration with percolating ground water at the present day or in the past. Present day interaction can be ruled out since the samples were taken at the surface and so the envisaged process would be indistinguishable from surface weathering. This leaves interaction with water at some time in the past, presumably at depth. The leucogranites have such high Rb/Sr ratios that their Sr^{87}/Sr^{86} ratios would have risen past the low value characteristic of groundwater (maximum 0.71-0.72, Faure and Powell, 1972) very soon after crystallisation. The resulting high contrast in Sr^{87}/Sr^{86} ratios render the leucogranite very susceptible to reductions in Sr^{87} content. It follows that all samples would be susceptible to such interaction and a general lowering of Sr^{87}/Sr^{86} ratios would result. If it is accepted that III has been produced by such a mechanism, then II could have been also and the age defined by I will be closer to the true age. As a result, the age and initial Sr isotopic composition of the Vioolsdrif leucogranite is considered to be more closely approximated by regression I.

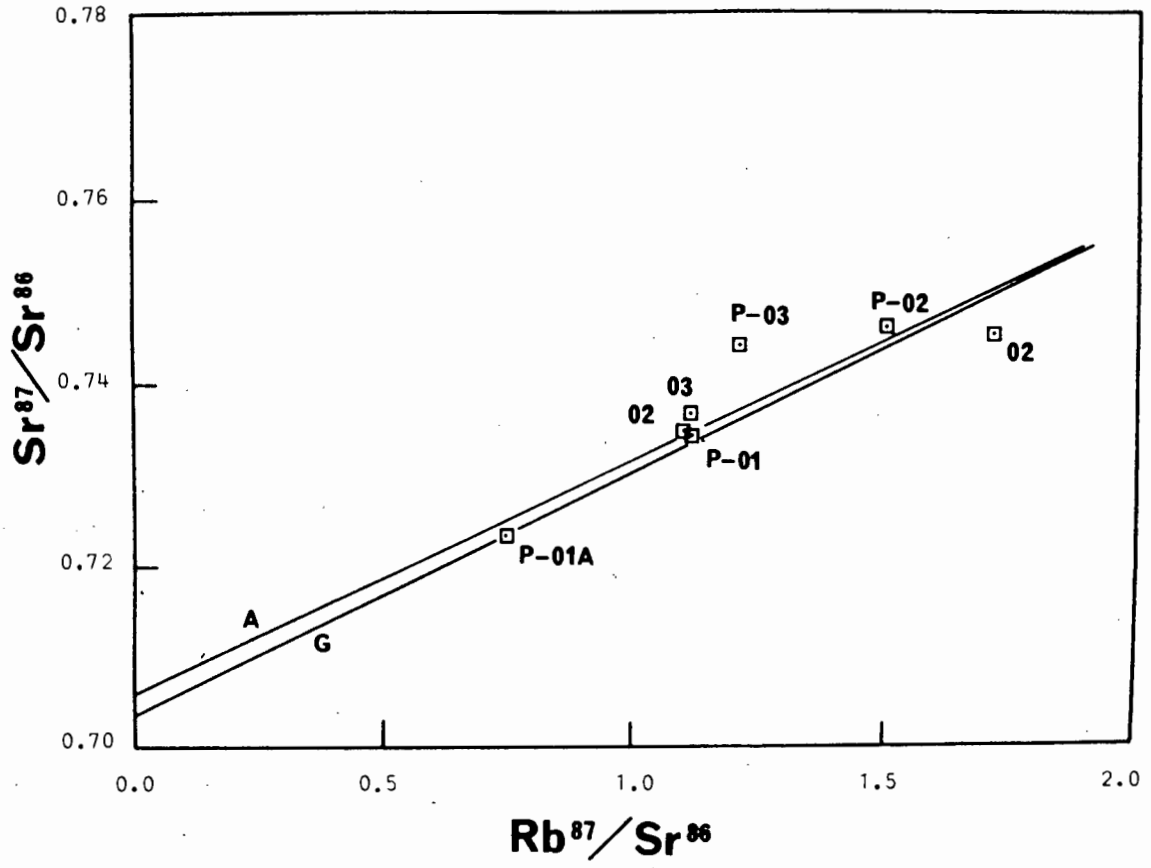

Fig. 11. Rb-Sr diagram for the Haib porphyry. Reference isochrons for the Vioolsdrif granodiorite (G) and adamellite (A) are shown.

3.2.11. Combined Rb-Sr isochron for the VIS

The results of three independent regressions for the Vioolsdrif diorite, tonalite and granodiorite all overlap at the one sigma level. This suggests that the three rock types became closed to Rb-Sr migration over a short period of time corresponding to the range in overlap. Initial Sr^{87}/Sr^{86} ratios also overlap at the one sigma level. A combined regression of 23 samples (two aberrant granodiorite samples have been excluded) yields an age of 1940 ± 30 Ma and an initial Sr^{87}/Sr^{86} ratio of .7030 ± 2. The MSUM of 1.4 is obviously lower than those for the three individual regressions.

This combined age for the diorite (D), tonalite (T) and granodiorite (G) has been subsequently referred to as the D/T/G age.

3.2.12. Haib porphyry

A porphyritic intrusion in the Tsams River area acts as host to extensive, low grade, porphyry copper type mineralisation. Widespread alteration associated with the base metal mineralisation has rendered the rocks unsuitable for dating by the Rb-Sr whole rock technique. Seven of the freshest samples have been analysed for their Sr isotopic composition (Table 4) and the data are plotted in Fig. 11. The porphyry exhibits compositional similarities to both the Vioolsdrif granodiorite and adamellite and the reference isochrons for these two rock types are included in Fig. 11 for comparison. Unfortunately the points do not define a good isochron but do however, roughly conform to a 1800-1900 Ma evolution line. This may be taken as indicating an approximate age of the host porphyry, but provides no clear information on the age of mineralisation. Porphyry copper type mineralisation is usually syngenetic (Hutchinson and Hodder, 1972), but more work needs to be done on the mineralised rocks (e.g. Pb isotope systematics on the sulphides), before any firm conclusions can be made.

3.3. Total rock U-Th-Pb

3.3.1. Haib Volcanic Group

Lavas ranging in composition from basaltic andesite to rhyolite have been analysed for their U, Th and Pb concentrations, together with their Pb isotopic compositions, in order to provide an independent estimate of their radiometric age. The mafic lavas have a similar Rb-Sr age and initial Sr isotopic composition to the felsic lavas, which suggests that they may be cogenetic; this possibility is evaluated further in Chapter 15. For purposes of this part of the study, all the lavas have

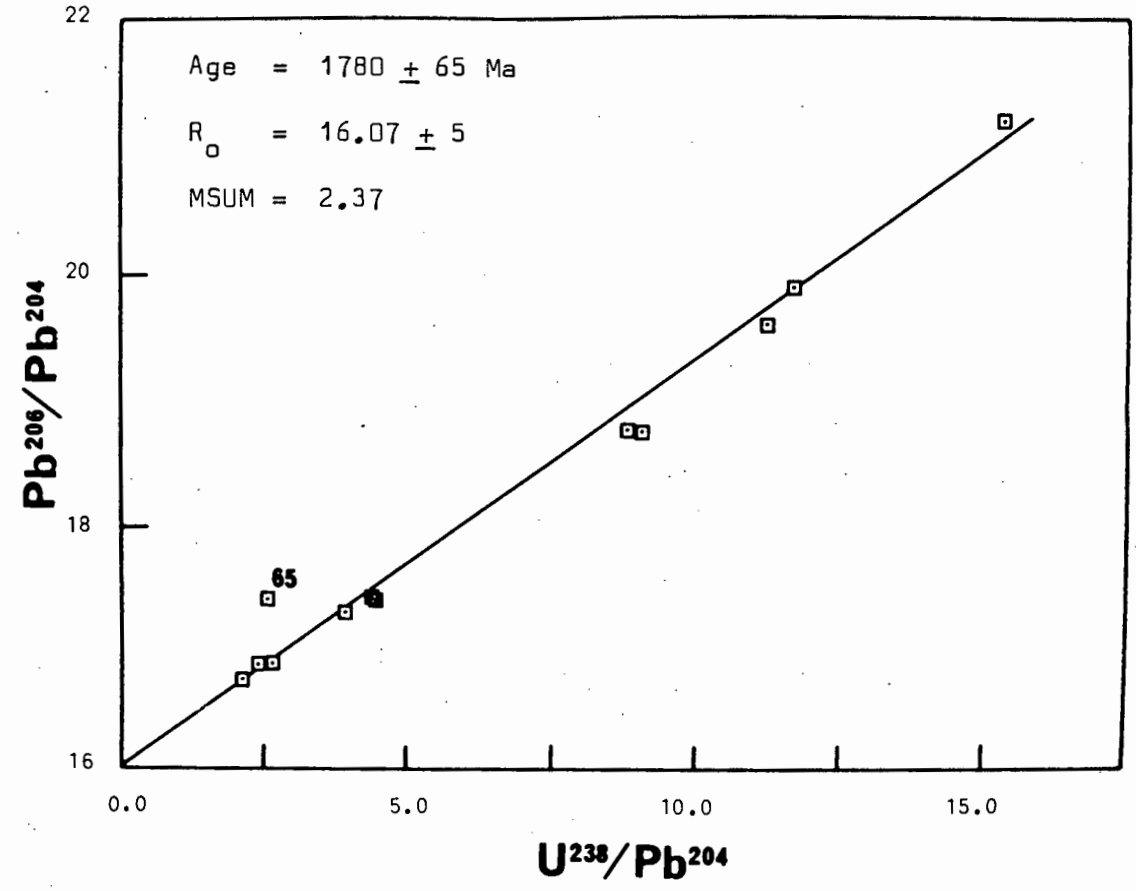

Fig. 12. U^{238}-Pb^{206} diagram for the combined HVG.

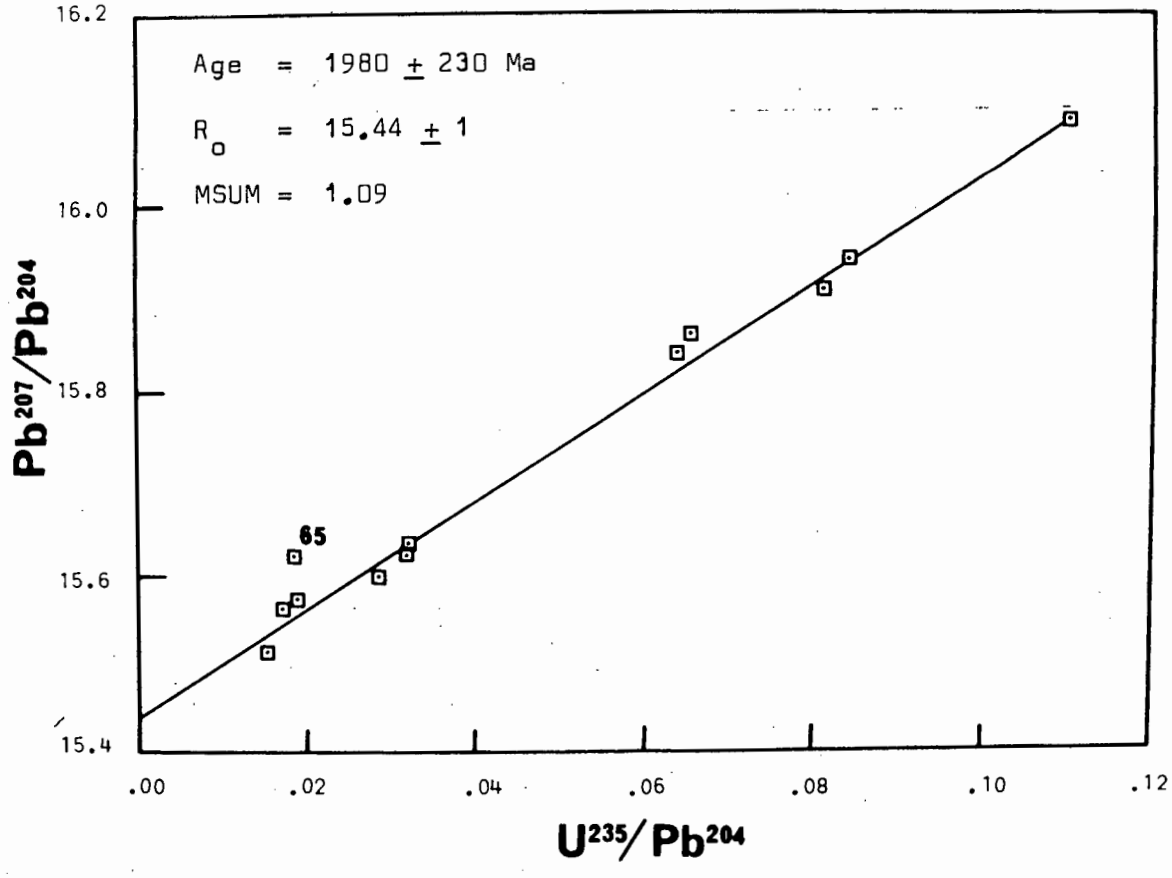

Fig. 13. U^{235}-Pb^{207} diagram for the combined HVG.

been combined in order to generate a reasonable spread in U/Pb and Th/Pb ratios so that meaningful U-Th-Pb evolution diagrams could be constructed. All the relevant atomic ratios are listed in Table 5 and the various diagrams (see 3.1) are displayed in Figs 12-14.

3.3.1.1. U^{238}-Pb^{206}

Regression of 11 data points yields an age of 1780 ± 65 Ma and an initial Pb^{206}/Pb^{204} ratio of 16.07 ± 5. The MSUM is 2,4 which is lower than the maximum allowable value of 2,5. One aberrant sample (65) lies significantly above the line of best fit and was rejected from the regression analysis. Sample 65 seems to be consistently aberrant on all the U-Th-Pb diagrams and will be discussed in 3.3.1.4.

3.3.1.2. U^{235}-Pb^{207}

If the aberrant sample 65 is excluded, a regression of the data for 11 samples yields an age of 1980 ± 230 Ma and an initial Pb^{207}/Pb^{204} ratio of 15.444 ± 13. Although the MSUM is 1.1, the regression does not define a very precise age. This is a function of the very low U^{235}/Pb^{204} ratios, which though useful for determining the initial Pb^{207}/Pb^{204} ratio, are unsatisfactory for defining precise ages. This is also apparent in the Rb-Sr study, where the ages of rock types with high average Rb/Sr ratios (leucogranite, adamellite) are better defined than those with low average Rb/Sr ratios (Swartkop basic-ultrabasic complex). The extremely low U^{235} contents (<0.05 ppm) result in very little radiogenic enrichment of Pb^{207} and it is for this reason that the total rock U^{235}-Pb^{207} system is of little use in geochronology (Hamilton, 1965).

3.3.1.3. Th-Pb

The majority of analysed samples fall on a well defined isochron

(Fig. 14) which yields an age of 2015 ± 60 Ma and an initial Pb^{208}/Pb^{204} ratio of 34.86 ± 9. Regression of the data for 8 samples yields an acceptably low MSUM of 1.3. Three samples (41, 65 and 113) seem to define a parallel isochron which intersects the ordinate at a higher Pb^{208}/Pb^{204} ratio. The presence of sample 65 on this isochron casts some doubt as to its validity, in view of the aberrant nature which this sample displays on the U-Pb diagrams. Three possible explanations for the second isochron are:

(i) Introduction of Pb with the same isotopic composition as the rock, such that the Th^{232}/Pb^{204} ratio is lowered by increases in Pb^{204}.

Since three samples are involved, the Pb introduced must have had different isotopic compositions for each sample. This is considered highly unlikely and it is concluded that the aberrant nature of the samples is not due to Pb contamination.

(ii) The existence of lavas of the same age but derived from a different source having a higher Pb^{208}/Pb^{204} ratio.

The aberrant nature of sample 65 on all U-Th-Pb isochrons has already been noted. Samples 41 and 113 have compositions that fall on U-Pb isochrons and on the Pb^{207}/Pb^{206} isochron, so a different source is not indicated by Pb^{207}/Pb^{204} or Pb^{206}/Pb^{204} ratios. It follows that the two sources have the same U/Pb ratio, but different Th/U ratios. At present only two samples seem to suggest a separate source region and it is concluded that there is insufficient evidence to establish its presence.

(iii) Equal amounts of Th removal such that the samples are displaced toward lower Th^{232}/Pb^{204} ratios.

Th appears to be less susceptible to removal during weathering or groundwater interaction than U (Rosholt et al., 1971; Rogers and Adams, 1969).

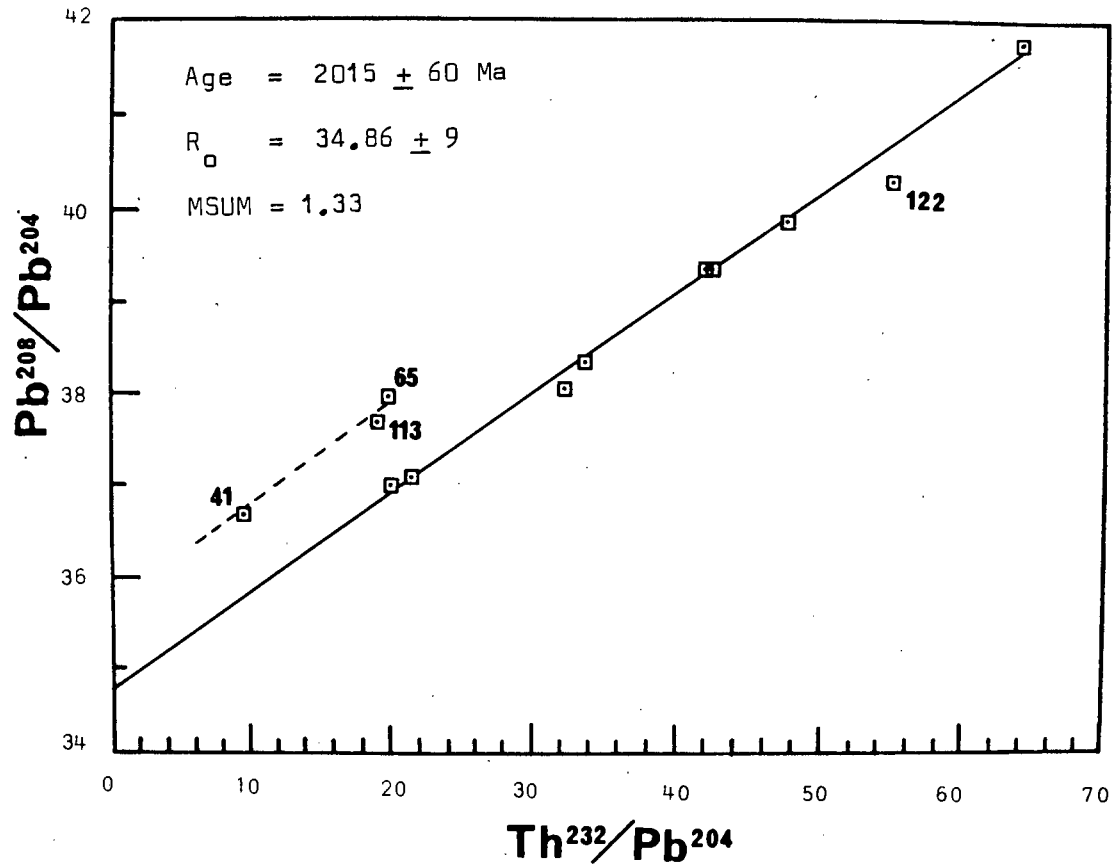

Fig. 14. Th-Pb isochron for the combined HVG.

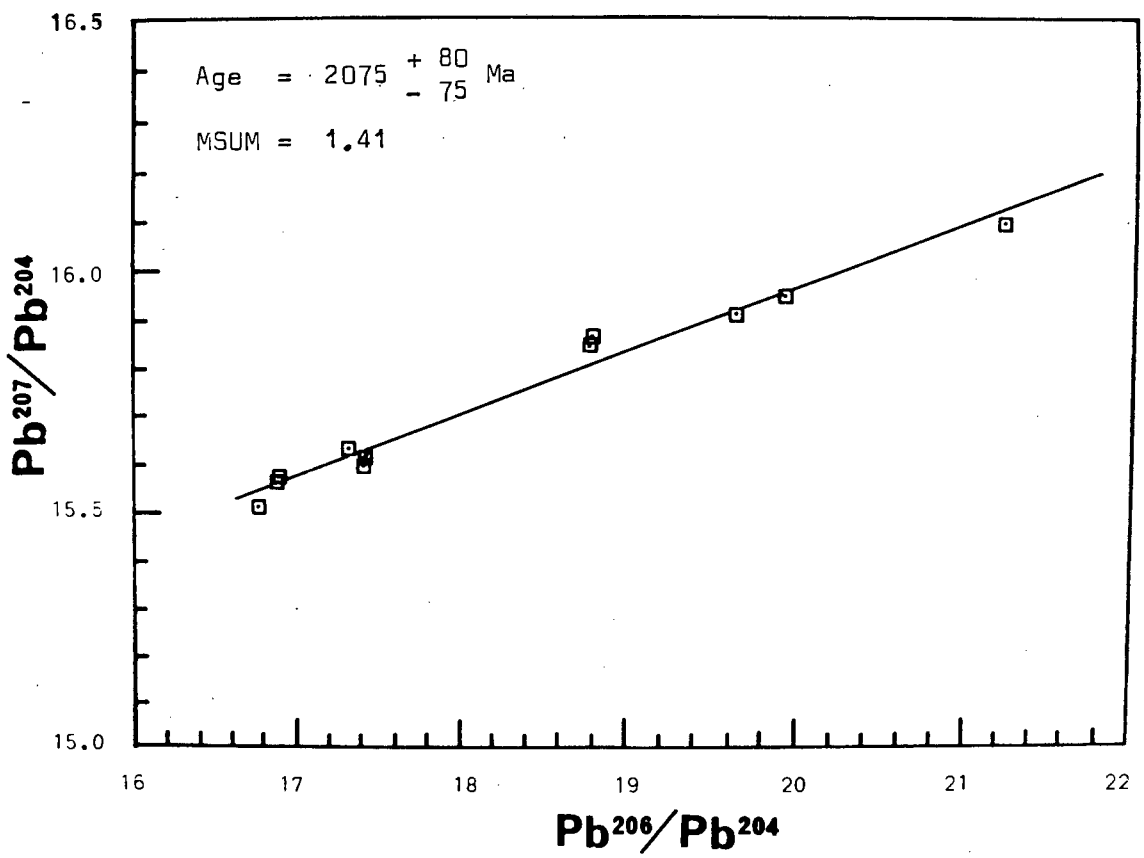

Fig. 16. Pb^{207}-Pb^{206} isochron for the combined HVG.

However, the positions of 41 and 113 on a Th-U plot (Fig. 15) suggest that they may have suffered loss of Th. There is rough correlation between Th and U for all samples that lie on the Th-Pb isochron. The aberrant samples lie distinctly to the left of the line of best fit, indicating a Th content too low for the observed U content. A similar technique has been used by Black and Richards (1972) to detect U removal in rocks. Sample 65 falls on the line in Fig. 15, but it must be remembered that this sample has a composition that also falls above the U-Pb isochrons. This latter feature may be due to U removal and, if coupled with Th removal, may result in the sample retaining its original Th/U ratio. It is therefore concluded that the aberrant nature of samples 41 and 113 has been caused by Th removal. Sample 65 has probably suffered U as well as Th removal so its aberrant nature cannot be detected using a Th-U plot.

3.3.1.4. Pb^{207}-Pb^{206}

A close linear correlation between Pb^{207}/Pb^{204} and Pb^{206}/Pb^{204} is apparent in Fig. 16. Such a correlation is predicted if all the rocks had the same Pb isotopic composition some time in the past, but experienced strong U-Pb fractionation. Closed system enrichment in Pb^{207} and Pb^{206} by decay of U isotopes would tend to spread the individual samples along an isochron (Kanasewich, 1968). The slope of the isochron depends on the period for which the closed system conditions prevailed.

Regression of the data for 12 samples yields a slope age of $2075 \pm {}^{80}_{75}$ Ma and an MSUM of 1.4. An important point is that all samples conform to the isochron, including 65, which has been shown to be aberrant on all U-Th-Pb diagrams. U removal has been suspected for this sample since it has a composition that lies above the line of best fit in both U-Pb diagrams. Removal of U must have occurred in recent times (~10 Ma) because an earlier period of U removal would have resulted in the composition of 65 falling off the Pb^{207}-Pb^{206} isochron as well. Assuming that 65 should have a composition

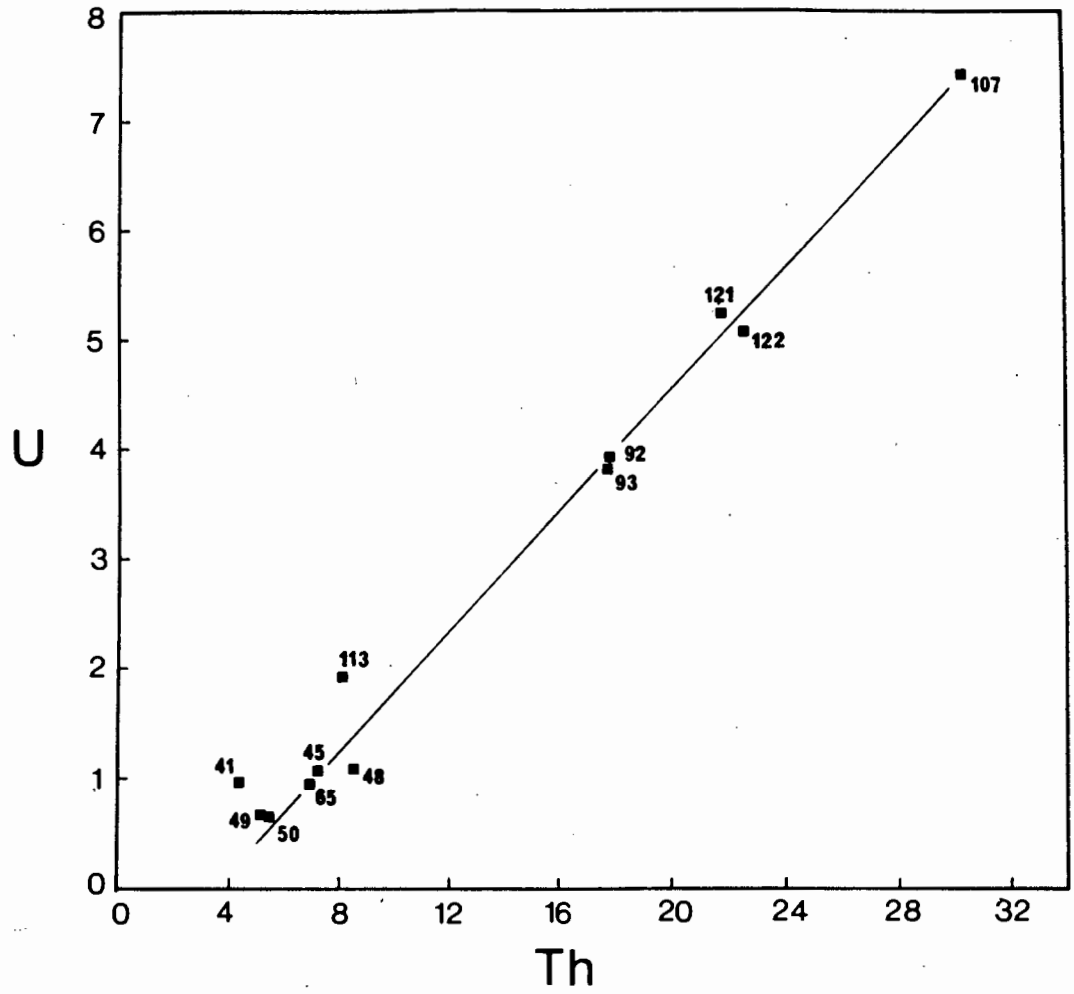

Fig. 15. Plot of Th versus U for the samples analysed in the U-Th-Pb geochronological study. Note that the line of best fit through the data does not pass through the origin.

that falls on the U-Pb isochrons, about 40 percent of its total U must have been removed. The mobility of U is well known and there are many examples where total rock U-Pb systems have been rendered unusable because of recent U removal (Rosholt et al., 1969, 1971, 1973; Rogers and Adams (1969); Moorbath et al., 1975; Barbier and Ranchin, 1969; Oversby, 1975; Manton, 1973). U migration must have been an extremely localised phenomenon in the HVG, since only one sample in twelve shows this feature.

3.3.1.5. Discussion

The U^{235}-Pb^{207}, Th-Pb and Pb^{207}-Pb^{206} ages all overlap at the one sigma level, while the U^{238}-Pb^{206} age is slightly lower. In view of the very low U^{235}-Pb^{204} ratios, the U^{235}-Pb^{207} age is imprecise and little weight can be assigned to it. The slightly lower U^{238}-Pb^{206} age is interesting because it suggests that small amounts of Pb may have been lost very recently. In order to maintain a linear array, a constant amount of Pb, irrespective of the U^{238}-Pb^{204} ratio and original Pb content, must have been removed from each sample. However, such Pb loss would be inconsistent with the agreement between the Th-Pb and Pb^{207}-Pb^{206} ages. In view of the unsatisfactory results which other workers have obtained for the U-Pb system, more weight is put on the agreement between the Th-Pb and Pb^{207}-Pb^{206} ages than on their disagreement with the U^{238}-Pb^{206} age. At present the problem of the lower U^{238}-Pb^{206} age remains unresolved.

3.3.2. Vioolsdrif leucogranite

It was not possible to investigate all the intrusive rock types in the time available, so the leucogranite was chosen because it would provide a check on the minimum age of the VIS.

3.3.2.1. U-Pb

Figs. 17 and 18 show the two U-Pb plots and the wide scatter exhibited by six analysed samples of the Vioolsdrif leucogranite. All the data points lie on or above a reference isochron which corresponds to an age of 1800 Ma (based on Rb-Sr and Pb^{207}-Pb^{206} ages). The initial Pb isotopic ratios are those obtained for the HVG. The most likely mechanism to explain the scatter is recent U removal, because the Pb^{207}-Pb^{206} plot (Fig. 20) is quite regular. It has already been noted that recent U removal in whole rock samples is very common and the scatter in Figs. 17 and 18 confirms its

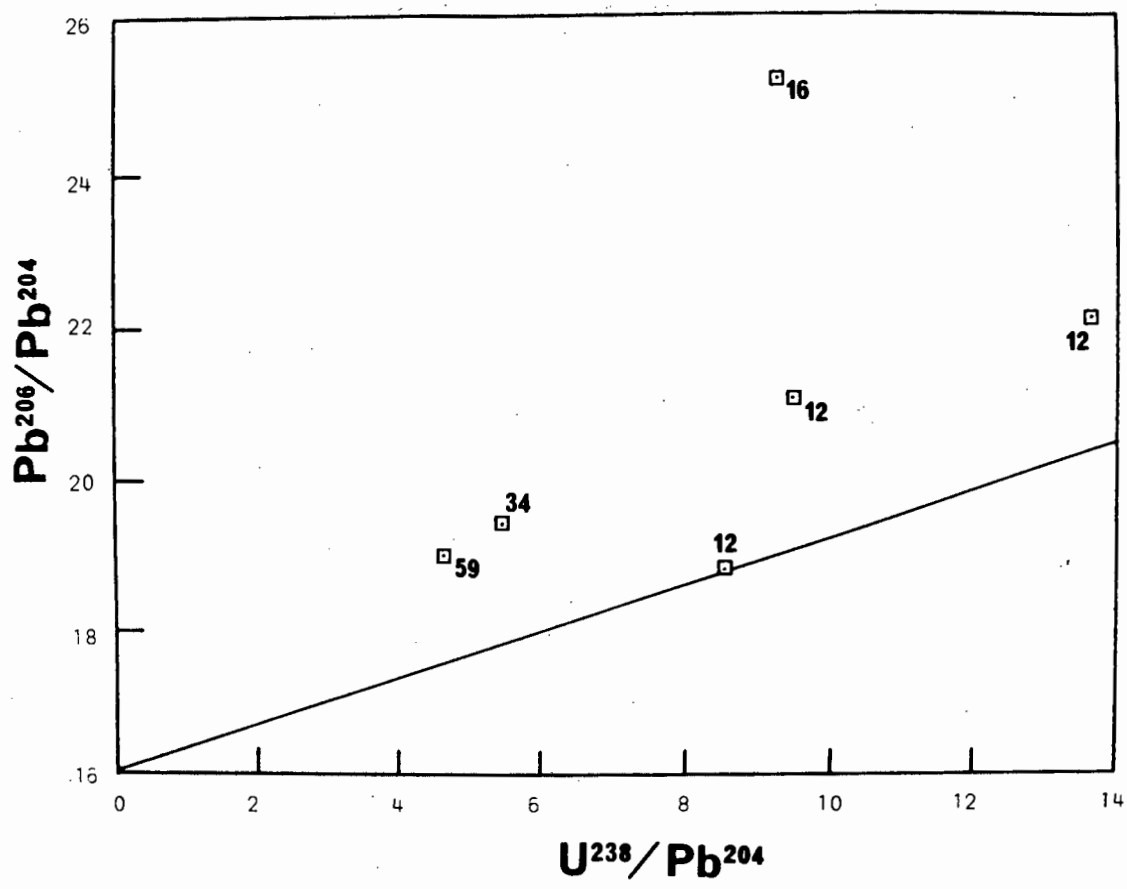

Fig. 17. U^{238}–Pb^{206} diagram for the Vioolsdrif leucogranite. Solid line represents a 1800 Ma reference isochron with $(Pb^{206}/Pb^{204})_o = 16$.

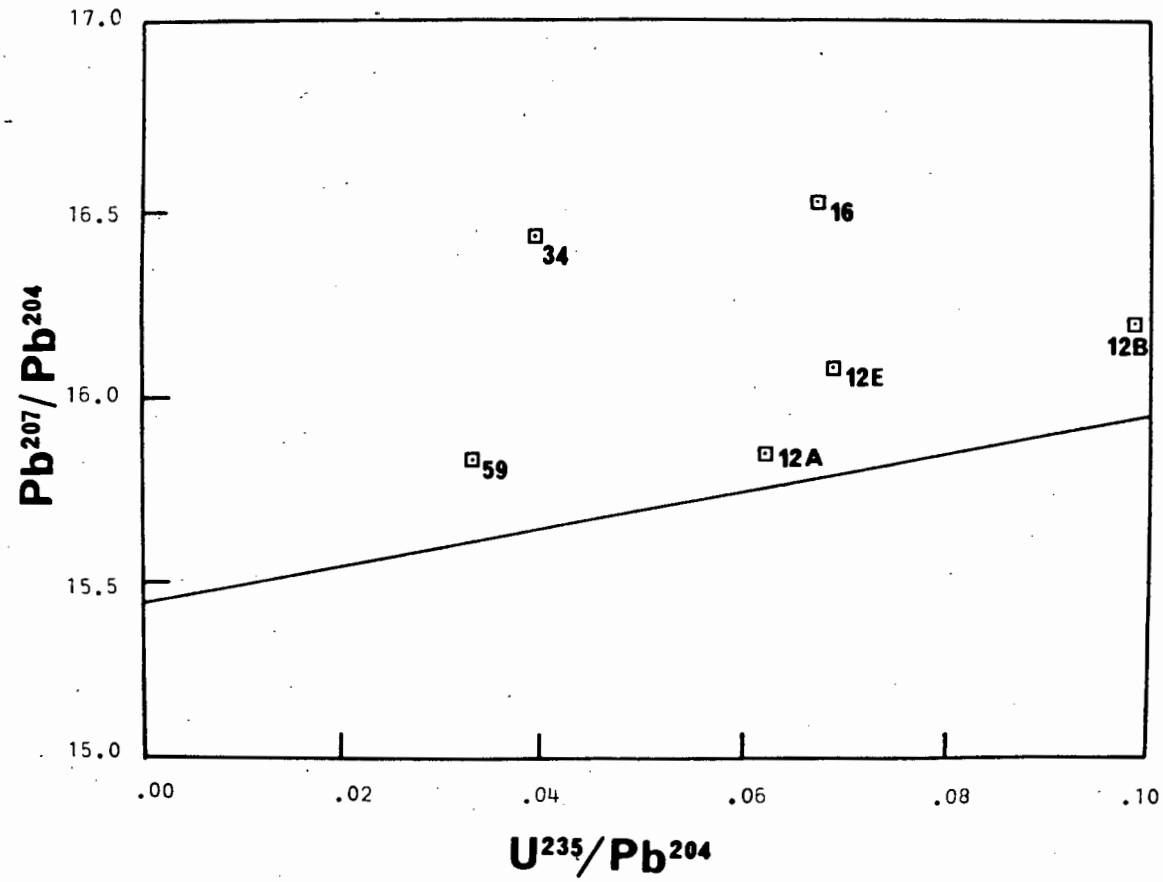

Fig. 18. U^{235}–Pb^{207} diagram for the Vioolsdrif leucogranite. Solid line represents a 1800 Ma reference isochron with $(Pb^{207}/Pb^{204})_o = 15.44$.

widespread prevalence.

Table 6. Comparison between observed U content (U_o) and that predicted assuming an age of 1800 Ma (U_p). The difference has been expressed as a percentage of the predicted U content.

Sample	Uo	Up	Δ%
DRV - 12A	5.85	5.85	0
DRV - 12B	6.42	8.98	28.5
DRV - 12E	4.89	8.08	39.5
DRV - 16	6.17	19.02	67.6
DRV - 34	3.01	5.78	47.8
DRV - 59	2.44	4.82	49.4

Since the Pb isotopic ratios appear to have remained constant during the period of U removal, the amount of U removed may be calculated if the 1800 Ma age and initial Pb isotopic ratios for the HVG are adopted. The results are listed in Table 6 and show a wide range in degree of U removal from near zero to nearly 70 percent. In view of the degree to which U has been removed from the Vioolsdrif leucogranites, the U abundance data reported for the other granitic rocks in the VIS must be considered only as minimum values. Published data for U in any granitic rocks must therefore be treated with caution, unless U-Pb isotopic work has been carried out in order to evaluate the possibility of U migration.

The predicted U abundances listed in Table 6 depend on the age and initial Pb isotopic ratios adopted. The age of 1800 Ma is reasonably justified, in view of the concordant results of the Rb-Sr and Pb^{207}-Pb^{206} isochrons. Changing the value for the Pb^{206}/Pb^{204} ratio by one unit (i.e. 16 ± 1), results in a change in predicted U content of 1-2 ppm. The predicted U values in Table 6 are considered therefore to be only accurate to about 2 ppm.

3.3.2.2. Th-Pb plot

The Th-Pb plot also shows considerable scatter (Fig. 19). All data points fall above a 1800 Ma reference isochron (using the initial Pb^{208}/Pb^{204} ratio for the HVG). Three samples define a roughly parallel line, which yields a slope age of 1730 ± 50 Ma and an initial Pb^{208}/Pb^{204} ratio of 36.01 ± 14. This may be pure coincidence and little reliance is assigned to this data. The aberrancy could be caused by Th removal, but it is difficult to determine when and how this removal took place. The analagous Pb-Pb plots (e.g. Pb^{208}/Pb^{204} versus Pb^{206}/Pb^{204}) will not necessarily define a straight line, except in the unlikely case where all the samples have the same Th/U ratio. The Th-U plot is, of course, modified by the effects of U removal, so no predictions about Th migration can be made. The relative immobility of Th in rocks argues against this element being removed in a manner similar to U (Adams and Rogers, 1959; Rosholt et al., 1971) during surface weathering. Although recent Th loss is suspected, further work is necessary to furnish proof.

3.3.2.3. Pb^{207}-Pb^{206}

Five out of six analysed samples conform to a well defined isochron which yields an age of 1770 ± 50 Ma (Fig. 20) and an acceptably low MSUM of 0.8. One sample (34) falls appreciably above the line of best fit, but since the Pb isotope analytical run was unstable, the Pb isotopic data are unreliable. Judging from the position of the aberrant sample, the Pb^{207}/Pb^{204} ratio appears to be the one at fault. This probably contributed a great deal to the position of 34 in the U^{235}-Pb^{207} diagram, but the other atomic ratios are relatively insensitive to changes in Pb isotopic ratios.

3.3.2.4. Discussion

The effect of recent U (and perhaps Th) removal has resulted in

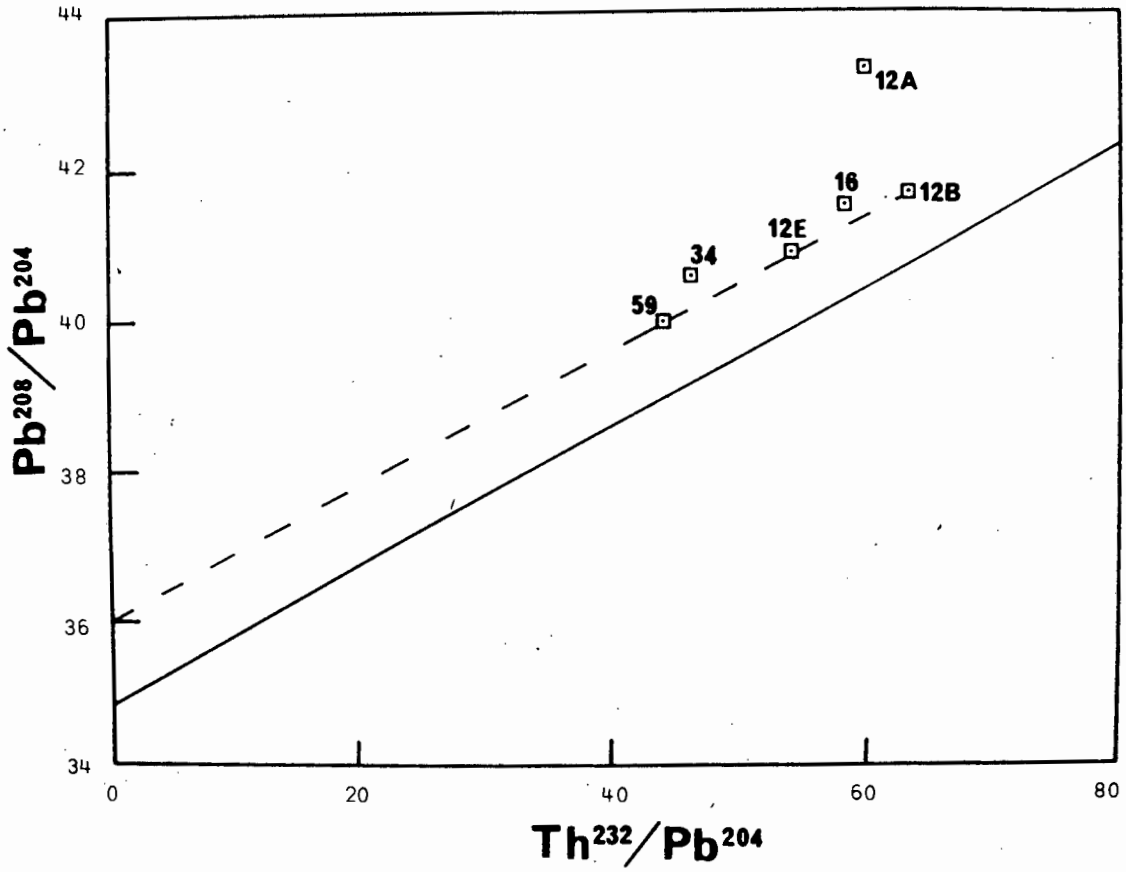

Fig. 19. Th-Pb diagram for the Vioolsdrif leucogranite. Solid line represents a 1800 Ma reference isochron with $(Pb^{208}/Pb^{204})_o = 34.86$.

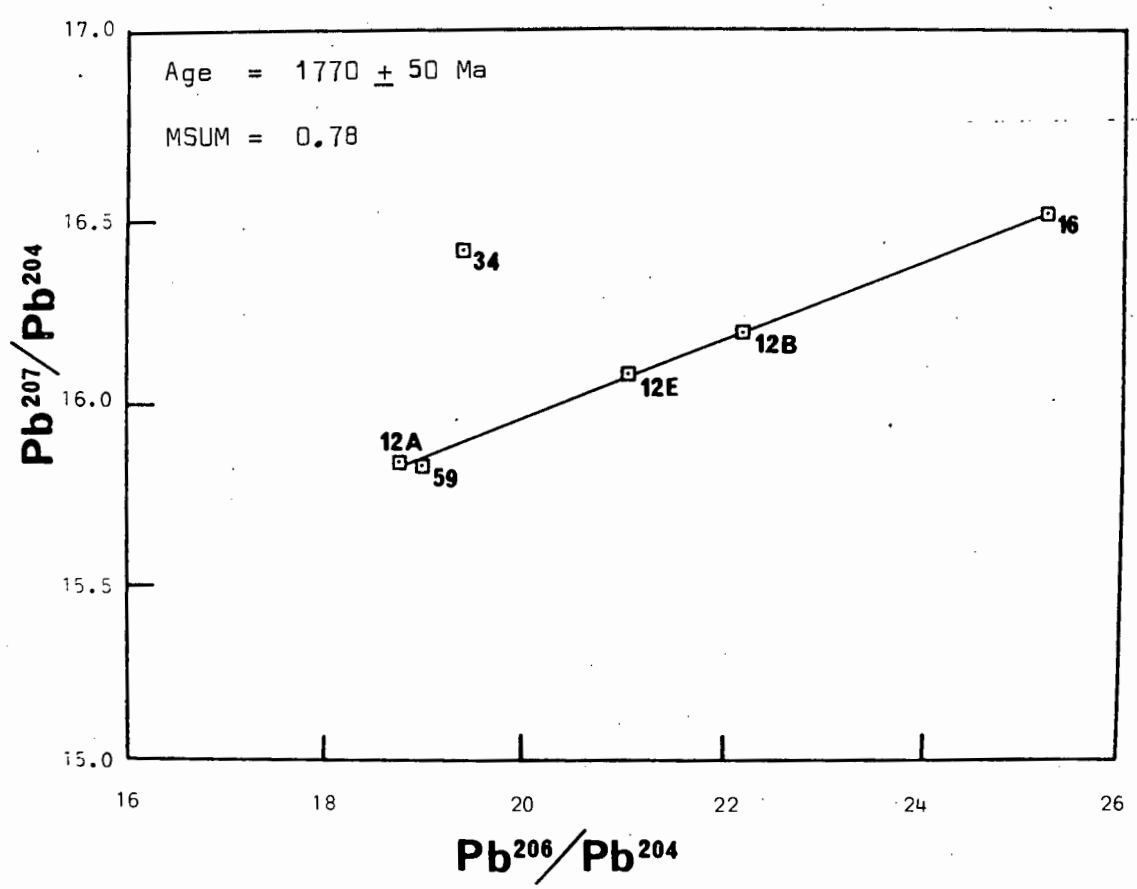

Fig. 20. Pb^{207}-Pb^{206} isochron for the Vioolsdrif leucogranite.

considerable scatter in the U-Pb and Th-Pb diagrams. Only the Pb^{207}-Pb^{206} system appears to have remained unaffected and is therefore the only system which produces a reliable age. In view of published results of similar isotopic studies, such unsystematic behaviour is not unexpected. Published U abundance data for rocks must be treated with caution unless the effects of recent U removal have been evaluated.

3.4. Comparison between Rb-Sr and U-Th-Pb ages

3.4.1. Haib Volcanic Group

Rb-Sr and U-Th-Pb ages are summarised in Table 7 and illustrated in Fig. 21. The combined Rb-Sr, Th-Pb and Pb^{207}-Pb^{206} (subsequently abbreviated to Pb-Pb) ages all overlap at the one sigma error level. Such concordancy between independent radioactive systems implies one of two possibilities:

(i) The apparent age defined by these systems is very close to the age of eruption of the lavas.

(ii) Closure occurred after isotopic homogenisation during an intense thermal event.

The latter process implies medium to high grade metamorphism, which must have occurred on a regional scale since the samples were collected over a very wide area. No petrographic or mineralogical evidence exists to suspect such grades of metamorphism (see Chapter 6) and it is concluded that the concordant age pattern exhibited by the HVG is probably not the result of closure immediately on cooling after an intense thermal event. It may be argued that even the relatively low grade metamorphic readjustment experienced by the HVG may have resulted in isotopic resetting, especially for the Rb-Sr system. Allsopp et al., (1973) have reported a reset Rb-Sr

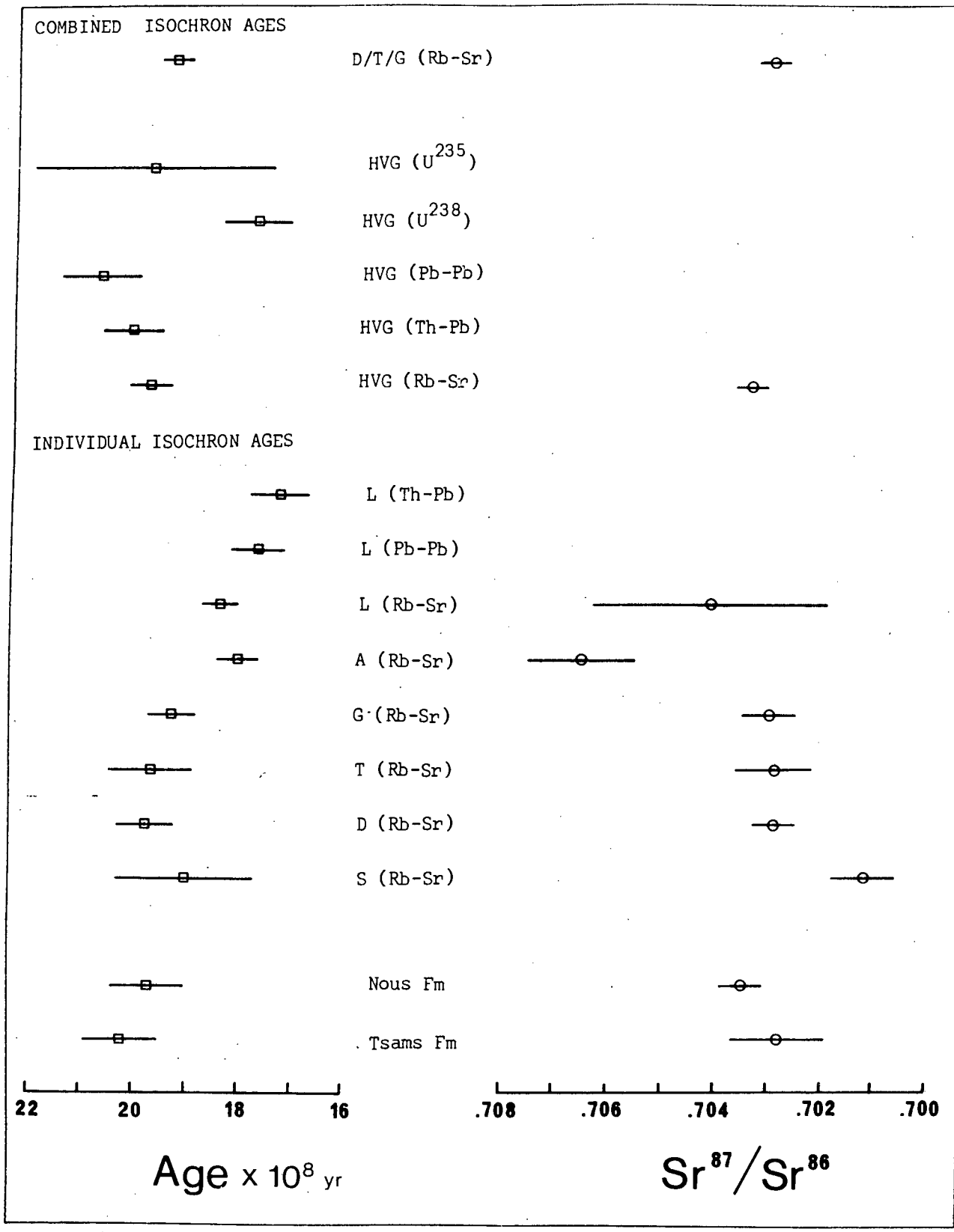

Fig. 21. Summary of radiometric ages and initial Sr isotopic ratios for the HVIP.

total rock age for Archaean greenstones in the Barberton Mountainland that have only suffered low grade greenschist facies metamorphism. Possible resetting of the Rb-Sr system during metamorphism is evaluated further in 3.5.

3.4.2. Vioolsdrif Intrusive Suite

At present only the leucogranite can be evaluated and the effects of U and Th migration make few conclusions possible. The Rb-Sr age of 1835 ± 35 Ma overlaps at the one sigma level with the Pb-Pb age of 1770 ± 50 Ma, indicating a concordant age of about 1800 Ma. The unmetamorphosed nature of the leucogranite suggests that such concordancy is probably the result of closure soon after intrusion.

3.5. Test for Sr isotopic resetting

The possible effect of Sr isotopic resetting during a later metamorphic event can be tested by calculating the maximum possible Rb-Sr ages that the various rocks can have. Maximum Rb-Sr ages critically depend on two assumptions:

(i) There is a minimum possible Sr^{87}/Sr^{86} ratio and this is equal to that of the upper mantle at the time of the igneous activity.

(ii) The average Rb/Sr ratio of the rock system under investigation did not change drastically during the metamorphic event.

The rock system in question is the HVG, since it has been suggested (see Chapter 6) that the metamorphism which affected the volcanics occurred during the regional emplacement of the Vioolsdrif batholith. This implies that the HVG could be significantly older than 1800-1900 Ma, despite the predictions based on the concordant age pattern discussed in 3.4.1. Figure 22 illustrates the procedure whereby the maximum Rb-Sr age for the HVG may be calculated. The line A-B represents a linear approximation to the

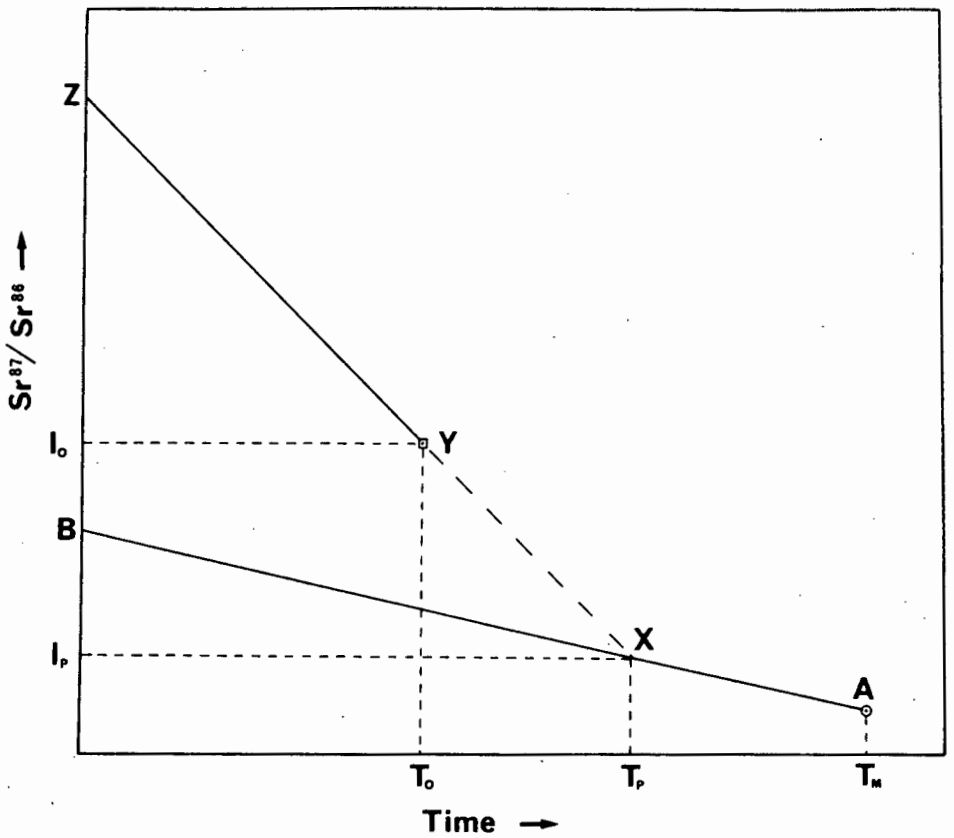

Fig. 22. Graphical illustration of the maximum possible Rb-Sr age of a particular system. Explanation in text.

evolution of Sr in the upper mantle between T_m (age of the Earth), and the present day. Point Y represents isochron data (observed age = T_o, observed initial Sr^{87}/Sr^{86} = I_o) for the rock system under investigation and the line Y-Z represents the increase in average Sr^{87}/Sr^{86} ratio of the system until the present day. The extrapolation of line Z-Y meets the upper mantle evolution line at X, which defines the maximum possible Rb-Sr age for the rock system (predicted age = T_p, predicted Sr^{87}/Sr^{86} = I_p).

The age of the earth has been taken as 4.57×10^9 years (Stacey and Kramers, 1975). A primordial Sr^{87}/Sr^{86} ratio of 0.699 has been adopted and is based on the value (BABI) derived by Papanastassiou and Wasserburg (1969)

for basaltic achondrites. The value for the present day upper mantle is based on the range found in modern oceanic basalts and a minimum value of 0.703 has been adopted (Faure and Powell, 1972). The results for the Haib lavas are listed in Table 8 and it can be seen that on this basis, the maximum possible Rb-Sr age of the volcanics is only 260 Ma greater than the observed Rb-Sr age. It is concluded that the HVG does not represent a significantly older volcanic pile that has been reset by metamorphism during the emplacement of the Vioolsdrif batholith. The average Rb/Sr ratio for the HVG is an arithmetic mean of all analysed lavas (55 samples). If the average was weighted towards the more abundant lavas (andesites, dacites) then the Rb/Sr ratio would be higher, resulting in an even smaller period of time between eruption and the postulated resetting event.

Maximum ages for the various intrusive rocks have also been calculated and it can be seen that the difference between T_p and T_o is only 100-200 Ma. The predicted ages for the VIS have no real significance because the rocks have not been metamorphosed. Rb-Sr systematics of deformed and metamorphosed VIS is briefly discussed in 3.7.

Table 8. Comparison between the observed Rb-Sr age (T_o) and initial Sr^{87}/Sr^{86} ratio (I_o), with the predicted maximum Rb-Sr age (T_p) and minimum initial ratio (I_p) for various rock units within the HVIP.

ROCK TYPE	RB/SR	Rb^{87}/Sr^{86}	Sr^{87}/Sr^{86}	To	Io	Tp	Ip
LEUCOGRANITE	2.429	7.137	.8859	1810	.7041	1840	.7014
ADAMELLITE	.699	2.029	.7579	1800	.7065	1985	.7013
GRANODIORITE	.371	1.075	.7321	1925	.7030	2045	.7012
TONALITE	.237	.685	.7219	1965	.7029	2150	.7011
DIORITE	.208	.601	.7196	1975	.7029	2190	.7011
SWARTKOP	.162	.468	.7137	1900	.7012	-	-
HAIB VOLCANICS	.362	1.048	.7330	2010	.7034	2270	.7010

3.6. Zircon U-Pb chronology

Zircon has been separated from a Vioolsdrif granodiorite (DRV-15) and adamellite (DRV-01), and from a porphyritic rhyolite in the Tsams Formation of the HVG (DRL-92). An aliquot representing the total population of each zircon separate has been analysed for U and Pb concentrations and Pb isotopic ratios. The data obtained are listed in Table 9, together with analyses of zircon separates from rocks collected by other workers. One of the granodiorite samples (VG-1) has also yielded sufficient apatite for analysis and data for this mineral are also included.

The ages calculated from the isotopic data have been corrected for initial Pb, using the initial Pb isotopic ratios determined for the HVG. These values are considered to be more realistic than arbitrary values generally used for zircon age determinations. Model ages are listed in Table 9 and it can be seen that all zircons are discordant. However, the Pb^{207}-Pb^{206} ages are all very similar and it is not surprising that when plotted on a concordia diagram (Fig. 23) the points define a chord passing through the origin and an upper intercept corresponding to an age of 1860 $\pm$ 25 Ma. A seven point regression yields a lower intercept of -0.003 $\pm$ 0.002 (which can be regarded as zero) and an upper intercept which yields a Pb^{207}/Pb^{206} ratio of 0.110375 $\pm$ 0.001616. The MSUM of the best fit line is 0.72.

The seven points on the chord represent data for four adamellites, two granodiorites and one rhyolite. Two of the adamellites (DRV-01 and JPW-19) come from the same pluton near the banks of the Orange River at Vioolsdrif. Adamellite in this pluton is porphyritic, undeformed and unmetamorphosed. Contrasting with these rocks, are the adamellite samples DRV-33 and BB-3. The former was collected from a road cutting about 30 km south of Vioolsdrif, where the adamellite has been deformed and recrystallised into gneiss. BB-3 was collected by H.J. Blignault from outcrops of porphyroblastic adamellite gneiss north of the present study area and considered by Blignault (1975) to be reconstituted Vioolsdrif batholith. Granodiorite

	CONCENTRATIONS		ISOTOPIC RATIOS			ATOMIC RATIOS			AGES (Ma)		
Sample	U	Pb	206/204	207/204	208/204	206/238	207/235	207/206	206/238	207/235	207/206
DRV-01	587.5	78.7	780.88	102.80	248.68	.104928	1.651255	.114136	643	990	1869
DRV-15	489.7	119.6	1486.55	176.14	274.57	.215224	3.241641	.109238	1257	1467	1788
JPW-19	604.4	153.1	385.24	56.58	146.89	.184026	2.822951	.111256	1090	1361	1820
GBW-3	282.7	41.91	2142.70	253.91	592.89	.122386	1.892016	.112122	745	1080	1835
GBW-4	660.9	136.3	3073.14	355.26	467.42	.187959	2.880528	.111150	1100	1380	1820
BB-3	354.3	119	618.43	83.18	181.76	.265542	4.115714	.112412	1520	1660	1850
DRV-33	434	91.9	612.75	83.31	218.69	.160124	2.508764	.113632	957	1275	1860
VG-1	879.4	275.4	2380.95	265.68	415.29	.307635	4.487835	.105803	1730	1730	1740
VG-1A	34.60	12.47	67.93	19.29	47.50	.159813	1.608178	.072983	956	973	1013
DRL-92	232.7	74.7	2343.02	282.24	736.93	.257802	4.074511	.114627	1480	1650	1875

Table 9. U and Pb concentrations (ppm), Pb isotopic ratios, relevant atomic ratios and model ages of zircons and one apatite separated from various rock units within the HVIP.

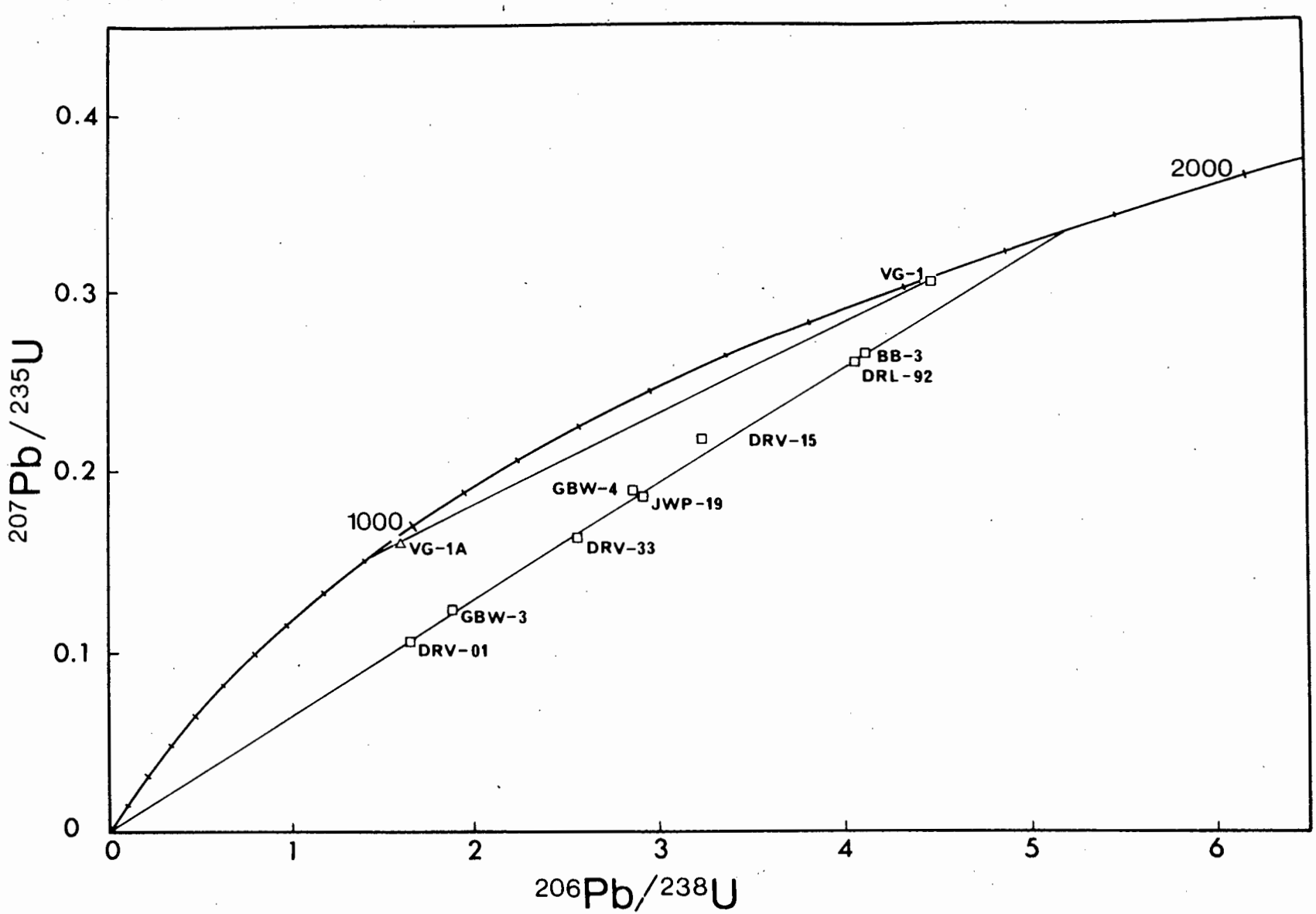

Fig. 23. Pb-U concordia diagram containing data for zircons (plus one apatite) separated from various rock units within the HVIP.

samples GBW-3 and 4 were collected by G.J. Beukes further to the east of the present study area. The samples apparently come from even-grained unmetamorphosed granodiorite cutting correlatives with the HVG (Beukes, 1973). The rhyolite zircon (DRL-92) also has an isotopic composition that falls on the chord, suggesting that the intercept age (1860 Ma) represents the time when this zircon finally became closed to U and Pb migration. The rhyolite from which the zircon was separated has an isotopic composition which falls on the Rb-Sr and U-Th-Pb isochrons described previously. The crystallisation age of the rhyolite zircon was probably $\pm$ 2000 Ma, but this mineral remained open to U and Pb migration during the emplacement of the Vioolsdrif batholith. Only in the final stages of emplacement, when the temperature cooled sufficiently for closure to be attained, did the zircon begin to retain radiogenic Pb. The spectrum of ages derived from the total rock study of the VIS suggests that emplacement began soon after eruption of the HVG at 2000 Ma and ended with the leucogranites at about 1800 Ma. The most voluminous intrusive rock types are the tonalite, granodiorite and adamellite; the later leucogranite is volumetrically insignificant. The thermal maximum was probably attained during the emplacement of the most voluminous rocks and the later rocks were probably emplaced as the temperature was gradually decreasing. The sequence of intrusion is towards the lower temperature magma (i.e. diorite -- tonalite -- granodiorite -- adamellite). It is probable that zircons crystallising from the earlier granitic magmas (tonalite, granodiorite) exhibited open system behaviour until the closing stages of intrusive activity. The upper intercept age shown in Fig. 23 is significantly lower than the total rock Rb-Sr age of the granodiorite, but is within the range of that established for the adamellite and leucogranite. It is suggested that zircons in the granitic rocks became closed to U and Pb migration at 1860 $\pm$ 25 Ma.

The zircon U-Pb system was only disturbed in very recent times when a significant amount of Pb was lost, thereby producing a chord which passes through the origin of the Pb-U concordia diagram. Despite the fact that some of the data points represent Vioolsdrif plutonic rocks deformed and

recrystallised during a later metamorphic event, no impression was apparently made on the U-Pb system of the constituent zircon.

3.7. "Xenolith in xenolith" exposure

An isolated exposure of granitic rocks about 10 km south of the present study area displays an interesting association. An adamellite encloses xenoliths of granodiorite, which in turn contain tiny xenoliths of fine-grained biotite-rich, hornfels. The order of incorporation is similar to the sequence of intrusion in the Vioolsdrif batholith. The inner xenolith probably represents hornfelsed country rock and is similar to the numerous fine-grained xenoliths which characterise the Vioolsdrif granodiorite. Although isolated, the exposure is considered to represent a southern extension of the Vioolsdrif batholith. However, in this region the plutonic rocks are strongly deformed and a foliation, defined by orientation of biotite, passes through host and xenoliths alike.

Zircon has been separated from the host adamellite, while zircon and apatite have been separated from the granodiorite xenolith. Whole rock samples of adamellite, granodiorite and inner xenolith have been analysed for their Sr-isotopic compositions. The mineral data are included in Table 9 and have been plotted in Fig. 23. Zircon from the host adamellite (DRV-33) has already been described in 3.6., and has an isotopic composition that falls on the chord reflecting recent loss of Pb. Zircon and apatite from the granodiorite xenolith yield very different, but individually concordant, age patterns. Petrographic evidence suggests that both are primary minerals and the chord defined indicates that the zircon became closed to U and Pb migration at about 1740 Ma, whereas the apatite lost practically all its radiogenic Pb during a later event at $\pm$ 1000 Ma. Although the host adamellite is just as deformed and metamorphosed as the granodiorite xenolith, there is no suggestion that zircon DRV-33 ever experienced the 1000 Ma event.

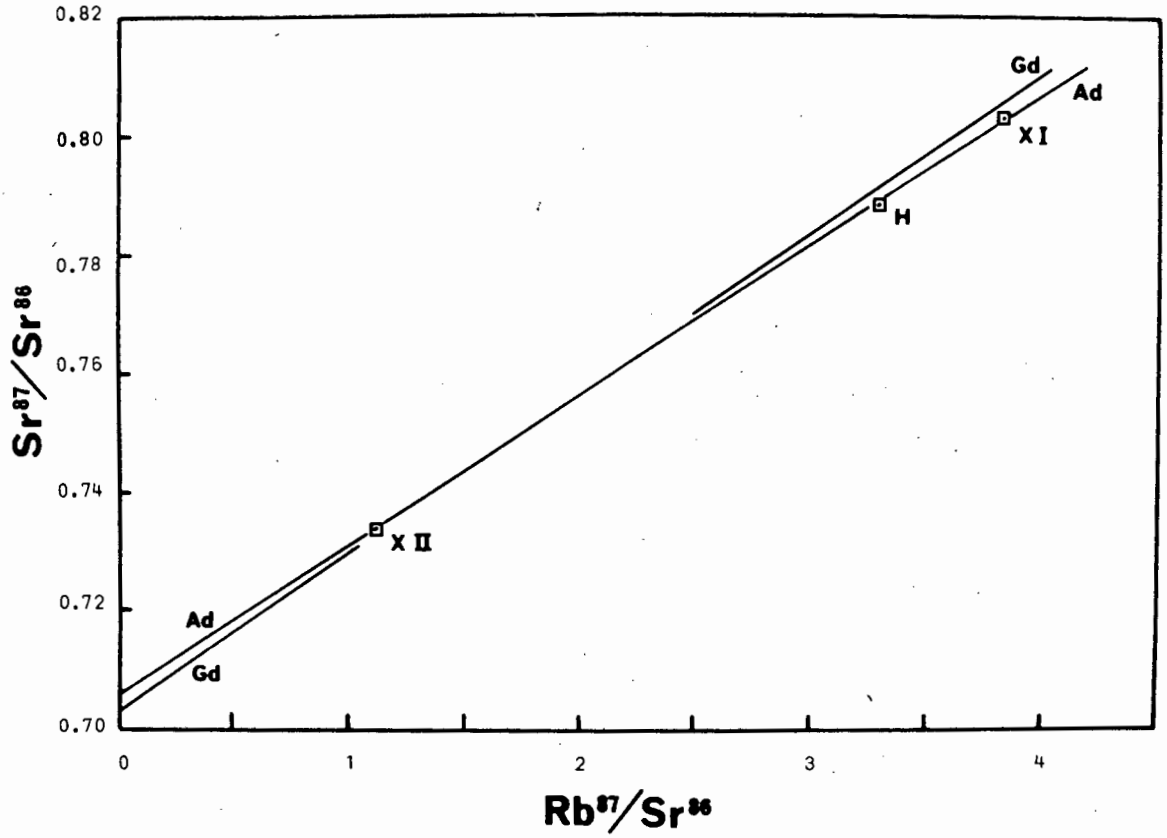

Fig. 24. Rb-Sr diagram for the components within the "xenolith in xenolith" exposure.

The three whole rock samples have been plotted on a Rb-Sr diagram (data in Table 4), together with reference isochrons corresponding to the Vioolsdrif granodiorite and adamellite (Fig. 24). The three points conform closely to the adamellite isochron and indicate that the xenoliths were isotopically reset during their incorporation in the host adamellite. The subsequent deformation and recrystallisation did not in any way disturb the total rock Rb-Sr system.

To summarise, zircon from the host adamellite has an isotopic composition which falls on a chord reflecting recent loss of Pb, but retains the

closure age of ± 1860 Ma exhibited by zircons from unmetamorphosed rocks further north in the batholith. Zircon from the granodiorite xenolith yields a concordant but anomalously low Pb-Pb age of ± 1740 Ma. Apatite from the granodiorite xenolith records the effect of a later thermal event at about 1000 Ma. This later event may have been accompanied by the deformation and recrystallisation exhibited by the rocks in this southern region. The total rock Rb-Sr system was unaffected by the later 1000 Ma event and retains the age of the host adamellite.

4

THE HVG GENERAL DESCRIPTION

4.1 Distribution

As mentioned previously in 2.2, volcanic rocks cropping out in the Haib-Vioolsdrif region and in the adjacent Richtersveld, were correlated with the Wilgenhoutsdrif Series by De Villies and Söhnge (1959). Since no detailed geochemical work has been done on the volcanics in the Richtersveld, their inclusion within the HVG (as defined in the present study) is open to question. However, in order to show the *possible* distribution of the HVG in the lower Orange River region, they have been included in Fig. 25, which indicates an areal distribution of at least 4000 square kilometres (1500 square miles). This could be further increased if the volcanics in the north-east Richtersveld (previously correlated with the Marydale Series) also prove to be part of the HVG. They have been given the provisional name of De Hoop Volcanic Group (Blignault, 1974b).

4.2 Stratigraphy within the HVG

Detailed stratigraphy within the HVG is very difficult to establish because of (1) local tight folding, (2) extensive faulting and shearing and (3) pervasive metamorphic recrystallisation. Where sections of 1-2 km could be measured and the original character of the rocks possible to determine, no systematic pattern could be recognised. It is likely that the volcanic succession comprises a suite of lavas, pyroclastics and volcanogenic sediments (produced by local reworking of the volcanic pile) in an almost random juxtaposition. Such a juxtaposition of different rock types is not unusual in volcanic fields, especially those erupting abundant intermediate and acid material. Eruptions are typically explosive and may issue from a great number of short-lived vents, thereby producing a plexus of volcanic material varying greatly in texture and composition.

Despite the stratigraphic complexity, a very rough two-fold division of the HVG is possible. Dacitic and rhyolitic material seem to predominate lower in the exposed succession, whereas basaltic-andesitic material increases towards the top. As a result of this rough compositional difference between the top and bottom of the exposed succession, two formations have been defined (Blignault, 1975). These are (1) the Nous Formation (after the Nous River), which comprises the upper, more basic part of the HVG and (2) the Tsams Formation (after the Tsams River), which includes the more felsic rocks in the lower part of the HVG.

4.3 Structure of the HVG

4.3.1 Attitude of flows and beds

Unfortunately, there are few primary volcanic or sedimentary features preserved in the HVG that could provide irrefutable evidence for the attitude of flows or beds. Features such as flow forms, flow banding, pyroclastic and sedimentary bedding are quite common, but in many cases it was impossible to determine which way up the structures were. Criteria upon which the attitude of flows or beds was deduced and which allowed conclusions to be made regarding the relative positions of the Tsams and Nous Formations, are described below.

(i) Mantled bedding in primary airfall deposits

Large blocks often occur in crudely bedded, unsorted primary airfall deposits. Finer grained material may deposit in thin beds mantling the large block. Since the mantling beds will be convex upwards, the attitude of the sequence can be readily deduced.

(ii) Size grading in fragmental beds

Coarse to fine grading may occur in both primary airfall or subaqueous sedimentary deposits. Provided the original fragmental texture has not been obliterated by metamorphic recrystallisation, the grading reveals the attitude of the sequence. Reverse grading may occur when fragments of a permeable

material (e.g. pumice) fall into still water. Smaller particles get water-logged quicker and sink first, thereby forming fine to coarse upwards size grading. This causes problems in interpretation when no other criteria accompany size grading. Outcrops displaying only size graded beds were left unresolved.

(iii) Bed thickening towards topographic lows

Primary airfall and subaqueous sediments often show beds that thicken towards topographic lows that existed prior to eruption. Thickening is probably caused by gravitational instability of material deposited on the slopes of the lows. This criterion suffers from the problem that the original attitude of the beds may be modified by folding. However, in localities where the volcanic sequence was near horizontal, it was possible to make out original topographic relief.

(iv) Soft sediment deformation

Subaqueous deposits in relatively small pools of water (e.g. lakes, ponds) may slump from the slopes of these topographic lows into the centre. Structural features that accompany such slumping may be small scale overfolding and thrusting.

4.3.2. Pre-intrusion deformation

Prior to the emplacement of the VIS, the HVG was deformed into a series of open folds striking more or less E-W. Evidence for this early folding has been partly obliterated by forceful intrusion and later deformation. The best preserved structure is a major syncline that is well exposed between Vioolsdrif and the Namma Keinam Weir. The axis of the syncline strikes ESE across the Orange River about 2-3 km upstream from Vioolsdrif but swings around to ENE and crosses the Orange River again between the Noujaseep and Uranoop confluences. Near Vioolsdrif the syncline is open, with the southern limb much steeper than the northern limb. Further eastwards the northern limb steepens until it is overfolded, so that both limbs dip northwards. The axis

is more or less horizontal at Vioolsdrif but plunges more and more to the west as it traced eastwards and plunges at an angle of about 70^{o} at Haakiesdoorn.

Evidence that this major syncline predates the emplacement of the VIS is that plutons of adamellite, granodiorite, tonalite and diorite intrude the base of the syncline. An adamellite pluton cuts the syncline at Vioolsdrif, while an extensive plutonic complex cuts the syncline at the Haib River mouth. Upstream from the junction between the Noujaseep and Orange Rivers, plutons cut the southern limb of the syncline and send irregular sheets and dikes into the dipping volcanic sequence.

4.3.3. Deformation during intrusion

Some of the plutons have been emplaced forcefully by updoming the HVG so that sedimentary beds and lava flows dip away from the contacts. Good examples of this are around the plutons of adamellite cropping out in the area between the Warmklip and Krom Rivers. Steep dips away from the NE contact of an adamellite pluton near Vioolsdrif are well exposed on the north bank of the Orange River in this vicinity. In some plutons, the last stages of emplacement occurred when the rocks were almost completely consolidated and gneissic structures are developed parallel to the contacts. Another common feature, especially when the rock type is tonalite or granodiorite (less commonly adamellite), is for the contacts to be brecciated and to have hundreds of xenoliths of country rock crowding the margins of the plutons. Such a feature indicates that a considerable amount of stoping occurred along with updoming during emplacement.

4.3.4. Later deformation

After the consolidation of the VIS, the HVIP as a whole behaved more or less rigidly towards later deformation. Much of the stress was released along zones of intense shearing which ramify the region in a rough E-W pattern. Some of the zones are over 5 km wide, such as that which crosses the northern part

of the study area near the Witputs River. Volcanic and plutonic rocks of the HVIP have been reduced to schists and mylonites within the shear belts. A very common effect of the shearing is for lava flows and sedimentary beds in the HVG to become distorted and tightly folded as they approach the shear zone. At present the age of this deformation is not known.

The tectonic conditions that prevailed during the development of the shear zones described above, were followed by periods of tension that resulted in the development of regional fracture patterns. An E-W fracture pattern was followed by the Namaqualand Pegmatite Swarm, while SSW-NNE fractures were followed by the Gannakouriep basic dike swarm.

A relatively late series of N-S trending faults, possibly associated with the development of the Neint Nababeep plateau, traverse the region. The most prominent N-S trending fault is that which forms the eastern boundary of the Neint Nababeep plateau. The faults are obviously post-Nama, but are pre-Karroo since the eastern boundary fault of the Neint Nababeep plateau disappears under the Karroo as it is traced across the Orange River west of Vioolsdrif. Another regional fracture pattern must have developed after the deposition of the Karroo Supergroup in order to provide feeder dikes to the Karroo dolerites. No Karroo dikes have been found in the present study area, although Von Backström and De Villiers (1972) report an E-W trending basic dike cutting Nama strata in the Neint Nababeep plateau. This may indicate that the Karroo magma rose along E-W striking fractures.

4.4 Field relationships

4.4.1 Nous Formation

Basaltic andesite and andesite lavas in the Nous Formation are best exposed in the region between the Nous River and Vioolsdrif. Excellent exposures of lavas interbedded with fragmental rock types occur in the gorge of the Koubank River and on both sides of the Orange River near the Namma Keinam Weir. Uninterrupted sections of lavas are seldom thick (less than 300 m) and all reasonably continuous sequences show alternating flows, pyro-

clastics and lenses of volcanogenic sediments. The latter fragmental rocks weather more readily than the lavas and it is common to find massive flow units separated by strongly etched beds of pyroclastics or sediments. Fine-grained recrystallised tuffs appear massive in hand specimen and resemble aphyric lavas. However, outcrops of tuffaceous rocks are generally bedded and can therefore be distinguished from true lavas. In fact, aphyric lavas seem to be very rare in the HVG.

Boundaries to individual flows are difficult to locate, since they seldom weather out. However, with careful inspection, flow boundaries may be seen in some sections and are characterised by discontinuous jointing parallel to the presumed attitude of the flow (usually defined by pyroclastic or sedimentary interbeds). The lava within this boundary zone sometimes displays a fragmental texture (flow breccia), but it is always obscured by metamorphic recrystallisation. Amygdales are difficult to recognise, again because of recrystallisation, since they resemble altered phenocrysts. Obvious amygdales containing quartz and/or carbonate are rare. Pillow structures indicative of quiet subaqueous extrusion have not been recognised.

Dacite lavas occur sporadically throughout the Nous Formation, but are definitely subordinate to basaltic andesite and andesite. A single porphyritic dacite flow, associated with sheared tuffaceous beds, crops out in the Koubank gorge and separates two massive units of basaltic andesite lava flows. The dacite displays an internal fracture pattern which resembles deformed cooling joints, although an alternative interpretation is that the joints have formed as a response to shearing in the underlying tuffaceous beds. The pattern is confined to the dacite flow and the overlying basaltic andesite flows show only very crude discontinuous jointing normal to the dipping contact. Although deformed cooling joints have been described in basalt flows (e.g. Waters, 1960), description of dacite flows developing this feature is unknown to the author. Due to the lack of any other useful features, the problem of the origin of the jointing remains unresolved. However, if it is accepted that the fracture pattern is in fact deformed cooling joints, then it is possible to determine the attitude of the flow and the direction of movement. The latter

deduction may give an indication of the direction to the source of the lavas in this locality. According to Waters (1960), cooling basalt flows develop jointing normal to their surfaces, which are usually horizontal. Although the flow may be largely consolidated before jointing develops, it is possible that a little plastic deformation may occur during final movement. The cooling joints would be deformed in such a way as to be convex in the direction of flow, but with their tops displaced further than the bottoms. In the case of the Nous dacite, the geometry of the joint surfaces indicate that the flow is right way up and the exposed portion moved in a direction opposite to which it now dips. The attitude is consistent with that deduced from volcanogenic sediments displaying size grading, soft sediment deformation and thickness variation, which crop out about 800 m further down the Koubank gorge.

No rhyolite lava was recognised in the Nous Formation, although acid material in the form of pyroclastic beds and volcanogenic sediments is not uncommon. A conspicuous rhyolitic to dacitic unit crops out in the north bank of the Orange River at the Namma Keinam Weir, forming an interbed about 100 m thick which separates two massive flow units of basaltic andesite. The acid unit is bedded down to the centimetre scale and displays size grading.

The contact between the Nous Formation and the underlying Tsams Formation is arbitrarily placed at the point where basaltic andesitic and andesitic volcanic products become abundant. North of the Orange River, this contact is exposed in the upper reaches of the Witloop River where the volcanic succession dips very steeply (about 70°) to the south. South of the Orange River the contact is exposed in the lower reaches of the Noujaseep River, where finely bedded pyroclastics are conformably overlain by a thick sequence of basaltic andesitic tuffs and interbedded lavas all of which are strongly sheared. In most areas however, the contact has been disrupted by intrusion. The Nous Formation is disconformably overlain by quartzites of the Nama Group. Good exposures of this unconformity occur in the lower Koubank gorge and Charliesfontein River in the western part of the study area. In the mountains immediately north of the Namma Keinam Weir, mafic lavas and pyroclastics of the Nous Formation, cut by irregular bodies of porphyritic adamellite, dis-

appear under the flat-lying shales and glacial beds of the Dwyka Group.

4.4.2 Tsams Formation

The Tsams Formation comprises mainly dacitic to rhyolitic volcanic products, but also contains a significant amount of andesitic material. More mafic material is confined to relatively thin units containing a few porphyritic basaltic andesite flows and mafic pyroclastics. Despite metamorphic recrystallisation, which tends to obliterate primary textures, it seems that pyroclastic debris may be more abundant than true lava.

Sheets of coarse pumice that may be in excess of 100 m thick are well-exposed in the mountains between the Warmklip and Krom Rivers. The pale-grey pumice clasts are usually flattened parallel to bedding either because of shearing or tight folding, but can be easily distinguished in weathered outcrops. More massive units that persist for great distances along strike are more difficult to interpret. They may be ignimbrites, but their primary textures have been almost completely obliterated. Some of the units have a profile similar to modern ignimbrites, in that a massive, sparsely porphyritic interior grades both upwards and downwards into partly welded tuffaceous material. Unfortunately, it is not possible to distinguish partly welded tops and bottoms of ignimbrites from discrete beds of coarse pyroclastic tuff. Possible eutaxitic texture was observed in one locality in the middle of a thick acid unit in the lower Noujaseep River. This unit represents the top of the Tsams Formation in this area, as it grades up into bedded pyroclastic acid tuffs which in turn are overlain by the basal basaltic andesitic debris of the Nous Formation. This possible rhyolitic ignimbrite is at least 300 m thick, although metamorphic recrystallisation may have obliterated boundaries between individual sheets. The presumed base of the acid unit is cut by granodiorite.

Dacitic and rhyolitic lavas occur sporadically throughout the voluminous volcaniclastic sequence. The positive identification of true lava is difficult and involves the arbitrary decision that all rock types which are obviously porphyritic and massive, are lavas. Most porphyritic dacite lavas with a

dark groundmass can be distinguished from andesites by the presence of quartz phenocrysts accompanying plagioclase. However, a significant number of dacites investigated contained only microphenocrysts of quartz, so it is not possible to accurately distinguish dacites from andesites in the field. A sack name such as "quartz-feldspar porphyry" may be useful for field mapping but unfortunately the andesite-dacite boundary, as defined in Chapter 5, falls within the rocks called feldspar porphyry (Blignault, 1975). In other words, some feldspar porphyries are andesitic, others are dacitic.

Lavas that crop out in the rugged terrain surrounding the Tsams River are andesites and dacites, although it is only possible to map them as one unit under the name of feldspar porphyry. Quartz-phyric dacites occur in the mountains at the head of the Krom River, where they form a large resistant mass in a major shear zone.

Light coloured porphyritic dacites are difficult to distinguish from porphyritic rhyolites and their separation is only achieved by comparing bulk chemical composition. The most impressive development of porphyritic rhyolite lava occurs in the mountains between the Matjies and Nous Rivers, where they build a large mass centred around the Nous trigonometrical beacon. The mass pinches out westwards and is faulted against basaltic andesite lavas and andesitic tuffs in the east. A sheared contact with porphyritic adamellite of the VIS forms the southern boundary of the mass, while it is overlain by porphyritic andesite flows in the north. The whole volcanic succession dips steeply to the north. Dispersed throughout the mass of porphyritic rhyolite are patches of agglomerate which are made up of blocks of porphyritic rhyolite set in a felsitic matrix. Individual flows of rhyolite are not recognisable. Although faulting and intrusion have foreshortened the mass and preclude accurate estimation of its original extent, its massive nature and dispersed agglomerates suggest that it may be part of a rhyolite dome complex.

4.5 Thicknesses and proportions of rock types

The thickness of the Nous Formation is very difficult to estimate because

the top has been removed by erosion prior to the deposition of the Nama Group. Other features which hamper thickness estimations include the presence of intrusions and the lack of continuous exposures exhibiting regular dips over distances greater than 500 m. The section exposed in the Koubank - Charliesfontein gorges near Vioolsdrif is at least 1500 m thick. The northern limb of a major syncline in the Nous Formation in the lower Matjies River - Namma Keinam Weir area comprises a sequence of flows and interbedded fragmental rocks which is at least 3100 m thick. A conservative estimate for the minimum thickness of the Nous Formation is about 3000 m.

The only section in the Tsams Formation exhibiting regular dips occurs in the mountains between the Warmklip and lower Krom Rivers. The thickness of this section is about 4.5 - 5.0 km and this may be taken as the minimum thickness of the Tsams Formation.

The estimated minimum thickness of the HVG in the study area is about 8000 m (26,000 feet), with the Tsams Formation being at least 5000 m (16,000 feet) thick and the Nous Formation about 3000 m (10,000 feet) thick.

Traverses through the study area yielded an impression that a very large proportion of the HVG consisted of fragmental rock types (pyroclastics, volcanogenic sediments), which exhibit a range in composition as wide as that for the lavas. At least 50-60 % of the Tsams Formation is probably made up of fragmental rock types and points to sustained explosive eruptions and reworking of the volcanic pile. Moreover, this figure does not include acid ignimbrite sheets, which together with acid pyroclastics (pumice sheets, bedded tuffs) probably makes up about 40 % of the entire exposed succession.

Andesitic lava forms an important constituent in both the Nous and Tsams Formations and is probably the most abundant lava type in the HVG. It is dangerous to cite figures because they are usually prone to revision, but of the remaining 60% of the HVG that is not acid ignimbrite and related fragmental rock types, about 30% (i.e. half) is probably andesitic lava. The remaining 30% is made up of 10% basaltic andesitic to dacitic fragmental rock types, 10% basaltic andesite lava, 5% dacite lava and 5% porphyritic rhyolite lava.

5

THE HVG PETROGRAPHY

5.1 Classification

Problems of classification exist mainly with the systematic description of lavas within the HVG, although it must be remembered that subdividing a rock series that displays continuous bulk chemical variation is only useful when individual members are to be referenced. Metamorphic recrystallisation precludes any detailed classification based solely on petrographic properties (e.g. Streckeisen, 1967, 1976), so a scheme based on bulk chemical composition has been used in this study.

Many classificatio schemes are available, ranging from very elaborate (Irvine and Baragar, 1971; Le Maitre, 1976a), to very simple (Taylor, 1969, Peccerillo and Taylor, 1976; Nicholls, 1971; Carmichael *et al.*, 1974). Unfortunately, the results obtained from different schemes are inconsistent. To illustrate this inconsistency, three schemes were chosen and 55 analysed samples of HVG lavas were classified according to their respective criteria. It is obvious from the results displayed in Table 10 that, any particular sample to be classified, for example as a basalt, depends very strongly on which scheme is chosen.

The scheme of Irvine and Baragar (1971) does not separate basaltic andesites from basalts, so the disproportionate number of basalts is not surprising. What is surprising however, is the fact that many of the samples classified as basalts have in excess of 56% SiO_2. This discrepancy is probably caused by a high normative plagioclase composition (commonly caused by calcic plagioclase phenocrysts) which results in the sample plotting in the basalt field. This is obviously the case with some of the intermediate lavas of the HVG, so this particular scheme has been rejected. The results of the schemes of Peccerillo and Taylor (1976) and Nicholls (1971) are more comparable, except for the more basic lavas. An important criticism of the scheme of Peccerillo

Table 10

Classification of the Haib lavas according to three schemes.

SCHEME	ROCK TYPE				
	BASALT	BASALTIC ANDESITE	ANDESITE	DACITE	RHYOLITE
NICHOLLS	3	12	11	15	14
I and B	20	0	21	18	8
TAYLOR	0	5	18	6	14

The details of the classification schemes are as follows :

Nicholls (1971)

DI less than 35	=	Basalt
DI between 35 and 50	=	Basaltic andesite
DI between 50 and 65	=	Andesite
DI between 65 and 80	=	Dacite
DI greater than 80	=	Rhyolite

DI = Differentiation Index (Thornton and Tuttle, 1960)

Irvine and Baragar (1971)

CI between 70 and PLAG	=	Basalt
CI between 30 and PLAG x 0.6	=	Andesite
CI between 20 and PLAG	=	Dacite
CI less than (20-PLAG)	=	Rhyolite

CI = Normative colour index
PLAG = Normative plagioclase composition

Taylor (amended by Peccerillo and Taylor, 1976)

SiO_2 less than 52%	=	Basalt
SiO_2 between 52% & 56%	=	Basaltic andesite
SiO_2 between 56% & 63%	=	Andesite
SiO_2 between 63% & 70%	=	Dacite
SiO_2 greater than 70%	=	Rhyolite

NB - All major element compositions are re-calculated to 100% volatile free with both FeO and Fe_2O_3 reported

and Taylor (1976) is that it is too simple, as it is based on only one major element oxide. The scheme of Nicholls (1971) uses all the major element oxides, as it is based on normative mineralogy. However, many people use a scheme either the same as, or similar to, that of Peccerillo and Taylor (1976) and furthermore report abundant trace element data. By adhering to the scheme of Peccerillo and Taylor, trace element data can be more readily compared. Serious discrepancies in trace element compositions may arise when different groups of rocks are included under one name using different major element criteria.

It was finally decided to use the scheme of Nicholls for purposes of nomenclature and reference, but the scheme of Taylor was used to compute average bulk chemical data discussed in later chapters.

CIPW weight percent norms from which DI was determined, have been calculated from major element analyses expressed as oxides, recast to 100% volatile free and with the Fe_2O_3/FeO adjusted (see Chapter 7).

5.2 Petrographic descriptions

Pervasive metamorphic recrystallisation has resulted in almost complete replacement of the original igneous mineralogy and a partial obliteration of primary textures. Recrystallised phenocrysts in porphyritic rocks are sometimes difficult to distinguish from the granoblastic matrix, which makes it impossible to determine accurate modes. The following petrographic descriptions are presented as if the rocks are igneous, although most of the minerals mentioned are metamorphic in origin. A more detailed account of the metamorphic minerals, their chemical composition and estimation of metamorphic grade, is given in Chapter 6.

The primary fragmental texture of pyroclastics and volcanogenic sediments has been almost completely obliterated by metamorphic recrystallisation. As a result, any detailed description or classification of textures (e.g. tuffs, breccias, agglomerates) is not possible, nor is it crucial to this study. In many cases, the only evidence for their original fragmental nature is the etching out of individual clasts on weathered surfaces. Fine-grained re-

crystallised tuffs are very difficult to tell from aphyric lavas in hand specimen, but most outcrops of fragmental rocks show some evidence of bedding and may be distinguished from true lavas.

5.3 Basaltic andesite

Basaltic andesite lavas are porphyritic, with conspicuous dark mafic phenocrysts of plagioclase set in a fine-grained dark-green groundmass. In thin section, the groundmass is completely reconstituted to a granoblastic mosaic of metamorphic minerals which include albite, epidote, actinolite, chlorite and biotite with accessory amounts of quartz and sphene.

Mafic phenocrysts are replaced by various mineral assemblages, which commonly occur as decussate aggregates bounded by the outline of the original igneous mineral. There seems to be at least two distinct mineral assemblages; one dominated by actinolite, the other by a complex intergrowth of chlorite - biotite - epidote $\pm$ magnetite $\pm$ sphene $\pm$ albite $\pm$ quartz. A mafic phenocryst pseudomorphed by actinolite may occur next to a pseudomorph containing the chlorite-biotite rich intergrowth, so it is possible that at least two mafic minerals may occur in basaltic andesite lavas. No unaltered cores or relicts within any of the mafic pseudomorphs were found, so it is not possible to identify the original igneous phases.

A few samples of basaltic andesite lava contain small subhedral microphenocrysts of an opaque mineral, probably a Fe-Ti oxide. Many of the opaque grains are surrounded by what seems to be a reaction rim of pale green chlorite, tiny granules of sphene and less commonly green biotite. It is possible to observe the change from a primary subhedral Fe-Ti oxide microphenocryst, through partial replacements, to a complete pseudomorph of chlorite, sphene and biotite. The sphene often forms a halo of tiny grains surrounding a decussate aggregate of chlorite. Many basaltic andesites studied under the microscope contain these chlorite-sphene-biotite pseudomorphs after Fe-Ti oxide.

Prismatic plagioclase phenocrysts are replaced by a fine-grained, turbid intergrowth of epidote and sericite. With advancing recrystallisation, the

grain size of the intergrowth increases until short, stubby prisms of pale lemon-yellow epidote are visible, set in a mosaic of sericite flakes. Unaltered cores and relic patches of the original plagioclase are not uncommon and display distinctive lamellar twinning.

5.4 Andesite

Andesitic lavas cannot be easily distinguished from basaltic andesites in the field, since they are also dark-green, porphyritic rocks with mafic minerals and plagioclase forming conspicuous phenocrysts set in a dense, aphanitic groundmass. The only petrographic difference between the two is the dominance of plagioclase over mafic minerals as a phenocryst phase. There is however, a complete gradation from lavas in which mafic phenocrysts predominate to those containing abundant plagioclase.

Mineral assemblages that occur in the mafic pseudomorphs are dominated either by actinolite or by the complex biotite-chlorite-epidote intergrowth, suggesting the existence of two mafic phenocryst phases. The complex multimineral intergrowth is more common.

Biotite-sphene pseudomorphs after Fe-Ti oxide microphenocrysts also occur, with the sphene grains arranged in a trellis-like pattern which may reflect an exsolved Ti-rich phase in the original igneous mineral. A trellis-like intergrowth of magnetite and ilmenite often results during post-consolidation. In contrast, the same pseudomorphs in basaltic andesite lavas have chlorite as a very subordinate phase and green-brown biotite is common.

Abundant plagioclase phenocrysts show characteristic prismatic outline and are either partially or completely replaced by a turbid epidote-sericite intergrowth. Glomeroporphyritic aggregates are not uncommon and often include actinolite-rich mafic pseudomorphs.

The reconstituted groundmass contains contains abundant albite, epidote, biotite and quartz with lesser amounts of actinolite, chlorite and sphene. Compared to the basaltic andesite lavas, the andesite groundmass contains more biotite, quartz and albite.

Apatite occurs as short stubby crystals, often included within the biotite-chlorite pseudomorphs, but also as possible microphenocrysts in the groundmass.

The more acid varieties (DI= 60-65) contain a few micro-phenocrysts of quartz, which can only be recognised in thin section. These andesites are essentially transitional toward dacites (DI greater than 65).

5.5 Dacite

Dacite lavas are characteristically porphyritic, with abundant phenocrysts of plagioclase and quartz set in a dark green to pale green groundmass. Not all dacites have quartz phenocrysts which are conspicuous in hand specimen, but this mineral can always be found in thin section. A very distinctive feature of all quartz-phyric dacites, is the pale opalescent blue colour of the quartz phenocrysts.

Pseudomorphs after mafic phenocryst minerals, include the complex biotite-chlorite-epidote intergrowth and another containing chlorite and sphene after biotite. In the latter case, relic patches of the original biotite still remain. However, investigation with the Electron Microprobe (EMP) shows extensive removal of K during incipient alteration. Partly replaced biotite phenocrysts still show euhedral shapes, with basal sections showing a characteristic pseudohexagonal outline. Sections parallel to the c-axis appear as flat, tubular crystals. Short, stubby prisms of apatite often occur both within the complex biotite-chlorite-epidote intergrowths and in the biotite phenocrysts. Partly replaced Te-Fi oxide microphenocrysts also occur, showing reaction with the groundmass to form green-brown biotite, sphene and a little chlorite.

Plagioclase is by far the predominant phenocryst phase, but is extensively replaced by epidote/sericite intergrowths. Crystal outline is often preserved and is invariably prismatic with the elongation parallel to 010. Relic patches display fine lamellar twinning parallel to 010, which indicates the albite twin law. Glomeroporphyritic aggregates up to 10 mm across are not

uncommon.

Quartz occurs as subhedral to highly embayed crystals, ranging in size from 4 mm across down to groundmass dimensions. The phenocrysts are normally free from inclusions, but where present the included material is similar in texture and composition to the adjacent groundmass. In every sample inspected, the quartz phenocrysts show pronounced undulose extinction and are very commonly fractured into a mosaic of irregularly shaped domains. It appears that all the quartz-phyric rocks have suffered some deformation, although no directional texture can be observed in hand specimen.

5.6 Porphyritic rhyolite

Porphyritic rhyolite lavas are pale grey to pinkish grey with conspicuous phenocrysts of opalescent-blue quartz, greenish-grey plagioclase and a green altered mafic mineral.

Some of the mafic phenocrysts are biotite, now extensively replaced by green secondary biotite, sphene and chlorite. Primary phenocrystic biotite occurs as tabular crystals up to 0.5 mm in length, flattened parallel to the prominent basal cleavage (001). Tiny microphenocrysts of an opaque mineral (magmetite?) also occur, but invariably show replacement by chlorite and green biotite.

Plagioclase occurs as prismatic phenocrysts up to 1 mm in length, elongated parallel to the albite twin planes. Replacement by epidote and sericite is well advanced. Quartz builds large subhedral to deeply embayed phenocrysts up to 3 mm across. Undulose extinction is common and most crystals are cracked into irregular mosaics.

The groundmass is made up of a fine-grained granoblastic mosaic of quartz and alkali-feldspar, with lesser amounts of epidote, green biotite, chlorite and muscovite. The quartz-feldspar matrix often shows strongly sutured grain boundaries.

5.7 Non-porphyritic rhyolite

Non-porphyritic rhyolites include all those fine-grained acid units that may be ignimbrite sheets. In thin section these "lavas" are simply granoblastic mosaics of quartz, alkali feldspar, sodic plagioclase, epidote and muscovite. An opaque mineral (magnetite?) and chlorite occur as accessories. The chlorite is prominent in the possible eutaxites within the acid unit in the Noujaseep River. Very rare phenocrysts of alkali feldspar up to 1 mm across occur in some of the acid rocks, their boundaries being invariably ragged and carrying numerous inclusions of the groundmass. It is possible that these alkali feldspar "phenocrysts" could be metamorphic in origin.

6

THE HVG METAMORPHISM

6.1 General statement

Apart from relict plagioclase and quartz, none of the primary igneous minerals remain. This section is concerned with the composition of some of the constituent metamorphic minerals, in the hope that they may indicate the grade of metamorphism. This is by no means an exhaustive study, which must await further work, but may serve as an introduction to a systematic investigation. Only metalavas of basaltic andesite composition have been investigated in this study, but since the samples come from flows throughout the entire succession in the study area, they are considered to represent the grade of metamorphism attained by the HVG. The following sections will describe each individual mineral and evaluate its importance as an index mineral. All EMP analyses are listed in Appendix 2.

6.2 Amphibole

Amphibole is confined to rocks of basaltic andesite and andesite composition. In lavas, it replaces mafic phenocrysts and is an important constituent of the granoblastic groundmass. Fragmental rocks with the appropriate bulk composition contain abundant amphibole, which often occurs as a felted mass of fine to medium-grained, prismatic crystals.

Colour zoning is marked, especially in the pseudomorphed phenocrysts, varying from very pale green (non-pleochroic) to blue green (pleochroic) and as a result, the pseudomorphs appear mottled in thin section. Deeper coloured varieties of amphibole have the pleochroic scheme X = very pale straw yellow, Y = pale olive green, Z = pale bluish green. Although the colour zoning is usually irregular, some of the more recrystallised rocks near intrusive contacts show the deeper coloured amphibole forming continuous rims around paler amphibole in the pseudomorph. Groundmass amphibole is usually coloured

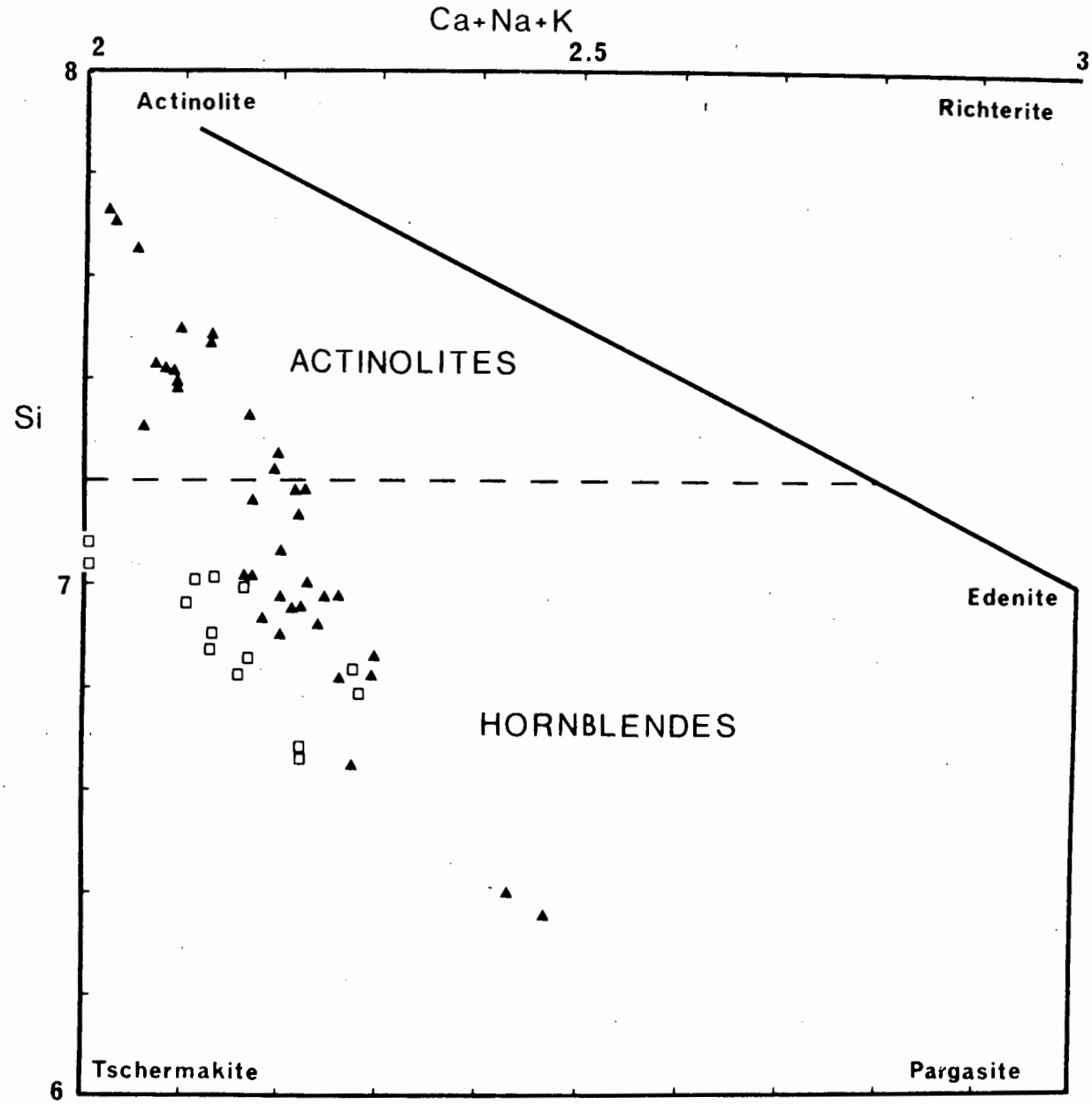

Fig. 26. Plot of Si against (Ca+Na+K) for amphiboles. Atomic proportions based on 23 oxygens. Scheme after Miyashiro (1973).
▲ = metamorphic amphibole in Haib basaltic andesites;
□ = primary igneous hornblende in a Vioolsdrif diorite.

as deeply as the deepest coloured amphibole in the pseudomorphed phenocrysts.

The mottled colour zoning in the amphibole pseudomorphs reflects variation in chemical composition. Deeper colours are associated with higher FeO^*/MgO (FeO^* is total Fe as FeO), higher TiO_2, Al_2O_3 and (Ca + Na + K) contents. Pale coloured non-pleochroic to faintly pleochroic zones have a composition appropriate to actinolite, according to the classification scheme of Miyashiro (1973), since they have Si contents (calculated on the basis of 23 oxygens) of greater than 7.2 (Fig.26). Deeper coloured, strongly pleochroic zones have Si contents that fall in the hornblende field. Although (Ca + Na + K) increases with decreasing Si content, the actual increase is in (Na + K), while Ca remains essentially constant (or perhaps slightly lowered). By inspection of the EMP analyses, it can be seen that the increasing amount of Al in the Z sites is accompanied by increasing (Na + K). The sum in the X site (SX) becomes increasingly greater than 2 (based on 23 oxygens) and reflects increasing occupation in the A site (Deer *et al.*, 1962). While the passage to hornblende compositions is essentially a function of Al content, the deepening colour is controlled by the FeO^*/MgO ratio (Fig. 27) and also probably TiO_2 content (Fig. 28).

Individual zones do not always have sharp boundaries, since no marked Becke bright line (cf. Cooper and Lovering, 1970) can be consistently recognised. However, X-ray intensities for Al, Mg and Fe were monitored with the EMP across a boundary between a pale and a deeper coloured zone and revealed a very rapid increase in Al and Fe/Mg ratio. Individual analyses of adjacent pale and dark zones in a mottled amphibole pseudomorph may differ in Al_2O_3 content by as much as 6 wt %. Large, complexly-zoned pseudomorphs have an interior of actinolite (Al_2O_3 = 2,49%, FeO^*/MgO = 0,548) and a rim of hornblende (Al_2O_3 = 12,42, FeO^*/MgO = 1,532).

The wide range in chemical composition and the mottled colour zoning, may be due to one of at least three processes;

(i) Coexistence of actinolite and hornblende; the apparent lack of sharp boundaries being a function of imperfect recrystallisation under

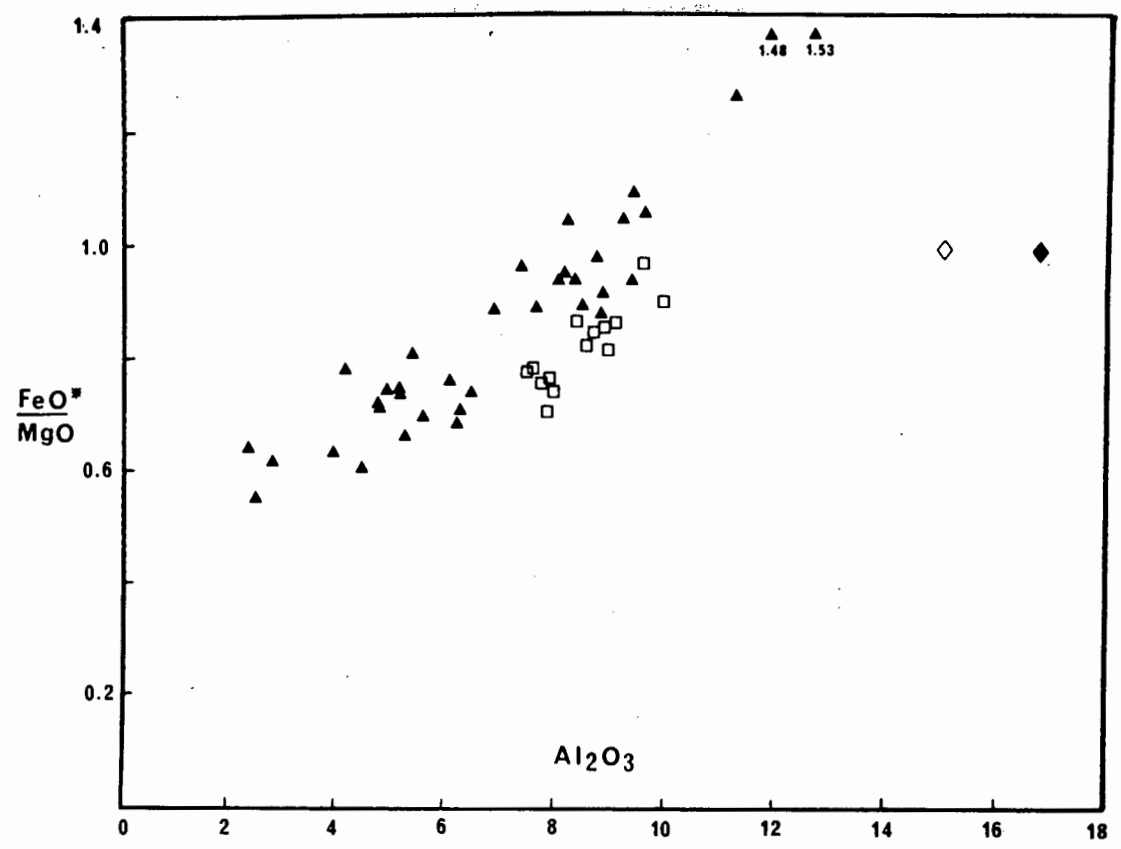

Fig. 27. Plot of FeO^*/MgO against Al_2O_3 for amphiboles. Symbols as in Fig. 26. ◇ = average Al_2O_3 content of Haib basaltic andesites; ◆ = Al_2O_3 content of Vioolsdrif diorite.

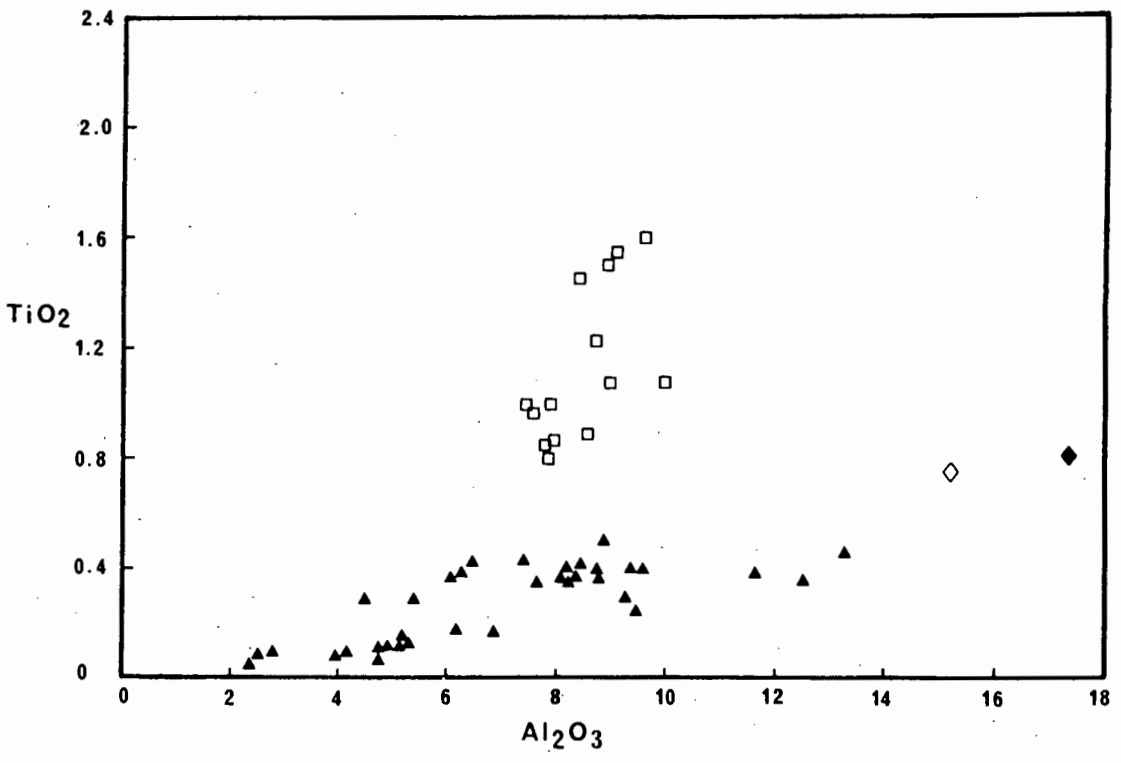

Fig. 28. Plot of TiO_2 against Al_2O_3 for amphiboles. Symbols as in Fig. 27.

low grade metamorphic conditions.

Coexisting actinolite and hornblende in metabasites is not uncommon and have been described in greenschist facies metabasites by Cooper and Lovering (1970), Shido and Miyashiro (1959) and Compton (1958). These authors suggest that coexisting calcic amphiboles mark the transition from greenschist to amphibolite facies metamorphism, although Miyashiro (1968, 1973) later regards this phenomenon as characteristic of upper greenschist facies assemblages. Winkler (1976) includes this intergrowth texture with his "low grade" metamorphism of basic rocks. Imperfect recrystallisation is to be expected in the lower grades of metamorphism, especially when there is very little accompanying deformation (Spry, 1969). This is consistent with the preservation of the primary igneous porphyritic texture. Inspection of Fig. 25 however, does not reveal any distinctive grouping of the amphibole compositions which is difficult to reconcile with the coexisting amphibole hypothesis. The only possible explanation is that the intergrowth is on a submicron scale and unresolveable with the EMP. This is not uncommon, since Klein (1969), Cooper and Lovering (1970) and Ross *et al.*, (1968) report exceedingly fine lamellae of coexisting actinolite and hornblende in metamorphic amphibole from greenschist metabasites.

(ii) Partial replacement of actinolite by hornblende as a readjustment to a higher grade of metamorphism.

Replacement of actinolite by hornblende during prograde metamorphism is accepted as standard (Turner, 1968). However, it is difficult to distinguish between poorly formed, coexisting amphiboles described previously and an arrested state in the replacement of actinolite by hornblende. The latter case implies that the rock has been subjected to conditions appropriate to amphibolite facies, but the mineralogical readjustment was not complete. This may be contrasted with the attainment of upper greenschist facies and the production of a two amphibole intergrowth. Amphibolite facies is ruled out because of the presence of abundant chlorite and albitic plagioclase coexisting with the amphibole. The assemblage albitic plagioclase-chlorite-actinolitic amphibole is considered to be diagnostic of the greenschist facies (Turner, 1968; Miyashiro, 1973; Winkler, 1976).

(iii) Partial metamorphic replacement of an original igneous hornblende by actinolite. This third possibility is only considered since in some cases it is difficult to ascertain which of the two amphiboles is the replacement.

The hornblende component in the amphibole may in fact be primary, representing relict patches surrounded by secondary amphibole. Figs. 25 and 26 show that its composition is roughly similar to igneous hornblendes in a diorite of the VIS. However, there is a marked difference in their TiO_2 contents (Fig. 28). The diorite has an FeO^*/MgO ratio and TiO_2 content similar to those of the basaltic andesites, so the difference cannot be due to contrasting bulk composition. Cawthorn (1976a) has shown that for a given bulk composition, volcanic hornblendes contain more TiO_2 than their plutonic counterparts. It follows that primary igneous hornblende in a Haib basaltic andesite will probably be higher in TiO_2 when compared with that in the Vioolsdrif diorite. The very low TiO_2 contents observed for the hornblende in the basaltic andesites suggest that this mineral is not primary and is most likely metamorphic in origin.

6.3 Chlorite

Chlorite occurs in metalavas and associated fragmental rock types of all compositions, throughout the study area. Chlorite disappears from the rocks as they are followed out of the study area, so the boundaries displayed in Fig. 25, define a chlorite zone of metamorphism. Chlorite free metavolcanics outside the study area may indicate a higher grade of metamorphism, but whether this higher grade was impressed upon the volcanics at the same time is open to question, since the associated VIS is also affected.

The composition of the chlorite also appears to be useful, since Cooper (1972) found that the Mg/Fe ratio increases with metamorphic grade (within the greenschist facies). Analysed chlorites are plotted on an Al-Mg-Fe diagram (atomic wt %) (Fig. 29). The broken line is from Cooper (1972) and indicates the change in composition of chlorites in the Haast Schist Group with increas-

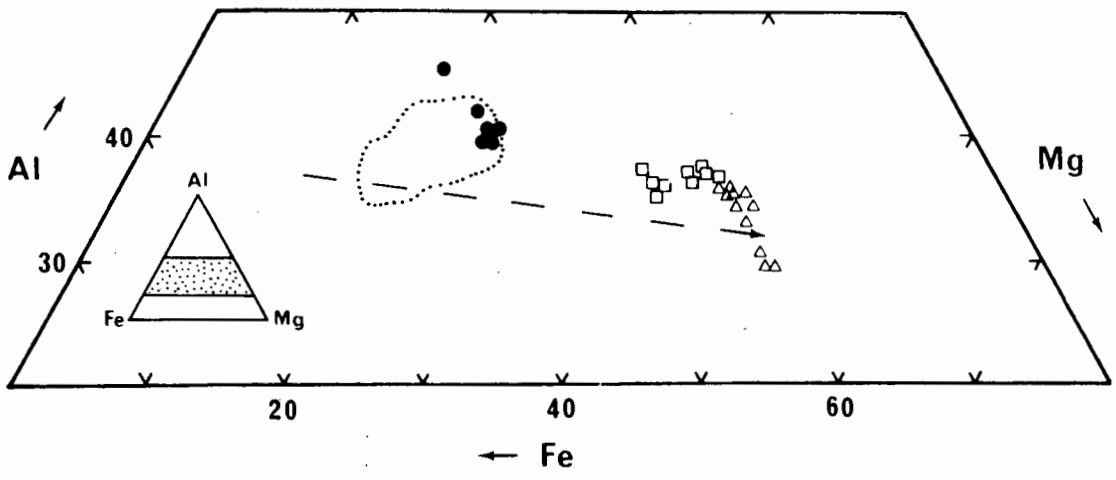

Fig. 29. Al-Mg-Fe plot for metamorphic chlorites and biotites in the Haib basaltic andesites. Original atomic proportions (Al^{3+}, Mg, total Fe as Fe^{2+}) based on 23 oxygens. △ = chlorites, □ = biotites, ● = bulk composition of basaltic andesites. Dotted field is that occupied by the Haast metabasites (Cooper, 1972). Broken line indicates change in chlorite composition in the Haast metabasites with increasing metamorphic grade.

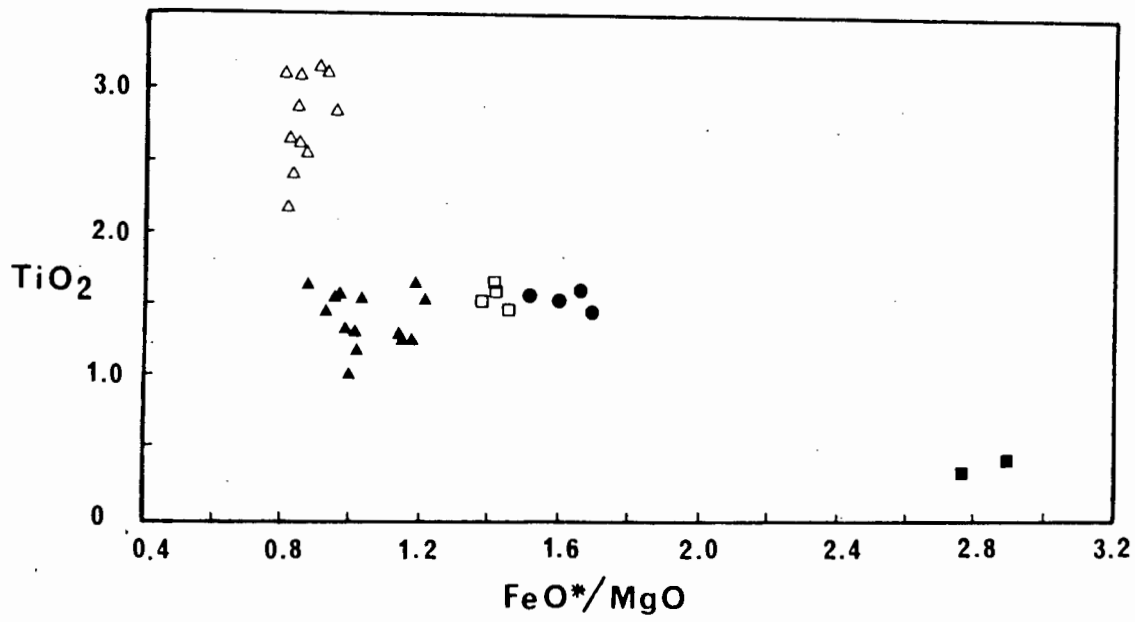

Fig. 30. Plot of TiO_2 against FeO^*/MgO for biotites. ▲ = metamorphic biotite in the Haib basaltic andesites; △, □, ●, ■ = primary igneous biotite from Vioolsdrif diorite, granodiorite, adamellite and leucogranite respectively.

ing metamorphic grade. Chlorites in the Haib basaltic andesite metalavas are similar in composition to chlorite from the oligoclase zone (uppermost greenschist facies) of the Haast Schist Group. This is in agreement with Turnock (1959) who found that Mg-chlorite is stable at higher temperatures than Fe-chlorite. Also displayed in Fig. 29, are the bulk compositions of the basaltic andesite metalavas in which the analysed chlorites occur, together with the range of metabasite composition observed for the Haast Schist Group (Cooper and Lovering, 1970).

6.4 Epidote

Epidote occurs in all rocks of all compositions throughout the study area. This mineral is secondary after plagioclase and forms an important component in pseudomorphs after phenocrysts of this mineral. Epidote also forms a component in pseudomorphs in at least one type of mafic phenocryst and is abundant in the reconstituted groundmass of all metalavas. Migration of the components of epidote has occurred throughout the volcanic pile, since veins, pods and large domains of country rock replaced by epidote are common.

Information on the variation in epidote composition with metamorphic grade is confusing. Sethuraman and Moore (1973) report on epidotes in metamorphosed calc-alkaline volcanics that increase in Fe content with increasing grade. On the other hand, Holdaway (1965) has described epidotes that show the opposite behaviour, becoming poorer in Fe with increasing grade. Since most of the Fe in epidote is in the trivalent state, the composition of this mineral must be controlled by the availability of oxidised Fe. Cooper (1972) has shown that the Fe content (expressed as Pistacite (Ps) content) is controlled by the oxygen fugacity maintained during metamorphism, a factor which may or may not be a function of metamorphic grade. This conclusion is consistent with experimental evidence (Liou, 1973). The results of Sethuraman and Moore (1973) seem to be fortuitous in this respect, since the bulk rock oxidation ratio ($OR = 2Fe_2O_3.100/(2Fe_2O_3+FeO)$ mole.%) does in fact increase with metamorphic grade. The dependance of epidote composition on the bulk rock oxidation ratio is illustrated in Table 11 which compares the results

Table 11

Relationship between bulk oxidation ratio
and Ps content of constituent metamorphic epidotes

OR = $2Fe_2O_3.100/(2Fe_2O_3+FeO)$ mole %

Ps = Pistacite ($Ca_2Fe^{3+}_3 Si_3O_{12}.OH$) content of epidote (mole %)

Sources : Grenville (Sethuraman and Moore, 1973), Haast (Cooper, 1972)

	GRENVILLE	HAAST	HAIB
OR	2.88-16.98	13.63-71.10	38.45
Ps	16.63-24.87	14-30	25-32.95

of the two abovementioned studies, with analysed epidotes in the Haib basaltic andesites.

It is interesting to note that the rocks described by Sethuraman and Moore (1973) pass from greenschist facies (Epidote with Ps = 16.63%) to upper amphibolite facies (epidote with Ps = 24.87% and coexists with diopside). Metabasites described by Cooper (1972) range from lower greenschist to lower amphibolite, but there is no correlation between grade and epidote composition. It is very probable that epidote composition is insensitive to metamorphic grade, unless it can de demonstrated that the rocks become more oxidised with increasing metamorphism. Finally, no general rule linking the bulk rock oxidation ratio and epidote composition can be formulated, a fact made clear by the data given in Table 11. The Haib basaltic andesite metalavas have a bulk rock oxidation ratio of 38.45, yet contain epidote with a Ps content higher than that in metabasites from the Haart Schist Group, which have bulk oxidation ratios almost twice as high.

6.5 Biotite

Biotite occurs as a metamorphic mineral in all rocks of the HVG. It is

subordinate in the reconstituted groundmass of the most basic rocks (basaltic andesites), but rapidly increases in abundance at the expense of other mafic sillicates (amphibole and chlorite) in the more acid rocks. Biotite is the most abundant mafic metamorphic mineral in rock of andesitic to rhyolitic composition. It occurs as an important constituent in pseudomorphed mafic phenocrysts (in metalavas), including those after primary igneous biotite in some of the dacites and rhyolites.

Colours range from pale green to pale greenish brown, with a pleochroic scheme X = Y = pale greenish yellow, Z = deeper greenish brown. Inclusions of granular or sagenitic sphene are common, especially in the secondary biotite pseudomorphs after primary igneous biotite. The presence of these Ti-bearing inclusions suggests that the secondary biotite cannot hold as much Ti in solid solution as the primary phase. This is borne out by the chemistry of biotite in the basaltic andesite metalavas. Analytical data are listed in Appendix 2 and their TiO_2 contents and FeO^*/MgO values illustrated in Fig. 30. For comparative purposes, igneous biotites from various rock types in the VIS are also included in the plot. The plutonic rock with the most comparable bulk composition to the basaltic andesites is the Vioolsdrif diorite and it is obvious that for rocks with similar bulk composition, low grade metamorphic biotite contains far less TiO_2 than igneous biotite.

As in the case for epidote, information on biotite composition in metamorphic rocks is also confusing. Although many studies show that the Mg/Fe ratio and Ti contents of biotite increase systematically with metamorphic grade (e.g. Engel and Engel, 1960), there are others that show the reverse (e.g. Miyashiro, 1958). Cooper (1970) found that there is no systematic variation in biotite composition with metamorphic grade, but like epidote, it is probably controlled by bulk composition and may also depend on the nature of other ferromagnesian phases present (c.f. Deer *et al.*, 1962). It is particularly interesting in this respect, to note the similar Al-Mg-Fe contents of the co-existing biotites and chlorites (Fig. 29).

There is however, a general consensus of opinion (e.g. Miyashiro, 1973)

that green to green-brown biotite is characteristic of low grade metamorphism, whereas brown and red-brown colours appear with increasing grade. According to Engel and Engel (1960), the colour is mainly controlled by the Ti content of the biotite, implying that it increases in abundance with increasing temperature of formation.

6.6. Feldspars

Feldspar in basaltic andesite metalavas is confined to the turbid patches in pseudomorphed plagioclase phenocrysts and in the reconstituted groundmass. This mode of occurrence is common to all volcanic rocks in the HVG. Inspection with the EMP shows that these turbid patches are probably mixtures of relict primary igneous plagioclase, metamorphic plagioclase and sericite. EMP analyses are listed in Appendix 2 and calculated mole proportions of An, Ab and Or are plotted in Fig. 31. The analyses show a rough grouping into Ab rich feldspar, An rick (and Or poor) feldspar and Or rich but variable "feldspar". The Ab rich feldspar is probably metamorphic in origin and represents part of the simplified greenschist facies reaction:-

plagioclase + water = albite + epidote (Miyashiro, 1973)

The scatter of An rich feldspars along the An-Ab join, may represent primary igneous calcic plagioclase in the arrested state of alteration. Orthoclase rich feldspars are probably mixtures of albite, calcic plagioclase and sericite; the intergrowth being finer than the 1-2 micron EMP beam. An accompanying possibility is that some of the An rich plagioclase may be metamorphic also (Crawford,1966). Cooper (1972) and Crawford (1966) report coexisting plagioclase (An_4 and An_{20-25}) in greenschist metabasites and suggest that this is evidence of plagioclase immiscibility. Though it is obvious that more detailed work needs to be done on these feldspars in order to establish the full picture, the important point is that a significant portion of the feldspar in the basaltic andesite metalavas is albitic, which is an important factor in defining the grade of metamorphism. Even if further work reveals the presence of two coexisting metamorphic plagioclases (albite and calcic oligoclase), it will not alter the present estimation of metamorphic grade, since this inter-

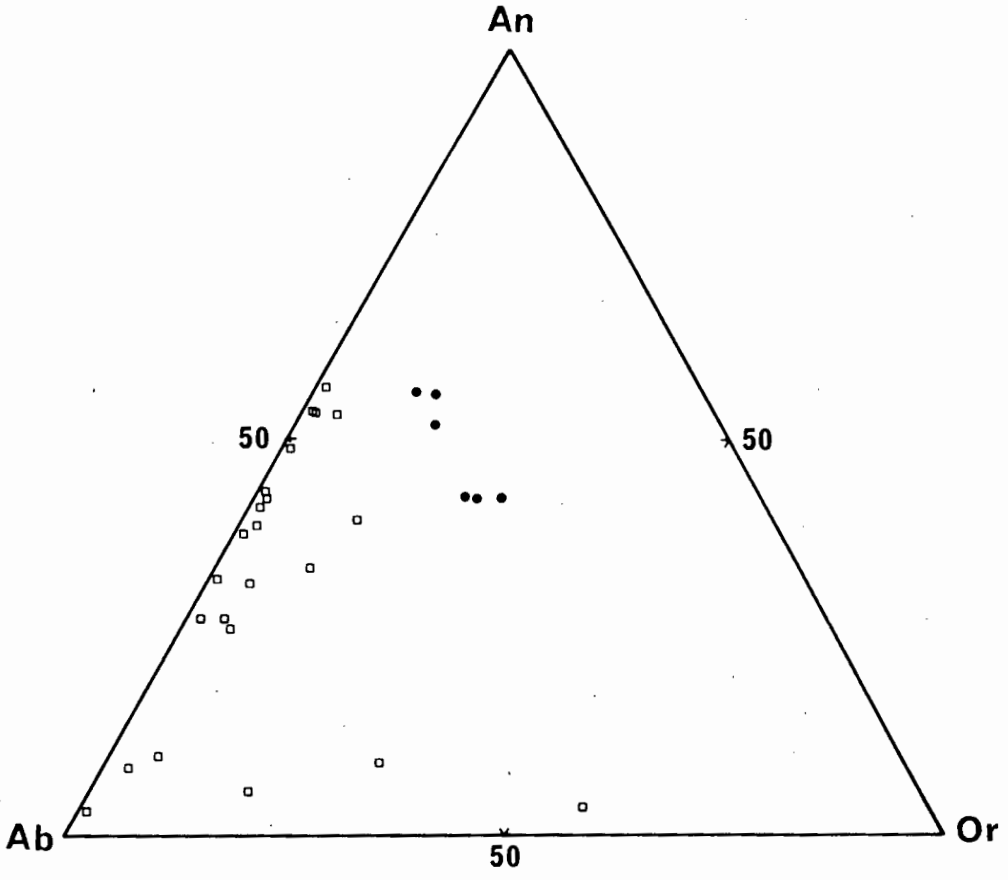

Fig. 31. Ternary feldspar plot. □ = "feldspar" from basaltic andesite metalavas; ● = normative feldspar composition of host basaltic andesites.

growth is considered by Turner (1968), Cooper (1972) and Miyashiro (1973) to be characteristic of upper greenschist conditions.

6.7 Discussion

Although detailed mineralogical work is confined to metalavas of basaltic andesite composition, their sporadic occurrence throughout the volcanic pile indicates that conclusions based on their parageneses may be representative of the whole volcanic group in the study area. The mineral assemblages described previously, indicate that the volcanic rocks have been subjected to conditions appropriate to upper greenschist facies metamorphism

Thick volcanic piles often suffer mild metamorphic recrystallisation in their lower regions, probably due to heat produced by devitrification of abundant glassy material and subjacent magma chambers. Although the grade of metamorphism may attain lower greenschist facies (Smith, 1969; Jolly, 1972), it is generally lower, with predominance of zeolites and prehnite-pumpellyite assemblages (Jolly and Smith, 1972; Jolly, 1970). The grade of metamorphism suffered by the HVG seems slightly higher than that usually attributed to simple burial metamorphism.

A volcanic pile is seldom free from intrusion and is often ramified by a great plexus of sheets, dikes and plugs, representing magma that failed to reach the surface. Intrusion may occur on a regional scale with the voluminous production of a composite batholith. Certainly there is ample opportunity for metamorphic recrystallisation under these circumstances. Three features suggest that heat provided by intrusions has caused the metamorphism of the HVG; (1) large tracts of these volcanics are seldom free from intrusion, (2) there is an increase in degree of recrystallisation in the volcanics as an intrusive contact is approached (this is not universally developed however) and (3) the rocks in the plutons are generally unmetamorphosed. The implication is that metamorphism is a contact phenomenon, but since intrusion is on a regional scale (the entire study area is probably underlain by a batholith), the recrystallisation is pervasive. It can be regarded as a regional contact phenomenon (cf. Hamilton and Myers, 1967) where separate contact aureoles have merged due to sustained intrusion.

7

THE HVG. ASSESSMENT OF ALTERATION

7.1. General statement

Chemical alteration is regarded here as any process by which the chemical composition of the original igneous rocks considered in this study have been changed. This applies to all components; major elements, trace elements, degree of oxidation, isotope ratios and water content.

Alteration may be discussed from the point of view of type, e.g. hydrothermal, contact metasomatism, sub-aerial weathering, sub-aqueous weathering, or with regard to individual components, e.g. alkali, ferric-ferrous ratio, normative corrundum. With regards alteration type, it is pertinent to note that the HVG has been folded, metamorphosed, uplifted, locally sheared, intruded and exposed to at least three periods of sub-aerial (and possibly subaqueous) weathering. The latter corresponds to pre-Nama, pre-Karroo and present day periods. It is therefore difficult to avoid the conclusion that a significant portion of the HVG has had ample opportunity to be affected by some sort of alteration process. The following section involves the assessment of chemical alteration and possible techniques to overcome the associated problems.

7.2. Field evidence for alteration

Apart from the effects of present day sub-aerial weathering (brown surface encrustations of clays and limonite) and the metamorphism which has affected these rocks (which may or may not be isochemical), only two types of alteration may be recognised with certainty; (1) rock decomposition associated with sulphide mineralisation and (2) metasomatism within shear zones. These two types are described separately in sections 7.3. and 7.4. respectively. There is, however, abundant field evidence for widespread alteration which is not obviously related to sulphide mineralisation or shear zones. This alteration is in the form of diffuse, pale coloured zones

immediately surrounding veins of silica, carbonate, albite, chlorite and epidote. The veins have sometimes developed such a closely spaced intersecting network that it is impossible to secure "fresh" volcanic rock from some outcrops. Veins containing the aforementioned minerals vary in size from 10 cm wide right down to sub-millimetre dimensions. The inspection of a significant proportion of "fresh" looking rocks revealed the presence of microscopic veinlets. Alteration associated with these veinlets is commonly the replacement of the country rock by the minerals in the vein, resulting in epidote-quartz, heavily carbonated, silicified and chloritised rocks.

No obvious relationship could be established between the concentration of veins and degree of alteration with proximity to intrusions (except for the distinctive effects associated with sulphide mineralisation). Furthermore, this alteration does not increase towards the unconformities with Nama or Karroo sediments, indicating that there is no obvious link between alteration and pre-Nama or pre-Karroo weathering.

Fragmental rock types are particularly susceptible to alteration, especially epidotisation, characteristically appearing as pale green, hard, brittle, fine-grained rocks showing relict bedding. Flow boundaries are also heavily altered, probably reflecting greater permeability, since it has been demonstrated by Smith (1969) and Jolly and Smith (1972), that water is the controlling agent in all processes of alteration.

Important features of the alteration are the intimate association with veins or originally permeable rocks (pyroclastic beds, waterlain tuffs, brecciated flow boundaries) and the regional extent. Such alteration is undoubtedly the result of the migration of aqueous solutions through the volcanic pile, as demonstrated elsewhere (e.g. Jolly, 1972). Practically every presently active volcanic field contains a complex subsurface hydrothermal system, which involves the movement of heated meteoric water, with subordinate juvenile water (Ellis, 1967), through channelways such as fractures or permeable rock. The hydrothermal system is obviously sustained

by heat from the cooling lava pile and subjacent intrusions, but does not need to show any obvious relationship with specific intrusions within the volcanic field (White, 1957). This may result in the permanent effects of regional hydrothermal activity - altered country rock appearing pervasive throughout the eroded volcanic pile, spatially unassociated with separate intrusions. This, of course, must be qualified with the observation that intense hydrothermal alteration such as that described later in section 7.3., may represent localised activity definitely associated with a particular intrusion. This pervasive alteration in and around joints and fractures, appears analagous to the metamorphic reconstitution in that it may well have been ultimately caused by intrusive activity, but since intrusion has been regional in extent, so too is the alteration.

7.3. Alteration associated with sulphide mineralisation

Only a brief account of alteration associated with sulphide mineralisation is included in this report, since, because of the obvious economic importance, other more detailed studies are at present in progress (R. Minnitt, pers comm,1976). Alteration of country rock (volcanics of the Tsams Formation, HVG) around and within a porphyritic to equigranular adamellite-granodiorite pluton of the VIS in the Tsams River area, has been accompanied by low grade, finely disseminated Fe-Cu-Pb-Zn mineralisation. Degree of alteration increases into the pluton, which contains most of the sulphide. Hydrothermal solutions have reacted with feldspar and mafic minerals in the pluton and country rock, forming a bleached sericite-quartz-sulphide rock. Extreme alteration has produced small areas of kaolinite-sericite-quartz rocks (so-called "white bodies"). The rock types involved (porphyritic intrusive, volcanic country rock), the type of alteration and the characteristics of the mineralisation (low grade, disseminated Cu sulphides) suggest a porphyry-copper type deposit (Titley and Hicks, 1966; Hollister, 1975; Lowell and Guilbert, 1970).

Alteration of this type seems to be confined to the Tsams river area, since no comparable effects of intrusion are to be found anywhere else in the Haib-Vioolsdrif region. The only other Cu sulphide mineralisation definitely associated with Vioolsdrif intrusive activity is in the lower Krom River, where a small quantity of sulphides occur within hydrothermally altered leucogranite. A few samples of altered lava from the Tsams River area were collected, but were not included in the geochemical investigations.

7.4. Alteration associated with shear zones

Extensive shearing accompanied tectonic deformation after the consolidation of the HVIP. The various recognisable periods of shearing have been mentioned briefly in Chapter 2. The most conspicuous shear zones are the wide belts of schistose and mylonitic rocks that ramify the study area in a rough E-W pattern. Apart from the directional textures developed, the shear zones have acted as channels for migrating solutions, since veins and pods of carbonate, chlorite and silica are very common. The region immediately surrounding Nous Wells is underlain by intensely sheared volcanics and intrusives which have been reduced to chlorite-biotite schists seamed with milky white quartz veins. An important accessory mineral associated with quartz and other carbonates is pale green malachite. Concentration of the Cu mineral has attracted attention in the form of numerous prospecting pits. It is important to contrast this type of Cu mineralisation (exclusively carbonate) with the sulphide ores in the Tsams River area. The latter is probably a syngenetic deposit while the former is probably epigenetic, being generated by solutions precipitating carbonate during migration along the shear zone.

7.5. Criteria for selection

The main criterion used for selecting samples for analytical work was

based on appearance in hand specimen and under the microscope. Weathered samples were easily recognised by their friable nature and brown clay-rich encrustation. Altered samples within the Tsams River area were easily avoided because of their bleached appearance and the presence of disseminated pyrite replacing the primary mafic minerals. Any rocks displaying penetrative schistosity or foliation were rejected, since they may have been altered during the period in which they were sheared. Hard, unweathered, unfoliated rocks containing conspicuous veins, pods or stringers or silica, chlorite, epidote and carbonate were rejected. Samples containing "abnormally high" amounts of any one of the above secondary minerals were also rejected, even though no veins could be seen. "Abnormally high" usually meant volume percentages greater than 10%.

Samples that passed through all the above tests were hard, unweathered, unfoliated rocks containing very few or no veins, but which were composed of metamorphic and relict igneous minerals. The possibility that these samples may have been affected by cryptic alteration (alteration not detected in hand specimens or thin sections) has been evaluated in the following sections, in terms of selected chemical components.

7.6. Volatile content

Most of the volatile material (expressed as "loss on ignition" is probably H_2O^+ (water lost above 110°C) and CO_2. The former is probably more abundant, since carbonated samples were rejected after visual and microscopic examination. Although separate determinations of H_2O^+ and CO_2 were not carried out, the modal proportions of hydrous (metamorphic) minerals in the lavas suggest that water must be the most significant volatile component.

The maximum loss on ignition is that corrected for oxidation of Fe. In the XRF analyses listed in Appendix 3, Fe is expressed as Fe_2O_3, although a significant proportion is present as FeO. Oxidation of Fe during the

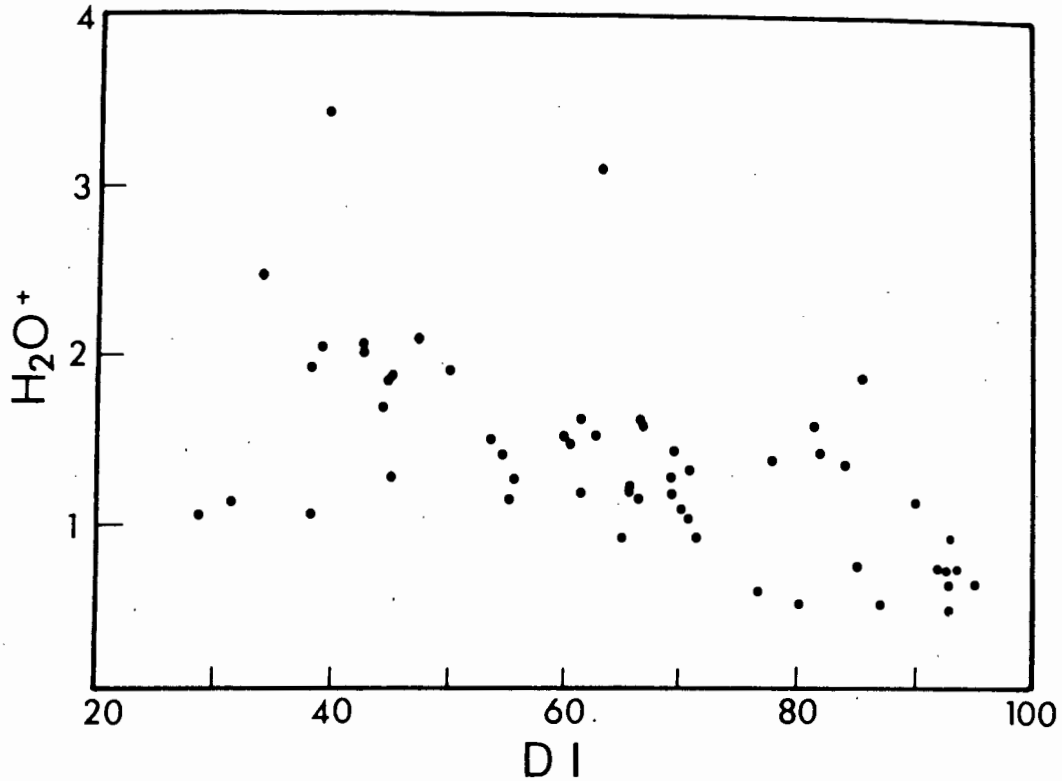

Fig. 32. Plot of H_2O^+ (corrected L.O.I.) against DI (Differentiation Index) for the Haib lavas.

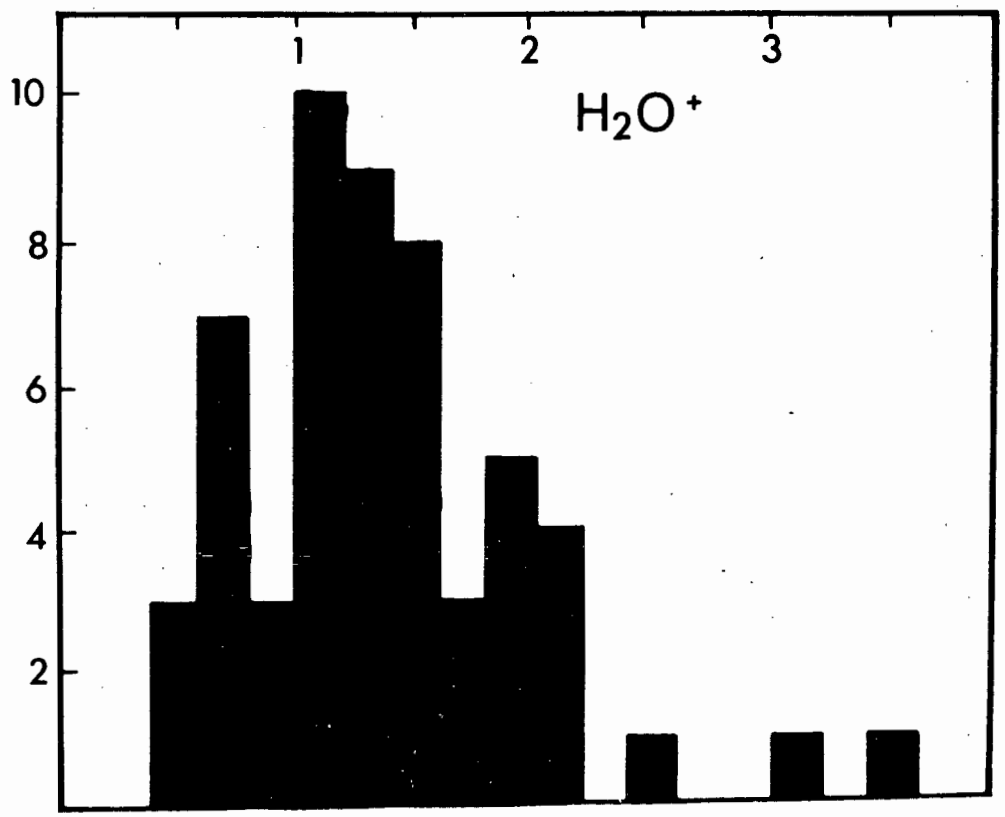

Fig. 33. Frequency histogram illustrating the range in H_2O^+ content in the Haib lavas.

ashing process (prior to casting fusion discs) is incomplete (about 80%), so the correction applied to the loss on ignition figure is as follows:-

Corr. loss = Calc. loss + 0,8 (Total Fe as Fe_2O_3 - (Actual Fe_2O_3 + Actual FeO)). Corrected loss was always greater than calculated loss, since there were no cases of a gain on ignition (usually confined to materials very rich in FeO).

Values for corrected loss have been plotted against D.I. and on a frequency histogram (Figs. 32 and 33). It is clear from the plots, that the loss (referred to hereafter as water content) in all lavas, except for a few outliers, is not unacceptably high. Reconstituted volcanic piles containing zeolites or prehnite-pumpellyite assemblages commonly contain greater than 4 per cent water (Jolly, 1972). Higher grades of metamorphism (greenschist facies) involve progressive dehydration of the rock, with the production of minerals containing lower water contents (epidote, biotite, amphibole). Rocks such as these contain 0.5 - 3 per cent water (Jolly, 1972), but may retain a bulk chemical composition similar to the unmetamorphosed igneous parent. Chayes (1969a) found no striking contrast in compositions between volcanic rocks containing more or less than 2% water. Rejection criteria used by Baragar (1966, 1968), Baragar and Goodwin (1969) and Irvine and Baragar (1971) in their studies of the Precambrian greenstones of the Canadian Shield, involved a cut-off value for H_2O^+ of about 2 - 2.5 per cent. Rocks containing H_2O^+ greater than 2.5 per cent were considered to be more prone to alteration. Those with less than 2.5 per cent H_2O^+ were subsequently recalculated to 100 per cent water free, apparently in the belief that at this level, water had been merely added, rather than being a replacement component. In view of the comparable H_2O^+ contents (mostly less than 2.5%) in the lavas of the HVG, the analyses listed in Appendix 3 have been retained. In other words, no analyses could be obviously rejected on the grounds that they contained extreme quantities of water. It is interesting to note that Smith (1968, 1969) has found that bulk composition of reconstituted volcanics, recalculated to 100 per cent water free, were comparable to fresh, unaltered zones, even

though the reconstituted rocks contained up to 10-12 per cent H_2O^+. This suggests that water content may not always be useful as a check for alteration. Based upon this uncertainty, even the outlying samples (H_2O^+ greater than 2.5%) have not been rejected.

7.7. Bulk Fe_2O_3/FeO ratio

The ubiquitous presence of epidote throughout the exposed volcanic pile indicates a significant Fe_2O_3 content, since all Fe in this mineral is trivalent. Furthermore, the work of Watkins and Haggerty (1967) has clearly demonstrated post consolidation modification of the bulk ferric/ferrous ratio in young, apparently fresh lavas. Since the Fe_2O_3/FeO ratio influences the CIPW norm (Le Maitre, 1976b), some estimate of the original value for this ratio must be attempted.

The Fe_2O_3 content of a rock is always difficult to measure. Its derivation is invariably by calculation after FeO has been determined by some wet chemical technique, commonly involving titration (e.g. Shapiro and Brannock, 1956; Rigg and Wagenbauer, 1964; Schafer, 1966a, 1966b). These authors emphasise the problems with partial oxidation of FeO to Fe_2O_3 during dissolution and titration, resulting in the calculated Fe_2O_3/FeO always being slightly high. Prolonged grinding of rock powders also result in slight oxidation (Fitton and Gill, 1970).

Analytical difficulties, together with possible oxidation immediately after consolidation, and obvious oxidation as indicated by the growth of abundant epidote, caused the author to dispense with direct FeO determination. The remainder of this section will deal with the problem of determining a Fe_2O_3/FeO that is considered to more closely resemble that displayed by the original freshly crystallised rock.

An important petrographic feature which has bearing on this problem is the ubiquitous presence of phyric Fe-Ti oxide. In the basaltic andesite lavas, this mineral forms discrete subhedral microphenocrysts, or, less

commonly, is partly enclosed in pseudomorphed mafic silicate phenocrysts, a feature pointing to their early appearance. Unfortunately, metamorphic reconstitution has resulted in their extensive reaction with the groundmass, the Ti-phase now being represented by sphene and a residual opaque phase of nearly pure magnetite. Further reaction with the groundmass has produced chlorite and biotite at the expense of magnetite. The magnetite composition was revealed with the EMP, and the analyses total 100 per cent when the Fe is calculated as FeO and Fe_2O_3 according to the theoretical spinel formula. This information suggests that the original opaque phase was probably a member of the magnetite - Ulvöspinel series (β phase of Buddington and Lindsley, 1964; Carmichael and Nicholls, 1967).

The presence of a phyric Fe-Ti oxide in all the lavas, must reflect the Fe_2O_3/FeO ratio prevailing during crystallisation. Wager (1960) and Carmichael et al., (1974) suggest that basic magmas require at least 2.0 - 3.5 weight per cent Fe_2O_3 for magnetite to precipitate. The absence of a coexisting α phase (ilmenite-hematite series) in the Haib lavas is probably a function of their uniformly low TiO_2 content (less than 0.8%) (cf. Marsh, 1976).

The results of Fudali (1965) indicate that for basic to andesitic silicate melts equilibrated at or near liquidus temperatures under constant oxygen fugacity, the Fe_2O_3/FeO ratio increases with total alkali content. The increase is more marked if K/Na ratios are high, suggesting that K is more "oxidising". Total alkali contents are not abnormally high in the Haib lavas, however, K/Na ratios are relatively high (>1.0) which judging from the conclusions of Fudali (1965), will tend to result in a higher Fe_2O_3/FeO ratio for a given total alkali content.

The high K/Na ratios and the ubiquitous presence of phyric magnetite, suggest that Fe_2O_3/FeO ratio of all the Haib lavas was relatively high. Just how high is difficult to establish, but if the figures quoted by Wager (1960) and Carmichael et al., (1974) can be adopted, then Fe_2O_3 contents of at least 3% (in the basic to intermediate lavas) seem to be required.

A constant Fe_2O_3 throughout the lava series is unrealistic, since total Fe as FeO falls below 3% at about D I = 75. An arbitrary Fe_2O_3/FeO is also unsatisfactory, because it has been demonstrated that Fe_2O_3 is influenced by bulk composition (Fudali, 1965). Different values for the various rock types (e.g. 0.2 for basaltic andesite, 0.4 for andesite, and so on), will necessarily produce artificial step-like variations in Fe_2O_3 and FeO contents. Irvine and Baragar (1971) have suggested that the maximum $Fe_2O_3 = TiO_2 + 1.5$ wt %. Le Maitre (1976b) has suggested that a mean value rather than a maximum value is more realistic and has put forward a scheme based on multiple regression analysis of nearly 26,000 igneous rock analyses, which involves the calculation of the oxidation ratio ($Ox = FeO/(FeO + Fe_2O_3)$ weight per cent) from the formula (for volcanic rocks):-

$$Ox = 0.93 - 0.0042\ SiO_2 - 0.022\ (Na_2O + K_2O)$$

Testing this formula, a Haib basaltic andesite containing abundant magnetite microphenocrysts (total Fe as Fe_2O_3 = 8.77%) was selected. The calculated Fe_2O_3 content is 3.37%, and the Fe_2O_3/FeO ratio is 0.69. The Fe_2O_3 content is above the limiting value for the early appearance of Fe-Ti oxide (for basic lavas), so it seems that the Le Maitre scheme may be acceptable for estimating Fe_2O_3 in the Haib lavas.

7.8. Normative Corundum

Corundum appears in the CIPW weight percent norm when there is a molecular excess of Al_2O_3 over ($Na_2O + K_2O + CaO$). Rocks containing normative corundum have often been explained as being altered (cf. Chayes, 1969a), specifically involving the removal of alkalis. Volcanic glasses are very prone to such alkali loss during hydration and devitrification (Noble, 1967, Lipman et al., 1969; Wilkinson, 1971; Heming and Carmichael, 1973), and their CIPW norms often reflect this by containing corundum. Higher viscosities of more siliceous magmas result in a greater abundance of glassy

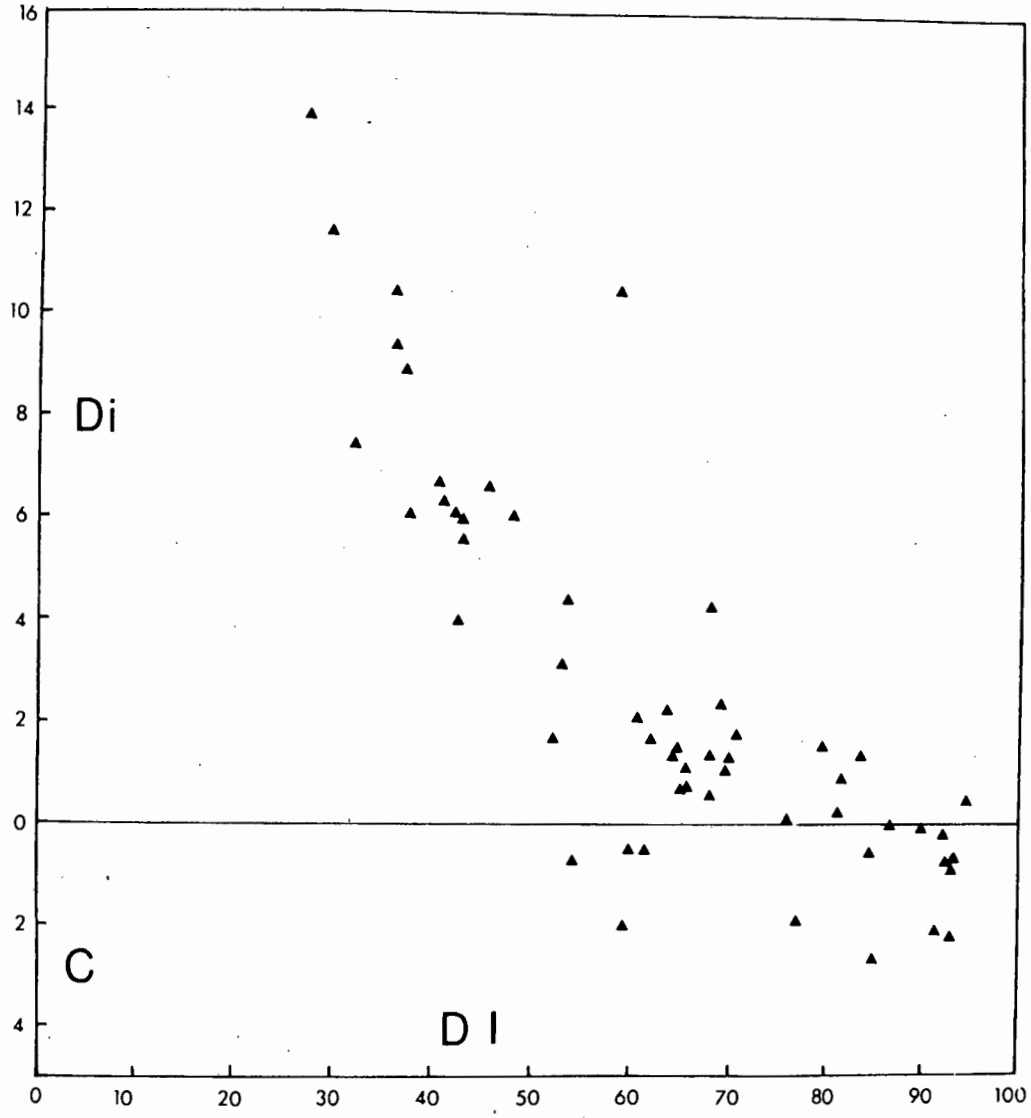

Fig. 34. Plot of normative corundum (C) and diopside(Di) against DI for the Haib lavas.

material and hence render such lavas more prone to alkali leaching. In other words, it is to be expected that alteration will produce more corundum normative acid lavas than basic types. This may have to be kept in mind when studying Fig. 33, where Di and C are plotted versus D I. The regular variation in normative composition may be controlled by alteration, rather than by a systematic process such as fractional crystallisation (Cawthorn et al., 1976; Cawthorn and Brown, 1976) or progressive assimilation (Ewart and Stipp, 1968).

If alkali removal has occurred in the more siliceous lavas, then it has not been general or extreme, since Na_2O and K_2O increase with D I. The acid lavas contain the highest alkali contents, yet are quite commonly corundum normative. The total alkalis - D I plot (Fig. 35a) and the K_2O - D I plot (Fig. 35b) may indicate that a few of the more acid lavas have lost alkalis, especially three rhyolitic lavas with D I greater than 80 but K_2O contents less than 4%. The rhyolite with the lowest K_2O is a flow banded acid glass from the Tsams Formation. It has extremely high SiO_2 ($> 80\%$) which suggests some post consolidation silicification. The glassy nature of this particular rock renders it susceptible to alkali loss, especially in the light of the age and geologic history of the HVG. All those analyses which plot below the average trend in K_2O variation have been ignored in the subsequent discussion on petrologic modelling.

Normative corundum may be produced by Ca leaching, while the alkalis have remained static. Alteration may remove Ca in solution as carbonate, but it is difficult to conceive of such a process not affecting the alkalis to some extent. In situations where Ca has been affected, primary Ca-silicates have been replaced by secondary Ca-silicates (e.g. epidote) or Ca-carbonate, with little or no migration of Ca at all (Smith and Smith, 1976).

The data presented above suggest that the presence of normative corundum in the more siliceous lavas of the HVG has not been produced by any leaching process, except in a few cases. The production of rocks with these

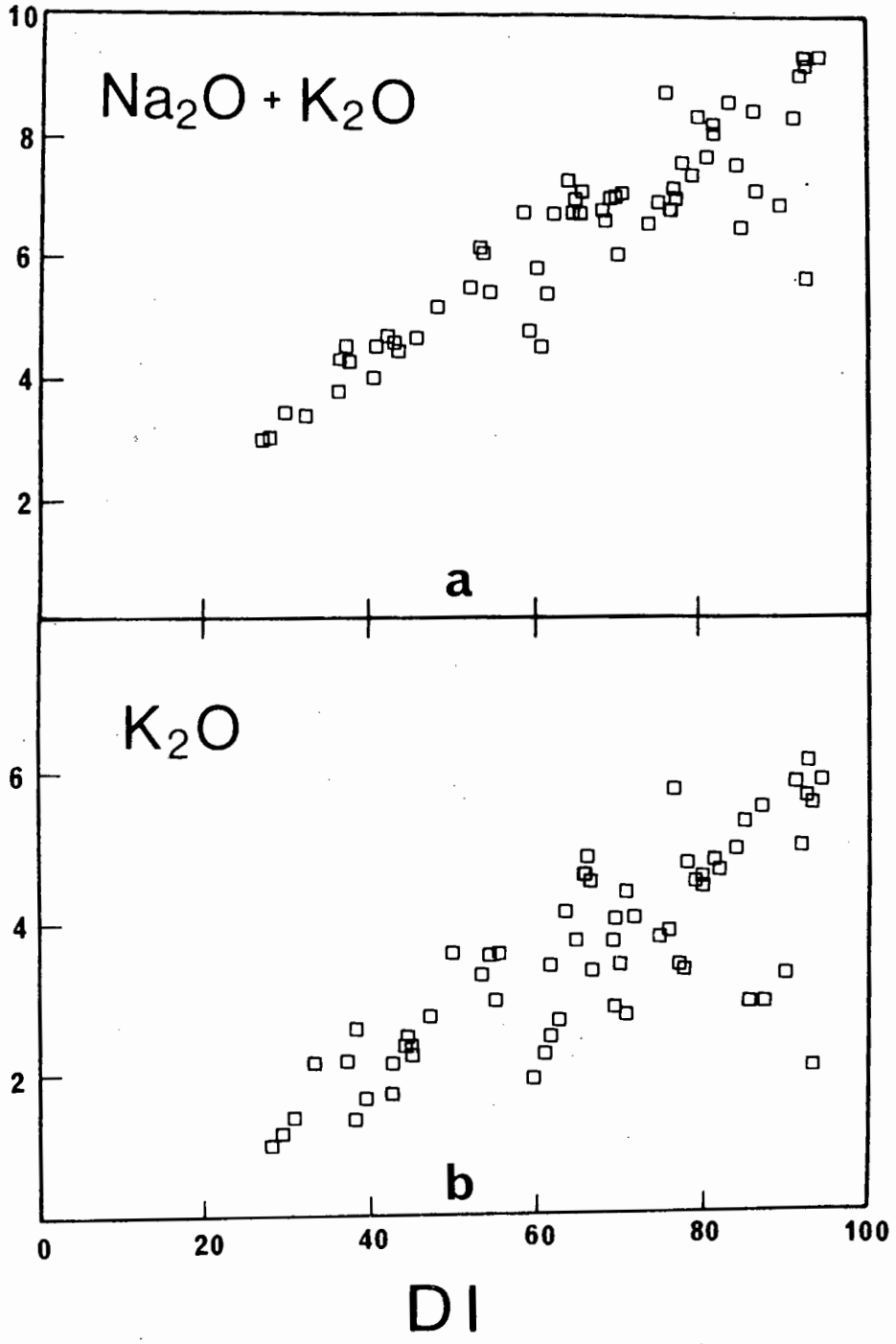

Fig. 35. Plot of total alkalis (a) and potassium (b) against DI for the Haib lavas.

normative characteristics is more likely to be a primary igneous process.

7.9. Sr isotopes

Sr^{87}/Sr^{86} ratios have been measured in a large number of lava samples in order to determine their Rb-Sr age. It has been shown in Chapter 3, that despite metamorphic reconstitution, the Rb-Sr isochron age is probably very close to the extrusion age of the volcanic pile. The good correlation between Sr^{87}/Sr^{86} and Rb^{87}/Sr^{86} suggests that the lavas have essentially remained as closed systems with regard to Sr and Rb migration. Since Sr replaces Ca in plagioclase and K in K-feldspar, the Rb-Sr isochrons indicate that Sr has behaved in a similar manner to these major elements during metamorphic reconstitution. Rb, which is contained in biotite, K-feldspar and glass, has presumably behaved in a similar manner to K during metamorphism. As far as the bulk rock is concerned, no major migration of Sr and Rb and, by inference, Ca and K, has occurred since the time of eruption.

7.10 U and Pb isotopes

U, Pb concentrations and Pb isotopic ratios have been measured in selected lava samples of all bulk compositions, in order to determine U-Th-Pb ages (Chapter 3). Pb-Pb and Th-Pb isochron ages are both very similar to the Rb-Sr isochron age discussed briefly in Section 7.9. This suggests that (1) no influx of Pb with significantly different isotopic ratios has occurred, (2) no extensive U migration has occurred between the age of extrusion and the present day, and (3) no significant Th migration has occurred. U-Pb isochron plots show slightly more scatter, and the calculated ages are therefore less accurately known. However, estimated mean U-Pb ages are not very different from the more reliable Rb-Sr, Th-Pb and Pb-Pb ages. In view of the well documented mobility of U during practically any type of alteration process involving solutions (especially sub-aerial

weathering), the near concordancy in the U-Th-Pb radiometric system, and the agreement with the Rb-Sr radiometric system, indicates that very little migration of any of the above elements has occurred.

7.11. Discussion

The Haib lavas have not entirely escaped alteration but the effects associated with weathering, hydrothermal activity, contact metasomatism and shearing, can all be avoided by careful visual and petrographic examination. Samples remaining after these tests were only a small fraction of the total number collected. Cryptic alteration in the samples finally analysed is not widespread. The ferric/ferrous ratio was adjusted to some more realistic value since there was petrographic evidence in the form of abundant epidote to show that all the rocks have been oxidised. Investigation of other components such as K_2O content, Sr and Pb isotope ratios, resulted in a few more samples being rejected from final discussion and petrogenetic modelling.

8

THE HVG. MAJOR ELEMENT COMPOSITION

8.1 General statement

Inspection of the bulk major element analyses listed in Appendix 3 is sufficient to establish the extremely wide compositional range displayed by lavas in the HVG. The range is considered to reflect some primary igneous characteristic and has not been produced by metamorphism, metasomatism or some other alteration process. An important feature to note is the scatter displayed by the data on appropriate variation diagrams (Figs. 36 to 44), when considering the question of average compositions. The latter abound in modern literature, probably because space requirements prohibit the inclusion of all analytical data. Comparison of average data may be of dubious significance because (1) the widely differing schemes of classification which define the boundary conditions used for calculating the averages (e.g. Chayes' (1969b) criticism of Nockolds' (1954) average andesite) and (2) the ever-present uncertainty as to whether the sample population is statistically balanced. Average compositions of the various lavas within the HVG given in Table 12 are arithmetic means of samples falling in each of the classes defined in the scheme of Peccerillo and Taylor (1976) (see Chapter 5). The accompanying uncertainties are single standard deviations.

In the following section, reference is made to major oxide compositions recalculated to 100 per cent volatile free, in order to minimize differences caused only by variable water contents. In addition, the Fe_2O_3/FeO ratio has been adjusted according to the scheme of Le Maitre (1976b), following the conclusion set out in Chapter 7. CIPW weight percent norms have been calculated from recalculated analyses.

8.2 Lavas

8.2.1. Normative Quartz

Table 12. Average major element composition of the Haib lavas. Classification based on SiO_2 content (see Table 10). Recalculated on a volatile free basis, with all Fe as FeO. CIPW norms have been calculated with Fe_2O_3 and FeO estimated using the method of Le Maitre (see Appendix 4).
N = number of samples; $\overline{X}$ = mean composition; sd = standard deviation about the mean (1σ)

	Basaltic andesite N=5		Andesite N=18		Dacite N=18		Rhyolite N=14	
	$\overline{X}$	sd	$\overline{X}$	sd	$\overline{X}$	sd	$\overline{X}$	sd
SiO_2	54.95	1.02	59.10	2.05	65.68	1.73	73.77	2.75
TiO_2	.73	.03	.74	.07	.59	.11	.36	.16
Al_2O_3	14.94	.20	16.10	.85	15.73	.68	13.75	.94
FeO	8.55	.38	6.84	.98	4.48	.62	1.84	.28
MnO	.16	.01	.12	.03	.09	.04	.04	.01
MgO	8.09	.43	4.90	1.69	2.26	.89	.60	.35
CaO	8.29	.90	6.35	.93	4.16	.88	1.31	.82
Na_2O	1.87	.34	2.59	.78	2.81	.56	3.33	.51
K_2O	1.86	.64	2.74	.82	3.82	.96	4.83	1.22
P_2O_5	.23	.04	.23	.04	.16	.04	.07	.03
Qz	7.30		12.04		22.02		34.09	
C	.00		.00		.00		.72	
Or	10.99		16.19		22.59		28.54	
Ab	15.82		21.92		23.78		28.18	
An	26.83		24.22		19.03		1.95	
Di	11.26		5.47		1.03		.00	
Hy	21.29		13.68		6.95		1.68	
Il	1.39		1.41		1.10		.68	
Mt	4.83		4.36		3.29		1.57	
Ap	.50		.50		.35		.15	
DI	34.11		50.55		68.37		90.81	

The oversaturated nature of the Haib lavas is reflected in the appearance of normative quartz (Qz). Even though Qz is partly controlled by the adopted Fe_2O_3/FeO ratio (Le Maitre, 1976b), none of the Haib lavas approach saturated or undersaturated compositions by decreasing this ratio. Metamorphic reconstitution has produced quartz in the groundmass of even the most basic lavas (basaltic andesites, Qz = 6-10%), although it was probably not present in the original igneous mode. Phyric quartz appears in many of the dacites and certainly all of the porphyritic rhyolites. The appearance and subsequently increasing amounts of modal quartz is consistent with the progressive increase in normative quartz from basaltic andesite through to rhyolite.

8.2.2. Iron enrichment

Of the many different diagrams used in the literature to illustrate degree of iron enrichment in igneous rocks, three are shown in Figs. 36 and 37.

To facilitate comparison, average data listed in Table 12 are plotted (Fig. 36b), but may be checked against a plot of all individual analyses of the Haib lavas (Fig. 36a), in order to confirm that the averages plot on the trend defined by all the data. All three diagrams illustrate the same effect, but indicate the degree of Fe enrichment against different parameters in order to show that this trend is a fundamental characteristic.

Fig. 37 clearly illustrates the lack of iron enrichment in the Haib lava series, which is in contrast to that exhibited by the Thingmuli volcano (Carmichael, 1964). On the other hand, the Haib trend corresponds very closely to that displayed by the Cascade volcanic province (averages cited by Carmichael, 1964, based on data from Anderson (1941), Williams (1932, 1935, 1942) and Yoder and Tilley (1962)). The Thingmuli trend is considered to be an example of the so-called tholeiitic series, whereas the Cascades are representative of the calc-alkaline series. Based on the AFM variation, the Haib lavas show affinity to calc-alkaline type volcanics.

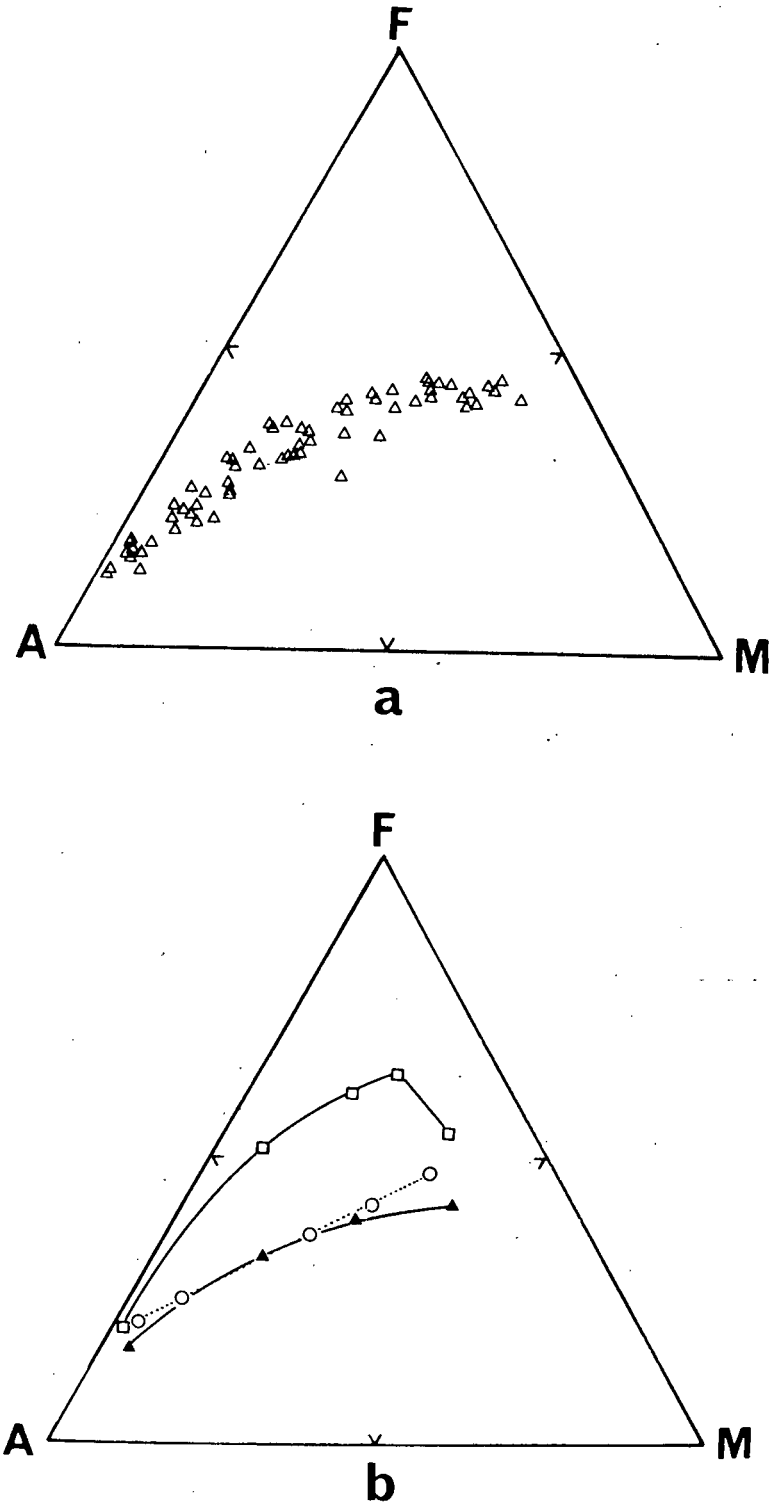

Fig. 36. A (Na_2O + K_2O) - F (Total Fe as FeO) - M (MgO) plots for the Haib lavas. a = all individual data points; b = average trend; ▲ = HVG; ○ = Cascades trend; □ = Thingmuli trend. Average data for Cascades and Thingmuli from Carmichael (1964).

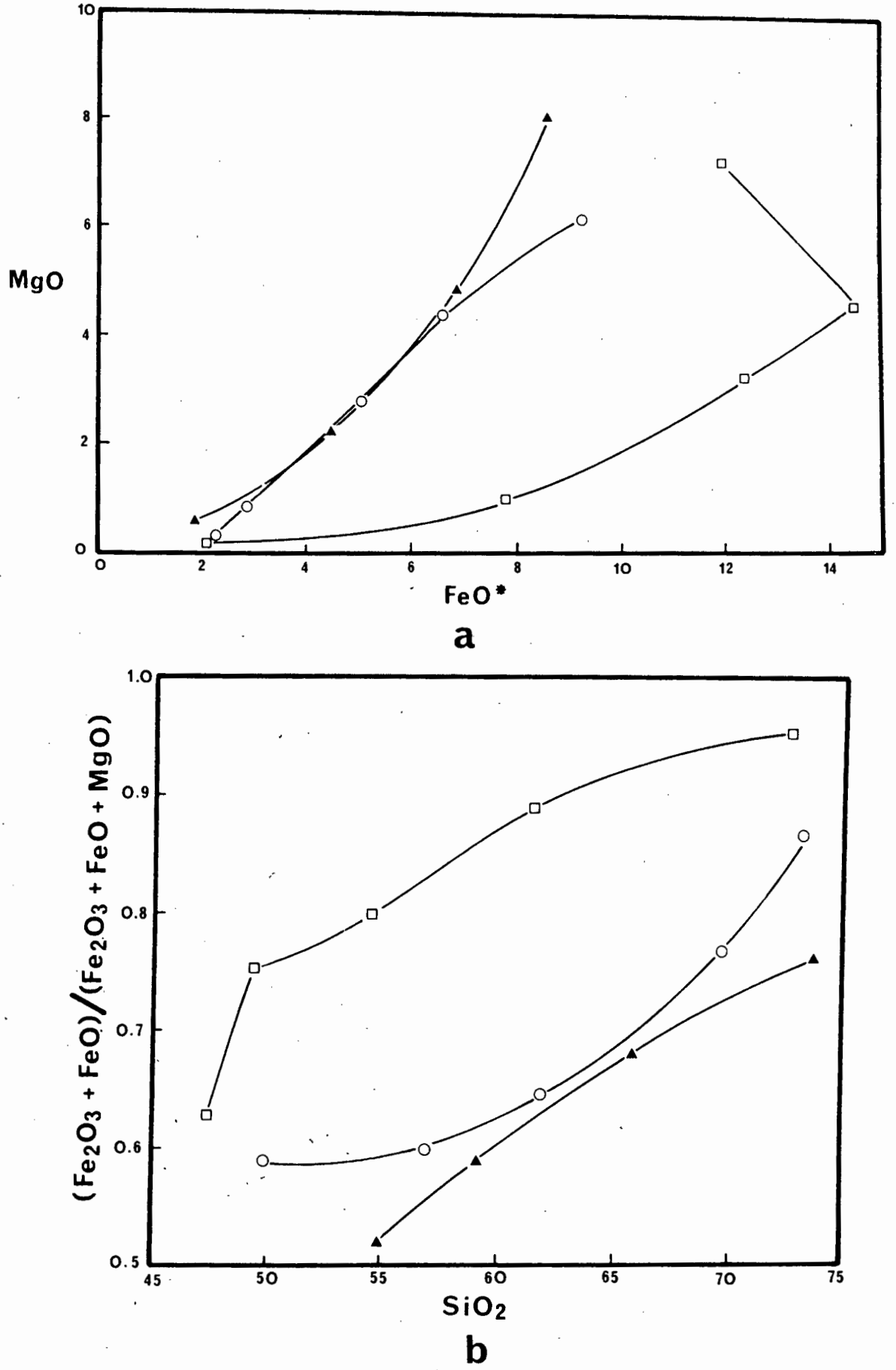

Fig. 37. Plot of MgO against FeO^* (a) and $(Fe_2O_3 + FeO)/ (Fe_2O_3 + FeO + Mg)$ against SiO_2 (b) illustrating the average trends for a typical calc-alkaline suite (Cascades) and a tholeiitic suite (Thingmuli). Symbols as in Fig. 36.

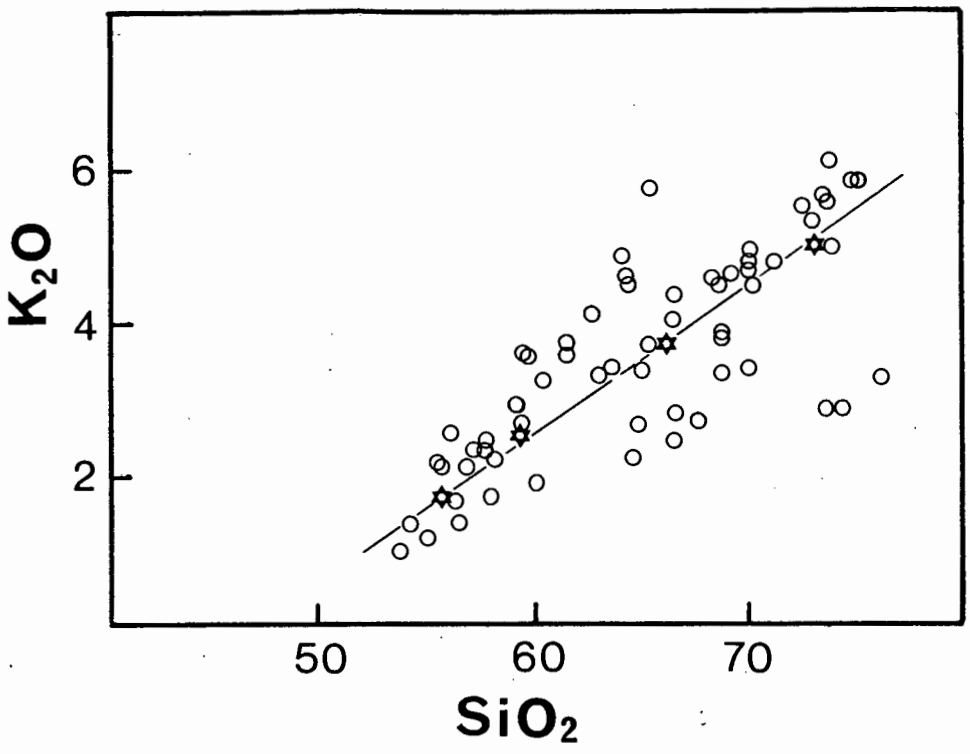

Fig. 38. Plot of K_2O against SiO_2 for the Haib lavas. The stars represent average compositions listed in Table 12. Solid line is an estimate of the average trend for the HVG.

8.2.3. Potassium-Silica variation

Fig. 38 contains all available K_2O abundance data for the Haib lavas, together with an estimate of the average trend. This average trend may be compared with those displayed by various Cenozoic circum-Pacific volcanic provinces (based on a compilation by Gill, 1970) and other selected provinces (Fig. 39). Predictably, there is a continuum of trends and any subdivision would be arbitrary (e.g. Peccerillo and Taylor, 1976; McKenzie and Chappell, 1972; Taylor, 1969). However, the Haib average trend is distinctly steeper than that displayed by many calc-alkaline provinces, despite comparable degrees of iron-enrichment. Such K-rich calc-alkaline provinces are not unknown and the Haib lavas may be compared with the Ordovician Borrowdale volcanics (trend 22 in Fig. 39, Fitton, 1972; Oliver, 1961) and the late Precambrian Guperas volcanics in south-west Africa (trend 21, Watters, 1974). Cenozoic volcanics in the circum-Pacific region showing similar K_2O-SiO_2 varia-

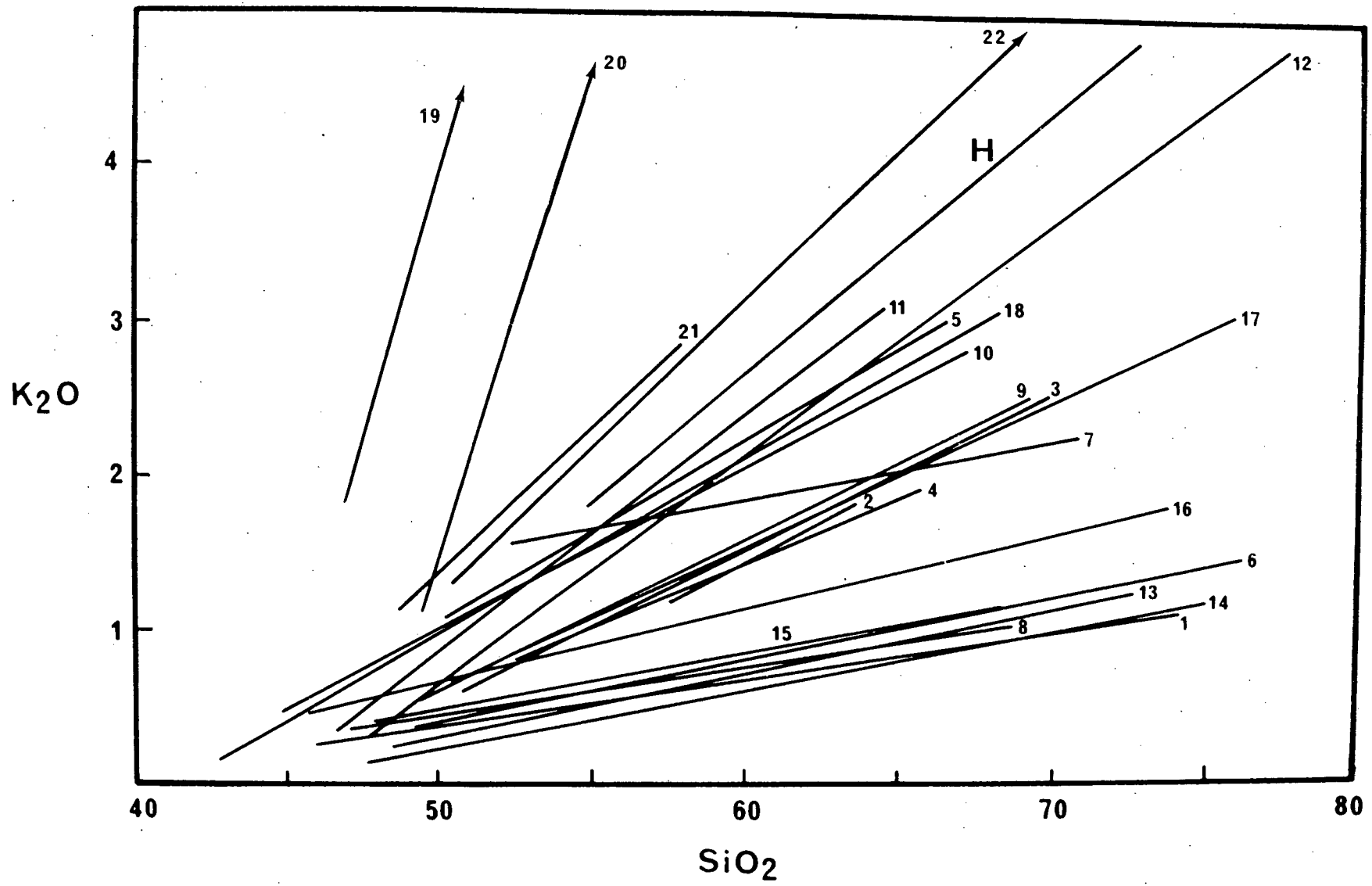

Fig. 39. Comparison between the Haib average K_2O-SiO_2 trend (H) and other volcanic provinces. Trends 1-18 are for Cenozoic suites in the circum Pacific region (compilation in Gill, 1970). 19 = Shoshonitic suite of Fiji (Gill, 1970); 20 = Barby shoshonitic lavas (Watters, 1974); 21 = Salina (Keller, 1974); 22 = Borrowdale (Fitton, 1972).

tion occur in the Aleutians (trend 11, Coates, 1952). The Haib average trend falls in the so-called "high-K calc-alkaline" field of Peccerillo and Taylor, (1976), although other schemes (e.g. McKenzie and Chappell, 1972) would regard them as shoshonites. These latter K-rich rocks show quite variable compositions; the shoshonite-absarokite-banakite series in the type area (Yellowstone, Wyoming-Montana) do not display a regular correlation between K_2O and SiO_2 (Joplin, 1968; Nicholls and Carmichael, 1969; Protska, 1973; Beall, 1974), a feature which has contributed to the controversy over their petrogenesis. However, volcanic rocks subsequently referred to as shoshonites do in fact display quite regular K_2O-SiO_2 trends (trend 19 - Fiji, Gill, 1970 and trend 20 - Barby volcanics, South West Africa, Watters, 1974). The Haib lavas do not contain enough K to warrant their inclusion in the shoshonite series and seem to lie in a transitional field between the "normal" calc-alkaline field and shoshonites. Following this observation, the Haib lavas may be described as having affinities with high-K calc-alkaline volcanic provinces.

8.2.4. Total alkalis-silica variation

Kuno (1966, 1968) has demonstrated that a systematic increase in total alkalis at constant SiO_2 exists in the Cenozoic lavas of Japan as they are traced across the island arc from the oceanic to the continental side. With the chemical data available to him, Kuno has defined three fields in the total alkalis-silica diagram (Fig. 40) that correspond to (I) tholeiitic (lowest total alkalis), (II) high-alumina and (III) alkali (highest total alkalis). It was further demonstrated that high alumina basalt and its derivatives constituted the calc-alkaline series. Thus the calc-alkaline series was characterised by low iron enrichment, moderate K enrichment and moderate total alkali contents. Later work in other areas of the circum-Pacific region has confirmed that calc-alkaline volcanic provinces are characterised by moderate total alkali contents (Carmichael *et al.*, 1974). However, the intermediate field of the total alkalis-silica diagram is not exclusively occupied by calc-alkaline trends. For example, the Thingmuli volcano (cited previously as an example of the tholeiitic series) exhibits an average trend that lies entirely within the calc-

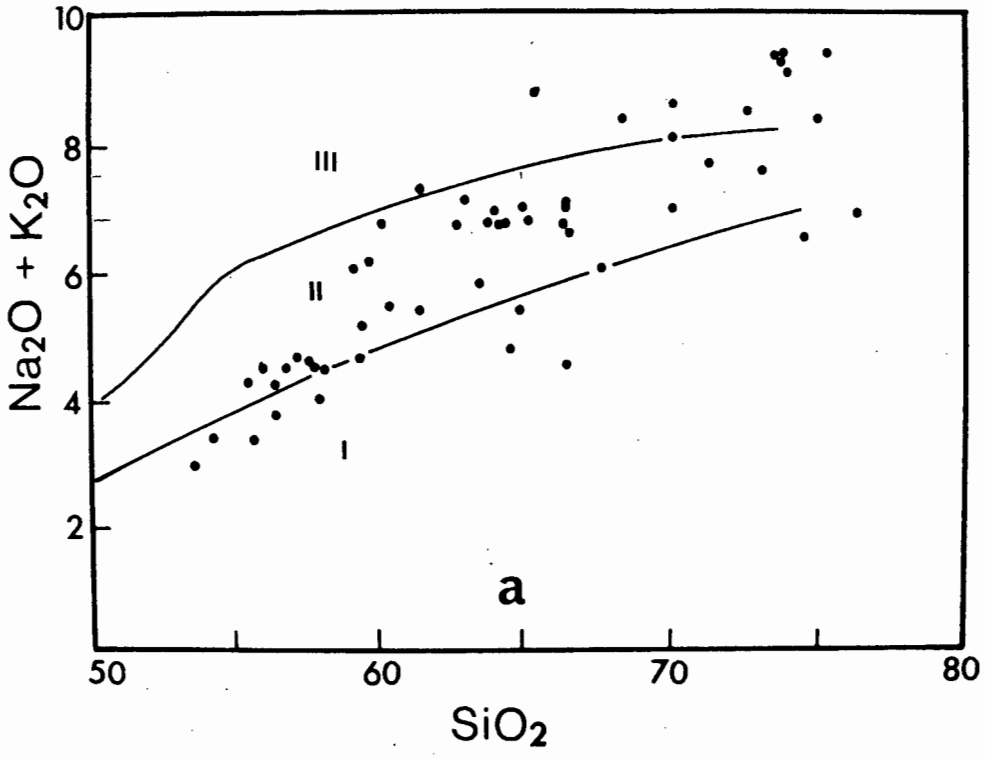

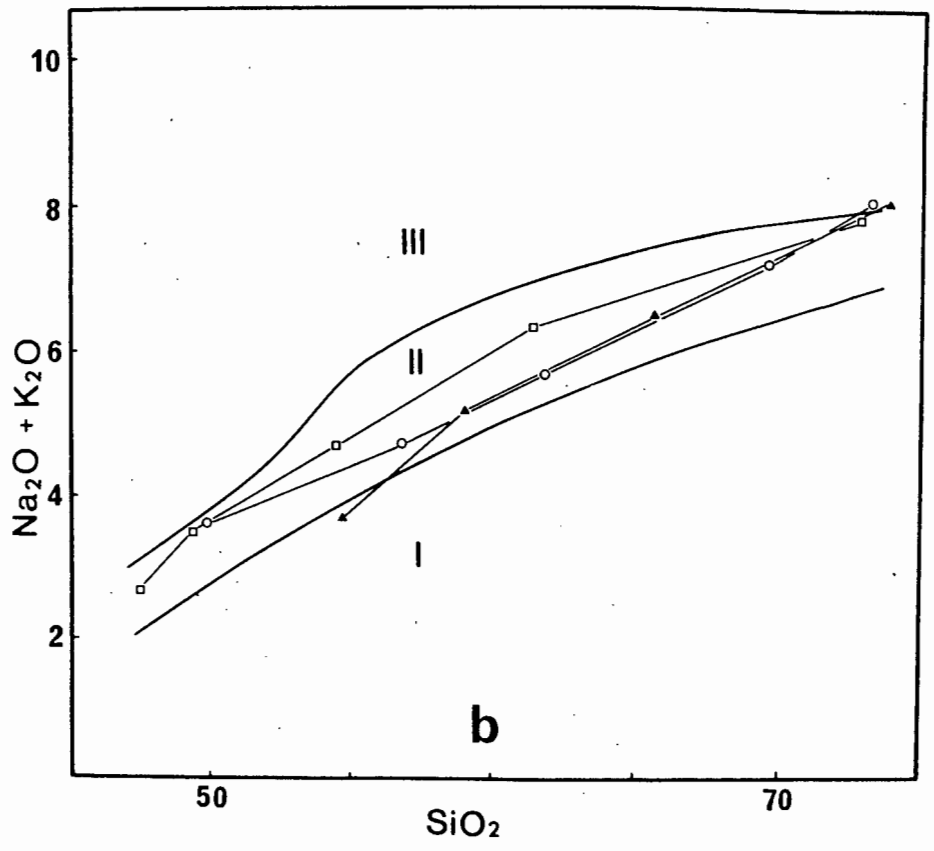

Fig. 40. Plot of ($Na_2O + K_2O$) against SiO_2 for the Haib lavas. a = individual samples; b = average trend. ▲ = HVG; O = Cascades; □ = Thingmuli. Fields are those defined for the Japanese arc by Kuno (1968) I = Tholeiitic field, II = High alumina (calc-alkaline) field, III = Alkaline field.

alkaline field. It can be seen that the Thingmuli (tholeiitic), Cascades (calc-alkaline) and Haib (possibly high-K calc-alkaline) volcanic provinces may not be readily distinguished on a total alkalis-silica diagram. While the total alkalis-silica variation exhibited by the Haib lavas is consistent with its calc-alkaline definition, this feature may not be invoked as independent evidence alone. This serves to illustrate the problems of extending simple chemical parameters from one province to another.

8.2.5. Alkali-lime index

The term "calc-alkali" was originally used by Peacock (1931) in his attempt to classify igneous rock series in terms of their major element variation. His concept of alkali-lime index involved the determination of the silica composition at which total alkalis ($Na_2O + K_2O$) equalled the lime content (CaO). Fig. 41 contains a partial Harker diagram where both the average ($Na_2O_2 + K_2O$) and average CaO contents for the Haib lavas are plotted against average SiO_2. The two trend lines intersect at SiO_2 = 60.8. Peacock's scheme makes arbitrary subdivisions and defines four fields;

alkalic	*ALI less than 51
alkali-calcic	ALI between 51 and 56
calc-alkalic	ALI between 56 and 61
calcic	ALI above 61

*Alkali-Lime Index

Based on this scheme the Haib lavas are calc-alkalic, a feature consistent with that obtained from the other chemical parameters. Peacock's scheme has not been followed rigorously, since many volcanic suites showing tholeiitic tendencies by other criteria (AFM variation, low K_2O-SiO_2 trends) have ALI of between 56 and 61. On the other hand, suites with ALI outside the 56-61 range may exhibit all the accepted chemical features of the calc-alkaline series (Carmichael *et al.*, 1974).

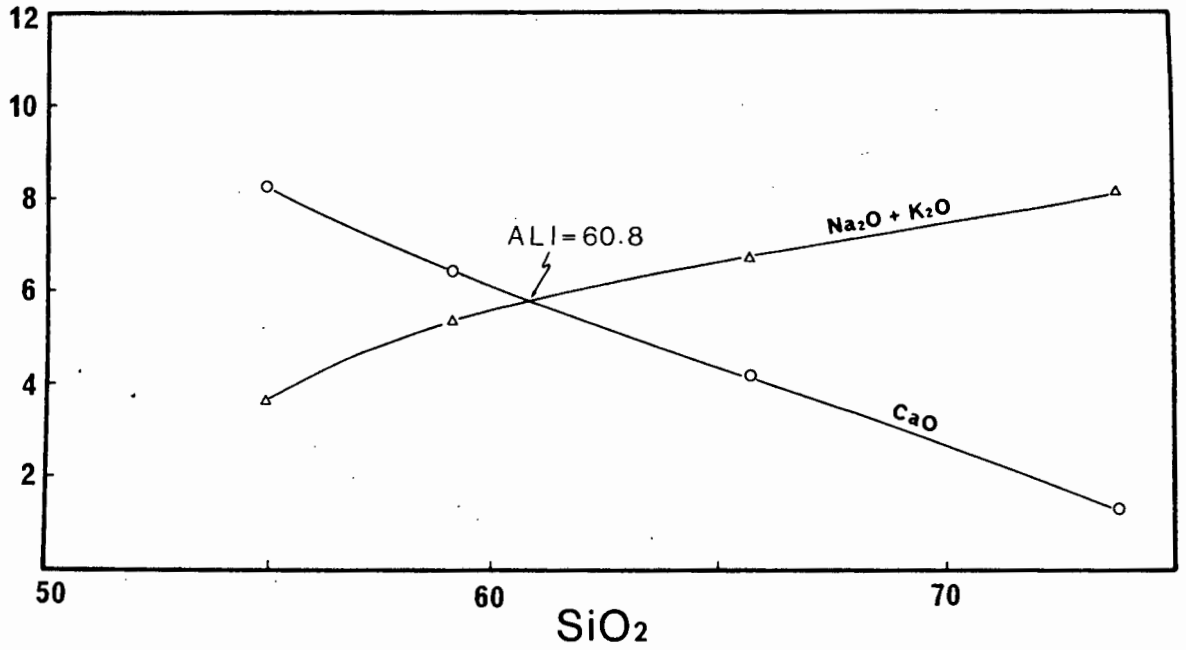

Fig. 41. Alkali-lime index for the Haib lavas.

8.2.6. TiO_2 content

Chayes (1964) has focussed attention on a systematic difference between TiO_2 contents in comparable Cenozoic volcanic rocks (basic-intermediate) in and around the oceans. In particular, he found that circum-oceanic volcanics generally have less than 1.75% TiO_2, whereas oceanic equivalents usually contain more than 1.75%. The subsequent discovery of abundant modern oceanic basalts with TiO_2 less than 1.75% (e.g. Engel *et al.*, 1965) tends to refute this distinction, but Carmichael *et al.*, (1974) and Jakes and White (1972a) have confirmed that circum-oceanic volcanics (island arcs and convergent plate margins) have uniformly low TiO_2 contents (less than 1.2%). Calc-alkaline volcanics are abundant in such an environment, but do not comprise the entire volcanic products (Jakes and White, 1972a). The range shown in Fig. 44 shows clearly that the Haib lavas are uniformly low in TiO_2 (less than 0.8%), which appears to reinforce their possible affinity with calc-alkaline provinces.

TiO_2 shows a reasonably regular variation with D I (Fig. 43). In the passage from basaltic andesite to rhyolite, the TiO_2 content rises slightly to a maximum (0.8% TiO_2 at D I = 40), then decreases progressively from 0.8%-0.2% in the most acid lavas (D I greater than 90). Three aberrantly high points in the D I range 70 - 85 may be a function of increased (accumulated?) amounts of titanomagnetite phenocrysts.

8.2.7. Al_2O_3 content

The work of Kuno (1960) attached some significance to the Al_2O_3 content of volcanic rocks, especially calc-alkaline types, since they are generally characterised by high values (16-20 percent Al_2O_3). Wilkinson (1967) later considered that the parental magma of the calc-alkaline series was a high alumina basalt. Subsequently, Taylor (1969); Taylor *et al.*, (1969a); Jakes and White (1972a); Cole (1973); Carmichael *et al.*, (1974) and others, have confirmed that basalts associated with cenozoic calc-alkaline lavas are relatively enriched in Al_2O_3. In fact, the entire calc-alkaline series is characterised by high Al_2O_3 contents. Average data plotted in Fig. 42 show

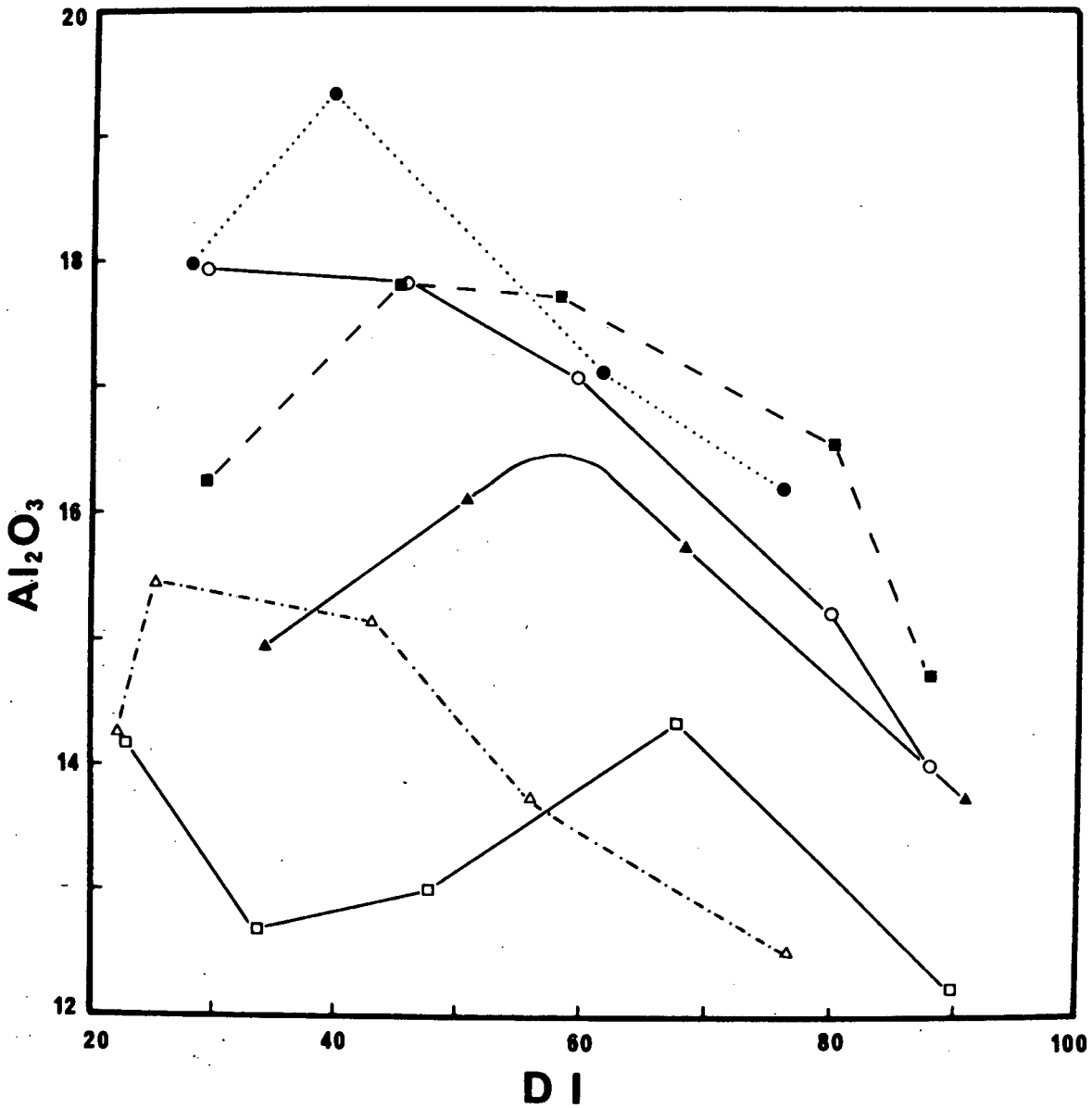

Fig. 42. Comparison of Al_2O_3 - DI trends for various igneous suites.
▲ = HVG; △ = Red Hill dolerite - granophyre (McDougall, 1962);
□ = Thingmuli (Carmichael, 1964); ■ = Borrowdale (Fitton, 1972);
○ = Cascades (Carmichael, 1964); ● = Salina (Keller, 1974)

clearly the high Al_2O_3 contents of calc-alkali volcanics (e.g. Cascades, Borrowdale, Salina) relative to tholeiites (e.g. Thingmuli, Red Hill). The distinction between calc-alkaline and tholeiitic lavas was considered to be so marked by Irvine and Baragar (1971) that they proposed it as a basis for separating the two trends.

Cenozoic calc-alkaline basalts, basaltic-andesites and even andesites seem to contain higher Al_2O_3 contents than equivalent rock types in the Haib series. Furthermore, the variation trend exhibited by the Cascades contrasts sharply with that of the Haib; the Cascade trend is one of progressive depletion in Al_2O_3 with differentiation, whereas the Haib trend involves an initial increase to a maximum of about 16.5% at D I = 60, followed by a decrease with increasing D I . Trends in Al_2O_3 variation exhibiting a maximum at some intermediate D I are not unknown in some calc-alkaline or tholeiitic provinces, three of which are included in Fig. 42. For example, Fitton (1972) describes a series of lavas in the Ordovician Borrowdale Group (N.W. England), that reaches a maximum Al_2O_3 content of 17% at D I = 45. Keller (1974) reports a calc-alkaline trend in the Salina volcanic series (Aeolian Islands), with a maximum Al_2O_3 (19.3%) at D I = 40. On the other hand, a typical tholeiitic trend such as that exhibited by the Red Hill dolerite intrusion, Tasmania (McDougall, 1962), has maximum Al_2O_3 = 15.5% at D I = 35. The tholeiitic Thingmuli volcano (Carmichael, 1964) shows a slightly different behaviour, with the least differentiated rocks having relatively high Al_2O_3 (olivine tholeiite), which decreases to a minimum at D I = 40 (basaltic andesite), then increases to a maximum at D I = 70 (icelandite) and finally decreasing to a low value of 12% Al_2O_3 in the rhyolites.

Two important features of the Haib Al_2O_3 variation trend are (1) the Al_2O_3 maximum is displaced towards a higher D I relative to most other calc-alkaline or tholeiitic provinces and (2) it apparently shows transitional Al_2O_3 contents. The latter illustrates the fact that the Haib series is not characterised by high Al_2O_3 contents, nor is it comparable to "normal" tholeiites. Inspection of the vast literature on igneous rocks, shows that there is a continuum of trends from uniformly low, to very high Al_2O_3 contents

and which may exhibit flat, inclined or convex upwards variation patterns. In other words, there are calc-alkaline trends with low alumina (e.g. Superior Province greenstones, Canada; Baragar and Goodwin, 1969) and high alumina tholeiites (e.g. Arc tholeiites of Tonga, Ewart *et al.*, 1973), hence alumina contents are not very informative for classification purposes.

8.2.8. Major oxides - D I variation

Major element variation is illustrated in Fig. 43, where all oxides are plotted against Differentiation Index (D I). The close correlation between SiO_2 and D I indicates that the major element variation trends resemble the conventional Harker diagram, parts of which have been used in the preceding sections. For example, the K_2O-SiO_2 plot (Fig. 38) is similar to the K_2O-DI plot. This is a predictable feature, since differentiation from basaltic andesite to rhyolite is dominated by progressive enrichment in silica. All plots show a reasonably regular variation and so average trend lines may be defined, which pass through, or are very close to, the bulk of the data points. On each plot there are a few aberrant points and since all samples shown were chosen for further study by their lack of visible alteration, the discrepant nature must be a function of cryptic metasomatism or some primary igneous process (phenocryst accumulation, fractionation). The aberrant points on each diagram have been labelled with their field number.

Three samples with high TiO_2 lying above the average trend were highlighted in section 8.2.7. The suggested titanomagnetite accumulation may be tested chemically in only a very general way, since the original opaque phase has been extensively reconstituted. Analysed titanomagnetite from lavas range in composition from $Mt_{20}USP_{80}$ - $Mt_{84}USP_{16}$ (Carmichael *et al.*, 1974). An average titanomagnetite ($Mt_{50}USP_{50}$) will have 17.9% TiO_2 and 79.14% total Fe as FeO, assuming the theoretical composition. One of the high TiO_2 rocks (DRL-93) has about 0.2% more TiO_2 than the average value (0.6) at this DI. The average FeO* (total Fe as FeO) content at the same D I is about 5%. This results in $(TiO_2)_{mt}/(TiO_2)_{rock} = 30$ and $(FeO^*)_{mt}/(FeO^*)_{rock} = 18$, which indic-

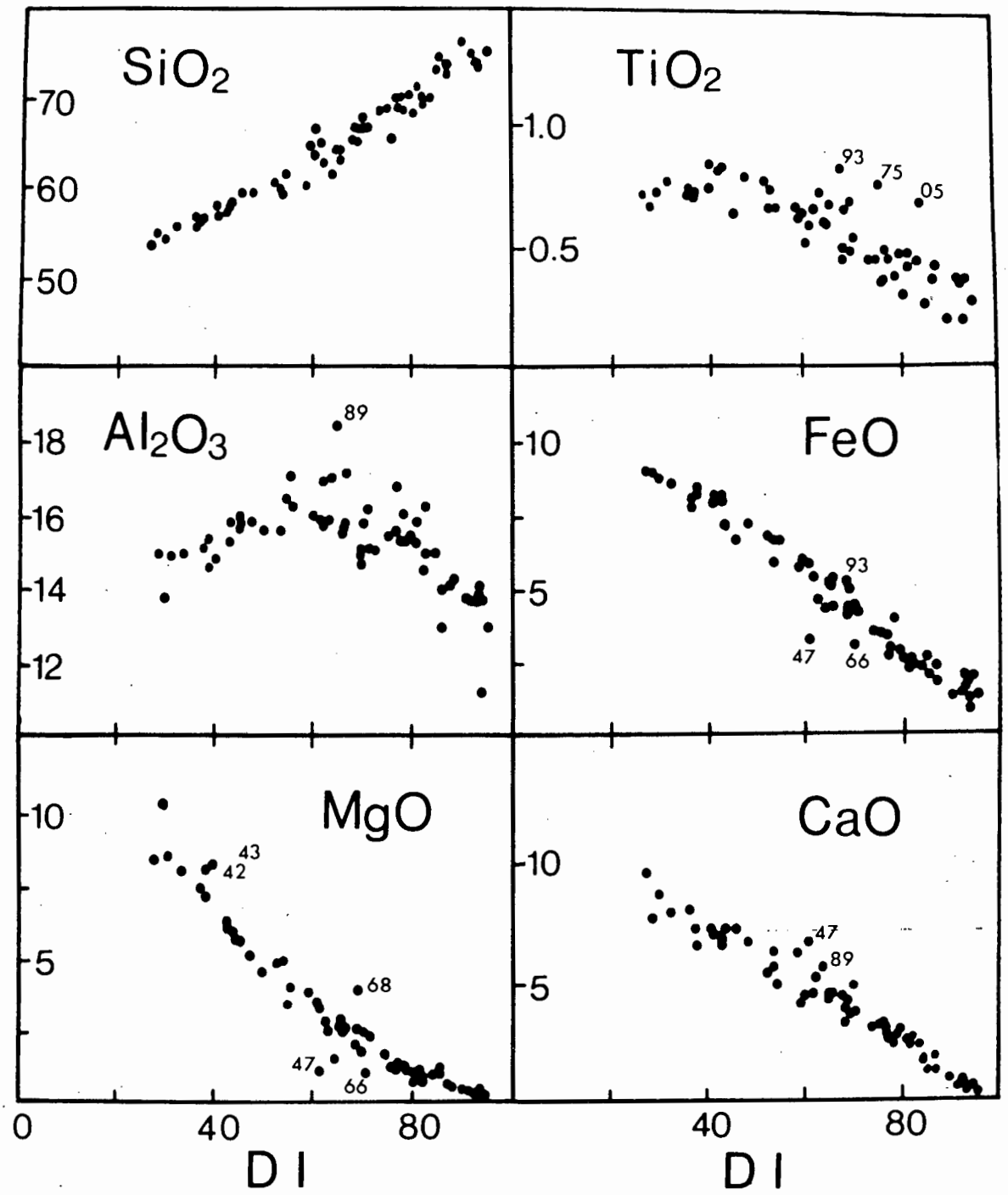

Fig. 43. Plot of major oxides against DI for the Haib lavas. All compositions are on a volatile free basis.

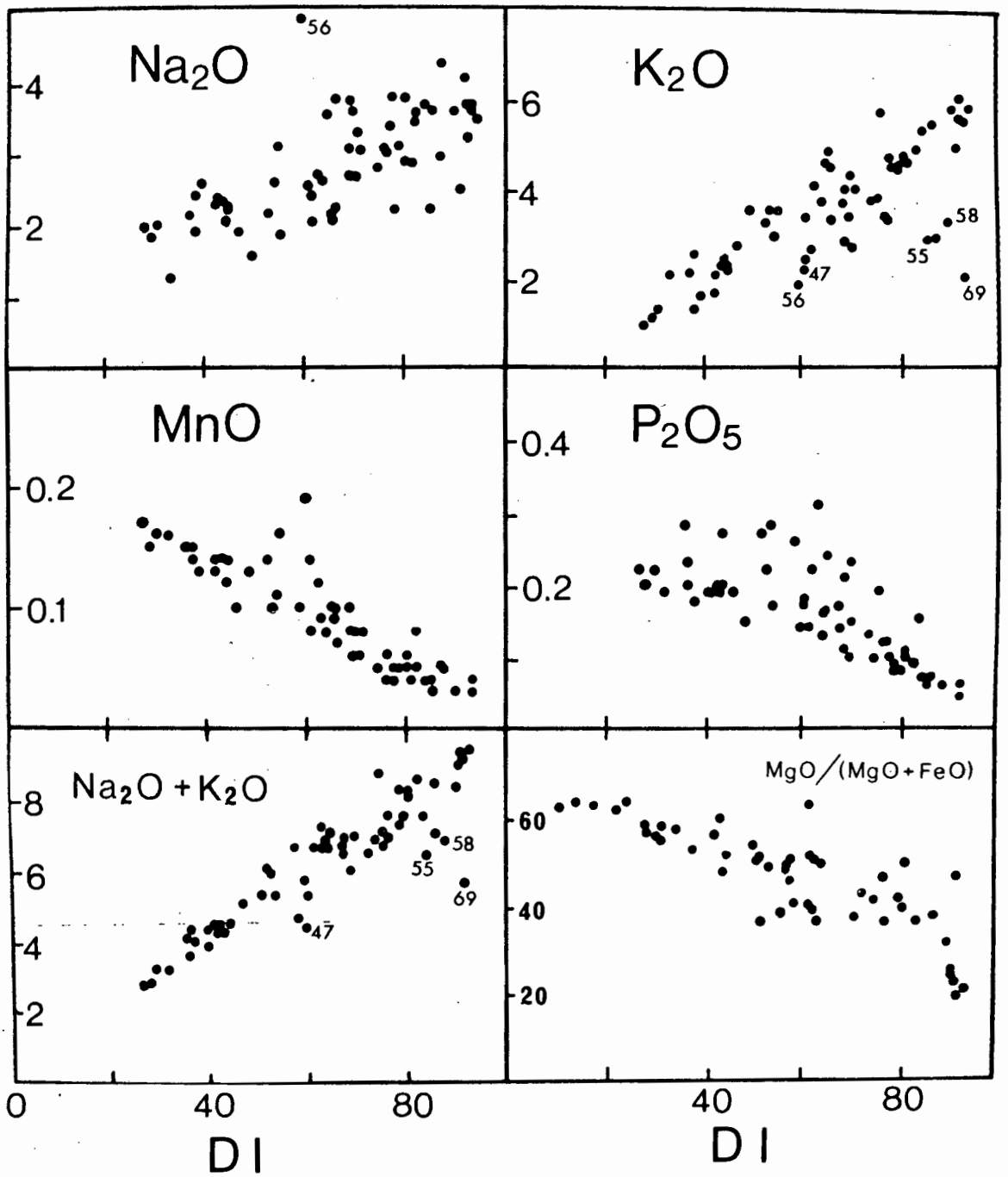

Fig. 43. Plot of major oxides against DI (continued).

ates that titanomagnetite accumulation would have a greater affect on TiO_2 content than on FeO* content. An increase of 0.2% TiO_2 in DRL-93 could result from about a 1.0% titanomagnetite addition, which would necessarily be accompanied by an increase in FeO* from 5% to 5.7%. This latter change is barely detectable in Fig. 43, hence would not result in sample 93 lying significantly above the average trend. The other two points represent lower bulk TiO_2 contents and hence would be more affected by titanomagnetite addition. Less titanomagnetite would be needed and hence no significant change in FeO* would be detected, a feature confirmed by inspection of Fig. 44.

The only aberrant sample in the Al_2O_3-DI plot is 89, which lies at least 1,5 wt % above the average trend line. The only mineral capable of producing such an enrichment is plagioclase, which will also require higher CaO and perhaps Na_2O contents. This sample has slightly high CaO, while the broad scatter in Na_2O contents prohibits the identification of mildly aberrant points. The normative plagioclase composition of DRL-89 is An_{55}, which represents a plagioclase with 28.9% Al_2O_3, 11.1% CaO and 5.3% Na_2O. The addition of 15% plagioclase (An_{55}) will result in the required Al_2O_3 content (i.e. sample 89 = 18.5%, Al_2O_3 "average trend" value = 16.5%). The accompanying change in Cao is from 5% (average trend value) to 5.9%, which agrees reasonably well with the observed value in DRL-93, of 5.7%. The quantitative argument above suggests that the aberrant point on the Al_2O_3 - DI plot is the result of plagioclase accumulation.

On the FeO* - DI diagram a porphyritic dacite lava (47) plots far below the average trend. In addition, this sample also has a low MgO concentration. In hand specimen and in thin section, the rock is similar to many of the Haib dacites, but has a DI of 60.6, which is very low. In addition to having low Fe and Mg contents, it also has a relatively low K_2O concentration, being one of a group of aberrant samples in the K_2O - DI plot. Petrographically, the rock is a dacite and its discrepant nature is considered to be caused by alkali leaching (especially K_2O). The groundmass of the lava is extremely fine-grained and was probably devitrified glass, before metamorphic recyrstallisation increased the grain size. Since alkalis are readily lost from glass

during hydration and devitrification (Noble, 1967; Lipman *et al.*, 1969), 47 may have undergone such a period of leaching, thereby lowering the K_2O concentration and hence its DI. The decrease in DI has resulted in the aberrant position of 47 in the variation diagrams. Another sample which shows a similar but less marked shift is 66 (also labelled on the appropriate diagram).

Two very discrepant points which are difficult to explain are 68 (on the MgO-DI plot) and 56 (on the Na_2O-DI plot). The high MgO content of 68 is not accompanied by high FeO*, which would have been expected if the relative enrichment was caused by accumulation of ferromagnesian minerals. A possible explanation for the discrepancy is to consider the DI as being too high for the MgO content. The hand specimen obtained from this andesite lava flow contains what are thought to be rounded enocrysts of quartz. It is quite possible that the material used for analysis includes some of this hidden xenocrystic quartz, thereby increasing SiO_2. Since the rock was already oversaturated, the additional SiO_2 would simply increase normative Qz and hence the DI. Certainly this particular rock is petrographically similar to basaltic andesites occurring in nearby flows and it was in fact surprising to find that it contains 66% SiO_2 instead of the expected 58-60%. The distribution of quartz xenocrysts was not found to be uniform throughout the outcrops or hand specimen of 68, so no accurate estimate of the amount of silica contamination was possible.

The sample containing high Na_2O (56) has relatively low K_2O, which results in a "normal" total alkalis content. The aberrant nature of this sample may be interpreted as having either a DI too low for its Na_2O content, or an Na_2O content too high for its DI. Judging from the other major oxide-DI diagrams, where 56 plots near the average trends, the former condition is unlikely. Addition of Na_2O from some outside source is a distinct possibility, since veins containing albite are quite common throughout the lave pile. However, it is difficult to explain why the K_2O should be low and apparently complementary to Na_2O, such that total alkalis appear normal. The effective addition of albite in veins will also increase the Al_2O_3 content and since the Al_2O_3/Na_2O formula weight ratio is 2, alumina should be affected to a greater extent. There is no evidence for an increased alumina content in 56

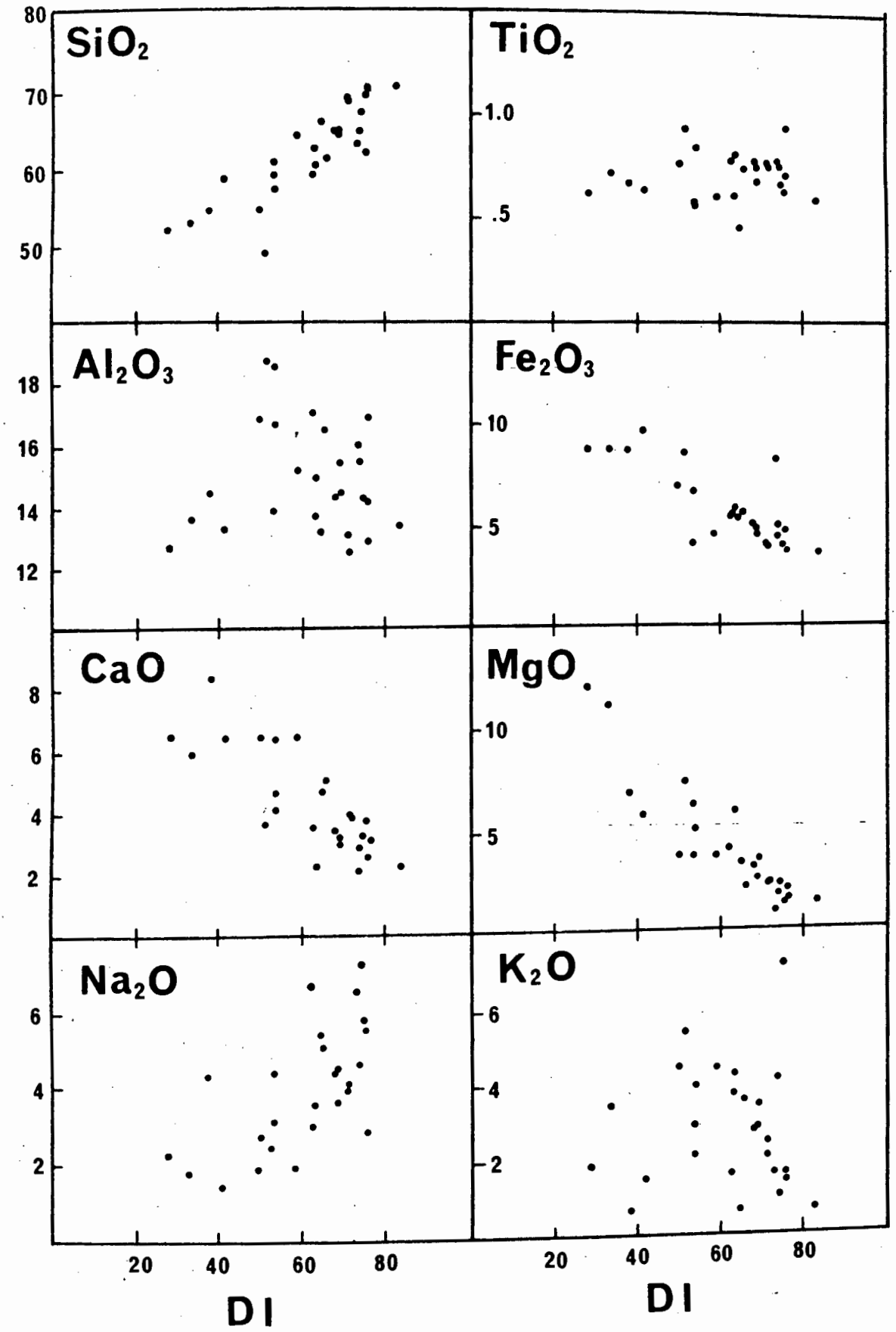

Fig. 44. Plot of major oxides against DI for fragmental rock types within the HVG. All compositions are on a volatile free basis.

and the problem of the aberrant nature of 56 remains unresolved. However, this single sample can be neglected without seriously affecting the overall picture.

Finally, it should be noted that two basaltic andesites (42 and 43) have slightly high MgO contents. Their FeO* contents are barely above the average trend. Slight accumulation of ferromagnesian minerals could account for this effect but since the primary minerals are metamorphosed, it is difficult to know which minerals are involved. Clinopyroxene addition would raise MgO and to a lesser extent FeO*, since the MgO/FeO* ratio of this mineral will be relatively high. However, such addition should increase the CaO content of the lava, but there is no evidence for this in the relevant diagram. The highly oversaturated nature of the lavas preclude olivine accumulation, but would be consistent with addition of orthopyroxene. The possibility of accumulating orthopyroxene is enhanced by the slightly low Al_2O_3 contents in these two lavas. Volcanic amphiboles commonly contain up to 12% Al_2O_3 (Cawthorn, 1976a; Jakes and White, 1972a), which is not far below the average basaltic andesite value (15% Al_2O_3), so small amounts of amphibole accumulation would not significantly depress the Al_2O_3 content of the lava.

8.3 Fragmental rock types

Fragmental rock types (pyroclastics, volcanogenic sediments) are essentially mechanical mixtures of the various lavas described previously. The wide range in lava compositions preclude any simple mixing models, because of the great variety of possible end members. In addition, the porous nature of the original volcanic debris has facilitated the migration of fluids, resulting in widespread alteration. Compositional variation caused by alteration has therefore been superimposed on that brought about by mechanical mixing. The diagrams in Fig. 44 illustrate the wide range in major element composition present in the fragmental rock types. The range is of the same order as that exhibited by the lavas, but shows much more scatter, which suggests that alteration has probably played a prominent part in producing the present compositions.

The variation diagrams require little comment, except for the K_2O-DI plot. Potassium shows no correlation with DI despite the fact that this parameter is influenced strongly by the amount of normative orthoclase. Acidic fragmental rocks (DI = 80) have similar K_2O contents to some basaltic andesitic lavas (DI = 40). In view of the absolute abundances involved (K_2O = 1.2%), the high DI rocks appear to have lost K_2O by some leaching process during alteration. The high DI fragmental rocks are dacitic to rhyolitic and must have lost a significant portion of their potassium. In view of the apparently common occurrence of high DI, low K_2O fragmental rock types in the HVG, these chemical peculiarities may be useful in identifying such rocks when metamorphic recrystallisation has rendered them indistinguishable from true lavas.

9

THE VIS. GENERAL DESCRIPTION

9.1. Distribution

9.1.1. Extent of batholith

Plutonic rocks included in the VIS probably underlie most of the study area in the form of a huge batholith, with the HVG forming a thin, discontinuous capping. The present cycle of erosion is unroofing the vast intrusive complex, so that excellent vertical exposures may be seen in the canyon of the Orange River and in the numerous tributary gorges both to the north and south of the main stream. Fig 25 shows the possible extent of the VIS in the study area and in the neighbouring Richtersveld. Correlation of intrusive rocks in the north-eastern Richtersveld (implied by De Villiers and Söhnge, 1959) with the VIS has been confirmed by recent work (Ritter, 1975). However, the correlation between "intrusive" rocks in the south-eastern Richtersveld (due west of the study area) and the VIS (implied by Middlemost, 1964) is somewhat dubious, since intense deformation and lithologic heterogeneity in this area make accurate identification impossible (Bertrand, 1975).

Deformed, metamorphosed and possibly remobilised VIS has been described to the north (Blignault, 1975), east (Bertrand, 1975) and south (Ward, 1974) of the present study area. The original extent of the batholith is at present unknown, mainly because of widespread cover strata, and the difficulty of recognising possible reworked VIS. A conservative estimate of the area underlain by the VIS is about 30,000 sq km (about 10,000 sq. miles). Comparison between this figure and estimates for other batholiths may be found in Table 13.

9.1.2. Distribution within the batholith

Relative proportions of the six major rock types in the batholith are

Table 13. Estimated area underlain by various batholiths throughout the world. 1. Joyce (1973a); 2. Hamilton and Myers (1967); 3. Cobbing and Pitcher (1972); 4. Turner and Verhoogen (1960).

BATHOLITH	AREA (KM^2)	REFERENCE
Vioolsdrif	30 000	
Murrumbidgee (Australia)	1 400	1
Boulder (USA)	5 000	2
Idaho (USA)	52 000	2
Sierra Nevada (USA)	55 000	2
Coastal (Peru)	88 000	3
Southern California	180 000	4
Coast Range (Alaska - Brit. Columbia)	280 000	4

listed in Table 14. The figures are, of course, very rough areal estimates, which should be confined to the present study area and the immediate surroundings. Accurate figures are difficult to give, since they would have to be based on very detailed mapping, involving the tracing of individual contacts of every single pluton within the complex. Such time consuming work is outside the scope of the present study. Furthermore, areal expression may bear no relationship to actual volumetric proportions.

It is clear that intermediate plutonic rocks (granodiorite, tonalite) are the most abundant. These two rock types are difficult to distinguish in the field, since they differ only in the amount of quartz. Moreover, the individual plutons often show variation from tonalite to granodiorite. Petrographic features are described more fully in Chapter 11. The preponderance of tonalitic-granodioritic rocks in composite batholiths (of any age), is not uncommon. Although rock names vary, it is clear that most batholiths are intermediate rather than acid in average composition. For example, Cobbing and Pitcher (1972) report that the most abundant rock type in the Coastal Batholith of Peru is tonalite. Bateman et al., (1963) have demonstrated that the Sierra Nevada Batholith is composed mainly of granodiorite, quartz-monzonite and quartz-diorite. The Southern California Batholith is mainly tonalite and granodiorite (Larsen, 1948).

Table 14. Relative proportions of individual rock types in the VIS. Applies to study area and immediate surroundings.

ROCK TYPE	AREA OCCUPIED (%)
Leucogranite	5
Adamellite	30
Granodiorite Tonalite	55
Diorite	5
Basic-Ultrabasic	5

No systematic zonation of the rock types could be defined in the study area. All the rock types are found in an almost random juxtaposition throughout. It is quite possible that the study area may be small compared to the original extent of the batholith, and large scale zonation may not be recognisable. One possibly significant feature in the zonation of individual rock types, is the greater abundance of gabbro-peridotite bodies in that part of the batholith exposed south of the Orange River. Since the bodies are only relicts, it is perhaps dangerous to attach any real importance to their assymetric distribution.

9.2. Intrusive form and mode of emplacement

9.2.1. Basic-ultrabasic complexes

Gabbro, peridotite and pyroxenite, together with their metamorphosed counterparts, occur as relict masses which have present shapes determined by (1) the outline of later intrusives and (2) subsequent shearing and faulting. Dimensions range from a few metres up to 3-4 km across. Despite the wide variety of shapes and sizes, all the bodies may be regarded as "xenoliths" within the later more felsic intrusions. It is quite probable that even the largest bodies do not persist to great depths, although detailed geophysical surveys are needed to establish this. Few contacts

between the HVG and basic-ultrabasic complexes were found, and are invariably strongly sheared. Middlemost (1965) and De Villiers and Söhnge (1959) report similar basic-ultrabasic bodies intrusive into metavolcanics (?HVG) in the neighbouring region of the south-eastern Richtersveld.

The largest mass in the present study area underlies the small group of hills of Swartkop, which can be easily recognised from the National Road about 30 km south of Vioolsdrif. The most common rock types are gabbro, gabbro-pegmatite with variable texture, peridotite and troctolite. The roughly circular body is surrounded on all sides by plutons of tonalite-granodiorite and adamellite. Numerous pegmatites, aplites and quartz veins transect the body.

Too little of the Swartkop complex remains to accurately describe its original form and internal structure. Isolated masses of metamorphosed gabbro and pyroxenite in the surrounding granitic rocks of the VIS may be part of the same large body. Other clusters may represent remnants of other bodies, e.g. the small masses of metagabbro, metapyroxenite and metaperidotites well exposed in the mountains between the Noujaseep and Uranoop Rivers.

No small scale layering has been recognised in the Swartkop complex, which could give a clue to the origin of the ultramafic rocks. Certainly the textures (described more fully in Chapter 10) of the peridotites are very similar to those in cumulate ultramafic rocks described by Wager, Brown and Wadsworth (1960).

9.2.2. Diorite

The largest single pluton of diorite crops out in the lower Nous River, and forms a highly irregular mass covering an area of about 6 sq km. To the north, east and west, the diorite is intruded by later plutons of the VIS and to the south it is in fault contact with the HVG. Irregular dikes and veins of tonalite, granodiorite and leucogranite transect the pluton. Diorite seems to be a relatively rare rock type in the batholith,

and occurs mainly as basic portions of tonalite plutons rather than as individual intrusions.

9.2.3. Tonalite and granodiorite

Tonalite and granodiorite are difficult to separate in the field, and can only be distinguished after thin section work. These two rock types together comprise more than half of the exposed batholith in the study area, and exhibit similar intrusive form. However, the plexus of intrusions in which these rock types occur obscures the original form of any individual pluton except where it cuts the HVG. Because of the sustained intrusive activity, the early plutons of tonalite and granodiorite now appear as discontinuous screens of variable width and extent, separated by later plutons of adamellite and leucogranite. Tonalite and granodiorite plutons that cut the HVG generally have irregular shape, but often have long axes that are concordant with the regional strike of the lava flows and volcaniclastic beds. Many contacts have been modified by shearing, although the trace of many such sheared contacts are also roughly parallel to the regional trend of the HVG. Later faults that strike roughly N-S, have also modified the shapes of many plutons.

The most conspicuous feature of the contacts is the abundance of xenoliths. Contacts between tonalite or granodiorite and the HVG are complex zones, sometimes up to 1-2 km wide and crammed full with xenoliths of country rock. Even at great distances from contacts, the plutons of tonalite and granodiorite are seldom free of xenoliths and may be contrasted with the later adamellites and leucogranites, which rarely contain inclusions. The prevalence of xenolith-choked contact zones suggests that emplacement of the early tonalite and granodiorite plutons was achieved in part by stoping.

Detailed investigations of some contacts indicate that emplacement was also achieved by block faulting, since numerous small faults pass out into the country rock at an angle to the contact. Many of the plutons seem

to have expanded by pushing aside the country rock, with the strain being resolved along closely spaced faults rather than up-arching. The brecciated nature of contacts probably reflects an advanced stage in the fracture of country rock during intrusion of the plutons.

9.2.4. Adamellite

Adamellite plutons may also be highly irregular, and often send protrusions into the country rock in the form of dikes and sheets. The shapes of most plutons are better preserved than the earlier tonalites and granodiorites since they appeared later in the emplacement history of the batholith and have not been obscur by subsequent intrusive activity. Intrusive form is best seen in those plutons in contact with the HVG rather than those in the composite intrusions, mainly because they are more easily traced on the air photographs.

The eastern part of a large adamellite pluton crops out in the lower Koubank Gorge and in the Orange River near Vioolsdrif. The western extension is covered by Nama and Karroo strata, but is sufficiently well exposed to suggest that the pluton is an elongate body at least 3 km across and which strikes parallel to the regional trend of the HVG. Along the northern contact of this particular pluton the adamellite extends into the country rock in the form of sills, the thickest being about 200 m thick. The roof zones of many adamellite plutons cropping out in the Orange River canyon are well exposed because of the great relief. Well bedded acid tuffs and pyroclastic flows cut by sills of medium grained adamellite crop out in the Noujaseep River. Another adamellite pluton sends up dikes that change abruptly into sills that follow planes within the volcanic sequence. It is clear that the emplacement of the adamellite magma was partly achieved by the filling of voids created by brittle fracture of the country rock. This tendency to form sills within the layered volcanic sequence, together with the numerous dikes, suggests a mode of emplacement similar to that envisaged by Du Toit (1920) and Bradley (1965) for the Karroo dolerites. The sills probably

represent the lifting of a roof built of denser mafic to intermediate lavas and pyroclastics by a light or adamellitic magma.

Roughly circular stocks of adamellite also occur, the best example of which underlies the mountain between the Warmklip and Krom Rivers. The stock has a diameter of about 2 km and is surrounded by lavas and pyroclastic beds that dip steeply away from the contacts. Immediately to the north of this small stock is a much larger adamellite pluton, which has a well exposed eastern contact with volcanics that also dip steeply away. Unfortunately, both the north and south contacts have been modified by later shearing and the western contact occurs in very inaccessible country and has not been located. This pluton covers an area of at least 30 sq km.

Contacts between adamellite and the HVG are often brecciated, and in this respect are similar to the earlier tonalites and granodiorites. However, the enclosed xenoliths are usually confined to the contact zones and are seldom encountered deep within any plutons. Moreover, the xenoliths tend to be highly angular, and do not exhibit the rounded shapes and advanced states of assimilation so characteristic of inclusions in the earlier tonalites and granodiorites.

Large plutons of adamellite have probably been emplaced by diapiric uprise, since the intruded volcanic sequence now dips away from the contacts. This mode of emplacement contrasts with that envisaged for the earlier tonalites and granodiorites, which have been emplaced by block faulting and stoping. Superimposed on diapiric uprise, the adamellitic magma has intruded further by extensive brittle fracture, especially in the roof zones of the uprising plutons. The fractures are largely sheet-like with the resulting intrusions occurring as dikes or irregular sills. Circuate fractures seem to be rare, and cone sheets or ring dikes of adamellite have not been recognised.

9.2.5. Leucogranite

Bodies of pink leucogranite represent the youngest intrusives within

the Vioolsdrif Batholith. Their contacts have been seen to cut the HVG and all the earlier more mafic rock types of the batholith. The greatest development of leucogranite occurs in the area between Nous Wells and the lower Uranoop River. A large number of bodies, ranging in size from thin dikes less than a metre across, up to elongate plutons 4 km by 1 km, are distributed in a very crudely defined flattened ring structure. The long axis of the structure is roughly parallel to the regional trend of the HVG and the composite intrusive bodies of the rest of the VIS. Apart from the Nous-Uranoop structure, no other arcuate distribution of leucogranite bodies have been recognised, probably because of the lack of large well defined plutons. Leucogranite plutons approaching the size of those in the Nous-Uranoop structure occur only in the Lower Haib River area, but do not define any arcuate distribution. The lower Haib plutons, however, are elongate masses which exhibit a slight curvature. Detailed mapping may result in the discovery of smaller bodies between the bigger plutons that would help to define a ring structure.

The best known example of ring structures and central complexes forming the final intrusive phase during the emplacement of a major batholith is the coastal batholith of Peru (Bussel et al., 1976; Cobbing and Pitcher, 1972). The final rock type in this batholith was adamellite and is confined to discrete centres of intrusive activity. In the Vioolsdrif Batholith the analagous rock type is the pink leucogranite. Adamellites in the Vioolsdrif Batholith have not been emplaced in the same way as their Peruvian counterparts, although the difference is only one of intrusive form (i.e. sheet-like instead of arcuate fractures).

Leucogranite sheets have often followed contacts between earlier intrusions and country rock, e.g. between adamellite and metagabbro, adamellite and HVG, tonalite and metapyroxenite, adamellite and tonalite-granodiorite. Brecciation of the contacts and incorporation of xenoliths is very rare and has only been observed in one locality. Patches of coarse-grained pegmatite within the larger leucogranite plutons are not uncommon and

are composed of essentially the same minerals as the main mass. Dikes of pegmatite passing from the leucogranite pluton into surrounding country rock also occur. These pegmatite bodies may be distinguished from later pegmatites of the 1000 Ma old Namaqualand swarm by the colour of their constituent alkali-feldspar; the Vioolsdrif pegmatites have flesh pink to brick red alkali feldspar, whereas the Namaqualand pegmatites usually contain white to buff-coloured alkali feldspar.

10

THE VIS. BASIC-ULTRABASIC COMPLEXES[1]

The widely scattered remnants of early Vioolsdrif basic-ultrabasic complexes consist chiefly of gabbroic rocks, together with peridotite, pyroxenite and their metamorphosed counterparts. Only the Swartkop complex has been studied in detail and has been found to consist of the four main rock types: (1) gabbro, (2) gabbro-pegmatite, (3) peridotite and (4) troctolite (see Fig. 45).

10.1 Gabbro and gabbro-pegmatite

Gabbroic rocks within the Swartkop complex are extensively reconstituted but often retain the original sub-ophitic to hypidiomorphic-granular textures. Grain size varies considerably from medium grained (0.5-1 mm) to very coarse-grained pegmatitic patches with amphibole prisms up to 5 cm long. Such a range in grain size may be seen in outcrops covering an area of only a few metres. Coarse-grained gabbro-pegmatite (characterised by elongate amphibole prisms) occurs as patches and veins within even-grained gabbro and peridotite.

Much of the original clinopyroxene has been replaced by actinolite, chlorite and epidote. Plagioclase shows partial replacement by a fine grained turbid aggregate of epidote and sericite. Clear areas of the feldspar exhibit fine lamellar twinning parallel to the prismatic axis. The amphibole pseudomorphs after clinopyroxene are often composed of stubby prisms in decussate arrangement. Opaque Fe-Ti oxides occur as irregular grains, sometimes moulded around plagioclase and pseudomorphed clinopyroxene. These grains are now composite, with thin lamellae of ilmenite contained in a host of magnetite. The original mineral was probably a titanomagnetite.

10.2 Peridotite

Peridotite is very widespread within the Swartkop complex and forms

---

1 The early basic-ultrabasic complexes within the Vioolsdrif batholith do not appear to be related to the later, more voluminous granitic suite (diorite - leucogranite). As a result, the basic-ultrabasic complexes have been described separately. However, conclusions drawn as to the nature and origin of these rocks are only preliminary. This was unavoidable, since, in the time available, it was impossible to do justice to all the major rock types in a plutonic complex as vast and variable as the VIS.

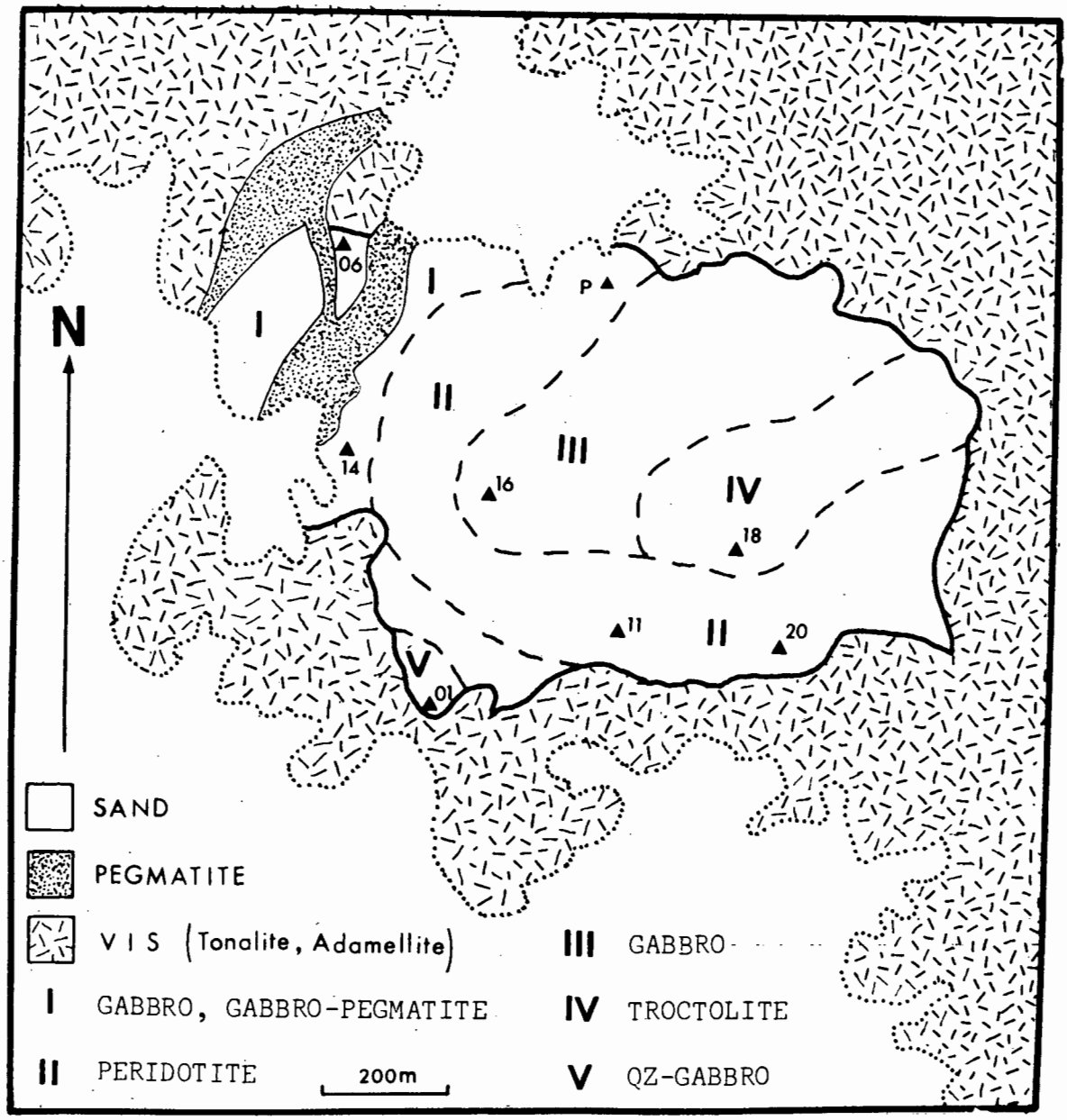

Fig. 45. Geological map of the Swartkop basic-ultrabasic complex.

a prominent, roughly semi-circular zone (Fig. 45). The contacts between it and gabbro are everywhere obscured by scree, so its relationship with other rocks in the complex is not clear. In the field, the peridotite is characterised by rusty red, deeply pitted weathered surfaces, which contrasts with the dark brown to black, smooth surfaces developed on gabbro. Fresh surfaces are black, but large oikocrysts of pyroxene enclosing olivine are conspicuous because their cleavage faces reflect the sunlight. Many samples of peridotite also contain variable amounts of white interstitial feldspar. Essential minerals are olivine and chromite with subordinate orthopyroxene, clinopyroxene, brown hornblende and plagioclase.

By far the most abundant mineral is olivine, which occurs as euhedral to slightly rounded grains which range in size from 1.5 mm to 0.2 mm. They are invariably serpentinised, with only irregular cores of the original olivine remaining. The pseudomorphs are choked with trains of powdery, secondary magnetite. Chromite forms equant, subhedral, opaque grains ranging in size from 0.1 up to 0.5 mm. Both olivine and chromite are poikilitically enclosed in orthopyroxene and occasionally plagioclase and clinopyroxene. Rare interstitial voids are filled with brown pleochroic hornblende (X = very pale straw brown, Y = pale brown, Z = deep reddish brown). Orthopyroxene is very faintly pleochroic with X = pale mauve, Y = Z = very pale greyish green. Clinopyroxene is colourless, but is commonly choked with slender inclusions aligned parallel to the c-axis. These inclusions may be incipient exsolution of a Ca-poor pyroxene on a sub-micron scale. The mineral appears homogeneous even to a 1-2μ EMP beam. Interstitial feldspar is invariably altered to a grey, turbid, fine-grained aggregate and no fresh material was observed. Qualitative analysis with the EMP showed that the turbid material was rich in Ca, Al and Si, suggesting that it may be after a very calcic plagioclase.

The overall igneous texture of the Swartkop peridotites is very similar to that of ultramafic rocks described by Wager *et al.*, (1960) as igneous cumulates. Using their nomenclature, olivine and chromite represent the cumulus minerals, while poikilitically enclosing orthopyroxene, clinopyroxene, plagioclase and hornblende constitute the intercumulus minerals.

	Peridotite					Troctolite				Pyroxenite	
	OL	CHR	OPX	CPX	AMPH	OL	PLAG	CPX	AMPH	CPX	AMPH
SiO_2	39.68	.05	55.03	50.00	41.95	38.47	48.31	50.82	41.66	52.54	43.64
TiO_2	.00	.62	.21	.57	3.96	.00	.00	.55	1.85	.17	.66
Al_2O_3	.00	23.67	3.01	4.60	13.41	.00	33.20	4.23	14.79	1.77	11.82
Cr_2O_3	.00	28.94	.00	1.05	.00	.00	.00	n.d	.00	.30	.00
Fe_2O_3	.00	15.36	.00	.00	.00	.00	.00	.00	.00	.00	.00
FeO	14.06	20.81	9.43	4.77	6.86	21.32	.10	6.75	9.74	4.85	11.44
MnO	0.23	0.65	0.23	0.14	0.10	.33	.00	.20	.10	.21	.17
MgO	45.76	9.67	31.01	17.11	16.51	40.16	.02	15.21	14.06	15.79	14.72
CaO	.00	.00	1.21	21.94	12.16	.00	16.13	21.85	12.11	24.45	12.91
Na_2O	.00	.00	.03	.61	2.64	.00	2.36	.35	1.72	.24	1.66
K_2O	.00	.00	.00	.00	1.13	.00	.00	.00	1.07	.00	.78
Total	99.73	99.77	100.16	100.79	98.72	100.28	100.12	99.96	97.10	100.32	97.80
No. of oxygens	4	32	6	6	23	4	32	6	23	6	23
Si	.995	.012	1.927	1.830	6.019	.993	8.833	1.880	6.112	1.934	6.402
Al	.000	7.036	.124	.198	2.267	.000	7.157	.185	2.559	.077	2.045
Ti	.000	.118	.005	.016	.428	.000	.000	.015	.205	.005	.073
Fe	.295	*	.276	.146	.823	.460	.015	.209	1.195	.149	1.403
Mn	.005	.139	.007	.004	.012	.007	.000	.006	.012	.007	.021
Mg	1.710	3.633	1.619	.933	3.531	1.546	.006	.839	3.074	.866	3.219
Cr	.000	5.768	.000	.030	.000	.000	.000	n.d	.000	.009	.000
Ca	.000	.000	.045	.860	1.869	.000	3.160	.866	1.903	.964	2.029
Na	.000	.000	.002	.043	.735	.000	.837	.025	.488	.017	.473
K	.000	.000	.000	.000	.207	.000	.000	.000	.201	.000	.146
	Fo_{85}	* Fe^{3+} =2.915 Fe^{2+} =4.388	Wo 2.4 En83.4 Fs14.2	Wo44.4 En48.1 Fs 7.5	Mg/Mg+ Fe=.811	Fo_{77}	An_{80}	Wo45.3 En43.8 Fs10.9	Mg/Mg+ Fe=.720	Wo48.8 En43.8 Fs 7.5	Mg/Mg+ Fe=.696

Table 15. Average compositions of constituent minerals in basic and ultrabasic rocks within the Swartkop complex. The pyroxenite sample was collected from another body (DRV-77)

More specifically, the euhedral habit of the cumulus minerals, together with the contrasting nature of the intercumulus minerals, suggest that the Swartkop peridotites are good examples of orthocumulates.

The Fo content of the olivine (Fo_{85}) is similar to the most magnesian olivines in stratiform peridotites (Fo_{88-80})(Wager and Brown, 1967). Olivine in alpine-type peridotites are usually more magnesian (Fo_{95-90}), but the distinction is not very strong (Green, 1964; Wyllie, 1967; Moores, 1973). More magnesian olivines may occur in the Swartkop body, but further work is needed to establish this.

The composition of the chromite may be more diagnostic and numerous authors (e.g. Irvine, 1965, 1967; Thayer, 1970; Dickey, 1975) have demonstrated a compositional distinction between chromite and stratiform and alpine-type peridotites. According to Thayer (1970), chromites with relatively low Cr_2O_3 (less than 40 wt %)from stratiform peridotites have higher total Fe contents and lower $Al/(Al+Cr+Fe^{3+})$ than alpine-type chromite with the same Cr_2O_3. The fields defined by Thayer (1970) are reproduced in Fig. 46 and from this it is clear that the Swartkop chromite is low in Cr_2O_3 and has affinities with stratiform types.

Irvine (1967) has suggested that the partitioning of Mg and Fe^{2+} between olivine and chromite may be influenced by temperature. The distribution coefficient

$$K_d = (X_{Mg}/X_{Fe})_{ol} \div (X_{Fe}/X_{Mg})_{chr}$$

is lower at higher temperatures. No quantitative model was presented by Irvine, but it was suggested that values for $\ln(K_d)$ of about 2 indicated high temperatures (early magmatic?) and that values of 3 indicated lower temperatures (late magmatic or subsolidus). The calculated value for $\ln(K_d)$ for the Swartkop olivine-chromite pair is 1.6, which suggests that final equilibration was achieved at relatively high temperatures.

Since orthopyroxene, clinopyroxene and hornblende occur in the interstitial areas, it is probable that they did not coprecipitate with olivine

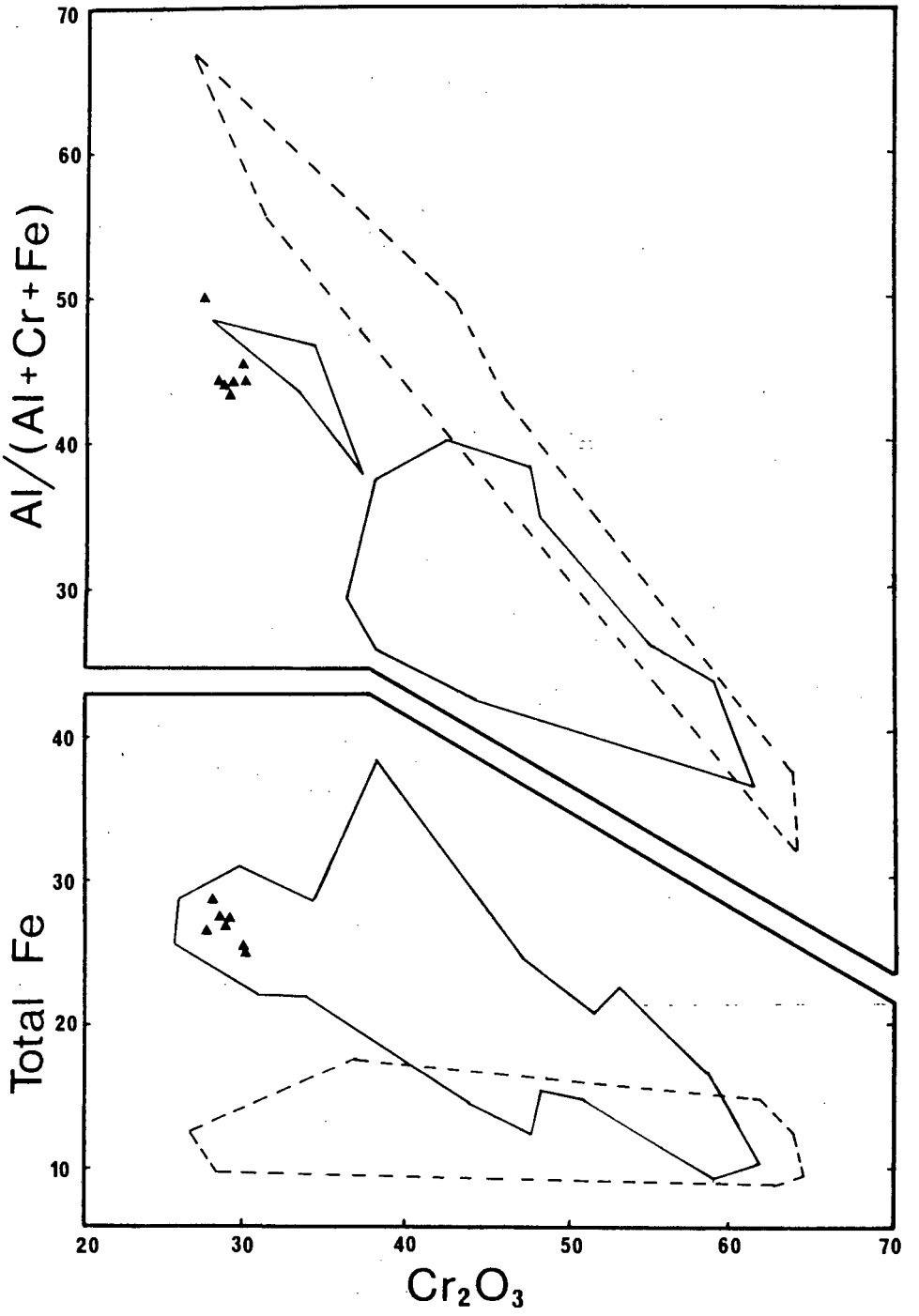

Fig. 46. Plot of total Fe and Al/(Al+Cr+Fe) against Cr_2O_3 for chromites. Fields for chromite from alpine type peridotites (broken lines) and stratiform type peridotites (solid lines) are from Thayer (1970).

and chromite. It is therefore not justifiable to apply any model Mg-Fe partitioning scheme (e.g. Duke, 1976; Medaris, 1969; Mueller, 1963; Powell and Powell, 1974), which assumes that orthopyroxene or clinopyroxene equilibrated with olivine and a mafic liquid. A trial calculation was carried out to see if subsolidus equilibration had occurred; according to Medaris (1969), the composition of an orthopyroxene coexisting with olivine can be calculated from the equation

$$\log (X_{Fe}/X_{Mg})_{ol} = 0.163 + 1.1128 \cdot \log (X_{Fe}/X_{Mg})_{opx}$$

If the olivine composition listed in Table 15 is adopted, then $(X_{Fe}/X_{Mg})_{ol} = 0.173$, which results in $(X_{Fe}/X_{Mg})_{opx} = 0.147$. The observed value for the orthopyroxene is 0.170, which is too Fe rich to be in equilibrium with the observed olivine if the relationship of Medaris is valid. Mg-Fe distribution appears to be independent of temperature and total pressure in the temperature range 700 - 1300°C. The results of this trial calculation suggest that there has been no subsolidus equilibration between intercumulus orthopyroxene and cumulus olivine.

Textural evidence suggests that ortho- and clinopyroxene coprecipitated from the intercumulus liquid and that model Mg-Fe distribution equations may be applied to this pair. The presence of hornblende however, raises difficulties with a rigorous application, since it will presumably affect the Mg-Fe distribution also. Hornblende seems to have appeared slightly later than the pyroxenes, since it fills small interstitial voids between them. In fact, the amphibole looks as if it represents the crystallisation of the final drop of intercumulus liquid and suggests that intercumulus pyroxenes may have crystallised in the absence of amphibole, except towards the final stages. Furthermore, the amount of amphibole is extremely small, making up less than 1 percent of the mode of most peridotites.

If the presence of the small quantity of hornblende is neglected as a first approximation, the Wood and Banno (1973) Mg-Fe distribution model yields an equilibration temperature of 1010°C for the coexisting pyroxenes. This temperature is not an unreasonable one and is compatible with the results

obtained when applying the diopside-enstatite solid solution model (Boyd and Shairer, 1964). The amount of En_{ss} in the clinopyroxene is only 3.8 mole percent, while the amount of Di_{ss} in the orthopyroxene is 5.9 percent. Such limited immiscibility between the pyroxenes only occurs at temperatures below about 1100°C. Considering the error of ± 60°C cited by Wood and Banno (1973) for their temperature estimates, the agreement between the two models is considered reasonable.

Intercumulus amphibole is a pargasitic hornblende relatively rich in TiO_2 (about 4 percent, see Table 15). Such a high Ti content probably contributes to the deep reddish brown colour, although an unknown amount of Fe^{3+} in the amphibole also affects the colour. Experimental work on the crystallisation of amphibole from hydrous basic melts (Helz, 1973; Hollaway and Burnham, 1972; Cawthorn and O'Hara, 1976) has demonstrated that brown pargasitic hornblende rich in TiO_2 is stable at high temperature (about 1000°C). Lower temperature hornblende was found to be poorer in TiO_2 and was green rather than brown.

The final appearance of pargasitic hornblende could represent either of two conditions : (1) the magma from which the peridotite was formed was hydrous, but only attained the minimum Na_2O content necessary to stabilise pargasitic amphibole (about 3 percent according to Cawthorn and O'Hara, 1976) after extensive crystallisation of pyroxene from the intercumulus liquid, or (2) the concentration of both H_2O and Na_2O required to stabilise amphibole was reached only in the confined pore spaces within the almost completely consolidated peridotite.

The two conditions depend essentially on the permeability of the early crystal aggregate. The lack of adcumulus modification in the form of overgrowths around olivine and chromite, suggests that the crystal aggregate was not easily permeated by fresh magma. The appearance of amphibole at a late stage is considered to be a consequence of crystallisation of the trapped intercumulus liquid. It is also considered that Na_2O increased by fractional crystallisation of Na-poor minerals (pyroxenes) and the low permeability

resulted in the increase in P_{H_2O} until amphibole was stable.

10.3 Troctolite

An interesting rock type found only in the Swartkop complex is troctolite. Similar rocks have not been identified in the few other basic-ultrabasic masses visited during the field work. The essential minerals are olivine and plagioclase, which form subhedral grains and prismatic crystals respectively. Clinopyroxene and brown hornblende build poikilitic plates enclosing olivine and plagioclase. Rarely, interstitial voids are filled with an opaque Fe-Ti oxide. Plagioclase forms euhedral prisms, whereas olivine appears to have been modified either by resorption or overgrowth. Again the texture is similar to cumulates described by Wager *et al.*, (1960). In this case the Swartkop troctolites resemble the so-called allivalites of Rhum (Brown, 1956). Olivine and plagioclase represent the cumulus minerals, while clinopyroxene, hornblende and Fe-Ti oxide constitute the intercumulus material.

Serpentinisation of the olivine has resulted in well developed expansion cracks in the surrounding plagioclase. Associated with the alteration to serpentine, is finely divided secondary magnetite. Closely spaced needle-like inclusions (or exsolution lamellae) cloud the intercumulus clinopyroxene and in this manner resemble the peridotite clinopyroxene. The troctolite hornblende has similar optic properties to that in the peridotite.

Olivine is fairly uniform in composition but is more Fe rich (Fo_{77}) than that in the peridotite. Crystal faces are not well developed and appear to have modified slightly by adcumulus growth rather than resorption, because some olivines are slightly moulded around prisms of plagioclase. Plagioclase is also quite uniform in composition (An_{80}), but shows slight normal zoning (An_{83-75}) near the edges of crystals.

The Mg-Fe distribution model of Duke (1976) has been used to test whether intercumulus clinopyroxene had equilibrated with cumulus olivine. The relevant equation for the distribution is :-

$$\log (X_{Fe}/X_{Mg})_{ol} = 0.198 + 1.30 \cdot \log (X_{Fe}/X_{Mg})_{cpx}$$

If the olivine composition in Table 15 is adopted, then $(X_{Fe}/X_{Mg})_{ol} = 0.298$, which results in $(X_{Fe}/X_{Mg})_{opx} = 0.278$. The observed value for $(X_{Fe}/X_{Mg})_{cpx}$ is 0.157, which is too magnesian to be in equilibrium with the observed olivine, provided the distribution model of Duke is valid. At present, the results of such a calculation should be treated with caution, because of the uncertainty in the Mg-Fe distribution model for coexisting olivine and clinopyroxene. Powell and Powell (1974) have maintained that $K_d^{ol/cpx}$ varies regularly with temperature, so that the mineral pair may be used as a geothermometer. This is in direct contradiction to the previously mentioned results of Duke (1976). Wood (1976) has severely criticised the Powell and Powell technique on thermodynamic grounds.

The clinopyroxene is slightly more Fe-rich than that in the peridotite, which is in accord with the slightly more Fe-rich olivine in the troctolite. Intercumulus amphibole is similar in appearance to that in the peridotite, but is lower in TiO_2 and Na_2O. The troctolite amphibole is also less magnesian and together with the lower Al(4) content (see Table 15) suggest lower temperatures of crystallisation relative to that in the peridotite.

The composition of the constituent mafic minerals in the troctolite suggests that the magma was more evolved than that which gave rise to the peridotite. The relationship between the troctolite and peridotite is difficult to determine from field evidence, but it is likely that they are comagmatic and were formed by crystal settling. The troctolite was possibly formed at a slightly later stage than the peridotite, during fractional crystallisation of a basic magma.

10.4 Pyroxenite

Although pyroxenite does not occur in the Swartkop complex, this rock type is extremely common within adjacent ultramafic bodies and indeed comprises a significant proportion of the bodies throughout the batholith. With increasing plagioclase, the pyroxenites merge with gabbros. Many discrete

bodies contain pyroxenite grading into gabbro.

Much of the original mineralogy has been replaced by metamorphic amphibole, chlorite, biotite and epidote. Similar rocks have been described as hornblendites by Middlemost (1965) in the neighbouring Richtersveld. Earlier work (e.g. Gevers *et al.*, 1937; De Villiers and Söhnge, 1959; Von Backström and De Villiers, 1972) suggested a variety of names including hornblendites, perknites, amphibolites and hyperites. In view of the extensive metamorphic reconstitution, it may be better to refer to these rocks as mafic metagabbros and metapyroxenites.

Apart from plagioclase, the essential igneous mineralogy includes clinopyroxene and hornblende. Relict patches of both mafic minerals are not uncommon, although the hornblende is invariably choked with opaque inclusions. Where the igneous texture is well preserved, the relationship between clinopyroxene and hornblende is analogous to that of olivine and clinopyroxene in the peridotites and troctolites (i.e. cumulus and intercumulus). The hornblende surrounds discrete subhedral crystals of clinopyroxene (now almost completely pseudomorphed) and builds large poikilitic plates.

The dominant secondary mineral is pale green actinolite after clinopyroxene. This metamorphic amphibole is easily distinguished from the deeper coloured igneous amphibole. Many pyroxenites have been formed by the accumulation of clinopyroxene to the extent that intercumulus material is virtually excluded. The original outline of the clinopyroxene crystals are often defined by narrow wedge-shaped patches of deep green, inclusion choked, primary igneous amphibole. In many cases the cumulus clinopyroxene has been replaced by a decussate aggregate of actinolite, but the outline of the original crystals is still preserved in the contrasting colours of the primary and secondary amphiboles.

Clinopyroxene is the only cumulus phase in most pyroxenites, but is joined by calcic plagioclase in rocks transitional to gabbros. Unfortunately, metamorphic reconstitution is well advanced in all pyroxenites examined and only cumulus clinopyroxene and intercumulus amphibole could be analysed.

Compared to intercumulus clinopyroxene in the peridotite and troctolite, cumulus clinopyroxene in the pyroxenite is lower in Al, Ti and Cr, but higher in Ca. There is very little difference in Mg/(Mg+Fe) between the peridotite and pyroxenite clinopyroxenes. The major difference can be expressed as a lower proportion of minor elements (Al, Ti, Cr) replacing Mg and Fe in the M1 site (Wood and Banno, 1973). This may be a function of temperature and suggests that the pyroxenite may have formed at a slightly lower temperature than the peridotite, because of the lower minor element content in the pyroxenite clinopyroxene.

Intercumulus amphibole is green and contrasts sharply with that in the peridotite and troctolite. The different colour is probably caused by the lower Ti content and perhaps by smaller amounts of Fe^{3+} (perhaps caused by lower total Fe rather than by lower Fe^{3+}/Fe^{2+} ratios). The green amphibole contains less Al_2O_3 (and as a result less Al(4) replacing Si), lower (Na+K) and lower Mg/(Mg+Fe). According to the experimental work of Helz (1973), green amphibole is a lower temperature analogue of brown titaniferous pargasitic hornblende. The implied lower temperature is consistent with qualitative estimates made previously when comparing clinopyroxene compositions.

10.5 Metamorphism

Olivine in the troctolite and peridotite has been replaced by pale yellowish green serpentine and secondary magnetite. An EMP analysis of serpentine is listed in Table 16. Expansion cracks in minerals enclosing serpentinised olivine (plagioclase and orthopyroxene) often contain serpentine. Occasionally the serpentine has been introduced along the cleavage planes of secondary actinolite after clinopyroxene. This feature suggests that the serpentine has been squeezed into the surrounding material during an increase in volume accompanying alteration. The composition of the secondary magnetite has been qualitatively investigated with the EMP; it contains no detectable Ti, Al, Mn, Cr or Mg and is probably pure Fe_3O_4.

Serpentine and chlorite replace orthopyroxene, with the latter being the most abundant. Chlorite is particularly abundant in altered pyroxenites

Specimen	PERIDOTITE						PYROXENITE			
Grain	SERPENTINE		CHLORITE		CR-MAGNETITE		ACTINOLITE			
SiO_2	40.72		30.87	SiO_2	.20	.02	SiO_2	54.85	56.19	55.04	56.47
TiO_2	.00		.07	TiO_2	1.00	.86	TiO_2	.12	.03	.07	.03
Al_2O_3	.06		17.25	Al_2O_3	.17	.17	Al_2O_3	3.08	1.18	2.25	.74
FeO*	4.17		5.00	Cr_2O_3	7.77	7.21	FeO*	6.31	5.77	6.70	5.82
MnO	.00		.03	Fe_2O_3	58.82	61.11	MnO	.16	.16	.14	.14
MgO	39.56		33.10	FeO	31.01	30.68	MgO	19.90	21.09	20.05	21.13
CaO	.03		.00	MnO	.22	.27	CaO	13.36	13.50	13.33	13.63
Na_2O	.00		.05	MgO	.73	.93	Na_2O	.40	.17	.30	.08
K_2O	.00		.11				K_2O	.10	.02	.06	.01
Total	84.54		86.48		99.91	101.25		98.77	98.11	98.18	98.07
No. of oxygens	7		28		32	32		23	23	23	23
Si	1.979	Si	5.920	Si	.061	.006	Si	7.638	7.806	7.701	7.849
Al	.003	Al (4)	2.080	Ti	.229	.194	Al (4)	.362	.194	.299	.122
SZ	1.982	SZ	8.000	Al	.061	.060	SZ	8.000	8.000	8.000	8.000
Fe	.170	Al (6)	1.821	Cr	1.872	1.714	Al (6)	.143	.000	.073	.000
Mg	2.865	Ti	.010	Fe^{3+}	13.486	13.825	Ti	.013	.003	.008	.003
Ca	.002	Fe	.802	SZ	15.709	15.799	Fe	.735	.670	.784	.677
SX	3.037	Mn	.005	Fe^{2+}	7.902	7.715	Mn	.019	.019	.017	.017
		Mg	9.460	Mn	.057	.069	Mg	4.130	4.367	4.181	4.377
		Na	.018	Mg	.332	.417	SY	5.040	5.059	5.063	5.074
		K	.027	SX	8.291	8.201	Ca	1.993	2.009	1.998	2.030
		SX	12.143				Na	.109	.045	.081	.022
							K	.018	.003	.010	.002
							SX	2.120	2.057	2.089	2.054

Table 16. Composition of metamorphic minerals within various ultramafic rocks in the Vioolsdrif batholith.

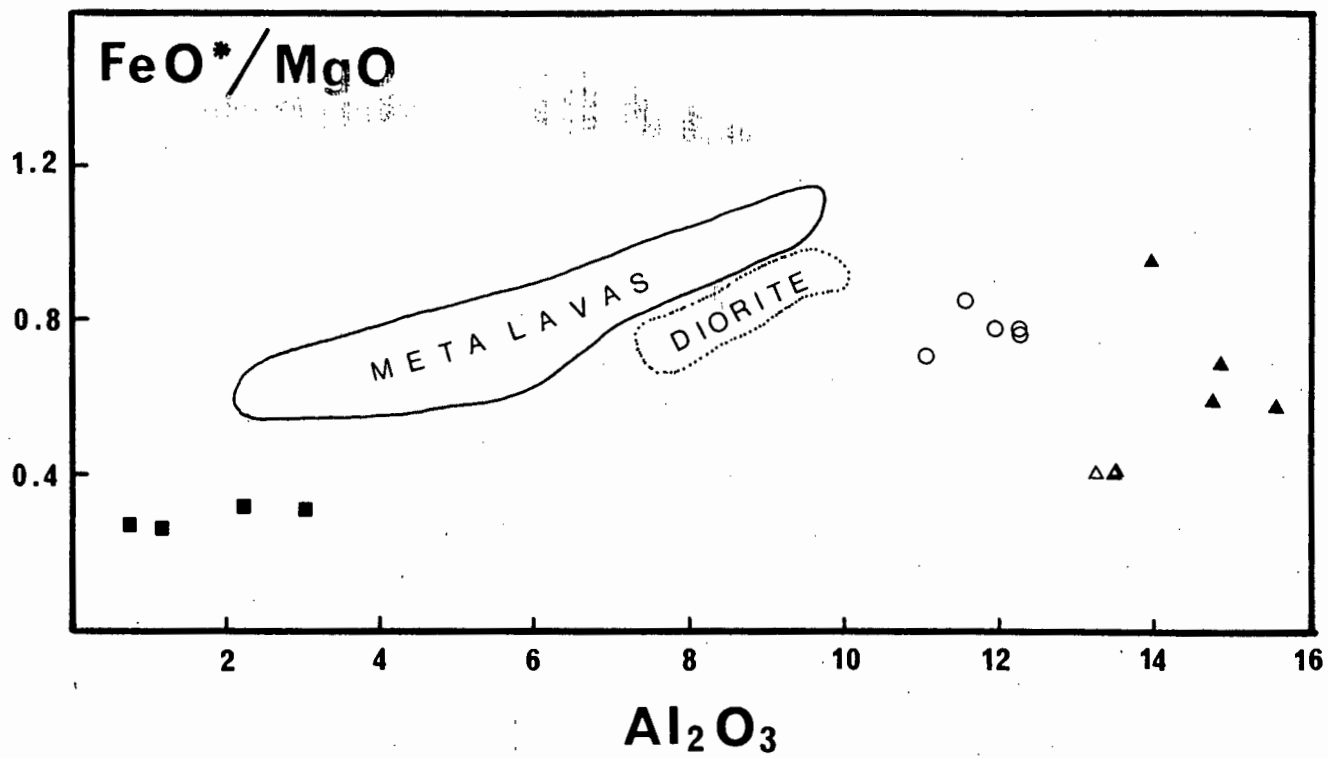

Fig. 47. Plot of FeO^*/MgO against Al_2O_3 for amphiboles. ■ = metamorphic actinolite after clinopyroxene in a metapyroxenite; ○ = primary igneous hornblende in a metapyroxenite; △, ▲ = primary igneous hornblende in a peridotite and troctolite respectively. Compositional fields occupied by metamorphic amphibole in basaltic andesite metalavas and by primary igneous hornblende in a diorite are also shown.

containing plagioclase and it is probably the feldspar that provides the Al necessary to produce this mineral after orthopyroxene. An analysis of chlorite after orthopyroxene in a peridotite is listed in Table 16.

Clinopyroxene is replaced by pale green to almost colourless actinolite which is characteristically low in Ti, Al and (Na+K). EMP analyses of this secondary actinolite are listed in Table 16. Compared to the metamorphic amphibole in the volcanic country rock, this actinolite has much lower FeO^*/MgO (Fig. 47). When plotted on Miyashiro's (1973)classification diagram, the actinolite in the early Vioolsdrif basic-ultrabasic rocks overlaps with the Si-rich amphiboles in the metavolcanics (Fig.48) There is also a distinct compositional difference between the actinolite and primary igneous amphibole (green hornblende) which both occur in the metapyroxenites.

Alteration of chromite is variable and depends on whether the surrounding mineral has been altered. For example, chromite poikilitically enclosed in fresh orthopyroxene is unaltered and the subhedral, equant grains are homogeneous. Chromite surrounded by serpentinised olivine or amphibolitised clinopyroxene is largely replaced by Cr-bearing magnetite. EMP scans over altered chromite grains show that Cr is extremely variable. In addition, other major components (Mg, Fe, Al) also vary considerably. Magnetite pseudomorphs after chromite often contain relict cores of Cr-bearing magnetite, analyses of which are listed in Table 16. Where the altered chromite is surrounded by altered plagioclase, a narrow rim of colourless chlorite(?) is developed. The secondary alteration of chromite obviously involves a complex series of reactions and further work is necessary to establish the pattern.

Although low-grade metamorphic reconstitution of the basic-ultrabasic rocks is well advanced, no re-equilibration of the relict mafic silicates (at least in terms of Mg-Fe distribution), at the lower temperatures involved, seems to have occurred. Hermes (1970) has described metagabbros which contain relict mafic silicates that have re-equilibrated at the lower temperature prevailing during metamorphism. Such low temperature re-equilibration is probably a precursor to metamorphic recrystallisation, but may depend on a variety

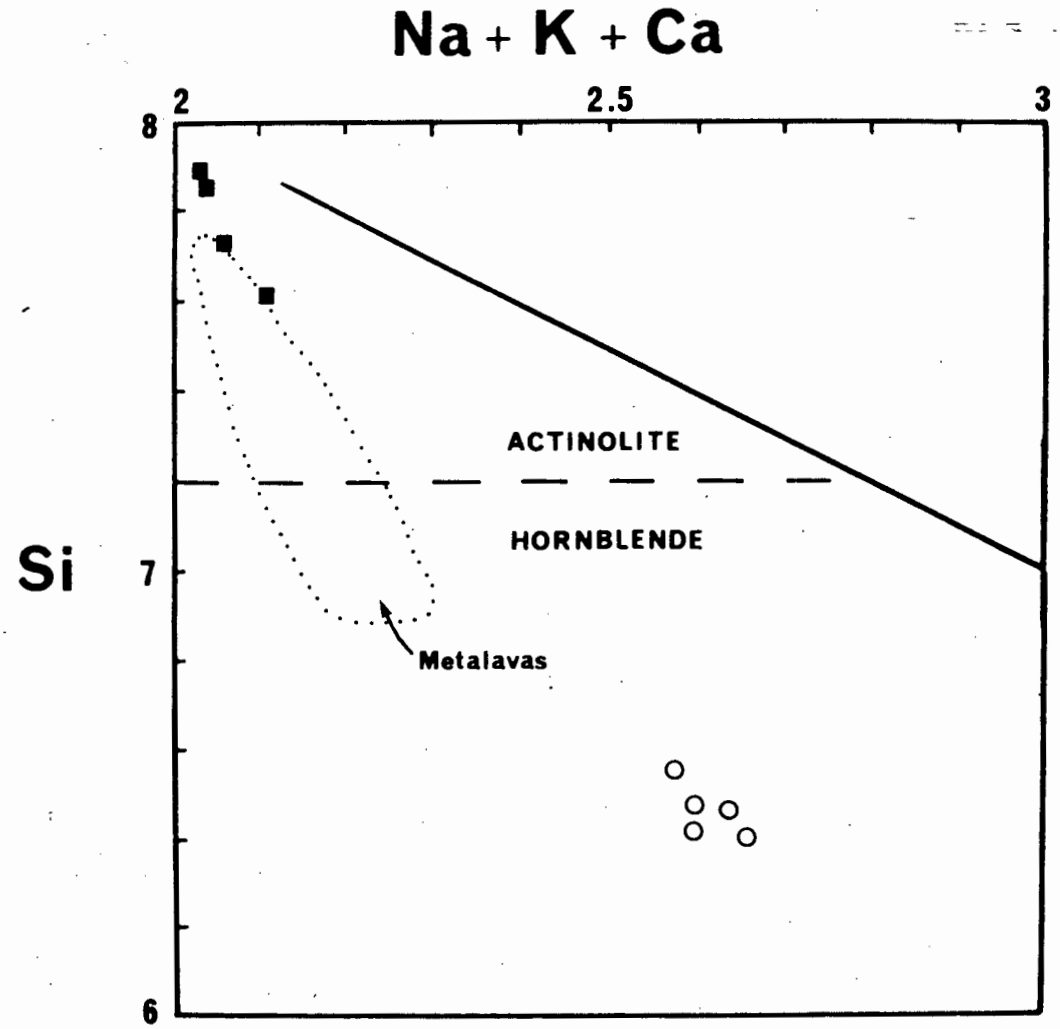

Fig. 48. Plot of Si against (Ca+Na+K) for amphiboles in a metapyroxenite. Atom proportions based on 23 oxygens. O = primary igneous hornblende; ■ = actinolite after primary clinopyroxene; field occupied by metamorphic amphiboles in basaltic andesites is bounded by the dotted line.

of factors. The metamorphic event which affected the Vioolsdrif basic-ultrabasic complexes may have been shorter-lived than that which affected the metagabbros described by Hermes (1970). An alternative is that water may not have been as active in the Vioolsdrif rocks, thereby retarding possible re-equilibration. However, the presence of serpentine, chlorite, secondary amphibole and epidote in the Vioolsdrif rocks indicates that water has had access.

The abundance of chlorite and low Al actinolite suggests that the grade of metamorphism suffered by the early Vioolsdrif basic-ultrabasic complexes is greenschist facies. This is similar to that experienced by the HVG. This suggests that the basic-ultrabasic complexes, together with the HVG, constitute the country rock into which the more voluminous granitic intrusives of the VIS were emplaced. The metamorphism of the basic-ultrabasic complexes is interpreted as part of the regional contact phenomenon that accompanied the emplacement of the later granitic batholith.

10.6 Major element chemistry

All the ultrabasic rocks are extensively modified by cumulus enrichment and can be regarded as essentially mixtures of early formed crystals and trapped intercumulus liquid. Chemical modes for a peridotite and troctolite in the Swartkop complex are listed in Table 17 and have been calculated using a least squares approximation method (Bryan *et al.*, 1969) and analysed minerals listed in Table 18 as input data. Some of the gabbros are also cumulus enriched and a significant part of the gabbro in the Swartkop complex has probably formed partly by crystal settling. Metamorphic reconstitution makes it difficult to distinguish cumulate rocks from gabbros formed by crystallisation in place. Non-cumulate gabbros in the Swartkop complex are probably those that display a patchy development and have been described as gabbro-pegmatites because of their relatively coarse textures and the common development of large prismatic pyroxenes and amphiboles.

Listed in Table 18 are the recalculated bulk analyses (volatile free basis

Results for Peridotite (DRS20)						Results for Troctolite (DRS18)				
	Obs.	Est.	Diff.		X_{mix}	Obs.	Est.	Diff.		X_{mix}
SiO_2	41.45	41.45	.00	Olivine	.69	46.79	46.30	.49	Olivine	.22
TiO_2	.14	.14	.00	Opx	.10	.22	.25	.03	Plag	.59
Al_2O_3	6.24	6.24	.00	Cpx	.04	20.92	21.27	.35	Cpx	.11
Cr_2O_3	.63	.71	.08	Chromite	.02	-	-	-	Hbl	.09
FeO*	11.79	11.71	.08	Plag	.13	6.57	6.41	.16	Total	1.01
MnO	.18	.19	.01	Hbl	.02	.10	.11	.01		
MgO	36.11	36.13	.02	Total	1.00	11.35	11.90	.55		
CaO	3.91	3.91	.00			12.21	12.95	.74		
Na_2O	.03	.08	.05			1.63	1.58	.05		
K_2O	.02	.03	.01			.15	.10	.05		
		$Diff^2$ =	.02				$Diff^2$ =	1.26		

Table 17. Chemical modes of a peridotite and a troctolite from the Swartkop complex.

Least squares approximation based on the method described in Bryan et al.,(1969). Mineral data from Table 15. Bulk compositions of the peridotite and troctolite are listed in Appendix 4 (Table A4.2). Plagioclase component in the peridotite is pure An.

None of the major oxides used in the mixing calculations have been weighted, but the least squares solution is biassed by the most abundant oxides (e.g. SiO_2 , Al_2O_3, MgO).

Obs. = observed composition; Est. = estimated composition; Diff. = Abs [Obs. - Est.]; X_{mix} = weight fraction of component in the mix.

$Diff^2$ = Sum of the squares of the absolute differences

Table 18

Recalculated anhydrous compositions of the Swartkop gabbros; DRS 06, DRS 14 are Ol-normative gabbro-pegmatites, DRS 01 is a Qz-normative gabbro.

	DRS06	DRS14	DRS01	1	2	3	4
SiO_2	50.8	50.4	54.8	50.6	52.8	51.2	52.5
TiO_2	.49	.29	.51	1.1	.83	.88	1.1
Al_2O_3	17.5	18.7	15.8	16.3	16.7	17.4	17.5
FeO*	7.5	5.6	9.2	8.4	7.6	9.3	8.3
MgO	8.9	9.3	6.8	9.0	9.7	6.1	5.9
CaO	11.3	12.5	9.6	9.5	8.2	10.3	8.8
Na_2O	2.0	1.5	1.8	2.9	3.2	2.6	3.2
K_2O	1.2	1.4	1.1	1.1	.26	.78	1.0

1 Typical Melanesian high-Al basalt (Jakes and White, 1972a)
2 Two-pyroxene gabbro (Mt Stuart batholith) (Erikson, 1977)
3 Average basalt of modern island arcs (Ewart, 1976a)
4 Average basalt of Quaternary provinces of W. America (Ewart, 1976a)

to 100 percent) of two samples of gabbro-pegmatite. The most salient features are the presence of Ol and Hy in the CIPW norm and the high Al_2O_3 content. The rock type may be regarded as a high alumina olivine tholeiite and is comparable to high alumina basaltic rocks occurring in modern orogenic provinces (Jakes and White, 1972a). Compared to average data reported by Ewart (1976a), the Swartkop gabbro-pegmatite contains higher MgO and lower Na_2O. Higher MgO contents have been reported for "typical" high alumina basalts by Jakes and White (1972a), which are more comparable to the Swartkop gabbro-pegmatite. Erikson (1977) has also reported gabbros with similar levels of MgO (8-10 percent) in the Mount Stuart composite batholith. The low Na_2O is interesting since many estimates of average high alumina basalt (Manson, 1967; Carmichael *et al.*, 1974; Kuno, 1968) show Na_2O to be invariably higher than 2 percent and usually between 2.5 and 3.5 percent.

A medium grained Qz-normative gabbro is locally developed in the southwest corner of the Swartkop complex. Although scree obscures field relation-

ships, this rock is probably a minor intrusive in a manner perhaps analogous to the gabbro-pegmatites. Compared to these latter gabbros, the Qz-normative gabbro is higher in SiO_2 and total Fe and lower in MgO, CaO and Al_2O_3. The FeO^*/MgO is higher (1.35 compared to 0.70 in the gabbro-pegmatite) and together with the aforementioned features, suggests that the Qz-normative gabbro may be a differentiate of the Ol-Hy-normative gabbros.

The relationship between the Ol- and Qz-normative gabbros in the Swartkop complex is illustrated in Fig. 49. A trend towards Fe enrichment is evident and may be compared with typical tholeiitic intrusive suites. The Swartkop trend may be contrasted with that displayed by the HVG and Vioolsdrif granitic rocks, which follow the typical calc-alkaline trend of zero Fe enrichment.

10.7 Petrogenesis

Ol- and Qz-normative gabbros in the Swartkop complex may represent late stage differentiates and suggest the development of quartz tholeiite from olivine tholeiite by fractional crystallisation. The progressive increase in FeO^*/MgO, together with little change in total alkalis and the depletion in Al_2O_3 and CaO, are consistent with the removal of olivine, plagioclase and possibly pyroxene. Ni and Cr show the expected decrease, while V and Co are enriched in the passage from saturated to oversaturated gabbro. The slight enrichment in Co is surprising, but is probably caused by the large proportion of a Co-poor mineral such as plagioclase crystallising with oliving and pyroxene. Incompatible trace elements such as Ba, Zr, Y and Pb show similar degrees of enrichment, suggesting an F value of 0.5 to 0.6. However, K and Rb are anomalous, in that they both decrease in the direction of presumed differentiation and their behaviour argues against the fractional crystallisation model. The possible influx of Rb during some alteration event long after crystallisation is ruled out because all the gabbros fall on a well defined Rb-Sr isochron, which yields a date very close to the accepted intrusion age. A possible explanation is that Rb (and by inference K) was introduced very soon after intrusion of the gabbros, before any significant change in Sr^{87}/Sr^{86} had occurred. The source of the Rb and K could have been the slightly later and more voluminous granitic rocks within which the

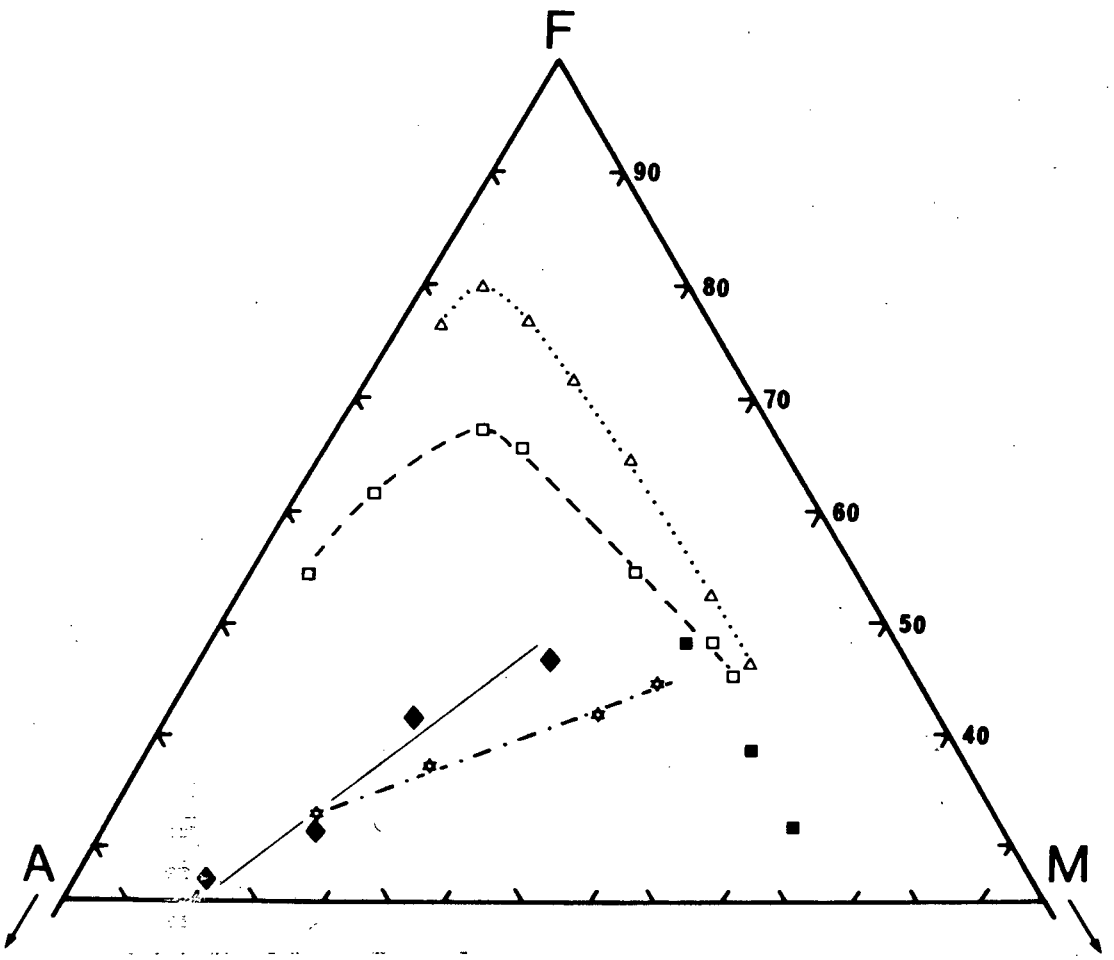

Fig. 49. $A(Na_2O+K_2O)$ - F (Total Fe as FeO) - M (MgO) diagram. All oxide compositions on a volatile free basis.
■ = Swartkop gabbros; ✡ = Haib lavas (average trend); ◆ = Vioolsdrif granitic suite (average trend); □ = Birds River complex (Eales and Robey, 1976); △ = Skaergaard liquid trend (Wager and Brown, 1968).

Swartkop complex is enclosed. It is possible that significant amounts of granitophile elements such as Rb and K may have been introduced during the widespread metamorphic reconstitution that accompanied the emplacement of the later batholithic rocks. Since the time difference between the Swartkop gabbros and the later granitic rocks is small (less than 50 Ma), the Rb-Sr system would not record the metasomatic event.

11

THE VIS. PETROGRAPHY

11.1. Classification

The bulk of the rocks in the VIS may be regarded as granitic in the broad sense of the word, i.e. compositions ranging from quartz diorite to granite (Turner and Verhoogen, 1960). Such rock types have been traditionally classified according to their relative modal proportions of alkali feldspar, plagioclase and quartz (Streckeisen, 1967). The coarse textures preclude the use of conventional size thin sections (25 mm x 45 mm) so a limited number of modes were determined on freshly cut rock slabs of 10 cm square.

A rectilinear grid consisting of 5 mm squares was drawn on a thin sheet of hard plastic 10 cm x 10 cm, giving 400 counting squares. A cut slab was overlain with the plastic grid and the minerals appearing in each square identified. Both sides of a slab were counted, resulting in an effective modal analysis based on 800 point counts. Where the grain size was considerably less than 5 mm, an estimate of the most abundant mineral in the square was made. The only components distinguished were quartz, alkali feldspar, plagioclase and dark minerals. Alkali feldspar was distinguished from plagioclase on colour, since the former was invariably flesh pink to brick red. Plagioclase often appeared pale green due to its incipient alteration to fine grained epidote. The marked colour difference between the two feldspars eliminated the need for staining.

Such a technique is obviously not the most accurate, but is sufficient for general classification purposes so that the major rock types in the VIS may be referred to by different names. Modal data are plotted on the QAP diagram (Fig. 50) (Streckeisen, 1967, 1974, 1976). Also included are normative (weight percent) estimates of the two feldspars and quartz. Values for A and P have been calculated from normative Ab, An and Or using the technique of Le Maitre (1976b) which is as follows:

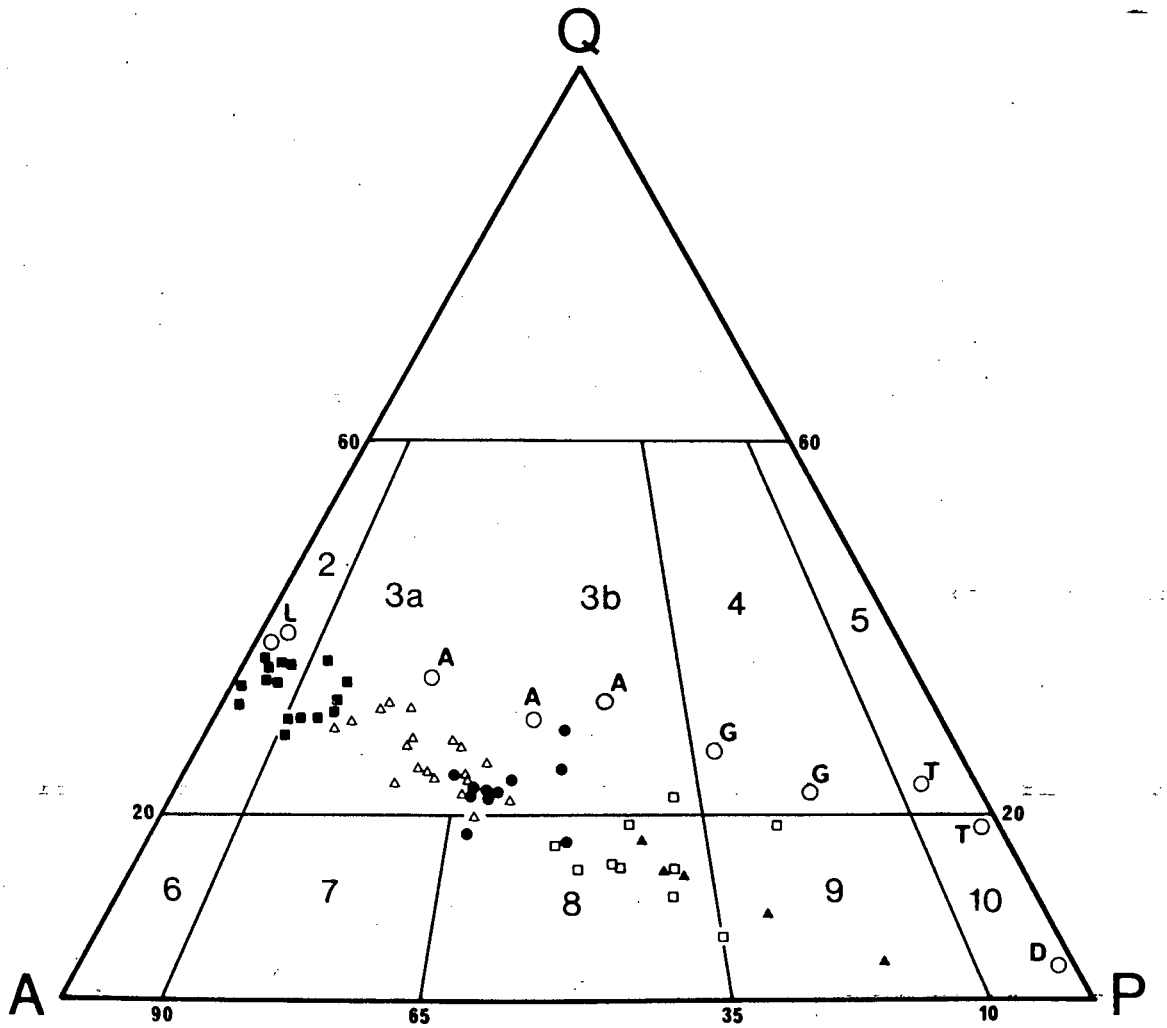

Fig. 50. Q (Quartz) - A (Alkali feldspar) - P (Plagioclase) diagram. Fields shown are for plutonic rocks (after Streckeisen, 1967). O = approximate modes of each rock type within the VIS. Other symbols are normative compositions, recast in the scheme of Le Maitre (1976b). ▲ = Diorite (D); □ = Tonalite (T); ● = Granodiorite (G); △ = Adamellite (A); ■ = Leucogranite (L).

$A = Or \times T$, $P = An \times T$

where $T = (Or + Ab + An)/(Or + An)$

Or, Ab, An are normative feldspar constituents (weight %).

The discrepancy between the modal analyses and the normative data is particularly bad in the case of the more mafic rocks (granodiorites, tonalites, diorites) and largely reflects the inability of the CIPW scheme to handle minerals such as hornblende and biotite. The CIPW norm recasts these mafic minerals as orthoclase, anorthite, hypersthene and diopside and, furthermore, results in a drastic under-estimation of the quartz content. Despite this discrepancy, the normative data does illustrate a more regular variation trend in the QAP diagram, and also serves to reflect the close chemical relationship between the various granitic rocks in the VIS much more effectively than modes.

The choice of the terms adamellite and leucogranite is necessary because they are separate mappable units within the batholith. Both are essentially granites, but differ in their relative proportions of alkali feldspar and plagioclase. Adamellite is still a commonly used term for two-feldspar granites (e.g. Cobbing and Pitcher, 1972), despite Streckeisen's (1967) recommendation to drop it. A highly leucocratic nature is the most characteristic feature of the other granite, hence leucogranite is considered to be more informative than alaskite and less cumbersome than alkali-feldspar granite. Leucocratic granites are normally rich in alkali feldspar, while quartz-bearing leucocratic rocks, in which plagioclase is the dominant feldspar, have been called trondhjémites (Williams et al., 1954).

To summarise, the rock names chosen are those recommended by Streckeisen (1967) using modal analyses. Two different granites may be distinguished in the VIS, and have been given the names of adamellite (two-feldspar granite) and leucogranite (alkali-feldspar granite). The use of normative data yields misleading results in terms of classification because of the presence of abundant biotite and hornblende in the mode, but reflects more effectively the regular compositional variation within the granitic rocks of the VIS.

11.2. Diorite

The Vioolsdrif Diorite is medium to coarse-grained, with an average grain size of 213 mm. The common variety is mottled, with creamy white crystals of plagioclase intergrown with dark grains of hornblende and biotite. More mafic varieties tend to be a uniform dull dark grey, including the plagioclase. Cleavage faces of large biotite flakes are conspicuous.

The essential minerals are plagioclase and green hornblende, but biotite, orthopyroxene, Fe-Ti oxide and quartz also occur in significant quantities. Slender prisms of apatite up to 1.5 mm long are a prominent accessory.

Prismatic plagioclase, subhedral hornblende and anhedral plates of biotite, build a hypidiomorphic granular intergrowth. In most mafic diorites, orthopyroxene occurs as stubby prisms included within the intergrowth, which attests to the early appearance of this mineral. Composite mafic aggregates are cored with orthopyroxene, which is mantled by green hornblende. The contact is often highly irregular and in extreme cases the orthopyroxene core is essentially an aggregate of tiny relict patches. Much of the orthopyroxene in the common variety of diorite occurs in this fashion, rather than as discrete grains. This suggests that the two minerals are in a reaction relationship. Surrounding these two inter-penetrating mafic minerals is a mantle of biotite. Hornblende and biotite sometimes occur in parallel growth. Orthopyroxene and biotite are never found in contact and a separating zone of hornblende is always present.

Orthopyroxene is slightly pleochroic with X = pale mauve, Y = Z = very pale greenish grey. It is optically negative and this, together with the colour, indicates a relatively high Fe content (this is confirmed by EMP analyses). Extremely fine exsolution lamellae (clinopyroxene) are always present, but are too fine even to be resolved with the EMP, so that the orthopyroxene appears homogeneous. The orientation of the

lamellae is parallel to the prominent prismatic cleavage, which suggests that it may be an example of Bushveld type exsolution (Hess, 1951).

Fine scale exsolution is also present in the green hornblende. Careful investigation of thin sections under high magnification, shows that the mineral is a fine scale lamellar intergrowth of two amphiboles, neither of which may be identified as the host. In crystals that are twinned along (100), the lamellae exhibit a "herring-bone" type orientation, and make an angle of about 110^{o} with the twin plane. This orientation is similar to lamellae described by Jaffe et al., (1968), which indicates exsolution parallel to $(10\bar{1})$. The amphibole lamellae are even finer than the pyroxene lamellae described previously and the mineral grains appear homogeneous under the EMP beam.

In addition to mantling hornblende, biotite also surrounds opaque Fe-Ti oxide grains which are deeply embayed, suggesting that a reaction relationship also exists between these two minerals. In reflected light, the opaque oxide consists of two phases which have the optic properties of magnetite and ilmenite. The latter is subordinate, and is confined to irregular patches scattered throughout the grain. Rarely does the ilmenite occur in lamellar form within the magnetite host. EMP analyses (listed in the next section) confirm the existence of the two Fe-Ti oxides. Quartz fills interstitial voids between the major minerals.

The textural evidence suggests that orthopyroxene and Fe-Ti oxide were the first minerals to crystallise, followed very closely by plagioclase. Hornblende replaced orthopyroxene and continued to crystallise after biotite appeared, the latter forming at the expense of early Fe-Ti oxide. The early appearance of small quantitites of apatite is suggested by its inclusion in both hornblende and biotite. Plagioclase continued to crystallise throughout the consolidation history and the most sodic material precipitated with quartz in the interstitial voids.

11.3. Tonalite

Tonalite differs from diorite by containing more biotite at the expense of hornblende, and in addition carries a little more quartz. Orthopyroxene is absent. Mafic tonalite merges with diorite, while leucocratic tonalite becomes indistinguishable from granodiorite. In fact, plutons of tonalite may show local variation from diorite to granodiorite.

The grain size is slightly larger than in the diorite, and fresh outcrops show a conspicuous mottled appearance, with creamy-white to pale greenish-grey plagioclase (3-4 mm) and abundant dark greenish-brown biotite and lesser amounts of dark-green hornblende. Small grains of interstitial quartz are also visible.

The major minerals are plagioclase, biotite and hornblende, together with significant amounts of quartz. Fe-Ti oxide, alkali feldspar, apatite and sphene occur as accessories. The major minerals build a hypidiomorphic granular intergrowth with subhedral biotite and minor hornblende crudely moulded around prismatic plagioclase. Mafic minerals often show the tendency to form aggregates of small grains rather than large crystals (cf. diorite).

Hornblende is similar to that in the diorite, except for the absence of exsolution lamellae, and a slightly more bluish pleochroic tint in the Z absorption direction. Biotite shows its characteristic strong pleochroism with Z = pale straw brown, Y = Z = very dark greyish brown. Alteration to green chlorite is not uncommon.

Plagioclase displays its characteristic prismatic habit, but the prisms are stouter than those in the diorite. Alteration to a turbid aggregate of fine-grained epidote and sericite is not uncommon. Clear patches of fresh plagioclase show well developed lamellar twinning.

Since hornblende, biotite and plagioclase occur in a hypidiomorphic intergrowth, all three must have co-precipitated. Biotite mantles opaque

Fe-Ti oxide, so the latter must have slightly preceded the former. It is quite probable that all four minerals - hornblende, biotite, plagioclase and Fe-Ti oxide, were crystallising when the tonalite magma was intruded. As in the diorite, apatite probably appeared early, since it occurs as inclusions in both hornblende and biotite. Sphene as well as biotite mantles Fe-Ti oxide, suggesting that it too has been formed by late stage reaction. Both reaction products often occur in association around a core of opaque Fe-Ti oxide.

11.4 Granodiorite

Granodiorite is a coarse-grained mottled rock with conspicuous pale greenish grey plagioclase and dark brown flakes of biotite, which build a hypidiomorphic granular intergrowth. The average grain size is 314 mm. Pale pink alkali feldspar is invariably present but in lesser amounts than plagioclase. Quartz occurs as very pale greyish blue grains which are generally smaller than the feldspars.

Plagioclase forms stout prisms up to 5-6 mm across, which show euhedral faces against quartz and alkali feldspar. Albite, pericline and combined Carlsbad-albite twinning are very common. Normal zoning is prevalent and extreme ranges involve a change from An_{65} in the core to An_{33} at the margins. Oscillatory zoning is rarely developed. Incipient alteration to a fine-grained aggregate of epidote and sericite is ubiquitous.

Biotite is the only mafic silicate mineral present and this feature distinguishes the granodiorite from tonalite. There is a tendency for biotite to occur as aggregates of small flakes as well as large single subhedral plates. The latter usually show euhedral faces in contact with quartz or alkali feldspar. Alkali feldspar is a microcline-microperthite and forms anhedral grains exhibiting cross hatched twinning and thin stringers of exsolved sodic plagioclase. The host is potash-rich. Small prisms of plagioclase, flakes of biotite and subhedral grains of opaque

Fe-Ti oxide are common inclusions.

Quartz fills interstitial voids between the plagioclase prisms and, where associated with alkali feldspar, builds fairly large anhedral grains with irregular boundaries against alkali feldspar.

Fe-Ti oxide, apatite, sphene and rare zircon are accessory minerals. All these minerals occur as inclusions in biotite. Fe-Ti oxide forms small anhedral to embayed grains. Apatite occurs as slender prisms with 6-sided sections. Sphene forms characteristic bipyramidal crystals and may itself contain tiny tubular inclusions. Zircon forms tiny equant grains, often surrounded by a narrow pleochroic halo developed in the host biotite.

Secondary minerals include epidote and sericite after plagioclase, and green biotite and chlorite after brown biotite. Basal sections of secondary green biotite contain needle-like inclusions arranged in an intersecting sagenitic network. The inclusions may be exsolved rutile, formed during the alteration of primary brown biotite (high TiO_2) to secondary green biotite (lower TiO_2).

11.5. Adamellite

A conspicuous and characteristic feature of the Vioolsdrif adamellite is the presence of large (up to 15 mm) phenocrysts of flesh pink alkali feldspar. Even-grained adamellite also occurs, but differs only in texture from the more common porphyritic variety. The porphyritic adamellite often grades into even-grained rock and it cannot be established whether the two textural types represent distinct mappable units.

Although alkali feldspar is the most conspicuous mineral, it is accompanied by an approximately equivalent amount of plagioclase, which forms slightly smaller, subhedral prismatic crystals that show incipient alteration to fine-grained epidote and sericite. The pink colour of the alkali feldspar is caused by partial sericitisation and the subsequent liberation of very

small amounts of finely divided hematite. The presence of Fe is confirmed by EMP analyses which show that the alkali feldspar contains up to 0.15% FeO*. The presence of well developed cross-hatched twinning, and the presence of narrow lamellae of albite, indicate that the alkali feldspar is a microcline-microperthite.

Plagioclase and biotite both show euhedral form against quartz and microcline-microperthite. The mafic mineral usually forms crystals flattened parallel to the a-axis and sections containing the c-axis usually exhibit the characteristic perfect basal cleavage. Inclusions of opaque Fe-Ti oxide, apatite, sphene and zircon are present in the larger biotite plates.

Microcline-microperthite and quartz often form a granular aggregate between the plagioclase prisms, although both minerals probably co-precipitated. Early quartz grains are sometimes poikilitically enclosed in large anhedral crystals of microcline-microperthite. In addition, small prisms of plagioclase, biotite flakes and Fe-Ti oxide may be enclosed in the alkali feldspar. Indeed, the large "phenocrysts" are really large oikocrysts of late stage alkali feldspar, and in this manner resemble the large plates of pyroxene enclosing olivine in the peridotite.

Sphene is a prominent accessory and forms subhedral crystals up to 0.4 mm across, with well developed faces against alkali feldspar and quartz, but is moulded around plagioclase and biotite.

11.6. Leucogranite

The most conspicuous feature of the Vioolsdrif leucogranite is its pink colour. This is caused by the colour of the most abundant constituent, alkali feldspar. Grain-size varies from medium-grained (1.5 - 2 mm) up to coarse (4 - 5 mm), the latter being confined to the central zones of the larger plutons. Pegmatitic patches may contain milky white quartz and brick red alkali feldspar crystals up to 3-4 cm across.

The essential minerals are microcline-microperthite and quartz. Other subordinate minerals are plagioclase, biotite, muscovite and Fe-Ti oxide. Interstitial patches of fine-grained intergrown albite, orthoclase and quartz are not uncommon.

The earliest minerals are plagioclase, Fe-Ti oxide and biotite, since they develop crystal faces against alkali feldspar and quartz. Alkali feldspar occurs in two forms: as large anhedral microcline-microperthite, and as small discrete grains of albite and orthoclase. This feature suggests that during the crystallisation of the leucogranite, the feldspar solvus was intersected (Tuttle and Bowen, 1958; Martin and Bonin, 1976).

Muscovite and biotite often occur in parallel growth, with adjacent crystals sharing a common c-axis such that their basal cleavage direction coincides.

11.7. Metamorphic effects

Metamorphic reconstitution of the volcanic country rock has been described in Chapter 6, where it was suggested that the pervasive recrystallisation was caused by regional intrusion of the Vioolsdrif batholith. Compared to the volcanics, the intrusives are quite fresh, except for the earliest plutons (gabbro-peridotite-pyroxenite, see Chapter 10). The granitic rocks exhibit incipient alteration with plagioclase replaced by a turbid aggregate of fine-grained epidote and sericite and with biotite replaced by green secondary biotite and chlorite. Such incipient recrystallisation need not necessarily be caused by a later metamorphic event, but may just as easily be the result of late stage deuteric activity (Hatch et al., 1961). Furthermore, the secondary alteration is only sporadically developed throughout the plutons and is quite often associated with vein networks filled with quartz, epidote and chlorite.

However, as the intrusive rocks are traced out of the study area, they show abundant evidence of being affected by a later superimposed meta-

morphic event which is accompanied by quite intense deformation. This metamorphism affects both the batholith and volcanic country rock alike, so the study area therefore contrasts with the surrounding region in having been unaffected by this later event. Localised deformation (E-W shear zones) that ramifies the study area may represent a tectonic manifestation of this later event. The absence of pervasive metamorphic recrystallisation may be a function of depth, the Vioolsdrif-Haib region representing a higher-level counterpart to the deformed, recrystallised rocks surrounding it. Description of these surrounding rocks and later superimposed metamorphisms is outside the scope of the present study, but forms a significant portion of other current studies (e.g. Blignault, 1977; Ritter, 1977).

To summarise, extensive metamorphic recrystallisation within the batholith is confined to the early basic-ultrabasic bodies, but is of the same grade as that experienced by the volcanic country rock. Both the volcanics and the basic-ultrabasic complexes may be regarded as country rock to the later more voluminous granite plutons. Recrystallisation of these later granitic rocks is restricted to turbid alteration of plagioclase and chloritisation of biotite, which was probably caused by late stage deuteric activity. A superimposed metamorphism and accompanying deformation affects both intrusives and volcanic country rock as they are traced out of the present study area. Incipient deformation associated with this later event may be represented by the localised E-W shear zones within the study area.

12

THE VIS. MINERALOGY

Fig. 51 summarises the major mineral content of the series diorite-tonalite-granodiorite-adamellite-leucogranite. Individual EMP analyses are listed in Appendix 2. Average compositions of the major minerals in the Vioolsdrif diorite are given in Table 19. Less mineral data are available for the other rock types and no separate tables of average compositions have been prepared.

12.1. Orthopyroxene

Orthopyroxene is confined to the diorite, occurring either as discrete grains (in the more mafic varieties) or as relict cores within green amphibole. Compositional variation is slight and the average orthopyroxene composition is $Wo_{1.3}En_{64.0}Fs_{34.7}$. Textural evidence indicates that orthopyroxene was the first mafic silicate to appear, but was subsequently replaced by discontinuous reaction with the surrounding liquid to produce green amphibole.

The amount of Di_{ss} in the orthopyroxene is only 4.4 mole percent, a factor which is probably responsible for the poorly developed exsolution features. The diorite orthopyroxene is much more Fe rich than that in the Swartkop peridotite.

12.2. Hornblende

Green calciferous amphibole occurs in the diorite and the tonalites, but does not show any marked variation in composition. Salient chemical features are illustrated in Figs. 52 and 53 and it can be seen that the amphibole may be regarded as a hornblende, using the scheme of Miyashiro (1973). In terms of Si and (Na+Ca+K) contents, the plutonic hornblendes

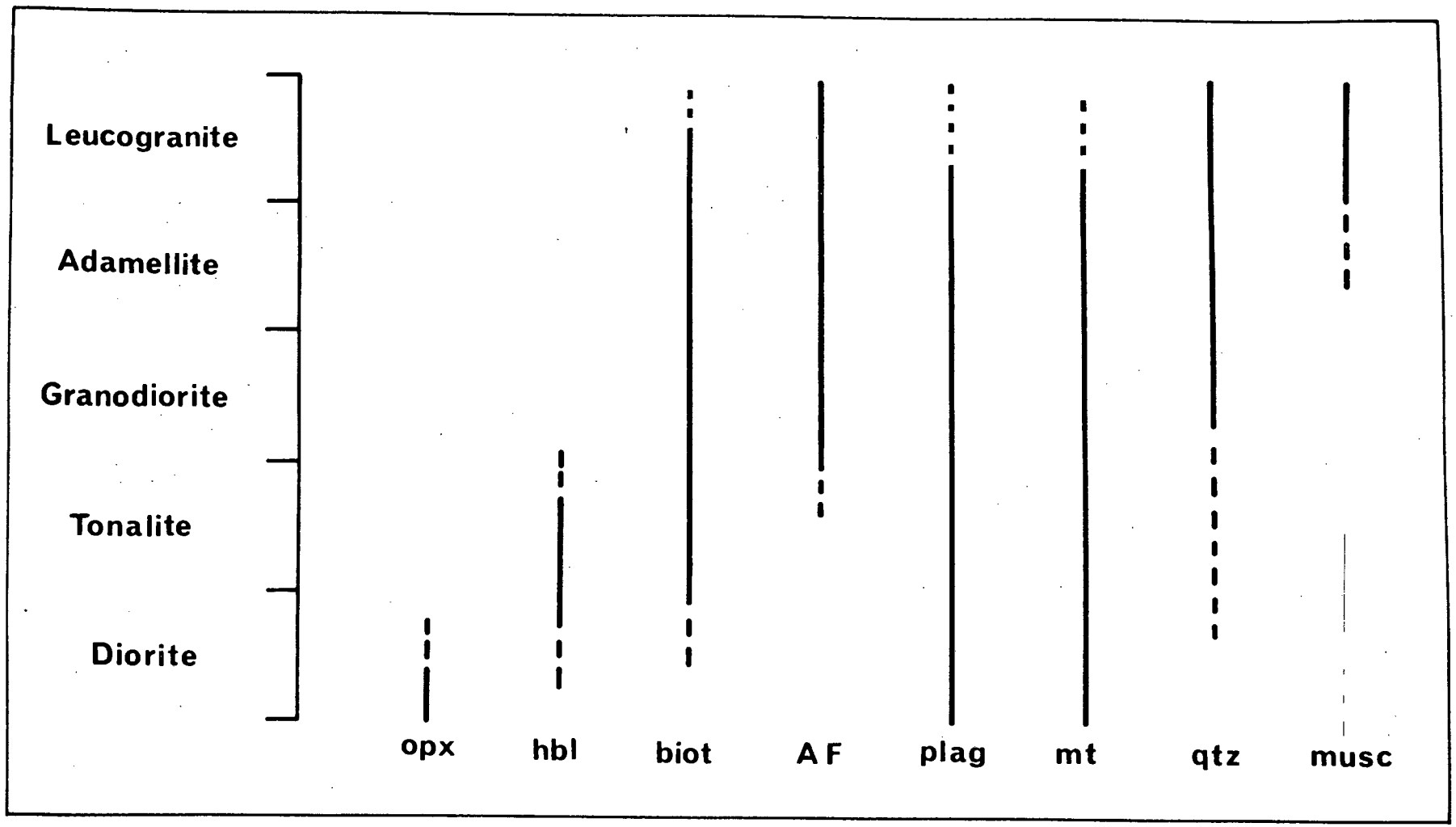

Fig. 51. Appearance of major minerals in the Vioolsdrif granitic suite.

Specimen Grain	OPX	HBL	BIOT	PLAG		MT	IL
SiO_2	51.93	47.75	38.47	51.50	SiO_2	.03	.17
TiO_2	.12	1.13	2.78	.00	TiO_2	.06	49.97
Al_2O_3	1.43	8.45	16.62	30.04	Al_2O_3	.12	.17
FeO*	22.18	12.45	14.04	.15	Fe_2O_3	68.42	4.97
MnO	.71	.23	.05	.00	FeO	30.88	40.94
MgO	23.00	15.31	17.00	.00	MnO	.04	3.73
CaO	.66	11.67	.01	12.34	MgO	.07	.14
Na_2O	.00	.89	.21	4.52	CaO	.00	.14
K_2O	.00	.52	9.26	.05			
Total	100.03	98.40	98.44	98.60		99.62	100.23
No. of oxygens	6	23	22	32		4	3
Si	1.939	6.896	5.504	9.477	Si	.002	.004
Al	.063	1.439	2.804	6.518	Al	.008	.005
Ti	.003	.122	.299	.000	Ti	.003	.946
Fe	.693	1.504	1.681	.023	Fe^{3+}	2.983	.094
Mn	.022	.028	.006	.000	Fe^{2+}	1.496	.862
Mg	1.280	3.295	3.625	.000	Mn	.002	.080
Ca	.026	1.806	.002	2.433	Mg	.006	.005
Na	.000	.250	.058	1.612	Ca	.000	.004
K	.000	.095	1.690	.011			

Table 19. Average compositions of the constituent minerals in the Vioolsdrif diorite.

have compositions which are similar to the metamorphic amphiboles in the basaltic andesite metalavas. However, plutonic hornblende may be readily distinguished from secondary amphibole by the relative contents of Ti and, less effectively, by their Mg/(Mg+Fe) ratios. Brown amphibole from the mafic-ultramafic rocks are also included for comparison.

Hornblende from the diorite and tonalite is green, whereas that in the mafic-ultramafic rocks is reddish-brown. The difference is probably a function of contrasting Ti contents and possibly different Fe^{3+} contents, although the latter feature cannot be tested. Another important difference is the amount of Al replacing Si (represented by Al(4) in Fig. 53). This corresponds with lower (Na+K) and suggests that green amphibole, with its lower Al(4) and (Na+K) contents, crystallised at lower temperatures than that in the ultrabasic rocks (cf. Helz, 1973; Harry, 1950).

Green hornblende in granitic rocks from elsewhere has a similar composition to that in the Vioolsdrif diorite and tonalite. Dodge et al., (1968) and Larsen and Draisen (1950) report similar Al(4), Ti and (Na+K) contents in hornblende from the Sierra Nevada and Southern California batholiths respectively. The compositional range reported by Dodge et al., (1968), which includes a compilation from other areas as well, is quite large, but no systematic variation between mineral composition and bulk rock was found to exist. Unfortunately, the restricted occurrence of hornblende in the Vioolsdrif granitic rocks precludes any evaluation of compositional variation with changing rock composition.

The composition of hornblende has often been recast in terms of the CIPW norm (e.g. Yoder and Tilley, 1962; Cawthorn, 1976a). The green hornblende in the diorite and tonalite is Ol-Hy normative, which is consistent with the predictions of Cawthorn (1976b) based on experimental evidence.

Presumed submicron scale exsolution features in the diorite hornblende may indicate immiscibility between Al-poor and Al-rich calciferous amphibole. The intermediate Al content of the diorite hornblende results in its com-

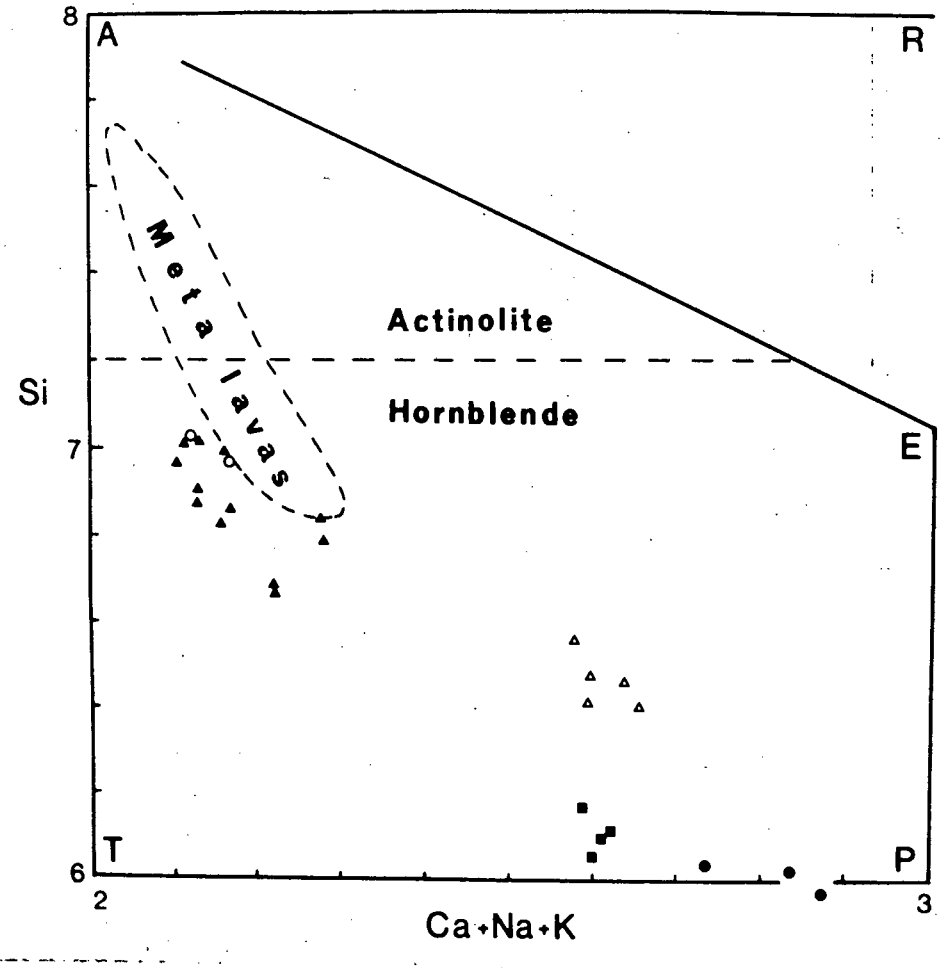

Fig. 52. Plot of Si against (Ca+Na+K) for amphiboles. Atomic proportions based on 23 oxygens. ▲ = Diorite; ○ = Tonalite; △ = Pyroxenite; ■ = Troctolite; ● = Peridotite. Field occupied by metamorphic amphibole in basaltic andesites is also shown.

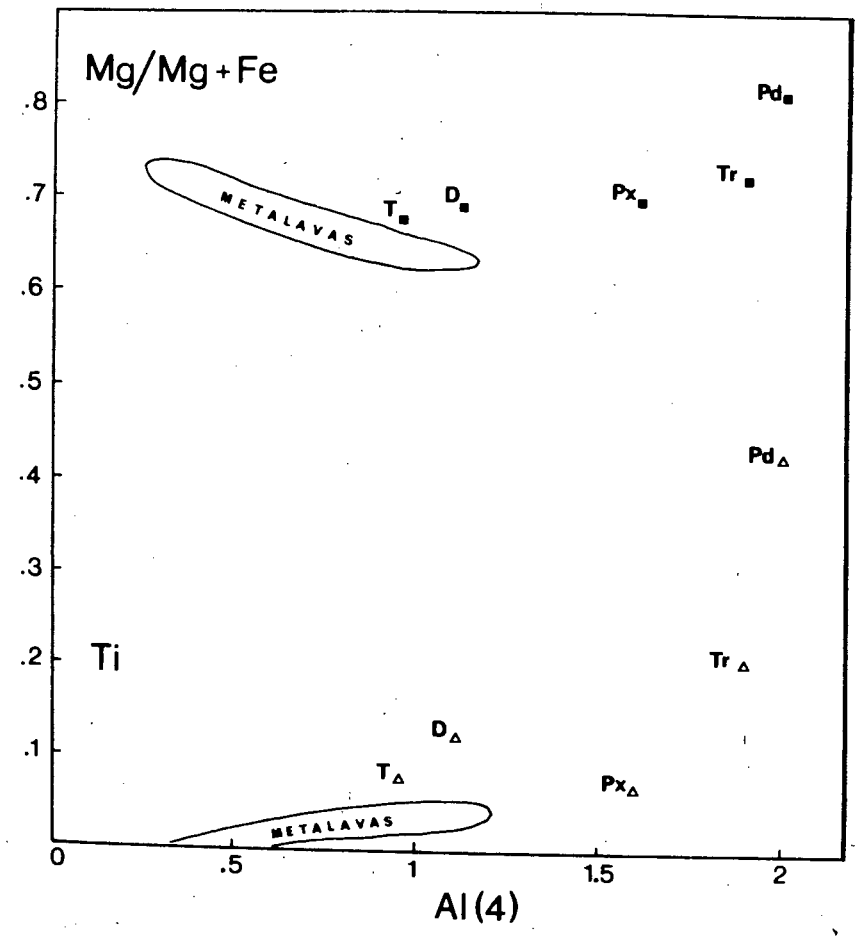

Fig. 53. Plot of Mg/Mg+Fe and Ti against AL(4) for amphiboles. Average compositions only are plotted. T = Tonalite; D = Diorite; Px = Pyroxenite; Pd = Peridotite. Field for amphibole in the basaltic andesite metalavas is also shown.

position falling very near the actinolite-hornblende boundary in Miyashiro's (1973) diagram (Fig. 52) and if immiscibility did exist, such an amphibole would be expected to show this. At the relatively high temperatures of magmatic crystallisation, the amphibole may have been homogeneous, but subsolidus readjustment of the amphibole structure could result in exsolution. The incipient nature of the exsolution could be caused either by rapid cooling or by limited immiscibility. The former is difficult to reconcile with the coarse texture, so the latter is considered more likely. Unfortunately, separate lamellae are impossible to resolve, even with a sharply focussed EMP beam and no estimation of the amphibole solvus could be made. Such exsolution structures are absent from the hornblende in the tonalite; this may be a function of a slightly lower Al content.

12.3. Fe-Ti oxide

Opaque Fe-Ti oxide is ubiquitous throughout the entire series from diorite to leucogranite. The grains are now completely oxidised and are composed of magnetite and small amounts of ilmenite. Ilmenite is often arranged as narrow plates intersecting at variable angles, depending on the orientation of the thin section, and provides the necessary evidence for exsolution of a Ti-rich phase from an originally homogeneous Fe-Ti oxide. The proportion of ilmenite in the grains is too variable to make an accurate estimate of the original Fe-Ti oxide composition. EMP analyses show that the Ti-poor and Ti-rich phases are almost pure magnetite and ilmenite respectively. The totals are very near 100 percent when Fe^{3+} and Fe^{2+} are calculated assuming the ideal spinel formula.

In the diorite and tonalite, Fe-Ti oxide forms relatively large grains, often mantled by biotite. This suggests that the latter was formed in part by discontinuous reaction, in a manner analagous to that of hornblende from orthopyroxene. In the more acid rocks, Fe-Ti oxide is often rimmed by sphene, as well as biotite. The original Fe-Ti oxide was probably a member of the magnetite-ulvöspinel series; the ulvöspinel content was not very high

(<40-50 mole percent), judging from the proportion of secondary ilmenite in the oxidised grains.

12.4. Biotite

Biotite is present in all rocks and appears to have crystallised continuously in the passage from diorite to leucogranite. The modal proportion of biotite falls regularly with degree of differentiation. Fig. 54 illustrates the progressive change in chemical composition of biotite throughout the rock series. In the passage from diorite (basic) to leucogranite (acid) there is a tendency for the constituent biotite to have less Al replacing Si, lower Ti and Mg/(Mg+Fe) ratios.

The reasonably systematic variation in biotite composition is consistent with a progressive drop in temperature of crystallisation (Deer et al., 1962). Variation in bulk composition is often invoked as an alternative to temperature changes, but it is difficult to de-couple liquid composition and temperature, since biotite will not appear at all unless both bulk composition and temperature are appropriate.

12.5. Plagioclase

Plagioclase probably crystallised throughout the entire series since it forms a significant modal fraction of all rock types. The most calcic plagioclase is found in the diorite and there is a progressive drop in An content through to the leucogranite. Fig. 55 summarises the range of An content of the plagioclase within each rock type and illustrates the progressive drop with degree of differentiation. The compositional ranges overlap, but the most calcic plagioclase in each rock type is poorer in An with increasing DI. Almost all crystals investigated were normally zoned, although a few cases of oscillatory zoning were observed. However, these involve reversals of only 1-2 mole percent.

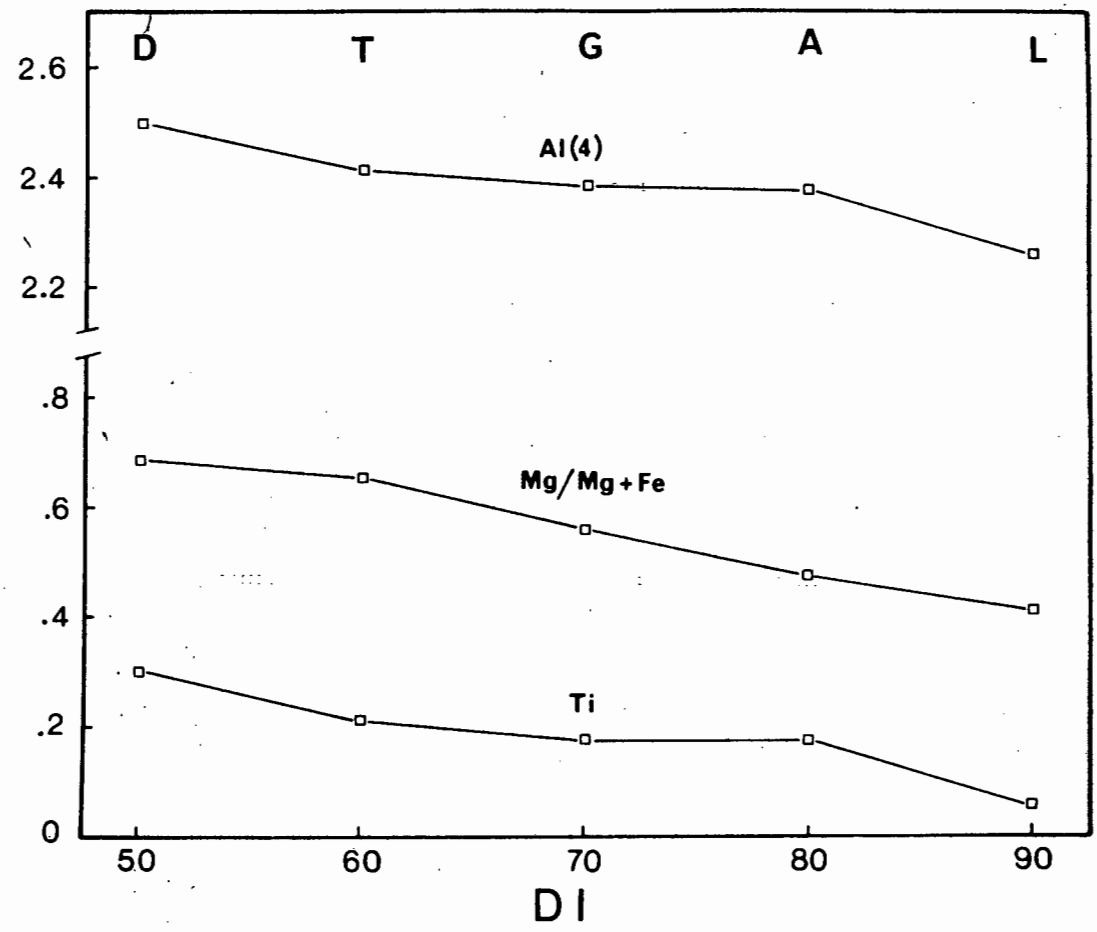

Fig. 54. Compositional variation exhibited by biotite in the Vioolsdrif granitic suite. All atomic proportions based on 22 oxygens. D = Diorite, T = Tonalite, G = Granodiorite, A = Adamellite, L = Leucogranite. DI = typical Differentiation Index for these rocks.

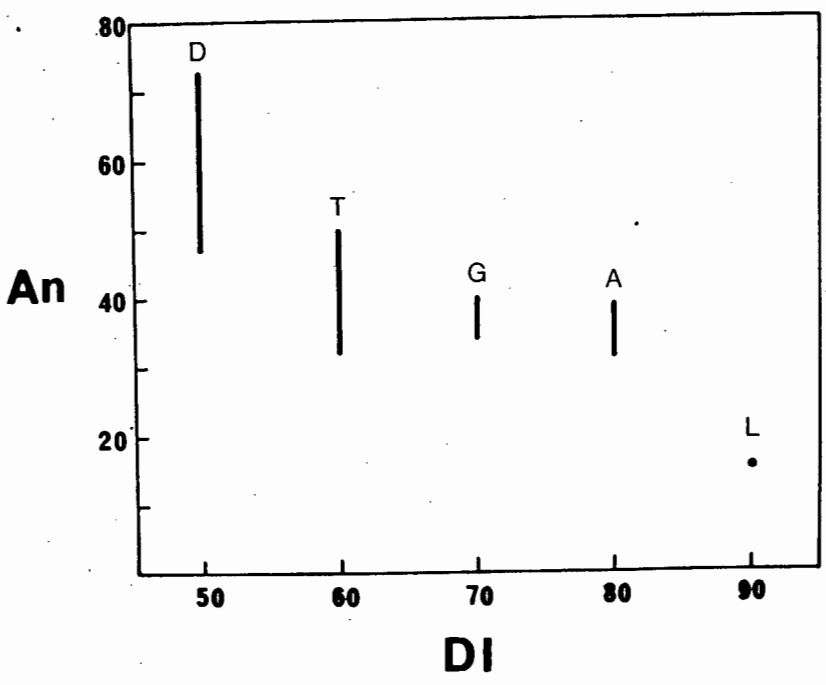

Fig. 55. Compositional variation exhibited by plagioclase in the various rock types within the Vioolsdrif granitic suite. Host rock types as in Fig. 54.

12.6. Alkali-feldspar

Alkali feldspar occurs as a minor accessory phase in the more acid tonalites, increasing progressively in abundance through the granodiorites and adamellites until it makes up nearly all the feldspar in the leucogranite. In the granodiorite and adamellite, the alkali feldspar is microcline-microperthite, with narrow stringers of almost pure albite within a host of almost pure K-feldspar which shows cross-hatched twinning. The albite lamellae are never wider than 20-30 microns and are widely spaced, suggesting that the original homogeneous phase was fairly potassic. Two generations of alkali feldspar occur in the leucogranite; an early microcline-microperthite similar to that in the granodiorite and adamellite and a later aggregate of discrete crystals of albite and orthoclase.

Granites containing a single alkali-feldspar phase (usually perthitic) have been distinguished from those containing two discrete alkali feldspar phases (one Na-rich, the other K-rich). They have been described as hypersolvus and subsolvus respectively (Martin and Bonin, 1976; Tuttle and Bowen, 1958) and reflect the influence of water pressure on the alkali feldspar solvus and solidus. The Vioolsdrif granodiorite and adamellite may be regarded as hypersolvus, suggesting that they did not crystallise under very high P_{H_2O}. Martin and Bonin (1976) have estimated from experimental data that if $P_{total} = P_{H_2O}$, the P_{H_2O} necessary for the alkali feldspar solidus to intersect the solvus is about 2.5 kbars. Under conditions where $P_{H_2O} < P_{total}$, the total confining pressure may be significantly higher than 2.5 kbars. The effect of CO_2 and other volatile components (B, Cl, F) are at present unknown, so no accurate estimate of the partial pressure of volatiles can be made.

In contrast with the earlier granitic rocks, the Vioolsdrif leucogranite is transitional in that it contains an early single perthitic alkali feldspar phase and a late interstitial intergrowth of albite, orthoclase and also quartz. Such trans-solvus granites appear to be rare,

but have been explained by at least two different mechanisms. The first involves the increase in P_{H2O} during crystallisation, presumably caused by closed system behaviour (Goldsmith and Newton, 1972). At an advanced stage of crystallisation, the final feldspathic liquid may solidify under extremely high P_{H_2O}, possibly equalling the total confining pressure, thereby producing a subsolvus assemblage as crystallisation proceeds. An alternative mechanism involves the introduction of meteoric water into a previously consolidated hypersolvus granite (Martin and Bonin, 1976). Such an influx of water may drive the solidus of the hypersolvus granite below its present temperature, resulting in partial refusion under higher P_{H_2O}. Subsequent recrystallisation may produce the required interstitial subsolvus assemblage. Martin and Bonin (1976) cite the presence of cross-cutting veins of subsolvus granites and oxygen isotopic data as evidence in favour of such a hydrous influx. No transecting veins or dikes of subsolvus granite cut the Vioolsdrif leucogranite and unfortunately no oxygen isotopic data are available, so the refusion hypothesis is difficult to test. Although Martin and Bonin do not mention features such as resorbed minerals or other replacement textures, it is probable that their proposed mechanism will lead to such petrographic effects. No effects of this kind have been observed in the Vioolsdrif leucogranite. On the other hand, the complete unmixing of Na- and K-feldspars, together with the high degree of structural ordering (as evidenced by the microcline-type cross hatched twinning), are more easily attained in a hydrous system (Tuttle and Bowen, 1958). Although cited by Martin and Bonin (1976) as evidence for high water content, the composition and structural state of the alkali feldspars cannot be used to distinguish between hypersolvus and subsolvus conditions. This is clear from the presence of microcline-microperthite in the granodiorite and adamellite, both of which crystallised under hypersolvus rather than subsolvus conditions. At present, the secondary refusion hypothesis is rejected in favour of that involving a progressive increase in P_{H_2O} in response to the increasing concentration of water during closed system crystallisation.

13

THE VIS. MAJOR ELEMENT CHEMISTRY

The granitic rocks of the VIS comprise the series diorite - tonalite - granodiorite - adamellite - leucogranite and constitute 95% of the exposed batholith. In view of the close spatial and temporal association between the VIS and the HVG, the following description of the intrusive suite will continuously refer to the comparable chemical characteristics of the lavas.

All individual analyses are listed in Appendix 3 and average compositions, recalculated to 100% volatile free, are listed in Table 20. Fe_2O_3 and FeO have been estimated using the method of Le Maitre (1976b) in order to calculate CIPW norms.

13.1 Fe enrichment

The lack of significant Fe enrichment in the passage from diorite to leucogranite (Fig. 56) indicates a close affinity with the calc-alkaline series. The average Vioolsdrif trend contrasts sharply with that displayed by typical tholeiitic series (e.g. Thingmuli), but closely resembles the average trend of the southern California batholith (Nockolds and Allen, 1953) and the Mount Stuart batholith (Erikson, 1976). The most basic intrusives (diorite and mafic tonalite) have slightly higher FeO*/MgO ratios than their extrusive counterparts (basaltic andesite and andesite). However, very few intrusive rocks sampled have compositions as basic as the basaltic andesites. Only one orthopyroxene-rich (accumulative?) diorite has a composition that approaches that of the Haib basaltic andesites.

13.2 Alkali-lime index

(Na_2O+K_2O) and CaO have been plotted against SiO_2 in Fig. 57 and intersection of the respective trends define an alkali-lime index of 60.0, which falls within Peacock's calc-alkalic field. This value for ALI is similar to that

Table 20. Average major element composition of the granitic rock types within the Vioolsdrif batholith. Recalculated on a volatile free basis, with all Fe as FeO. CIPW norms have been calculated with Fe_2O_3 and FeO estimated using the method of Le Maitre (1976b) (see Appendix 4).

N = number of samples; $\overline{X}$ = mean composition; sd = standard deviation about the mean (1σ)

	Diorite		Tonalite		Granodiorite		Adamellite		Leucogranite		Haib Porphyry	
	N=5		N=11		N=12		N=20		N=17		N=8	
	$\overline{X}$	sd	$\overline{X}$	sd	$\overline{X}$	sd	$\overline{X}$	sd	$\overline{X}$	sd	$\overline{X}$	sd
SiO_2	55.7	2.5	60.3	2.4	65.8	1.5	69.4	3.2	75.7	1.6	69.7	1.7
TiO_2	.95	.09	.88	.20	.57	.11	.47	.16	.19	.09	.43	.04
Al_2O_3	17.3	.67	17.2	.77	15.6	.51	14.7	1.0	13.0	.75	15.4	.60
FeO	8.1	.42	6.2	.77	4.3	.36	3.1	.66	1.1	.26	3.1	.36
MnO	.12	.01	.12	.03	.08	.01	.07	.02	.03	.01	.05	.01
MgO	4.6	.48	2.8	.69	2.2	.51	1.2	.56	.22	.19	1.1	.40
CaO	7.8	.91	6.0	.89	4.0	.43	2.7	.86	.83	.37	2.7	.63
Na_2O	2.6	.14	3.2	.24	3.0	.24	3.2	.45	3.5	.31	3.4	.49
K_2O	2.2	.68	2.9	.56	4.1	.44	4.8	.59	5.3	.39	3.9	.62
P_2O_5	.40	.04	.30	.10	.18	.05	.14	.06	.03	.03	.10	.02
Qz	8.2		13.5		20.4		24.9		32.5		27.3	
C	-		-		-		-		.02		1.0	
Or	13.0		17.3		24.4		28.2		31.5		22.9	
Ab	22.0		26.8		25.6		26.8		29.6		28.5	
An	29.0		24.2		16.9		11.9		4.0		12.7	
Di	5.9		3.0		1.5		.68		-		-	
Hy	15.1		9.4		7.2		4.2		1.1		4.6	
Il	1.8		1.7		1.1		.90		.36		.82	
Mt	4.1		3.5		2.7		2.1		.83		1.6	
Ap	.87		.66		.39		.31		.06		.22	
DI	43.2		57.5		70.3		79.9		93.6		78.8	

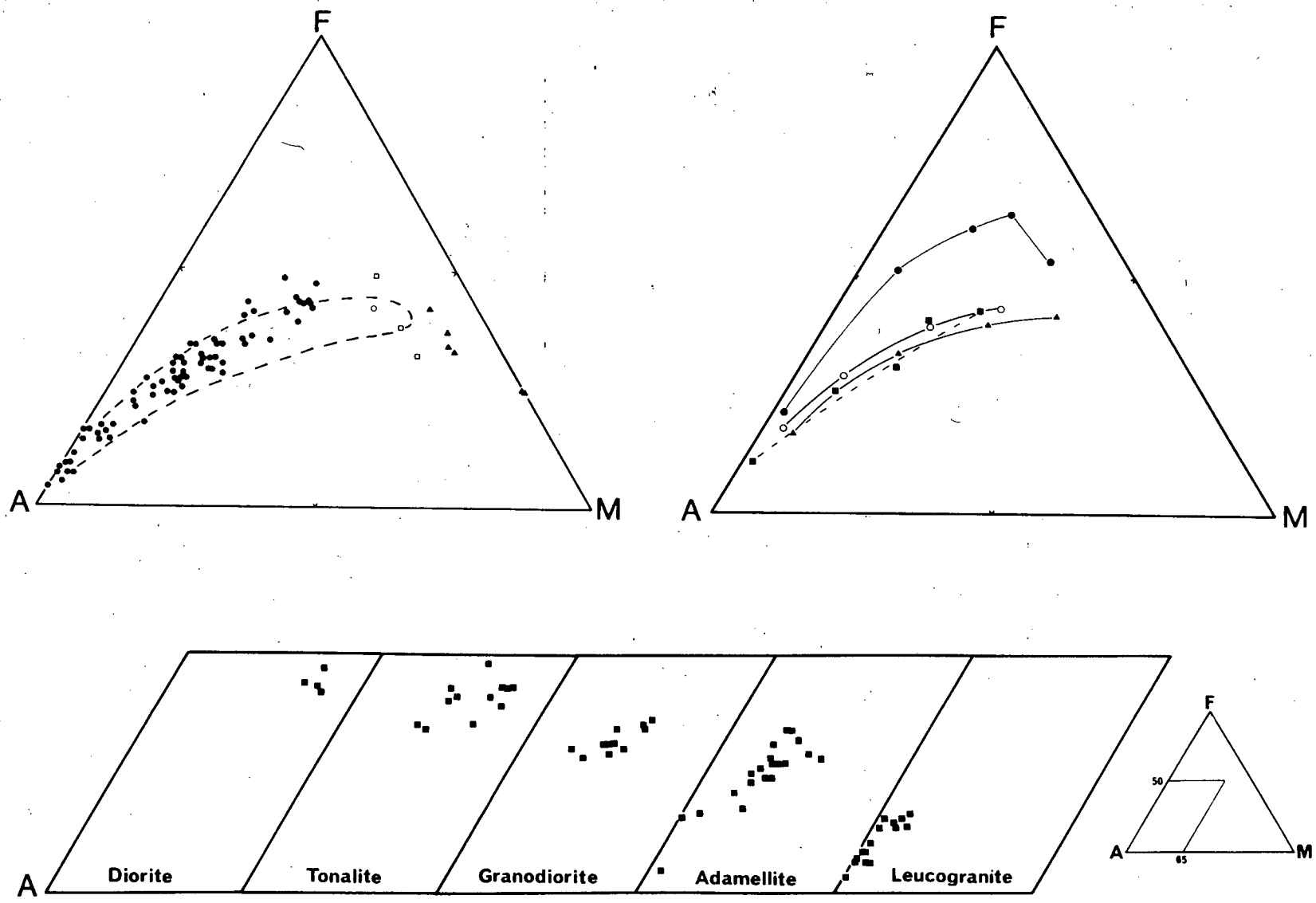

Fig. 56. A(Na_2O+K_2O) - F(Total Fe as FeO) - M(MgO) diagram for the Vioolsdrif Intrusive Suite. (a): individual compositions; ● = Vioolsdrif granitic suite, ○ = accumulative pyroxene diorite (DRV-08), □ = Swartkop gabbros, ▲ = accumulative rocks in the early basic-ultrabasic complexes, field occupied by lavas of the HVG is also shown (broken line). (b): average trends; ■ = Vioolsdrif granitic suite, ▲ = Haib lavas, ○ = southern Californian batholith (Nockolds and Allen (1953) and Mount Stuart batholith (Erikson, 1976); ● = typical tholeiitic trend (Thingmuli, Carmichael, 1964). (c): compositional field occupied by each individual rock type in the Vioolsdrif granitic suite.

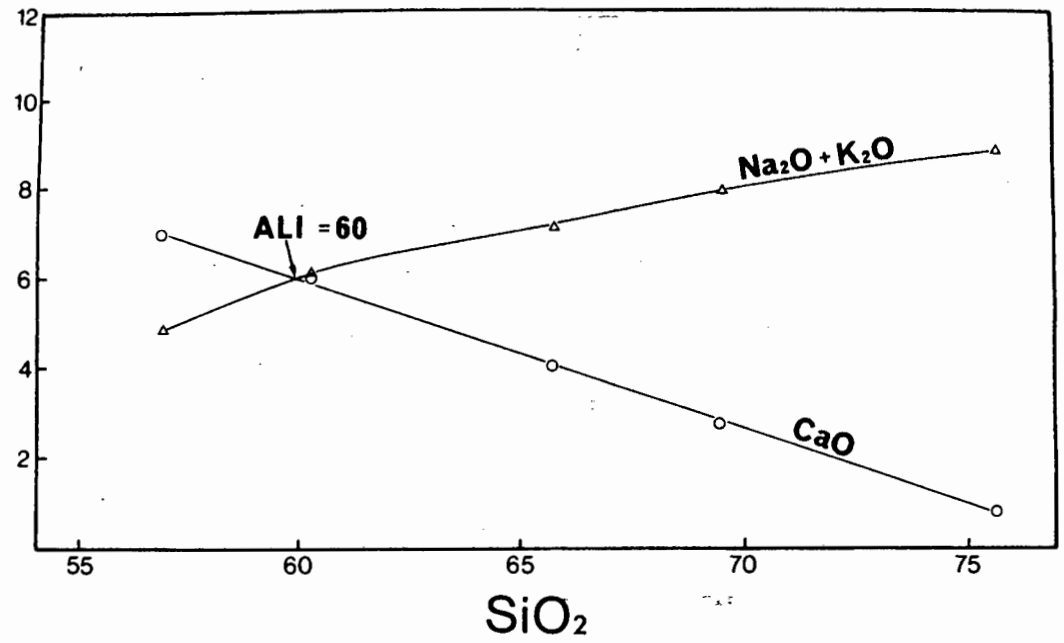

Fig. 57 Partial Harker diagram showing the average (Na_2O+K_2O) - SiO_2 and CaO - SiO_2 trends for the Vioolsdrif granitic suite. The alkali - lime index (ALI) for the suite is 60, which falls within the calc-alkalic field of Peacock (1931).

obtained for the Haib lavas (60.8).

13.3 K_2O - SiO_2 variation

Fig. 58 displays the variation between K_2O and SiO_2 for the Vioolsdrif granitic rocks; the rapid increase in K_2O suggests affinities with high-K calc-alkaline suites. The average trend is very similar to that displayed by the HVG, although the most felsic intrusives are slightly more enriched than their volcanic counterparts.

13.4 Total alkalis - SiO_2 variation

The average trend for the Vioolsdrif granitic suite falls within the field defined by Kuno (1960,1968) and Wilkinson (1967) as representing the calc-alkaline series (Fig. 59). It has already been shown (8.4) that the total alkalis - SiO_2 plot is not very diagnostic since typical tholeiitic provinces

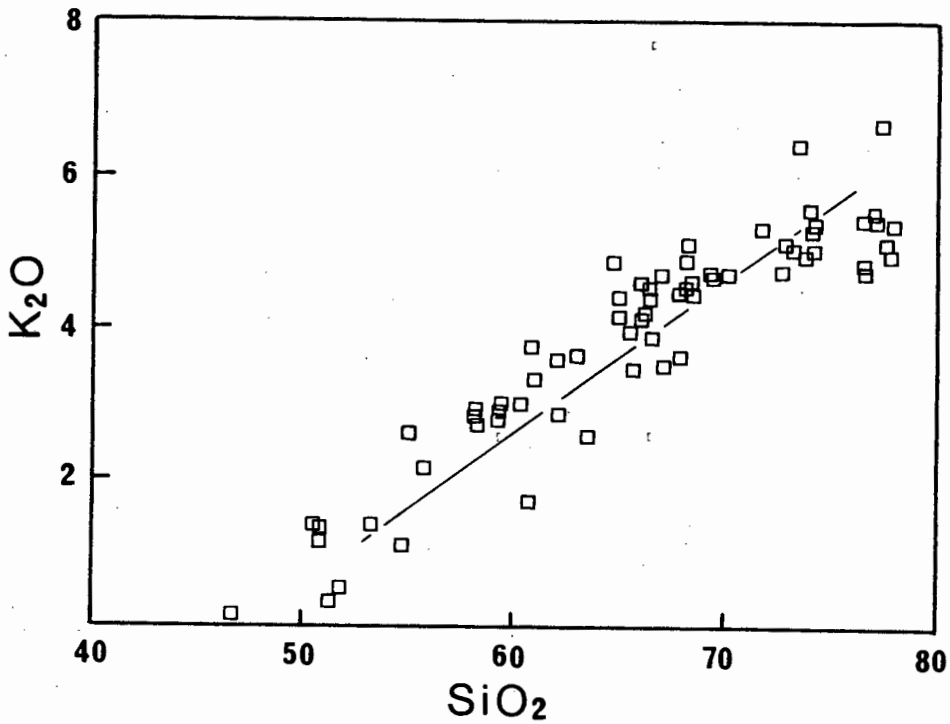

Fig. 58. Plot of K_2O against SiO_2 for the VIS. The average trend displayed by the HVG is also shown (solid line).

(e.g. Thingmuli) also fall in the calc-alkaline field. Compared with the Haib lavas, the Vioolsdrif granitic suite is slightly more enriched in total alkalis, although the fields defined by the scatter of individual points show considerable overlap.

13.5 TiO_2 content

All the Vioolsdrif granitic rocks are uniformly low in TiO_2 (less than 1.2%) and confirm the calc-alkaline affinity originally demonstrated by Chayes (1964). There is considerable overlap in the fields defined by the intrusives and the lavas except for the most basic rocks. Diorites and mafic tonalites have slightly higher TiO_2 contents than their volcanic counterparts. The

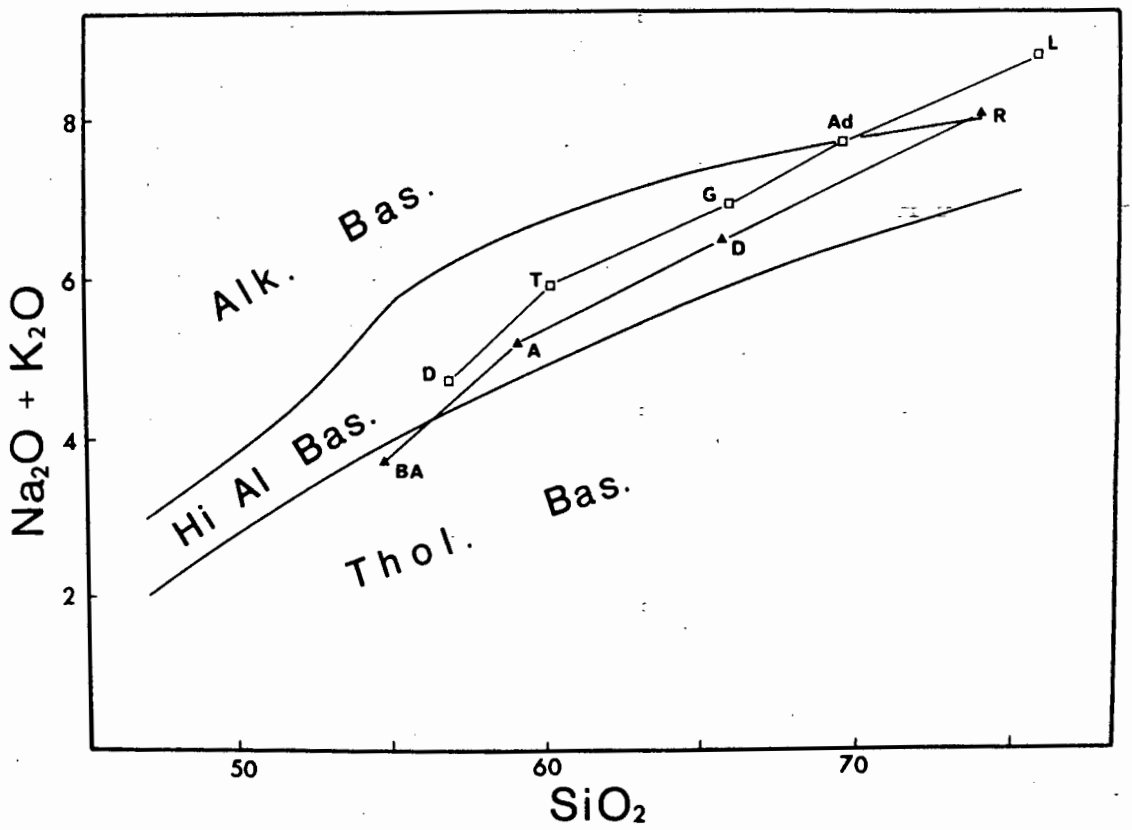

Fig. 59. Average trend in the total alkalis - SiO_2 plot. Fields are those defined by Kuno (1966) for the Japanese arc. □ = Vioolsdrif granitic suite, ▲ = Haib lavas. D,T,G,Ad,L = Diorite, Tonalite, Granodiorite, Adamellite, Leucogranite respectively; BA,A,D,R = Basaltic andesite, Andesite, Dacite, Rhyolite respectively.

average trend of the lavas peaks at about 58% SiO_2 (DI=40), whereas the intrusives show progressive depletion from diorite to leucogranite.

13.6 Al_2O_3 content

In the passage from diorite to leucogranite, the Al_2O_3 content falls progressively from 17% to 12% (Fig.60), which appears to be typical of many calc-alkaline suites. An important difference between the Vioolsdrif granitic suite and the Haib lavas is illustrated in Fig. 60, where their respective trends can be seen to overlap except for the most basic rocks. Lavas with SiO_2 contents less than about 65% have significantly lower Al_2O_3 than their intrusive counterparts. The intrusives show a progressive depletion in Al_2O_3, whereas the Al_2O_3 content in the lavas initially rise to a maximum of 17% Al_2O_3 at 60% SiO_2. A similar but less marked contrast has already been noted in the TiO_2 variation.

13.7 Major oxides - DI variation

The compositional variation within the granitic suite is summarised in the major oxide - DI plots (Fig.61). Apart from Al_2O_3 and to a lesser extent TiO_2, the major oxides show similar variation trends to those displayed by the Haib lavas. The Vioolsdrif average FeO* and MgO trends are slightly displaced below the average trends for the lavas.

There is a good correlation between K_2O and DI, which defines an average trend very similar to that of the Haib lavas. In the latter case, many lavas appeared to have lost K by some process of leaching. Coarse-grained rocks are less susceptible to alkali leaching than glassy materials and hence the lack of low K, high DI intrusive rocks in the VIS is not surprising.

The patterns of Na_2O variation is very interesting in that there is progressive increase up to a DI of about 60. Rocks with higher DI show very little change in Na_2O and appear to be slightly depleted in Na_2O. On average, the granodiorites (DI around 70) have lower Na_2O than the tonalites (DI around

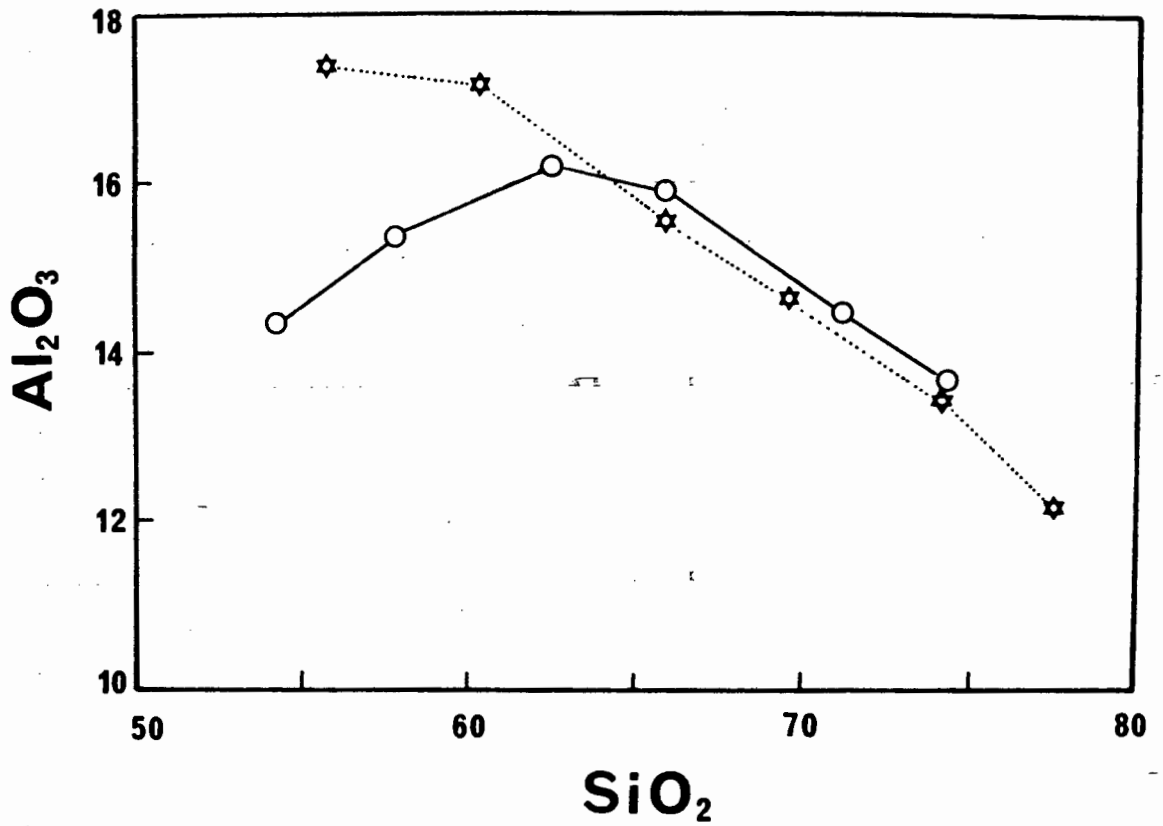

Fig. 60. Average Al_2O_3 - SiO_2 trends for the VIS and HVG. ✡ = Vioolsdrif granitic suite (data from Table 36), ○ = Haib lavas (data from Table 23).

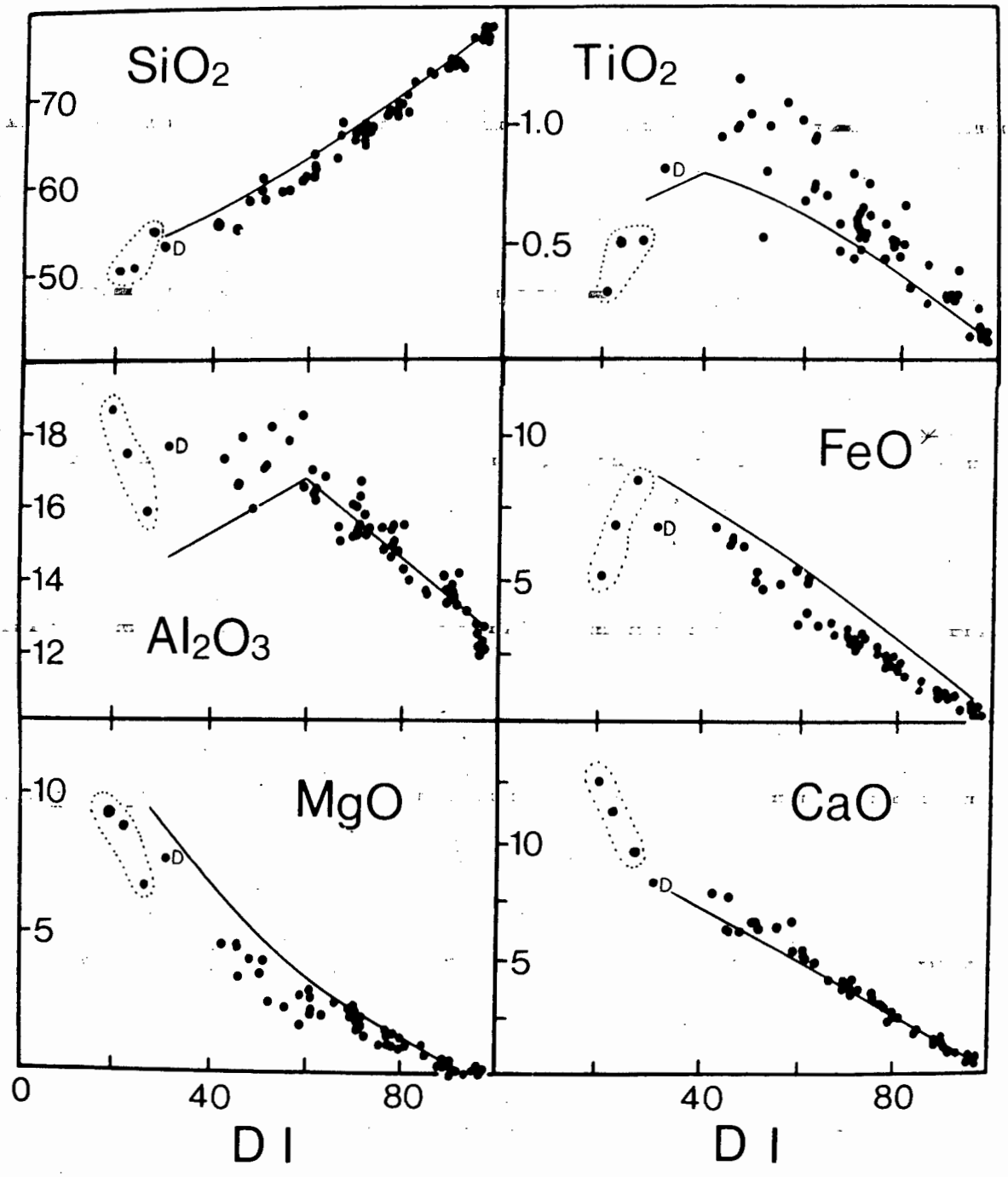

Fig. 61. Plot of major oxides against DI for the VIS. All oxides on a volatile free basis. Dotted line defines field occupied by gabbros in the Swartkop complex; D = accumulative pyroxene diorite (DRV-08), average trend for the Haib lavas also shown (solid line).

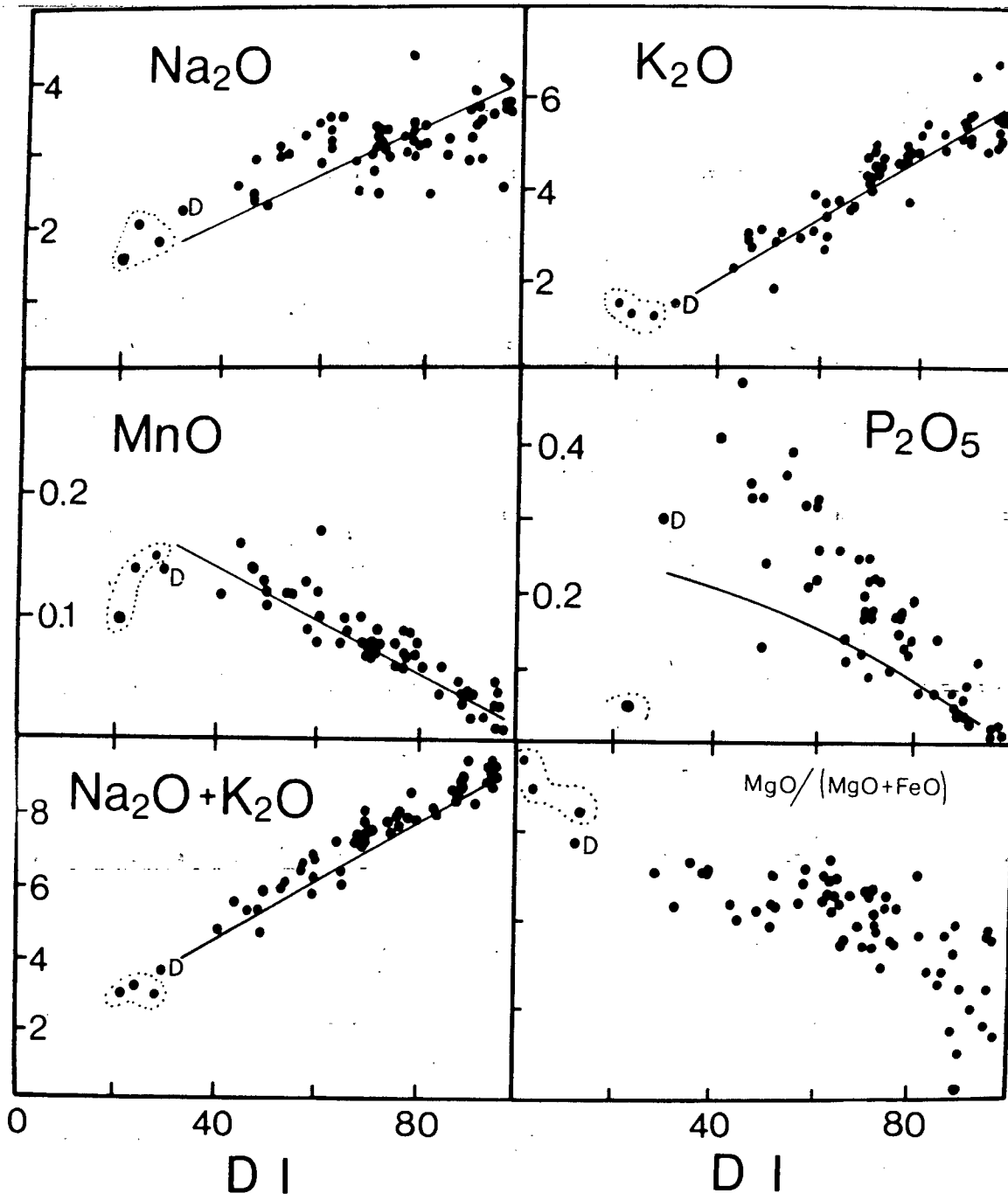

Fig. 61. Plot of major oxides aginst DI for the VIS (continued).

60). At DI greater than 75, Na_2O again increases until the highest contents are reached in the leucogranites. It has been noted by Bateman and Dodge (1970) that Na_2O does not show marked enrichment with differentiation and often behaves unsystematically in calc-alkaline intrusives.

The basic to intermediate intrusives contain slightly higher levels of P_2O_5 than their extrusive counterparts; the diorite and mafic tonalites contain about 0.3 to 0.4% P_2O_5, whereas the basaltic andesites contain 0.20 to 0.25%. Furthermore, the rate of depletion in P_2O_5 with DI is greater in the intrusives, which is shown by a steeper trend line.

13.8 Discussion

The Vioolsdrif granitic suite displays a chemical affinity with high K calc-alkaline igneous rocks and may be compared with similar batholithic complexes in western America. In many respects, the major element variation trends of the VIS parallel those observed for the Haib lavas. However, there are a few important differences, which include;

(i) If the early Vioolsdrif basic-ultrabasic complexes are excluded, the VIS does not seem to contain rock types as basic as the most basic lavas in the HVG.

(ii) The Vioolsdrif diorites and tonalites (DI=50-60) have higher Al_2O_3, TiO_2 and P_2O_5 contents than that in their extrusive counterparts (basaltic andesite - andesite).

(iii) The Vioolsdrif diorites have slightly higher FeO^*/MgO ratios than those observed for the Haib basaltic andesites. This is a function of lower MgO contents and results in the more basic intrusives displaying a variation trend in the AFM diagram that is displaced slightly above that of the lavas.

14

COMPARATIVE TRACE ELEMENT GEOCHEMISTRY

Despite many similarities within the extrusive and intrusive suites, the important differences in major element chemistry described in Chapter 13 make it pertinent to combine the respective descriptions of trace element variation. 15 trace elements reported in this study are listed in Appendix 4 and are plotted on a log scale against DI in Fig. 62. The respective trends of the two suites for each individual element have been placed alongside each other to facilitate comparison. Average trace element compositions for each rock type within the HVG and VIS are given in Tables 21 and 22 respectively. Estimates of uncertainty are expressed as standard deviations.

14.1. Systematic description

Barium

The lavas are uniformly high in Ba and show a two-fold enrichment in the passage from basaltic andesite (700 ppm) to rhyolite (1400 ppm). The increase is progressive and correlates with DI. Such high levels of Ba in calc-alkaline lavas seem to be confined to those characterised by relatively high K contents (Taylor et al., 1969a; Jakes and White, 1972a; Zielinkski and Lipman, 1976). Since the Haib lavas show affinity to high K calc-alkaline suites, the high Ba contents are not unexpected.

Ba seems to behave quite differently in the more acid members of the intrusive suite. Rocks with DI>80 (adamellite, leucogranite) are severely depleted in Ba relative to their extrusive counterparts. The variation trend is characterised by an initial increase in Ba to a broad maximum at DI = 60-70 (granodiorite). At higher DI, Ba drops from over 1000 ppm to less than 100 ppm. This latter feature is probably the most important difference between the two suites, with respect to Ba variation.

Table 21. Average trace element compositions of the Haib lavas. Classification scheme based on SiO_2 content (see Table 12).

N = number of samples; $\overline{X}$ = mean composition; sd = standard deviation about the mean (1σ)

	Basaltic andesite		Andesite		Dacite		Rhyolite	
	N=5		N=18		N=18		N=14	
	$\overline{X}$	sd	$\overline{X}$	sd	$\overline{X}$	sd	$\overline{X}$	sd
Ba	739	190	959	286	1070	295	1235	292
Rb	61	28	98	35	153	35	188	56
Zr	116	9	144	20	175	53	233	75
Nb	4.0	1.2	5.6	1.5	9.8	2.0	13.7	1.9
Th	6.6	2.5	8.9	3.5	18	5.6	20	7.1
Pb	18	3	23	8	34	11	30	12
Y	17	.5	17	3.1	21	4.7	28	9.9
Sr	471	113	531	121	406	104	177	89
Ni	110	14	58	38	20	20	4.1	4.4
Co	42	3.1	29	9.1	16	7.8	1.3	2.1
Cr	344	58	144	95	44	52	7.0	8.4
V	184	19	151	37	87	33	17	18
Zn	82	14	78	28	69	35	19	16
Cu	74	50	62	52	97	147	17	28
U	.8	.2	1.4	.8	3.4	1.5	3.4	1.6

Table 22. Average trace element composition of the granitic rocks within the Vioolsdrif batholith.

N = number of samples; $\overline{X}$ = mean composition; sd = standerd deviation about the mean (1σ)

	Diorite		Tonalite		Granodiorite		Adamellite		Leucogranite		Haib Porphyry	
	N=5		N=11		N=12		N=20		N=17		N=17	
	$\overline{X}$	sd	$\overline{X}$	sd	$\overline{X}$	sd	$\overline{X}$	sd	$\overline{X}$	sd	$\overline{X}$	sd
Ba	711	155	1060	301	1144	269	937	368	521	397	1136	506
Rb	80	33	122	25	161	31	195	32	246	57	147	46
Zr	161	30	167	55	130	36	168	59	124	51	157	52
Nb	9.1	2.6	8.3	3.2	8.9	1.6	11.5	2.1	16.7	5.2	7.8	3.0
Th	7.0	2.5	10.3	4.5	15.9	3.7	21	5.4	28	9.6	14.9	5.5
Pb	21	4.5	26	15.2	34	7	27	3.7	35	6.3	23	6.7
Y	20	2.1	21	5.7	16.7	5.2	21	4.9	25	9.2	13.0	6.2
Sr	504	60	514	82	434	70	279	75	101	58	37	11
Ni	102	2	22	9.7	13	6.6	10.7	6.6	0	0	10.8	4.2
Co	35	2.6	17.9	5.8	12.7	4.2	8.6	4.6	0	0	5.2	1.9
Cr	55	11.5	42	14	24	8.7	18.7	9.9	1.9	1.4	10.7	2.3
V	196	34	115	20	83	17	58	22	5	2	65	20
Zn	88	4	74	16	46	12	42	15	12	6	37	11
Cu	100	47	74	25	48	25	35	24	18	25	336	379
U	.6	.3	1.8	.55	2.1	.76	3.2	1.4	4.8	1.7	2.8	.6

The contrasting trends represent the two most commonly encountered in igneous rock suites. Nockolds and Allen (1953) found both trends in various calc-alkaline provinces in western U.S.A. Progressive enrichment in Ba with differentiation is shown by the volcanics of Lassen Peak, Crater Lake and Medicine Lake Highlands, and also the Southern California batholith. Severe depletion in Ba with increasing DI (above a value of 75-80) is exhibited by the E. central Sierra Nevada batholith. More modern studies confirm the contrasting behaviour of acid members of calc-alkaline suites (Baker, 1968 ; Lewis, 1968; Ewart et al., 1968; Taylor et al., 1968; Arculus, 1976). There seems to be no relationship between the behaviour of Ba and the observed abundance levels, since it can be seen from Fig. 61 that the two suites have fairly similar Ba contents at intermediate DI (50-80).

Rubidium

Both suites show a similar range in Rb abundances and also have very similar variation trends such that they could be superimposed without any major discrepancies. Two minor differences, are that the lavas show more scatter about the average trend and the most acid intrusives have slightly higher Rb (on average) than their extrusive equivalents.

As in the case of Ba, high K calc-alkaline suites usually have higher Rb contents than those observed in "normal" calc-alkaline suites. Inspection of typical high K calc-alkaline lava suites described by McKenzie and Chappell (1972), Jakes and Smith (1970), Jakes and White (1972a) confirm this compositional feature. The relatively high Rb content in the Haib basaltic andesites and andesites is compatible with the suspected high K-calc-alkaline affinity.

Zirconium

The lavas display a well defined increase in Zr with DI, but this is

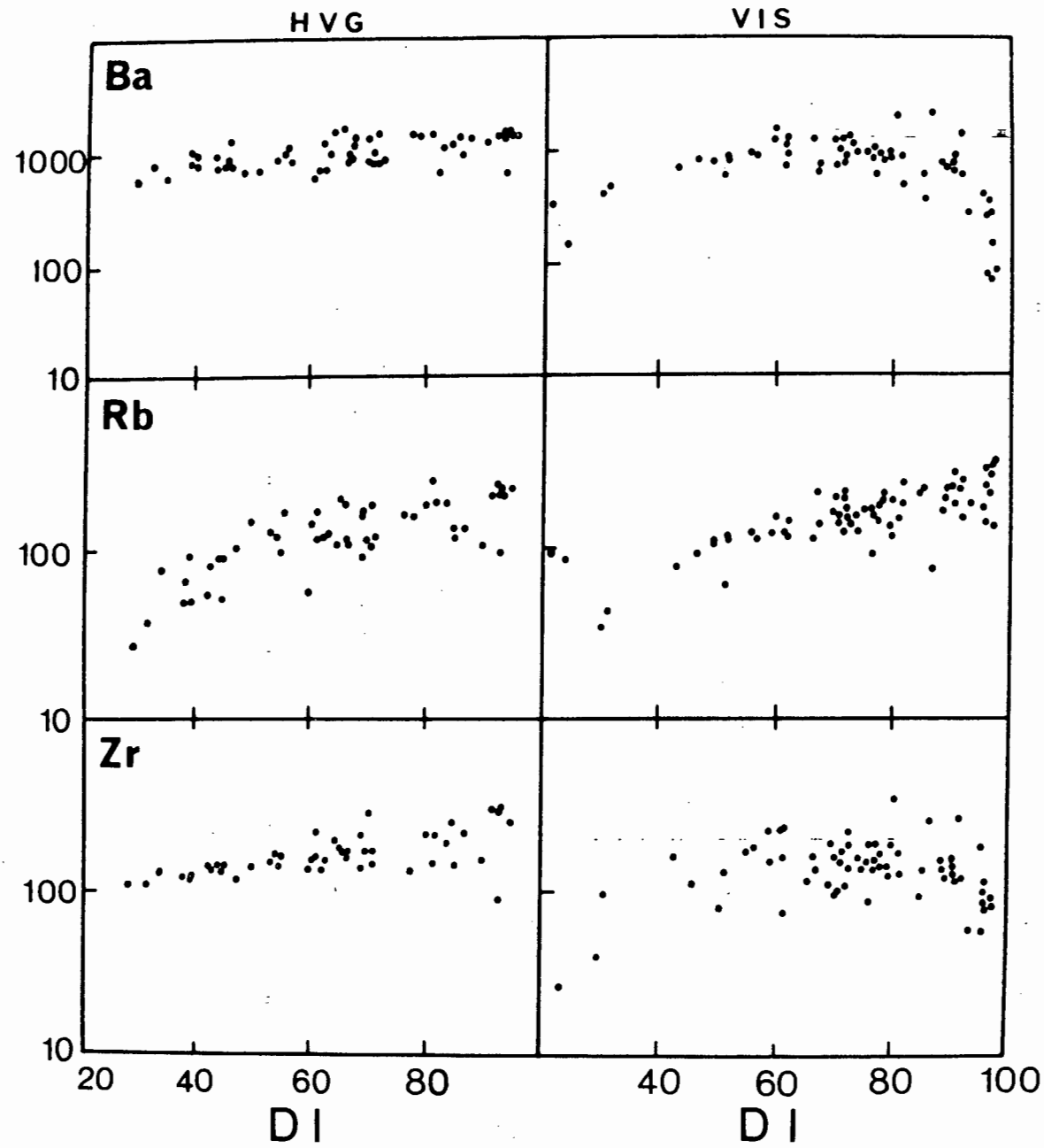

Fig. 62 Plot of trace elements against DI for the HVG and VIS. The trace element abundances have been plotted against a log scale in order to display average trends.

accompanied by an increase in degree of scatter. Zr contents between 100 and 200 ppm for the series basaltic andesite to dacite are typical of calc-alkaline suites (Taylor, 1969; Jakes and White, 1972a). Scatter is not confined to the acid members of the intrusives and the overall variation trend is not well defined. Despite the uncertainty, the variation exhibited by the intrusives appears to be different from the lavas in that the acid intrusives (adamellite, leucogranite) are lower in Zr than their extrusive equivalents. There is a suspicion that the Zr trend involves a maximum at intermediate DI (70-80, which corresponds to adamellite) in a manner analagous to Ba. Unfortunately, the initial increase in Zr with DI is poorly defined through lack of data on mafic intrusives.

Niobium

The lavas show a well defined increase in Nb with DI, which involves a rise from 3 ppm in the basaltic andesites to 16 ppm in the rhyolites. Mafic to intermediate intrusive rocks show a great deal of scatter and no significant trend can be observed. Intrusive rocks with DI greater than 60 have Nb contents similar to their extrusive equivalents, although some of the leucogranites contain over 20 ppm Nb as compared to the 15-16 ppm in the rhyolites. In general, both suites are characterised by Nb contents that increase with DI and which broadly occupy the same fields.

Thorium

Both suites contain similar levels of Th and show increasing Th with DI. The leucogranites are enriched slightly in Th relative to their extrusive counterparts. Data on Th in other calc-alkaline suites suggest that the levels observed in both extrusive and intrusive suites are relatively high. Jakes and White (1972a) quote levels of between 1 and 3 ppm for typical calc-alkaline lavas (basalt, andesite, dacite) in the circum-Pacific island arcs. Peccerillo and Taylor (1976) report levels of between 2 and 6 ppm Th in a suite consisting of basaltic andesites, andesites and

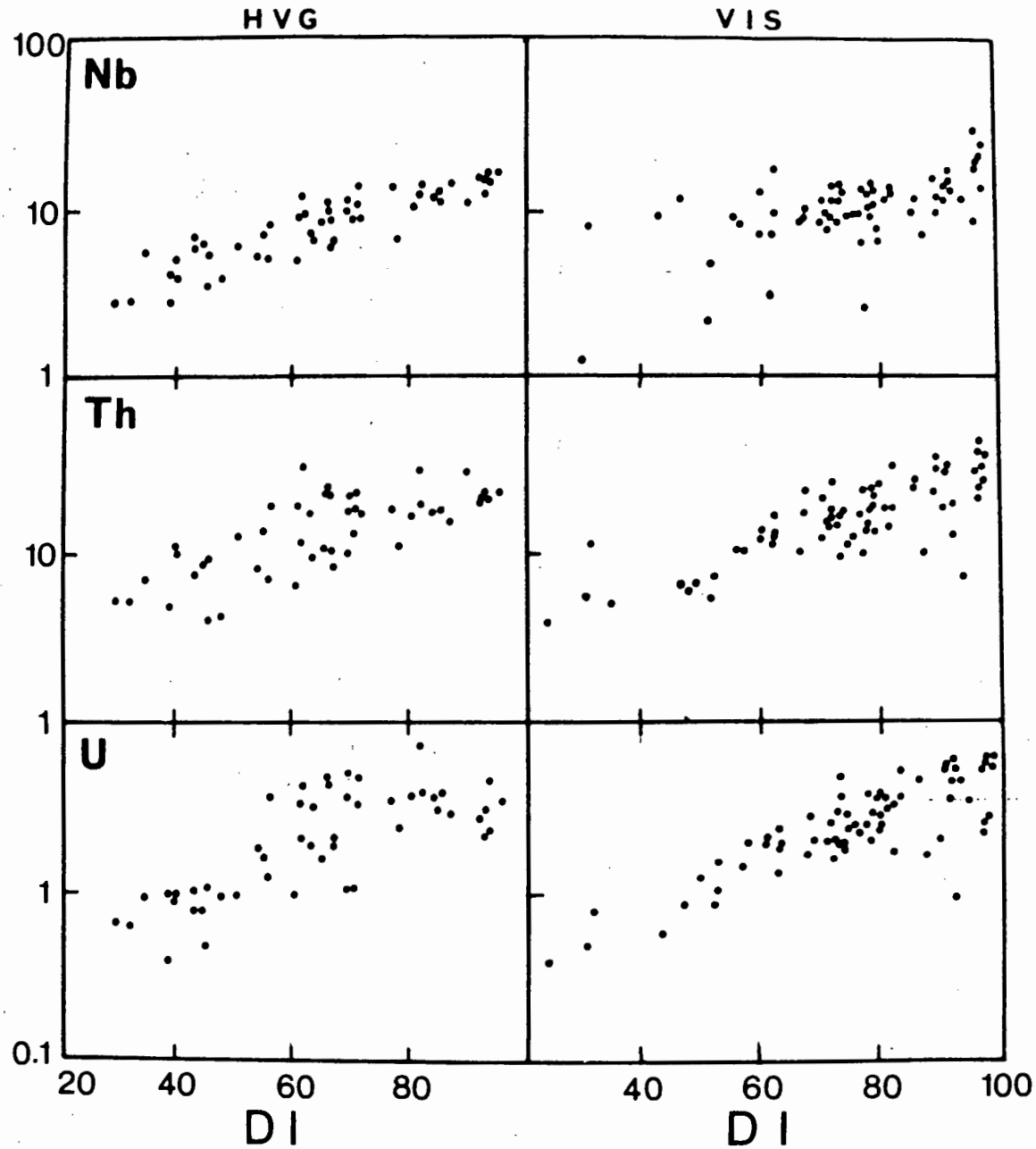

Fig. 62. Plot of trace elements against DI for the HVG and VIS (continued)

dacites. Similar levels of Th (5-15 ppm) are reported by Jakes and Smith (1970) in high K calc-alkaline lavas from New Guinea. Their data also showed a correlation between Th and DI.

The increase in Th with DI and the levels of Th in both suites are similar to those observed in high K calc-alkaline igneous suites and add weight to the previous suggestion of such an affinity.

Uranium

Both suites follow the same average trend of U enrichment with increasing DI. In addition, the fields defined by the scatter of individual data points overlap to a considerable extent. There are two groups of rocks that appear slightly different; the most acid intrusives have higher U than rhyolites, and lavas with DI between 60 and 70 (andesite, dacite) have higher U than their intrusive equivalents. Recent U removal has been noted in some leucogranites analysed in the U-Pb isotopic study (Chapter 3) and as a result, the interpretation of present day U abundances must be treated with caution. However, similar levels of U (1-9 ppm) have been reported in high K calc-alkaline lavas by Jakes and Smith (1970).

Lead

Pb increases with DI in both suites and is present in similar concentrations (15-35 ppm). The average trend is not so well defined in intrusives with low DI, mainly because of the lack of data. High Pb contents in some of the intrusives (three tonalites) are interesting, but cannot be related to any obvious petrographic feature.

Comparable Pb abundances are found in high K calc-alkaline lavas and intrusives (Taylor et al., 1969a; Taylor, 1969; Ewart et al., 1968). Increasing Pb content with DI is also a common feature in the other suites studied. Unfortunately, the amount of data on Pb is small, even though the

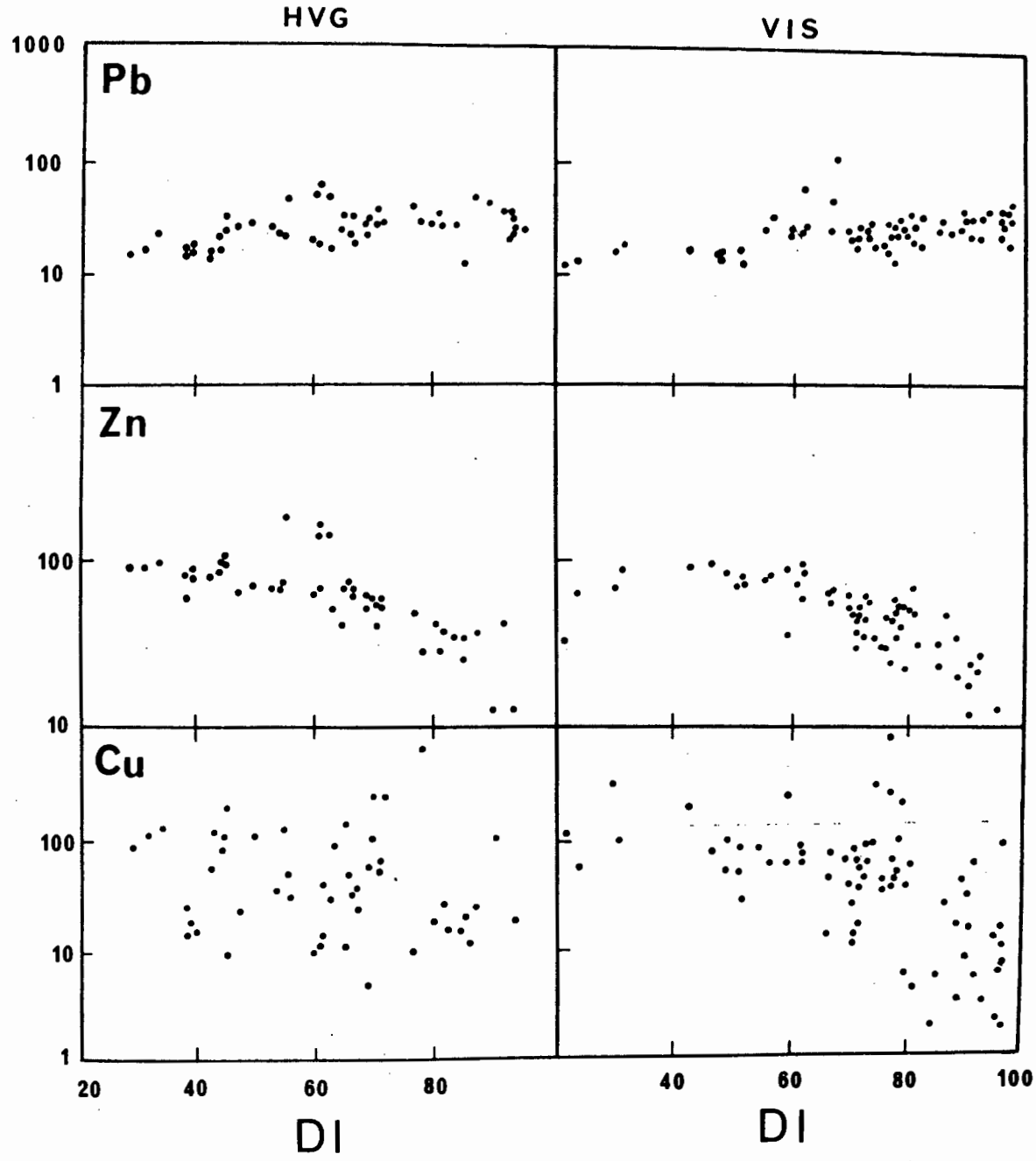

Fig. 62. Plot of trace elements against DI for the HVG and VIS (continued)

amount of Pb isotopic analyses is growing rapidly (e.g. Armstrong and Cooper, 1971; Meijer, 1976).

Zinc

Both suites exhibit similar ranges in Zn abundances and follow almost identical variation trends, which involve the progressive decrease of Zn with DI. Of particular interest are four lavas (porphyritic andesites) with anomalously high Zn contents (greater than 100 ppm). Inspection of the Pb-DI plot shows that the same samples are also high in Pb. All these samples come from the mineralised area near Tsams and this suggests that seemingly unaltered volcanics (see Chapter 7) may be mineralised, resulting in abnormally high Zn (and Pb) contents. Except for the much larger scatter in Zn values for rocks with DI~70-85 (granodiorite-adamellite), the intrusives show no abnormal characteristics similar to the Tsams lavas. Zn content and its behaviour in calc-alkaline suites are poorly known due to lack of data. Granitic rocks described by Sheraton and Black (1973) show decreasing Zn with DI. Taylor (1965) predicted that An should behave in a similar manner to Fe and decrease with differentiation, provided the mechanism of differentiation is fractional crystallisation involving common rock forming silicate minerals. The behaviour of Zn in both suites studied here obeys the empirical rule set up by Taylor. In view of the coherent trends obtained in this study, it is difficult to understand why the analysis of Zn in calc-alkaline lavas and intrusives is so rarely reported.

Copper

In contrast to Pb and Zn, Cu shows extremely wide scatter in both suites, with the lavas being the most striking. Despite the scatter, there is a suggestion of a negative correlation with DI, especially in the intrusives. Calc-alkaline suites where Cu behaves coherently (e.g. Baker, 1968 ; Lowder and Carmichael, 1970), show progressive depletion in Cu

with increasing DI. Erratic behaviour of Cu in calc-alkaline suites seems to be quite common and may be related to the occurrence of extensive, low-grade Cu mineralisation (so-called "porphyry coppers"). Many calc-alkaline suites with which the Haib lavas and Vioolsdrif intrusives may be compared (e.g. Andes, Melanesia, Western U.S.A., Canadian Cordillera) contain a great number of porphyry copper deposits. The Cu mineralisation in the Tsams area north of the Orange River has many lithologic and petrographic similarities with porphyry copper deposits. It is important to note that other base metals such as Pb, Zn and dual lithophile/chalcophile elements such as Ni and Co, behave in a reasonably coherent manner suggesting that their distribution has been controlled by the common rock forming silicates and Fe-Ti oxides. In contrast to these elements, Cu has probably been controlled by other factors such as sulphide phases or perhaps hydrothermal solutions. The latter may be disregarded because of the attempt to avoid samples obviously affected by hydrothermal activity. Although much of the Cu mineralisation is confined to the small area around Tsams, the presence of small quantities of Cu in the form of malachite staining is ubiquitous. There is no correlation between Cu and S, so the erratic behaviour may not be a function of variable Cu-sulphide content. A detailed study of Cu is outside the scope of this project but an important point in such a study would be the contrasting behaviour of Cu, Pb and Zn.

Yttrium

Despite the scatter in Fig. 62, Y shows slight enrichment in the lavas with DI. There are, however, acid lavas with Y contents similar to that of some basaltic andesites. Volcanic rocks most enriched in Y are the non-porphyritic rhyolites (?ignimbrite sheets) with values over 30 ppm. The intrusive suite exhibits a similar field of scatter and comparable lack of significant enrichment with DI.

The apparent narrow range in Y abundances is confirmed when average

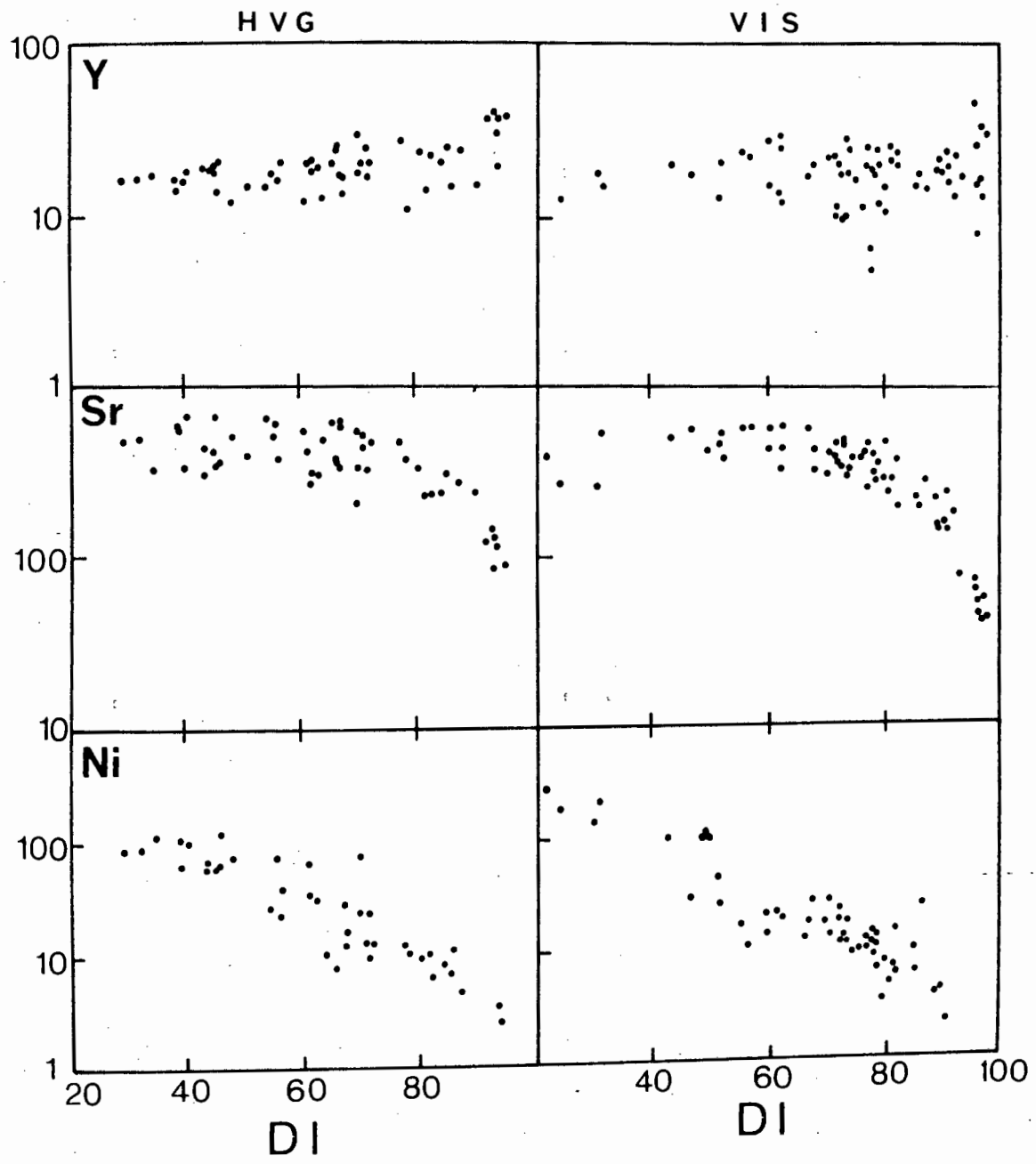

Fig. 62. Plot of trace elements against DI for the HVG and VIS (continued)

data for calc-alkaline suites are inspected (Taylor, 1969; Jakes and White, 1972a). However, Y may show significant enrichment with DI in some suites (e.g. Yeoval Complex, N.S.W., Gulson, 1972; Carboniferous calc-alkaline province of N.S.W., Wilkinson, 1971; Mount Ararat, Lambert et al., 1974). On the other hand, some calc-alkaline suites show depletion in Y with advanced differentiation (Lambert and Holland, 1974). No systematic relationship between Y and the average K content in calc-alkaline suites has been established and the observed levels in the Haib lavas and Vioolsdrif intrusives are similar to averages and ranges quoted in Jakes and White (1972a) and Lambert and Holland (1974).

Strontium

The most important feature of the Sr variation is the marked depletion in rocks with high DI. Both suites have similar ranges in Sr and also define the same average trend. The intrusives show greater depletion in Sr due simply to more advanced differentiation (some of the low Sr leucogranites have DI > 95). The basaltic andesites have, on average, slightly lower Sr than the andesites, which suggests that a maximum Sr content is reached at intermediate DI. A similar but less well defined maximum appears to be reached in the intrusive suite, since the diorites (DI = 45-50) have lower Sr than that in the tonalites (DI = 60).

The relatively high Sr contents in the intermediate rocks (andesite, tonalite) are comparable with those observed in high K calc-alkaline lavas. Sr levels in "normal" lower K calc-alkaline suites are somewhat less. Hence the observed Sr abundances confirm the high K calc-alkaline affinity suggested by the relatively high levels of Ba, Rb, Zr, Th and U.

Nickel

The behaviour of Ni in the two suites is very similar, both in terms of observed ranges (100 ppm to zero) and average trends. Compared to modern

calc-alkaline igneous rocks, the mafic to intermediate lavas and intrusives of the HVIP contain higher Ni contents. Taylor (1969) has highlighted the relatively low Ni contents in calc-alkaline lavas (commonly less than 30 ppm). Jakes and White (1972a) qualify this feature by confining the compositional distinction to rocks with $SiO_2 > 54.0\%$, which implies that less basic rocks such as basaltic andesite and especially andesite are typically low in Ni (<20-30 ppm). Miyashiro and Shido (1975) have demonstrated the relatively low Ni contents in calc-alkaline lavas compared with tholeiites, but appear cautious in following Taylor's assertion about the universally low Ni contents. Several exceptions have been subsequently described (e.g. Hedge, 1971; Zielinski and Lipman, 1976; Noble et al., 1975), so the HVIP mafic to intermediate igneous rocks cannot be regarded as a unique high Ni calc-alkaline suite. Baragar and Goodwin (1969) report high Ni values in "andesites" from the numerous Precambrian greenstone belts of the Canadian shield. These authors do state however, that these intermediate metalavas are transitional to tholeiites and therefore may not be strictly comparable. It still remains a problem as to whether calc-alkaline basaltic andesites and andesites (and their intrusive equivalents) are characteristically low in Ni because of the relative importance attached to this element in various petrogenetic models (e.g. Taylor, 1969; Nicholls and Ringwood, 1972).

Ni abundances in high K calc-alkaline rocks (with $SiO_2 > 54\%$) are more variable, but are often higher than in suites with lower K (McKenzie and Chappell, 1972; Jakes and Smith, 1970; Noble et al, 1975). High K tonalites (SiO_2 = 55-58%) described by Albuquerque (1971) have Ni contents ranging from 92-33 ppm, with an average of 51 ppm. This is similar to the average Ni content in the Haib andesites (58 ppm) but higher than that in the Vioolsdrif tonalites (22 ppm). The latter discrepancy is caused by the more basic nature of the tonalites described by Albuquerque (DI about 50) compared with the Vioolsdrif tonalites (DI about 60) and reflects the ever present problem of inconsistent nomenclature.

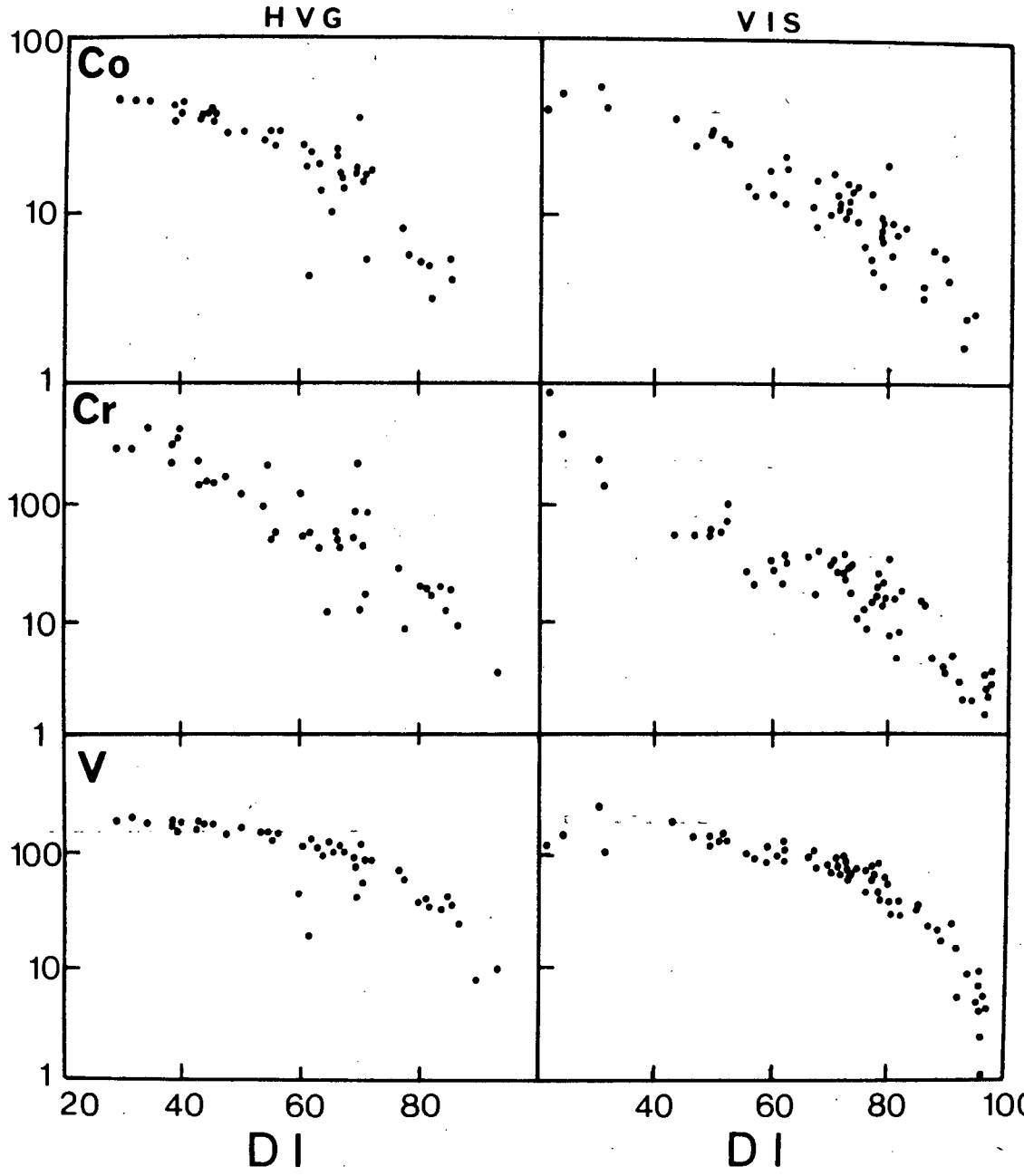

Fig. 62. Plot of trace elements against DI for the HVG and VIS (continued)

Cobalt

Average trends and the range in abundance of Co in both suites are similar. As is to be expected, the Co content drops progressively with increasing DI. Little variation in Co contents of calc-alkaline basaltic andesites and andesites seems to occur (Taylor, 1969; Taylor et al., 1969b; Jakes and White, 1972a), nor is a significant difference in Co content of high K calc-alkaline rocks apparent (Jakes and Smith, 1970).

Chromium

Cr behaves similarly in both suites and the plots may be superimposed with no serious discrepancy. As is expected, Cr drops progressively with increasing DI. Average Cr contents in basaltic andesites (85 ppm) and andesites (56 ppm) listed in Taylor et al., (1969b) are considerably lower than those observed in the Haib lavas and intrusives. The various calc-alkaline suites (both extrusive and intrusive) described by Nockolds and Allen (1953) show quite variable average trends, differing mainly in the Cr contents of the most basic members. Of the spectrum of trends presented by Nockolds and Allen, the most comparable to the HVIP is that displayed by the volcanics of the Medicine Lake Highlands.

Vanadium

Both suites show similar variation trends for V, including the severe depletion in the acid members. The acid intrusives are more depleted because of their greater DI (cf. Sr). The V content of the Haib mafic to intermediate lavas and Vioolsdrif diorites and tonalites are similar to the ranges found by most workers (Taylor et al., 1969b). Jakes and White (1972a) have suggested that high K calc-alkaline lavas and intrusives may have slightly lower V contents, but noted that the range of observed abundances is similar, irrespective of K content. Nockolds and Allen (1953) demonstrated

that various calc-alkaline suites follow a spectrum of average trends in a manner analagous to Cr. The average trend of the HVIP is similar to that displayed by the E. central Sierra Nevada batholith. It is interesting to note that the volcanics of the Medicine Lake Highlands have significantly lower V contents, although these lavas display a similar Cr variation trend to that observed for the HVIP.

14.2 Discussion

The abundances of Ba, Rb, Zr, Th, U and Sr in the Haib lavas are enriched relative to "average" calc-alkaline lavas (basaltic andesite to dacite), but are similar to high K calc-alkaline suites. The suspected affinity with high K suites is therefore confirmed by the observed trace element composition. The intrusive rocks show very similar trace element abundances to the lavas and may be regarded as a plutonic equivalent of a high K calc-alkaline suite.

Despite the general parallelism with the associated extrusives, the intrusives exhibit some important differences in trace element composition, such as severe depletion in Ba and to a lesser extent in Zr, at high DI. Trace elements that show a negative correlation with DI (Zn, Sr, Ni, Co, Cr, V) show almost identical behaviour in both intrusive and extrusive suites. In addition, the observed abundances are similar throughout the range of DI so that the individual plots may be superimposed without serious discrepancy. The observed range in Cr, V and Co abundances, together with average trends, are similar to other calc-alkaline suites. If the Ni data quoted by Taylor (1969) and Jakes and White (1972a) are taken as being typical for calc-alkaline suites, then the observed Ni contents of the HVIP mafic to intermediate rocks are significantly higher than typical basaltic andesites and andesites.

15

PETROGENESIS OF THE HAIB LAVAS

Eruption of lavas which vary from basaltic andesite to rhyolite, automatically implies the existence of magmas exhibiting the appropriate compositional range. The fundamental factors responsible for the variation in magma compositions are:

(1) Fractional crystallisation (includes crystal settling)

(2) Contamination (includes magma mixing)

(3) Partial fusion (includes variation in source composition)

Separating these processes is admittedly somewhat artificial, since magmas are initially generated by partial fusion and possibly experience variable amounts of fractional crystallisation during their ascent (O'Hara, 1968). Partial fusion alone is not considered to be responsible for the range in lava compositions encountered, because this implies that every lava constitutes a separate primary melt, which is considered highly unlikely. If the presence of a limited number of primary magmas is conceded, then the entire spectrum of lavas must have been produced by the superimposition of the other two processes (1 and 2 listed above) on the partial melting process.

Pervasive metamorphism (resulting in a lack of primary minerals amenable to analysis) and ill-defined variation trends, render the lava suite unsuitable for rigorous quantitative evaluation of possible petrogenetic models. As a result, a semi-quantitative approach has been adopted and the evaluated models have been restricted to those which offer the simplest explanation.

15.1 Models involving contamination

Porphyritic lavas ranging in composition from basaltic andesite to rhyolite have isotopic characteristics which fall on well-defined Rb-Sr, Th-Pb and Pb-Pb isochrons, which indicate that they all had the same Sr and Pb isotopic composition at the time of eruption. Possible contaminants are

therefore restricted to cogenetic igneous material of contrasting chemical composition, or material with no Sr or Pb. The latter is considered unlikely and there is no compelling evidence to suspect widespread contamination by solid material (e.g. presence of abundant xenoliths and xenocrysts).

The degree of scatter in the major element variation diagrams is such that it is equally feasible to fit smooth curves or straight lines to define the average trends. It is therefore not possible to discount the presence of mixing lines as opposed to trends produced by other processes. The pronounced changes in slope of the Al_2O_3 -DI and TiO_2-DI trends (Fig. 43) are difficult to explain by the mixing of two end members, but would be consistent with three mixing lines involving four separate magmas. An assumption underlying the process of magma mixing, is that the separate magmas have been derived independently and have only come into contact immediately prior to eruption (Anderson, 1976). This raises the question as to the origin of the different magmas, bearing in mind that they must be cogenetic in order to be consistent with the Sr and Pb isotopic data. That the different magmas have been derived from a common parent at separate times and/or places and mix subsequently, seems unnecessarily complicated and very difficult to recognise. Much of the evidence for magma mixing is petrographic (e.g. incompatible phenocryst assemblages, inter-mingling of two or more different glasses) and is therefore susceptible to being obscured by metamorphism.

No lava suite as complete as the HVG has ever been seriously explained entirely in terms of magma mixing; this process has usually been invoked for certain parts of a suite where there is abundant petrographic evidence for it (Larsen *et al.*, 1938). Certain lavas within the HVG may have been the result of magma mixing, but the badly preserved state of all the rocks preclude a positive identification of such a petrogenetic process and thus it will not be further discussed.

15.2 Models involving fractional crystallisation

Rigorous quantitative evaluation of possible petrogenetic models involving fractional crystallisation is seriously hampered by the lack of data

for phenocryst compositions. Apart from relict plagioclase and quartz, no fresh phenocrysts were encountered. This is particularly unfortunate in the case of mafic lavas, since it has not been possible to identify any mafic silicate phases, although their presence is indicated by abundant pseudomorphs.

A fundamental assumption upon which many models involving fractional crystallisation are based, is that the trends shown in Chapters 8 and 14 represent a liquid line of descent. In other words, for a given DI, the major and trace element composition for any liquid may be estimated from the trend lines. It is quite likely that many porphyritic lavas are phenocryst enriched, with the result that their compositions fall off the liquid line of descent. The effects of possible phenocryst accumulation may be overcome if a large number of samples are analysed, because these effects will probably appear as scatter about average trend lines. For the purposes of this study the average trend has been modelled, rather than the composition of any particular lava. The first model evaluated involves the assumption that the average trend represents a liquid line of descent. An alternative model for the origin of the most basic lavas in the HVG (basaltic andesite) by crystal accumulation, has also been evaluated.

Average trend lines have been fitted through the major and trace element plots (Figs. 43 and 62) and estimated liquid compositions have been read off at pre-determined intervals. The average trends were first estimated visually and then reproduced by polynomial regression analysis. All average trends approximated either first order (linear) or second order polynomial curves. Table 23 lists the estimated liquid compositions which correspond to the following natural magma types:

(i) BA Basaltic andesite
(ii) BA1 Basaltic andesite; maximum TiO_2 content
(iii) A Andesite; maximum Al_2O_3 content
(iv) D Dacite; arbitrarily chosen at DI = 70
(v) R Rhyolite; porphyritic variety, with DI = 80-93
(vi) NR Rhyolite; non-porphyritic variety, with highest DI (>90)

	BA	BA1	A	D	R	NR
SiO_2	54.6	58.0	62.6	65.8	71.1	74.2
TiO_2	.70	.80	.68	.60	.29	.34
Al_2O_3	14.4	15.8	16.2	15.9	14.5	13.7
FeO	9.3	7.5	5.6	4.4	2.3	1.3
MnO	.17	.14	.11	.10	.04	.03
MgO	8.5	5.8	3.3	2.10	1.1	.28
CaO	9.0	7.0	5.2	4.0	2.7	.71
Na_2O	1.8	2.3	2.7	3.0	2.9	3.4
K_2O	1.3	2.4	3.4	3.9	4.8	5.7
P_2O_5	.21	.23	.21	.18	.08	.03
DI	29.7	40.0	60.7	70.0	81.4	93.2
mg	62.0	58.0	51.2	46.1	46.0	27.7
Ba	719	830	960	1113	985	1468
Rb	40	82	128	154	218	227
Zr	109	132	152	167	188	305
Nb	3.2	5.0	7.3	8.9	12.9	15.4
Th	4.9	8.4	13.1	16.2	18.6	21
U	.7	1.0	2.3	2.9	4.0	2.9
Pb	15.3	22	30	26	29	32
Y	17.6	18.1	19.4	21	22	39
Sr	450	525	485	390	246	128
Ni	125	73	35	20	8.0	nd
Co	47	36	21	11	2.7	nd
Cr	420	165	63	35	18	nd
V	200	180	123	74	40	nd
Zn	92	86	72	58	33	39

Table 23. Liquid compositions used in the modelling study. All Fe has been expressed as FeO and the major element compositions have been recalculated to 100 percent volatile free.

Sources of data are the variation diagrams (Figs 43 and 62)

DI = Differentiation Index, mg = 100 MgO/(MgO + FeO) mole percent

The fractional crystallisation model has been subdivided into a series of steps (BA-BA1, BA1-A and so on), each of which has been evaluated separately. There have been a variety of approaches adopted towards petrogenetic modelling in recent literature (e.g. only major elements, Erikson, 1977; only trace elements, Allegre *et al.*,1977; Major and trace elements, Ewart *et al.*, 1973). The author believes that, ideally, the major elements should be modelled first and subsequently tested for consistency with trace elements. However, the metamorphosed nature of the lava has precluded this totally objective approach and trace element data have had to be used to obtain information on possible crystallising phases. As a result, certain sections involve the discussion of both major and trace elements together.

15.2.1 Basaltic andesite to Andesite (BA-BA1, BA1-A)

Inspection of thin sections of basaltic andesite reveals the presence plagioclase and a Fe-Ti oxide (magnetite) as subordinate primary phenocryst phases. The dominant phenocrysts are of some mafic silicate (or silicates) which are now replaced mainly by actinolite and chlorite. A clue to the possible identity of this phase (or phases) comes from inspection of Fig. 63, which summarises the change in major element composition in the passage from basaltic andesite (BA) to andesite (A).

Common phenocryst phases in modern, fresh basaltic andesites (in addition to plagioclase and magnetite) include olivine, orthopyroxene, clinopyroxene (augite) and sometimes hornblende. Olivine is probably not present because of the fairly strong quartz normative nature of the basaltic andesites and the absence of distinctive alteration products (e.g. serpentine, bowlingite, iddingsite, talc, Mg-Fe amphiboles, secondary magnetite). Since differentiation is in the direction of increasing normative quartz, it is unlikely that olivine will persist for any significant crystallisation interval without reacting with surrounding liquid to produce orthopyroxene. If average compositions of the other common phenocryst phases are adopted, it is possible to construct control lines which represent the behaviour of magmas affected by the removal of any of these phases. Table 24 lists the adopted major element

Table 24. Estimated compositions of the common phenocryst phases in basaltic andesites. The control lines in Fig. 63 and 64 were constructed using OPX(1), CPX(1), HBL(1), MT and PLAG (An_{60}).

	OPX		CPX		HBL		MT	PLAG	BIOT
	1	2	1	2	1	2			
SiO_2	53.0	53.2	50.0	50.7	46.5	48.9	0	53	39.0
TiO_2	.2	.2	.2 - 1.0		2.0	1.1	15	0	1.6
Al_2O_3	1.0	1.0	2.0	2.0	7.7	8.5	0	30	16.5
FeO	17.0	19.1	10.5	13.3	16.1	18.6	80	0	20.5
MgO	26.8	24.4	17.8	15.4	13.7	9.5	0	0	12.7
CaO	2.0	2.1	19.0	17.9	11.5	11.9	0	12.5	0
Na_2O	0	0	.2	.2	1.4	.9	0	4.5	.06
K_2O	0	0	0	0	1.1	.5	0	0	9.6

compositions of the various phenocryst phases. MgO and FeO^* contents of the pyroxenes have been calculated from the average compositions reported by Ewart (1976a). CaO in the clinopyroxene has been estimated from the pyroxene quadrilateral (Ewart, 1976a, Fig. 3a). Al_2O_3, TiO_2 and Na_2O in the clinopyroxene are typical values, as are TiO_2 and CaO in the orthopyroxene. Ewart (1976a) found that typical Fe-Ti oxides in basaltic andesite lavas are usually members of the magnetite-ulvöspinel series (sometimes referred to as titanomagnetite or simply magnetite) and are commonly poor in TiO_2 ($<Usp_{50}$). An arbitrary composition of $Mt_{60}Usp_{40}$ (TiO_2 = 15 %) was chosen for the control line diagrams, but the FeO^* and TiO_2 contents of any titanomagnetite are so much higher than the basaltic andesite (BA) that little change in slope results from varying the composition. The An content of the plagioclase is an average of a limited number of EMP analyses. Individual spot analyses yield compositions from An_{70} to An_{53} (average An_{60}), which is considered to represent a minimum range since advanced alteration precludes a systematic study.

The most difficult composition to estimate is that of hornblende, since MgO, FeO^*, Al_2O_3 and TiO_2 may vary quite considerably in rocks of this composition (Jakes and White, 1972b ; Cawthorn, 1976a). The composition listed in Table 24 has been estimated from published analyses, keeping in mind that $(MgO/FeO^*)_{hbl}$ is usually lower than that for pyroxenes crystallising from the same melt, but still higher than that for the magma. In addition, hornblendes from calc-alkaline extrusive rocks are commonly higher in TiO_2 but lower in Na_2O and K_2O, relative to the magma (Cawthorn, 1976a).

Since plagioclase and magnetite occur as phenocryst phases in the Haib basaltic andesites, they need to be considered first as possible fractionating phases. Simultaneous crystallisation of the two phases could produce the observed Al_2O_3-SiO_2 path (Fig. 63), provided magnetite was dominant. This is not consistent with the MgO-SiO_2 path, because any resultant controlled by these two phases would not coincide with that observed. It must be concluded that another phase (or phases) accompanied plagioclase and magnetite during the presumed fractionation process. The following combinations are possible:

(1) plag+mt+opx
(2) plag+mt+cpx
(3) plag+mt+hbl
(4) plag+mt+opx+cpx
(5) plag+mt+opx+hbl
(6) plag+mt+cpx+hbl
(7) plag+mt+cpx+opx+hbl

plag = plagioclase, mt = magnetite, opx = orthopyroxene, cpx = clinopyroxene, hbl = hornblende.

Combination (1) could produce the Al_2O_3-SiO_2 path, provided opx and mt were dominant. The latter mineral occurs as volumetrically insignificant microphenocrysts, so it must be assumed that opx is the dominating phase. This is inconsistent with the CaO-SiO_2 path, which implies that opx should be less important than plag. Combination (2) could also produce the Al_2O_3-SiO_2 path, but not the CaO-SiO_2 path, because the predicted depletion in CaO would be greater than that observed. Combination (3) is difficult to assess because of the wide range in possible hornblende compositions. Although the chosen hornblende control line lies slightly above the observed MgO-SiO_2

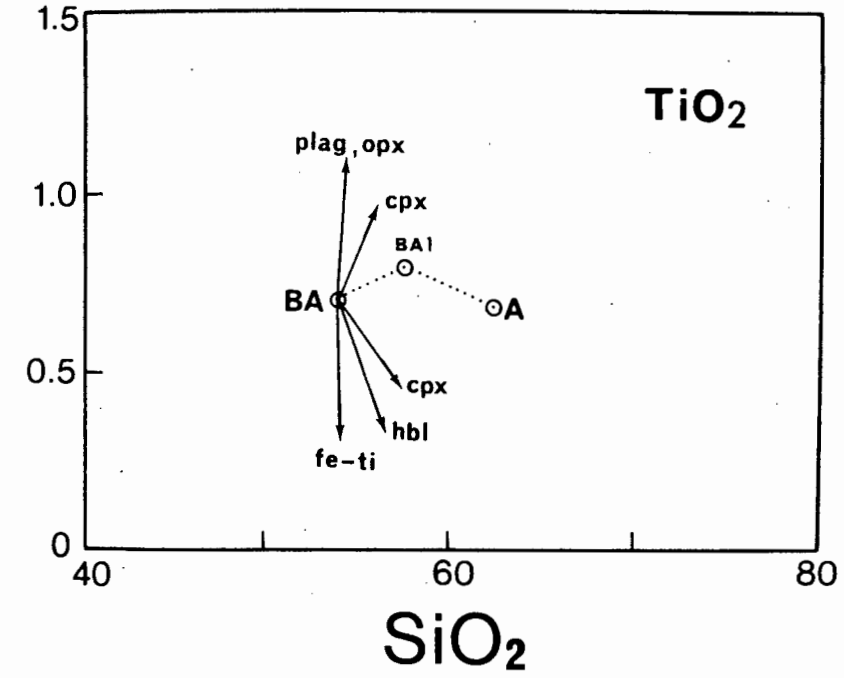

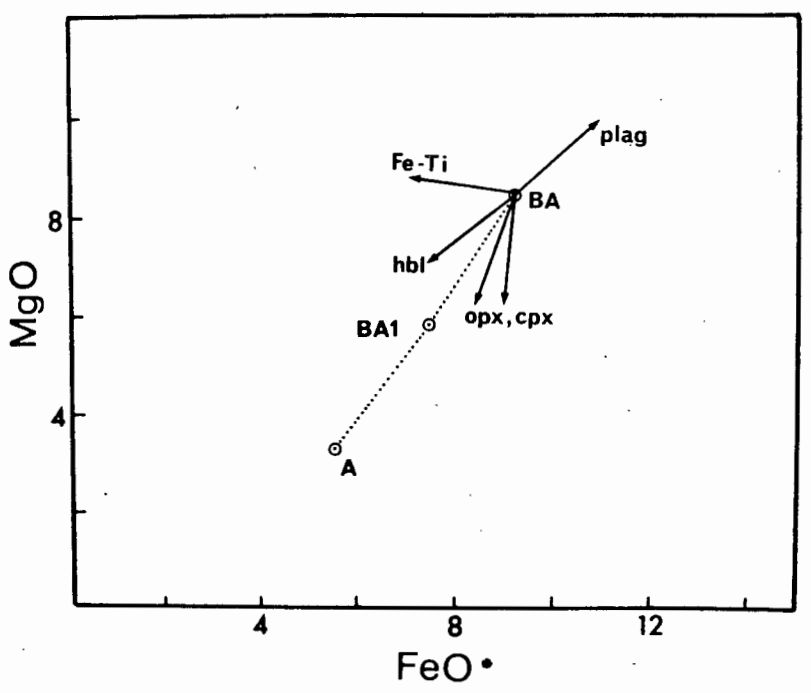

Fig. 63. Plot of average major oxide compositions against SiO_2 for the more basic lavas of the HVG (basaltic andesite, andesite). Vectors represent the path taken by the compositions of residual liquids during the removal of the appropriate mineral. opx = orthopyroxene; cpx = clinopyroxene (augite); hbl = hornblende; Fe-Ti = magnetite; plag = plagioclase.

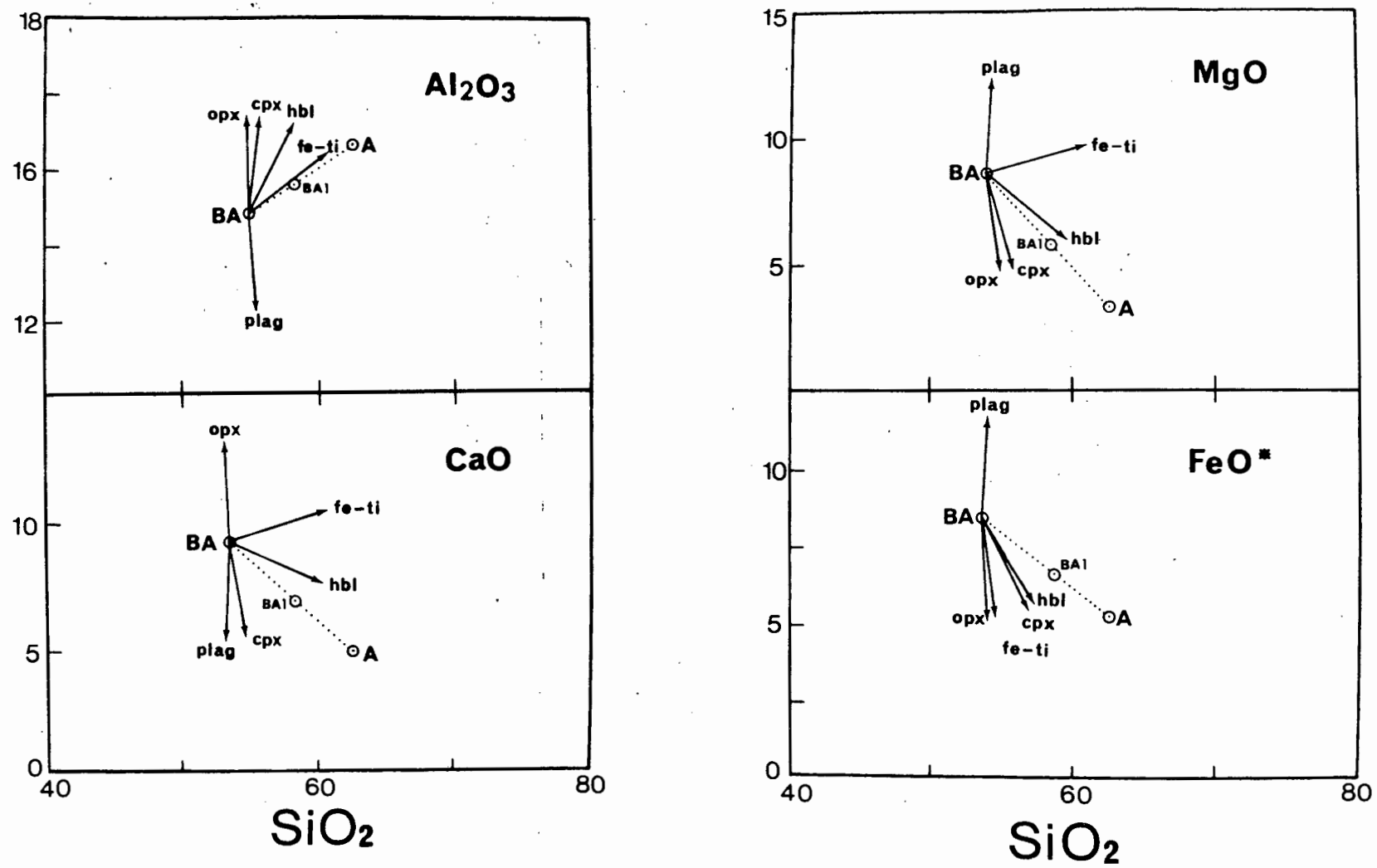

Fig. 63. Continued

path, the range in MgO content in natural hornblendes in basaltic andesites will probably result in a fan of control lines straddling the observed path (BA-A). This implies that the Haib andesite could have been derived by simple hornblende fractionation. Suitable choice of Al_2O_3, FeO^* and MgO contents in the predicted hornblende could produce control lines that coincide with the observed paths. However, the CaO content of most hornblendes in basic/intermediate lavas does not show similar variability (Jakes and White, 1972b, Cawthorn, 1976a) and the control line in the $CaO-SiO_2$ plot diverges significantly from the observed trend. Co-precipitation of plagioclase could shift the resultant nearer the observed $CaO-SiO_2$ path, but would upset the resulting control lines in the MgO- and FeO^* - SiO_2 plots. Furthermore, removal of large amounts of hornblende would deplete the magma in TiO_2, since this mineral contains more TiO_2 than BA. This is inconsistent with the initial increase in TiO_2 in the passage from BA to A. A more complex combination such as (4) is possible, involving two mafic silicate phases, provided cpx and opx together dominate over plagioclase. This condition will satisfy the $Al_2O_3-SiO_2$ path and the co-precipitation of opx will offset the depletion in CaO caused by cpx-plag fractionation. Combination (5) suffers from the inability to produce the observed depletion in CaO, because of the restriction on the relative proportions of plagioclase in the crystallate. Combination (6) could produce the required paths, provided cpx dominated over hbl. Pyroxenes must dominate over hbl if combination (7) is to be feasible. The final important feature of the major element variation, is the $MgO-FeO^*$ plot shown in Fig. 63. Since both pyroxenes will have higher MgO/FeO^* ratios than BA, removal of these minerals will enrich the residual magma in FeO^*, such that MgO/FeO^* will decrease. Plagioclase contains no significant FeO^* or MgO, so removal of this mineral will not affect the MgO/FeO^* ratio of the magma. If the MgO and FeO^* content of both pyroxenes are allowed to vary within the limits established by Ewart (1976a), the resulting fan of possible opx/cpx control lines corresponds to the wide arrow shown on the diagram. The observed path falls significantly away from the fan of pyroxene control lines, suggesting that a phase with lower MgO/FeO^* must have accompanied pyroxenes and plagioclase during fractionation. Possible low MgO/FeO^* minerals are

hornblende and magnetite and the separation of one or both of these phases will offset the Fe-enrichment caused by pyroxene-plagioclase fractionation. Since magnetite is present in the lavas, it is not unreasonable to conclude that this mineral is responsible for counteracting the Fe-enrichment. The effect of removing magnetite or hornblende can be more clearly evaluated by reference to Fig. 64, where the length of each control line represents 10% fractionation. Inspection of Fig. 64 reveals that magnetite is far more efficient in counteracting the Fe-enrichment than hornblende. Far less magnetite is necessary to produce the observed MgO-FeO* path than hornblende.

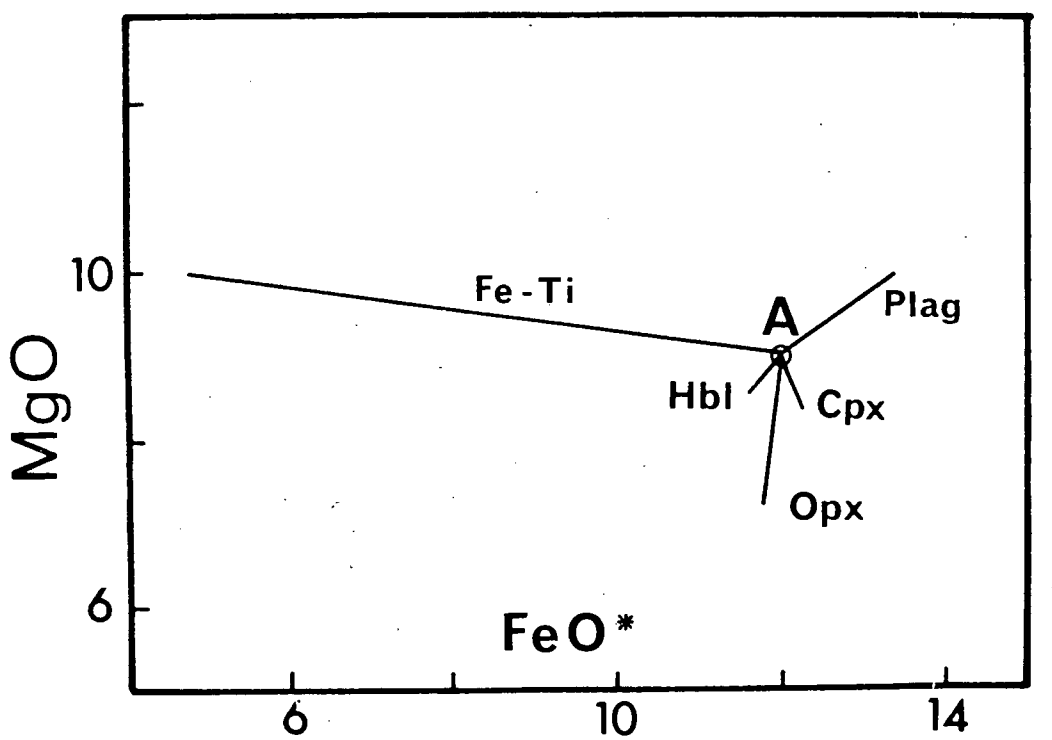

Fig. 64. Path followed by the composition of residual liquids during the removal of various minerals from a magma with composition A. The length of each control line represents removal of 10 percent of each phase. Mineral names abbreviated as in Fig. 63.

This latter point has an important bearing on the observed path in the TiO_2-SiO_2 plot. If magnetite separates along with two pyroxenes and plagioclase, the bulk TiO_2 content of the crystallate must be lower than 0.6 %. Such a value is obtained if the observed TiO_2-SiO_2 path (BA-BA1) is extrapolated back until

the bulk SiO_2 content of the crystallate is reached (45-50%, judging from the SiO_2 content of the pyroxenes and plagioclase; see Table 24). Almost all the TiO_2 in the crystallate removed from BA will be contributed by magnetite. Assuming the magnetite to contain about 15% TiO_2 (Usp_{40}), then the maximum weight fraction of the opaque oxide will be 0.4 (i.e. 4%). The actual weight fraction of BA that is required to crystallise as magnetite will be smaller, but depends on the relative amount of the other phases. It is clear however, that small quantities of magnetite will pull the resulting control lines nearer the observed $MgO-FeO^*$ path in Fig. 63.

The preferred fractional crystallisation model involves the removal of orthopyroxene, clinopyroxene and subordinate plagioclase and magnetite from BA to produce the transitional basaltic andesite BA1. Further fractionation involving the same minerals may produce the andesite (A), provided magnetite makes up a slightly greater proportion of the crystallate. The increased importance of magnetite is necessary to produce the slight change in slope of the $MgO-FeO^*$ path. In contrast to the passage from BA to BA1, derivation of the andesite (A) from BA1 involves progressive depletion in TiO_2. The bulk SiO_2 content of the crystallate removed from BA1 to produce A is probably very similar to the solid removed from BA to yield BA1. As a result, the TiO_2 content of the crystallate necessary to produce the observed depletion in the residual magma is about 1.0%, which corresponds to a maximum magnetite component of about 6.7%. This implies that the percentage of magnetite in the crystallate, in the passage from basaltic andesite to andesite, is initially about 4% (BA-BA1) and subsequently increases to 6.7% (BA1-A).

To summarise, if fractional crystallisation is invoked as a model to produce the Haib andesites, then the most likely mechanism is the progressive removal of two pyroxenes, plagioclase and magnetite. Choice of appropriate weight fractions can produce the observed variation trends in the major elements, in particular the progressive increase in Al_2O_3 and the lack of strong Fe-enrichment. These conditions are satisfied if pyroxenes dominate over plagioclase and magnetite makes up between 4 and 7 % of the solid material removed from the Haib basaltic andesite.

Fractionation of the above minerals suggests that certain trace elements, because of their very low crystal/liquid distribution coefficients, will be preferentially enriched in the residual magma. Such elements have been commonly referred to as "incompatible" (Ringwood, 1966) or "hygromagmatophile" (or simply H) elements (Allegre *et al.*, 1977) and in this case include Rb, Nb, Th, U and Pb. Other trace elements such as Ba, Zr and Y have crystal/liquid distribution coefficients that depart significantly from zero for some of the minerals involved (e.g. Ba in plagioclase, Zr and Y in clinopyroxene) but their average solid/liquid distribution coefficients may be effectively zero. Potassium will also behave as an incompatible element, since it is not a major constituent of the postulated fractionating minerals. Since $D^i_{xstal/liq} \simeq 0$, it follows that

$$\frac{C^i_l}{C^i_o} \simeq \frac{1}{F} \qquad (1)$$

$D^i_{xstal/liq}$ = crystal/liquid distribution coefficient for trace element i (subsequently abbreviated to D^i)

C^i_l = concentration of element i in residual liquid

C^i_o = concentration of element i in original liquid

F = weight fraction of original liquid remaining

It follows from equation (1) that the respective F values for the first two steps (BA-BA1, BA1-A) may be estimated from the incompatible elements by calculating the appropriate ratios (e.g. C^{Rb}_{BA}/C^K_{BA1}, C^K_{BA1}/C^K_A, etc.). Table 25 lists the various ratios and it is immediately obvious from the spread in values (especially for the first step BA-BA1) that either these elements have not behaved as truly incompatible elements, or some other processes have controlled their behaviour.

In the first step (BA-BA1), Rb and K show the greatest degree of enrichment, which therefore implies that they are the most incompatible. That K and Rb have D^i values < .1 for opx, cpx, plag and mt has been confirmed both by experiments (Shimizu, 1974) and by direct measurement of phenocryst/groundmass pairs (Hart and Brooks, 1974, Philpotts and Schnetzler, 1970).

Table 25. Ratios of various incompatible trace elements (e.g. C^i_{BA}/C^i_{BA1}) for the fractionation steps evaluated in this chapter.

	BA-BA1	BA1-A	A-D
K	0.54	0.71	0.87
Rb	0.50	0.64	0.83
Nb	0.64	0.69	0.82
Th	0.58	0.64	0.81
U	0.70	0.44	0.79
Pb	0.69	0.74	1.15
Ba	0.87	0.86	0.86
Zr	0.83	0.87	0.91
Y	0.97	0.93	0.92

Other incompatible trace elements such as Nb, Th and U are relatively low in abundance (<10 ppm) and show a great deal of scatter (see Fig. 62) about any presumed average trend line. The scatter is large compared to the absolute abundances and as a result, the ratios (e.g. C^{Nb}_{BA}/C^{Nb}_{BA1}, etc.) are subject to a great deal of uncertainty. Zr and Ba are much more abundant and although the absolute scatter may be greater than that observed for Th and U, the relative scatter is less. Furthermore, the ratios for these two incompatible elements are similar, being 0.83 and 0.87 respectively (Table 25). If an average F value of 0.85 is adopted, it automatically highlights a problem with K. This major element displays a degree of enrichment greater than that predicted for F = 0.85 and would imply that either BA has lost some of its K or BA1 has gained K. Inspection of Fig. 61, which displays the variation of K_2O with DI, reveals that the average trend for K is reasonably well defined, especially for the most basic lavas. The amount of scatter increases with DI and the points corresponding to BA1 and A are not so well defined as for BA, but are probably better defined than for most of the trace elements. K yields an F value of 0.54, which implies 46 percent crystallisa-

Results for Basaltic Andesite (BA1)

	Obs.	Est.	Diff.		X_{mix}	S.D.	X_{solid}
SiO_2	58.00	58.02	.02	BA	1.6958	.0927	
Al_2O_3	15.80	15.78	.02	OPX	-.1900	.0259	.2714
FeO	7.50	7.50	.00	CPX	-.2222	.0272	.3174
MgO	5.80	5.75	.05	PLAG	-.2507	.0281	.3581
CaO	7.00	6.99	.01	MT	-.0374	.0055	.0534
Na_2O	2.30	2.20	.10	TOTAL	.9956	.0655	
K_2O	2.40	2.20	.20				
		$Diff^2$ = .06			F = .5897		

Table 26. Least squares approximation to the Haib basaltic andesite (BA1) by subtracting the listed quantities (X_{mix}) of the suggested phenocryst phases from a parental basaltic andesite (BA).

Explanation

Method based on that described in Bryan et al., (1969), and has been followed in all least squares approximations reported in this study.

None of the major oxides used in the mixing calculations have been weighted, but the least squares solution is biassed by the most abundant oxides (e.g. SiO_2, Al_2O_3).

Obs. = observed composition of the derivative(subtraction) or cumulate (addition).
Est. = estimated composition
Diff. = Abs[Obs. - Est.]
$Diff^2$ = Sum of the squares of the absolute differences
X_{mix} = Weight fractions of the various components (minerals, parent magma) in the mix.
S.D. = uncertainty in X_{mix} expressed as a standard deviation
X_{solid} = recalculated weight fractions of mineral components in the solid removed or added.

Mineral compositions (see Table 24): OPX(1), CPX(1), PLAG(An_{60}), MT

tion to produce BA1 from BA. A least squares approximation to BA1, made using the calculation procedure of Bryan *et al.*, (1969), involves subtraction of the appropriate amounts of the observed and suspected phenocryst phases from BA. The results are listed in Table 26 and closely approximate the predicted relative proportions of pyroxenes, plagioclase and magnetite. The good fit for BA1 has not been taken as proof of fractional crystallisation because the mineral compositions are only approximations. However, the results probably yield a reasonable estimate for F, since the calculation procedure takes all the major elements into account. The calculated F in Table 26 agrees fairly well with that obtained by using the ratio C^K_{BA}/C^K_{BA1}. It is difficult to see how an F value of 0.85 (from Zr and Ba) could be obtained, even if the mineral compositions were allowed to vary within the limits defined in the previous graphical treatments. It is concluded that if fractional crystallisation did occur, then BA1 represents a residual magma after about 40-45 percent crystallisation of BA.

The results for the passage from BA1 to A seem more encouraging. The ratios of some incompatible elements listed in Table 25 show reasonable agreement and define an F value of 0.70 $\pm$ 0.05. The agreement shown by Nb and Th is probably fortuitous because of the great uncertainty in their respective ratios. The most salient feature is the agreement between K, Rb and Pb. Ba, Zr and Y are high again and have similar ratios to those obtained for these elements in the first step from BA to BA1. A least squares approximation to A, using the major elements and estimated mineral compositions, yields an F value of 0.68 (Table 27). This value is similar to that obtained by using K, together with some of the incompatible trace elements. It is concluded that if fractional crystallisation did occur, then the Haib andesite (A) represents the residual magma after about 30 percent fractionation of BA1.

The degree of fractionation implied by the behaviour of major and some incompatible trace elements may be tested further by using those trace elements that show affinity for the crystallising phases. If the distribution of a compatible trace element ($D^i > 1$) between crystals and surrounding liquid is controlled by Rayleigh type distillation (Rayleigh, 1896; Doerner and Hoskins, 1925), then

$$\frac{C_1^i}{C_o^i} = F^{\overline{D^i}} - 1 \qquad (2)$$

Rayleigh fractionation assumes surface equilibrium and allows for the possibility of zoning in crystals. Since volcanic phenocrysts are invariably zoned, this type of crystallisation mechanism is probably the most realistic. The symbols in equation (2) have already been defined, except for $\overline{D^i}$, which represents the average solid/liquid distribution coefficient of trace element i for the phenocryst assemblage, such that

$$\overline{D^i} = D_a^i \cdot X_a + D_b^i \cdot X_b + \ldots \qquad (3)$$

D_a^i = individual distribution coefficient of mineral a
X_a = weight fraction of mineral a in crystallate
By rearranging equation (2) and making $\overline{D^i}$ the subject,

$$\overline{D^i} = \frac{1 + \log(C_1^i/C_o^i)}{\log F} \qquad (4)$$

Table 28 lists $\overline{D^i}$ values for the two steps BA-BA1 and BA1-A, for Sr, Ni, Co, Cr, V and Zn. It is assumed that C_{BA}^i, C_{BA1}^i and C_A^i represent liquid concentrations and that individual distribution coefficients, together with the relative proportions of crystallising phases, remain constant within each step.

The subordinate role played by plagioclase in the first step (BA-BA1) is reflected by the $\overline{D^{Sr}}$ value of 0.75. It is interesting to note that although plagioclase is still subordinate to mafic phases, $\overline{D^{Sr}}$ in the second step (BA1-A) is greater than unity, which reflects a greater affinity of plagioclase for Sr relative to Al. The amount of Sr contained in orthopyroxene and magnetite is negligible compared to that found in clinopyroxene ($D_{cpx}^{Sr} = 0.1$). However, most of the Sr in these rocks is contained in plagioclase and D_{plag}^{Sr} probably makes the greatest contribution to $\overline{D^{Sr}}$. For an An content of between 60 and 70 mole %, Korringa and Noble (1971) estimate D_{plag}^{Sr} to be between

Table 27. Least squares approximation to the Haib andesite (A) by subtracting the listed quantities (X_{mix}) of the suggested phenocryst phases from a parental basaltic andesite (BA1).

Mineral compositions (see Table 24): OPX(1), CPX(1), PLAG(An_{60}), MT

Results for Andesite (A)

	Obs.	Est.	Diff.		X_{mix}	S.D.	X_{solid}
SiO_2	62.60	62.59	.01	BA1	1.4620	.0291	
Al_2O_3	16.20	16.21	.01	OPX	-.1450	.0103	.3142
FeO	5.60	5.60	.00	CPX	-.0866	.0102	.1872
MgO	3.30	3.33	.03	PLAG	-.2025	.0142	.4388
CaO	5.20	5.21	.01	MT	-.0275	.0022	.0596
Na_2O	2.70	2.76	.06	TOTAL	1.0005	.0363	
K_2O	3.40	3.50	.10				
		$Diff^2$ = .02			F = .6840		

Table 28. Average solid/liquid distribution coefficients for the listed trace elements in the various fractionation steps evaluated in this chapter.

	BA - BA1	BA1 - A	A - D	D - R
	F=.55	F=.70	F=.80	F=.73
Sr	.74	1.22	1.97	2.43
Ni	1.90	3.06	3.48	3.9
Co	1.45	2.51	3.87	4.2
V	1.18	2.07	3.26	3.4
Cr	2.56	3.70	3.61	3.1
Zn	1.11	1.50	1.97	2.78
Ba	-	-	-	1.38

Table 29. Crystal/liquid distribution coefficients for the listed trace elements determined for the phenocryst phases in the Tongan lavas. Averages have been calculated from data in Ewart et al., (1973). Inter-mineral relationships for opx, cpx and mt from the data in Ewart et al., (1969). Data for D_{hbl}/D_{biot} from Joyce (1973b).

	OPX	CPX	MT	D_{opx}/D_{cpx}	D_{mt}/D_{cpx}	$D_{hbl/biot}$
Ni	9.0	6.5	19	1.44	3.02	0.63
Co	3.7	1.9	6.2	2.0	2.6	0.80
Cr	15.7	28.6	58	-	-	1.06
V	0.54	1.1	24	0.47	20	0.96
Ba	-	-	-	-	-	0.034

3.8 and 2.5. The experimental data reported by Drake and Weill (1975) suggest a figure of about 2.3 - 2.5. If D^{Sr}_{plag} is taken to be 2.5, then the weight fraction of plagioclase (An_{60-70}) necessary to produce $D^{Sr} = 0.75$ can be calculated from the equation

$$D^{Sr}_{plag} \cdot X_{plag} = \overline{D^{Sr}} \qquad (5)$$

The contribution from clinopyroxene has been neglected because the term $D^{Sr}_{cpx} \cdot X_{cpx}$ is equivalent to $0.1 \cdot X_{cpx}$, which is very small irrespective of the value of X_{cpx}. The value of X_{plag} is 0.30 and this agrees well with that predicted, since it implies that pyroxenes and magnetite make up about 70% of the crystallate (i.e. they dominate the fractionation process).

It is more difficult to evaluate the other compatible trace elements (Ni, Co, Cr, V) because they all enter orthopyroxene, clinopyroxene and magnetite. A set of simultaneous equations may be set up, provided reasonable estimates of individual D^i values can be made, but this is where problems occur. Inspection of the literature reveals a wide range in crystal/liquid distribution coefficients for Ni, Co, Cr and V into pyroxenes and especially

Table 30. Estimated crystal/liquid distribution coefficients for the listed elements using equation (6) and the inter-mineral relationships listed in Table 29.

	Ni				Co				V			
	BA-BA1	BA1-A	A - D	D - R	BA-BA1	BA1-A	A - D	D - R	BA-BA1	BA1-A	A - D	D - R
OPX	3.2	5.4	7.6	-	2.9	5.2	10	-	0.4	0.6	1.3	-
CPX	2.2	3.7	5.3	-	1.4	2.6	5	-	0.8	1.4	2.7	-
MT	6.6	11.3	16	(16)	3.8	6.7	13	(13)	15.6	27	54	(54)
HBL	-	-	-	6.6	-	-	-	8.1	-	-	-	5.2
BIOT	-	-	-	10.4	-	-	-	10.1	-	-	-	5.4
	Sr				Ba							
PLAG	2.1	2.8	3.5	4.5	-	-	-	(0.4)				
BIOT	-	-	-	-	-	-	-	6.6				
HBL	-	-	-	-	-	-	-	0.2				

magnetites. Experimental studies have demonstrated the strong influence of temperature, bulk and mineral composition and oxygen fugacity on crystal/liquid distribution coefficients for pyroxenes and magnetite. This probably contributes to the large differences between experimentally derived D^i values and those determined from phenocryst/groundmass pairs.

For example, Mysen (1976) reports a D^{Ni}_{opx} of 1.3 for a synthetic basalt liquid crystallising both olivine and orthopyroxene. Leeman (1976) has utilised published D^{Ni}_{ol} (Leeman, 1974) and $D^{Ni}_{opx/ol}$ (Mercy and O'Hara, 1967) to calculate a D^{Ni}_{opx} value of 3.8. Ewart *et al.*, (1973) found a range in D^{Ni}_{opx} from 5.6 to 8.4 in basaltic andesites from Tonga. All these figures are subject to uncertainties which seriously limit their applicability. The same can be said for the other elements and minerals.

A commonly used method to attempt to overcome the possible effects of temperature, composition, etc., is to use D^i values obtained from similar lavas or from experimental systems closely approximating those of the rocks studied. If such a procedure is to be followed, the most likely choice is the study of Ewart *et al.*, (1973). The basaltic andesite lavas described by these authors show some similarities to the Haib lavas (e.g. presence of two pyroxenes and plagioclase as phenocryst phases). There are many important differences however, but the Tongan lavas still remain the best choice. Average D^i values for orthopyroxene and clinopyroxene in the Tongan basaltic andesites and andesites are listed in Table 29, together with some information on magnetite from a Tongan andesite.

The weight fractions X_{opx}, X_{cpx} and X_{mt} may be calculated from a series of equations of the type,

$$D^i_{opx} \cdot X_{opx} + D^i_{cpx} \cdot X_{cpx} + D^i_{mt} = \overline{D^i} \qquad (6)$$

where i = Ni, Co, Cr, V. The solutions have been estimated by least squares approximation (Bryan *et al.*, 1969) and were found to be impossible, since some of the weight fractions are negative. Similar results were obtained for the second step.

The unsatisfactory results may be a function of the relatively high D^i values used. If the weight fractions of the mafic minerals calculated in the major element approximations (Table 26, 27) are adopted, then it is clear that Ni, Co, Cr and V should all show greater depletion than that which is observed. For example, $\overline{D^{Ni}}$ for the first step (BA-BA1) may be calculated using the average D^{Ni} values listed in Table 29; the figure of 5.5 is far higher than the observed $\overline{D^{Ni}}$ of 1.9.

One possible source of error in the data quoted by Ewart *et al.*, (1973), is the assumption that the modal fractions of phenocryst phases closely approximates the relative proportions in which the phenocrysts crystallised. Addition or subtraction of phenocrysts will introduce serious error in the calculated individual D^i values, although the average D^i values may be correct. Furthermore, since plagioclase phenocrysts are very abundant in the Tongan lavas, incomplete removal of phenocrysts from the groundmass samples will dilute the Ni, Co, Cr and V concentrations. Distribution coefficients calculated from these data will be too high. Phenocryst compositions seem to be more representative, because there are reasonably good correlations between C^i_{opx} and C^i_{cpx}, such that C^i_{opx}/C^i_{cpx} = constant. Ewart *et al.*, (1973) have interpreted these correlations as indicating equilibrium distribution. Results of this type were obtained for Ni, Co and V, but not for Cr, which exhibited erratic behaviour. In view of possible uncertainties in the individual D^i values, more weight has been given to inter-mineral relationships. This implies that the ratio D^i_{opx}/D^i_{cpx} is better defined than the individual D^i values, because the value of the ratio is independent of groundmass concentration by the relationship

$$\frac{D^i_{opx}}{C^i_{opx}} = \frac{D^i_{cpx}}{C^i_{cpx}} \qquad (7)$$

This relationship may also extend to phenocrystic magnetite, although few data are available. The single lava analysed by Ewart *et al.*, (1973), which contained magnetite in addition to orthopyroxene and clinopyroxene, yields the only estimate of D^i_{mt}/D^i_{cpx}.

The inter-mineral relationships described above suggest an alternative approach. A series of equations linking D^i and $\overline{D^i}$ may be derived and solved for D^i rather than for weight fractions. The latter may be estimated from the major element approximations listed in Tables 26 and 27. Equations identical to (6) may be written and solved for D^i. The number of unknowns may be reduced to one per element if the inter-mineral relationships (Table 29) are adopted. The latter are based on the K_d values (= C^i_{opx}/C^i_{cpx}) determined by Ewart *et al.*, (1973). The resulting D^i values are listed in Table 30 and represent those necessary to produce the observed variation trends for Ni, Co and V, if the behaviour of these elements were controlled by simple fractional crystallisation.

Inspection of Table 30 reveals that the D^i values for Ni, Co and V necessary to produce the observed variation in the Haib basaltic andesites and andesites are not unreasonable, provided more weight is given to the lower values reported in the literature. However, there is quite a considerable difference between the two sets of distribution coefficients calculated for the two steps (BA-BA1, BA1-A). In order to remain consistent with fractional crystallisation, the D^i values must increase by nearly a factor of two in some cases. Experimental work has demonstrated the influence of temperature on D^i and predicts higher D^i values for Ni, Co and V for pyroxenes at lower temperatures (Hakli and Wright, 1967; Seward, 1971; Lindstrom, 1976). Although it cannot be proved in this study, the temperature of crystallisation of BA1 was probably lower than for BA and the apparent increase in D^i shown in Table 30 may be interpreted as the influence of temperature. The change in D^i seems to be somewhat excessive (e.g. D^V_{mt} changes from 15.6 to 27), because the crystallisation temperature of the two basaltic andesites (BA, BA1) cannot be all that different (less than 100°C) if the results of Ewart (1976b) are applicable.

To summarise, the results obtained are not altogether satisfactory, but serve to highlight the various difficulties. The uncertainties in distribution coefficients for many different elements between magma and common phenocryst phases also contribute to the problem. No definite conclusion as to the feasibility of the fractional crystallisation model can be made, although the observed behaviour of Ni, Co and V requires D^i_{opx} and D^i_{cpx} to be significantly lower than those obtained by Ewart *et al.*, (1973).

15.2.2 Porphyritic dacites and rhyolites (A-D-R)

The dominant phenocryst in the more acid lavas of the HVG is plagioclase, with subordinate quartz, magnetite and sometimes biotite. The latter mineral was never found in a sufficiently fresh state for analysis. Another mafic silicate (or silicates) occurs, but is completely pseudomorphed by metamorphic minerals.

The change in major element composition in the passage from andesite to rhyolite (DI = 60-83) is shown in Fig. 43. It is clear from the progressive decrease in Al_2O_3, that if the more acid lavas are products of fractional crystallisation of the andesite, then the process probably involves the removal of plagioclase. In addition, the progressive depletion in MgO, FeO^* and TiO_2 indicates the co-precipitation of mafic silicates. The presence of biotite infers that the water pressure was sufficiently high to stabilise hydrous minerals during intratelluric crystallisation. This suggests that amphibole may also have crystallised and perhaps played a significant role in the fractionation process.

The possible influence of amphibole and/or biotite would be reflected by elements such as K, Rb and Ba. In contrast with pyroxenes and plagioclase, removal of amphibole and/or biotite will fractionate K from Rb and Ba. Inspection of D^i values for the two hydrous phases reveals their very different affinities for the three elements. Compound distribution coefficients ($D^{i/j} = D^i/D^j$) are listed in Table 31 and have been calculated from individual D^i and D^j values listed in Arth (1976).

Table 31

Individual and compound distribution coefficients for hornblende and biotite; based on the compilation in Arth (1976)

	D^K	D^{Rb}	B^{Ba}	$D^{K/Rb}$	$D^{K/Ba}$
HBL	.081	.014	.044	5.79	1.84
BIOT	2.5	2.24	9.7	1.11	0.26

It is clear from Table 31 that fractionation of one of the two hydrous phases will produce quite different residual liquids in terms of their K/Rb and K/Ba ratios.

In the passage from andesite to dacite, K/Rb is only slightly lowered from 221 to 210, but decreases markedly in passing to the rhyolite (183). K/Ba remains constant from the andesite (29.4) to the dacite (29.1), but shows a sharp increase in the rhyolite (40.5). These results suggest that hornblende may not be the dominant fractionating phase in the passage from the andesite to the dacite and therefore cannot be responsible for the observed depletion in the ferromagnesian elements. It must be concluded that the other mafic silicates (e.g. pyroxenes) must be involved in the step A to D. On the other hand, amphibole and biotite appear to be important fractionating phases in the production of the rhyolite.

Table 32. Least squares approximation to the Haib dacite (D) by subtracting the listed quantities (X_{mix}) of the suggested phenocryst phases from a parental andesite (A).

Mineral compositions (see Table 24): OPX(2), CPX(2), PLAG(An_{60}), MT

Results for Dacite (D)

	Obs.	Est.	Diff.		X_{mix}	S.D.	X_{solid}	
SiO_2	65.80	65.76	.04	A	1.2525	.0245		
Al_2O_3	15.90	15.99	.09	OPX	-.0627	.0180	.1367	
FeO	4.40	4.40	.00	CPX	-.0343	.0170	.2498	
MgO	2.10	2.18	.08	PLAG	-.1405	.0186	.5598	An_{60}
CaO	4.00	4.04	.04	MT	-.0135	.0036	.0538	
Na_2O	3.00	2.78	.22	TOTAL	1.0016	.0397		
K_2O	3.90	4.26	.36					
		$Diff^2$ = .19		F = .7984				

The inferred absence or subordinate role of amphibole in the intermediate lavas (andesite-dacite) is perhaps surprising, but may be a function of the relatively low Na_2O content of all the Haib lavas. Cawthorn and O'Hara (1975) have concluded from their experiments (Cawthorn, 1976b) that typical calc-alkaline amphiboles (pargasitic hornblende) will only crystallise from liquids with more than 3% Na_2O. Of the presumed liquid compositions listed in Table 23, only the dacite has a Na_2O content that approaches 3%, although early crystallisation of Na-poor minerals may yield a transient interstitial liquid sufficiently high in Na to stabilise amphibole. The fact remains, however, that amphibole could not have been an early fractionating phase in any of the intermediate Haib magmas. It may have been stabilised at a late stage and perhaps a few microphenocrysts did appear, but not in sufficient quantity as to control the composition of successive residual liquids.

A least squares approximation to the Haib dacite is given in Table 32 and involves the removal of two pyroxenes, plagioclase and magnetite. The pyroxene compositions adopted are more Fe rich than those used for the basaltic andesite, in keeping with the well documented decrease in Mg/Fe ratio of pyroxenes with differentiation. The F value obtained for this step (A-D) is 0.80, which agrees reasonably well with the ratios of the incompatible elements (Table 25). Calculated $\overline{D^i}$ values for Sr, Ni, Co and V are listed in Table 28 and are based on $\overline{F} = 0.80$. Assuming that all Sr is contained in plagioclase, then D^{Sr}_{plag} necessary to produce the observed depletion in Sr (485-390) is 3.5, which is in reasonable agreement with that established by Korringa and Noble (1971) for intermediate plagioclase (An_{60}, $D^{Sr}_{plag} = 3.8$).

If the inter-mineral relationships established for the Tongan lavas are retained, individual D^i values may be calculated for opx, cpx and magnetite. These have been listed in Table 30 and it is noteworthy that the values obtained are still higher than those obtained for the earlier step (BA1-A). This implies that D^{Ni}, D^{Co} and D^V must increase with fractionation if the model is to adequately explain the behaviour of Ni, Co and V. There is abundant experimental evidence for the implied temperature dependence (e.g. Lindstrom , 1976; Seward, 1971) and it is to be expected that D^i will increase with

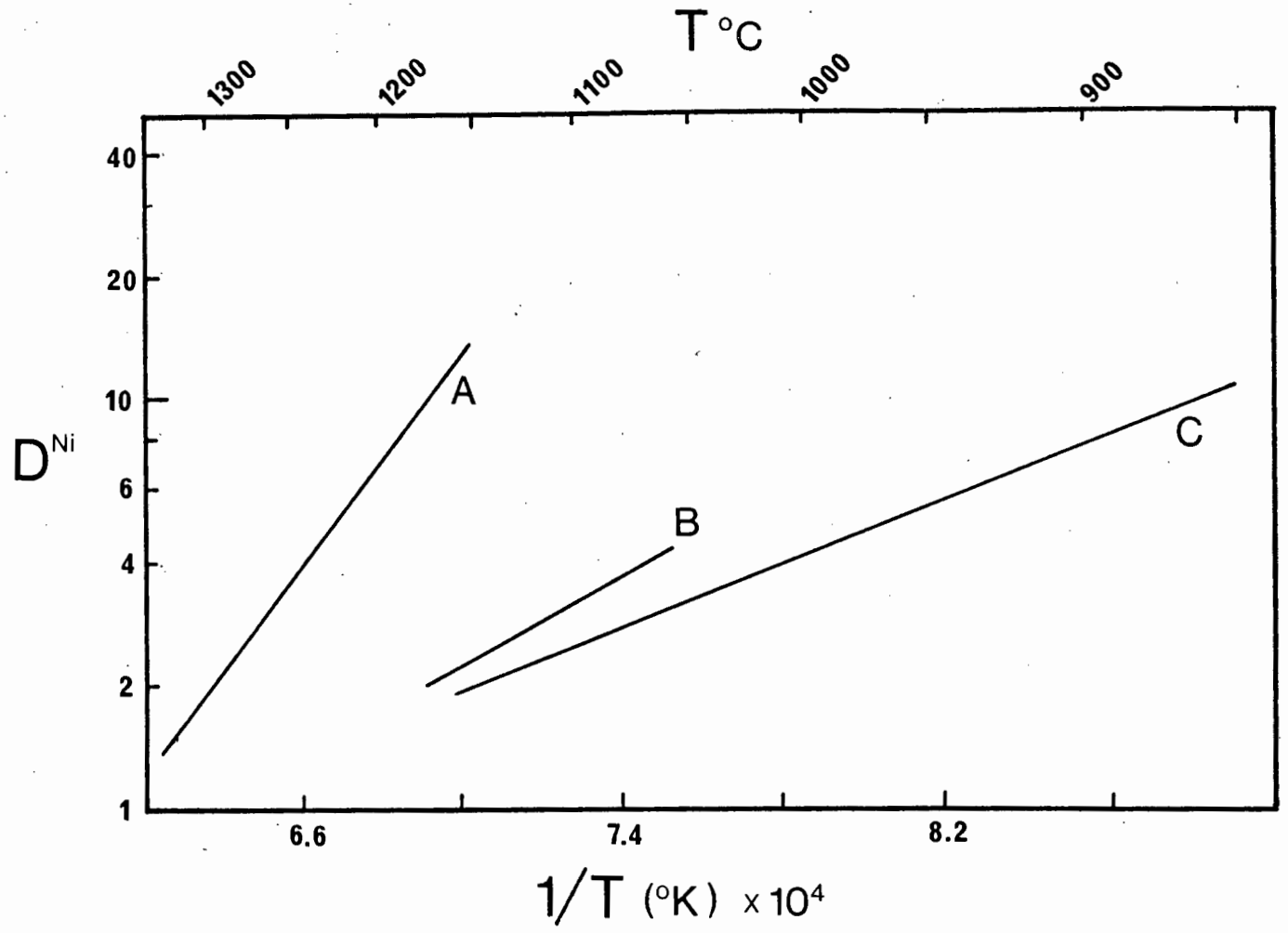

Fig. 65. Variation in D^{Ni}_{cpx} with temperature, as deduced from three independent studies. A = Lindstrom (1976); B = Hakli and Wright (1967); C = Seward (1971).

decreasing temperature of crystallisation. If minerals such as pyroxenes persist throughout a long temperature interval, as implied by their presence in all the Haib lavas from basaltic andesite to dacite, then D^i_{opx} and D^i_{cpx} would be expected to increase. The observed progressive increase in D^i_{opx} and D^i_{cpx} is encouraging and supports the fractional crystallisation model. However, the precise relationship between D^i and temperature is uncertain, because of the conflicting results published in recent literature. Fig. 65 illustrates the relationship between D^{Ni}_{cpx} and temperature, established by three independent studies. The synthetic system of Seward (1971) involved the behaviour of Ni in the binary system $CaMgSi_2O_6$(Diopside) - $Na_2Si_2O_5$, while the synthetic compositions employed by Lindstrom (1976) approach more closely those of natural rocks. The data of Hakli and Wright (1967) are from natural rocks, but which are much more basic than any of the Haib lavas. Many of the synthetic liquids used by Lindstrom (1976) often crystallised orthopyroxene and magnetite together with clinopyroxene and therefore probably represent the most applicable set of data. It is noteworthy that Lindstrom's data imply a fairly rapid increase in D^{Ni}_{cpx} for a relatively small decrease in temperature. For a decrease of 100^oC, D^{Ni}_{cpx} changes by over a factor of two, which is comparable with that suspected for the Haib lavas. Temperature estimates for the onset of crystallisation of basaltic andesites, andesites and dacites span 100^o-200^oC, judging from published data on mineral-mineral equilibration (Ewart, 1976b; Carmichael and Nicholls, 1967) and experimental work (Eggler, 1972; Brown and Shairer, 1968). The relationship between D^i_{cpx} and temperature established by Lindstrom (1976) suggests that the observed change in D^i_{cpx} (and by inference D^i_{opx} and D^i_{mt}) in the Haib lavas may be reasonable.

No plausible results were obtained by attempting to derive the Haib porphyritic rhyolite (R) by fractionation of pyroxenes. However, by substituting hornblende and biotite, a reasonable approximation to R was obtained and the results are listed in Table 33. Hornblende and biotite compositions in the least squares calculations are based on published analyses, with

Table 33. Least squares approximation to the Haib porphyritic rhyolite (R) by subtracting the listed quantities (X_{mix}) of the suggested phenocryst phases from a parental dacite (D).

Mineral compositions (see Table 24): HBL(2), BIOT, MT
Since no plagioclase was analysed in the dacites and rhyolites, pure end members (Anorthite and Albite, see Table 37) were used. The plagioclase composition listed is based on the individual weight fractions obtained by using the end members. The mix was subsequently run again with this plagioclase, in order to obtain an accurate S.D. value. This procedure has been adopted in all subsequent approximations using end members.

Results for Porphyritic Rhyolite (R)

	Obs.	Est.	Diff.		X_{mix}	S.D.	X_{solid}	
SiO_2	71.14	71.14	.00	D	1.3736	.0213		
Al_2O_3	14.54	14.62	.08	HBL	-.1053	.0181	.2781	
FeO	2.29	2.29	.00	BIOT	-.0638	.0152	.1685	
MgO	1.13	1.11	.02	PLAG	-.2023	.0160	.5342	An_{41}
CaO	2.66	2.63	.03	MT	-.0074	.0053	.0195	
Na_2O	2.87	2.59	.28	TOTAL	.9949	.0360		
K_2O	4.82	4.71	.11					
		$Diff^2$ = .10		F = .7280				

MgO/FeO^* adjusted so that it is compatible with that of the dacite. The MgO/FeO^* ratio of hornblende and biotite are near to or slightly higher than that of the magma from which they crystallise (Cawthorn, 1976a; Carmichael, 1967; Nockolds, 1947; Dodge *et al.*, 1969). An F value is difficult to obtain from incompatible trace elements, because of the uncertainty as to which elements have D^i_{hbl} and D^i_{biot} near zero. Certainly none of the investigated elements have D^i values known to be <0.1 and whose abundances are precisely defined in Fig. 62 ; Nb, Th and U show too much scatter to define precise F values. In the absence of any confirmation from trace elements, the F value determined from the least squares approximation (0.73) has been adopted.

Average $\overline{D^i}$ values for Sr, Ni, Co, Cr and V are listed in Table 28 and may be used to calculate individual D^i values provided some inter-mineral relationships are established. There is much data on coexisting hornblende and biotite in acid igneous rocks and thus it is possible to estimate the compound distribution coefficient $D^i_{hbl/biot}$ ($= C^i_{hbl}/C^i_{biot}$). Average $D^i_{hbl/biot}$ for Ba, Ni, Co, Cr and V are listed in Table 31 and have been calculated from published analytical data (Albuquerque, 1973, 1974; Dodge and Ross, 1971; Dodge *et al.*, 1968, 1969; Simon and Rollison, 1976). No data on the relationship between D^i_{mt} and D^i_{hbl} and D^i_{biot} could be found, except for Cr (Simon and Rollinson, 1976). In the absence of any estimates for D^i_{mt}, the values obtained for the previous step (A-D) have been arbitrarily adopted. $D^{Ba}_{plag/biot}$ values have been taken from the data of Joyce (1973b). Individual D^i values for plagioclase, hornblende, biotite and magnetite have been calculated using the weight fractions listed in Table 33 and the derived figures are listed in Table 30.

Assuming that all Sr is contained in plagioclase, then $D^{Sr}_{plag} = 4.5$, which is consistent with the figures reported by Korringa and Noble (1971) for plagioclase (An_{40}, $D^{Sr}_{plag} = 5$). Most of the Ba removed from the dacite during fractionation enters biotite and the value of 6.6 for D^{Ba}_{biot} is within the range obtained by Philpotts and Schnetzler (1970) who have reported values ranging from 6 to 9.

The very small proportion of magnetite in the solid removed, limits the

Table 34. Compilation of individual crystal/liquid distribution coefficients published recently.

	Ni	Co	Cr	V
OPX	1.3(1), 7-11(2), 3.8(3) 6.6(4)	3-6(2), 2.1(5), 3.2(4)	2.0(3), 9-17(2), 2.8(4)	0.4-0.6(2)
CPX	6-8(2), 1.8-4.5(7) 1.5-6(8), 1.4-2.1(9) 4(4,10)	1.7-2.1(2), 0.7-1.2(9) 1.0-1.8(8), 1.0-1.2(10) 1.5(4), 1.12(5)	12(10), 10.33(2), 10(11) 4.8-11.4(9), 15(4)	0.9-1.2(2), 5.5-10(10) 0.2-2.3(8)
MT	19(2), 20-80(11)	6.2,8.0(2), 6-17(11)	58(2), 100-620(11)	24,36(2), 18-22(11)
HBL	3.0(3), 7.2(12), 12(4)	0.9(3),7.5(12), 3.8(4)	12(3)	18(12)
BIOT	3.7(3)	1.1(3)	7 (3)	

Sources: (1) Mysen (1976); (2) Ewart et al.,(1973); (3) Leeman (1976); (4) Allegre et al.,(1977); (5) Onuma et al.,(1968); (6) Arth (1976); (7) Hakli and Wright (1967); (8) Duke (1976); (9) Dale and Henderson (1972); (10) Seward (1970); (11) Lindstrom (1976); (12) Ewart and Taylor (1969)

effect of changing D^i_{mt} in the equations linking D^i_{mt}, D^i_{hbl} and D^i_{biot} with $\overline{D^i}$. Calculated D^i values for Ni, Co, Cr and V have been compared with the limited published data available (Table 34) and the results are not encouraging, both in terms of the apparent discrepancy between predicted and published figures and the spread in the published figures. There are not sufficient data to make a quantitative test feasible and so the trace element behaviour is not considered to provide sufficiently strong evidence to refute the fractional crystallisation model.

15.3 Basaltic andesite (BA) as a cumulus enriched magma

Fractional crystallisation involves the progressive removal of phenocrysts from the magma as they are formed and implies the existence of three components; (1) parent liquid, (2) residual liquid and (3) complementary cumulates. Many published accounts of fractional crystallisation deal with one, perhaps two of the necessary components and tacitly assume the existence of the third. The preceeding discussion on fractional crystallisation assumed that the solid material removed presumably occurs as cumulate rocks in now consolidated magma chambers (intrusions) below the volcanic pile.

It is possible that the solid material removed from some magma during fractional crystallisation may be erupted as phenocryst enriched lavas rather than form cumulus piles in subterranean magma chambers. It is not surprising that Ewart (1976a) has noted the significant correlation between bulk lava composition and phenocryst contents in calc-alkaline volcanics. Bearing in mind the possibility of phenocryst enriched lavas, an alternative model involving both crystal accumulation and fractional crystallisation may be proposed for the origin of the Haib basaltic andesites. The model involves the accumulation of phenocrysts removed from BA1 into undifferentiated batches of the same magma to produce more mafic lavas such as BA. Products of the progressive removal of phenocrysts from BA1 are the andesites (represented by A).

The least squares approximation to BA listed in Table 35 is simply the

Table 35. Least squares approximation to the Haib basaltic andesite (BA) by the addition of the listed quantities (X_{mix}) of the suggested phenocryst phases to a magma with the composition of BA1.

Mineral compositions (see Table 24): OPX(1), CPX(1), MT
End member compositions for plagioclase were used.

Results for Basaltic Andesite (BA)

	Obs.	Est.	Diff.		X_{mix}	S.D.	X_{solid}	
SiO_2	54.60	54.58	.02	BA1	.5942	.0117		
Al_2O_3	14.40	14.42	.02	OPX	.1119	.0065	.2741	
FeO	9.30	9.30	.00	CPX	.1298	.0081	.3180	
MgO	8.50	8.53	.03	PLAG	.1447	.0076	.3545	An_{74}
CaO	9.00	9.01	.01	MT	.0218	.0014	.0534	
Na_2O	1.80	1.84	.04	TOTAL	1.0025	.0175		
K_2O	1.30	1.43	.13					
		$Diff^2$	= .02					

reverse mix of the step BA-BA1 given in Table 26. It is important to note that the bulk composition of the solid material added to BA1 to produce BA is not the same as the solid removed from BA1 to produce the andesites. In order for the required composition to be produced, the phenocryst assemblage separating from BA1 must have been sorted in such a way as to enable the necessary solid to accumulate. This would require special pleading, although it is clear from the existence of layered intrusions that the modes of cumulate rocks often bear no resemblance to the mode of the phenocryst assemblage that originally separated from the parent magma.

The necessary test will be to see if the trace element composition (Sr, Ni, Co and V) of BA is consistent with the accumulation of phenocrysts that originally crystallised from BA1. The trace element composition of the separating phenocrysts will be controlled by (1) the composition of BA1, (2) the magnitude of the average distribution coefficients ($\overline{D^i}$) and (3) the weight fractions of each phenocryst phase in the crystallate. The average concentration of trace element i in a phenocryst assemblage (C_s^i) may be determined from the following equation,

$$\overline{C_s^i} = C_o^i \cdot \frac{1 - F^{\overline{D^i}}}{1 - F} \qquad (8)$$

If Sr is taken as an example, $\overline{D^i}$ will be a weighted average of D^{Sr}_{plag} and D^{Sr}_{cpx}. The weight fractions of plagioclase and clinopyroxene in the crystallate from BA1 are listed in Table 27 and application of these figures, together with the D^{Sr} values used in the first model, give,

$$\overline{D^{Sr}} = 2.5 \cdot 0.44 + 0.1 \cdot 0.19 = 1.12$$

Since $C^i_o = 525$ (see Table 23),

$$\overline{C^{Sr}_s} = 525 \cdot \frac{1 - F^{1.12}}{1 - F}$$

It is possible to estimate the value for $\overline{C^{Sr}_{plag}}$ from the relationship,

$$X_{plag} \cdot \overline{C^{Sr}_{plag}} + X_{cpx} \cdot \overline{C^{Sr}_{cpx}} = \overline{C^{Sr}_s} \qquad (9)$$

$\overline{C^{Sr}_{plag}}$ and $\overline{C^{Sr}_{cpx}}$ are related by the expression

$$\frac{D^{Sr}_{plag}}{C^{Sr}_{plag}} = \frac{D^{Sr}_{cpx}}{C^{Sr}_{cpx}} \qquad \text{from equation (7)}$$

such that,

$$\frac{\overline{C^{Sr}_{cpx}}}{\overline{C^{Sr}_{plag}}} = \frac{D^{Sr}_{cpx}}{D^{Sr}_{plag}} \qquad \frac{0.1}{2.5}$$

therefore

$$\overline{C^{Sr}_{plag}} \cdot (X_{plag} + X_{cpx}/25) = \overline{C^{Sr}_s} \qquad (10)$$

Equation (10) illustrates the subordinate role of clinopyroxene in determining the bulk Sr content.

X_{plag} and X_{cpx} may be taken from Table 27 and equation (10) reduces to

$$\overline{C_s^{Sr}} = 0.45 \cdot \overline{C_{plag}^{Sr}} \quad (11)$$

$\overline{C_{plag}^{Sr}}$ may be determined from the requirement that BA is a weighted sum of BA1 (undifferentiated magma) and the accumulated phenocryst assemblage. The appropriate weight fractions are listed in Table 35, such that

$$0.59 \cdot 525 + 0.41 \cdot \overline{C_c^{Sr}} = 450 \quad (12)$$

where $\overline{C_c^{Sr}}$ is the average concentration of Sr in the accumulated phenocryst assemblage. The solution of equation (12) gives $\overline{C_c^{Sr}} = 338$. $\overline{C_{plag,c}^{Sr}}$ may be calculated from the relationship,

$$\overline{C_{plag,c}^{Sr}} \cdot X_{plag,c} + \overline{C_{cpx,c}^{Sr}} \cdot C_{cpx,c} = \overline{C_c^{Sr}} \quad (13)$$

where $\overline{C_{plag,c}^{Sr}}$ = concentration of Sr in plagioclase in the accumulated phenocryst assemblage.

$X_{plag,c}$ = weight fraction of plagioclase in accumulated phenocrysts

$\overline{C_{cpx,c}^{Sr}}$ and X_{cpx} are the analogous quantities for clinopyroxene.

Substituting $\overline{C_{plag,c}^{Sr}}/25$ for $\overline{C_{cpx,c}^{Sr}}$ and the weight fractions $X_{plag,c}$ and $X_{cpx,c}$ in equation (13), yields $\overline{C_{plag,c}^{Sr}} = 920$.

From equation (11), $\overline{C_s^{Sr}} = 0.45 \cdot 920 = 414$, which is less than C_{BA1}^{Sr} (525). Since $\overline{D^{Sr}}$ is greater than unity, the ratio $\overline{C_s^{Sr}}/\overline{C_o^{Sr}}$ can never be less than unity for any F. As a result, there is no F that will satisfy the requirement that $\overline{C_s^{Sr}}/\overline{C_o^{Sr}} = 414/525 = 0.79$. The accumulation model is therefore unlikely to produce the observed Sr abundance unless the values of various quantities are significantly different from those adopted. The results of the calculation procedure are particularly sensitive to the Sr content adopted for BA and BA1. If BA is slightly higher (e.g. 500 ppm Sr), the calculations yield $\overline{C_s^{Sr}} = 564$, which will produce a value for the ratio $\overline{C_s^{Sr}}/\overline{C_o^{Sr}}$ of 564/525 = 1.07. Solving equation (8) for F, yields a reasonable value of 0.5. However, the low $\overline{D^{Sr}}$ (near unity) renders equation (8) very insensitive to drastic changes in F. For example, changing F from 0.4 to 0.9, results in $\overline{C_s^{Sr}}$ increasing from 560 to 582. Since the aim of this exercise was

to estimate F in order to proceed to the other trace elements, this method fails to obtain a precise estimate of this crystallisation parameter.

If equation (8) through (13) are applied to Ni, a more precisely defined F value may be obtained because $\overline{D^{Ni}}$ (3.06) is higher than $\overline{D^{Sr}}$. By using the inter-mineral relationships shown in Table 29, the F value necessary to predict the Ni content in BA is 0.83. Both V and Co give different F values (0.25 and 0.51 respectively).

In other words, fractional crystallisation of BA1 will not produce solid phases with the required Sr, Ni, Co and V concentrations at the same degree of crystallisation. The unsatisfactory results suggest that the combined fractionation/accumulation model is unlikely, although no final conclusion may be reached.

15.4 Non-porphyritic rhyolites

Much of the acid fragmental material (bedded tuffs, pumice sheets, volcanogenic sediments) has probably been derived from the disaggregation (either by eruption or erosion) of the non-porphyritic rhyolites. Volume estimates given previously (Chapter 4) suggest that the non-porphyritic lavas (ignimbrites?) and related fragmental material make up about 40% of the exposed volcanic succession.

Compared with porphyritic rhyolites (R), the non-porphyritic rhyolites (NR) are higher in alkalis and silica, which is reflected in a higher DI of 85-95. The nature of the phenocryst assemblage in R suggests that the groundmass may approach the composition of NR in terms of major elements and suggests that they may be related by fractional crystallisation. However, a least squares approximation to NR, by removal of the phenocryst phases present in R, yields unsatisfactory results. Fractionation of a subset of the phenocryst assemblage in R is not possible because the residue would still be porphyritic, which is inconsistent with the aphyric nature of NR.

In a very general way, many of the trace element abundances are consistent with fractional crystallisation involving the phenocrysts present in R,

provided the relative proportions are retained. For example, Rb, Zr, Nb and Th are enriched and Sr, Ni, Co, Cr and V are depleted in NR relative to R. However, it has been shown that R is depleted in Ba relative to the Haib dacites, which is probably the result of biotite fractionation. It follows that the groundmass of R is probably even more depleted in Ba (less than 985 ppm) because of sustained biotite crystallisation. In contrast, NR contains 1400–1500 ppm Ba, which precludes its derivation from R by fractional crystallisation.

The inability to produce NR by fractional crystallisation is not surprising in view of its great volume compared with more basic lavas in the HVG. The most likely alternative to fractional crystallisation, is that NR and related fragmental rocks have been derived from a separate acid magma, possibly generated by partial fusion of crustal material. Unfortunately, the Sr isotopic data for NR vary irregularly and no correlation could be found between Sr^{87}/Sr^{86} and Rb^{87}/Sr^{86} (Chapter 3). Initial Sr^{87}/Sr^{86} ratios calculated by assuming an age of 2000 Ma are impossibly low (0.67–0.69) and suggest Rb and/or Sr migration sometime between extrusion and the present day. It is therefore not possible to establish the existence of a separate crustal derived acid magma on Sr isotopic evidence. Further isotopic analyses are hampered by the apparently unsuitable nature of the rocks, but is warranted by the major and trace element evidence together with the volume relationships.

15.5 Discussion

The Haib lavas may have been produced by fractional crystallisation of a basic magma (at least as basic as basaltic andesite) involving the separation of two pyroxenes, plagioclase and magnetite. The latter mineral is considered to have been responsible for the lack of significant Fe-enrichment in the passage from basaltic andesite to andesite.

A model for the production of the calc-alkaline suite, involving early magnetite fractionation, has been developed by Osborn (1959, 1962, 1969). This model predicts the appearance of andesite as the residual magma and alpine-

type peridotite as the complementary cumulate. The model has not yet met with general acceptance and appears to be inconsistent with the following petrographic and chemical features:

(1) Lack of magnetite phenocrysts in many calc-alkaline basic to intermediate lavas (Carmichael and Nicholls, 1967).

(2) The abnormally high oxygen fugacity necessary to stabilise magnetite as a liquidus or near liquidus phase (Eggler and Burnham, 1973; Thompson, 1973; Biggar, 1974).

(3) Oxygen fugacities do not remain constant and/or high in the passage from basalt to andesite (Meuller, 1969, 1971).

(4) The lack of severe depletion of elements that show a great affinity for magnetite, such as V (Taylor *et al.*, 1969b).

(5) The presence of Cr-spinel rather than magnetite as the characteristic opaque phase in alpine-type peridotites (Ringwood, 1975).

Although there is abundant experimental and petrographic evidence to indicate that magnetite is not the liquidus (or even a near liquidus) phase in basic magmas, when this mineral does appear it may have a profound effect on the chemistry of residual liquids. Ewart *et al.*, (1973) have noted that the ground mass of the Tongan basaltic andesite is enriched in V relative to the whole rock, which is consistent with lack of phyric magnetite. On the other hand, the Tongan andesite and dacite contain phyric magnetite and possess a groundmass that is depleted in V relative to the whole rock. Phenocrysts of two pyroxenes and plagioclase are present in all the Tongan lavas, but only the more acid varieties contain phyric magnetite, which suggests that the contrasting behaviour of V is a function of magnetite fractionation. The appearance of magnetite also coincides with an abrupt change in the direction of the trend in the AFM diagram.

Magnetite, though not necessarily an early crystallising phase, may appear long before the solidus is reached and will therefore be able to fractionate. This implies that basic magmas may experience an early stage of fractionation involving the removal of mafic silicates and possibly plagioclase, which may lead to strong Fe-enrichment (tholeiitic trend). At the point

where magnetite appears however, the liquid line of descent may change abruptly to display progressive enrichment in alkalis (and silica) without any significant Fe-enrichment (calc-alkaline trend).

The appearance of magnetite is primarily controlled by the availability of Fe_2O_3 (Wager, 1960; Carmichael and Nicholls, 1967), which is in turn controlled by a complex interplay of several factors including:

(1) Oxygen fugacity
(2) Temperature
(3) Composition (e.g. total alkalis, K/Na ratio, water content)
(4) Fractionation of other Fe-bearing phases

The effects of crystal fractionation and bulk composition are probably superimposed on the primary control of the Fe_2O_3 content by oxygen fugacity and temperature. These former effects are not negligible and may play a decisive role in the appearance of magnetite. Increased alkali content and/or increasing K/Na ratios appear to increase the Fe_2O_3/FeO ratio of melts at constant oxygen fugacity and temperature (Paul and Douglas, 1965; Carmichael and Nicholls, 1967). It is pertinent to note that much of the experimental work has been carried out on natural lavas with significantly lower K/Na ratios (but not total alkalis) to those observed for the Haib lavas. It follows that the Haib basaltic andesite may have crystallised at oxygen fugacities appropriate to the QFM or NNO buffer but would contain more Fe_2O_3 because of the higher K/Na ratio. As a result, magnetite could have been stabilised nearer the liquidus than in the rocks used in the experiments. More experimental data on high-K calc-alkaline and shoshonitic lavas are required to establish this possibility.

The compilation of Ewart (1976a) suggests that about 50% of modern orogenic basic lavas (basalt, basaltic andesite) and an even greater amount of andesites (up to 90%) contain phyric magnetite. It is clear therefore, that although magnetite fractionation cannot be invoked as a general model for the production of calc-alkaline suites, this process may be responsible for a significant proportion of such suites. Information on older calc-alkaline

suites is lacking, but may not reveal any marked differences to the compilation of Ewart (1976a). It is therefore assumed that the results of Ewart pertaining to the distribution of phyric magnetite may be applicable to Precambrian lava suites.

Fewer problems appear to exist with regard to the derivation of acid andesites and dacites by fractionation involving the removal of magnetite. Eggler (1974) has reported experimental results under controlled f_{O_2} and P_{H_2O} that predict the appearance of phyric magnetite in andesites and more differentiated lavas, which is consistent with the conclusions of Ewart (1976a) discussed previously.

If it is accepted that magnetite phenocrysts in the Haib basaltic andesite crystallised later than the more abundant pyroxenes and plagioclase, then the most basic lava in the HVG may represent a derivative liquid produced by an early stage of tholeiitic type fractionation, which was subsequently interrupted by the appearance of magnetite. This is difficult to test, because more basic magnetite free lavas have not been found. A possible alternative is that the basaltic magma was extensively crystallised before any nett removal of solid material occurred. Cox and Bell (1974) have suggested that a differentiating magma may experience compensated crystal settling, whereby the overall composition is maintained since crystals settling from a portion of the chamber are continually replaced by compositionally similar crystals which settle into it from higher levels. Variation in the efficiency of compensation will cause a nett loss or gain of phenocrysts, producing slightly fractionated or cumulus enriched magma respectively. The resulting magma chamber will be zoned with highly fractionated, phenocryst poor magma near the roof and cumulus enriched magma (crystal mush) near the floor. Magma from the central region of the zoned magma chamber may be fractionated, unchanged, or cumulus enriched, relative to the original magma, depending on the degree of compensation.

The results of the modelling presented previously suggest that much of the lava erupted in the HVG represents those portions of the magma chamber (or chambers) that experienced nett removal of phenocrysts. The tests involved in

recognising cumulus enriched magma were not entirely satisfactory, but yielded results that were inconsistent with the predictions of Rayleigh type crystallisation.

If the highly fractionated, phenocryst poor part of the magma chamber becomes isolated in some way, perhaps by consolidation of cumulus piles from below, or by intrusion into a separate chamber, further crystallisation may occur at increasing P_{H_2O}. This may be achieved if the water in the original magma was gradually concentrated into the remaining liquid fraction. Concentration of water appears necessary because the anhydrous mineral assemblage (two pyroxenes, plagioclase, magnetite) in the more basic precursors (basaltic andesite, andesite, dacite), implies low water content. The increase in P_{H_2O} at a late stage may have been sufficient to stabilise hydrous phases in the place of pyroxenes. Rhyolitic lavas with phenocrysts of amphibole and biotite, in addition to plagioclase, magnetite and quartz, would represent the final differentiation.

The proposed differentiation model need not be invalidated by the lack of correspondence between age of extrusion and composition. The volcanic plumbing system is seldom so systematic and efficient as to erupt magmas as soon as, or in the same proportion as, they have been produced in the differentiating source chambers. The irregular or inverse distribution within many volcanic provinces certifies to this behaviour and the fact that the most basic lavas in the HVG appear highest in the exposed succession is not unexpected.

16

PETROGENESIS OF THE VIOOLSDRIF INTRUSIVE SUITE

The serial variation in chemical and mineralogical composition, together with the intimate association in space and time, suggests that the series diorite - tonalite - granodiorite - adamellite - leucogranite may be comagmatic. In contrast to the lavas, the unmetamorphosed nature of the plutonic rocks enabled data to be obtained on the primary igneous minerals.

Various models involving fractional crystallisation are illustrated in Fig. 66, which includes a number of possible schemes whereby the entire granitic suite may be generated. The various schemes were evaluated first by modelling with major elements, which have been subsequently tested for consistency with trace elements. It was discovered that certain steps within the various schemes evaluated were not consistent with the observed behaviour of a few selected trace elements, and so further evaluation of these steps was not considered to be warranted.

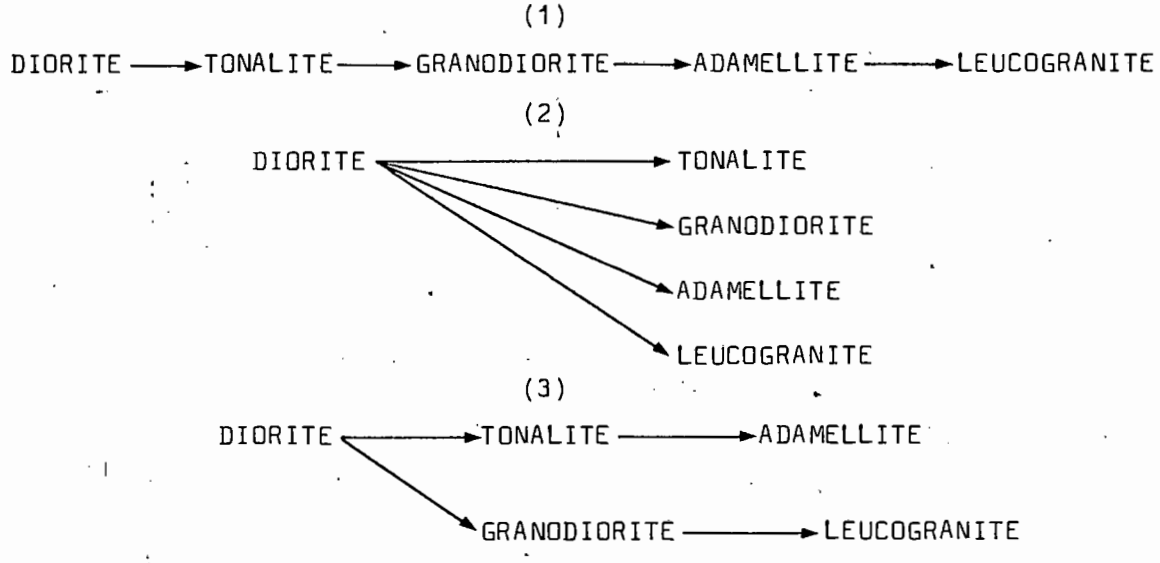

Fig. 66. Various schemes whereby the entire granitic suite may be derived by fractional crystallisation. (1) Stepwise fractionation; (2) Direct fractionation from a single parent; (3) Indirect fractionation

The simplest fractionation scheme involves a stepwise evolution whereby the first derivative magma acts as parent to the second derivative. Such a scheme has the advantage of relatively short crystallisation intervals, over which the mineral compositions, relative proportions of fractionating phases and crystal/liquid trace element distribution coefficients may be assumed to remain constant. An alternative scheme involving a direct production of all rocks from the most basic magma (diorite) is also possible, but suffers from the unrealistic assumption that the mineral species, their compositions and relative proportions and also crystal/liquid distribution coefficients remain constant over excessively long crystallisation intervals (e,g. diorite to leucogranite). More complex schemes involving combinations of the previous two may be possible and an example is included in Fig. 66.

16.1 Stepwise fractionation

Stepwise fractionation involves the removal of early formed crystals from the diorite to produce the tonalite, which in turn fractionates further to produce the granodiorite and so on. Least squares approximations to the major element composition of each proposed derivative rock have been calculated using the procedure of Bryan *et al.*, (1969) and input data from Tables 36 and 37. Average rock compositions have been used as the successive liquids in the fractionation model. All Fe has been expressed as Feo (FeO*) and the small quantities of MnO and P_2O_5 have been neglected. Mineral compositions are average data taken from EMP analyses listed in Appendix 2. End member compositions for plagioclase (pure anorthite and albite) and magnetite (pure magnetite and ulvöspinel) have been used instead of specific mineral compositions, because of the presence of marked zoning (plagioclase) and oxidation (magnetite).

16.1.1 Diorite - Tonalite (D - T)

Table 38a summarises the least squares approximation to the Vioolsdrif tonalite by removing orthopyroxene, hornblende, plagioclase and magnetite from

	D	T	G	A	L1	L2
SiO_2	55.7	60.3	65.8	69.4	74.0	77.4
TiO_2	.95	.88	.57	.47	.28	.11
Al_2O_3	17.3	17.2	15.6	14.7	13.5	12.2
FeO	8.1	6.2	4.3	3.1	1.7	.58
MnO	.12	.12	.08	.07	.03	.02
MgO	4.6	2.8	2.2	1.2	.43	.04
CaO	7.8	6.0	4.0	2.7	1.3	.67
Na_2O	2.6	3.2	3.0	3.2	3.3	3.6
K_2O	2.2	2.9	4.1	4.8	5.4	5.3
P_2O_5	.40	.30	.18	.14	.05	.01
DI	43.2	57.5	70.3	79.9	90.4	96.8
mg	50.3	44.6	47.7	40.8	31.6	10.9
Ba	711	1060	1144	970	797	83
Rb	80	122	161	195	246	325
Zr	161	167	130	168	135	84
Nb	9.1	8.3	8.9	11.5	12.6	21
Th	7.0	10.3	15.9	21	31	39
U	.6	1.8	2.1	3.2	5.7	6.2
Pb	21	26	34	27	34	43
Y	20	21	16.7	21	23	21
Sr	504	514	434	279	154	44
Ni	102	22	13	10.7	4	nd
Co	35	17.9	12.7	8.6	4	nd
Cr	55	42	24	18.7	3	nd
V	196	115	83	58	19	nd
Zn	88	74	46	42	13	5

Table 36. Average compositions of the main rock types in the Vioolsdrif granitic suite. Recalculated volatile free and with all Fe expressed as FeO. The two leucogranite compositions (L1 and L2) are explained in the text.

DI = Differentiation Index; mg = 100 MgO/(MgO + FeO) mole percent

Table 38 c. Least squares approximation to the Vioolsdrif adamellite (A) by subtracting the listed quantities (X_{mix}) of the suggested fractionating phases from a parental granodiorite (G).

Results for Adamellite (A)

	Obs.	Est.	Diff.		X_{mix}	S.D.	X_{solid}	
SiO_2	69.42	69.42	.00	G	1.2259	.0132		
TiO_2	.47	.47	.00	HBL	-.0761	.0127	.3341	
Al_2O_3	14.74	14.77	.03	BIOT	-.0209	.0114	.0917	
FeO	3.14	3.14	.00	PLAG	-.1208	.0111	.5303	An_{50}
MgO	1.21	1.16	.05	MT	-.0100	.0075	.0439	Usp_{23}
CaO	2.74	2.80	.06	TOTAL	.9981	.0252		
Na_2O	3.16	2.92	.24					
K_2O	4.78	4.82	.04					

$Diff^2 = .07$ F = .8157

Table 38 d. Least squares approximation to the Vioolsdrif leucogranite (L1) by subtracting the listed quantities (X_{mix}) of the suggested fractionating phases from a parental adamellite (A).

Results for Leucogranite (L1)

	Obs.	Est.	Diff.		X_{mix}	S.D.	X_{solid}	
SiO_2	74.00	74.05	.05	A	1.2194	.0394		
TiO_2	.28	.28	.00	BIOT	-.0612	.0412	.2844	
Al_2O_3	13.50	13.25	.25	PLAG	-.1424	.0402	.6617	An_{41}
FeO	1.70	1.70	.00	MT	-.0117	.0101	.0514	Usp_{20}
MgO	.43	.85	.42	TOTAL	1.0042	.0595		
CaO	1.30	1.66	.36					
Na_2O	3.30	3.44	.14					
K_2O	5.40	5.09	.31					

$Diff^2 = .49$ F = .8201

Table 38 a. Least squares approximation to the Vioolsdrif tonalite (T) by subtracting the listed quantities (X_{mix}) of the suggested fractionating phases from a parental diorite (D).

Results for Tonalite (T)

	Obs.	Est.	Diff.		X_{mix}	S.D.	X_{solid}	
SiO_2	60.29	60.28	.01	D	1.4739	.0246		
TiO_2	.88	.88	.00	OPX	-.0242	.0208	.0511	
Al_2O_3	17.22	17.25	.03	HBL	-.2255	.0250	.4757	
FeO	6.16	6.16	.00	PLAG	-.1955	.0185	.4124	An_{74}
MgO	2.75	2.77	.02	MT	-.0287	.0050	.0605	Usp_{25}
CaO	5.98	5.98	.00	TOTAL	.9999	.0452		
Na_2O	3.16	2.97	.19					
K_2O	2.92	3.08	.16					
		$Diff^2$ =	.06		F = .6785			

Table 38 b. Least squares approximation to the Vioolsdrif granodiorite (G) by subtracting the listed quantities (X_{mix}) of the suggested fractionating phases from a parental tonalite (T).

Results for Granodiorite (G)

	Obs.	Est.	Diff.		X_{mix}	S.D.	X_{solid}	
SiO_2	65.76	65.77	.01	T	1.4268	.0067		
TiO_2	.57	.57	.00	HBL	-.1148	.0028	.2696	
Al_2O_3	15.62	15.60	.02	PLAG	-.2732	.0097	.6416	An_{57}
FeO	4.28	4.28	.00	MT	-.0379	.0028	.0890	Usp_{41}
MgO	2.19	2.16	.03	TOTAL	1.0010	.0086		
CaO	4.00	4.03	.03					
Na_2O	3.02	3.03	.01					
K_2O	4.12	4.10	.02					
		$Diff^2$ =	.003		F = .7009			

Table 38 e. Least squares approximation to the Vioolsdrif leucogranite (L2) by subtraction of the listed quantities (X_{mix}) of the suggested fractionating phases from a parental leucogranite (L1).

Results for Leucogranite (L2)

	Obs.	Est.	Diff.		X_{mix}	S.D.	X_{solid}	
SiO_2	77.40	77.41	.01	L1	1.1552	.0133		
TiO_2	.11	.11	.00	BIOT	-.0372	.0144	.2356	
Al_2O_3	12.19	12.19	.00	PLAG	-.0757	.0093	.4755	
FeO	.58	.58	.00	KSPR	-.0377	.0159	.2368	
MgO	.04	.04	.00	MT	-.0083	.0060	.0521	Usp_{21}
CaO	.67	.74	.07	TOTAL	.9960	.0277		
Na_2O	3.60	3.36	.24					
K_2O	5.30	5.25	.05					

$Diff^2$ = .06 F = .8657

Table 40. Average solid/liquid distribution coefficients for the listed elements in the various fractionation steps evaluated in this chapter. F = weight fraction of parental magma remaining; D-T, etc = Diorite to Tonalite, etc.

	D-T	T-G	G-A	A-L1	L1-L2	D-G	T-A
F	.68	.70	.82	.82	.87	.49	.59
Sr	.95	1.47	3.17	4.00	9.7	1.21	2.14
Ni	4.95	2.48	-	-	-	3.90	-
Co	2.73	1.96	-	-	-	2.44	-
Cr	1.70	3.81	-	-	-	2.80	2.51
V	2.37	1.92	3.30	-	-	2.22	2.28
Zn	1.45	2.33	1.45	-	-	1.92	2.06
Ba	-	.79	1.98	1.99	16.7	.33	1.17

the parent diorite. The predicted plagioclase composition is as calcic as the core compositions determined for this mineral in the diorite. The low TiO_2 content of the magnetite is consistent with the subordinate proportion of ilmenite in the oxidised grains. The crystallisation interval is not excessive and suggests that 32% of a diorite liquid needs to solidify before the residual liquid has the composition of the average tonalite. Although biotite is an important modal mineral in the diorite, it appears to have taken little part in fractionation, which is consistent with this mineral appearing later than orthopyroxene, hornblende and magnetite. Biotite usually forms semi-poikilitic patches surrounding orthopyroxene, hornblende, plagioclase and magnetite.

The F value obtained from the least squares approximation may be compared with the degree of enrichment experienced by incompatible trace elements, such as Ba, Rb, Zr, Nb, Th, U and Pb. Table 39 lists the ratios C_D^{Rb}/C_T^{Rb}, etc., that should be approximately equal to F if $\overline{D^i}$ is < 0.1.

Table 39

Ratio of various incompatible trace elements (C_D^i/C_T^i) in the passage from diorite (D) to the tonalite (T)

	Diorite - Tonalite
Ba	0.67
Rb	0.66
Th	0.68
Zr	0.96
Nb	1.10
U	0.33
Pb	0.81

Values for Ba, Rb and Th are very close to the predicted F value but Zr, Nb, U and Pb yield discrepant results. These latter elements either do not show very coherent trends for the basic - intermediate intrusives (Zr, Pb) or are very low in abundance (Nb, U) such that the observed scatter introduces large uncertainties in the concentration ratios (see Fig. 62). Those incompatible

elements that show relatively high abundances (>10 ppm) and regular variation trends (between diorite and tonalite) yield degrees of enrichment that confirm the degree of crystallisation necessary to produce the tonalite.

The depletion in compatible elements ($\overline{D^i}>1$) may be evaluated in a manner similar to that used for the Haib lavas. $\overline{D^i}$ values have been calculated for Sr, Ni, Co, Cr, V and Zn using equation (4) and are listed in Table 40. Individual D^i values are more difficult to estimate because of the lack of information on inter-mineral relationships. In order to proceed further with the evaluation, some assumptions are necessary and are discussed below.

The situation with Sr is simplified because only plagioclase has $D^{Sr} > 1$ and so $\overline{D^{Sr}}$ will essentially reflect the contribution from D^{Sr}_{plag}. The contribution from D^{Sr}_{hbl}, D^{Sr}_{opx}, and D^{Sr}_{mt} is negligible. If X_{plag} (in the solid) is taken from the least squares approximation in Table 38a and $\overline{D^{Sr}}$ is taken from Table 40, the application of equation (5) gives $D^{Sr}_{plag} = 2.3$, which is the same as that reported by Korringa and Noble (1971) for calcic plagioclase ($An_{75} = 2.3$).

D^i_{hbl} values for Ni, Co and V have been calculated assuming D^i_{opx} and D^i_{mt} have those values obtained for the Haib basaltic andesites. The composition of the Vioolsdrif diorite is intermediate between BA and BA1 (see Chapter 15) and average values for D^i_{opx} and D^i_{mt} have been calculated from the data listed in Table 30, for the steps BA - BA1 and BA1 - A. Weight fractions of the minerals have been obtained from Table 38a and D^i_{hbl} for Ni, Co and V have been calculated using equation (6) and are listed in Table 41. D^{Ni}_{hbl} and D^{Co}_{hbl} fall within the range reported by other workers (see Table 32), but D^V_{hbl} seems significantly lower than the single figure reported by Ewart & Taylor (1969) (See Fig.34). The possible presence of minute magnetite inclusions in the hornblende phenocrysts analysed by Ewart and Taylor will seriously affect D^V_{hbl} and their very high figure of 18 is open to question.

Calculated D^{Ni}_{hbl} and D^{Co}_{hbl} values are not unreasonable, bearing in mind that they are partly based on assumed D^i values for the coexisting mafic silicates. These results, taken with those for Sr and the major element modelling, suggest that the production of the tonalite by fractional crystalli-

Table 41. Predicted individual crystal/liquid distribution coefficients for the suggested fractionating phases in the various steps evaluated in this chapter. The figures in brackets are assumed values and have been used to calculate the other unbracketed values.

	Sr	Ni	Co	V	Ba
Diorite - Tonalite					
Plag	2.3	-	-	-	-
Opx	-	(4.3)	(4.1)	(0.5)	-
Mt	-	(9.0)	(5.3)	(20)	-
Hbl	-	8.8	4.6	2.4	-
Tonalite - Granodiorite					
Plag	2.3	-	-	-	-
Mt	-	-	-	(20)	-
Hbl	-	-	-	0.5	-
Granodiorite - Adamellite					
Plag	6.0	-	-	-	(0.35)
Mt	-	-	-	(20)	-
Hbl	-	-	-	5.6	0.6
Biot	-	-	-	5.9	17
Adamellite - Leucogranite (L1)					
Plag	6.0	-	-	-	(0.4)
Biot	-	-	-	-	6.1
Diorite - Granodiorite					
Plag	2.5	-	-	-	-
Opx	-	(4.3)	(4.1)	(0.5)	-
Mt	-	(9.0)	(5.3)	(20)	-
Hbl	-	7.9	4.8	1.9	-
Tonalite - Adamellite					
Plag	3.5	-	-	-	(0.3)
Mt	-	-	-	(20)	-
Hbl	-	-	-	2.2	0.3
Biot	-	-	-	2.3	7.7

sation of the diorite is a feasible mechanism.

16.1.2 Tonalite - Granodiorite (T - G)

Table 38b lists the least squares approximation to the granodiorite which may be produced by removal of hornblende, plagioclase and magnetite from the tonalite. The absence of orthopyroxene is to be expected, because this mineral is in reaction relationship with hornblende in the diorite and is not found in the tonalite. The predicted plagioclase composition is as calcic as the core compositions determined for this mineral in the tonalite, but is lower than that which separated from the diorite. This latter feature is consistent with the well documented decrease in An content of plagioclase with falling temperature of crystallisation. The absence of biotite from the calculation is surprising, since this mineral is the dominant mafic silicate in the tonalite and granodiorite. Least squares approximations including biotite as a fractionating phase, either with hornblende and magnetite or with magnetite alone, yield unsatisfactory results.

Average $\overline{D^i}$ values for selected trace elements, assuming an F of 0.70 (Table 38b) are listed in Table 40. Since Sr enters only plagioclase, the $\overline{D^{Sr}}$ value of 1.47 implies that a significant proportion of plagioclase must be removed. This is satisfied in the least squares approximation, which requires X_{plag} in the solid to be 0.64. If the values of $\overline{D^{Sr}}$ and X_{plag} are substituted in equation (5), the resulting D^{Sr}_{plag} is 2.3, which is the same as that obtained for the first step (D - T). Since the plagioclase removed in this second step (T - D) is less calcic, D^{Sr}_{plag} should be slightly higher than 2.3, if the results of Korringa and Noble (1971) are correct. According to their data, D^{Sr}_{plag} depends on An content and for a plagioclase An_{67} their curve predicts $D^{Sr}_{plag} = 4$.

The very low levels of Ni and Co (< 20 ppm) render these trace elements of little use in the evaluation of this step in the fractionation scheme. Small uncertainties of 2-3 ppm are large relative to the absolute concentration

(e.g. 20 ± 2 ppm is 10 percent uncertainty). The source of uncertainty at this low abundance level includes the scatter about the average trend lines and analytical error. As a result, $\overline{D^{Ni}}$ and $\overline{D^{Co}}$ values calculated from such low abundances of Ni and Co will be very sensitive to seemingly small changes in concentration.

Only V persists at sufficiently high levels (~100 ppm) to warrant further evaluation. The estimated $\overline{D^{V}}$ for this step is 1.92, which appears to be low, considering the solid removed contains nearly 9% magnetite. D^{V}_{mt} is probably 30 to 50, judging from the results for the Haib lavas (see Table 30) and even if it is assumed that all V was removed in magnetite, the maximum D^{V}_{mt} = 21.6. Apart from temperature, D^{V}_{mt} may depend on oxygen fugacity, since only V^{3+} enters magnetite (and presumably hornblende), while more oxidised species (V^{4+} and V^{5+}) may show preference for the liquid (Lindstrom, 1976). The tendency for D^{V} to increase with decreasing temperature may be counteracted by fluctuations in f_{O_2} (which will control the amount of V^{3+} in the liquid) such that D^{V}_{mt} may not change. Lindstrom's preliminary experimental data suggests that oxygen fugacities appropriate to the QFM buffer at 1130°C will result in significant amounts of V^{4+} and possibly V^{5+} in natural magmas. It has been demonstrated by Carmichael and Nicholls (1967) that the range in natural oxygen fugacities in magmas closely approximate that of the QFM buffer. D^{V}_{mt} under oxygen fugacities of the QFM buffer was found by Lindstrom to be 15-20, which is comparable to those values obtained for the Haib basaltic andesites. In order for the behaviour of V to be consistent with the stepwise fractionation model, at least in the passage from diorite, through tonalite to the granodiorite, D^{V}_{mt} is required to remain fairly constant at 15-20. This could be achieved if the tendency for D^{V} to increase with decreasing temperature is counterbalanced by f_{O_2}, such that D^{V} is controlled by the V^{3+}/V^{4+} (or V^{5+}) ratio in the liquid.

The behaviour of Ba is slightly anomalous, in that the degree of enrichment in G is not as high as expected. $\overline{D^{Ba}}$ is 0.79 for (T - G) and should be < 0.1 if the fractionating mineral assemblage required to produce the granodiorite

is retained. Korringa and Noble (1971) have shown that D^{Ba}_{plag} for composition An_{57} is about 0.3. The compilation in Arth (1976) lists D^{Ba}_{hbl} in rhyolitic rocks at about 0.2, but may be as high as 0.7 in basic rocks. Even if the maximum D^{Ba} values are adopted, combined fractionation of plagioclase and hornblende will not produce $\overline{D^{Ba}}$ as high as that observed. Biotite fractionation could raise $\overline{D^{Ba}}$ because D^{Ba}_{biot} is very high (6-9; according to Arth, 1976). However, the role of biotite in the passage from tonalite to granodiorite seems to be a very minor one, because of the results obtained in the major element modelling discussed previously.

To summarise, the behaviour of Sr, Ba and possibly V in the passage from the tonalite to granodiorite, appear to be inconsistent with the stepwise fractionation model. If the granodiorite has been derived from a tonalite magma by fractional crystallisation, as the major element modelling and Rb-Sr isotopic data suggest, then the behaviour of Sr, Ba and possibly V have been controlled, in part, by some additional process. Alternatively, the granodiorite has been derived from some parent other than its immediate predecessor in the batholith.

16.1.3 Granodiorite - Adamellite (G - A)

Despite the present uncertainty as to the origin of the granodiorite, fractionation of this magma may have produced the adamellite and a least squares approximation to the latter rock type is given in Table 38c. The dominance of hornblende over biotite should be noted, since the former mineral is very rare in the granodiorite and is absent in the adamellite. A possible explanation for this anomalous behaviour is that if fractionation was achieved by crystal settling, then the platey habit of early formed biotite crystals (as shown by phenocrysts in acid lavas) may prevent them sinking as fast as prismatic hornblendes. There is no great density contrast between the two minerals and therefore differential removal can only be achieved by a contrast in settling velocities brought about by radically different crystal shape.

The observed depletion in Sr (434 to 279 ppm) implies that D^{Sr}_{plag} is

about 6, if all the Sr is removed in plagioclase. The predicted D^{Sr}_{plag} for An_{50} is 5 (Korringa and Noble, 1971) and this discrepancy casts doubt over the crystal fractionation model. A similar problem exists with Ba, which is depleted in the adamellite relative to the granodiorite, although the only fractionating phase with D^{Ba} significantly greater than unity (biotite) makes up less than 10% of the solid removed. D^{Ba}_{biot} may be calculated using equation (6) and by adopting $D^{Ba}_{plag} = 0.35$ (from the curve of Korringa and Noble, 1971) and $D^{Ba}_{hbl/biot} = 0.034$ (see Table 32). The resulting value for D^{Ba}_{biot} necessary to produce the observed depletion in Ba is about 17, which is much higher than any published figure (e.g. the compilation in Arth, 1976). Berlin and Henderson (1969) have suggested that D^{Ba}_{biot} may be as high as 15 and Philpotts and Schnetzler (1970) have reported a D^{Ba} for phlogopitic mica of 15. These latter data are bulk distribution ratios and have not been corrected for Rayleigh type crystallisation (cf. Korringa and Noble, 1971; Ewart *et al.*, 1973; Albarede and Bottinga, 1972), so may be over-estimates. Although little data are available, the D^{Ba}_{biot} necessary to produce the observed depletion in Ba, appears to be too high and confirms the suspicion that the observed trace element behaviour is not consistent with the proposed fractionation scheme.

The behaviour of V seems to add weight to the above suspicion. For $D^{V}_{mt} = 20$, D^{V}_{hbl} and D^{V}_{biot} are 5.9 and 5.6 respectively, which appear to be too high because D^{V}_{hbl} in the previous steps was about 2.5. This problem may be overcome if it is postulated that, in contrast to the previous step (T - G), D^{V} is allowed to increase with fractionation, presumably because the oxygen fugacity ceased to counteract the tendency for D^{V} to increase with decreasing temperature. This verges on special pleading and there is no obvious feature to suggest that D^{V} may have behaved in such a complicated manner. It appears that V does not satisfy the requirements of the stepwise fractionation model either.

To summarise, the behaviour of Sr, Ba and V does not appear to be consistent with the model involving the production of the adamellite from the granodiorite by fractional crystallisation. If the Vioolsdrif granodiorite and adamellite have been produced by fractional crystallisation, then their

respective parental magmas are not those predicted by the stepwise fractionation model.

16.1.4 Adamellite - Leucogranite

Since both rock types are composed almost entirely of feldspar and quartz, the passage from adamellite to leucogranite may be traced within the salic tetrahedron(Qz-An-Ab-Or) or a projection thereof. The ternary feldspar system (An-Ab-Or) is a projection of the salic tetrahedron from the Qz apex and is shown in Fig. 67, together with the two feldspar cotectic under anhydrous and hydrous conditions. The points plotted in Fig. 67 represent the normative feldspar compositions of all analysed adamellites and leucogranites from the VIS. The distribution suggests that alkali feldspar may have joined plagioclase at an intermediate stage in the passage from adamellite to leucogranite. Leucogranites that fall on or very near the two feldspar cotectic, may be distinguished from those that fall significantly above it. The latter group represents the link between the adamellites (which crystallised only plagioclase) and the former group of leucogranites that may have experienced two feldspar fractionation.

Average compositions of the two groups (L1 and L2) are listed in Table 36 and the passage from adamellite to leucogranite has been broken into two steps (A - L1, L1 - L2) in order to allow for the appearance of alkali feldspar. Least squares approximations to the major element compositions of L1 and L2 are listed in Table 38 d and e and the reasonably good agreements suggest that such a stepwise fractionation scheme may be feasible. The predicted plagioclase composition for the first step is similar to the most calcic plagioclase analysed in the adamellite. Early plagioclase in the leucogranites is extensively sericitised and the only composition obtained was An_{15}, which was situated near the rim of the analysed crystal. Judging from the zoning present in all plagioclase investigated, the cores of the leucogranite plagioclase could well be as calcic as An_{30} and therefore the predicted value in Table 38e may not be unreasonable.

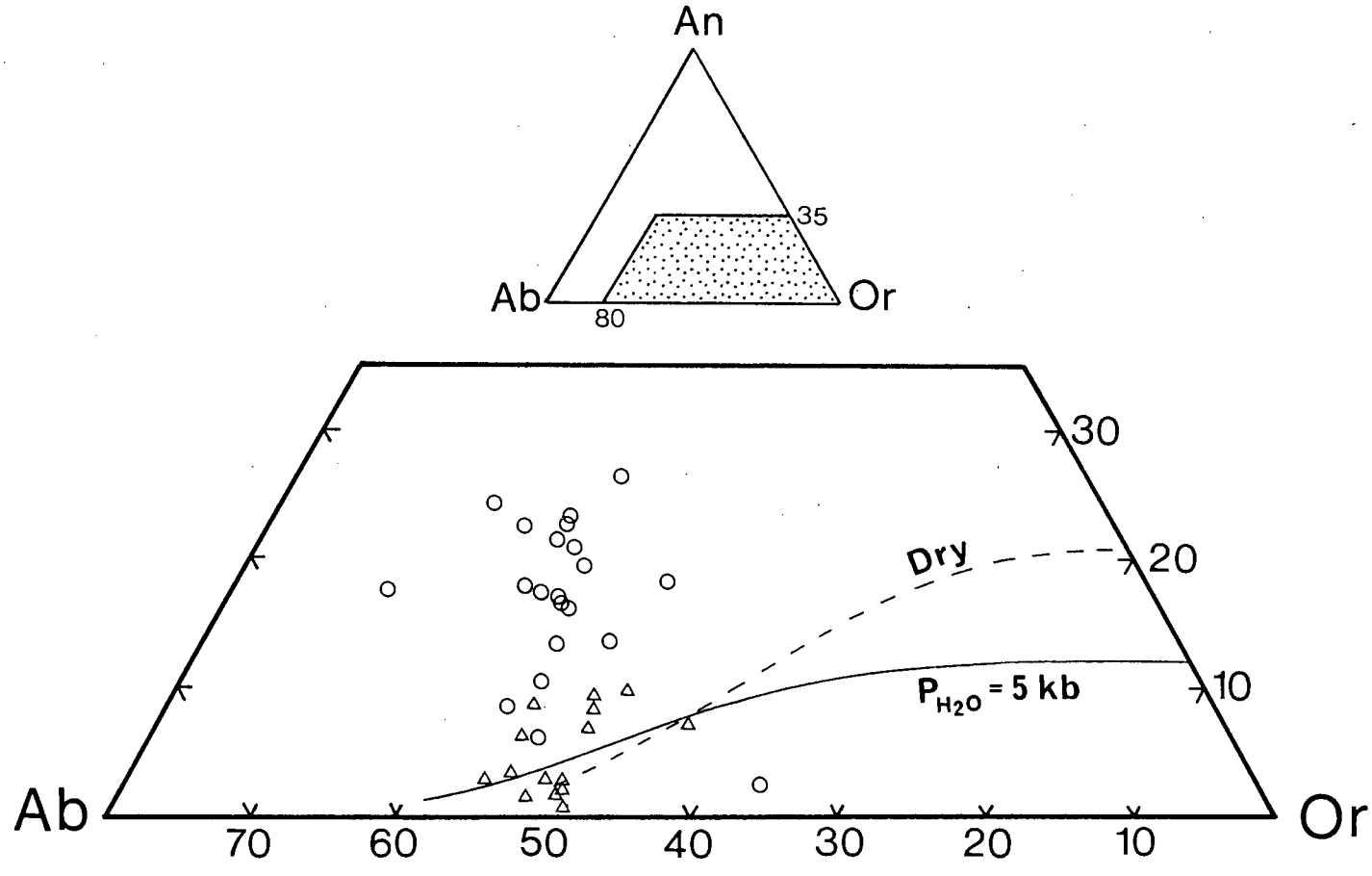

Fig. 67. Ternary feldspar diagram. Two feldspar cotectic curves after Franco and Shairer (1951) and Yoder et al., (1957). Normative feldspar compositions of the Vioolsdrif adamellites (O) and leucogranites (Δ) are shown.

Since all the ferromagnesian trace elements (Ni, Co, Cr and V) are very low in abundance (<20 ppm), they are of very little use in monitoring these two fractionation steps and only Ba and Sr provide any useful information.

16.1.4.1 First step : Adamellite - L1

$\overline{D^i}$ values for the first step are listed in Table 40 and together with values for X_{solid} in Table 38d, may be used to calculate individual D^i values for the fractionating phases (Table 41). Assuming that plagioclase took up all Sr removed, then D^{Sr}_{plag} must be about 6, which is consistent with the predictions of Korringa and Noble (1971). The curve of Korringa and Noble linking D^{Ba}_{plag} with An content suggests that for plagioclase with composition An_{41}, D^{Ba}_{plag} is about 0.4. If this D^{Ba}_{plag} is adopted, then D^{Ba}_{biot} must be about 6, if fractionation of these minerals is responsible for the depletion in Ba in the passage to L1. This falls within the range compiled by Arth (1976) but contrasts sharply with that predicted for D^{Ba}_{biot} in the earlier step (G - A).

16.1.4.2 Second step : L1 - L2

Inspection of Table 36 reveals that L2 is strongly depleted in Sr and Ba relative to L1 and this is reflected in the very high $\overline{D^i}$ values listed in Table 40. In order to achieve the observed depletion in Sr (154 - 44 ppm) over the predicted crystallisation interval, at least one of the fractionating feldspars must have D^{Sr} greater than 10. The curve of Korringa and Noble (1971) predicts $D^{Sr}_{plag} = 7$ for An_{30}, so if $\overline{D^{Sr}}$ is to be 9.7, then, using the proportions given in Table 38e, D^{Sr}_{Kspr} must be 27, which is far higher than any published value. Severe depletion in Sr is consistent with two feldspar fractionation in a qualitative sense and has been demonstrated in a number of fractionated salic igneous suites (e.g. Paresis, Siedner, 1965; Bouvet, Verwoerd et al., 1974; Luderitz, Marsh, 1976). However, the application of quantitative modelling using published estimates of D^{Sr} as a guide, shows that that the most evolved Vioolsdrif leucogranites seem to contain far less Sr than predicted. The same conclusion may be reached with Ba, since $\overline{D^{Ba}}$ is higher than any published

individual D^{Ba} for biotite (maximum 15, Philpotts and Schnetzler, 1970), plagioclase (less than unity, Korringa and Noble, 1971; Drake and Weill, 1975) and alkali feldspar (maximum 9, Berlin and Henderson, 1969).

The anomalously low Sr and Ba abundances may be explained in at least three possible ways :

(i) D^{i} values are higher than published figures.

(ii) Ba and Sr may have been lost to an escaping vapour phase.

(iii) Crystallisation interval is longer than that predicted.

The first explanation must await further work on establishing the range in possible D^{i} values, particularly for Ba in alkali feldspar. The severe depletion in Ba could have been achieved if the fractionating alkali feldspar had a significant Celsian component. Such Ba rich alkali feldspars are known from granitic pegmatites (Deer *et al.*, 1962) but appear to be more characteristic of manganese deposits (Spencer, 1942). Furthermore, the EMP analyses of alkali feldspar in the leucogranite total near 100%, suggesting the presence of only trace amounts of other components such as Ba.

Transport of significant quantities of Ba and Sr in post magmatic hydrothermal fluids is suggested by the presence of barite ($BaSO_4$) and celestite ($SrSO_4$) in solfataric deposits and as gangue in some ore deposits associated with mineralised plutons (Holland, 1967). However, the magmatic origin for the Sr and Ba in many of the above type of deposits has never been proved conclusively (Bateman, 1950). The presence of a vapour phase coexisting with a late stage leucogranite liquid is suggested by at least two other features. Many of the leucogranites studied contain normative corundum, which is reflected in the presence of minor amounts of modal muscovite. The implied peraluminous nature of the magma has been considered by Burnham (1967) to be the result of interaction with an aqueous vapour phase; the purging effect of a coexisting vapour phase on alkalis has been established by experiment (Orville, 1963; Luth *et al.*, 1964). There is petrographic evidence to suggest that the leucogranite crystallised initially under hypersolvus conditions, changing to subsolvus conditions during final consolidation. The experimental work of

Yoder *et al.*, (1957) and Martin and Bonin (1976) indicates that the alkali feldspar solvus is intersected only at very high water pressures (P_{H_2O} = P_{Total} = 2.5 - 5 kbars). It is unlikely that P_{H_2O} is ever much less than P_{Total} during subsolvus crystallisation, because of the very high confining pressures necessary (Martin and Bonin, 1976). The observed petrographic features and the results of experimental work on feldspars, suggest that a vapour phase probably existed during the period of subsolvus crystallisation of the leucogranite.

The crystallisation interval necessary to produce L2 from L1 has been determined from major element requirements in the least squares approximation (Table 38e). Judging from the low S.D. values, the uncertainty in F is fairly small (less than $\pm$ 0.1) and may not be invoked as a source of fluctuation in the crystallisation interval. The only way that F may change significantly, is if radically different mineral compositions are used. Another alternative is to change the fractionating mineral assemblage. The composition of biotite, plagioclase and magnetite are very close to that observed in the leucogranites. The alkali feldspar used in the least squares approximation is pure K feldspar; the presence of albite lamellae suggests that the original alkali feldspar contained a significant proportion of Na. Judging from the size and abundance of the lamellae, the amount of Ab_{ss} in the original homogeneous alkali feldspar was probably less than 10% and the use of the pure end member in the major element modelling calculations is considered justifiable. In any case, the substitution of an alkali feldspar with composition $Or_{90}Ab_{10}$ produced unsatisfactory results and predicted an F value slightly higher than that listed in Table 38e, which is the reverse of that required.

To summarise, none of the possible mechanisms capable of producing the strong depletion in Sr and Ba are particularly attractive. The choice between the three is hampered mainly by lack of information. However, the first two appear to be better candidates than the third and it is concluded that the observed depletion in Sr and Ba is either a function of two feldspar fractionation alone (with very high D^{Sr} and D^{Ba} implied) or two feldspar fractionation supplemented by loss to a coexisting vapour phase.

16.1.5 Summary

Only the first (D - T) and the last (A - L) steps of the stepwise fractionation model appear to be feasible and the intermediate rocks (G, A) require different parents than those predicted. The failure of this model to produce the entire granitic suite suggests that the emplacement history of the batholith did not involve the periodic tapping of a progressively differentiating batch of dioritic magma.

16.2 Indirect fractionation

16.2.1 Origin of the granodiorite

It has already been stated that direct production of the more acid rocks (adamellite, leucogranite) by prolonged fractionation of the diorite is unrealistic. However, the granodiorite is a less differentiated rock compared to the adamellite and it may be feasible to produce this rock directly from the diorite. Table 42a lists the least squares approximation to the granodiorite and involves the removal of the same mineral assemblage (opx-hbl-plag-mt) as that invoked to explain the derivation of the tonalite. As is expected, the crystallisation interval necessary to produce the granodiorite is greater than that required to produce the tonalite. The granodiorite represents the residual liquid after 51% crystallisation, while the tonalite represents that after 32%. The relative proportions of the fractionating phases are not drastically different; the opx/hbl ratio is 9.31 and 9.24 for the steps (D - T) and (D - G) respectively. The main difference is the amount of plagioclase, which makes up 41% of the solid removed for the step (D - T), but increases to 49% for (D - G).

In contrast to the step (T - G), where the Ni and Co abundances are too low to be of any use, these elements may be included in the evaluation of the step (D - G) and their average distribution coefficients have been included in Table 40. Individual D^i values have been calculated assuming D^i_{opx} and D^i_{mt} for Ni, Co and V to be the same as those determined for the Haib basaltic

Table 42 a. Least squares approximation to the Vioolsdrif granodiorite (G) by subtracting the listed quantities (X_{mix}) of the suggested fractionating phases from a parental diorite (D).

Results for Granodiorite (G)

	Obs.	Est.	Diff.		X_{mix}	S.D.	X_{solid}	
SiO_2	65.76	65.75	.01	D	2.0250	.0159		
TiO_2	.57	.57	.00	OPX	-.0432	.0099	.0422	
Al_2O_3	15.62	15.63	.01	HBL	-.3990	.0122	.3901	
FeO	4.28	4.28	.00	PLAG	-.5058	.0180	.4946	An_{70}
MgO	2.19	2.21	.02	MT	-.0748	.0066	.0731	Usp_{33}
CaO	4.00	4.00	.00	TOTAL	1.0023	.0135		
Na_2O	3.02	3.05	.03					
K_2O	4.12	4.18	.06					

$Diff^2 = .01$ F = .4938

Table 42 b. Least squares approximation to the Vioolsdrif adamellite (A) by subtracting the listed quantities (X_{mix}) of the suggested fractionating phases from a parental tonalite (T).

Results for Adamellite (A)

	Obs.	Est.	Diff.		X_{mix}	S.D.	X_{solid}	
SiO_2	69.42	69.42	.00	T	1.7095	.0142		
TiO_2	.47	.47	.00	HBL	-.1391	.0063	.1961	
Al_2O_3	14.74	14.75	.01	BIOT	-.0862	.0047	.1215	
FeO	3.14	3.14	.00	PLAG	-.4285	.0212	.6041	An_{59}
MgO	1.21	1.22	.01	MT	-.0555	.0062	.0783	Usp_{37}
CaO	2.74	2.71	.03	TOTAL	1.0002	.0188		
Na_2O	3.16	3.12	.04					
K_2O	4.78	4.73	.05					

$Diff^2 = .01$ F = .5850

andesites and are listed in Table 41. The results may be compared with those obtained for the step (D - T). D^{Sr}_{plag} is slightly higher in the passage to the granodiorite, which is consistent with the slightly lower An content required in the least squares approximation. The predicted D^{i}_{hbl} values are similar to those predicted for the passage to tonalite, which is to be expected since both steps involve fractionation of the same parent magma, probably under similar P, T conditions. These consistent results suggest that the fractionation scheme, whereby both the tonalite and granodiorite are derived from a common parental diorite magma, is feasible and more likely than the stepwise scheme discussed previously. Furthermore, the common initial Sr^{87}/Sr^{86} ratio of the three intrusive rock types is consistent with this particular scheme.

16.2.2 Origin of the adamellite

Derivation of the adamellite by direct fractionation of the diorite is unrealistic because the average distribution coefficients are not constant over this crystallisation interval. The diorite initially crystallises orthopyroxene, which subsequently disappears by reaction; biotite probably appears after a significant interval following the disappearance of orthopyroxene. The passage from diorite to adamellite probably involves three steps; the first in which the solid removed contains orthopyroxene as a component, a second containing neither orthopyroxene nor biotite and a third containing biotite as a component. These significant changes in the assemblage probably have a pronounced effect on $\overline{D^{i}}$.

The only other possible parent magma for the adamellite is the tonalite and a least squares approximation to the former is given in Table 42b. The solid material removed from the tonalite contains significant amounts of hornblende and biotite, which is consistent with the observed modal mineralogy of this rock type. The predicted plagioclase composition is more calcic than that observed in the granodiorite, but less calcic than the cores of plagioclase present in the diorite.

The observed depletion in Sr is reflected in the $\overline{D^{Sr}}$ value of 2.14 (Table 40) and corresponds to a D^{Sr}_{plag} of 3.5, which is similar to that predicted for An_{59} (3.8) by Korringa and Noble (1971). The observed Ni and Co abundances are too low to be of any use and only V can be evaluated further. D^{V} for hornblende and biotite may be calculated assuming a D^{V}_{mt} of 20 and the inter-mineral relationship $D^{V}_{hbl/biot}$ given in Table 29. The results are listed in Table 41 and indicate that for a D^{V}_{mt} of 20, D^{V}_{hbl} and D^{V}_{biot} must be about 2.2 and 2.3 respectively in order for the behaviour of V to be consistent with this particular fractionation scheme. The value for D^{V}_{hbl} is similar to that obtained for the steps (D - T) and (D - G) (see Table 41) and since D^{V}_{mt} is the same as that adopted for those steps, the results obtained for the step (T - A) appear reasonably consistent. The behaviour of Ba may also be predicted by the fractionating assemblage; by adopting D^{Ba}_{plag} = 0.3 (for An_{59}, Korringa and Noble, 1971) and the inter-mineral relationship $D^{Ba}_{hbl/biot}$ given in Table 29, the values for D^{Ba}_{hbl} and D^{Ba}_{biot} are 0.3 and 7.7 respectively, which are within the range compiled by Arth (1976).

The observed behaviour of major and selected trace elements appear to be compatible with the production of the adamellite by fractionation of the proposed mineral assemblage hbl-biot-plag-mt from a parental tonalite. However, the results of the Rb-Sr isotopic study indicate that the adamellite has a significantly higher initial Sr^{87}/Sr^{86} ratio. Inspection of Table 7 in Chapter 3 reveals that the adamellite is also significantly younger than the tonalite by about 165 Ma. This latter feature may provide a clue as to the reason why the adamellite is anomalous in terms of its initial Sr isotopic composition. The combined Rb-Sr isochron (D/T/G) probably yields the best estimate of the initial Sr^{87}/Sr^{86} ratio (0.7030) and the age of intrusion (1940 Ma) of the tonalite. If the adamellite magma was formed at this time by fractional crystallisation of a tonalite, then the increase in Rb/Sr ratio caused by plagioclase fractionation may be sufficient to "age" the derivative magma during the lull in intrusive activity. The average Rb/Sr ratio of the adamellite is 0.70 (from Table 36), which yields an Rb^{87}/Sr^{86} ratio of 2.02. Assuming that the adamellite had an initial Sr^{87}/Sr^{86} ratio of 0.7030 at 1940 Ma, then this ratio would have increased to 0.7069 by 1800 Ma, which is very similar

to the observed initial Sr^{87}/Sr^{86} ratio (0.7065). Since there is a significant time interval between intrusion of the D/T/G complex and the later adamellite, such a process of magmatic "aging" appears feasible. An alternative process, is contamination of adamellite magma (originally produced by fractional crystallisation) by material with a significantly higher Sr^{87}/Sr^{86} ratio. No likely candidates occur in the study area because the HVIP is the oldest known group of rocks in the Lower Orange River region . Older basement rocks presumably underlie the HVIP but their composition is unknown. However, if it is assumed that this underlying basement is broadly granitic in composition, then at the time of the Vioolsdrif magmatism the basement rocks may have had a high Sr^{87}/Sr^{86} (>0.71?) which, if assimilated by the adamellite, may have produced the anomalously high initial Sr^{87}/Sr^{86} of 0.7065. The composition of the magma and contaminant will probably be very similar, since they are both granitic, but differ only in their respective Sr^{87}/Sr^{86} ratios. Contamination of the adamellite with old granitic basement is therefore a feasible mechanism, but suffers from the fact that a quantitative evaluation cannot be carried out.

The mean initial Sr^{87}/Sr^{86} ratio of the leucogranite is lower than that of the adamellite but the uncertainty for both initial ratios is so great that no conclusions may be reached. The one sigma error range is such that the leucogranite initial Sr^{87}/Sr^{86} ratio can fall between .7021 and .7063 and this range overlaps with that of the D/T/G and the adamellite. If the fractionation scheme to produce the leucogranite is accepted, then the probable initial Sr^{87}/Sr^{86} is near 0.7065. In view of the high Rb/Sr ratios of the leucogranite there is little use in further total rock Rb-Sr investigations; however, analysis of low Rb/Sr minerals (e.g. plagioclase) may help in solving this problem.

16.3 Adamellite from a different source

Another alternative is that the adamellite represents magma derived directly or indirectly from a different source. Since indirect derivation

implies the existence of precursors (i.e. parental magmas), the absence of more basic rocks in the batholith with initial Sr^{87}/Sr^{86} of .7065 renders this alternative model impossible to evaluate. If the adamellite magma was derived directly (i.e. was a primary magma), then the most likely source is the lower crust. It has become increasingly clear that many acid intrusive rocks in calc-alkaline batholiths have initial Sr^{87}/Sr^{86} ratios of .705 - .708 (Kistler, 1974; Brown, 1977). Early estimates of the Sr isotopic composition of potential crustal source rocks (e.g. Hurley *et al.*, 1965; Gast, 1960; Faure and Powell, 1972) have contributed to the apparent enigma of granitic magmas with initial Sr^{87}/Sr^{86} ratios less than about .708.

Continental crust has possibly generated in a manner similar to that proposed by Taylor (1967) and Ringwood (1974), involving irreversible differentiation of the mantle which is brought about by island arc magmatism. While the operation of a process such as island arc magmatism in Precambrian times is debatable, the Sr isotopic composition of any portion of newly formed continental crust will not be far removed from its mantle derived precursor (cf. Moorbath, 1975). The degree of enrichment in Sr^{87} will depend on the Rb/Sr ratio and the age of that particular portion of crust. In view of the low Sr^{87}/Sr^{86} ratios implied by crustal derived granitic magmas (.705 - .708), the crustal source rocks must either be very young (i.e. consolidated shortly before magma generation) or have Rb/Sr ratios significantly lower than those values adopted by Gast (1960); Hurley *et al.*, (1965) and Faure and Powell (1972).

Lower crustal material, such as some high pressure granulite terrains, have low Rb/Sr ratios (<0.2, Lambert and Heier, 1968) but are also usually low in Rb, K, Ba, U and Th. This feature has been interpreted as evidence for an earlier depletion event, often equated with removal of a granitic magma. If granulite terrains showing such depletion in granitophile elements owe their geochemical characteristics to a previous history of melt removal, then it is difficult to believe that such low Rb/Sr rocks could produce more granitic magma.

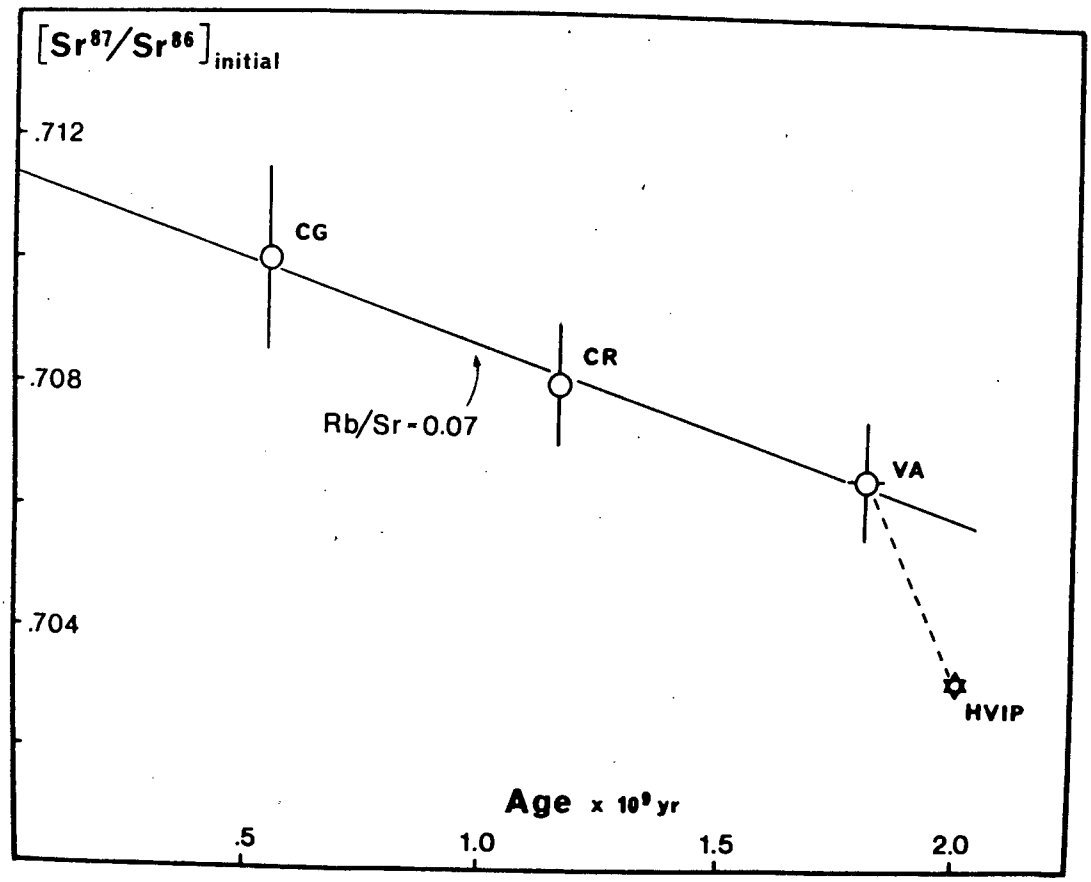

Fig. 68. Plot of initial Sr^{87}/Sr^{86} ratios against geologic age for various granites in the lower Orange River region.

Symbol	Rock suite	Age (Ma)	(Sr^{87}/Sr^{86})	Source
CG	Cape Granite	553 ± 4	.710 ± 15	Allsopp and Kolbe (1965)
CR	Concordia and Rietberg Granites	1166 ± 10	.708 ± 1	Clifford et al., (1975)
VA	Vioolsdrif adamellite			
HVIP	Haib - Vioolsdrif Igneous Province (parental magma)			

Data for VA and HVIP from Table 7.

Recent estimates for the average composition of island arcs and continental crust (e.g. Taylor, 1967, 1969; Jakes and White, 1971; Jakes, 1973) are andesitic rather than rhyolitic. The average andesite in island arcs studied by Taylor (1969) has a Rb/Sr ratio of .081. The data reported by Jakes and White (1971) yield an average Rb/Sr ratio for the rocks comprising modern island arcs, of .052. An average Rb/Sr ratio of .091 for the lower crust has been estimated by Shaw (1972). An overall average of these average values is .075, which is significantly lower than previous estimates (e.g. 0.25, Hurley *et al.*, 1965; Gast, 1960; 0.18, Faure and Powell, 1972). These higher values have been interpreted by Shaw (1972) as representing the upper crust, which has experienced a more protracted history of Rb-Sr fractionation than the lower crust.

Bearing this estimate of the Rb/Sr ratio of potential lower crust source rocks in mind, it is pertinent to ask if there is any evidence for such material underlying the lower Orange River region. Sr isotopic data on granitic rocks from this region are few, but Fig. 68 contains estimates of initial Sr isotopic compositions of granitic magma ranging in age from 550 Ma to 2000 Ma. Although the 550 Ma granites in the lower Orange River region (Kuboos-Bremen line of intrusives, Söhnge and De Villiers, 1948) have not been investigated, rocks of similar age and composition occur in the south-western Cape (the Cape granites of Allsopp and Kolbe, 1965). Scholtz (1946) and Kolbe (1966) have regarded the Kuboos-Tatasberg-Bremen intrusives as part of a 500-550 Ma granite province, which includes the Cape granites and similar rocks near George in the southern Cape.

The initial Sr^{87}/Sr^{86} ratios for the Cape granite, post-tectonic granites of the Springbok district (Clifford *et al.*, 1975) and the Vioolsdrif adamellite, conform to a line which has a slope appropriate to a Rb/Sr ratio of about .07. The uncertainties are quite large but the data indicate that these three granites of different ages may have been derived from a common source with Rb/Sr ratios similar to that estimated for the lower crust.

At present, the only justification for considering such an alternative for the origin of the Vioolsdrif adamellite is that provided by Sr isotopic data.

The alternative model involving Rb-Sr aging is a consequence of the conclusions reached after an evaluation of all major elements and selected trace elements. The magmatic aging model is currently preferred to that which invokes a different source purely because it may be tested more rigorously with the information available. However, the implications of the alternative source model certainly warrant further study.

16.4 Discussion

The observed major and trace element composition of the five granitic magma types within the VIS may have been produced by fractional crystallisation of the dioritic parental magma. The dominant minerals crystallising include plagioclase, hornblende and biotite, which constitute the main modal components in all rock types. Hornblende and magnetite fractionation may have been responsible for the lack of Fe enrichment in the passage from diorite to tonalite and granodiorite, thereby producing a suite of calc-alkaline intrusives. That the early Vioolsdrif granitic rocks (diorite, tonalite and granodiorite) are linked by fractional crystallisation is consistent with their common initial Sr^{87}/Sr^{86} ratio.

More evolved granitic magmas may also be produced by fractional crystallisation involving the removal of the same phases mentioned above. However, the adamellite has a significantly higher initial Sr^{87}/Sr^{86} ratio than the early granitic rocks. The more radiogenic differentiates may have been the result of Rb-Sr " aging", since the adamellite is significantly younger than the earlier, more basic rocks. High Rb/Sr ratios produced by plagioclase fractionation provide the means whereby Sr^{87}/Sr^{86} may be significantly increased over the time interval ($\sim$150 Ma) between the early Vioolsdrif granitic rocks (diorite, tonalite, granodiorite) and the later differentiates (adamellite, leucogranite). The youngest Vioolsdrif granite, the leucogranite, has a Rb/Sr age close to that of the adamellite, but the uniformly high Rb/Sr ratios result in a very poorly estimated initial Sr^{87}/Sr^{86} ratio, but which falls in the range of initial Sr^{87}/Sr^{86} ratio for the adamellite. The production of leucogranite by fractionation of the adamellite is therefore not ruled out on

the basis of the Sr isotopic evidence.

A potential problem with this fractional crystallisation model is the relative proportions of the various granitic rock types at present exposed. The presumed parent - diorite - is volumetrically insignificant compared to the later tonalites and granodiorites. Furthermore, the model predicts large bodies of complementary cumulates at depth. The question of volume and complementary cumulates is not a new problem (e.g. Turner and Verhoogen, 1960) and has been used as evidence against the simple fractional crystallisation model.

To overcome the volume problem it is possible to invoke the presence of more basic rocks at depth, which implies that the surface exposures do not yield realistic estimates of the actual volumetric proportions. Continued erosion of the batholith may reveal a greater proportion of diorites and even gabbros. Hamilton and Myers (1967) have suggested that granitic batholiths do not persist to very great depths and Fyfe (1971, 1973) has suggested that granitic plutons in batholiths are the result of diapiric intrusion. Batholiths may be relatively thin and their shape governed by gravity, in that lighter granitic fractions rise and spread out near the surface of the crust. Light fractions such as adamellite may form a thin veneer over a predominantly basic to intermediate batholithic complex.

Geophysical investigations, to establish the presence of complementary basic-ultrabasic cumulate bodies under the Vioolsdrif batholith, have yet to be carried out. In regions where such work has been undertaken, the geophysical data usually provide no evidence for the presence of basic-ultrabasic bodies beneath granitic batholiths (e.g. Turner and Verhoogen, 1960; Carmichael *et al.*, 1974). A possible reason for the lack of any geophysical expression of complementary cumulates is that they occur near the base of the crust and therefore display very little chemical and physical contrast with the surrounding rocks (Erikson, 1976; Osborn, 1969).

An alternative model involving the production of all granitic rocks by fractional crystallisation of a tonalitic parent is attractive because it may

explain the diorites as cumulate enriched material, while the more acid rocks represent the differentiates. Tonalite is probably the most abundant rock type in the batholith at the present erosion level. Unfortunately, a tonalite parent must be ruled out because it is not possible to derive the later differentiate - granodiorite - by simple fractional crystallisation (see 16.1.2). The predicted mineral assemblage removed from the tonalite is inconsistent with both petrographic data and observed trace element abundances.

More complex models have not been evaluated in this study and further work may result in the simple fractional crystallisation model presented here being discarded. At least the implications of the preferred model are reasonably clear and able to be tested. Models involving contamination, magma mixing, crustal and mantle derived magmas and polybaric crystal fractionation must await further work on this vast intrusive complex.

17

MAGMA GENESIS AND SOURCE CHARCTERISTICS

17.1 Basaltic andesite (BA) as primary magma

It has been suggested in Chapter 15, that the most basic lavas (BA) in the HVG represent magma that was parental to the differentiated suite basaltic andesite (BA1) - andesite - dacite - porphyritic rhyolite. The possibility that BA represents a primary magma is evaluated here; the term "primary" is used in the sense of Carmichael et al., (1974), as describing an unmodified, unfractionated liquid formed directly by partial fusion of a pre-existing solid.

The basic nature of BA is taken to preclude its derivation from any crustal source and the relatively high MgO content suggests that most basaltic source materials are also excluded. Although BA has been regarded as a basaltic andesite on the grounds of its relatively high SiO_2 and DI, the observed abundances of MgO and ferromagnesian trace elements (Ni, Co, Cr) are more typical of basalts. Most natural and synthetic basaltic systems investigated experimentally do not contain more than 10-11% MgO, and to produce a liquid with 8.5% MgO requires excessively high degrees of partial fusion. Such high degrees are theoretically possible, but it is difficult to envisage the retention of a gravitationally unstable system such as a partial melt until 80-90% of the basaltic source rock has fused; segregation and uprise of a magma diapir will probably occur long before such high degrees of partial fusion are attained. A more likely model involves lower degrees of partial fusion of some ultrabasic source material in the upper mantle.

An important prerequisite of any mantle derived primary magma is that it must be in eqilibrium with the solid residue (mainly olivine). Kesson (1973) formulated a criterion for equilibrium using the empirical relationship between olivine and mafic liquid established by Roeder and Emslie (1970). Kesson (1973) introduced the parameter "Mg number" (= 100 MgO/(MgO + FeO) mole percent) by which the distribution of Mg and Fe between upper mantle olivine

and primary melt may be expressed. Liquids in equilibrium with upper mantle olivine (Mg number = 87.5-92) should have Mg numbers ranging from 67 to about 77. The Mg number of BA will depend on the amount of FeO, which in turn depends on the Fe_2O_3/FeO ratio of the primary magma. Kesson (1973) adopted a value of 0.25 for Fe_2O_3/FeO in alkaline lavas and if this figure is used, then the FeO content of BA is 7.59 and the Mg number is 67, which is just within the range for primary melts. In Chapter 7, it was concluded that the average Fe_2O_3/FeO predicted by the method of Le Maitre (1976b) yielded reasonable results in view of the presence of phyric magnetite, which implied Fe_2O_3 contents at least as high as 3%. The resulting Fe_2O_3/FeO ratio using the method of Le Maitre on BA is 0.57, which yields a higher Mg number of 71. In terms of the predicted distribution of MgO and FeO between upper mantle olivine and liquid, BA fulfils the requirement of a primary magma.

Another salient feature of BA is the relatively high K_2O and K/Na ratio, which suggests that the origin of BA is probably related to the genesis of high K calc-alkaline magmas and, in particular, the factors controlling the K content of primary melts. In addition, recent work on modern high K calc-alkaline lavas in island arcs and active continental margins has shown that Mg, Ni and Cr are variable, but are generally higher than in "normal" calc-alkaline lavas (Jakes and White, 1972a; Jakes and Smith, 1970; McKenzie and Chappell, 1972). The geochemical constraints placed on the genesis of calc-alkaline magmas by Taylor (1969) are therefore not strictly applicable to high K varieties. The major compositional differences between high and lower K basaltic andesites are shown in Table 43.

Potassium occurs in the upper mantle either as a trace element (<100 ppm) in the major minerals (olivine, pyroxene, garnet, spinel), along grain boundaries, or as a stoichiometric component in minor phases such as phlogopite and amphibole (Gast, 1968 ; Erlank, 1970; Oxburgh, 1964). It is likely that K will be strongly partitioned into the liquid during melting, and that K bearing phases such as phlogopite or amphibole will disappear very close

Table 43. Major and trace element abundances in high and low K basaltic andesites.

	BA	1	2	3	4
SiO_2	54.6	54.9	56.4	52.4	54.2
TiO_2	.70	.82	1.0	1.0	1.5
Al_2O_3	14.4	17.5	15.7	16.3	15.7
FeO*	9.3	8.2	6.7	8.3	7.5
MgO	8.5	4.7	6.5	6.4	6.0
CaO	9.0	8.5	7.3	8.5	8.1
Na_2O	1.8	3.4	3.7	3.1	3.9
K_2O	1.3	1.1	1.9	2.5	2.9
Ba	719	200	603	561	3050
Rb	40	14	52	62	74
Zr	109	92	187	122	--
Th	4.9	1.3	7.1	--	7.4
U	.7	.4	1.9	--	1.8
Sr	450	438	611	973	2100
Ni	125	28	166	54	74
Cr	420	85	387	147	172
V	200	200	139	214	195

1 Average low Si andesite of Taylor (1969)
2 High K basaltic andesite, Papua New Guinea (Jakes and Smith, 1970)
3 High K basaltic andesite (shoshonite) New Guinea highlands (McKenzie and Chappell, 1972)
4 Low Si latite, central Peruvian Andes (Noble et al., 1975)

to the solidus. This has been questioned by Forbes and Flower (1974) and Beswick (1976), who suggest that under hydrous conditions, phlogopite may be a refractory phase in the upper mantle. Experimental studies of hydrous melting of upper mantle materials have shown that under certain conditions, phlogopite may coexist with a mafic liquid and therefore buffer the K content of primary melts (Modreski and Boettcher, 1972; Bravo and O'Hara, 1974; Mysen and Boettcher, 1975a,b). However, the maximum K content of undepleted upper mantle (garnet lherzolite) is probably 1000 ppm (Engel et al., 1965; Gast, 1965) which limits the amount of phlogopite (K = 9.4%) to about 1%, assuming that all K is contained in this mineral. The experimental charges studied by the above authors contained at least 3% phlogopite, which seriously limits their applicability unless the maximum K content cited previously for the upper mantle is a gross underestimate.

If it is assumed that all K in the source enters the liquid during partial melting, then in order to attain a concentration similar to that in BA (1.3% K_2O = 1.08% K), 9.3% of the source material needs to be melted. Under anhydrous conditions and low pressures (< 15kbar), the partial melt will be a saturated (ol-hy-normative) tholeiitic basalt (Kushiro, 1973). Qz-normative andesitic & basaltic magmas may be produced from the same source material under vapour present conditions up to 25 kbar, provided $X_{H_2O}^{vap}$ (mole fraction of H_2O in vapour phase) is greater than 0.6 (Mysen and Boettcher, 1975b). Lower water contents tend to result in saturated and undersaturated partial melts. Inspection of liquid compositions reported by Mysen and Boettcher (1975b), reveal that they are much lower in MgO (< 5%) than BA, although no data on the extent of melting in their experimental charges were given.

The extent of melting suggested by the K content of BA may be used to predict the behaviour of Ni, using equations expressing trace element distribution during anatexis developed by Gast (1968) and Shaw (1970). Assuming that the liquid has remained in equilibrium with the solid residue throughout the melting interval, and that the relative proportions of minerals contribu-

ting to the melt remain constant, then

$$\frac{C_l^i}{C_o^i} = \frac{1}{\overline{D^i} + F(1-\overline{D^i})} \qquad (14)$$

where, C_l^i = concentration of i in liquid

C_o^i = concentration of i in original solid

$\overline{D^i}$ = average solid/liquid distribution coefficient

F = weight fraction of liquid

The assumption of modal melting is not strictly justifiable, since minor phases (e.g. phlogopite, amphibole) are considered to disappear very near the solidus. However, the phases controlling the behaviour of Ni will be the major components (olivine, pyroxenes, garnet) which may not experience any drastic change in their relative proportions with up to 10 percent melting. Recent estimates for C_o^{Ni} range from 1600 ppm (Harris et al., 1967) to 2800 ppm (Reid et al., 1974) and substitution in equation (14) yields $\overline{D^{Ni}} = 14$ for F = 0.093, $C_o^{Ni} = 1600$, $C_l^{Ni} = 125$; and $\overline{D^{Ni}} = 25$ for $C_o^{Ni} = 2800$. Both the maximum and minimum possible $\overline{D^{Ni}}$ values are higher than individual D^i values for the residual phases (olivine, pyroxenes, garnet). Olivine probably has the highest D^{Ni}, and the empirical relationship of Hart et al., (1977) suggests that

$$\ln D_{ol}^{Ni} = 3.325 - 0.0885 \cdot MgO \qquad (15)$$

For a liquid with MgO = 8.5 percent (that for BA), D_{ol}^{Ni} will be about 13, and since D_{opx}^{Ni}, D_{cpx}^{Ni} and D_{gt}^{Ni} will all be significantly lower than D_{ol}^{Ni}, the behaviour of Ni is inconsistent with the idea that BA represents a 10 percent partial melt of undepleted upper mantle material.

A similar conclusion may be reached with Cr; recent estimates for C_o^{Cr} range from 2050 to 3350 ppm (Harris et al., 1967; Hutchison et al., 1970; Reid et al.,1974). Substitution in equation (14) yields $\overline{D^{Cr}} = 5.3$ for $C_o^{Cr} = 2050$ and $\overline{D^{Cr}} = 8.7$ for $C_o^{Cr} = 3350$. These figures appear high

because the residual mantle is dominated by minerals with low D^{Cr} (about 1-2, e.g. olivine and orthopyroxene). Minerals with high D^{Cr} (>> 2, e.g. clinopyroxene, garnet and Cr-spinel), probably make up less than 10 percent of the residual mantle and therefore will not contribute enough to produce $\overline{D^{Cr}}$ values of 5 or more, even with the small contributions from olivine and orthopyroxene. Modal estimates of depleted mantle indicate that clinopyroxene and garnet may be either absent, or present in very small amounts (2-3 percent); Cr-spinel probably makes up about 1 percent (Reid et al, 1974; Gurney et al., 1974; Kuno and Aoki, 1970). If values of 20, 30 and 300 are taken for D^{Cr}_{cpx}, D^{Cr}_{gt} and D^{Cr}_{spinel} respectively, then the contribution to $\overline{D^{Cr}}$ will be

$$0.03 \cdot 20\ (cpx) + 0.03 \cdot 30\ (gt) + 0.01 \cdot 300\ (Cr\text{-}spinel) = 4.5$$

This is probably the maximum possible contribution to $\overline{D^{Cr}}$ from Cr-bearing phases in the residual mantle, but is still not sufficient to produce the high $\overline{D^{Cr}}$ predicted by the observed Cr content of BA.

To summarise, certain chemical features of BA are consistent with a primary nature, while others are not. If a reasonable estimate for the Fe_2O_3 content in BA is made, then the Mg number is sufficiently high (67-71) to fulfil the requirements of a primary magma. Assuming a K content of 1000 ppm for undepleted upper mantle, the melt fraction necessary to produce a magma with 1.08 percent K is about 9%. This is consistent with the prediction of Kushiro (1973) and Mysen and Boettcher (1975b), that low degrees of partial melting of hydrous garnet lherzolite could produce oversaturated andesitic-basaltic magmas. However, the MgO content of BA is significantly higher than that in any of the liquid compositions reported by the above authors. Furthermore, the Ni and Cr contents of BA are too low for this magma to have been in equilibrium with those minerals considered to be present in the residual mantle (olivine, orthopyroxene). The evidence is too conflicting to conclude that BA represents a primary magma, and other models involving a primary precursor to BA must be considered.

17.2. Basaltic andesite (BA) as a derivative magma

The derivative nature of BA is difficult to evaluate, because of the uncertainty in identifying the mafic phenocrysts which could have shed some light on any pre-history (e.g. high pressure phenocrysts, xenocrysts). The dominant mafic phenocryst phases could have been orthopyroxene and augite, since fractionation of these two minerals, together with plagioclase and magnetite, can produce a reasonably close approximation to the observed major element variation trends. Such an assemblage is characteristic of low pressure crystallisation (Ewart et al., 1973), although it is quite possible that BA had precursors that were produced by polybaric fractionation (O'Hara, 1968). Evaluation of complex models involving polybaric fractionation is not justified by the information available, but certain petrographic and chemical features place constraints on the composition of possible precursors. The subordinate nature of plagioclase as a phenocryst phase in BA suggest that this mineral was also subordinate in the precursor. It follows that magma parental to BA was even lower in Al_2O_3 (< 14 percent) as well as being higher in MgO (> 8.5 percent) and probably Ni (> 125 ppm). Such high Mg, Ni, low Al basaltic magmas appear to be rare in modern island arcs and active continental margins, although they are well developed in the fairly primitive island arc of the Solomons (Stanton and Bell, 1969; Cox and Bell, 1972). Cox and Bell (1972) have argued that the olivine-phyric picritic basalts of the Solomon arc are not cumulates and owe their phenocryst rich nature to a process they term "compensated crystal setting". This mechanism has been discussed in 15.5. According to Jakes and Gill (1970) and Ringwood (1974), the earliest volcanic products of modern island arc magmatism are tholeiitic (island arc tholeiitic series), with basalt and basaltic andesite dominant. In contrast to the earliest tholeiitic basalts in the Solomon arc, typical island arc tholeiites are alleged to be low in MgO (< 5 percent), Ni (< 30 ppm) and contain relatively low K_2O (compared to calc-alkaline and shoshonitic basalts). It is clear that the high Mg, Ni, K, low Al basalts of

the Solomon arc are anomalous, at least in terms of currently held theories of island arc magmatism. Fractionation of such a basic magma however, involving the removal of suitable amounts of the observed phenocryst phases (olivine, clinopyroxene, minor plagioclase), could possibly produce a residual magma similar to BA. Nicholls and Whitford (1976) have come to a similar conclusion and postulate the presence of a primary basaltic magma that fractionated olivine to produce the Cenozoic basaltic andesite and andesite lavas in the Indonesian island arc. Table 44 lists the average compositions of picritic and high Mg basalts from the Solomon arc, compared with a 'typical' arc tholeiite and high-Al basalt from the Melanesian arcs. Also included are possible primary magma compositions estimated by Nicholls and Whitford (1976) for the Indonesian island arc. An interesting point, is the relatively high K_2O content of the Solomon picrite. Assuming an upper mantle source with 1000 ppm K, then in order to produce a primary magma with 0.66 percent K, the melt fraction required is 15.3 percent (assuming all K in the source enters the melt). This fraction appears small in view of the high MgO content of the liquid. Picritic liquids are thought to represent at least 30 percent partial melting of mantle source material (pyrolite, Green, 1972; hydrous garnet lherzolite, Mysen and Boettcher, 1975a,b), and in order to reconcile the high K content, some other process acting on the liquid, subsequent to generation, must be invoked. Jamieson and Clarke (1970) have concluded that high K contents in some continental basaltic rocks are probably the result of mantle wall rock reaction (cf. zone refining, Harris, 1957). High K picritic basalts studied by Cox and Jamieson (1974) and Kristanamurthy and Cox (1977) have been interpreted in a similar fashion.

To summarise, BA may have been derived from a high Mg, low Al basaltic magma, by olivine ± pyroxene ± minor plagioclase fractionation. This precursor is probably not a primary magma, since it would have to contain too much K to be produced by about 30 percent partial melting of a mantle source with only 1000 ppm K. The ultimate primary melt probably gained K by some process

Table 44. Major oxide composition of various basaltic magmas observed or postulated in modern island arcs.

	BA	1	2	3	4	5
SiO_2	54.6	47.2	50.0	50.6	51.6	56.0-47.3
TiO_2	.70	.42	.54	1.1	.8	.7- 1.4
Al_2O_3	14.4	8.5	13.0	16.3	15.9	19.0-14.5
FeO*	9.3	9.9	10.3	8.4	9.5	8.1-10.8
MgO	8.5	23.2	11.1	9.0	6.7	6.7-12.1
CaO	9.0	8.1	11.0	9.5	11.7	11.2- 6.5
Na_2O	1.8	1.3	2.1	2.9	2.4	3.1- 2.4
K_2O	1.3	.79	1.4	1.1	.44	1.7- 0.3

1 Picrite basalt, Solomon island arc (Stanton and Bell, 1969)

2 Basalt, Solomon island arc (Stanton and Bell, 1969)

3 "Typical" high Al basalt, Melanesian arcs (Jakes and White, 1972a)

4 "Typical" island arc tholeiite, Melanesian arcs (Jakes and White, 1972a)

5 Range of possible primary magmas, Indonesian island arc (Nicholls and Whitford, 1976)

involving wall rock interaction during diapiric uprise through the overlying mantle. Finally, the most likely precursor to BA probably resembles high Mg basalts erupted during the early stage of evolution of the Solomon island arc, or the postulated primary basaltic magma for the Indonesian island arc. However, such high Mg, low Al basalts seem to be rare in modern orogenic igneous provinces.

17.3. Vioolsdrif diorite (D) as a primary magma.

Compared to BA, the Vioolsdrif diorite (D) is significantly higher in Al_2O_3 and lower in MgO and more closely resembles modern high alumina calc-alkaline quartz diorites and volcanic equivalents (basaltic andesite).

Because of these differences, the more basic members of the Vioolsdrif plutonics and the Haib volcanics may not, strictly speaking, be comagmatic.

It has been demonstrated in Chapter 16, that diorite could be parental to the entire granitic suite; the possibility that the diorite represents a primary magma will be considered here. Oversaturated, high alumina, low Mg calc-alkaline magmas (diorite, tonalite) may be formed by partial melting of hydrous garnet lherzolite under P,T conditions present in the upper mantle (Kushiro, 1973; Mysen and Boettcher, 1975a,b). On the other hand, similar liquids may be formed by partial fusion of basaltic material (oceanic crust, amphibolite, eclogite) under hydrous conditions (Helz, 1973, 1976; Hollaway and Burnham, 1972; Ito and Kennedy, 1974; Lambert and Wyllie, 1972; Green and Ringwood, 1968).

It is unlikely that the diorite (D) represents a mantle derived primary magma because the various chemical criteria outlined in 17.1 are not satisfied. The Mg number of the diorite is 55, if the Fe_2O_3/FeO ratio is taken as 0.25 (Kesson, 1973) and 60 if the Fe_2O_3/FeO ratio is estimated using the method of Le Maitre (1976b). In the latter case the Fe_2O_3/FeO ratio is 0.51. The Ni and Cr contents (102 and 55 ppm respectively) are too low for a liquid with the composition of D to have been in equilibrium with an olivine rich residual mantle. Moreover, to produce a primary liquid with 1.83 percent K (that of D), only 5.5 percent of the upper mantle source (with 1000 ppm K) may be melted. This melt fraction appears too low to produce sufficient magma to generate a batholithic complex with the size of the VIS.

The composition of liquids formed by partial melting of basalt must be similar to those formed by equilibrium crystallisation of a basaltic magma under the same P,T conditions. The locus of liquid compositions formed by equilibrium batch melting will be indistinguishable from a liquid line of descent. The same mineralogical controls as those invoked for crystallisation differentiation must operate during partial melting. It follows that calc-alkaline liquids produced by partial melting of a basaltic source must be in equilibrium with residual magnetite and/or amphibole.

Liquids in equilibrium with amphibole, analysed by Helz (1976) during a study of hydrous melting of basalt, are very low in MgO (< 2 percent). Higher MgO liquids were produced only when amphibole broke down in response to increasing temperature ($\geqslant 1000^{o}C$). Liquids with SiO_2 about 55 percent, Al_2O_3 = 16-18 percent and MgO about 4 percent were generated either above or near to the stability limit of amphibole. Liquid compositions similar to D were produced by about 50-60 percent melting of hydrous olivine tholeiite (1921 Kilauea tholeiite) leaving a residue of amphibole, clinopyroxene and olivine (QFM buffer, $1045^{o}C$, $P_{H_2O} = P_{total}$ = 5 kbars) and clinopyroxene, Fe-Ti oxide and olivine (HM buffer, $1000^{o}C$, $P_{H_2O} = P_{total}$ = 5 kbars).

The melt fraction necessary to produce D by partial melting of the 1921 Kilauea tholeiite may be calculated by a least squares approximation, assuming that

Partial melt (D) + Residual phases = 1921 Kilauea tholeiite

The relevant input data and results are listed in Tables 45 and 46 and suggest that 44% melting could produce a liquid similar in major element composition to D. The residual mineral assemblage (amphibole, clinopyroxene, olivine) is that produced under oxygen fugacities appropriate to the QFM buffer. A residual assemblage containing Fe-Ti oxide in place of amphibole (HM buffer), produced unsatisfactory results.

The nature of the residual assemblage suggests that certain trace elements will be strongly partitioned into the liquid. The concentration of these incompatible elements in the source may be estimated using the relationship

$$C_o^i = C_1^i \cdot F \qquad (16)$$

where C_o^i = trace element content in source, C_1^i = trace element content in D and F is the melt fraction. The results are listed in Table 47 and may be compared with published data for Hawaiian tholeiites. Unfortunately, no trace element data are available for the 1921 Kilauea tholeiite but similar

Table 45. Composition of residual phases in possible source material (oceanic crust). HBL, OL and CPX for hydrous basalt (Helz, 1973); GARN and OMPH (garnet and omphacite) for eclogite (Gill, 1974; Green, 1972)

	HBL	OL	CPX	GARN	OMPH
SiO_2	40.08	37.9	51.56	39.7	49.3
TiO_2	4.27	0	.96	.95	.87
Al_2O_3	13.34	0	2.24	21.9	12.5
FeO	15.68	23.3	6.99	11.9	5.2
MgO	9.92	38.1	16.0	15.4	12.8
CaO	11.24	0	21.53	7.8	15.6
Na_2O	2.30	0	.32	0	2.0
K_2O	.50	0	0	0	0

Table 46. Least squares approximation to a possible basaltic source (Hawaiian tholeiite) as a linear addition of the Vioolsdrif diorite (D) to the presumed residual phases

Results for 1921 Kilauea tholeiite

	Obs.	Est.	Diff.		X_{mix}	S.D.	X_{solid}
SiO_2	49.11	49.06	.05	D	.4406	.0285	
TiO_2	2.51	2.08	.43	HBL	.3542	.0413	.6218
Al_2O_3	12.74	12.70	.04	OL	.0563	.0137	.0988
FeO	11.35	11.56	.21	CPX	.1591	.0210	.2793
MgO	10.3	10.23	.08	TOTAL	1.0102	.0561	
CaO	10.73	10.86	.13				
Na_2O	1.97	1.99	.02				
K_2O	.49	1.14	.65				

$Diff^2$ = .67 F(Melt fraction) = .4406

Table 47. Predictions of the basaltic source model. Obs. = observed trace element composition of a possible basaltic source (Hawaiian tholeiite, data from Gunn, 1971 and Murali et al., 1977); Est. = estimated composition using equation (16) and the composition of the Vioolsdrif diorite (D); C_s = concentration in the basaltic source; C_d = concentration in the Vioolsdrif diorite; $\overline{D_c}$ = predicted average solid/liquid distribution coefficient using equation (4) and the data from Table 46.

	Obs.	Est.		C_s	C_d	$\overline{D_c}$
Rb	10	35	Ni	210	102	2.9
Ba	170	313	Co	60	35	2.3
Zr	110	71	Cr	500	55	15.4
Y	23	7.7	V	300	196	2.0
Sr	330	222				

Table 48. Least squares approximation to a possible eclogitic source (composition of average modern oceanic tholeiite, Gill, 1974) as a linear addition of the Vioolsdrif diorite (D) to the presumed residual phases.

Results for Eclogite

	Obs.	Est.	Diff.		X_{mix}	S.D.	X_{solid}
SiO_2	49.90	49.79	.11	D	.3591	.1001	
TiO_2	1.40	1.40	.00	OMPH	.4412	.0441	.7073
Al_2O_3	16.00	15.58	.42	GARN	.1772	.0236	.2841
FeO	9.30	9.26	.04	RUT	.0054	.0008	.0087
MgO	8.70	8.21	.49	TOTAL	.9937	.0266	
CaO	11.30	11.59	.29				
Na_2O	2.75	1.95	.80				
K_2O	.27	.79	.52				

$Diff^2 = 1.42$ F(Melt fraction) = .3591

basalts (9-10 percent MgO, 12-13 percent Al_2O_3) have been analysed by Gunn (1971) and Murali et al., (1977). Abundance data from these studies have been used in the comparison. It is clear from Table 46 that the predicted incompatible trace element composition of the source is very different from that observed for the Hawaiian tholeiites; Rb and Ba contents are high, while the Zr, Y and Sr contents are low. Alteration and/or incorporation of small amounts of sediment could raise the Rb and Ba contents of the source prior to the melting episode but would have little effect on the Zr and Y contents (Hart et al., 1974). These discrepancies argue against the primary magma model.

Further evaluation making use of the compatible trace elements is summarised in Table 47 . Average $\overline{D^i}$ values have been calculated using equation (4) and the most salient feature is the similar $\overline{D^{Ni}}$ and $\overline{D^{Co}}$, which is inconsistent with the predicted behaviour of these two elements in the residual phases. Individual D^{Ni} values for the three residual mafic minerals (olivine, clinopyroxene, amphibole) are significantly higher than D^{Co} (Gunn, 1971; Henderson and Dale, 1970; Mysen, 1976; Ewart and Taylor, 1968) and for the given assemblage $\overline{D^{Ni}}$ should be much higher than $\overline{D^{Co}}$, irrespective of the absolute values. The anomalous behaviour of Ni or Co (or both) confirm the unlikelihood of deriving the Vioolsdrif diorite by partial melting of hydrous basalt at low pressures.

An alternative basaltic source is eclogite, which implies partial melting under higher pressures (> 25 kbar) and which has been advocated by Green and Ringwood (1968). In this case the major residual phases are omphacite and garnet. The evaluation follows that of Gill (1974), from which the relevant data have been obtained. The eclogite source model involves the transformation of oceanic crust (oceanic tholeiite composition) to a high pressure garnet-clinopyroxene assemblage which subsequently melts under hydrous conditions (Green, 1972).

The melt fraction necessary to produce D from an eclogitic source may also be calculated by a least squares approximation, provided that

Partial melt (D) + residual phases = Eclogite

Gill (1974) has compiled recent estimates of the composition of modern oceanic tholeiites, together with the most likely compositions of residual garnet and omphacite (based on experimental work by Green (1972)); these data are listed in Table 45. The least squares approximation is given in Table 48 and suggests that 36 percent melting of an eclogite, with the composition of average modern oceanic tholeiite, may produce a liquid similar in major element composition to D.

The predicted incompatible trace element composition of the eclogite source (Fig. 49) is very different from that observed, since Rb, Ba, Sr Pb and Th contents are all high, while the Zr content is low. Furthermore, the Co content of D is higher than that in the proposed source. If D^i values for Ni, Cr and V quoted by Gill (1974) are used, then the calculated $\overline{D^{Cr}}$ and $\overline{D^{Ni}}$ are significantly higher than those predicted, while $\overline{D^{V}}$ is low. The trace element composition of the Vioolsdrif diorite is therefore inconsistent with its derivation from an eclogite source with the composition of average modern oceanic tholeiite.

To summarise, liquids similar in major element composition to D may be produced by suitable degrees of partial melting of either hydrous basalt or eclogite. However, the predicted abundances of the incompatible trace elements in the source materials are very different to published estimates. Furthermore, the behaviour of compatible trace elements such as Ni, Co, Cr and V are also inconsistent with the primary magma model. This latter feature precludes the possibility of choosing other basaltic source material (e.g. altered basalt, basalt + sediment, alkali basalt). It is concluded that the Vioolsdrif diorite does not represent a primary magma and other models involving a primary precursor to the diorite must be considered.

17.4. Vioolsdrif diorite (D) as a derivative magma

It is probably fortuitous that, in spite of not being co-magmatic, the Vioolsdrif diorite has a similar initial Sr^{87}/Sr^{86} ratio

Table 49. Predictions of the eclogitic source model. Obs. = observed trace element composition of a possible eclogitic source (average oceanic tholeiite, Gill, 1974); Est. = estimated composition using equation (16) and the composition of the Vioolsdrif diorite (D); C_s = concentration in source; C_d = concentration in Vioolsdrif diorite; $\overline{D}_p$ = average solid/liquid distribution coefficient predicted for the residual mineral assemblage; $\overline{D}_c$ = average solid/liquid distribution coefficient using equation (4) and the data from Table 48.

	Obs.	Est.		C_s	C_p	$\overline{D}_p$	$\overline{D}_c$
Rb	1.8	29	Ni	120	102	2.52	1.28
Sr	110	181	Co	32	35	2.55	-
Ba	13	256	Cr	300	55	29.6	8.0
Pb	.5	7.6	V	290	196	.8	1.8
Th	.15	2.5					
U	.08-.30	.2					
Zr	100	58					

(.7030 ± 3) to the Haib basaltic andesite (.7034 ± 3). At the one sigma error level, the two initial ratios are indistinguishable and this fact argues strongly that both suites may have stemmed from a common parent. It was concluded in 17.2 that the basaltic andesite (BA) could have been derived by fractionation of a high Mg, low Al basaltic magma. In order to produce the Vioolsdrif diorite from the same parent magma, a different fractionation scheme is necessary, because the Al_2O_3 content of the diorite is far higher than any of the Haib lavas with similar DI. The significant difference in Al_2O_3 between the more mafic members of the two suites has been discussed in Chapter 13.

Possible schemes are illustrated in Fig. 69 , which shows schematically the proposed lineages stemming from a common parent, but differing in the rate of increase in Al_2O_3. In order to produce two derivatives with very different Al_2O_3 contents at about the same DI, a mechanism whereby plagioclase in suppressed is needed. A possible mechanism involves the effect of water on the crystallisation of basaltic magmas. Yoder (1965) and Kushiro (1974) have demonstrated that in the simple systems Diopside-Anorthite-H_2O and Forsterite-Plagioclase-Silica-H_2O respectively, the plagioclase field is drastically reduced relative to mafic phases at high water pressures. These simple systems serve as a basis to explain the relative behaviour of plagioclase and mafic silicates in more complex systems. Increasing water pressure may change the order of appearance of the crystallising phases and increase the temperature interval between them. Yoder and Tilley (1962) have demonstrated this in the system olivine tholeiite-H_2O and their P,T diagram is reproduced in Fig. 70 . Later studies have confirmed this effect in other basalt-H_2O systems (e.g. Eggler, 1972; Helz, 1973, 1976, Gandy, 1973).

High Mg basalts probably have olivine as the liquidus silicate phase, which is followed by either a pyroxene or plagioclase. At low water pressures, the results of Yoder and Tilley (1962) suggest that the temperature interval between the olivine and plagioclase liquidii is relatively small (about 80°C).

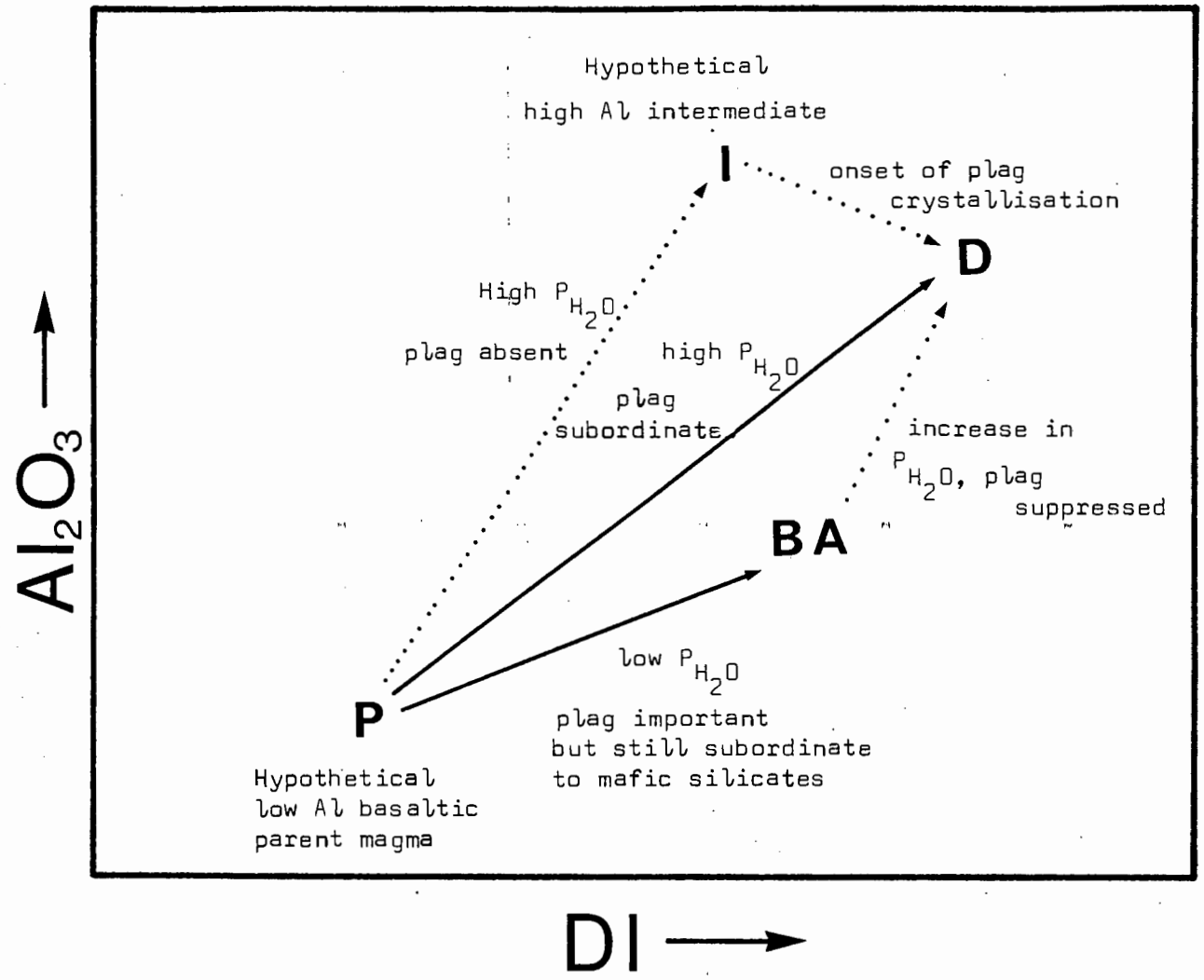

Fig. 69. Derivation of the Haib basaltic andesite (BA) and the Vioolsdrif diorite (D) from a common basaltic parent (P).

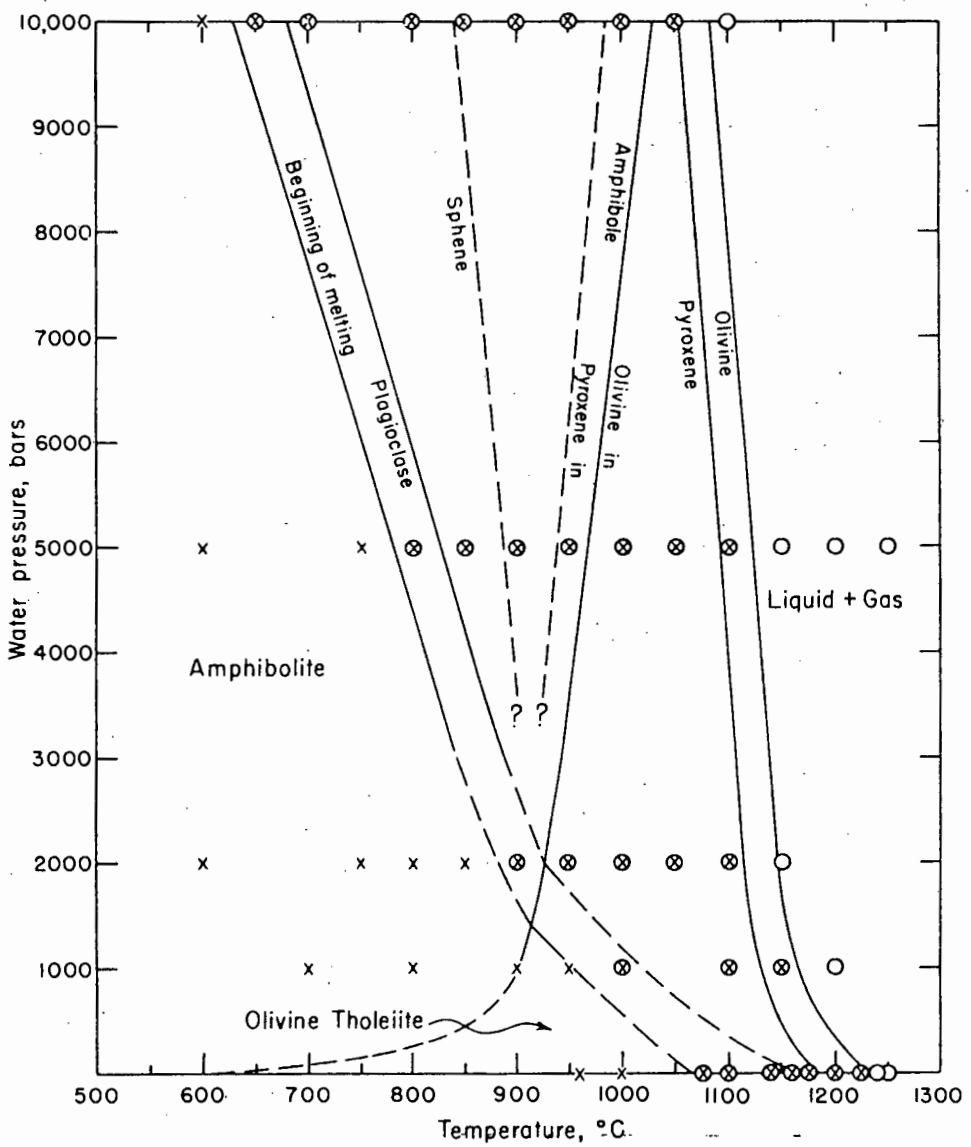

Fig. 70. Mineral stabilities in the system olivine tholeiite - H_2O as a function of P_{H_2O} and T. Data for the 1921 Kilauea tholeiite (Yoder and Tilley, 1962). Note the suppression of plagioclase relative to olivine and pyroxene with increasing P_{H_2O}.

As a result, low pressure fractionation is unlikely to involve removal of only olivine, unless cooling is extremely slow. On the other hand, at higher water pressures, the temperature interval between the olivine and plagioclase liquidii is substantially increased, thereby allowing the possibility of extensive fractionation of olivine (and perhaps pyroxenes) before the appearance of feldspar.

Fractionation of the same basaltic magma at different water pressures would differ only in the relative importance of plagioclase. Residual liquids produced by low pressure fractionation may be depleted, unaffected or slowly enriched in Al_2O_3, depending on the amount of plagioclase removed. The suppression of plagioclase at high water pressures may result in its absence or greatly diminished importance as a fractionating phase. Residual liquids produced by high pressure hydrous fractionation could be enriched in Al_2O_3 relative to liquids formed at lower pressures.

Crystallisation at high water pressure to produce the diorite is consistent with the presence of hornblende and biotite and their subsequent control over the composition of the evolved magmas (tonalite, granodiorite, etc). In contrast, a close approximation to the major element variation trend exhibited by the lavas may be produced by the progressive removal of two pyroxenes, plagioclase and magnetite; an essentially anhydrous assemblage appropriate to low water pressures.

A least squares approximation to D has been made by removing olivine and diopside from the average Solomon picrite-basalt; the results are not very satisfactory and suggest that the Al_2O_3 of residual liquids produced from the picrite will be even higher than 17 percent (about 19 percent). This problem may be overcome if the diorite and the picrite are linked through a high Al_2O_3 intermediate, which by fractionation involving plagioclase, produces lower Al_2O_3 residual liquids similar to the diorite. An alternative process involves fractionation of a magma similar in composition to BA at elevated water pressures, such that the absence or very

subordinate role of plagioclase will result in high Al residual liquids. The various possible schemes are illustrated in Fig. 69.

17.5. Discussion

The most feasible model to explain the Sr isotopic systematics, major and trace element compositions, petrographic characteristics and the intimate spatial and temporal association of the HVG and VIS, involves the effect of water pressure on the fractional crystallisation of a common high Mg basaltic magma. The lava suite basaltic andesite - andesite - dacite may be produced by fractionation at low water pressures while the intrusive suite diorite - tonalite - granodiorite - adamellite - leucogranite may have been generated at higher water pressures. The initial separation of the two lineages from a common parent is believed to be the result of the suppression of plagioclase relative to olivine and pyroxene at high water pressures.

The postulated presence of a high Mg basaltic magma may have some bearing on the origin of the early basic-ultrabasic complexes in the VIS. Gabbro-pegmatites which cut the cumulate pile in the Swartkop complex contain 8-9 percent MgO and 17-18 percent Al_2O_3, and are considered to be differentiates of a more basic magma. The possibility that the basic-ultrabasic complexes may represent the complementary culmulate material produced during fractionation of the hypothetical parent magma is attractive. However, preliminary Rb-Sr isotopic analyses on the Swartkop complex suggest that the basaltic magma responsible for the basic-ultrabasic rocks within the batholith has a significantly lower initial Sr^{87}/Sr^{86} ratio (.7012 as compared with .7034 for the granitic rocks). More work is necessary on the basic-ultrabasic rocks in order to evaluate the possibility of their complementary nature.

The different initial Sr^{87}/Sr^{86} ratios mentioned above raise the question as to the nature of the upper mantle sources. If it is assumed that isotopic equilibrium was maintained during the partial melting event, it

follows that the basic magma which was parental to the early Vioolsdrif basic-ultrabasic complexes was derived from a different upper mantle source than that which gave rise to the lavas and other intrusives. Recent work has made it increasingly clear that the upper mantle is probably not homogeneous and that regional differences in Sr isotopic composition appear to have persisted for long periods of geologic time (Hart and Brooks, 1977). Although the data on the basic-ultrabasic complexes are only preliminary, they suggest that the upper mantle may have been laterally heterogeneous (at 2000 Ma) on the scale of the lower Orange River region. An alternative is that the upper mantle was heterogeneous in a vertical sense and the two parental magmas were derived from different depths. Further evaluation must await the confirmation of the lower initial Sr^{87}/Sr^{86} ratio for the basic-ultrabasic complexes.

A compilation of published initial Sr^{87}/Sr^{86} ratios for all ± 2000 Ma old basaltic igneous rocks throughout southern Africa is given in Table 50 and illustrated in Fig. 71. It is clear that if Sr^{87}/Sr^{86} is reflective of source regions, then the subcontinental mantle under southern Africa was homogeneous at that time and possessed Sr^{87}/Sr^{86} ratios ranging from .701 to .708. In each idividual case, the workers have argued on geochemical grounds that the initial Sr^{87}/Sr^{86} ratio had not been modified by crustal interaction.

It is interesting to note that, neglecting the Swartkop basic-ultrabasic complex, the HVIP has the lowest initial Sr^{87}/Sr^{86} ratio of all the ± 2000 Ma igneous suites studied. Hamilton (1977) has argued convincingly that the range in initial Sr isotopic composition exhibited by the Bushveld Mafic Phase, could not have been produced by either bulk or selective crustal contamination. This infers that basic igneous rocks of the same age elsewhere in southern Africa with lower initial Sr^{87}/Sr^{86} ratios may have had even less chance of being contaminated. Hamilton (1977) developed a model whereby the subcontinental mantle under southern Africa evolved with a significantly higher Rb/Sr ratio (about 0.2) than the mantle which would give rise to modern oceanic basalts

Table 50. Sr isotopic data for ± 2000 Ma basic igneous rocks in southern Africa.

	AGE (Ma)	$(Sr^{87}/Sr^{86})_o$	Ref.
Bushveld Mafic Phase	2095 ± 24	.70563 ± 2 to .70769 ± 6	1
Great Dyke	2514 ± 16	.70261 ± 4	1
Que Que (microgabbros)	2700 (adopted)	.7013 - .7019	2
Matsap lavas	2070 ± 90	.7044 ± 3	3
Marydale (Soetvlei)	1901 ± 63	.7042 ± 4	4
Losberg complex	1881 ± 282	.7064 ± 24	5
HVIP	2000 (adopted)	.7032 ± 2	This study
Swartkop complex	1980 ± 130	.7012 ± 6	This study

1 Hamilton (1977)
2 Hawkesworth et al.,(1975)
3 Crampton (1974)
4 Cornell (1975)
5 Davies et al., (1970)

B Mineral isochron, Barberton greenstone belt
A Clinopyroxene, Abitibi greenstone belt
M Pseudo-isochron, modern oceanic basalts

Data above compiled by Hart and Brooks (1977)

(Rb/Sr about 0.02). The implied enrichment in Rb relative to Sr was considered to have taken place at about 2.8 Ga because initial Sr isotopic ratios of the Bushveld Mafic Phase and older basic igneous rocks defined a line that intersected the oceanic mantle evolution line at this date. It is clear from Fig. 71 that basic igneous rocks of the same age as the Bushveld in southern Africa, occurring further to the west (Marydale, Haib-Vioolsdrif), have not been derived from mantle sources that conform to Hamilton's model.

An important question arises as to the validity of distinct evolution lines, such as the three shown in Fig. 71. The spread in initial Sr^{87}/Sr^{86} ratios displayed by ± 2000 Ma basic igneous rocks in southern Africa suggests that the isotopic composition of Sr in the upper mantle may have evolved in a

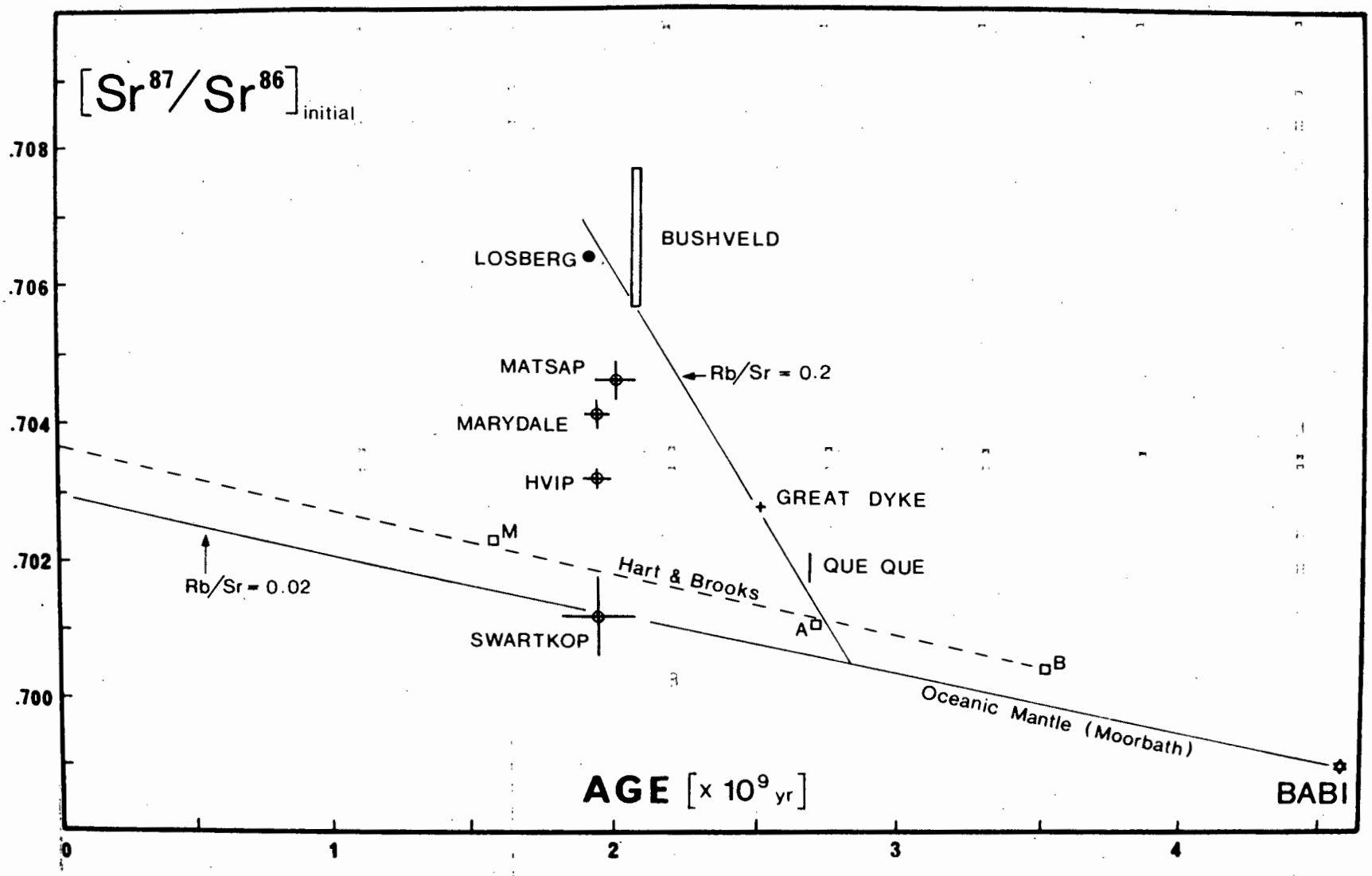

Fig. 71. Plot of initial Sr^{87}/Sr^{86} ratios against geologic age. See Table 50 and text for explanation.

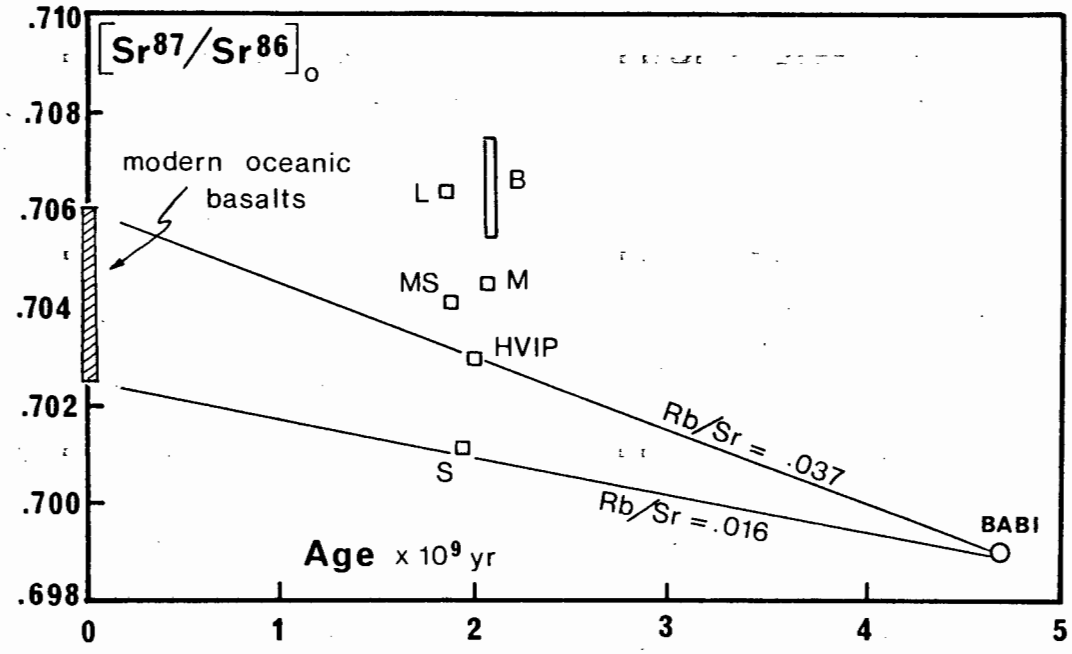

Fig. 72. Single stage Sr isotopic evolution model. Maximum and minimum Rb/Sr ratios for the upper mantle are fixed by the range in Sr^{87}/Sr^{86} found in modern, fresh oceanic basalts. B = Bushveld Mafic Phase; L = Losberg; M = Matsap; MS = Marydale (Soetvlei); HVIP = parental magma to the HVIP; S = Swartkop complex.

manner similar to that suggested by Faure and Hurley (1965). Data from modern, fresh oceanic basalts suggest that the Sr^{87}/Sr^{86} ratio of the present day oceanic upper mantle may range from .7025 to .7060 (Jahn and Nyquist, 1976; Hart and Brooks, 1977). If a primordial Sr^{87}/Sr^{86} ratio of .6990 is adopted (BABI, Papanastassiou and Wasserburg, 1969), then upper mantle Sr could have evolved in a fashion similar to that shown in Fig. 72. The initial Sr^{87}/Sr^{86} of the HVIP can be considered to be consistent with this single stage model, allowing for uncertainties in its estimation.

The Sr isotopic data are consistent with the conclusions drawn previously from major and trace element considerations, that the primary magma that was parental to the differentiated lava suite of the HVG and the Vioolsdrif batholith, was generated in the upper mantle. It follows that a significant proportion of the 2000-1800 Ma igneous rocks in the lower Orange River region

represent juvenile addition from the upper mantle. A different (crustal?) source is suspected for the voluminous acid volcanics (non-porphyritic rhyolites and related fragmental rock types) in the HVG. At present, the only justification for considering an alternative source for the acid volcanics is based mainly on negative evidence, i.e. these rocks do not seem to be related to the more basic lavas (dacite, andesite) in the HVG.

18

SUMMARY AND CONCLUSIONS

18.1 Evolution of the HVIP

It has been noted previously (Chapter 4) that the upper part of the HVIP has been removed by erosion and, as a result, the following conclusions should be regarded as being applicable only to the Haib-Vioolsdrif region. The initial stage in the development of the HVIP was dominated by the eruption of lavas and related fragmental rock types. The earliest volcanics were predominantly andesitic-rhyolitic, being made up of two distinct components: (1) non-porphyritic rhyolites (?ignimbrites) and related pumice sheets and bedded tuffs; (2) a differentiated suite of porphyritic lavas ranging in composition from andesite to rhyolite, with andesite being the most abundant. Later extrusive activity was characterised by an increased proportion of basaltic-andesitic and andesitic material, in the form of porphyritic lavas, pyroclastic beds and volcanogenic sediments.

The differentiated suite of porphyritic lavas follows a calc-alkaline trend, ranging in composition from basaltic-andesite, through andesite-and dacite, to rhyolite. Andesite is the most abundant rock type. Major and trace element modelling suggest that this suite could have been produced by fractional crystallisation of a basaltic andesite parent. The most basic lava (basaltic andesite) is probably not a primary magma, and a more basic precursor is preferred. The early non-porphyritic rhyolites do not appear to be related to the porphyritic lava suite through fractional crystallisation, and may represent a separate, crustal derived, primary magma. This suggests that a significant proportion of the volcanic pile (about 40 percent, see 4.5) represents remobilised continental crust, while the remaining 60 percent may be juvenile addition from the upper mantle. Strong evidence for such a contribution from the upper mantle is the basic nature of the presumed parental magma and the low initial Sr^{87}/Sr^{86} ratio (.7034) of the porphyritic lava suite.

Sustained intrusion of magma into the volcanic pile resulted in the development of a composite batholith. The compositional variation exhibited

by the batholith broadly parallels that of its volcanic envelope, but certain chemical features argue against the two suites being entirely comagmatic. The earliest rocks of the batholith are differentiated basic-ultrabasic complexes exhibiting tholeiitic affinities and compositions which are more basic than those displayed by the lavas. Intrusion of granitic rocks that form 95 percent of the batholith resulted in the fragmentation of the early basic-ultrabasic complexes, such that they now appear as scattered relicts. The radiometric age pattern exhibited by the intrusive rocks suggests an emplacement period of about 200 Ma, starting soon after eruption of the volcanic pile ($\pm$ 2000 Ma) and ending at about 1800 Ma. Field relationships suggest that emplacement involved the intrusion of progressively more differentiated magma, such that the suite diorite - tonalite - granodiorite-adamellite - leucogranite also represents a temporal sequence.

Major and trace element modelling of the intrusive suite suggest that the tonalite and granodiorite could have been produced by fractional crystallisation of a dioritic parent. The adamellite and leucogranite could have been produced by stepwise fractionation of a tonalitic parent. Such a fractionation scheme is corroborated by Sr isotopes, at least for the more basic intrusives (diorite, tonalite, granodiorite). In order for the adamellite to be a derivative of the tonalite, enrichment in radiogenic Sr^{87} must have occurred, because the ademellite has a significantly higher Sr^{87}/Sr^{86} ratio (.7065 $\pm$ 10) than the tonalite (.7030 $\pm$ 3). The required increase in Sr^{87}/Sr^{86} could have been achieved in the time between intrusion of the tonalite (about 1940 Ma) and the adamellite (about 1800 Ma), provided the latter formed as a magma by fractional crystallisation at 1940 Ma.

The initial Sr isotopic composition of the diorite is the same as that for the basaltic andesite, suggesting that the two suites could have been produced from a common, mantle derived parent. The contrasting major and trace element compositions of the more basic members of the two suites can be explained by the effect of P_{H_2O} on the crystallisation behaviour of a basaltic magma. The suppression of plagioclase at high P_{H2O} could have been responsible for the production of the high Al diorites and tonalites. Fractionation of the same parental magma at lower P_{H_2O} may result in the increased importance of

plagioclase as a crystallising phase, with the result that derivative magmas (such as the lava suite) will not be as high in Al as those produced at higher P_{H_2O}.

In contrast with the volcanics, the more acid members of the intrusive suite have major and trace element compositions which are consistent with extreme fractional crystallisation of a more basic parent. Furthermore, the adamellites and leucogranites do not display the same disproportionate development as that observed for the non-porphyritic rhyolites and related fragmental rock types. If the Rb-Sr aging mechanism to explain the Sr isotopes is accepted, then the entire batholith represents juvenile addition from the upper mantle.

18.2 Status of the so-called Richtersveld Province

Kröner and Blignault (1977) defined a tectonic province as "... a geographic region that is characterised by a combination of such parameters as lithology, structure, metamorphism and predominant radiometric age differing significantly from those of adjacent areas." The use of the term "Richtersveld Province" implies that the type area exhibiting the required geologic and radiometric features may be found in the geographic region commonly known as the Richtersveld (Fig. 73). However, it appears that much of the geologic evidence cited by Kröner and Blignault (1977) has been obtained from regions surrounding the Richtersveld, in the lower Fish River area (Blignault, 1974a) and the present study area between Vioolsdrif and the Haib River (Blignault, 1974b; Reid, 1974).

The only radiometric evidence for the presence of pre-1000 Ma old igneous rocks in the Richtersveld, is a single unpublished total rock Rb-Sr isochron age of 1700-1800 Ma (Corner, 1971). Petrographic descriptions suggest that the rocks analysed by Corner (1971) are probably similar to the gneissic adamellite described in 3.10 ("xenolith in xenolith" exposure) and may therefore represent the VIS in the Richtersveld. In view of the few radiometric data available on the basement rocks in the Richtersveld (compared with that reported in this study), and the comments made above regarding the

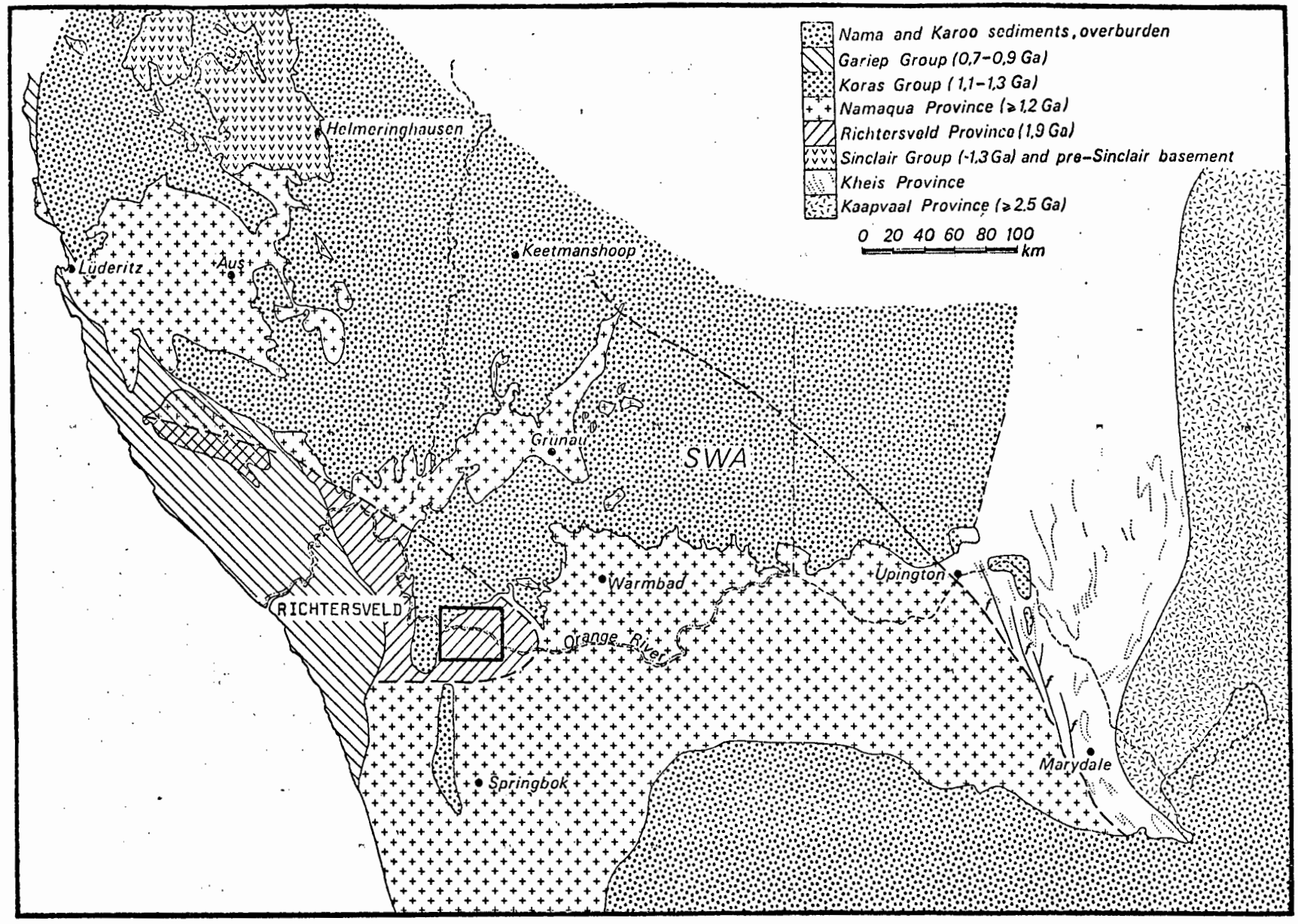

Fig. 73. Tectonic provinces in the lower Orange River region, as defined by Kröner and Blignault (1977). The present study area is shown within the heavy square.

source of geologic evidence used by Kröner and Blignault (1977), it is suggested that the use of the term "Richtersveld Province" is incorrect, or at best, premature.

Nevertheless, the basic requirements of a tectonic province may be found in the present study area. It has been shown in this study that the HVG and VIS constitute distinctive lithologic units, which exhibit a structural style, metamorphic history and radiometric age pattern quite different from that observed in the neighbouring Namaqua or Gariep provinces. It is concluded that the basement rocks in the Vioolsdrif-Haib region fulfil the requirements set down by Kröner and Blignault (1977) to justify the use of the term "province". However, to be consistent with the geographic connotation, their term "Richtersveld" must be replaced with "Vioolsdrif" or "Haib". The latter terms readily suggest the locations of the type area for the province. The author therefore suggests that the term "Vioolsdrif Province" be used when referring to basement rocks that display a distinctive structural-geochemical-radiometric pattern, indicative of a fundamental pre-1000 Ma crust-producing event in the Precambrian history of the lower Orange River region.

REFERENCES

ADAMS, J.A.S., ROGERS, J.J.W., 1959 - The geochemistry of thorium and uranium. In: Ahrens, L.H., Press, F., Rankama, K., Runcorn, S.K. (Eds) Physics and Chemistry of the Earth, 3, 298.

ALBAREDE, F., BOTTINGA, Y., 1972 - Kinetic disequilibrium in trace element partitioning between phenocrysts and host lava. Geochim. Cosmochim. Acta 36, 141.

ALBUQUERQUE, C.A.R., 1971 - Petrochemistry of a series of granitic rocks from northern Portugal. Bull. Geol. Soc. Amer. 82, 2783.

_____, 1973 - Geochemistry of biotites from granitic rocks, northern Portugal. Geochim. Cosmochim. Acta 37, 1779.

_____, 1974 - Geochemistry of actinolitic hornblendes from tonalitic rocks, northern Portugal. Geochim. Cosmochim. Acta 38, 789.

ALLEGRE, C.J., TREUIL, M., MINSTER, J., MINSTER, B., ALBAREDE, F., 1977 - Systematic use of trace element in igneous process. Part I. Fractional crystallisation processes in volcanic suites. Contrib. Mineral. Petrol. 60, 57.

ALLSOPP, H.L., KOLBE, P., 1965 - Isotopic age determinations on the Cape Granite and intruded Malmesbury sediments. Geochim. Cosmochim. Acta 29, 1115.

_____, VILJOEN, M.J., VILJOEN, R.P., 1973 - Strontium isotopic studies of the mafic and felsic rocks in the Onverwacht Group of the Swaziland Sequence. Geol. Rundschau 62, 902.

ANDERSON, A.T., 1976 - Magma mixing: petrological process and volcanological tool. J. Volcan. Geotherm. Res. 1, 3.

ANDERSON, C.A., 1941 - Volcanoes of the Medicine Lake highland, California. Univ. Calif. Dept. Geol. Sci., 25, 347.

ARCULUS, R.J., 1976 - Geology and geochemistry of the alkali basalt - andesite association of Granada, lesser Antilles island arc. Bull. Geol. Soc. Amer. 87, 612.

ARMSTRONG, R.L., COOPER, J.A., 1971 - Lead isotopes in island arcs. Bull. Volc. 35, 27.

ARTH, J.G., 1976 - Behaviour of trace elements during magmatic processes. A summary of theoretical models and their applications. J. Res. U.S. Geol. Surv. 4, 41.

BADSGAARD, H., VAN BREEMEN, O., 1970 - Thermally induced migration of Rb and Sr in adamellite. Eclogae geol. Helv. 63, 31.

BAIRD, A.K., 1961 - A pressed specimen die for the Norelco vacuum - path X-ray spectrograph. Norelco Rep. 8, 108.

BAKER, P.E., 1968 - Petrology of the Mt Misery volcano, St Kitts, West Indies. Lithos 1, 124.

BARAGAR, W.R.A., 1966 - Geochemistry of the Yellowknife volcanic rocks. Can. J. Earth Sci. 3, 9.

_____, 1968 - Major element geochemistry of the Noranda volcanic belt, Quebec - Ontario. Can. J. Earth Sci. 5, 773.

_____, GOODWIN, A.M., 1969 - Andesites and Archaean volcanism of the Canadian shield. In: McBirney, A.R., (Ed) Proceedings of the andesite conference. Oregon Dept. Geol. Mineral Ind. 65, 121.

BARBIER, J., RANCHIN, G., 1969 - Influence de l'alteration meteorique sur l'uranium a l'etat de traces dans le granite a deux micas de St-Sylvestre. Geochim. Cosmochim. Acta 33, 39.

BATEMAN, A.M., 1950 - Economic mineral deposits. Second Ed., Wiley, New York.

BATEMAN, P.C., DODGE, F.C.W., 1970 - Variations of major chemical constituents across the central Sierra Nevada batholith. Bull. Geol. Soc. Amer. 81, 409.

_____, CLARK, L.D., HUBER, N.K., MOORE, J.G. RINEHART, C.D., 1963 - The Sierra Nevada batholith - a synthesis of recent work across the central part. U.S. Geol. Surv. Prof. Pap. 414-D.

BEALL, J.J., 1974 - Hybrid origin of the Absarokite - Shoshonite - Banakite series, Absaroka volcanic field, Wyoming : Discussion. Bull. Geol. Soc. Amer. 85, 1003.

BERLIN, R., HENDERSON, C.M.B., 1969 - The distribution of Sr and Ba between alkali feldspar, plagioclase and groundmass phases of porphyritic trachytes and phonolites. Geochim. Cosmochim. Acta 33, 189.

BERTRAND, J.M., 1975 - Granitoids and deformation sequence in the Goodhouse-Henkries area. In: Thirteenth Ann. Rep. Precamb. Res. Unit, Univ. Cape Town, 61.

BESWICK, A.E. 1976 - K and Rb relations in basalts and other mantle derived. Is phlogopite the key? Geochim. Cosmochim. Acta 40, 1167.

BEUKES, G.J., 1973 - 'n Geologiese ondersoek van die gebied suid van Warmbad, Suid-wes Afrika, met speciale verwysing na die metamorf-magmatiese assosiasies van die Voorkamriese gesteentes. Unpub. D.Sc. thesis, Univ. Orange Free State.

BIGGAR, G.M., 1974 - Phase equilibrium studies of the chilled margins of some layered intrusions. Contrib. Mineral. Petrol. 46, 159.

BLACK, L.P., RICHARDS, J.R., 1972 - Rock lead isotopes in north-east Queensland. J. Geol. Soc. Australia 19, 321.

BLIGNAULT, H.J., 1974a - The tectonic zonation of part of the Namaqua Province in the lower Fish River/Narubis cross-section. In: Tenth and Eleventh Ann. Reps., Precamb. Res. Unit, Univ. Cape Town, 43.

_____, 1974b - Aspects of the Richtersveld Province. Bull. Precamb. Res. Unit, Univ. Cape Town, 15, 49.

BLIGNAULT, H.J., 1975 - Basement geology of the Haib area. Bull. Precamb. Res. Unit, Univ. Cape Town, 19, Annexure 3.

_____, 1977 - The tectonic evolution of the Richtersveld and Namaqua Provinces in the Ais-ais and Haib River areas, south-west Africa. Bull. Precamb. Res. Unit, Univ. Cape Town, 19, (in preparation).

BOTTINO, M.L., FULLAGAR, P.D., 1968 - The effects of weathering on whole rock Rb-Sr ages of granitic rocks. Amer. J. Sci. 266, 661.

BOYD, F.R., FINGER, L.W., CHAYES, F., 1968 - Computer reduction of electron probe data. Carnegie Inst. Wash. Year Book, 67, 210.

_____, SHAIRER, J.F., 1964 - The system $MgSiO_3$-$CaMgSi_2O_6$. J.Petrol. 5, 275.

BRADLEY, J., 1965 - Intrusion of major dolerite sills. Trans. Roy. Soc. N.Z., 3, 27.

BRAVO, M.S., O'HARA, M.J., 1974 - Partial melting of phlogopite-bearing synthetic spinel- and garnet-lherzolites. In: Ahrens, L.H., Dawson, J. B., Duncan, A.R., Erlank, A.J., (Eds) Phys. Chem. Earth 9, 845.

BROOKINS, D.G., CHAUDHURI, S., DOWLING, P.L., 1969 - The isotopic composition of strontium in Permian limestones, central Kansas. Chem. Geol. 4, 439.

BROOKS, C., HART, S.R., WENDT, I., 1972 - Realistic use of two error regression treatments as applied to Rb-Sr data. Rev. Geophys. Sp. Phys. 10, 551.

BROWN, G.C., 1977 - Mantle origin of Cordilleran granites. Nature 265, 21.

BROWN, G.M., 1956 - The layered ultrabasic rocks of Rhum, Inner Hebredies. Phil. Trans. Roy. Soc. Lond. B 240, 1.

_____, SHAIRER, J.F., 1968 - Melting relations of some calc-alkaline volcanic rocks. Mem. Geol. Soc. Amer. 130, 139.

BRYAN, W.B., FINGER, L.W., CHAYES, F., 1969 - Estimating proportions in petrogenetic mixing equations by least squares approximation. Science 163, 926.

BUDDINGTON, A.F., LINDSLEY, D.H., 1964 - Iron-titanium oxide minerals and synthetic equivalents. J. Petrol. 5, 310.

BURGER, A.J., COERTZE, F.J., 1973 - Radiometric age measurements on rocks from southern Africa to the end of 1971. Bull. Geol. Surv. S.Afr. 58.

BURNHAM, C.W., 1967 - Hydrothermal fluids at the magmatic stage. In: Barnes, H.L., (Ed) Geochemistry of hydrothermal ore deposits, Holt, Rinehardt and Winston, 34.

BUSSEL, M.A., PITCHER, W.S., WILSON, P.A., 1976 - Ring complexes of the Peruvian coastal batholith: a long standing subvolcanic regime. Can. J. Earth Sci. 13, 1020.

CARMICHAEL, I.S.E., 1964 - The petrology of Thingmuli, a Tertiary volcano in eastern Iceland. J.Petrol. 5, 435.

CARMICHAEL, I.S.E., 1967 - The iron-titanium oxides of salic volcanic rocks and their associated ferromagnesian phenocrysts. Contrib. Mineral. Petrol. 14, 36.

_____, NICHOLLS, J., 1967 - Iron-titanium oxides and oxygen fugacities in volcanic rocks. J. Geophys. Res. 72, 4665.

_____, TURNER, F.J., VERHOOGEN, J., 1974 - Igneous Petrology. McGraw - Hill.

CAWTHORN, R.G., 1976a - Some chemical controls on igneous amphibole compositions. Geochim. Cosmochim. Acta 40, 1319.

_____, 1976b - Melting relations in part of the system CaO - MgO - Al_2O_3 - SiO_2 - Na_2O - H_2O under 5 kb pressure. J. Petrol. 17, 44.

_____, BROWN, P.A., 1976 - A model for the formation and crystallisation of corundum-normative calc-alkaline magmas through amphibole fractionation. J. Geol. 84, 467.

_____, O'HARA, M.J., 1976 - Amphibole fractionation in calc-alkaline magma genesis. Amer. J. Sci. 276, 309.

_____, STRONG, D.F., BROWN, P.A., 1976 - Origin of corundum-normative intrusive and extrusive calc-alkaline magmas. Nature 259, 102.

CHAYES, F., 1964 - A petrographic distinction between Cenozoic volcanics in and around the open oceans. J. Geophys. Res. 69, 573.

_____, 1969a - On the occurrence of corundium in the norms of the common volcanic rocks. Carnegie Inst. Wash. Year Book 74, 179.

_____, 1969b - The chemical composition of Cenozoic andesite. In: McBirney, A.R. (Ed) Proceedings of the andesite conference. Oregon Dept. Geol. Mineral Ind. 65, 1.

CHERRY, R.D., HOBBS, J.B.M., ERLANK, A.J., WILLIS, J.P., 1970 - Thorium, Uranium, Potassium, Lead, Strontium and Rubibium in silicate rocks by Gamma-Spectroscopy and/or X-ray Fluorescence. Can. Spec. 15, 1.

CLIFFORD, T.N., GRONOW, J., REX, D.C., BURGER, A.J., 1975 - Geochronological and petrogenetic studies of high grade metamorphic rocks and intrusives in Namaqualand, South Africa. J.Petrol. 16, 154.

COATES, R.R., 1952 - Magmatic differentiation in Tertiary and Quaternary volcanic rocks from Adak and Kanaga islands, Aleutian Islands, Alaska. Bull. Geol. Soc. Amer. 63, 485.

COBBING, E.J., PITCHER, W.S., 1972 - The coastal batholith of Peru. J. Geol. Soc. Lond. 128, 421.

COLE, J.W., 1973 - High-alumina basalts of Taupo volcanic zone, New Zealand. Lithos 6, 53.

COMPTON, R.R., 1958 - Significance of amphibole paragenesis in the Bidwell Bar region, California. Amer. Mineral. 43, 890.

COOPER, A.F., 1972 - Progressive metamorphism of metabasic rocks from the Haast Schist Group of southern New Zealand. J. Petrol. 13, 457.

_____, LOVERING, J.F., 1970 - Greenschist amphiboles from Haast River. Contrib. Mineral. Petrol. 27, 11.

CORNELL, D.H., 1975 - Petrology of the Marydale metabasites. Unpub. Ph.D. thesis, Univ. Cambridge.

CORNER, B., 1971 - Rb-Sr isotopic study of the old granite at Helskloof, south-eastern Richtersveld. Unpub. B.Sc. Hons. thesis, Univ. Witwatersrand.

COX, K.G., BELL, J.D., 1972 - A crystal fractionation model for the basaltic rocks of the New Georgia Group, British Solomon Islands. Contrib. Mineral. Petrol. 37, 1.

_____, JAMIESON, B.G., 1974 - The olivine-rich lavas of Nuanetsi : a study of polybaric magmatic evolution. J.Petrol. 15, 269.

CRAMPTON, D., 1974 - A note on the age of the Matsap Formation of the northern Cape Province. Trans. Geol. Soc. S.Afr. 77, 71.

CRAWFORD, M.L., 1966 - Composition of plagioclase and associated minerals in some schists from Vermont, U.S.A. and south Westland, New Zealand, with inferences about the peristerite solvus. Contrib. Mineral. Petrol. 13, 269.

DALE, I.M., HENDERSON, P., 1972 - The partition of transition elements in phenocryst-bearing basalts and the implications about melt structure. 24th Int. Geol. Congress 10, 105.

DAVIES, R.D., ALLSOPP, H.L., ERLANK, A.J. MANTON, W.I., 1970 - Sr isotopic studies on various layered mafic intrusions in southern Africa. Spec. Publ. Geol. Soc. S.Afr. 1, 576.

DEER, W.A., HOWIE, R.A., ZUSSMAN, J., 1962 - Rock Forming Minerals, 5 volumes. Longmans.

DE LAETER, J.R., ABERCROMBIE, I.D., 1970 - Mass spectrometric isotope dilution analyses of rubidium and strontium in standard rocks. Earth Planet. Sci. Lett. 9, 327.

DE VILLIERS, J., 1968 - Fifth Ann. Rep., Precamb. Res. Unit, Univ. Cape Town.

_____, BURGER, A.J., 1967 - Note on the minimum age of certain granites from the Richtersveld area. Ann. Geol. Surv. S.Afr. 6, 83.

_____, SÖHNGE, P.G., 1959 - The geology of the Richtersveld. Mem. Geol. Surv. S.Afr. 48.

DICKEY, J.S., 1975 - A hypothesis of origin for podiform chromite deposits. Geochim. Cosmochim. Acta 39, 1061.

DODGE, F.C.W., PAPIKE, J.J., MAYS, R.E., 1968 - Hornblendes from granitic rocks of the central Sierra Nevada batholith, California. J.Petrol. 9, 378.

DODGE, F.C.W., ROSS, D.C., 1971 - Coexisting hornblendes and biotites from granitic rocks near the San Andreas fault, California. J. Geol. 79, 158.

_____, SMITH, V.C., MAYS, R.E., 1969 - Biotites from granitic rocks of the central Sierra Nevada batholith, California. J.Petrol. 10, 250.

DOERNER, H.A., HOSKINS, W.M., 1925 - Coprecipitation of radium and barium sulfates. J. Amer. Chem. Soc. 47, 662.

DRAKE, M.J., WEILL, D.F., 1975 - Partition of Sr, Ba, Ca, Y, Eu^{2+}, Eu^{3+} and other REE between plagioclase feldspar and magmatic liquid: an experimental study. Geochem. Cosmochim. Acta 39, 689.

DUKE, J.M., 1976 - Distribution of the period four transition elements among olivine, calcic clinopyroxene and mafic silicate liquid : Experimental results. J. Petrol. 17, 499.

DU TOIT, A.L., 1920 - The Karroo dolerites. Trans. Geol. Soc. S.Afr. 33, 1.

EALES, H.V., ROBEY, J.van A., 1976 - Differentiation of tholeiitic Karroo magma at Birds River, South Africa. Contrib. Mineral. Petrol. 56, 101.

EGGLER, D.H., 1972 - Water saturated and undersaturated melting relations in a Paricutin andesite and an estimate of water content in the natural magma. Contrib. Mineral. Petrol. 34, 261.

_____, 1974 - Application of a portion of the system $CaAl_2Si_2O_8$ - $NaAlSi_3O_8$ - SiO_2 - MgO - Fe - O_2 - H_2O - CO to genesis of the calc-alkaline suite. Amer. J. Sci. 274, 297.

_____, BURNHAM, C.W., 1973 - Crystallisation and fractionation trends in the system andesite - H_2O - CO_2 - O_2 at pressures to 10 kb. Bull. Geol. Soc. Amer. 84, 2517.

ELLIS, A.J., 1967 - The chemistry of some explored geothermal systems. In: Barnes, H.L. (Ed) Geochemistry of hydrothermal ore deposits. Holt, Rinehart and Winston, 465.

ENGEL, A.E.J., ENGEL, C.G., 1960 - Progressive metamorphism and granitization of the major paragneiss, north-west Adirondack Mountains, New York. Part II. Mineralogy. Bull. Geol. Soc. Amer. 71, 1.

_____, ENGEL, C.G., HAVENS, R.G., 1965 - Chemical characteristics of oceanic basalts and the upper mantle. Bull. Geol. Soc. Amer. 76, 719.

ERIKSON, E.H., 1977 - Petrology and petrogenesis of the Mount Stuart batholith-plutonic equivalent of the high alumina basalt association. Contrib. Mineral. Petrol. 60, 183.

ERLANK, A.J., 1970 - Distribution of potassium in mafic and ultramafic nodules. Carnegie Inst. Wash. Ann. Rep. 68, 433.

EWART, A., 1976a - Mineralogy and chemistry of modern orogenic lavas - some statistics and implications. Earth Planet. Sci. Lett. 31, 417.

EWART, A., 1976b - A petrological study of the younger Tongan andesites and dacites and the olivine tholeiites of Niva Fo'ou Island, S.W. Pacific. Contrib. Mineral. Petrol. 58, 1.

_____, BRYAN, W.B., GILL, J.B., 1973 - Mineralogy and geochemistry of the younger islands of Tonga. J. Petrol. 15, 429.

_____, STIPP, J.J., 1968 - Petrogenesis of the volcanic rocks of the central North Island, New Zealand, as indicated by a study of Sr^{87}/Sr^{86} ratios and Sr, Rb, K, U and Th abundances. Geochim. Cosmochim. Acta 32, 699.

_____, TAYLOR, S.R., 1969 - Trace element geochemistry of the rhyolitic volcanic rocks, central North Island, New Zealand. Contrib. Mineral. Petrol. 22, 127.

_____, TAYLOR, S.R., CAPP, A.C., 1968 - Trace and minor element geochemistry of the rhyolitic volcanic rocks, central North Island, New Zealand. Contrib. Mineral. Petrol. 18, 76.

FAIRBAIRN, H.W., HURLEY, P.M., 1971 - Evaluation of X-ray fluorescence and mass spectrometric analyses of Rb and Sr in some silicate standards. Geochim. Cosmochim. Acta 35, 149.

FAURE, G., POWELL, J.L., 1972 - Strontium isotope geology. Springer Verlag.

_____, HURLEY, P.M., 1963 - The isotopic composition of strontium in oceanic and continental basalt : Application to the origin of igneous rocks. J. Petrol. 4, 31.

FITTON, J.G., 1972 - The genetic significance of almandine - pyrope phenocrysts in the calc-alkaline Borrowdale volcanic group, northern England. Contrib. Mineral. Petrol. 36, 231.

_____, GILL, R.C.O., 1970 - The oxidation of ferrous iron in rocks during mechanical grinding. Geochim. Cosmochim. Acta 34, 518.

_____, HUGHES, D.J., 1970 - Volcanism and plate tectonics in the British Ordovician. Earth Planet. Sci. Lett. 8, 223.

FLEISCHER, M., 1969 - U.S. Geological Survey standards-I. Additional data on rocks G-1 and W-1, 1965-1967. Geochim. Cosmochim. Acta 33, 65.

FORBES, W.C., FLOWER, M.F.J., 1974 - Phase relations of titan-phlogopite, $K_2Mg_4TiAl_2Si_6O_{20}(OH)_4$: A refractory phase in the upper mantle? Earth Planet. Sci. Lett. 22, 60.

FRANCO, R.R., SHAIRER, J.F., 1951 - Liquidus temperatures in mixtures of the feldspars of soda, potash and lime. J. Geol. 59, 259.

FUDALI, R.F., 1965 - Oxygen fugacities of basaltic and andesitic magmas. Geochim. Cosmochim. Acta 29, 1063.

FYFE, W.S., 1971 - Some thoughts on granitic magmas. In: Newall, G., Rast, N. (Eds) Mechanism of igneous intrusion, Gallery Press.

_____, 1973 - The generation of batholiths. Tectonophys. 17, 273.

GALE, N., 1967 - Development of delayed neutron technique as rapid and precise method for determination of uranium and thorium at trace levels in rocks and minerals, with applications to isotope geochronology. Radioactive dating and methods of low-level counting. International Atomic Energy Agency, Vienna.

GANDY, M.K., 1973 - Melting relations of some calc-alkaline lavas from the eastern Sidlaw Hills, Perthshire. Earth Planet. Sci. Lett. 19, 230.

GAST, P.W., 1960 - Limitation on the composition of the upper mantle. J. Geophys. Res. 65, 1287.

_____, 1965 - Terrestrial ratio of potassium to rubidium and the composition of the Earth's mantle. Science 147, 858.

_____, 1968 - Trace element fractionation and the origin of tholeiitic and alkaline magma types. Geochim. Cosmochim. Acta 32, 1057.

GERMS, G.J.B., 1972 - The stratigraphy and palaeontology of the lower Nama Group, south-west Africa. Bull. Precamb. Res. Unit, Univ. Cape Town. 12.

GEVERS, T.W., PARTRIDGE, F.C., JOUBERT, G.K., 1937 - The pegmatite area south of the Orange River in Namaqualand. Mem. Geol. Surv. S.Afr. 31.

GIDSKEHAUG, A., CREER, K.M., MITCHELL, J.G., 1975 - Palaeomagnetism and K-Ar ages of the South-west African basalts and their bearing on the time of initial rifting of the south Atlantic Ocean. Geophys. J. Roy. Astronom. Soc. 42, 1.

GILL, J.B., 1970 - Geochemistry of Viti Levu, Fiji and its evolution as an island arc. Contrib. Mineral. Petrol. 27, 179.

_____, 1974 - Role of underthrust oceanic crust in the genesis of a Fijian calc-alkaline suite. Contrib. Mineral. Petrol. 43, 29.

GILLULY, J., 1971 - Plate tectonics and magmatic evolution. Bull. Geol. Soc. Amer. 82, 2383.

GOLDSMITH, J.S., NEWTON, R.C., 1972 - An experimental determination of the alkali feldspar solvus. In: MacKenzie, W.S., Zussman, J. (Eds) The Feldspars. Proceedings of a NATO advanced study institute. Manchester Univ. Press, 337.

GREEN, D.H., 1964 - The petrogenesis of the high-temperature peridotite intrusion in the Lizard area, Cornwall. J.Petrol. 5, 134.

_____, 1973 - Experimental melting studies on a model upper mantle composition at high pressure under water saturated and water undersaturated conditions. Earth Planet. Sci. Lett. 19, 37.

GREEN, T.H., 1972 - Crystallisation of calc-alkaline andesite under controlled high pressure hydrous conditions. Contrib. Mineral. Petrol. 34, 150.

GREEN, T.H., RINGWOOD, A.E., 1968 - Genesis of the calc-alkaline igneous rock suite. Contrib. Mineral. Petrol. 18, 105.

GULSON, B.L., 1972 - The high-K diorites and associated rocks of the Yeoval diorite complex, N.S.W. Contrib. Mineral. Petrol. 35, 173.

GUNN, B.M., 1971 - Trace element partition during olivine fractionation of Hawaiian basalts. Chem. Geol. 8, 1.

GURNEY, J.J., HARTE, B., COX, K.G., 1974 - Mantle xenoliths in the Matsoku kimberlite pipe. In: Ahrens, L.H., Dawson, J.B., Duncan, A.R., Erlank, A.J., (Eds) Phys. Chem. Earth 9, 507.

HART, S.R., ERLANK, A.J., KABLE, E.J.D., 1974 - Seafloor basalt alteration: some chemical and Sr isotopic effects. Contrib. Mineral. Petrol. 44,219.

HAKLI, T., WRIGHT, T.L., 1967 - The fractionation of Ni between olivine and augite as a geothermometer. Geochim. Cosmochim. Acta 31, 877.

HAMILTON, E.I., 1965 - Applied geochronology. Academic Press.

HAMILTON, J., 1977 - Sr isotope and trace element studies of the Great Dyke and Bushveld Mafic Phase and their relation to early Proterozoic magma genesis in southern Africa. J.Petrol. 18, 24.

HAMILTON, W., MYERS, W.B., 1967 - The nature of batholiths. U.S. Geol. Surv. Prof. Pap. 554-C.

HARRIS, P.G., 1957 - Zone refining and the origin of potassic basalts. Geochim. Cosmochim. Acta 12, 195.

_____, REAY, A., WHITE, I.G., 1967 - Chemical composition of the upper mantle. J. Geophys. Res. 72, 6359.

HARRY, W.T., 1950 - Aluminium replacing silicon in some silicate lattices. Mineral. Mag. 29, 142.

HART, S.R., BROOKS, C., 1974 - Clinopyroxene-matrix partitioning of K, Rb, Cs, Sr and Ba. Geochim. Cosmochim. Acta 38, 1799.

_____, BROOKS, C., 1977 - The geochemistry and evolution of the early Precambrian mantle. Contrib. Mineral. Petrol. 61, 109.

_____, DAVIS, K.E., KUSHIRO, I., WATSON, E.B., 1976 - Partitioning of Nickel between olivine and silicate liquid. (Abstract) Ann. Meet. Geol. Soc. Amer., Denver, Colo., 906.

HATCH, F.H., WELLS, A.K., WELLS, M.K., 1961 - Petrology of the igneous rocks. 12th Ed. Thomas Murby and Co.

HAWKESWORTH, C.J., MOORBATH, S., O'NIONS, R.K., 1975 - Age relationship between greenstone belts and "granites" in the Rhodesian Archaean craton. Earth Planet. Sci. Lett. 25, 251.

HEDGE, C.E., 1971 - Ni in high alumina basalts. Geochim. Cosmochim. Acta 35, 522.

HELZ, R.T., 1973 - Phase relations of basalts in their melting range at P_{H_2O} = 5 kb as a function of oxygen fugacity. Part I. Mafic phases. J. Petrol. 14, 249.

_____, 1976 - Phase relations of basalts in their melting ranges at P_{H_2O} = 5 kb. Part II. Melt compositions. J.Petrol. 17, 139.

HEMING, R.G., CARMICHAEL, I.S.E., 1973 - High temperature pumice flows from the Rabaul caldera, New Guinea. Contrib. Mineral. Petrol. 38, 1.

HENDERSON, P., DALE, I.M., 1970 - The partition of selected transition element ions between olivine and groundmass of oceanic basalts. Chem. Geol. 5, 267.

HERMES, O.D., 1970 - Petrochemistry of coexistent mafic silicates from the Meckelenburg gabbro-metagabbro complex, north Carolina. Bull. Geol. Soc. Amer. 81, 137.

HESS, H.H., 1952 - Orthopyroxenes of the Bushveld type, ion substitutions and changes in unit cell dimensions. Amer. J.Sci. Bowen Vol., 173.

HOLDAWAY, M.J., 1965 - Basic regional metamorphic rocks in part of the Klamath Mountains, northern California. Amer. Mineral. 50, 953.

HOLLAND, H.D., 1967 - Gangue minerals in hydrothermal deposits. In: Barnes, H.L. (Ed) Geochemistry of hydrothermal ore deposits. Holt, Rinehart and Winston, 382.

HOLLISTER, V.F., 1975 - An appraisal of the nature and source of porphyry copper deposits. Minerals Sci. Eng. 7, 225.

HOLLOWAY, J.R., BURNHAM, C.W., 1972 - Melting relations of basalt with equilibrium water pressure less than total pressure. J.Petrol. 13, 1.

HURLEY, P.M., BATEMAN, P.C., FAIRBAIRN, H.W., PINSON, W.H., 1965 - Investigation of initial Sr^{87}/Sr^{86} ratios in the Sierra Nevada plutonic province. Bull. Geol. Soc. Amer. 76, 165.

HUTCHINSON, R.W., HODDER, R.W., 1972 - Possible tectonic and metallogenic relationships between porphyry copper and massive sulphide deposits. Can. Inst. Met. Trans. 75, 16.

HUTCHINSON, R., PAUL, D.K., HARRIS, P.G., 1970 - Chemical composition of the upper mantle. Mineral. Mag. 37, 726.

IRVINE, T.N., 1965 - Chromian spinel as a petrogenetic indicator. Part I. Theory. Can. J. Earth Sci. 2, 648.

_____, 1967 - Chromian spinel as a petrogenetic indicator. Part II. Applications. Can. J. Earth Sci. 4, 71.

_____, BARAGAR, W.R.A., 1971 - A guide to the chemical classification of the common volcanic rocks. Can. J. Earth Sci. 8, 523.

ITO, K., KENNEDY, G.C., 1974 - The comparison of liquids formed by partial melting of eclogites at high temperatures and pressures. J.Geol. 82, 383.

JAHN, B.M., NYQUIST, L.E., 1976 - Crustal evolution in the early Earth-Moon system: Constraints from Rb-Sr studies. In: Windley, B.F. (Ed.) The Early History of the Earth. John Wiley and Sons, 55.

JAFFE, H.W., ROBINSON, P., KLEIN, C., 1968 - Exsolution lamellae optic orientation of clinoamphiboles. Science 160, 776.

JAKES, P., 1973 - Geochemistry of continental growth. In: Tarling, D., Runcorn, S., (Eds) Implication of continental drift to the Earth Sciences, Academic Press, 2, 999.

_____, GILL, J.B., 1970 - Rare earth elements and the island arc tholeiitic series. Earth Planet. Sci. Lett. 9, 17.

_____, SMITH, I.S.E., 1970 - High potassium calc-alkaline rocks from Cape Nelson, Eastern Papua. Contrib. Mineral. Petrol. 28, 259.

_____, WHITE, A.J.R., 1971 - Composition of island arcs and continental growth. Earth Planet. Sci. Lett. 12, 224.

_____, WHITE, A.J.R., 1972a - Major and trace element abundances in volcanic rocks of orogenic areas. Bull. Geol. Soc. Amer. 83, 29.

_____, WHITE, A.J.R., 1972b - Hornblendes from calc-alkaline volcanic rocks of island arcs and continental margins. Amer. Mineral. 57, 887.

JAMIESON, B.G., CLARKE, D.B., 1970 - Potassium and associated elements in tholeiitic basalts. J. Petrol. 11, 183.

JOLLY, W.T., 1970 - Zeolite and prehnite-pumpellyite facies in south central Puerto Rico. Contrib. Mineral. Petrol. 27, 204.

_____, 1972 - Degradation (hydration) - Aggradation (dehydration) and low rank metamorphism of mafic sequences. 24th Int. Geol. Cong. 2, 11.

_____, SMITH, R.E., 1972 - Degradation and metamorphic differentiation of the Keeweenawan tholeiitic lavas of northern Michigan, U.S.A., J. Petrol. 13, 273.

JOPLIN, G.A., 1968 - The shoshonite association : A review. J. Geol. Soc. Australia 15, 275.

JOYCE, A.S., 1973a - Petrogenesis of the Murrumbidgee batholith, A.C.T., J. Geol. Soc. Australia, 20, 179.

_____, 1973b - Chemistry of the minerals of the granitic Murrumbidgee batholith, Australian Capital Territory. Chem. Geol. 11, 271.

KANASEWICH, E.R., 1968 - The interpretation of lead isotopes and their geological significance. In: Hamilton, E.I., Farquhar, R.M., (Eds) Radiometric dating for geologists. Interscience Publishers, 147.

KELLER, J., 1974 - Petrology of some volcanic rock series of the Aeolian arc, south Tyrrhenian Sea : Calc-alkaline and shoshonitic associations. Contrib. Mineral. Petrol. 46, 29.

KESSON, S.E., 1973 - The primary geochemistry of the Monaro alkaline volcanics, S.E. Australia - Evidence of upper mantle heterogeneity. Contrib. Mineral. Petrol. 42, 93.

KISTLER, R.W., 1974 - Phanerozoic batholiths in western North America. In: Donath, F.A., (Ed) Ann. Rev. Earth Planet. Sci. 2, Annual Rev. Inc. 403.

KLEIN, C., 1969 - Two amphibole assemblages in the system actinolite - hornblende - glaucophane. Amer. Mineral. 54, 212.

KOLBE, P., 1966 - Geochemical investigations of the Cape Granite, south-western Cape Province, South Africa. Trans. Geol. Soc. S.Afr. 69, 161.

KORRINGA, M.K., NOBLE, D.C., 1971 - Distribution of Sr and Ba between natural feldspar and igneous melt. Earth Planet. Sci. Lett. 11, 147.

KOSTLIN, E.O., 1971 - The Rb/Sr radiometric ages of the Richtersveld complex and neighbouring bostonite dikes. Unpub. M.Sc. Thesis, Univ. Witwatersrand.

KRISTANAMURTHY, P., COX, K.G., 1977 - Picritic basalts and related lavas from the Deccan traps of western India. Contrib. Mineral. Petrol. 62, 53.

KRÖNER, A., BLIGNAULT, H.H., 1977 - Towards a definition of some tectonic and igneous provinces in western South Africa and southern South-west Africa. Trans. Geol. Soc. S.Afr. 79, 232.

KUNO, H., 1960 - High-alumina basalt. J.Petrol. 1, 121.

_____, 1966 - Lateral variation of basalt magma type across continental margins and island arcs. Bull. Volc. 29, 195.

_____, 1968 - Differentiation of basalt magmas. In: Hess, H.H., (Ed) Basalts. The Poldervaart treatise on rocks of basaltic composition. 2,Interscience, 623.

_____, AOKI, K., 1970 - Chemistry of ultramafic nodules and their bearing on the origin of basaltic magma. Phys. Earth Planet. Inter. 3, 273.

KUSHIRO, I., 1973 - Origin of some magmas in oceanic and circum-oceanic regions. Tectonophys. 17, 211.

_____, I., 1974 - The system forsterite - anorthite - albite - silica - H_2O at 15 kbar and the genesis of andesitic magmas in the upper mantle. Carnegie Inst. Wash. Year Book 73, 244.

LAMBERT, I.B., HEIER, K.S., 1968 - Geochemical investigation of deepseated rocks in the Australian shield. Lithos 1, 30.

_____, WYLLIE, P.J., 1972 - Melting of gabbro (quartz eclogite) with excess water to 35 kilobars, with geological applications. J. Geol. 80, 693.

LAMBERT, R.S., HOLLAND, J.G., 1974 - Yttrium geochemistry applied to petrogenesis, utilising calcium - yttrium relationships in minerals and rocks. Geochim. Cosmochim. Acta 38,

_____, HOLLAND, J.G., OWEN, P.F., 1974 - Chemical petrology of a suite of calc-alkaline lavas from Mount Ararat, Turkey. J. Geol. 82, 419.

LARSEN, E.S., 1948 - Batholith and associated rocks of Corona, Elsinore and San Luis Rey quadrangles, southern California, Mem. Geol. Soc. Amer. 29,

_____, DRAISIN, W.M., 1950 - Composition of the minerals in the rocks of the southern California batholith. 18th Int. Geol. Cong. 2, 66.

LARSEN, E.S., IRVING, J., GONYER, F.A., 1938 - Petrologic results of a study of minerals from the Tertiary volcanic rocks of the San Juan region, Colorado. Amer. Mineral. 23, 227.

LEEMAN, W.P., 1974 - Experimental determination of partitioning of divalent cations between olivine and basaltic liquid. Unpub. Ph.D. Thesis, Univ. Oregon.

_____, 1976 - Petrogenesis of McKinney (Snake River) olivine tholeiite in light of rare-earth element and Cr/Ni distributions. Bull. Geol. Soc. Amer. 87, 1582.

LE MAITRE, R.W., 1976a - A new approach to the classification of igneous rocks using the basalt - andesite- rhyolite suite as an example. Contrib. Mineral. Petrol. 56, 191.

_____, 1976b - Some problems of the projection of chemical data into mineralogical classifications. Contrib. Mineral. Petrol. 56, 181.

LEWIS, J.F., 1968 - Trace elements, variation in alkalis and the ratio Sr^{87}/Sr^{86} in selected rocks from the Taupo volcanic zone. N.Z. J. Geol. Geophys. 11, 608.

LINDSTROM, D.J., 1976 - Experimental study of the partitioning of the transition metals between clinopyroxene and coexisting silicate liquids. Unpub. Ph.D. Thesis, Univ. Oregon.

LIOU, J.G., 1973 - Synthesis and stability relations of epidote, $Ca_2Al_2FeSi_3O_{12}(OH)$. J. Petrol. 14, 381.

LIPMAN, P.W., CHRISTIANSEN, R.L., VAN ALSTINE, R.E., 1969 - Retention of alkalis by calc-alkali rhyolites during crystallisation and hydration. Amer. Mineral. 54, 286.

LOWDER, G.G., CARMICHAEL, I.S.E., 1970 - The volcanoes and caldera of Talasea, New Britain : Geology and Petrology. Bull. Geol. Soc. Amer. 81, 17.

LOWELL, J.D., GUILBERT, J., 1970 - Lateral and vertical alteration mineralisation zoning in porphyry ore deposits. Econ. Geol. 65, 373.

LUTH, W., JAHNS, R.H., TUTTLE, O.F., 1964 - The granite system at pressures of 4 to 10 kilobars. J. Geophys. Res. 69, 759.

MACKENZIE, D.E., CHAPPELL, B.W., 1972 - Shoshonitic and calc-alkaline lavas from the highlands of Papua New Guinea. Contrib. Mineral. Petrol. 35, 50.

MANSON, V., 1967 - Geochemistry of basaltic rocks : Major elements. In: Hess, H.H., (Ed) Basalts. The Poldervaart treatise of rocks of basaltic composition. 1, Interscience, 215.

MANTON, W.I., 1973 - Whole rock Th-Pb age for the Masuke and Dembe-Divula complexes, Rhodesia. Earth Planet. Sci. Lett. 19, 83.

MARSH, B.D., 1976 - Some Aleution andesites : their nature and source. J. Geol. 84, 27.

MARSH, J.S., 1976 - Distribution of Ca in highly fractionated peralkaline magmas. Earth Planet. Sci. Lett. 31, 153.

MARTIN, H., 1965 - Precambrian geology of South-west Africa and Namaqualand. Precamb. Res. Unit, Univ. Cape Town.

MARTIN, R.F., BONIN, B., 1976 - Water and magma genesis : The association hypersolvus granite - subsolvus granite. Can. Mineral. 14, 228.

McDOUGALL, I., 1962 - Differentiation of the Tasmanian dolerites : Red Hill dolerite - granophyre association. Bull. Geol. Soc. Amer. 73, 279.

MEDARIS, L.G., 1969 - Partitioning of Fe^{++} and Mg^{++} between coexisting synthetic olivine and orthopyroxene. Amer. J. Sci. 267, 945.

MEIJER, A., 1976 - Pb and Sr isotopic data bearing on the origin of volcanic rocks from the Mariana island arc system. Bull. Geol. Soc. Amer. 87, 1358.

MERCY, E., O'HARA, M.J., 1967 - Distribution of Mn, Cr, Ti and Ni in coexisting minerals of ultramafic rocks. Geochim. Cosmochim. Acta 31, 2331.

MIDDLEMOST, E.A.K., 1964 - Petrology of the plutonic and dyke rocks of the southeastern Richtersveld. Trans. Geol. Soc. S.Afr. 67, 227.

_____, 1965 - Ultramafic rocks of the south-eastern Richtersveld. Trans. Geol. Soc. S.Afr. 68, 53.

MIYASHIRO, A., 1958 - Regional metamorphism of the Gosaiyo - Takanuki district in the central Abukuma Plateau. J. Fac. Sci. Tokyo Univ. II. 11, 219.

_____, 1968 - Metamorphism of mafic rocks. In: Hess, H.H. (Ed) Basalts. The Poldervaart treatise on rocks of basaltic composition. 2, Interscience, 799.

_____, 1973 - Metamorphism and metamorphic belts. George Allen and Unwin.

_____, SHIDO, F., 1975 - Tholeiitic and calc-alkaline series in relation to the behaviours of Ti, V, Cr and Ni. Amer. J. Sci. 275, 265.

MODRESKI, P.J., BOETTCHER, A.L., 1972 - The stability of phlogopite + enstatite at high pressures : a model for micas in the interior of the Earth. Amer. J. Sci. 272, 852.

MOORBATH, S., 1975 - Evolution of Precambrian crust from strontium isotopic evidence. Nature 254, 395.

_____, O'NIONS, R.K., PANKHURST, R.J., 1975 - The evolution of early Precambrian crustal rocks at Isua, west Greenland - geochemical and isotopic evidence. Earth Planet. Sci. Lett. 27, 229.

MOORES, E.M., 1973 - Geotectonic significance of ultramafic rocks. Earth Sci. Rev. 9, 241.

MUELLER, R.F., 1963 - Interaction of chemistry and mechanics in magmatism. J. Geol. 71, 759.

MUELLER, R.F., 1969 - Hydration, oxidation and the origin of the calc-alkaline series. NASA Tech. Note D-5400.

_____, 1971 - Oxidative capacity of magmatic components. Amer. J.Sci. 270, 236.

MURALI, A.V., LEEMAN, W.P., MA, M.S., SCHMITT, R.A., 1977 - Evaluation of fractionation and hybridisation models for Kilauea eruptions and possible mantle source of Kilauea and Mauna Loa tholeiitic basalts, Hawaii, J. Petrol. (in press).

MYSEN, B.O., 1976 - Partitioning of samarium and nickel between olivine, orthopyroxene and liquid : Preliminary data at 20 kbar and 1025°C. Earth Planet. Sci. Lett. 31, 1.

_____, BOETTCHER, A.L., 1975a - Melting of hydrous mantle. I. Phase relations of natural peridotite at high pressures and temperatures with controlled activities of water, carbon dioxide and hydrogen. J. Petrol. 16, 520.

_____, BOETTCHER, A.L., 1975b - Melting of hydrous mantle. II. Geochemistry of crystals and liquids formed by anatexis of mantle peridotite at high pressures and high temperatures as a function of controlled activities of water, hydrogen and carbon dioxide. J. Petrol. 16, 549.

NICHOLLS, I.A., 1971 - Petrology of Santorini volcano, Cyclades, Greece. J. Petrol. 12, 67.

_____, RINGWOOD, A.E., 1972 - Production of silica-saturated tholeiitic magmas in island arcs. Earth Planet. Sci. Lett. 17, 243.

_____, WHITFORD, D.J., 1976 - Primary magmas associated with Quaternary volcanism in the western Sunda arc. In: Johnson, R.W., (Ed) Volcanism in Australasia, Elsevier, 77.

NICHOLLS, J., CARMICHAEL, I.S.E., 1969 - A commentary on the absarokite - shoshonite - banakite series of Wyoming U.S.A. Schwiez. Mineral. Petrog. Mitt. 49, 47.

NICOLAYSEN, L.O., 1962 - Stratigraphic interpretation of age measurements in southern Africa. Geol. Soc. Amer. Buddington Vol., 569.

_____, BURGER, A.J., 1965 - Note on an extensive zone of 1000 million year old metamorphic and igneous rocks in southern Africa. Sci. Terre 10, 497.

NOBLE, D.C., 1967 - Sodium, potassium and ferrous iron contents of some secondarily hydrated natural silicic glasses. Amer. Mineral. 52, 280.

_____, BOWMAN, H.R., HEBERT, A.J., SILBERMAN, M.L., HEROPOULOS, C.E., FABBI, B.P.,HEDGE, C.E., 1975 - Chemical and isotopic constraints on the origin of low-Si latite and andesite from the Andes of central Peru. Geology 3, 501.

NOCKOLDS, S.R., 1947 - The relation between chemical composition and paragenesis in the biotite micas of igneous rocks. Amer. J. Sci. 245, 401.

NOCKOLDS, S.R., 1954 - Average chemical compositions of some igneous rocks. Geol. Soc. Amer. Bull. 65, 1007.

_____, ALLEN, R., 1953 - The geochemistry of some igneous rock series. Geochim. Cosmochim. Acta 4, 105.

NORRISH, K., HUTTON, J.T., 1969 - An accurate X-ray spectrographic method for the analysis of a wide range of geological samples. Geochim. Cosmochim. Acta 33, 431.

O'HARA, M.J., 1968 - The bearing of phase equilibria studies in synthetic and natural systems on the origin and evolution of basic and ultrabasic rocks. Earth Sci. Rev. 4, 69

OLIVER, R.L., 1961 - The Borrowdale volcanic and associated rocks of the Scafell area, English Lake district. Quart. J. Geol. Soc. Lond. 117, 377.

ONUMA, N., HIGUCHI, H., WAKITA, H., NAGASAWA, H., 1968 - Trace element partition between two pyroxenes and the host lava. Earth Planet. Sci. Lett. 5, 47.

O'NIONS, R.K., PANKHURST, R.J., 1974 - Petrogenetic significance of isotope and trace element variations in volcanics from the Mid-Atlantic. J. Petrol. 15, 603.

ORVILLE, P.M., 1963 - Alkali ion exchange between vapor and feldspar phases. Amer. J. Sci. 261, 201.

OSBORN, E.F., 1959 - Role of oxygen pressure in the crystallisation and differentiation of basaltic magma. Amer. J. Sci. 257, 609.

_____, 1962 - Reaction series for subalkaline igneous rocks based on different oxygen pressure conditions. Amer. Mineral. 47, 211.

_____, 1969 - The complementariness of orogenic andesite and alpine peridotite. Geochim. Cosmochim. Acta 33, 307

OVERSBY, V.M., 1975 - Lead isotope systematics and ages of Archaean acid intrusives in the Kalgoorlie-Norseman area, western Australia. Geochim. Cosmochim. Acta 39, 1107.

OXBURGH, E.R., 1964 - Petrological evidence for the presence of amphibole in the upper mantle and its petrogenetic and geophysical implications. Geol. Mag. 101, 1.

PANKHURST, R.J., O'NIONS, R.K., 1973 - Determination of Rb/Sr and $^{87}Sr/^{86}Sr$ ratios of some standard rocks and the evaluation of X-ray fluorescence spectrometry in Rb-Sr geochemistry. Chem. Geol. 12, 127.

PAPANASTASSIOU, D.A., WASSERBURG, G.J., 1969 - Initial strontium isotopic abundances and the resolution of small time differences in the formation of planetary objects. Earth Planet. Sci. Lett. 5, 361.

PAUL, A., DOUGLAS, R.W., 1965 - Ferrous-ferric equilibrium in binary alkali silicate glasses. Phys. Chem. Glasses 6, 207.

PEACOCK, M.A., 1931 - Classification of igneous rock series. J. Geol. 39,54.

PEARCE, J.A., CANN, J.R., 1973 - Tectonic setting of basic volcanic rocks determined using trace element analyses. Earth Planet. Sci. Lett. 19, 290.

PECCERILLO, A., TAYLOR, S.R., 1976 - Geochemistry of Eocene calc-alkaline volcanic rocks from the Kastamonu area, northern Turkey. Contrib. Mineral. Petrol. 58, 63.

PHILPOTTS, J.A., SCHNETZLER, C.C., 1970 - Phenocryst-matrix partition coefficients for K, Rb, Sr and Ba, with applications to anorthosite and basalt genesis. Geochim. Cosmochim. Acta 34, 307

POWELL, M., POWELL, R., 1974 - An olivine-clinopyroxene geothermometer. Contrib. Mineral. Petrol. 48, 249.

PROSTKA, H.J., 1973 - Hybrid origin of the absarokite - shoshonite- banakite series, Absaroka volcanic field, Wyoming. Bull. Geol. Soc. Amer. 84, 697.

RAYLEIGH, J.W.S., 1896 - Theoretical considerations respecting the separation of gasses by diffusion and similar processes. Phil. Mag. 42, 77.

REID, A.M., DONALDSON, C.H., BROWN, R.W., RIDLEY, W.I., DAWSON, J.B., 1974 - Mineral chemistry of peridotite xenoliths from Lashaine volcano, Tanzania. In: Ahrens, L.H., Dawson, J.B., Duncan, A.R., Erlank, A.J., (Eds) Phys. Chem. Earth 9, 525.

REID, D.L., 1974 - Preliminary report on petrologic studies of volcanic and intrusive rocks in the Vioolsdrif region. Bull. Precamb. Res. Unit, Univ. Cape Town, 15, 57.

RIGG, T., WAGENBAUER, H.A. 1964 - Analysis of silicate rocks. Part I. Routine determination of major constituents. Res. Council Alberta. Prelim. Rep. 64.

RINGWOOD, A.E., 1966 - Chemical composition and origin of the Earth. In: Hurley, P.M., (Ed) Advances in Earth Sciences, M.I.T. Press, 287.

_____, 1974 - The petrological evolution of island arc systems. J. Geol. Soc. Lond. 130, 183.

_____, 1975 - Composition and petrology of the Earth's mantle. McGraw-Hill.

RITTER, U., 1975 - Preliminary report on the geology of the north-eastern Richtersveld. Thirteenth Ann. Rep. Precamb. Res. Unit, Univ. Cape Town, 42.

_____, 1977 - Bull. Precamb. Res. Unit, Univ. Cape Town, 29 (in preparation).

ROEDER, P.L., EMSLIE, R.F., 1970 - Olivine - liquid equilibrium. Contrib. Mineral. Petrol. 29, 275.

ROGERS, A.W., DU TOIT, A.L., 1908 - Report on the geology of parts of Prieska, Hay, Britstown, Canarvon and Victoria West. Ann. Rep. Geol. Comm. C.G.H. 13, 7.

ROGERS, J.J.W., ADAMS, J.A.S., 1969 - Uranium and Thorium. In: Wedepohl, K. H., (Ed) Handbook of Geochemistry, II/1, Springer Verlag.

ROSHOLT, J.N., BARTEL, A.J., 1969 - Uranium, thorium and lead systematics in Granite Mountains, Wyoming. Earth Planet. Sci. Lett. 7, 141.

_____, PRIJANA, NOBLE, D.C., 1971 - Mobility of uranium and thorium in glassy and crystallised silicic volcanic rocks. Econ. Geol. 66, 1061.

_____, ZARTMAN, R.E., NKOMO, I.T., 1973 - Lead isotope systematics and uranium depletion in the Granite Mountains, Wyoming. Bull. Geol. Soc. Amer. 84, 989.

ROSS, M., PAPIKE, J.J., WEIBLEN, P.W., 1968 - Exsolution in clinoamphiboles. Science 159, 1099.

SCHAFER, H.N.S., 1966a - The determination of iron (II) oxide in silicate and refractory materials. Part I. Review. The Analyst 91, 755.

_____, 1966b - The determination of iron (II) oxide in silicate and refractory materials. Part II. A semi-micro titrimatric method for determining iron (II) oxide in silicate materials. The Analyst 91, 763.

SCHOLTZ, D.L., 1946 - On the younger pre-Cambrian plutons of the Cape Province. Proc. Geol. Soc. S.Afr. 49, 35.

SCHUTTE, I.C., 1972 - The main pegmatites of the area between Steinkopf, Vioolsdrif and Goodhouse, Namaqualand. Mem. Geol. Surv. S.Afr. 60.

SETHURAMAN, K., MOORE, J.M., 1973 - Petrology of metavolcanic rocks in the Bishop Corners - Donaldson area, Grenville Province, Ontario. Can. J. Earth Sci. 10, 589.

SEWARD, T.M., 1971 - The distribution of transition elements in the system $CaMgSi_2O_6$ - $Na_2Si_2O_5$ - H_2O at 1000 bars pressure. Chem. Geol. 7, 73.

SHAPIRO, L., BRANNOCK, W.W., 1956 - Rapid analysis of silicate rocks. Bull. U.S. Geol. Surv. 1036-C.

SHAW, D.M., 1970 - Trace element fractionation during anatexis. Geochim. Cosmochim. Acta 34, 237.

_____, 1972 - Development of the early continental crust. Part I. Use of trace element distribution coefficient models for the protoarchaean crust. Can. J. Earth Sci. 9, 1577.

SHERATON, J.W., BLACK, L.P., 1973 - Zinc content in granites from central Queensland and northern New South Wales. Mineralum Deposita 4, 66.

SHIDO, F., MIYASHIRO, A., 1959 - Hornblendes of basic metamorphic rocks. J. Fac. Sci. Tokyo Univ. II, 12, 85.

SHIMIZU, N., 1974 - An experimental study of the partitioning of K, Rb, Cs, Sr and Ba between clinopyroxene and liquid at high pressures. Geochim. Cosmochim. Acta 38, 1789.

SIEDNER, G., 1965 - Geochemical features of a strongly fractionated alkali igneous rock suite. Geochim. Cosmochim. Acta 29, 113.

SIMON, F.O., ROLLINSON, C.L., 1976 - Chromium in rocks and minerals from the southern California batholith. Chem. Geol. 17, 73.

SMITH, R.E., 1968 - Redistribution of major elements in the alteration of some basic lavas during burial metamorphism. J. Petrol. 9, 191.

_____, 1969 - Zones of progressive regional burial metamorphism in part of the Tasman geosyncline, eastern Australia. J. Petrol.10, 144.

_____, SMITH, S.E., 1976 - Comments on the use of Ti, Zr, Y, Sr, K, P and Nb in the classification of basaltic magmas. Earth Planet. Sci. Lett. 32, 114.

SÖHNGE, P.G., DE VILLIERS, J., 1948 - The Kuboos pluton and its association line of intrusives. Trans. Geol. Soc. S.Afr. 51, 1.

SPENCER, L.J., 1942 - Barium-feldspars (celsian and paracelsian) from Wales. Mineral. Mag. 26, 231.

SPRY, A., 1969 - Metamorphic textures. Pergamon Press.

STACEY, J.A.S., KRAMERS, J.D., 1975 - Approximation of terrestrial lead isotope evolution by a two-stage model. Earth Planet. Sci. Lett. 26, 207.

_____, STEARNS, T.W., 1973 - Revised tables for the calculation of lead isotope ages. Natl. Tech. Information Service, Springfield, Virginia.

STANTON, R.L., BELL, J.D., 1969 - Volcanic and associated rocks of the New Georgia Group, British Solomon Islands Protectorate. Overseas Geol. Mineral. Res. 10, 113.

STRECKEISEN, A., 1967 - Classification and nomenclature of igneous rocks. N. Jb. Miner. Abh. 107, 144.

_____, 1974 - Classification and nomenclature of plutonic rocks. Geol. Rundschau 63, 773.

_____, 1976 - To each plutonic rock its proper name. Earth Sci. Rev. 12,1.

TAYLOR, S.R., 1965 - The application of trace element data to problems of petrology. In:Ahrens, L.H., Press, F., Runcorn, S.K., Urey, H.C. (Eds) Phys. Chem. Earth 6, 133.

_____, 1967 - The origin and growth of continents. Tectonophys. 4, 17.

_____, 1969 - Trace element chemistry of andesites and associated calc-alkaline rocks. In: McBirney, A.R., (Ed) Proceedings of the andesite conference. Bull. Oregon Dept. Mineral Ind. 65, 43.

_____, CAPP, A.C., GRAHAM, A.L., BLAKE, D.H., 1969a - Trace element abundances in andesites. II. Saipan, Bougainville and Fiji. Contrib. Mineral. Petrol. 23, 1.

TAYLOR, S.R., EWART, A., CAPP, A.C., 1968 - Leucogranites and rhyolites : Trace element evidence for fractional crystallisation and partial melting. Lithos 1, 179.

_____, KAYE, M., WHITE, A.J.R., DUNCAN, A.R., EWART, A., 1969b - Genetic significance of Co, Cr, Ni, Sc and V content of andesites. Geochim. Cosmochim. Acta 33, 275.

THAYER, T.P., 1970 - Chromite segregations as petrogenetic indicators. Spec. Pap. Geol. Soc. S.Afr. 1, 380.

THOMPSON, R.N., 1973 - One atmosphere melting behaviour and nomenclature of terrestrial lavas. Contrib. Mineral. Petrol. 41, 197.

THORNTON, C.P., TUTTLE, O.F., 1960 - Chemistry of igneous rocks. I. Differentiation Index. Amer. J. Sci. 258, 664.

TITLEY, S.R., HICKS, C.L., 1966 - (Eds) : Geology of the porphyry copper deposits, south-western North America. Univ. Ariz. Press.

TURNER, F.J., 1968 - Metamorphic petrology. McGraw-Hill.

_____, VERHOOGEN, J., 1960 - Igneous and metamorphic petrology. 2nd Ed. McGraw-Hill.

TURNOCK, A.C., 1959 - Stability range of iron chlorite. Bull. Geol. Soc. Amer. 70, 1690.

TUTTLE, O.F., BOWEN, N.L., 1958 - Origin of granite in the light of experimental studies in the system $NaAlSi_3O_8$ - $KAlSi_3O_8$ - SiO_2 - H_2O. Mem. Geol. Soc. Amer. 74.

VERWOERD, W.J., ERLANK, A.J., KABLE, E.J.D., 1974 - Geology and geochemistry of Bouvet Island. Proc. Symp. Andean Antarctic Volc. IAVCEI. Bull. Volc., 204.

VON BACKSTRÖM, J. W., DE VILLIERS, J., 1972 - The geology along the Orange River between Onseepkans and the Richtersveld. Explan. Sheets 2817D (Vioolsdrif), 2818C and D (Goodhouse) and 2819C (Onseepkans). Geol. Surv. S.Afr.

WAGER, L.R., 1960 - The major element variation of the layered series of the Skaergaard Intrusion. J. Petrol. 1, 364.

_____, BROWN, G.M., 1967 - Layered igneous rocks. Oliver and Boyd.

_____, BROWN, G.M., WADSWORTH, W.J., 1960 - Types of igneous cumulates. J. Petrol. 1, 73.

WARD, J.H.W., 1974 - The Vioolsdrif pegmatite belt. Tenth and eleventh Ann. Rep., Precamb. Res. Unit, Univ. Cape Town. 38.

WATERS, A.C., 1960 - Determining direction of flow in basalts. Amer. J. Sci. 258A, 350.

WATKINS, N.D., HAGGERTY, S.E., 1967 - Primary oxidation variation and petrogenesis in a single lava. Contrib. Mineral. Petrol. 15, 251.

WATTERS, B.R., 1974 - Stratigraphy, igneous petrology and evolution of the Sinclair Group in southern South-west Africa. Bull. Precamb. Res. Unit, Univ. Cape Town, 16,

WHITE, D.E., 1957 - Thermal waters of volcanic origin. Bull. Geol. Soc. Amer. 68, 1637.

WILKINSON, J.F.G., 1967 - The petrography of basaltic rocks. In: Hess, H.H., (Ed) Basalts. The Poldervaart treatise on rocks of basaltic composition. 1, Interscience, 163.

_____, 1971 - The petrology of some vitrophyric calc-alkaline volcanics from the Carboniferous of New South Wales. J. Petrol. 12, 587.

WILLIAMS, H., 1932 - Geology of Lassen national park, California. Univ. Calif. Dept. Geol. Sci. 21, 195.

_____, 1935 - Newberry volcano of central Oregon. Bull. Geol. Soc. Amer. 46, 253.

_____, 1942 - The geology of Crater Lake national park. Carnegie Inst. Wash. Publ. 540.

_____, TURNER, F.J., GILBERT, C.M., 1954 - Petrography. W.H. Freeman.

WILLIS, J.P., AHRENS, L.H., DANCHIN, R.V., ERLANK, A.J., GURNEY, J.J., HOFMEYR, P.K., McCARTHY, T.S., ORREN, M.J., 1971 - Some inter-element relationships between lunar rocks and fines and stony meteorites. In: Levinson, A.A., (Ed) Proc. Second Lunar Sci. Conf. M.I.T. Press, 1123.

_____, ERLANK, A.J., GURNEY, J.J., THEIL, R.H., AHRENS, L.H., 1972 - Major, minor and trace element data for some Apollo 11, 12, 14 and 15 samples. In: Heymann, L. D., (Ed) Proc. Third Lunar Sci. Conf. M.I.T. Press, 1269.

WINKLER, H.G.F., 1976 - Petrogenesis of metamorphic rocks. (4th Ed.) Springer Verlag.

WOOD, B.J., 1976 - An olivine-clinopyroxene geothermometer. A discussion. Contrib. Mineral. Petrol. 56, 297.

_____, BANNO, S., 1973 - Garnet-orthopyroxene and orthopyroxene - clinopyroxene relationships in simple and complex systems. Contrib. Mineral. Petrol. 42,109.

WORDEN, J.M., COMPSTON, W., 1973 - A Rb-Sr isotopic study of weathering in the Mertondale granite, western Australia. Geochim. Cosmochim. Acta 37, 2567.

WYLLIE, P.J., 1967 - (Ed) Ultramafic and related rocks. Wiley.

YODER, H.S., 1965 - Diopside-anorthite-water at 5 and 10 kb and its bearing on explosive volcanism. Carnegie Inst. Wash. Year Book 64, 82.

_____, STEWART, D.B., SMITH, J.R., 1957 - Ternary feldspars. Carnegie Inst. Wash. Year Book, 56, 206.

YODER, H.S., TILLEY, C.E., 1962 - Origin of basalt magmas : An experimental study of natural and synthetic rock systems. J. Petrol. 3, 342.

YORK, D., 1966 - Least squares fitting of a straight line. Can. J. Phys. 44, 1079.

_____, 1967 - The best isochron. Earth Planet. Sci. Lett. 2, 479.

ZEILINSKI, R.A., LIPMAN, P.W., 1976 - Trace element variations at Summer Coon volcano, San Juan Mountains, Colorado and the origin of continental interior andesite. Bull. Geol. Soc. Amer. 87, 1477.

Appendix 1

SAMPLE LOCALITIES

Sample localities have been plotted on three maps included in this Appendix (Figs A1.1-3). The map in Fig. A1.1 contains the major geological boundaries defined by Blignault (1975). The map in Fig. A1.2 contains the geological boundaries defined in the S.A. Geological Survey Sheet 2917D (Vioolsdrif), compiled by Von Backstrom and De Villiers (1972), plus some modifications the author. The section through the Nous Formation exposed in the Charliesfontein - Koubank gorge is shown in Fig. A1.3. Samples collected from the Swartkop basic-ultrabasic complex are plotted on the map shown in Fig. 45 (Chapter 10). Samples of the Haib porphyry (RT-01, RT-02 and RT-03) are specimens of drill core from the upper Tsams River area, which were kindly provided by Rio Tinto (Pty) Ltd. Samples of dacitic lava intruded by the Haib porphyry in the upper Tsams River area (RT-04, RT-05 and RT-06) are also specimens of drill core supplied by the above company.

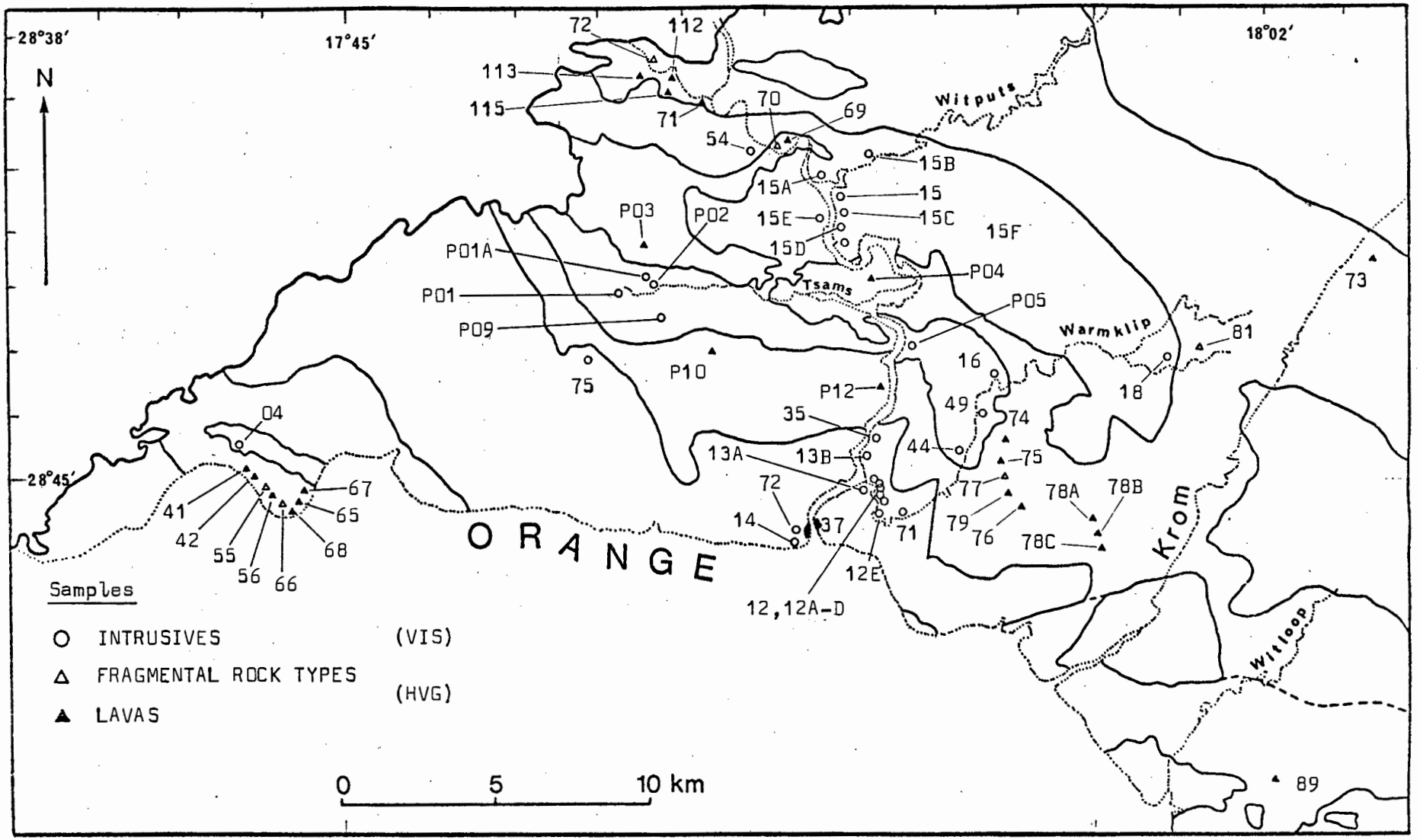

Fig. A1.1 Sample localities in the HVIP north of the Orange River in South-west Africa. Geological boundaries after Blignault (1975).

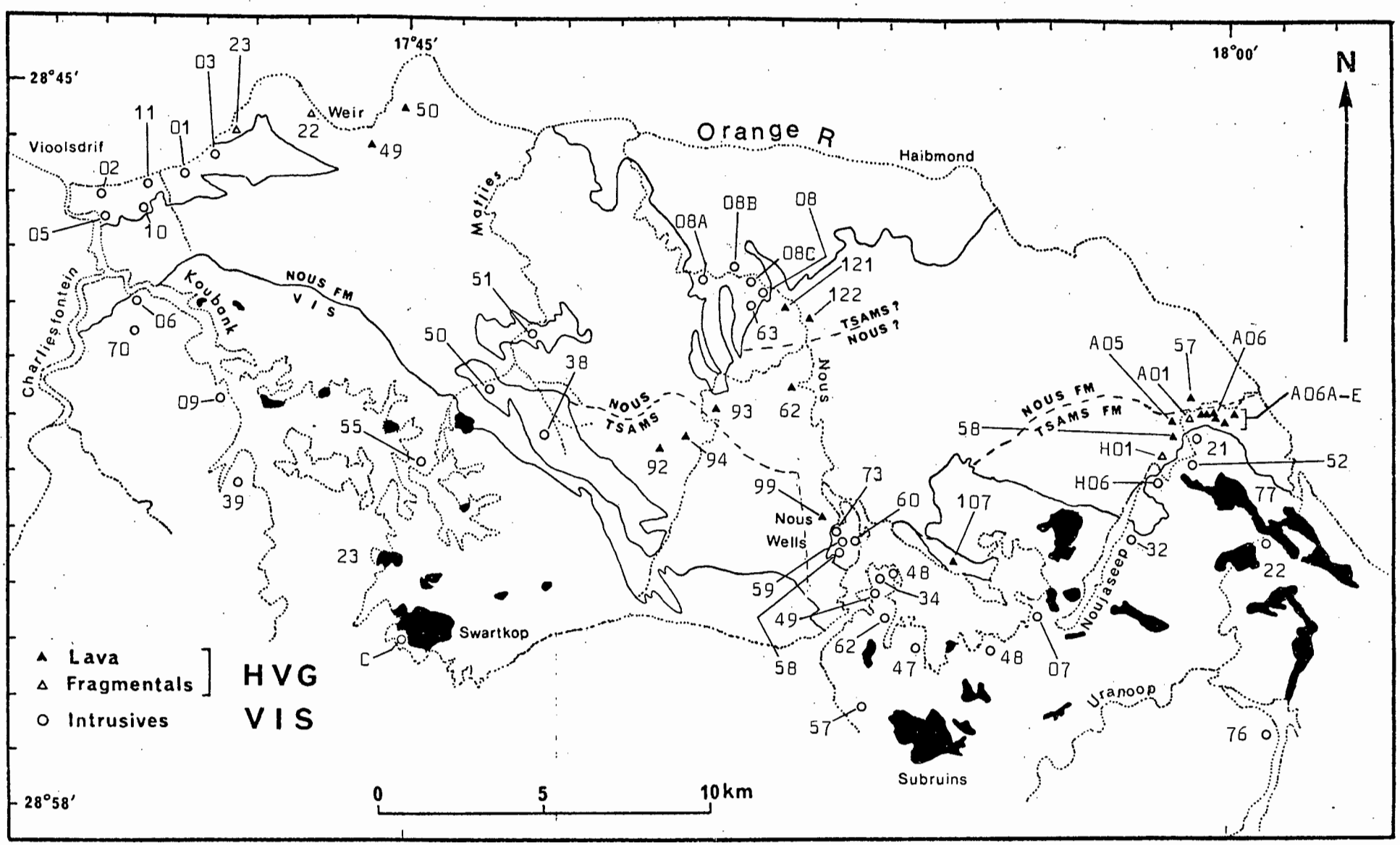

Fig. A1.2 Sample localities in the HVIP south of the Orange River in the Republic of South Africa. Geological boundaries based on Von Backstrom and De Villiers (1972), plus some modifications by the author.

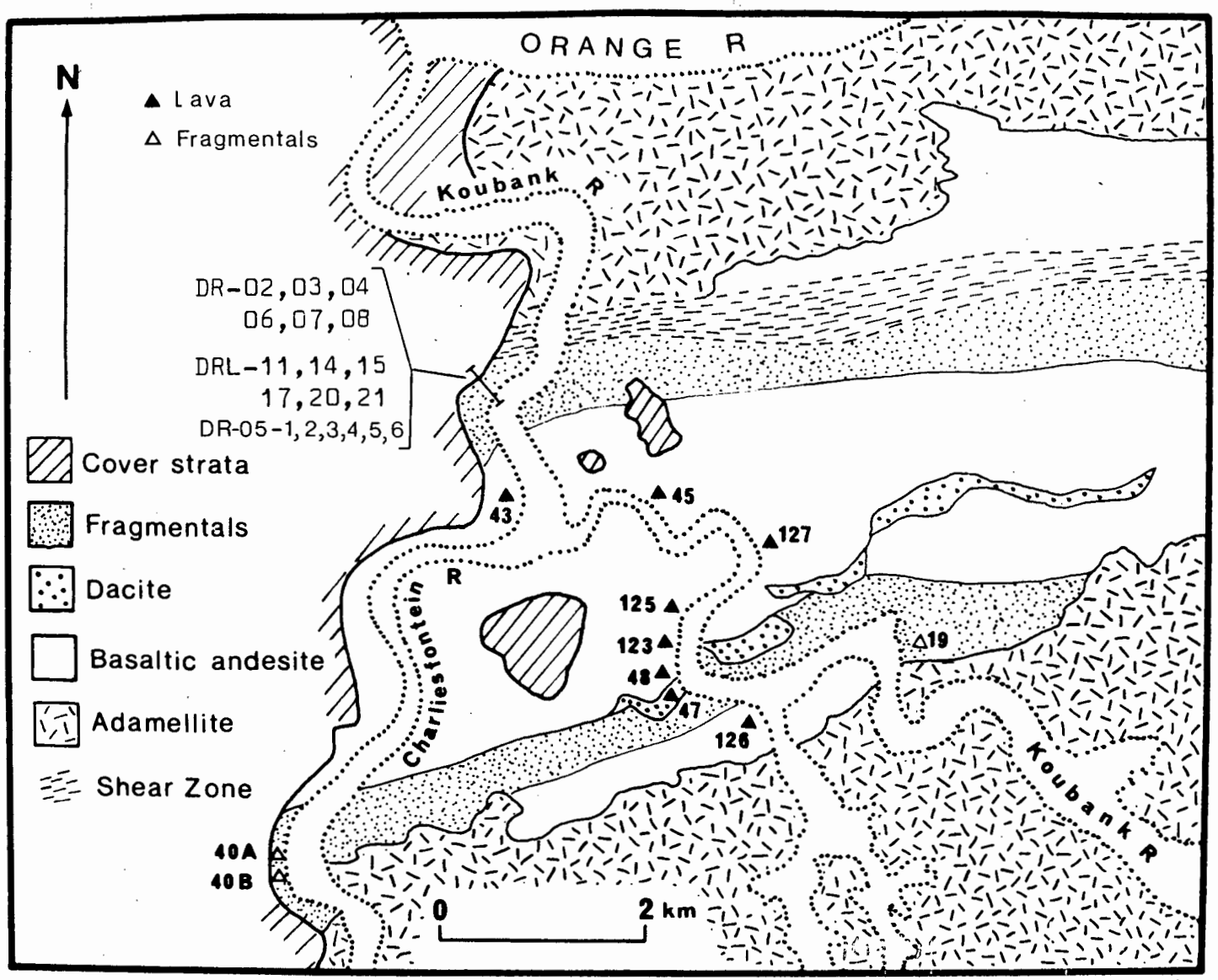

Fig. A1.3 Details of the Charliesfontein - Koubank gorge section through the Nous Formation.

Appendix 2

MINERAL ANALYSES

A2.1 Analytical techniques

Mineral compositions have been determined with an electron microprobe (EMP), on polished thin sections, previously coated with finely divided carbon to aid conduction. No comprehensive account of the operating procedures used in the Department of Geochemistry has been formerly published, so a brief account is given below:

Instrument : Cambridge Microscan 5 with two wavelength dispersive spectrometers
Beam Current : 0.15μA at specimen
Accelerating voltage : 15 kV
Analysing crystals : RAP (Si, Al, Mg, Na) ; QUARTZ (Fe, Mn, Cr, Ca, Ti, K)
Detection : Flow counters with Ar/CO_2 gas mixture

A finely focussed (1-2μ diameter) beam was used for all elements, except when analysing feldspars, when a 10μ defocussed beam was used. Calibration was achieved with natural mineral standards, which had previously been analysed by wet chemical or XRF techniques (e.g. Kakanui mineral suite - hornblende, augite, pyrope). Raw counts were corrected for dead time and background. Nominal concentrations were calculated from standard data obtained at the beginning of each analytical run, and subsequently corrected using the method of Boyd et al.,(1968).

The precision of the technique was estimated by replicate analysis of pargasitic amphibole in a peridotite from the Swartkop complex. The standard deviation about the mean of 10 analyses of the same spot has been compared with the uncertainty caused by counting statistics in Table A2.1. The relatively large S.D. value for Na_2O is caused in part by volatisation of this element during prolonged exposure to the EMP beam. Inspection of Table A2.1 suggests that the overall precision of the technique is determined by counting statistics.

The accuracy of the technique is difficult to establish, because of the

Table A2.1 An estimate of the precision of the analytical technique.

$\bar{X}$ = Mean of 10 replicate analyses of the same spot within a pargasitic hornblende in a peridotite from the Swartkop complex

S.D. = Standard deviation about the mean

ERR = 2 σ error (95 percent confidence limits) due to counting statistics

DL = Theoretical detection limit (99 percent confidence)

All quantities expressed in weight percent of the oxide

OXIDE	$\bar{X}$	S.D.	ERR	DL
SiO_2	41.97	.08	.08	.06
TiO_2	3.92	.08	.10	.07
Al_2O_3	13.51	.06	.06	.04
FeO	6.82	.15	.16	.10
MgO	16.34	.07	.10	.05
CaO	12.10	.07	.08	.05
Na_2O	2.71	.12	.14	.09
K_2O	1.18	.06	.10	.07
TOTAL	98.55	.20		

MnO and Cr_2O_3 were not analysed, but the estimated precisions are as follows:

MnO - ERR = .10, DL = .07 at 0.75 percent level
Cr_2O_3 - ERR = .10, DL = .05 at 1.25 percent level
Data for MnO from an orthopyroxene, Cr_2O_3 from a clinopyroxene

possibility that natural mineral standards are not homogeneous at the micron scale. Nevertheless, good agreement was achieved when analysing one natural mineral standard against another, using abundance data obtained by another method (XRF data provided by B.W. Chappell, Australian National University). A less objective approach was to inspect the totals for analyses of those minerals where the sum of the oxides should be near 100 percent (e.g. olivine, pyroxenes, feldspars). Inspection of the following tables suggest that the accuracy of the technique is satisfactory for the purposes of this study.

Notes on the tables:

All Fe is reported as FeO (FeO*), except in the case of magnetite, ilmenite and chromite, where Fe_2O_3 and FeO have been estimated assuming perfect spinel stoichiometry; n.d. = not determined

METAMORPHIC AMPHIBOLES - HAIB BASALTIC ANDESITES

Specimen	DRL-65						DRL-49			
Grain	1	2	3	4	5	6	1	2	3	4
SiO_2	49.99	52.33	52.00	47.74	53.59	51.98	51.32	48.41	47.41	54.36
TiO_2	.17	.13	.07	.30	.08	.18	.12	.38	.25	.10
Al_2O_3	6.89	5.27	4.75	9.23	3.97	6.20	5.19	8.16	9.43	2.80
FeO*	13.30	11.04	12.04	14.26	11.09	11.29	12.14	13.69	14.57	10.80
MnO	.28	.28	.27	.28	.26	.27	.28	.28	.32	.28
MgO	15.04	16.72	16.75	13.68	17.56	16.56	16.29	14.46	13.40	17.47
CaO	12.63	12.84	12.90	12.49	12.97	12.55	12.67	12.55	12.50	13.03
Na_2O	.75	.47	.38	.84	.50	.54	.72	.99	1.17	.27
K_2O	.14	.12	.13	.17	.10	.13	.18	.24	.17	.07
Cr_2O_3	.00	.00	.00	.00	.00	.00	.00	.00	.00	.00
Total	99.19	99.20	99.29	98.99	100.12	99.70	98.91	99.16	99.22	99.18
No. of oxygens	23	23	23	23	23	23	23	23	23	23
Si	7.162	7.391	7.381	6.901	7.496	7.308	7.329	6.976	6.861	7.652
Al (4)	.838	.609	.619	1.099	.504	.692	.671	1.024	1.139	.348
SZ	8.000	8.000	8.000	8.000	8.000	8.000	8.000	8.000	8.000	8.000
Al (6)	.326	.268	.176	.474	.151	.336	.203	.362	.470	.117
Ti	.018	.014	.007	.033	.008	.019	.013	.041	.027	.011
Fe	1.594	1.304	1.429	1.724	1.297	1.327	1.450	1.650	1.763	1.271
Mn	.034	.033	.032	.034	.031	.032	.034	.034	.039	.033
Mg	3.211	3.519	3.543	2.947	3.661	3.470	3.467	3.105	2.890	3.554
Cr	.000	.000	.000	.000	.000	.000	.000	.000	.000	.000
SY	5.183	5.138	5.187	5.212	5.148	5.184	5.167	5.192	5.189	5.097
Ca	1.939	1.943	1.962	1.935	1.944	1.891	1.939	1.938	1.938	1.965
Na	.208	.129	.105	.235	.136	.147	.199	.277	.328	.074
K	.026	.022	.024	.031	.018	.023	.033	.044	.031	.013
SX	2.173	2.094	2.091	2.201	2.098	2.061	2.171	2.259	2.297	2.051

METAMORPHIC AMPHIBOLES - HAIB BASALTIC ANDESITES

Specimen	DRL-49									
Grain	5	6	7	8	9	10	11	12	13	14
SiO_2	52.54	48.18	54.63	49.16	48.44	48.55	48.28	45.34	51.76	46.40
TiO_2	.10	.37	.05	35	.37	.40	.40	.45	.12	.40
Al_2O_3	4.17	8.37	2.35	7.67	8.07	8.17	8.75	11.21	4.78	9.60
FeO*	12.46	13.43	11.19	13.13	13.49	13.49	13.63	15.38	11.69	14.12
MnO	.30	.00	.28	.32	.31	.30	.00	.32	.25	.33
MgO	15.98	14.42	17.29	14.80	14.42	14.26	13.98	12.22	16.35	13.38
CaO	12.98	12.43	13.07	12.42	12.42	12.48	12.44	12.14	12.64	12.10
Na_2O	.49	.99	.19	.92	.96	.73	.89	1.11	.46	1.09
K_2O	.07	.21	.01	.18	.19	.19	.14	.26	.08	.23
Cr_2O_3	.00	.00	.00	.00	.00	.00	.00	.00	.00	.00
Total	99.09	98.40	99.06	98.95	98.67	98.57	98.51	98.43	98.13	97.65
No. of oxygens	23	23	23	23	23	23	23	23	23	23
Si	7.481	6.976	7.706	7.065	7.003	7.017	6.977	6.652	7.415	6.816
Al (4)	.519	1.024	.294	.935	.997	.983	1.023	1.348	.585	1.184
SZ	8.000	8.000	8.000	8.000	8.000	8.000	8.000	8.000	8.000	8.000
Al (6)	.181	.405	.097	.365	.378	.409	.468	.591	.222	.478
Ti	.011	.040	.005	.038	.040	.043	.043	.050	.013	.044
Fe	1.484	1.626	1.320	1.578	1.631	1.631	1.647	1.887	1.401	1.735
Mn	.036	.000	.033	.039	.038	.037	.000	.040	.030	.041
Mg	3.391	3.112	3.635	3.170	3.107	3.072	3.011	2.672	3.491	2.929
Cr	.000	.000	.000	.000	.000	.000	.000	.000	.000	.000
SY	5.103	5.183	5.090	5.190	5.194	5.192	5.169	5.240	5.157	5.227
Ca	1.980	1.928	1.976	1.913	1.924	1.933	1.926	1.908	1.940	1.905
Na	.135	.278	.052	.256	.269	.205	.249	.316	.128	.310
K	.013	.039	.002	.033	.035	.035	.026	.049	.015	.043
SX	2.128	2.245	2.030	2.202	2.228	2.173	2.201	2.273	2.083	2.258

METAMORPHIC AMPHIBOLES - HAIB BASALTIC ANDESITES

Specimen	DRL-49	DRL-50					DRL-42			
Grain	15	1	2	3	4	5	1	2	3	4
SiO_2	51.03	47.98	48.15	48.72	48.23	50.39	52.16	50.02	49.54	49.84
TiO_2	.12	.50	.40	.42	.37	.20	.29	.39	.42	.37
Al_2O_3	4.86	8.84	9.35	8.44	8.74	5.57	4.43	6.23	6.42	6.07
FeO*	11.78	13.27	13.14	13.01	12.77	11.48	10.08	11.48	11.87	11.80
MnO	.27	.30	.27	.31	.27	.28	.30	.30	.27	.31
MgO	15.85	14.47	14.01	14.64	14.65	16.58	16.77	16.26	16.11	15.65
CaO	12.41	12.03	12.23	11.85	12.53	12.63	12.82	12.62	12.61	12.36
Na_2O	.49	1.01	1.12	1.12	.87	.72	.47	.77	.73	.75
K_2O	.11	.19	.23	.13	.18	.26	.15	.33	.36	.34
Cr_2O_3	.00	.00	.00	.00	.00	.00	.00	.00	.00	.00
Total	96.92	98.59	98.90	98.64	98.61	98.11	97.47	98.40	98.33	97.49
No. of oxygens	23	23	23	23	23	23	23	23	23	23
Si	7.411	6.930	6.927	7.011	6.951	7.249	7.472	7.181	7.136	7.227
Al (4)	.589	1.070	1.073	.989	1.049	.751	.528	.819	.864	.773
SZ	8.000	8.000	8.000	8.000	8.000	8.000	8.000	8.000	8.000	8.000
Al (6)	.243	.435	.513	.443	.436	.194	.220	.235	.226	.265
Ti	.013	.054	.043	.045	.040	.022	.031	.042	.045	.040
Fe	1.431	1.603	1.581	1.566	1.539	1.381	1.208	1.378	1.430	1.431
Mn	.033	.037	.033	.038	.033	.034	.036	.036	.033	.038
Mg	3.430	3.115	3.004	3.140	3.146	3.555	3.580	3.479	3.458	3.382
Cr	.000	.000	.000	.000	.000	.000	.000	.000	.000	.000
SY	5.150	5.244	5.174	5.232	5.194	5.186	5.075	5.170	5.192	5.156
Ca	1.931	1.862	1.885	1.827	1.935	1.947	1.968	1.941	1.946	1.920
Na	.138	.283	.312	.313	.243	.201	.131	.214	.204	.211
K	.020	.035	.042	.024	.033	.048	.027	.060	.066	.063
SX	2.089	2.180	2.239	2.164	2.211	2.196	2.126	2.215	2.216	2.194

METAMORPHIC AMPHIBOLES - HAIB BASALTIC ANDESITES

Specimen	DRL-99				DRL-123		
Grain	1	2	3	4	1	2	3
SiO_2	48.62	42.24	53.56	41.40	51.60	48.46	47.59
TiO_2	.28	.38	.08	.35	.15	.43	.35
Al_2O_3	5.35	11.61	2.49	12.42	5.18	7.38	8.20
FeO*	12.71	16.89	9.46	16.47	11.62	13.68	14.49
MnO	.27	.29	.27	.27	.25	.33	.33
MgO	15.73	11.44	17.27	10.75	15.86	14.25	13.91
CaO	12.59	12.37	12.64	12.08	12.31	12.33	12.08
Na_2O	.60	1.12	.23	1.26	.52	.77	.87
K_2O	.30	.48	.02	.54	.15	.47	.45
Cr_2O_3	.00	.02	.05	.00	.00	.00	.00
Total	96.45	96.84	96.07	95.54	97.64	98.10	98.27
No. of oxygens	23	23	23	23	23	23	23
Si	7.183	6.405	7.730	6.355	7.420	7.062	6.954
Al (4)	.817	1.595	.270	1.645	.580	.938	1.046
SZ	8.000	8.000	8.000	8.000	8.000	8.000	8.000
Al (6)	.115	.481	.154	.603	.298	.330	.367
Ti	.031	.043	.009	.040	.016	.047	.038
Fe	1.570	2.142	1.142	2.115	1.397	1.667	1.771
Mn	.034	.037	.033	.035	.030	.041	.041
Mg	3.463	2.585	3.715	2.459	3.399	3.095	3.029
Cr	.000	.002	.006	.000	.000	.000	.000
SY	5.213	5.290	5.059	5.252	5.140	5.180	5.246
Ca	1.993	2.010	1.955	1.987	1.897	1.925	1.891
Na	.172	.329	.064	.375	.145	.218	.246
K	.057	.093	.004	.106	.028	.087	.084
SX	2.222	2.432	2.023	2.468	2.070	2.230	2.221

METAMORPHIC CHLORITES - HAIB BASALTIC ANDESITES

	DRL-42	DRL-65			DRL-49		
	1	1	2	3	1	2	3
SiO_2	26.73	29.42	30.44	29.76	26.95	27.02	26.88
TiO_2	.07	.05	.05	.07	.08	.07	.07
Al_2O_3	21.42	18.69	18.11	18.25	21.78	22.25	22.72
FeO*	16.45	18.20	17.62	17.52	18.07	18.52	18.33
MnO	.26	.27	.26	.00	.25	.24	.27
MgO	21.67	24.17	24.24	24.53	21.35	22.08	22.28
CaO	.06	.06	.07	.06	.03	.01	.03
Na_2O	.04	1.33	.03	.03	.07	.03	.00
K_2O	.00	.02	.27	.04	.04	.00	.00
Cr_2O_3	.00	.00	.00	.00	.00	.00	.00
Total	86.70	92.21	91.09	90.26	88.62	90.22	90.58
No. of oxygens	28	28	28	28	28	28	28
Si	5.431	5.689	5.905	5.818	5.398	5.323	5.269
Al (4)	2.569	2.311	2.095	2.182	2.602	2.677	2.731
SZ	8.000	8.000	8.000	8.000	8.000	8.000	8.000
Al (6)	2.561	1.950	2.047	2.024	2.541	2.491	2.520
Ti	.011	.007	.007	.010	.012	.010	.010
Fe	2.795	2.943	2.859	2.864	3.027	3.051	3.005
Mn	.045	.044	.043	.000	.042	.040	.045
Mg	6.561	6.965	7.008	7.147	6.373	6.483	6.509
Cr	.000	.000	.000	.000	.000	.000	.000
Ca	.013	.012	.015	.013	.006	.002	.006
Na	.016	.499	.011	.011	.027	.011	.000
K	.000	.005	.067	.010	.010	.000	.000
SX	12.002	12.425	12.057	12.079	12.038	12.088	12.095

METAMORPHIC CHLORITES - HAIB BASALTIC ANDESITES

	DRL-49		DRL-123			DRL-74
	4	5	1	2	3	1
SiO_2	26.88	27.17	26.48	26.44	27.04	26.55
TiO_2	.07	.08	.13	.08	.16	.08
Al_2O_3	22.36	21.47	20.96	21.35	20.56	20.84
FeO*	17.84	18.06	17.76	18.12	17.53	17.08
MnO	.29	.27	.29	.32	.29	.26
MgO	21.72	22.62	22.56	22.06	23.05	22.34
CaO	.04	.01	.05	.05	.10	.04
Na_2O	.00	.04	.06	.01	.06	.04
K_2O	.00	.02	.01	.02	.00	.00
Cr_2O_3	.00	.00	.00	.00	.00	.00
Total	89.20	89.74	88.30	88.45	88.79	87.23
No. of oxygens	28	28	28	28	28	28
Si	5.338	5.375	5.332	5.321	5.404	5.389
Al (4)	2.662	2.625	2.668	2.679	2.596	2.611
SZ	8.000	8.000	8.000	8.000	8.000	8.000
Al (6)	2.573	2.382	2.307	2.386	2.248	2.376
Ti	.010	.012	.020	.012	.024	.012
Fe	2.963	2.988	2.991	3.050	2.930	2.899
Mn	.049	.045	.049	.055	.049	.045
Mg	6.429	6.669	6.770	6.616	6.865	6.758
Cr	.000	.000	.000	.000	.000	.000
Ca	.009	.002	.011	.011	.021	.009
Na	.000	.015	.023	.004	.023	.016
K	.000	.005	.003	.005	.000	.000
SX	12.033	12.118	12.174	12.139	12.160	12.115

METAMORPHIC BIOTITES - HAIB BASALTIC ANDESITES

	DRL-49		DRL-50			DRL-42	
	1	2	1	2	3	1	2
SiO_2	37.27	37.34	37.16	37.40	36.39	37.43	37.65
TiO_2	1.30	1.25	1.54	1.62	1.55	1.32	1.42
Al_2O_3	17.26	16.99	17.53	17.21	16.87	17.21	17.32
FeO*	16.78	17.45	14.81	14.06	14.61	15.29	14.20
MnO	.19	.18	.15	.15	.12	.17	.19
MgO	14.83	14.87	15.62	16.25	15.07	15.58	15.29
CaO	.08	.14	.00	.07	.18	.01	.06
Na_2O	.07	.06	.10	.18	.00	.08	.07
K_2O	9.15	9.07	9.85	9.25	9.00	9.32	9.39
Cr_2O_3	.00	.00	.00	.00	.00	.00	.00
Total	96.93	97.35	96.76	96.19	93.79	96.41	95.59
No. of oxygens	22	22	22	22	22	22	22
Si	5.492	5.495	5.457	5.488	5.496	5.509	5.559
Al (4)	2.508	2.505	2.543	2.512	2.504	2.491	2.441
SZ	8.000	8.000	8.000	8.000	8.000	8.000	8.000
Al (6)	.490	.442	.492	.465	.500	.495	.574
Ti	.144	.138	.170	.179	.176	.146	.158
Fe	2.068	2.148	1.819	1.725	1.846	1.882	1.753
Mn	.024	.022	.019	.019	.015	.021	.024
Mg	3.257	3.261	3.419	3.554	3.392	3.418	3.364
Cr	.000	.000	.000	.000	.000	.000	.000
SY	5.983	6.011	5.919	5.942	5.929	5.962	5.873
Ca	.013	.022	.000	.011	.029	.002	.009
Na	.020	.017	.028	.051	.000	.023	.020
K	1.720	1.703	1.845	1.732	1.734	1.750	1.769
SX	1.753	1.742	1.873	1.794	1.763	1.775	1.798

METAMORPHIC BIOTITES - HAIB BASALTIC ANDESITES

	DRL-42	DRL-99		DRL-74			DRL-123	
	1	1	2	1	2	3	1	2
SiO_2	37.38	37.58	38.12	36.46	37.61	37.03	35.70	36.20
TiO_2	1.32	1.66	1.53	1.52	1.52	1.22	.96	1.15
Al_2O_3	17.10	17.18	17.39	16.20	16.35	16.62	16.63	16.46
FeO*	14.80	17.18	17.29	15.50	15.70	15.08	16.05	16.12
MnO	.13	.17	.19	.14	.18	.10	.22	.20
MgO	14.68	14.46	14.20	14.98	15.22	13.13	16.21	15.48
CaO	.03	.00	.00	.00	.00	.14	.07	.18
Na_2O	.08	.13	.22	.12	.22	.15	.04	.04
K_2O	9.24	9.21	9.60	9.82	9.98	10.02	9.20	8.76
Cr_2O_3	.00	.00	.00	.00	.00	.00	.00	.00
Total	94.76	97.62	98.54	94.74	96.78	93.49	95.08	94.59
No. of oxygens	22	22	22	22	22	22	22	22
Si	5.581	5.506	5.539	5.507	5.554	5.648	5.539	5.463
Al (4)	2.419	2.494	2.461	2.493	2.446	2.352	2.621	2.537
SZ	8.000	8.000	8.000	8.000	8.000	8.000	8.000	8.000
Al (6)	.591	.473	.518	.392	.401	.637	.333	.392
Ti	.148	.183	.167	.173	.169	.140	.109	.131
Fe	1.848	2.105	2.101	1.958	1.939	1.924	2.023	2.035
Mn	.016	.021	.023	.018	.023	.013	.028	.026
Mg	3.266	3.157	3.075	3.372	3.350	2.985	3.640	3.482
Cr	.000	.00	.000	.000	.000	.000	.000	.000
SY	5.869	5.945	5.884	5.913	5.882	5.699	6.133	6.066
Ca	.005	.000	.000	.000	.000	.023	.011	.029
Na	.023	.037	.062	.035	.063	.044	.012	.012
K	1.760	1.722	1.780	1.892	1.880	1.950	1.769	1.687
SX	1.788	1.759	1.842	1.927	1.943	2.017	1.792	1.728

METAMORPHIC EPIDOTES - HAIB BASALTIC ANDESITES

	DRL-65 1	2	3	4	5	6	7	DRL-42 1
SiO_2	36.79	35.65	38.10	36.82	37.11	37.02	36.35	37.90
TiO_2	.03	.07	.07	.15	.13	.12	.13	.03
Al_2O_3	24.87	24.59	25.35	22.96	23.19	22.94	23.49	23.46
Fe_2O_3*	11.07	11.52	12.89	14.40	13.74	13.62	13.04	14.52
MnO	.22	.21	.24	.21	.18	.22	.15	.15
MgO	.03	.03	.05	.05	.05	.45	.05	.07
CaO	23.23	23.21	23.56	23.23	23.13	22.66	23.40	23.42
Na_2O	.00	.00	.00	.00	.00	.00	.00	.04
K_2O	.00	.00	.00	.00	.00	.00	.00	.00
Cr_2O_3	.00	.00	.00	.00	.00	.00	.00	.00
Total	96.24	95.28	100.26	97.82	97.53	97.03	96.61	99.59
No. of oxygens	25	25	25	25	25	25	25	25
Si	5.925	5.826	5.908	5.905	5.950	5.960	5.855	5.955
Al (4)	.075	.174	.092	.095	.050	.040	.145	.045
SZ	6.000	6.000	6.000	6.000	6.000	6.000	6.000	6.000
Al (6)	4.648	4.563	4.543	4.246	4.333	4.313	4.338	4.301
Ti	.004	.009	.008	.018	.015	.015	.016	.004
Fe	1.341	1.416	1.504	1.739	1.657	1.650	1.590	1.716
Cr	.000	.000	.000	.000	.000	.000	.000	.000
SY	5.993	5.988	6.055	6.003	6.005	5.978	5.944	6.021
Mn	.030	.030	.032	.029	.024	.030	.020	.020
Mg	.007	.007	.011	.012	.012	.108	.012	.016
Ca	4.009	4.064	3.915	3.992	3.973	3.909	4.060	3.943
Na	.000	.000	.000	.000	.000	.000	.000	.006
K	.000	.000	.000	.000	.000	.000	.000	.000
SX	4.046	4.101	3.958	4.033	4.009	4.047	4.092	3.985

METAMORPHIC EPIDOTES - HAIB BASALTIC ANDESITES

	DRL-42 2	DRL-99 1	DRL-74 1	2	3	4	DRL-123 1	2
SiO_2	37.66	38.41	37.53	36.53	38.34	38.55	38.01	38.46
TiO_2	.10	.07	.05	.08	.10	.10	.17	.44
Al_2O_3	24.27	25.04	26.03	21.86	24.10	24.69	22.89	24.66
Fe_2O_3*	13.86	12.76	11.22	14.59	13.71	12.29	14.15	12.84
MnO	.18	.21	.27	.14	.24	.09	.17	.27
MgO	.07	.00	.00	.02	.00	.16	.04	.00
CaO	23.29	23.41	22.93	20.77	22.68	23.01	23.50	22.80
Na_2O	.03	.06	.01	.00	.00	.03	.13	.06
K_2O	.00	.00	.00	.03	.01	.00	.05	.06
Cr_2O_3	.00	.00	.00	.00	.00	.00	.00	.00
Total	99.46	99.96	98.04	94.02	99.18	98.92	99.11	99.59
No. of oxygens	25	25	25	25	25	25	25	25
Si	5.911	5.967	5.915	6.126	6.071	6.084	6.065	6.048
Al (4)	.089	.033	.085	.000	.000	.000	.000	.000
SZ	6.000	6.000	6.000	6.126	6.071	6.084	6.065	6.048
Al (6)	4.402	4.559	4.751	4.322	4.499	4.594	4.306	4.572
Ti	.012	.008	.057	.010	.012	.012	.020	.052
Fe	1.637	1.492	1.331	1.657	1.470	1.314	1.529	1.367
Cr	.000	.000	.000	.000	.000	.000	.000	.000
SY	6.051	6.059	6.139	5.989	5.981	5.920	5.855	5.991
Mn	.024	.028	.037	.020	.032	.012	.023	.036
Mg	.016	.000	.000	.005	.000	.038	.010	.000
Ca	3.917	3.896	3.872	3.732	3.848	3.891	4.018	3.842
Na	.011	.018	.004	.000	.000	.009	.040	.018
K	.000	.000	.000	.006	.002	.000	.010	.012
SX	3.968	3.942	3.913	3.763	3.882	3.950	4.101	3.908

FELDSPAR (METAMORPHIC AND PRIMARY) - HAIB BASALTIC ANDESITES

	DRL-49						DRL-65			
	1	2	3	4	5	6	1	2	3	4
SiO_2	54.22	64.73	60.73	61.82	59.06	58.47	58.12	61.56	55.64	54.30
TiO_2	.03	.03	.02	.03	.12	.07	.05	.03	.05	.03
Al_2O_3	29.21	22.45	24.82	24.93	24.98	25.91	26.56	24.22	29.27	28.59
FeO*	.39	.97	.30	.22	1.45	.50	.55	.41	.47	.30
MnO	.03	.01	.01	.01	.01	.00	.00	.01	.00	.00
MgO	.17	.28	.08	.22	.60	.13	.09	.11	.09	.13
CaO	11.12	1.62	5.70	5.59	6.65	6.95	8.24	5.19	7.82	11.42
Na_2O	4.94	5.71	7.77	7.94	7.36	6.35	6.90	7.57	4.55	5.30
K_2O	.80	4.47	.68	.21	.76	1.81	.35	.92	2.96	.17
Cr_2O_3	.00	.00	.00	.00	.00	.00	.00	.00	.00	.00
Total	100.91	100.27	100.11	100.97	100.99	100.19	100.86	100.02	100.85	100.24
No. of oxygens	32	32	32	32	32	32	32	32	32	32
Si	9.750	11.472	10.806	10.863	10.538	10.497	10.355	10.944	9.985	9.810
Ti	.004	.004	.003	.004	.016	.009	.007	.004	.007	.004
Al	6.192	4.690	5.207	5.164	5.255	5.485	5.577	5.077	6.191	6.089
Fe	.059	.144	.045	.032	.216	.075	.082	.061	.071	.045
Mn	.005	.002	.002	.001	.002	.000	.000	.002	.000	.000
Mg	.046	.074	.021	.058	.160	.035	.024	.029	.024	.035
Ca	2.143	.308	1.087	1.052	1.271	1.337	1.573	.989	1.504	2.211
Na	1.722	1.962	2.681	2.705	2.546	2.211	2.384	2.610	1.583	1.857
K	.184	1.011	.154	.047	.173	.415	.080	.209	.678	.039
Cr	.000	.000	.000	.000	.000	.000	.000	.000	.000	.000
An	52.93	9.39	27.72	27.66	31.85	33.74	38.96	25.97	39.95	53.83
Ab	42.53	59.80	68.36	71.11	63.81	55.79	59.05	68.54	42.05	45.22
Or	4.54	30.81	3.93	1.24	4.34	10.47	1.98	5.49	18.01	.95

FELDSPAR (METAMORPHIC AND PRIMARY) - HAIB BASALTIC ANDESITES

	DRL-42			DRL-99	DRL-50						DRL-123		DRL-74
	1	2	3	1	1	2	3	4	5	6	1	2	1
SiO_2	56.65	66.05	56.61	67.68	56.88	54.79	63.38	64.87	58.11	53.93	54.53	52.16	60.48
TiO_2	.02	.00	.00	.02	.00	.00	.03	.00	.00	.00	.07	.10	.03
Al_2O_3	28.37	22.20	28.20	21.42	27.98	29.06	25.07	22.81	26.49	31.69	29.09	29.15	25.06
FeO*	.20	.17	.14	.14	.13	.10	.52	.12	.14	1.33	.51	1.29	.24
MnO	.00	.00	.00	.00	.00	.01	.00	.01	.03	.01	.00	.00	.00
MgO	.05	.06	.03	.06	.05	.03	.00	.06	.00	.06	.08	.33	.03
CaO	8.23	1.75	7.97	.68	8.00	9.37	1.12	2.03	8.18	.61	11.15	11.79	6.73
Na_2O	5.86	9.80	6.07	10.97	5.79	5.30	7.89	9.38	7.13	3.59	5.39	5.07	7.71
K_2O	.05	.43	.05	.02	.06	.02	2.82	.94	.06	7.80	.08	.19	.08
Cr_2O_3	.00	.00	.00	.00	.00	.00	.02	.02	.00	.02	.00	.00	.00
Total	99.43	100.46	99.07	100.99	98.89	98.68	100.85	100.24	100.14	99.04	100.90	100.08	100.36
No. of oxygens	32	32	32	32	32	32	32	32	32	32	32	32	32
Si	10.169	11.535	10.194	11.716	10.246	9.945	11.129	11.395	10.393	9.904	9.782	9.523	10.734
Ti	.003	.000	.000	.003	.000	.000	.004	.000	.000	.000	.009	.014	.004
Al	6.004	4.570	5.987	4.371	5.942	6.219	5.189	4.724	5.586	6.861	6.153	6.276	5.244
Fe	.030	.025	.021	.020	.020	.015	.076	.018	.021	.204	.077	.197	.036
Mn	.000	.000	.000	.000	.000	.002	.000	.001	.005	.002	.000	.000	.000
Mg	.013	.016	.008	.015	.013	.008	.000	.016	.000	.016	.021	.090	.008
Ca	1.583	.327	1.538	.126	1.544	1.822	.211	.382	1.568	.120	2.143	2.307	1.280
Na	2.040	3.318	2.119	3.682	2.022	1.865	2.686	3.195	2.473	1.278	1.875	1.795	2.653
K	.011	.096	.011	.004	.014	.005	.632	.211	.014	1.828	.018	.044	.018
Cr	.000	.000	.000	.000	.000	.000	.003	.003	.000	.003	.000	.000	.000
An	43.56	8.74	41.93	3.31	43.13	49.35	5.98	10.08	38.67	3.72	53.10	55.64	32.40
Ab	56.14	88.69	57.77	96.59	56.48	50.51	76.11	84.35	60.99	39.62	46.46	43.29	67.15
Or	.30	2.57	.30	.10	.39	.14	17.91	5.57	.35	56.66	.45	1.06	.46

OLIVINE (SWARTKOP BASIC-ULTRABASIC COMPLEX)

Rock	Peridotite (DRS-20)				Peridotite (DRV-P)		
Grain	1	2	3	4	1	2	3
SiO_2	39.78	39.87	40.11	39.91	38.87	39.69	39.53
TiO_2	.00	.00	.00	.00	.00	.00	.00
Al_2O_3	.00	.00	.00	.00	.00	.00	.00
FeO*	13.74	13.90	13.89	14.15	13.89	14.30	14.33
MnO	.22	.23	.19	.23	.22	.24	.23
MgO	46.47	46.02	46.12	46.16	45.14	45.61	45.13
CaO	.00	.00	.00	.00	.00	.00	.00
Na_2O	.00	.00	.00	.00	.00	.00	.00
K_2O	.00	.00	.00	.00	.00	.00	.00
Cr_2O_3	.00	.00	.00	.00	.00	.00	.00
Total	100.21	100.02	100.31	100.45	98.12	99.84	99.22
No. of oxygens	4	4	4	4	4	4	4
Si	.991	.996	.998	.994	.991	.995	.998
Ti	.000	.000	.000	.000	.000	.000	.000
Al	.000	.000	.000	.000	.000	.000	.000
Fe	.286	.290	.289	.295	.296	.300	.302
Mn	.005	.005	.004	.005	.005	.005	.005
Mg	1.726	1.713	1.711	1.713	1.716	1.705	1.697
Ca	.000	.000	.000	.000	.000	.000	.000
Na	.000	.000	.000	.000	.000	.000	.000
K	.000	.000	.000	.000	.000	.000	.000
Cr	.000	.000	.000	.000	.000	.000	.000
Fo	86.8	85.5	85.6	85.3	85.3	85.0	84.9

OLIVINE (SWARTKOP BASIC-ULTRABASIC COMPLEX)

Rock	(DRV-P)	Serpentine	Troctolite			
Grain	4	1	1	2	3	4
SiO_2	39.69	40.72	38.55	38.44	38.42	38.47
TiO_2	.00	.00	.00	.00	.00	.00
Al_2O_3	.00	.06	.00	.00	.00	.00
FeO*	14.24	4.17	21.22	21.35	21.36	21.33
MnO	.26	.00	.33	.33	.30	.33
MgO	45.43	39.56	39.94	40.30	40.33	40.08
CaO	.00	.03	.00	.00	.00	.00
Na_2O	.00	.00	.00	.00	.00	.00
K_2O	.00	.00	.00	.00	.00	.00
Cr_2O_3	.00	.00	.00	.00	.00	.00
Total	99.62	84.54	100.04	100.42	100.41	100.21
No. of oxygens	4	7	4	4	4	4
Si	.997	1.979	.997	.992	.991	.994
Ti	.000	.000	.000	.000	.000	.000
Al	.000	.004	.000	.000	.000	.000
Fe	.299	.169	.459	.461	.461	.461
Mn	.006	.000	.007	.007	.007	.007
Mg	1.701	2.866	1.540	1.549	1.550	1.544
Ca	.000	.002	.000	.000	.000	.000
Na	.000	.000	.000	.000	.000	.000
K	.000	.000	.000	.000	.000	.000
Cr	.000	.000	.000	.000	.000	.000
Fo	85.1	-	77.0	77.1	77.1	77.0

CHROMITE (SWARTKOP BASIC-ULTRABASIC COMPLEX)

Rock	Peridotite (DRS-20)						Peridotite (DRV-P)	
Grain	1	2	3	4	5	6	1	2
SiO_2	.02	.00	.00	.04	.17	.07	.20	.02
TiO_2	.50	.40	1.13	.39	.75	.55	1.00	.86
Al_2O_3	24.23	23.24	22.28	22.55	23.20	26.51	.17	.17
Cr_2O_3	30.04	28.51	28.17	29.15	30.08	27.66	7.77	7.21
Fe_2O_3	14.71	17.12	16.11	16.41	14.44	13.38	58.82	61.11
FeO	19.69	20.31	22.39	20.91	19.48	22.06	31.01	30.68
MnO	.62	.63	.64	.62	.79	.61	.22	.27
MgO	10.39	9.72	8.56	9.15	10.40	9.12	.73	.93
Total	100.20	99.94	99.27	99.22	99.31	99.96	99.91	101.25
No. of oxygens	32	32	32	32	32	32	32	32
Si	.005	.000	.000	.010	.043	.017	.061	.006
Ti	.094	.076	.218	.075	.142	.103	.229	.194
Al	7.120	6.910	6.738	6.788	6.894	7.792	.061	.060
Cr	5.922	5.687	5.716	5.887	5.997	5.455	1.872	1.714
Fe(3)	2.760	3.251	3.110	3.154	2.739	2.512	13.486	13.825
SY	15.901	15.924	15.784	15.914	15.815	15.879	15.709	15.799
Fe(2)	4.106	4.285	4.804	4.467	4.107	4.601	7.902	7.715
Mn	.131	.135	.139	.134	.169	.129	.057	.069
Mg	3.862	3.656	3.275	3.484	3.909	3.391	.332	.417
SX	8.099	8.076	8.218	8.085	8.185	8.121	8.291	8.201

ORTHOPYROXENE (SWARTKOP BASIC-ULTRABASIC COMPLEX)

Rock	Peridotite (DRS-20)		
Grain	1	2	3
SiO_2	54.68	55.12	55.30
TiO_2	0.18	0.20	0.25
Al_2O_3	2.93	3.11	2.99
FeO*	9.28	9.55	9.46
MnO	0.21	0.27	.22
MgO	30.95	31.08	31.00
CaO	1.50	1.05	1.08
Na_2O	0.05	0.03	.00
K_2O	0.00	0.00	0.00
Cr_2O_3	0.00	0.00	0.00
Total	99.78	100.41	100.30
No. of oxygens	6	6	6
Si	1.924	1.926	1.932
Al (4)	.076	.074	.068
SZ	2.000	2.000	2.000
Al (6)	.046	.054	.055
Ti	.005	.005	.007
Fe	.273	.279	.276
Mn	.006	.008	.007
Mg	1.623	1.618	1.614
Ca	.057	.039	.040
Na	.003	.002	.000
K	.000	.000	.000
Cr	.000	.000	.000
SY	2.013	2.005	1.999
Wo	2.9	2.0	2.1
En	83.1	83.6	83.6
Fs	14.0	14.4	14.3

CLINOPYROXENE (SWARTKOP BASIC-ULTRABASIC COMPLEX)

Rock	Peridotite (DRS-20)				Pyroxenite (DRV-23)		
Grain	1	2	3	4	1	2	3
SiO_2	49.41	51.27	49.49	49.81	52.19	53.32	53.07
TiO_2	.50	.84	.46	.46	.21	.09	.07
Al_2O_3	4.20	4.69	4.81	4.71	1.97	1.36	1.06
FeO*	4.61	4.46	4.81	5.19	4.49	5.07	4.86
MnO	.16	.13	.14	.13	.20	.22	.22
MgO	18.82	16.40	16.38	16.83	15.63	15.96	15.88
CaO	21.47	21.86	22.30	22.11	24.98	23.84	24.95
Na_2O	.50	.64	.64	.65	.22	.20	.25
K_2O	.00	.00	.00	.00	.01	.00	.00
Cr_2O_3	1.00	1.09	1.17	.94	.34	.35	.37
Total	99.67	100.58	100.20	100.83	100.24	100.41	100.73
No. of oxygens	6	6	6	6	6	6	6
Si	1.811	1.856	1.825	1.827	1.927	1.956	1.948
Al (4)	0.181	0.144	.175	.173	.073	.044	.046
SZ	1.992	2.000	2.000	2.000	2.000	2.000	1.994
Al (6)	-	.056	.034	.031	.013	.015	-
Ti	.014	.023	.013	.013	.001	.002	.002
Fe	.141	.135	.148	.159	.139	.156	.149
Mn	.005	.004	.004	.004	.006	.007	.007
Mg	1.028	.885	.901	.920	.860	.873	.869
Ca	.843	.848	.881	.869	.988	.937	.981
Na	.036	.045	.046	.043	.016	.014	.018
K	.000	.000	.000	.000	.000	.000	.000
Cr	.029	.031	.034	.027	.010	.010	.011
SY	2.096	2.027	2.061	2.066	2.033	2.014	2.037
Wo	41.9	45.4	45.6	44.6	49.7	47.7	49.1
En	51.1	47.4	46.7	47.2	43.3	44.4	43.5
Fs	7.0	7.2	7.7	8.2	7.0	7.9	7.5

CLINOPYROXENE (SWARTKOP BASIC-ULTRABASIC COMPLEX)

Rock	Pyroxenite (DRV-23)			Troctolite (DRS-18)					
Grain	4	5	6	1	2	3	4	5	6
SiO_2	52.10	52.29	52.29	50.19	50.12	51.41	51.28	51.06	50.86
TiO_2	.22	.21	.24	0.75	.73	.19	.49	.58	.56
Al_2O_3	2.07	2.07	2.09	4.77	5.00	3.30	4.05	4.10	4.16
FeO*	5.04	4.80	4.86	6.79	6.78	7.92	7.44	5.14	6.43
MnO	.22	.21	.21	.17	.19	.25	.22	.13	.21
MgO	15.82	15.67	15.79	13.80	14.92	16.87	16.53	15.02	14.14
CaO	24.39	24.43	24.11	23.07	21.85	19.98	19.42	23.65	23.13
Na2O	.26	.30	.21	.36	.34	.40	.33	.24	.45
K_2O				.00	.00	.00	.00	.00	.00
Cr_2O_3	.26	.34	.16	n.d.	n.d.	n.d.	n.d.	n.d.	n.d.
Total	100.38	100.32	100.96	99.90	99.93	100.32	99.76	99.92	99.96
No. of oxygens	6	6	6	6	6	6	6	6	6
Si	1.919	1.925	1.942	1.866	1.856	1.910	1.892	1.884	1.886
Al (4)	.081	.075	.058	0.134	.144	.090	.108	.116	.114
SZ	2.000	2.000	2.000	2.000	2.000	2.000	2.000	2.000	2.000
Al (6)	.009	.015	.032	.075	.074	.044	.040	.060	.068
Ti	.006	.006	.007	.021	.020	.005	.014	.016	.016
Fe	.155	.148	.148	.211	.210	.246	.230	.159	.199
Mn	.007	.007	.006	.005	.006	.008	.007	.004	.007
Mg	.869	.860	.858	.765	.824	.933	.959	.909	.782
Ca	.963	.964	.941	.919	.867	.795	.768	.935	.919
Na	.091	.021	.015	.026	.024	.022	.024	.017	.032
K	.000	.000	.000	.000	.000	.000	.000	.000	.000
Cr	.008	.010	.005	n.d.	n.d.	n.d.	n.d.	n.d.	n.d.
SY	2.036	2.031	2.012	2.022	2.025	2.053	2.042	2.100	2.023
Wo	48.5	48.9	48.3	48.5	45.6	40.3	39.2	46.7	48.4
En	48.5	43.6	44.1	40.4	43.3	47.3	49.0	45.4	41.2
Fs	7.8	7.5	7.6	11.1	11.1	12.4	11.8	7.9	10.4

PRIMARY AMPHIBOLE (SWARTKOP BASIC-ULTRABASIC COMPLEX)

Specimen	Peridotite			Troctolite		
Grain	1	2	3	1	2	3
SiO_2	41.97	41.75	42.12	41.63	41.94	41.49
TiO_2	3.92	4.36	3.61	2.19	1.66	1.58
Al_2O_3	13.51	13.51	13.22	13.98	14.71	15.60
FeO*	6.82	6.77	7.00	11.92	8.94	8.52
MnO	.09	.10	.09	.10	.08	.10
MgO	16.34	16.17	17.01	12.43	15.08	14.79
CaO	12.10	12.29	12.10	12.17	12.00	12.14
Na_2O	2.71	2.81	2.40	1.53	1.84	1.79
K_2O	1.18	1.11	1.11	1.12	.94	1.05
Cr_2O_3	n.d	n.d	n.d	n.d	n.d	n.d
Total	98.64	98.87	98.66	97.07	97.19	97.06
No. of oxygens	23	23	23	23	23	23
Si	6.026	5.987	6.042	6.174	6.119	6.055
Al (4)	1.974	2.013	1.958	1.826	1.881	1.945
SZ	8.000	8.000	8.000	2.000	2.000	2.000
Al (6)	.312	.270	.278	.618	.649	.739
Ti	.424	.470	.390	.244	.182	.173
Fe	.819	.812	.840	1.478	1.091	1.040
Mn	.011	.012	.011	.013	.010	.012
Mg	3.496	3.455	3.637	2.747	3.279	3.217
Cr	n.d	n.d	n.d	n.d	n.d	n.d
SY	5.062	5.019	5.156	5.100	5.211	5.181
Ca	1.862	1.889	1.860	1.934	1.876	1.898
Na	.754	.781	.667	.440	.521	.507
K	.216	.203	.203	.212	.175	.195
SZ	2.832	2.873	2.730	2.586	2.572	2.600

PRIMARY AMPHIBOLE (BASIC-ULTRABASIC COMPLEXES)

Specimen	Troctolite	Pyroxenite				
Grain	4	1	2	3	4	5
SiO_2	41.57	43.20	44.36	43.32	42.99	43.33
TiO_2	1.96	.92	.49	.82	.39	.67
Al_2O_3	14.86	12.27	11.03	12.27	11.92	11.59
FeO*	9.59	11.15	10.91	11.37	11.55	12.24
MnO	.10	.15	.15	.17	.21	.18
MgO	13.95	14.53	15.29	14.63	14.90	14.24
Cao	12.13	12.94	12.88	12.90	12.82	12.99
Na_2O	1.71	1.81	1.53	1.65	1.61	1.69
K_2O	1.15	.74	.83	.71	.92	.71
Cr_2O_3	n.d	.05	.16	.05	.11	.02
Total	97.02	97.76	97.63	97.89	97.42	97.66
No. of oxygens	23	23	23	23	23	23
Si	6.103	6.341	6.506	6.350	6.355	6.397
Al (4)	1.897	1.659	1.494	1.650	1.645	1.603
SZ	2.000	8.000	8.000	8.000	8.000	8.000
Al (6)	.675	.465	.413	.471	.432	.414
Ti	.216	.101	.054	.091	.044	.075
Fe	1.178	1.368	1.338	1.394	1.429	1.512
Mn	.012	.019	.019	.021	.027	.022
Mg	3.052	3.179	3.342	3.196	3.283	3.133
Cr	n.d	.006	.019	.006	.013	.003
SY	5.133	5.138	5.185	5.179	5.228	5.159
Ca	1.908	2.034	2.025	2.026	2.031	2.055
Na	.487	.515	.435	.469	.462	.434
K	.215	.139	.155	.132	.174	.133
SZ	2.610	2.688	2.615	2.627	2.667	2.672

ORTHOPYROXENE (DIORITE DRV-08)

Specimen								
Grain	1	2	3	4	5	6	7	8
SiO_2	53.44	52.43	51.82	52.32	50.68	51.40	51.88	51.47
TiO_2	.06	.06	.10	.13	.11	.08	.24	.16
Al_2O_3	1.02	1.32	1.34	1.52	1.64	1.20	1.77	1.59
FeO*	21.71	21.77	22.50	22.19	22.33	22.86	22.34	21.73
MnO	.70	.67	.72	.68	.79	.73	.71	.69
MgO	23.20	22.94	23.17	23.15	22.87	22.97	22.89	22.83
Cao	.33	.37	.35	.98	.47	.43	1.09	1.22
Na_2O	.00	.00	.00	.00	.00	.00	.00	.00
K_2O	.00	.00	.00	.00	.00	.00	.00	.00
Cr_2O_3	.00	.00	.09	.11	.09	.03	.05	.08
Total	100.46	99.56	101.09	101.08	98.98	99.70	100.97	99.77
No. of oxygens	6	6	6	6	6	6	6	6
Si	1.974	1.958	1.936	1.934	1.919	1.933	1.923	1.928
Al (4)	.026	.042	.059	.066	.073	.053	.077	.070
SZ	2.000	2.000	1.995	2.000	1.992	1.986	2.000	1.998
Al (6)	.018	.016	-	-	-	-	-	-
Ti	.002	.002	.003	.004	.003	.002	.007	.005
Fe	.671	.680	.703	.686	.707	.719	.693	.681
Mn	.022	.021	.023	.021	.025	.023	.022	.022
Mg	1.277	1.277	1.290	1.275	1.291	1.288	1.264	1.275
Cr	.000	.000	.003	.003	.003	.001	.001	.002
Ca	.013	.015	.014	.039	.019	.017	.043	.049
Na	.000	.000	.000	.000	.000	.000	.000	.000
K	.000	.000	.000	.000	.000	.000	.000	.000
SX	2.003	2.011	2.031	2.028	2.040	2.036	2.030	2.032
Wo	.66	.76	.70	1.95	.94	.84	2.15	2.44
En	65.12	64.76	64.28	63.75	64.01	63.64	63.20	63.59
Fs	34.22	34.48	35.03	34.30	35.05	35.52	34.65	33.97

HORNBLENDE (DIORITE - DRV-08)

Specimen Grain	1	2	3	4	5	6	7
SiO_2	47.98	46.63	45.11	47.20	50.10	47.89	47.83
TiO_2	.97	1.23	1.60	.89	.99	1.45	1.50
Al_2O_3	7.51	8.67	9.59	8.54	7.43	8.37	8.88
FeO*	12.07	12.39	13.39	12.35	12.48	13.23	12.65
MnO	.22	.22	.21	.20	.26	.23	.23
MgO	15.47	14.65	13.91	15.05	16.10	15.28	14.85
CaO	11.48	11.42	11.42	11.74	11.53	11.31	11.95
Na_2O	.82	.96	.94	.78	.71	.94	1.10
K_2O	.45	.50	.72	.38	.33	.69	.77
Total	96.97	96.67	96.89	97.13	99.93	99.39	99.76
No. of oxygens	23	23	23	23	23	23	23
Si	7.010	6.861	6.688	6.907	7.081	6.873	6.838
Al	.990	1.139	1.312	1.093	.919	1.127	1.162
SZ	8.000	8.000	8.000	8.000	8.000	8.000	8.000
Al	.304	.365	.364	.380	.319	.289	.335
Ti	.107	.136	.178	.098	.105	.157	.161
Fe	1.475	1.525	1.660	1.511	1.475	1.588	1.512
Mn	.027	.027	.000	.000	.031	.028	.028
Mg	3.369	3.213	3.074	3.282	3.391	3.268	3.164
SY	5.282	5.266	5.276	5.271	5.321	5.330	5.200
Ca	1.797	1.801	1.814	1.841	1.746	1.739	1.830
Na	.232	.274	.270	.221	.195	.262	.305
K	.084	.094	.136	.071	.060	.126	.140
SX	2.113	2.169	2.220	2.133	2.001	2.127	2.275

HORNBLENDE (DIORITE - DRV-08)

Specimen Grain	8	9	10	11	12	13	14
SiO_2	49.43	47.56	49.71	47.97	46.63	49.40	45.08
TiO_2	.99	1.55	.80	.85	1.07	.87	1.08
Al_2O_3	7.85	9.07	7.83	7.73	8.91	7.94	9.94
FeO*	12.03	12.83	11.68	12.00	12.31	11.90	12.96
MnO	.22	.23	.23	.22	.22	.25	.27
MgO	15.80	14.94	16.62	15.98	15.14	16.07	14.44
CaO	12.07	12.00	11.59	11.52	11.45	12.30	11.60
Na_2O	.74	1.08	.70	.81	.95	.88	1.01
K_2O	.51	.80	.32	.45	.50	.30	.51
Total	99.64	100.06	99.48	97.53	97.18	99.91	96.89
No. of oxygens	23	23	23	23	23	23	23
Si	7.018	6.790	7.036	6.968	6.823	6.993	6.660
Al	.982	1.210	.964	1.032	1.177	1.007	1.340
SZ	8.000	8.000	8.000	8.000	8.000	8.000	8.000
Al	.332	.317	.343	.292	.360	.318	.391
Ti	.106	.166	.085	.093	.118	.093	.120
Fe	1.428	1.532	1.383	1.458	1.506	1.409	1.601
Mn	.026	.028	.028	.027	.027	.030	.034
Mg	3.343	3.179	3.506	3.459	3.302	3.390	3.179
SY	5.235	5.222	5.345	5.329	5.313	5.240	5.325
Ca	1.836	1.836	1.758	1.793	1.795	1.866	1.836
Na	.204	.299	.192	.228	.270	.242	.289
K	.092	.146	.058	.083	.093	.054	.096
SX	2.132	2.281	2.008	2.104	2.158	2.162	2.221

BIOTITE (DIORITE - DRV-08)

Specimen Grain	1	2	3	4	5	6	7	8	9	10	11
SiO_2	37.48	37.66	37.68	37.54	39.19	38.98	38.63	38.93	39.11	39.24	38.68
TiO_2	2.65	2.17	2.53	3.08	2.60	3.16	2.84	2.86	3.11	2.42	3.17
Al_2O_3	16.24	16.29	16.30	16.32	16.96	16.91	16.51	16.78	16.69	17.14	16.65
FeO*	13.41	13.54	13.87	13.82	14.31	14.41	14.89	14.05	13.75	13.98	14.45
MnO	.06	.05	.04	.08	.08	.06	.05	.05	.05	.06	.05
MgO	16.65	16.82	16.78	16.87	17.40	16.97	17.06	17.19	17.13	17.24	16.93
CaO	.00	.00	.00	.00	.01	.03	.03	.00	.03	.00	.00
Na_2O	.19	.20	.20	.16	.23	.20	.22	.20	.24	.28	.22
K_2O	9.23	9.24	9.64	9.81	9.30	9.18	9.09	9.26	9.03	8.99	9.06
Total	95.91	95.97	97.04	97.68	100.08	99.90	99.32	99.32	99.14	99.35	99.21
No. of oxygens	.22	.22	.22	.22	.22	.22	.22	.22	.22	.22	.22
Si	5.504	5.527	5.492	5.445	5.512	5.494	5.494	5.513	5.533	5.538	5.493
Al (4)	2.496	2.473	2.508	2.555	2.488	2.506	2.506	2.487	2.467	2.462	2.507
SZ	8.000	8.000	8.000	8.000	8.000	8.000	8.000	8.000	8.000	8.000	8.000
Al (6)	.315	.345	.293	.236	.324	.304	.262	.315	.317	.390	.280
Ti	.293	.239	.277	.336	.275	.335	.304	.305	.331	.257	.339
Fe	1.647	1.662	1.691	1.676	1.683	1.699	1.771	1.664	1.627	1.650	1.716
Mn	.007	.006	.000	.000	.010	.007	.006	.006	.006	.007	.006
Ma	3.644	3.679	3.645	3.646	3.647	3.565	3.616	3.628	3.612	3.626	3.583
SY	5.906	5.931	5.906	5.894	5.939	5.910	5.959	5.918	5.893	5.930	5.924
Ca	.000	.000	.000	.000	.002	.005	.005	.000	.005	.000	.000
Na	.054	.057	.057	.045	.063	.055	.061	.055	.066	.077	.061
K	1.729	1.730	1.793	1.815	1.669	1.651	1.649	1.673	1.630	1.619	1.641
SX	1.783	1.787	1.850	1.860	1.734	1.711	1.715	1.728	1.701	1.696	1.702

PLAGIOCLASE (DIORITE - DRV-08)

Specimen Grain	1	2	3	4	5	6
SiO_2	47.89	54.04	48.24	53.60	48.21	53.59
TiO_2	.00	.00	.00	.00	.00	.00
Al_2O_3	31.54	28.09	31.78	28.70	31.96	29.15
FeO*	.16	.18	.14	.09	.16	.17
MnO	.00	.00	.00	.00	.00	.00
MgO	.00	.00	.00	.00	.00	.00
CaO	14.83	10.15	14.97	10.81	14.65	10.98
Na_2O	3.12	5.92	3.40	5.37	3.05	5.15
K_2O	.02	.05	.04	.07	.04	.06
Total	97.56	98.43	98.57	98.64	98.07	99.10
No. of oxygens	16	16	16	16	16	16
Si	4.491	4.953	4.483	4.904	4.491	4.881
Ti	.000	.000	.000	.000	.000	.000
Al	3.487	3.036	3.482	3.096	3.510	3.130
Fe	.013	.014	.011	.007	.012	.013
Mn	.000	.000	.000	.000	.000	.000
Mg	.000	.000	.000	.000	.000	.000
Ca	1.490	.997	1.491	1.060	1.462	1.072
Na	.567	1.052	.613	.953	.551	.910
K	.002	.006	.005	.008	.005	.007
An	72.37	48.52	70.70	52.45	72.45	53.90
Ab	27.54	51.19	29.07	47.15	27.30	45.75
Or	.10	.29	.24	.40	.25	.35

PLAGIOCLASE (DIORITE - DRV-08)

Specimen Grain	7	8	9	10	11	12
SiO_2	52.10	49.63	53.86	48.14	54.12	54.58
TiO_2	.00	.00	.00	.00	.00	.00
Al_2O_3	29.60	31.12	29.26	32.21	28.96	28.13
FeO*	.12	.14	.27	.12	.13	.13
MnO	.00	.00	.00	.00	.00	.00
MgO	.00	.00	.00	.00	.00	.00
CaO	11.82	13.78	10.85	14.87	10.55	9.80
Na_2O	4.66	3.63	5.37	2.97	5.55	5.97
K_2O	.06	.04	.05	.04	.07	.07
Total	98.36	98.34	99.66	98.35	99.38	98.68
No. of oxygens	16	16	16	16	16	16
Si	4.794	4.598	4.881	4.473	4.912	4.980
Ti	.000	.000	.000	.000	.000	.000
Al	3.211	3.399	3.126	3.529	3.099	3.026
Fe	.009	.011	.020	.009	.010	.010
Mn	.000	.000	.000	.000	.000	.000
Mg	.000	.000	.000	.000	.000	.000
Ca	1.166	1.368	1.054	1.481	1.026	.958
Na	.832	.652	.944	.535	.977	1.056
K	.007	.005	.006	.005	.008	.008
An	58.15	67.56	52.59	73.28	51.02	47.38
Ab	41.50	32.20	47.11	26.47	48.58	52.23
Or	.35	.25	.30	.25	.40	.40

FE-TI OXIDE (DIORITE - DRV-08)

Specimen Grain	MAGNETITE 1	2	ILMENITE 1	2
SiO_2	.02	.04	.00	.34
TiO_2	.11	.00	51.47	48.46
Al_2O_3	.12	.12	.06	.28
Fe_2O_3	68.34	68.49	2.82	7.12
FeO	30.91	30.85	42.09	39.78
MnO	.04	.03	3.95	3.51
MgO	.07	.05	.11	.17
CaO	.00	.02	.00	.27
Total	99.61	99.59	100.50	99.93
No. of oxygens	4	4	3	3
Si	.001	.002	.000	.009
Ti	.003	.000	.972	.920
Al	.005	.005	.002	.008
Fe^{3*}	1.987	1.991	.053	.135
Fe^{2*}	.999	.997	.884	.839
Mn	.001	.001	.084	.075
Mg	.004	.003	.004	.006
Ca	.000	.001	.000	.007

TONALITE (DRV-13B)

Mineral	Hornblende			Biotite			Plagioclase		
Grain	1	2	Av	1	2	Av	1	2	3
SiO_2	48.01	48.66	48.34	37.66	36.91	37.29	55.44	56.68	60.29
TiO_2	.72	.69	.71	1.90	1.86	1.88	.01	.00	.00
Al_2O_3	8.00	8.13	8.07	16.29	16.33	16.31	28.34	27.51	25.11
FeO*	12.76	12.43	12.60	14.88	14.55	14.72	.11	.15	.12
MnO	.20	.19	.20	.30	.31	.31	.00	.00	.00
MgO	15.01	14.62	14.82	14.88	15.98	15.43	.06	.09	.10
CaO	11.89	12.01	11.95	.00	.00	.00	10.48	9.47	6.65
Na_2O	.80	.66	.73	.11	.15	.13	5.63	6.13	7.84
K_2O	.49	.40	.45	9.80	9.91	9.82	.07	.19	.12
Total	97.88	97.79	97.87	95.81	96.00	95.88	100.14	100.22	100.23
No. of oxygens	23	23	23	22	22	22	32	32	32
Si	6.976	7.046	7.009	5.590	5.479	5.536	Si 9.971	10.162	10.716
Al (4)	1.024	.954	.991	2.410	2.521	2.464	Al 6.009	5.815	5.261
SZ	8.000	8.000	8.000	8.000	8.000	8.000	Ti .001	.000	.000
Al (6)	.347	.435	.389	.441	.337	.390	Fe .016	.023	.018
Ti	.079	.075	.078	.212	.208	.210	Mn .000	.000	.000
Fe	1.551	1.505	1.528	1.847	1.806	1.828	Mg .016	.024	.027
Mn	.024	.023	.024	.037	.039	.037	Ca 2.020	1.820	1.267
Mg	3.250	3.155	3.203	3.291	3.535	3.414	Na 1.963	2.131	2.702
SY	5.251	5.193	5.222	5.828	5.925	5.879	K .015	.043	.028
Ca	1.851	1.864	1.857	.000	.000	.000	An 50.5	45.6	31.7
Na	.225	.184	.206	.032	.043	.037	Ab 49.1	53.4	67.6
K	.091	.073	.084	1.855	1.877	1.859	Or 0.4	1.0	0.7
SX	2.167	2.121	2.147	1.887	1.920	1.896			

GRANODIORITE (DRV-15E)

Mineral	Biotite						
Grain	1	2	3	4	5	6	7
SiO_2	36.72	37.52	36.97	36.93	37.01	37.04	37.58
TiO_2	1.66	1.53	1.52	1.46	1.61	1.51	1.36
Al_2O_3	16.12	16.34	16.17	16.06	16.13	16.18	16.12
FeO*	17.69	17.96	18.09	18.36	17.96	17.54	17.30
MnO	.29	.28	.28	.31	.31	.32	.28
MgO	12.56	13.06	12.75	12.66	12.74	12.77	13.06
CaO	.00	.00	.00	.00	.00	.00	.00
Na_2O	.14	.14	.14	.08	.13	.13	.10
K_2O	9.52	9.64	9.79	9.69	9.67	9.64	9.45
Total	94.70	96.51	95.71	95.55	95.59	96.03	95.25
No. of oxygens	22	22	22	22	22	22	22
Si	5.594	5.604	5.587	5.595	5.594	5.678	5.663
Al (4)	2.406	2.396	2.413	2.405	2.406	2.322	2.337
SZ	8.000	8.000	8.000	8.000	8.000	8.000	8.000
Al (6)	.489	.481	.468	.464	.468	.532	.526
Ti	.190	.172	.173	.166	.183	.170	.154
Fe	2.254	2.244	2.286	2.327	2.270	2.195	2.180
Mn	.037	.035	.036	.040	.040	.041	.035
Mg	2.852	2.907	2.872	2.859	2.870	2.848	2.933
SY	5.822	5.839	5.835	5.856	5.831	5.786	5.828
Ca	.000	.000	.000	.000	.000	.000	.000
Na	.041	.041	.041	.024	.038	.038	.029
K	1.850	1.837	1.888	1.873	1.865	1.840	1.816
SX	1.891	1.878	1.929	1.897	1.903	1.878	1.845

GRANODIORITE (DRV-15E)

Mineral	Plagioclase			K-Feldspar		Na-Feldspar
Grain	1	2	3	1	2	1
SiO_2	59.17	58.23	59.55	64.16	63.33	68.57
TiO_2	.03	.03	.00	.00	.00	.00
Al_2O_3	26.38	26.40	26.11	19.25	19.44	20.59
FeO*	.30	.30	.20	.12	.12	.12
MnO	.00	.00	.00	.00	.00	.00
MgO	.06	.05	.03	.03	.02	.02
CaO	7.53	8.10	6.96	.00	.00	.27
Na_2O	7.22	6.73	7.26	.42	.56	10.46
K_2O	.12	.13	.22	16.18	16.09	.42
Total	100.45	100.97	100.33	100.16	99.48	100.33
No. of oxygens	32	32	32	32	32	32
Si	10.509	10.483	10.580	11.852	11.787	11.900
Al	5.523	5.509	5.469	4.192	4.266	4.213
Ti	.004	.004	.000	.000	.000	.000
Fe	.043	.044	.030	.019	.019	.020
Mn	.000	.000	.000	.000	.000	.000
Mg	.012	.010	.008	.008	.005	.004
Ca	1.433	1.536	1.325	.000	.000	.050
Na	2.486	2.310	2.501	.150	.202	3.415
K	.027	.029	.050	3.813	3.821	.090
An	36.3	39.6	34.2	0	0	1.4
Ab	63.0	59.6	64.5	3.7	5.0	96.1
Or	0.7	0.8	1.3	96.3	95.0	1.4

ADAMELLITE (DRV-01)

Mineral	Biotite				Plagioclase			
Grain	1	2	3	4	1	2	3	4
SiO_2	37.30	37.37	36.97	37.10	58.23	59.55	60.16	57.68
TiO_2	1.57	1.52	1.62	1.48	.03	.00	.00	.00
Al_2O_3	16.05	15.65	15.98	15.68	27.40	26.11	25.68	26.56
FeO*	19.15	19.42	19.81	20.06	.30	.20	.05	.27
MnO	.36	.34	.35	.37	.00	.00	.00	.00
MgO	12.65	12.12	12.01	11.85	.05	.03	.00	.06
CaO	.00	.01	.03	.00	8.10	6.96	6.75	8.38
Na_2O	.06	.06	.09	.03	6.73	7.27	8.12	7.28
K_2O	9.21	9.38	9.27	9.40	.13	.22	.10	.11
Total	96.35	95.87	96.13	95.97	100.97	100.33	100.86	100.34
No. of oxygens	22	22	22	22	32	32	32	32
Si	5.603	5.656	5.593	5.632	10.319	10.580	10.639	10.326
Al (4)	2.397	2.344	2.407	2.368	5.725	5.469	5.354	5.606
SZ	8.000	8.000	8.000	8.000	.004	.000	.000	.000
Al (6)	.445	.449	.443	.438	.045	.030	.007	.040
Ti	.177	.173	.184	.169	.000	.000	.000	.000
Fe	2.406	2.458	2.506	2.547	.013	.008	.000	.016
Mn	.046	.044	.045	.048	1.538	1.325	1.279	1.607
Mg	2.832	2.734	2.708	2.681	2.313	2.501	2.784	2.527
SY	5.906	5.858	5.886	5.883	.030	.050	.023	.025
Ca	.000	.002	.005	.000	39.6	34.2	31.3	38.6
Na	.017	.018	.026	.009	59.6	64.5	68.1	60.8
K	1.765	1.811	1.789	1.820	0.8	1.3	0.6	0.6
SX	1.782	1.831	1.820	1.829				

ADAMELLITE (DRV-01)

Mineral	K-Feldspar		Na-Feldspar			Sphene	
Grain	1	2	1	2	3	1	2
SiO_2	63.91	63.95	67.22	67.06	67.20	29.53	29.47
TiO_2	.00	.00	.00	.00	.00	38.93	39.50
Al_2O_3	18.66	18.62	19.39	20.25	20.61	1.48	1.52
FeO*	.05	.04	.03	.03	.00	1.73	1.79
MnO	.00	.00	.00	.00	.00	.17	.13
MgO	.00	.00	.00	.00	.00	.03	.05
CaO	.00	.25	.20	.21	.24	27.68	27.30
Na_2O	.51	.50	9.78	12.27	12.25	.00	.00
K_2O	16.35	16.50	3.20	.27	.12	.00	.00
Total	99.48	99.78	99.82	100.09	100.42	99.55	99.76
No. of oxygens	32	32	32	32	32	20	20
Si	11.906	11.891	11.918	11.775	11.747	3.898	3.878
Al	4.097	4.083	4.053	4.191	4.248	.230	.236
Ti	.000	.000	.000	.000	.000	3.864	3.910
Fe	.008	.007	.004	.004	.000	.191	.197
Mn	.000	.000	.000	.000	.000	.019	.014
Mg	.000	.000	.000	.000	.000	.005	.009
Ca	.000	.050	.038	.039	.044	3.915	3.850
Na	.185	.181	3.362	4.132	4.107	.000	.000
K	3.662	3.894	.724	.061	.026	.000	.000
An	0	1.2	0.9	0.9	1.0		
Ab	4.5	4.4	81.5	97.7	98.3		
Or	95.5	94.4	17.6	1.4	0.7		

LEUCOGRANITE (DRV-128)

Mineral	Biotite			Plagioclase	Na-Feldspar	K-Feldspar
Grain	1	2	3			
SiO_2	37.13	37.37	37.41	63.68	66.62	63.95
TiO_2	.46	.44	.50	.00	.00	.00
Al_2O_3	16.10	16.59	16.02	22.83	20.48	18.61
FeO*	24.34	22.17	22.29	.05	.04	.01
MnO	.33	.20	.31	.00	.00	.00
MgO	9.70	8.53	8.60	.03	.00	.00
CaO	.04	.04	.02	3.43	.58	.00
Na_2O	.17	.13	.10	10.53	11.77	.50
K_2O	9.68	9.91	9.88	.07	.09	16.18
Total	97.95	95.38	95.23	100.62	99.58	99.25
No. of oxygens	22	22	22	32	32	32
Si	5.637	5.763	5.794	Si 11.212	11.740	11.923
Al (4)	2.363	2.237	2.206	Al 4.739	4.255	4.092
SZ	8.000	8.000	8.000	Ti .000	.000	.000
				Fe .007	.006	.001
Al (6)	.518	.779	.720	Mn .000	.000	.000
Ti	.053	.051	.059	Mg .008	.000	.000
Fe	3.091	2.860	2.887	Ca .647	.110	.000
Mn	.043	.026	.041	Na 3.595	4.022	.182
Mg	2.195	1.961	1.985	K .016	.020	3.850
SY	5.900	5.677	5.692			
Ca	.006	.006	.004	An 15.2	2.7	0
Na	.049	.039	.030	Ab 84.4	96.9	4.5
K	1.876	1.950	1.952	Or 0.4	0.4	95.5
SX	1.931	1.995	1.986			

Appendix 3

MAJOR AND TRACE ELEMENT ANALYSES

A3.1 Major elements

All major elements (with the exception of Na) were analysed by X-ray fluorescence spectrometry (XRF), using the lithium tetraborate fusion method of Norrish and Hutton (1969). Na was analysed by XRF on pressed powder briquettes, prepared using the method of Baird (1961). The operating conditions used are routine procedures adopted in the Department of Geochemistry for the analysis of terrestrial, lunar and meteoritic samples (Willis et al., 1971, 1972).

Estimates of the precision and detection limit for each major oxide are given in Table A3.1. Natural rock standards were used for calibration, and included the USGS standard set and four local standards originally calibrated against the USGS set. The operating conditions for each major element analytical run was adjusted so that the scatter about the standard calibration curves was within the precision limits given in Table A3.1.

A3.2 Trace elements

With the exception of U, all trace elements were analysed by XRF, using pressed powder briquettes. Routine operating conditions similar to those outlined in Willis et al., (1971, 1972) and Cherry et al., (1970) were used. Estimates of the uncertainties due to counting statistics are given in Table A3.2. Natural rock standards were used, including the USGS standard set and local standards originally calibrated against the USGS set. The operating conditions for each analytical run was adjusted until the scatter about the standard calibration curves was within that predicted by counting statistics given in Table A3.2. The quality of the Rb, Sr, Th and Pb abundance data have an important bearing on the geochronological study and have been discussed further in Appendix 5.

U was analysed at the A.E.B., Pelindaba, by Delayed Neutron Activation. About 200 mg of sample powder was accurately weighed out (in duplicate) into small (2 cm long) polyethylene ampoules. Each ampoule was loaded into a larger polyethylene container ("rabbit") and irradiated. One aliquot of each

Table A3.1 Estimated precision and detection limits for the major oxides. Precision is expressed as a percentage of the average concentration. Detection limits expressed as weight percent of oxide.

Na on a pressed powder briquette; all other major elements on Norrish fusion discs.

OXIDE	AVERAGE	PRECISION	DETECTION LIMIT
Fe_2O_3	5	0.3	.04
MnO	0.20	2.5	.006
TiO_2	0.5	0.4	.004
CaO	5.0	0.3	.01
K_2O	2.5	0.8	.002
SiO_2	55	0.5	.05
Al_2O_3	15	0.5	.03
MgO	4.0	1.0	.05
Na_2O	3.0	1.3	.08

duplicate pair was covered with a Cd shield during irradiation, in order to provide data for a Th correction (Gale, 1967). Standard calibration was achieved by running specially prepared aqueous solutions containg a known amount of U. The delayed neutron flux is so penetrative that there is very little matrix contrast between solutions and geological materials. The precision of this technique, for a single analysis, is 10-15 percent relative, at the 1-10 ppm abundance level. Further information about the technique is documented in an unpublished internal A.E.B. report, by M.C.B. Smit, Chemistry Division, Pelindaba. The quality of the U abundance data is further discussed in Appendix 5.

A3.3 Notes on the tables

The analysed samples have been grouped according to rock type and the following abbreviations have been used:

BA = Basaltic andesite D = Dacite P R = Porphyritic rhyolite

A = Andesite NR = Non-porphyritic rhyolite

Table A3.2 Counting errors and detection limits for trace elements analysed by XRF. All data in ppm.

SD(100) = 2 σ error (95 percent cofidence) at 100 ppm
SD(10) = 2 σ error at 10 ppm
DL = Detection limit at 99 percent confidence
G = Granitic matrix
B = Basaltic matrix

ELEMENT		SD(100)	SD(10)	DL
Ba	G	2.0	2.0	3
	B	6.2	4.0	7
Rb	G	0.6	0.4	0.8
	B	0.6	0.5	1.0
Zr	G	1.0	0.9	2.0
	B	1.4	1.2	2.6
Nb	G	1.2	1.1	2.3
	B	1.6	1.4	2.9
Th	G	0.8	0.5	1.9
	B	1.0	0.7	2.1
Pb	G	0.8	0.5	1.9
	B	1.0	0.7	2.1
Y	G	1.0	0.9	1.9
	B	1.2	1.1	2.2
Zn	G	0.8	0.5	1.0
	B	1.0	0.7	1.0
Sr	G	0.6	0.4	0.7
	B	0.6	0.5	0.9
Cu	G	1.0	0.8	1.7
	B	1.2	1.0	2.0
Co	G	3.4	3.2	7
	B	4.4	4.2	9
Ni	G	1.2	1.0	2.1
	B	1.6	1.2	2.6
Cr	G	1.6	1.2	2.5
	B	2.0	1.5	3.1
V	G	2.6	2.2	4.8
	B	3.0	2.8	5.6

No specific fragmental rock types have been distinguished.

BB = Basic-ultrabasic complexes DT = Diorite T = Tonalite
G = Granodiorite AD = Adamellite L = Leucogranite
HP = Haib Porphyry

The name of the first sample in each rock group is labelled with the appropriate abbreviation. The tables should be read from right to left in order to determine the number of samples in each rock group.

The decimal fractions in the trace element data are not significant, but have been included in order to allow accurate rounding off.

	BA									
	DRL-49	DRL-50	DRL-65	DRL-74	DRL-42	DRL-57	DRL-43	DRL-45	DRL-48	DRL-67
SIO2	52.40	53.04	53.93	54.27	54.32	54.79	54.58	56.35	57.21	56.98
TIO2	.70	.71	.75	.72	.68	.69	.70	.72	.81	.80
AL2O3	14.64	14.62	14.55	14.81	14.17	14.91	14.36	14.90	15.83	15.38
FE2O3	9.80	9.52	9.27	8.86	8.89	8.47	9.03	8.57	8.77	7.72
FEO	.00	.00	.00	.00	.00	.00	.00	.00	.00	.00
MNO	.17	.16	.16	.15	.15	.14	.13	.14	.14	.12
MGO	8.22	8.36	7.76	7.27	7.83	6.94	8.03	6.09	5.63	5.50
CAO	9.37	8.53	7.68	7.86	7.00	7.81	6.36	7.03	6.62	6.98
NA2O	1.93	1.99	1.25	2.10	1.87	2.35	2.52	2.25	2.03	2.18
K2O	1.00	1.36	2.06	2.13	2.52	1.34	1.62	1.68	2.47	2.18
P2O5	.22	.22	.19	.28	.20	.23	.18	.19	.19	.27
H2O-	.03	.03	.04	.04	.03	.05	.05	.04	.05	.05
LOI	.69	.80	2.20	.76	1.80	1.67	3.18	1.80	1.17	1.57
TOTAL	99.17	99.34	99.84	99.25	99.46	99.39	100.74	99.76	100.92	99.03
BA	555.00	764.00	581.00	1030.00	767.00	825.00	976.00	948.00	858.00	1275.00
RB	27.80	38.30	77.40	67.20	94.90	51.00	52.00	57.20	93.20	53.30
ZR	108.00	108.00	128.00	120.00	116.00	119.00	123.00	139.00	142.00	136.00
NB	2.80	2.90	5.50	4.00	5.00	2.80	3.90	6.80	5.40	3.50
TH	5.24	5.26	6.95	4.85	10.80	4.75	10.10	7.38	8.58	4.00
PB	15.41	16.60	22.85	17.60	15.90	14.80	18.40	14.31	17.10	23.60
Y	17.00	17.10	17.90	16.90	16.50	14.80	18.30	19.60	20.40	14.60
ZN	87.00	87.00	95.00	59.00	83.00	80.00	76.00	78.00	90.00	92.00
SR	507.00	521.00	353.00	615.00	357.00	596.00	696.00	465.00	370.00	704.00
CU	87.00	110.00	129.00	24.00	17.80	14.00	15.20	58.00	108.00	8.30
CO	44.00	44.00	44.00	41.00	37.00	34.00	42.00	35.00	39.00	35.00
NI	95.00	99.00	127.00	120.00	110.00	69.00	115.00	76.00	70.00	137.00
CR	295.00	299.00	433.00	320.00	371.00	222.00	421.00	237.00	156.00	150.00
V	187.00	206.00	181.00	192.00	155.00	181.00	183.00	163.00	182.00	170.00
U	.67	.65	.95	1.00	.90	.40	1.00	1.06	1.09	.50

	BA					A				
	DRL-41	DRL-123	DRL-125	DRL-126	DRL-127	DRL-62	DRP-04	DRL-73	DRL-56	DRL-99
SIO2	57.20	55.83	56.28	55.16	58.26	58.11	59.67	58.00	58.26	60.60
TIO2	.62	.80	.81	.82	.77	.65	.65	.73	.64	.71
AL2O3	15.27	15.34	15.32	15.40	15.32	16.03	15.79	16.74	15.54	18.19
FE2O3	7.17	8.88	8.89	8.86	7.88	6.42	7.18	7.22	6.24	4.77
FEO	.00	.00	.00	.00	.00	.00	.00	.00	.00	.00
MNO	.10	.14	.14	.13	.13	.10	.16	.11	.10	.08
MGO	4.91	5.79	5.50	5.93	4.47	4.01	3.94	3.38	3.75	1.53
CAO	6.95	6.73	6.66	6.91	6.55	5.50	4.83	6.16	6.04	5.57
NA2O	1.85	2.29	2.22	2.32	1.57	2.54	1.82	3.02	4.70	3.49
K2O	2.60	2.30	2.29	2.08	3.53	3.48	3.47	2.93	1.86	3.72
P2O5	.19	.20	.20	.19	.15	.22	.17	.28	.26	.31
H2O-	.04	.08	.09	.08	.10	.02	.06	.06	.03	.09
LOI	2.14	1.40	1.58	1.76	1.64	1.22	1.30	.92	1.72	.77
TOTAL	99.10	99.78	99.98	99.64	100.37	99.10	99.04	99.55	99.14	99.76
BA	676.00	768.00	766.00	741.00	703.00	951.00	851.00	1135.00	590.00	1630.00
RB	106.00	90.70	92.30	82.50	151.00	122.00	173.00	100.00	59.00	111.00
ZR	116.00	139.10	139.60	135.58	136.06	165.00	158.00	142.00	135.00	203.00
NB	3.90	6.18	5.27	5.94	5.97	7.10	8.00	5.10	4.90	8.00
TH	4.23	8.64	9.30	7.43	12.45	13.60	18.60	7.20	6.51	10.50
PB	27.28	21.88	31.59	15.82	28.99	23.60	46.80	22.50	20.20	25.80
Y	12.40	19.38	21.13	19.42	15.16	18.40	21.00	16.90	12.30	21.00
ZN	62.00	85.00	101.00	78.00	69.00	67.00	172.00	71.00	61.00	41.00
SR	537.00	446.15	381.29	332.00	416.00	532.00	404.00	632.00	573.00	630.00
CU	23.00	80.00	195.00	117.00	111.00	125.00	32.00	53.00	10.70	11.10
CO	29.00	37.76	37.38	36.02	28.74	29.00	29.00	24.00	24.00	10.10
NI	88.00	67.31	70.34	67.54	62.12	82.00	42.00	26.00	69.00	8.70
CR	176.00	154.89	155.52	146.51	123.53	212.00	58.00	52.00	124.00	12.30
V	151.00	179.02	178.38	188.27	165.40	150.00	149.00	142.00	47.00	124.00
U	.96	.80	1.10	.80	1.00	1.70	3.90	1.30	1.00	1.70

	A							D		
	DRL-113	DRL-78C	DRL-47	DRP-10	DRP-12	DRL-115	DRL-78B	DRL-71	DRL-68	DRL-66
SIO2	59.35	62.77	65.87	63.14	62.03	60.59	63.79	62.62	65.28	66.56
TIO2	.76	.60	.51	.57	.62	.63	.65	.65	.44	.68
AL2O3	15.34	15.42	16.82	15.44	15.41	16.46	15.50	16.75	14.40	15.92
FE2O3	7.43	6.46	3.69	5.84	6.42	5.00	5.48	5.17	4.47	3.64
FEO	.00	.00	.00	.00	.00	.00	.00	.00	.00	.00
MNO	.14	.19	.08	.12	.14	.09	.08	.06	.06	.06
MGO	6.82	3.40	1.08	2.78	3.31	2.46	1.79	1.81	3.82	1.01
CAO	5.32	4.04	6.66	4.45	4.33	5.07	4.17	4.55	3.24	4.80
NA2O	2.13	2.49	2.05	2.64	2.35	2.54	3.53	3.13	3.67	3.25
K2O	3.25	2.18	2.47	2.64	3.35	3.98	3.35	3.51	2.81	2.72
P2O5	.27	.14	.18	.14	.17	.22	.21	.24	.14	.23
H2O-	.10	.04	.05	.09	.10	.12	.03	.05	.04	.03
LOI	1.24	1.31	1.47	1.38	1.01	3.01	.93	1.42	1.05	.92
TOTAL	100.15	99.04	100.93	99.23	99.24	100.17	99.51	99.96	99.42	99.62
BA	880.00	694.00	1210.00	1010.00	696.00	1520.00	1010.00	1390.00	1370.00	1470.00
RB	131.00	143.00	120.00	121.00	172.00	123.86	119.00	114.00	94.00	108.00
ZR	148.67	157.00	225.00	138.00	162.00	156.30	176.00	172.00	220.00	287.00
NB	5.20	9.00	11.70	7.19	9.26	6.57	8.70	6.50	9.70	13.20
TH	8.10	19.10	11.60	17.24	30.68	9.43	13.00	8.41	9.96	17.00
PB	27.07	51.40	19.20	48.74	60.32	17.32	31.00	20.70	23.01	37.00
Y	15.35	21.00	22.00	19.60	19.05	13.18	21.00	17.30	18.40	26.00
ZN	67.00	131.00	66.00	131.00	156.00	51.00	58.00	59.00	51.00	80.00
SR	683.00	435.00	289.00	322.17	330.94	518.25	466.00	620.00	574.00	536.00
CU	37.00	11.40	13.90	30.50	40.90	87.00	234.00	24.00	100.00	57.00
CO	26.18	18.60	4.30	18.78	22.18	13.24	14.90	13.60	18.00	5.30
NI	29.34	38.00	15.86	34.57	36.17	10.99	14.10	17.80	84.00	10.60
CR	96.39	54.00	2.90	60.10	57.07	43.04	12.60	43.00	221.00	16.70
V	154.65	122.00	19.70	114.16	128.84	99.11	126.00	102.00	76.00	57.00
U	1.92	3.60	2.20	3.40	4.50	2.00	1.10	2.20	1.10	3.60

	D									
	DRL-75	RT-04	RT-05	RT-06	DRL-93	DRL-112	DRL-121	DRL-122	DRL-78A	DRP-03
SIO2	65.02	61.56	63.01	63.24	65.33	62.65	65.88	65.86	65.36	68.91
TIO2	.76	.57	.59	.59	.82	.68	.50	.49	.53	.36
AL2O3	16.68	15.07	15.28	15.51	14.97	17.07	14.97	14.95	14.85	15.09
FE2O3	3.84	5.47	5.71	5.81	5.83	4.90	4.89	4.87	4.66	3.33
FEO	.00	.00	.00	.00	.00	.00	.00	.00	.00	.00
MNO	.05	.09	.10	.10	.10	.07	.08	.08	.08	.05
MGO	1.18	2.78	2.69	2.47	2.05	2.58	2.59	2.47	2.31	1.29
CAO	3.30	4.18	4.37	4.22	4.49	4.49	3.89	3.64	3.71	2.64
NA2O	3.00	2.03	2.11	2.21	3.07	3.76	2.68	2.65	3.00	2.10
K2O	5.72	4.67	4.52	4.45	3.75	3.34	4.01	4.34	3.98	4.60
P2O5	.19	.16	.16	.13	.17	.24	.11	.10	.15	.12
H2O-	.03	.06	.02	.07	.08	.11	.08	.12	.03	.04
LOI	.47	2.15	1.03	.97	.35	1.02	1.24	1.14	.79	1.28
TOTAL	100.25	98.79	99.59	99.77	101.01	100.91	100.92	100.71	99.45	99.90
BA	1490.00	976.00	830.00	898.00	832.00	1170.00	796.00	812.00	849.00	1430.00
RB	168.00	203.00	202.00	191.00	167.00	119.00	172.00	189.00	124.00	161.00
ZR	280.00	179.00	184.00	172.00	216.50	162.90	145.93	149.06	176.00	135.00
NB	13.30	9.96	10.79	8.44	11.19	6.07	11.47	10.39	8.70	6.70
TH	18.20	23.84	22.25	21.94	17.80	10.22	21.67	22.67	17.30	11.10
PB	41.72	33.77	32.45	32.88	28.51	22.44	31.15	28.60	29.40	29.30
Y	28.00	26.30	25.40	17.60	30.63	13.91	18.12	17.19	21.00	11.20
ZN	46.00	69.00	67.00	74.00	60.00	65.00	51.80	51.90	58.00	28.00
SR	487.00	371.00	390.00	353.33	218.00	644.00	355.00	344.00	477.00	388.00
CU	9.40	50.00	141.00	33.00	5.00	35.00	57.80	64.50	234.00	615.00
CO	6.00	21.53	22.67	16.46	17.22	15.93	35.08	16.40	17.20	5.70
NI	13.10	30.16	37.10	32.25	26.62	13.81	26.20	25.97	14.10	11.60
CR	29.00	62.30	55.21	59.10	52.88	49.21	86.35	43.86	86.00	8.60
V	72.00	106.57	111.57	114.59	96.70	100.31	44.18	89.52	89.00	58.00
U	3.70	5.00	4.90	4.60	3.88	2.00	5.29	5.00	.00	2.60

	NR									
	DRA-06A	DRA-06B	DRA-06C	DRA-06D	DRA-06E	DRL-79	DRA-05	DRL-55	DRL-76	DRL-58
SIO2	73.80	74.06	74.00	74.45	74.92	66.99	72.26	72.36	71.09	75.19
TIO2	.38	.35	.37	.37	.27	.46	.68	.25	.36	.23
AL2O3	14.09	13.73	14.05	13.79	13.12	15.49	12.86	13.63	14.04	13.60
FE2O3	1.40	1.90	1.29	1.68	1.50	2.89	2.95	2.24	2.05	1.47
FEO	.00	.00	.00	.00	.00	.00	.00	.00	.00	.00
MNO	.03	.03	.07	.04	.03	.06	.04	.03	.05	.03
MGO	.22	.33	.28	.39	.20	1.05	.99	1.16	.61	.45
CAO	.86	.86	.52	.67	.65	2.97	1.78	1.27	1.86	.97
NA2O	3.23	4.07	3.73	2.54	3.53	3.72	2.21	3.52	2.94	3.56
K2O	6.11	5.00	5.74	5.89	5.91	4.50	5.29	2.84	5.47	3.37
P2O5	.04	.05	.05	.04	.02	.09	.15	.07	.06	.06
H2O-	.07	.07	.06	.06	.05	.04	.05	.03	.03	.04
LOI	.44	.59	.64	.68	.59	.47	.67	1.82	.47	1.08
TOTAL	100.65	101.04	100.80	100.60	100.79	98.73	99.93	99.22	99.93	100.12
BA	1560.00	1410.00	1540.00	1410.00	1420.00	1480.00	1380.00	987.00	1365.00	1240.00
RB	248.00	217.00	219.00	214.00	237.00	188.00	138.00	121.00	136.00	108.00
ZR	317.00	310.00	317.00	315.00	264.00	221.00	263.00	148.00	226.00	153.00
NB	14.90	16.00	16.10	15.30	16.30	10.40	12.40	11.00	14.00	11.10
TH	21.50	22.70	20.10	20.20	22.70	16.50	22.01	18.00	15.60	29.80
PB	36.00	35.50	26.30	36.80	25.00	28.90	37.03	13.30	49.70	43.70
Y	39.00	40.80	34.40	37.90	38.60	24.00	26.00	15.10	25.00	15.60
ZN	38.23	35.16	37.02	40.11	30.01	40.00	34.00	26.00	36.00	12.80
SR	148.00	152.00	119.00	128.00	92.00	349.00	325.00	210.00	287.00	251.00
CU	29.15	20.13	20.13	28.65	21.22	19.00	21.00	12.40	25.00	106.00
CO	.00	.00	.00	.00	.00	5.20	5.30	4.10	.00	.00
NI	.00	.00	.00	.00	.00	10.30	7.80	11.60	4.80	.00
CR	.00	.00	.00	.00	.00	19.70	12.40	18.30	8.80	.00
V	9.31	8.11	7.02	6.11	4.13	40.00	42.00	38.00	25.00	8.00
U	3.30	2.40	2.40	2.90	3.70	3.90	3.30	4.00	3.10	.00

	NR		PR		
	DRL-69	DRA-06	DRL-92	DRL-94	DRL-107
SIO2	80.59	73.40	69.43	67.87	69.96
TIO2	.20	.36	.44	.46	.29
AL2O3	11.18	13.62	14.83	14.49	14.30
FE2O3	.96	2.12	2.55	2.83	2.50
FEO	.00	.00	.00	.00	.00
MNO	.03	.04	.04	.05	.04
MGO	.43	.31	.93	.82	1.11
CAO	.53	.59	2.40	2.62	2.62
NA2O	3.59	3.64	3.64	3.34	2.82
K2O	2.06	5.54	4.90	4.51	4.74
P2O5	.06	.04	.09	.11	.08
H2O-	.07	.02	.07	.09	.12
LOI	.90	.66	1.27	1.98	1.52
TOTAL	100.60	100.34	100.59	99.17	100.10
BA	649.00	1370.00	1190.00	1110.00	656.00
RB	99.00	237.00	195.00	196.00	262.00
ZR	93.00	286.00	199.00	217.13	149.00
NB	12.40	14.20	11.86	13.95	12.17
TH	23.00	21.20	17.78	19.44	30.34
PB	22.70	33.80	28.11	29.19	33.87
Y	19.60	31.00	21.10	23.01	14.43
ZN	12.60	39.00	33.00	38.00	29.00
SR	90.00	133.00	252.00	244.00	242.00
CU	18.80	29.10	16.00	16.00	26.00
CO	.00	.00	1.14	3.17	4.94
NI	3.60	2.60	8.74	6.85	10.98
CR	.00	3.60	19.63	16.70	18.88
V	.00	10.10	34.50	36.31	41.47
U	4.80	2.50	3.93	4.10	7.48

HAIB FRAGMENTALS BULK ANALYSES

	DRL-21	DRL-70	DRL-72	DR-08	DRL-81	DR-05-1	DRL-40B	DRL-22	DRL-77	DRL-15
SIO2	61.60	53.06	52.19	53.00	54.69	49.26	58.75	54.76	59.40	59.21
TIO2	.62	.65	.62	.72	.67	.93	.64	.76	.58	.78
AL203	15.79	13.36	12.79	13.63	14.48	18.73	13.36	16.92	18.55	17.08
FE203	5.02	9.60	8.91	8.86	8.83	8.70	9.77	7.12	4.27	5.61
FEO	.00	.00	.00	.00	.00	.00	.00	.00	.00	.00
MNO	.07	.15	.16	.17	.16	.19	.15	.12	.07	.11
MGO	3.33	9.89	12.00	11.13	6.84	7.32	5.80	3.73	3.74	4.12
CAO	4.10	7.42	6.55	5.97	8.44	3.77	6.49	6.54	6.47	3.63
NA20	2.70	1.78	1.76	1.38	3.32	2.11	1.12	1.49	3.36	5.11
K20	3.58	1.15	1.84	3.44	.66	5.39	1.50	4.44	2.12	1.64
P205	.23	.20	.18	.20	.24	.24	.23	.30	.21	.18
H20-	.00	.06	.07	.07	.04	.37	.03	.07	.05	.31
LOI	2.32	1.87	1.95	1.20	.65	2.11	2.58	3.88	1.25	1.86
TOTAL	99.36	99.19	99.02	99.77	99.02	99.12	100.42	100.13	100.07	99.64
BA	986.00	627.00	506.00	936.00	399.00	2480.00	569.00	1620.00	1030.00	854.00
RB	147.00	43.00	69.00	115.00	14.80	200.00	70.00	134.00	82.00	49.00
ZR	193.00	91.00	123.00	126.00	98.00	297.00	105.00	152.00	158.00	260.00
NB	12.10	3.50	4.70	8.00	3.10	12.70	3.50	6.60	8.50	11.00
TH	.00	6.00	7.84	4.70	5.95	14.60	.00	.00	9.16	12.00
PB	.00	16.20	13.40	9.30	25.00	22.00	.00	.00	23.10	16.30
Y	20.10	14.70	16.90	17.30	16.60	34.00	14.60	19.00	21.00	29.00
ZN	56.00	63.00	88.00	100.00	68.00	157.00	86.00	73.00	37.00	76.00
SR	363.00	505.00	445.00	318.00	525.00	448.00	408.00	427.00	792.00	423.00
CU	6.60	3.80	60.00	26.00	175.00	105.00	.00	149.00	31.00	64.00
CO	18.60	44.00	51.00	57.00	37.00	33.00	57.00	24.00	18.40	21.00
NI	65.00	228.00	414.00	345.00	89.00	833.00	180.00	20.30	77.00	59.00
CR	102.00	866.00	871.00	958.00	381.00	605.00	695.00	13.90	81.00	76.00
V	110.00	177.00	147.00	173.00	186.00	69.00	136.00	186.00	71.00	76.00

	DRL-23	DR-05-5	DR-02	DR-03	DRL-17	DR-07	DRL-19	DRL-20	DRL-40A	DRH-01
SIO2	61.35	57.41	60.96	60.50	65.91	64.99	64.47	63.53	63.04	64.83
TIO2	.74	.84	.57	.81	.46	.77	.68	.60	.77	.76
AL203	16.55	16.77	13.96	14.97	13.26	14.37	15.47	15.01	16.09	15.51
FE203	5.76	6.75	6.79	5.97	5.53	5.18	4.97	4.76	8.31	5.15
FEO	.00	.00	.00	.00	.00	.00	.00	.00	.00	.00
MNO	.10	.14	.11	.09	.07	.09	.10	.12	.03	.08
MGO	2.21	5.08	6.30	5.90	3.33	3.21	2.61	3.68	1.04	1.80
CAO	5.14	4.77	4.16	2.38	4.78	3.54	3.25	6.46	2.23	3.02
NA20	3.89	2.43	1.88	2.74	4.15	3.38	2.79	4.47	5.02	3.57
K20	3.56	3.94	2.91	4.28	.66	2.80	3.44	4.39	1.64	4.14
P205	.27	.20	.15	.19	.11	.20	.17	.30	.28	.24
H20-	.02	.27	.03	.07	.01	.07	.02	.02	.02	.09
LOI	1.36	1.05	2.29	1.90	2.37	1.62	1.94	.88	.92	1.46
TOTAL	100.95	99.65	100.11	99.80	100.64	100.22	99.91	101.22	99.39	100.65
BA	1180.00	2276.00	1170.00	1676.00	239.00	1310.00	1260.00	.00	1100.00	831.00
RB	78.00	137.00	115.00	154.00	20.20	96.00	144.00	.00	58.00	216.00
ZR	194.00	283.00	174.00	249.00	110.00	238.00	242.00	.00	156.00	236.00
NB	8.10	13.40	8.40	13.30	5.10	12.40	10.90	.00	6.20	15.30
TH	13.20	11.90	8.10	6.60	.00	8.80	.00	.00	.00	.00
PB	20.10	20.10	16.70	8.80	.00	12.80	.00	.00	.00	.00
Y	23.00	33.00	21.00	28.00	14.90	25.00	26.00	.00	18.30	29.00
ZN	57.00	105.00	79.00	78.00	43.00	72.00	76.00	.00	14.60	57.00
SR	353.00	610.00	497.00	323.00	612.00	416.00	313.00	356.00	321.00	310.00
CU	5.20	211.00	33.00	3.70	303.00	77.00	23.00	11.00	5.70	103.00
CO	16.10	21.00	31.00	23.00	22.00	18.20	13.50	17.50	7.60	16.00
NI	17.80	460.00	190.00	164.00	41.00	52.00	34.00	63.00	56.00	6.80
CR	24.00	486.00	514.00	427.00	47.00	81.00	102.00	156.00	214.00	8.60
V	144.00	75.00	94.00	66.00	122.00	81.00	72.00	98.00	122.00	66.00

HAIB FRAGMENTALS BULK ANALYSES

	DRL-11	DRA-01	DR-05-2	DR-05-6	DR-06	DR-04	DRL-14	DR-05-3	DR-05-4
SIO2	67.22	62.13	64.99	62.72	69.25	70.23	70.65	68.91	69.10
TIO2	.67	.94	.75	.61	.63	.71	.59	.75	.76
AL2O3	14.26	16.97	14.45	13.77	14.25	12.98	13.51	12.57	13.16
FE2O3	4.66	4.79	4.77	5.84	4.15	3.94	3.86	4.26	4.22
FEO	.00	.00	.00	.00	.00	.00	.00	.00	.00
MNO	.08	.08	.10	.13	.07	.08	.07	.09	.09
MGO	2.25	1.52	3.54	5.91	1.34	2.03	1.38	2.38	2.31
CAO	3.37	2.69	3.09	2.37	3.82	3.18	2.31	4.03	4.00
NA2O	5.53	2.22	3.48	2.34	4.45	4.25	6.39	3.15	3.02
K2O	1.05	7.14	2.86	3.72	1.63	1.43	.63	2.07	2.38
P2O5	.17	.29	.17	.14	.17	.15	.17	.17	.18
H2O-	1.29	.10	.38	.32	.07	.03	.21	.26	.32
LOI	.00	1.22	1.19	1.46	1.20	1.21	.85	.99	1.14
TOTAL	100.57	100.09	99.77	99.33	101.03	100.22	100.62	99.63	100.68
BA	547.00	2090.00	1490.00	1360.00	1030.00	898.00	293.00	1235.00	1402.00
RB	35.00	234.00	99.00	142.00	48.00	42.00	16.00	70.00	73.00
ZR	242.00	336.00	229.00	222.00	238.00	26.00	209.00	242.00	250.00
NB	12.00	17.20	11.40	10.50	12.60	266.00	9.80	9.20	10.00
TH	.00	26.00	7.80	13.90	15.30	13.40	7.60	7.20	4.30
PB	.00	43.00	11.60	12.10	22.00	16.60	13.40	15.60	14.00
Y	27.00	34.00	23.00	26.00	29.00	10.20	25.00	21.00	23.00
ZN	54.00	58.00	75.00	124.00	38.00	.00	44.00	50.00	46.00
SR	520.00	252.00	392.00	364.00	532.00	439.00	277.00	511.00	474.00
CU	298.00	151.00	32.00	83.00	31.00	45.00	56.00	163.00	98.00
CO	13.10	12.10	15.60	28.00	7.90	8.00	4.80	.00	.00
NI	55.00	18.50	122.00	421.00	30.00	18.10	14.00	44.00	51.00
CR	130.00	.00	114.00	408.00	41.00	36.00	31.00	.00	.00
V	58.00	89.00	46.00	80.00	40.00	38.00	26.00	.00	.00

	BB							DT		DT
	DRS-01	DRS-06	DRS-14	DRS-16	DRS-18	DRS-20	DRS-11	DRV-37	DRV -77	DRV-08A
SIO2	54.05	50.25	49.33	50.40	44.98	36.12	37.13	48.26	51.04	58.31
TIO2	.50	.49	.28	.53	.21	.12	.13	.68	.53	1.03
AL203	15.63	17.29	18.24	15.99	20.11	5.44	5.44	11.69	9.60	15.64
FE203	10.06	8.25	6.13	9.79	7.02	11.42	11.37	9.97	10.35	7.95
FEO	.00	.00	.00	.00	.00	.00	.00	.00	.00	.00
MNO	.15	.14	.10	.15	.10	.16	.15	.23	.20	.13
MGO	6.67	8.78	9.10	10.07	10.91	31.47	32.05	15.23	14.11	4.04
CAO	9.48	11.21	12.24	10.22	11.74	3.41	2.65	7.16	12.33	6.08
NA20	1.76	1.99	1.50	1.63	1.57	.03	.02	1.23	1.47	2.24
K20	1.12	1.16	1.35	.33	.14	.02	.02	1.30	.53	2.97
P205	.00	.05	.00	.00	.00	.00	.00	.16	.12	.32
H20-	.04	.09	.08	.07	.37	.31	.26	.19	.05	.10
LOI	.94	1.11	1.87	1.10	1.96	11.07	10.98	3.20	.76	1.23
TOTAL	100.46	100.81	100.22	100.28	99.11	99.57	100.20	99.30	101.09	100.04
BA	416.00	150.00	338.00	122.00	42.20	10.10	29.60	413.00	93.00	857.00
RB	35.24	87.90	94.90	15.10	3.60	1.63	1.48	48.86	19.90	123.00
ZR	46.24	26.45	20.00	28.00	4.70	.00	.00	81.63	62.80	170.00
NB	1.26	.00	.00	.00	.00	.00	.00	4.37	2.53	9.60
TH	5.82	4.17	4.20	4.00	3.00	.00	.00	8.00	5.18	7.30
PB	16.83	13.50	12.70	9.00	9.00	.00	.00	11.53	13.42	22.00
Y	18.07	12.94	8.20	12.60	2.10	.00	.00	18.43	16.61	22.00
ZN	67.26	61.04	31.70	64.40	3.60	53.04	42.60	121.51	75.66	78.06
SR	288.70	274.79	390.00	226.00	259.00	20.60	29.60	217.25	365.35	387.00
CU	298.19	54.67	113.00	121.00	40.70	22.14	19.40	6.80	14.35	79.69
CO	52.28	49.46	40.00	56.00	59.00	136.00	133.00	71.31	71.88	26.00
NI	148.07	194.55	284.00	303.00	382.00	1680.00	1870.00	633.47	175.80	102.00
CR	248.44	396.79	899.00	576.00	247.00	4280.00	4130.00	1510.98	1114.84	75.00
V	247.19	148.39	120.00	156.00	64.00	56.00	60.00	172.68	162.64	156.00
U	.50	.40	.04	.01	.01	.01	.03	.00	.00	1.10
	DT				T					
	DRV-08B	DRV-08C	DRV-08	DRV-63	DRV-62	DRV-13A	DRV-13B	DRV-44	DRV-50	DRV-52
SIO2	57.04	57.38	52.83	55.03	58.34	60.77	54.14	60.40	57.88	57.82
TIO2	.97	.98	.80	.94	.98	.93	1.18	.93	1.07	.79
AL203	16.33	16.35	17.52	17.09	17.91	15.76	17.59	16.28	17.37	17.00
FE203	8.07	8.17	8.90	8.92	6.60	7.07	9.11	7.02	6.80	7.49
FEO	.00	.00	.00	.00	.00	.00	.00	.00	.00	.00
MNO	.14	.14	.14	.12	.12	.17	.16	.12	.12	.11
MGO	4.52	4.51	7.69	4.55	2.56	2.28	3.46	2.74	2.33	4.01
CAO	6.15	6.11	8.21	7.74	6.20	4.90	7.54	5.06	6.22	6.49
NA20	2.37	2.31	2.18	2.53	2.93	3.23	2.84	3.45	3.16	3.04
K20	2.77	2.88	1.39	2.14	2.90	2.80	2.58	3.29	2.75	2.73
P205	.34	.32	.30	.40	.35	.32	.47	.32	.38	.24
H20-	.12	.05	.05	.00	.13	.10	.13	.02	.02	.06
LOI	1.67	1.58	.54	1.16	1.56	1.06	1.38	.94	1.45	.83
TOTAL	100.49	100.78	100.55	100.62	100.58	99.39	100.58	100.57	99.55	100.61
BA	808.00	830.00	477.00	711.00	992.00	952.00	845.00	1340.00	934.00	901.00
RB	111.00	114.00	43.00	80.27	128.00	152.00	96.00	124.99	119.98	118.84
ZR	164.00	165.00	97.00	161.01	178.00	161.00	112.50	242.61	182.54	131.75
NB	9.10	9.20	7.80	9.08	8.88	16.90	11.40	9.22	8.13	4.71
TH	8.00	6.00	11.70	7.00	10.61	16.90	9.90	13.35	10.50	7.45
PB	20.00	24.00	19.10	24.88	26.30	27.00	20.10	62.31	34.22	13.30
Y	20.00	22.00	15.60	20.58	24.40	29.90	18.30	25.81	23.13	21.82
ZN	83.32	83.53	85.00	88.87	74.77	92.90	83.00	77.85	72.41	
SR	426.00	423.00	529.00	504.35	573.00	336.00	559.00	436.09	583.13	529.78
CU	56.81	96.68	95.00	177.68	77.48	81.33	76.46	61.17	59.00	27.77
CO	24.00	30.00	40.00	35.82	14.50	21.00	25.00	18.45	13.16	25.20
NI	105.00	108.00	216.00	102.41	16.60	20.00	31.00	19.47	11.30	26.64
CR	56.00	61.00	153.00	55.74	26.30	33.00	56.00	36.45	21.16	102.29
V	148.00	121.00	108.00	196.26	108.00	93.00	147.00	115.65	100.33	140.58
U	1.30	1.30	.80	.60	1.50	2.60	.90	2.10	2.10	1.60

	T					G				
	DRV-73	DRV-75	DRV-49	DRV-C	DRV-55	DRV-15	DRV-15A	DRV-15C	DRV-15D	DRV-15E
SIO2	59.35	62.27	58.96	59.18	62.60	65.48	65.25	65.46	64.75	61.18
TIO2	1.01	.72	.66	.52	.70	.54	.52	.55	.57	.74
AL2O3	16.22	16.70	17.92	16.62	16.73	15.06	15.19	15.20	15.01	16.14
FE2O3	7.46	5.44	4.87	6.82	5.34	4.58	4.32	4.47	4.60	5.04
FEO	.00	.00	.00	.00	.00	.00	.00	.00	.00	.00
MNO	.13	.08	.09	.12	.08	.08	.07	.07	.07	.10
MGO	2.76	2.16	1.75	3.50	2.16	1.80	2.50	1.86	2.24	3.03
CAO	5.31	5.28	6.36	6.44	4.80	3.83	3.81	4.02	3.88	5.13
NA2O	3.33	3.09	2.74	2.85	3.47	2.99	3.18	3.09	3.03	3.01
K2O	2.96	2.54	3.66	1.68	3.63	4.33	4.06	3.83	4.09	3.55
P2O5	.31	.22	.20	.13	.26	.18	.18	.18	.20	.26
H2O-	.05	.02	.09	.05	.10	.09	.05	.05	.03	.05
LOI	.92	1.45	1.91	1.20	.34	.01	1.19	1.33	.98	1.06
TOTAL	99.81	99.97	99.21	99.11	100.21	99.77	100.32	100.11	99.44	100.17
BA	1320.00	765.00	1610.00	636.00	1355.00	1320.00	1280.00	1265.00	1360.00	1240.00
RB	130.29	129.53	156.21	63.09	122.00	145.00	146.10	128.00	139.00	125.00
ZR	234.50	237.60	152.92	79.94	120.00	139.00	101.49	102.11	98.16	76.00
NB	12.21	3.02	6.96	2.19	8.21	11.10	7.61	5.24	7.36	7.00
TH	13.50	11.87	12.54	5.68	10.40	9.50	17.68	14.69	14.32	13.03
PB	24.25	25.56	27.13	17.42	27.05	25.60	22.99	20.82	27.76	25.15
Y	26.42	14.04	15.67	13.41	10.00	18.80	11.79	10.35	10.47	13.57
ZN	87.53	71.50	36.30	98.99	60.90	44.00	37.45	36.91	30.03	50.53
SR	440.35	581.25	572.83	476.05	572.00	476.00	377.12	482.00	463.00	584.00
CU	80.10	81.97	227.69	48.92	12.94	54.00	11.26	13.87	75.66	72.70
CO	18.05	11.61	12.97	20.53	10.80	14.60	12.72	12.90	11.78	21.17
NI	22.32	21.51	14.34	45.55	13.30	13.00	14.00	16.00	12.00	28.00
CR	33.78	22.05	29.08	64.53	37.90	28.00	29.00	33.00	30.00	40.00
V	126.31	102.19	90.20	135.77	102.00	75.00	86.55	73.23	95.85	133.36
U	2.30	1.40	3.10	.90	1.80	1.90	2.20	2.10	1.70	2.00

	G							AD		
	DRV-15F	DRV-09	DRV-32	DRV-33	DRV-38	DRV-57	DRV-39	DRV-01	DRV-02	DRV-03
SIO2	64.16	64.00	65.82	64.20	65.51	63.80	65.66	69.36	68.19	64.89
TIO2	.55	.43	.46	.65	.58	.79	.43	.49	.50	.74
AL2O3	16.28	14.78	14.78	16.60	15.40	15.79	14.92	14.15	14.80	15.14
FE2O3	4.50	4.62	4.72	4.07	5.42	5.10	4.03	3.20	3.37	5.07
FEO	.00	.00	.00	.00	.00	.00	.00	.00	.00	.00
MNO	.07	.08	.09	.07	.10	.10	.06	.07	.07	.09
MGO	2.21	2.34	2.55	1.72	2.58	2.05	1.06	1.35	1.05	1.37
CAO	3.63	3.93	3.99	4.04	4.06	3.65	3.39	2.66	2.93	3.63
NA2O	3.41	2.65	2.41	3.11	2.87	2.93	3.12	3.08	2.88	2.87
K2O	4.33	4.48	3.45	4.83	3.47	4.10	4.35	4.67	4.60	4.66
P2O5	.18	.12	.11	.25	.14	.25	.10	.14	.13	.22
H2O-	.04	.03	.03	.09	.02	.06	.07	.03	.08	.10
LOI	1.10	1.92	2.00	.79	.53	1.45	2.06	1.02	1.09	1.20
TOTAL	100.44	99.38	100.41	100.42	100.68	100.07	99.25	100.22	99.69	99.58
BA	1380.00	783.00	772.00	1410.00	681.00	1300.00	942.00	922.00	987.00	1165.00
RB	149.00	209.00	145.91	176.42	221.47	171.79	177.14	202.00	223.00	166.00
ZR	111.00	111.50	137.46	175.19	164.21	197.88	149.95	193.00	172.00	232.00
NB	6.25	11.20	9.92	11.23	8.62	8.32	9.41	11.20	13.20	13.00
TH	14.47	20.90	23.11	16.58	17.48	12.36	16.51	17.90	22.10	16.50
PB	22.64	27.50	117.23	25.38	49.47	22.40	17.11	22.00	27.40	26.00
Y	10.17	22.10	20.32	19.17	20.91	23.25	20.82	26.00	26.00	30.00
ZN	34.87	50.00	66.02	44.36	56.80	60.34	30.42	50.00	40.00	50.00
SR	447.00	324.00	338.90	462.69	421.03	420.75	417.07	245.00	292.00	315.00
CU	79.56	37.00	71.63	16.77	42.51	61.56	41.30	39.00	50.00	47.00
CO	11.97	17.00	15.86	10.21	8.51	9.99	5.39	8.80	9.00	13.60
NI	19.00	27.40	27.00	12.02	17.49	18.29	10.30	7.10	10.90	15.10
CR	22.00	34.00	39.68	24.05	17.31	32.78	8.94	16.40	14.50	18.20
V	90.52	73.00	85.38	99.45	108.58	87.33	78.28	42.00	43.00	62.00
U	2.10	2.80	2.20	2.30	3.00	2.20	2.70	3.50	2.60	3.10

	AD									
	DRV-04	DRV-05	DRV-06	DRV-14	DRV-18	DRV-21	DRV-15R	DRV-07	DRV-10	DRV-33A
SIO2	65.03	67.09	69.81	72.10	68.63	67.10	67.58	68.20	75.01	72.22
TIO2	.61	.57	.31	.28	.45	.48	.51	.67	.10	.41
AL2O3	15.03	14.58	13.63	13.94	14.65	15.32	14.85	15.49	11.79	13.60
FE2O3	4.91	4.09	2.80	1.99	3.88	3.95	3.83	3.50	.54	2.64
FEO	.00	.00	.00	.00	.00	.00	.00	.00	.00	.00
MNO	.08	.08	.06	.05	.09	.09	.07	.08	.01	.06
MGO	1.37	1.09	1.05	.36	1.47	1.36	1.37	1.00	.16	.78
CAO	3.63	3.31	2.39	1.52	2.31	2.80	3.01	2.61	.82	1.01
NA2O	2.87	2.93	2.36	3.52	3.06	4.26	3.38	3.35	2.47	3.17
K2O	4.46	4.36	5.20	4.97	4.71	3.60	4.51	5.13	6.58	4.74
P2O5	.22	.17	.07	.07	.12	.17	.18	.19	.01	.14
H2O-	.09	.09	.11	.12	.10	.09	.08	.04	.10	.00
LOI	1.69	1.07	1.76	.59	.52	.85	.82	.71	1.05	.58
TOTAL	99.99	99.43	99.55	99.51	99.99	100.07	100.19	100.97	99.53	100.34
BA	1175.00	996.00	531.00	856.00	936.00	885.00	866.00	2195.00	428.00	392.00
RB	165.00	165.00	255.00	182.00	142.00	211.00	204.00	157.00	151.04	236.78
ZR	193.00	197.00	138.00	157.00	143.00	154.00	141.98	364.00	56.06	136.54
NB	12.40	13.00	13.40	15.00	7.50	10.30	13.90	11.30	8.52	11.28
TH	17.50	23.00	31.90	22.40	24.70	13.30	23.29	14.00	29.83	26.70
PB	31.50	30.40	33.60	29.00	24.00	25.30	32.68	30.40	24.41	31.28
Y	26.00	27.00	21.00	19.30	15.60	21.00	19.22	23.00	8.32	18.70
ZN	56.00	44.00	31.00	34.00	51.00	55.00	51.25	64.00	.23	31.82
SR	337.00	264.00	201.00	224.00	293.00	359.00	312.00	302.00	62.73	200.00
CU	57.00	35.00	4.40	16.20	5.90	89.00	44.24	54.00	15.42	5.30
CO	14.30	13.10	8.30	5.50	19.20	9.60	7.92	7.50	2.50	3.33
NI	17.90	12.50	14.70	4.10	3.50	9.90	13.62	5.10	3.30	6.24
CR	31.00	15.00	18.90	4.00	35.00	16.00	22.03	4.90	3.59	14.46
V	68.00	49.00	39.00	23.00	69.00	51.00	66.33	32.00	9.99	38.33
U	2.60	4.00	5.50	2.20	3.90	2.70	4.10	1.90	4.20	4.00

	AD							L		
	DRV-47	DRV-48	DRV-51	DRV-54	DRV-70	DRV-72	DRV-76	DRV-11	DRV-12	DRV-22
SIO2	64.57	67.99	64.29	67.10	72.01	73.28	65.28	76.05	74.21	72.10
TIO2	.64	.51	.59	.51	.25	.27	.47	.11	.27	.38
AL2O3	16.21	15.38	15.72	14.35	13.58	13.81	15.09	13.07	13.76	13.85
FE2O3	4.57	3.33	4.64	3.92	2.19	1.85	4.45	.88	1.88	1.71
FEO	.00	.00	.00	.00	.00	.00	.00	.00	.00	.00
MNO	.08	.07	.08	.06	.04	.04	.07	.02	.04	.04
MGO	2.27	1.46	1.97	1.62	1.12	.02	1.63	.38	.04	.11
CAO	3.45	2.99	3.88	2.96	1.91	1.62	3.84	.92	1.32	.07
NA2O	3.29	3.15	3.30	3.22	2.93	3.84	2.37	3.50	2.89	2.86
K2O	4.39	4.88	3.90	4.53	5.08	4.94	4.61	4.70	5.38	6.34
P2O5	.22	.17	.17	.15	.07	.04	.09	.11	.05	.03
H2O-	.17	.09	.09	.09	.09	.07	.09	.09	.44	.11
LOI	1.12	.76	1.98	.81	1.07	.57	1.25	.50	.21	.43
TOTAL	100.98	100.80	100.61	99.32	100.34	100.35	99.24	100.07	100.83	99.02
BA	926.00	1040.00	1060.00	1030.00	653.00	900.00	806.00	309.00	720.00	1545.00
RB	209.44	216.62	165.48	193.15	230.76	199.11	225.74	196.00	209.00	161.00
ZR	153.44	159.24	166.25	199.68	96.78	158.74	152.72	61.20	146.00	277.00
NB	13.69	10.29	9.32	12.64	9.61	11.45	8.83	11.30	9.60	14.60
TH	15.84	14.65	15.00	18.21	24.00	18.32	25.80	7.09	35.10	12.50
PB	24.32	25.82	19.96	25.59	27.90	24.23	26.09	39.70	34.20	24.20
Y	21.20	18.66	23.42	20.05	15.52	16.70	20.35	18.10	23.00	23.50
ZN	51.58	34.11	47.81	46.28	23.22	23.32	42.33	10.00	16.00	26.00
SR	356.98	316.75	400.99	281.50	226.41	241.23	346.39	78.50	159.00	187.00
CU	60.44	63.55	24.46	36.69	1.86	14.85	33.17	3.20	3.20	59.00
CO	9.59	7.12	10.61	7.57	3.70	.92	12.41	2.60	4.00	1.70
NI	14.21	13.24	13.94	13.94	9.52	2.20	23.60	.00	4.20	.00
CR	27.46	26.17	27.26	21.54	15.16	5.12	36.77	2.10	3.70	2.10
V	99.25	71.77	78.58	66.62	36.27	25.52	77.96	9.10	19.00	5.90
U	3.90	3.10	3.20	3.90	4.90	3.90	5.10	3.80	5.70	1.00

	L									
	DRV-12A	DRV-12B	DRV-12C	DRV-12D	DRV-12E	DRV-16	DRV-34	DRV-35	DRV-58	DRV-59
SIO2	77.35	73.60	73.92	73.79	73.68	78.31	76.25	77.27	77.80	75.78
TIO2	.12	.29	.29	.28	.25	.09	.12	.13	.13	.15
AL2O3	12.35	13.50	13.35	13.29	13.63	12.20	12.86	12.21	12.35	12.30
FE2O3	.79	1.83	2.04	1.80	1.67	.38	.85	1.05	.86	.87
FEO	.00	.00	.00	.00	.00	.00	.00	.00	.00	.00
MNO	.03	.04	.03	.02	.04	.01	.03	.01	.04	.03
MGO	.00	.18	.60	.58	.41	.00	.24	.09	.00	.27
CAO	.71	1.40	1.27	1.18	1.31	.69	.45	.51	.54	.43
NA2O	3.67	3.61	3.20	3.42	3.39	3.58	4.01	3.72	3.74	3.54
K2O	5.43	5.02	5.30	5.57	5.55	5.39	5.50	5.56	5.01	5.40
P2O5	.01	.09	.04	.08	.04	.01	.02	.00	.00	.02
H2O-	.06	.07	.07	.06	.06	.04	.06	.07	.11	.16
LOI	.40	.53	.56	.67	.57	.25	.26	.45	.29	.35
TOTAL	100.92	100.13	100.67	100.74	100.60	100.95	100.65	101.07	100.87	99.30
BA	76.60	765.00	775.00	746.00	979.00	90.00	301.00	160.00	291.00	385.00
RB	324.00	245.00	241.00	242.00	292.00	337.00	288.00	145.85	225.00	255.00
ZR	81.76	133.07	126.78	120.93	151.14	84.00	95.82	93.08	102.60	117.85
NB	20.02	13.89	11.73	17.03	13.96	24.00	20.72	13.04	19.79	17.50
TH	44.26	31.69	31.13	31.09	28.36	36.40	25.55	31.94	20.92	23.45
PB	43.19	35.40	35.01	34.83	34.63	43.80	32.55	20.98	30.91	32.59
Y	17.40	20.52	19.59	24.81	24.84	31.40	34.75	14.08	35.26	28.56
ZN	3.50	17.16	9.90	10.65	11.32	4.20	10.75	5.42	10.42	8.09
SR	45.40	162.00	153.00	149.00	149.60	42.20	41.60	56.45	46.40	55.10
CU	.96	29.51	39.05	15.05	8.11	89.00	6.93	1.89	6.26	10.15
CO	.00	.00	.00	.00	.00	.00	.00	.00	.00	.00
NI	.00	.00	.00	.00	.00	.00	.00	.00	.00	.00
CR	.00	.00	.00	.00	.00	3.00	3.72	3.03	2.74	2.63
V	4.20	10.18	11.00	12.16	9.22	1.10	4.44	5.79	2.64	4.48
U	5.85	6.42	5.90	5.70	4.89	6.17	3.01	6.60	2.90	2.44

	L			HP							
	DRV-60	DRV-71	DRH-06	DRP-01	RT-01	RT-02	RT-03	DRP-01A	DRP-09	DRP-05	DRP-02
SIO2	76.83	77.39	73.74	67.46	67.31	67.04	66.94	69.01	69.03	71.89	68.10
TIO2	.23	.13	.19	.44	.48	.44	.44	.36	.37	.41	.41
AL2O3	12.87	12.14	14.09	15.17	15.70	15.00	15.15	15.12	14.97	13.89	15.96
FE2O3	1.25	.80	1.65	3.89	3.29	4.36	3.81	3.07	3.20	2.59	2.64
FEO	.00	.00	.00	.00	.00	.00	.00	.00	.00	.00	.00
MNO	.05	.03	.04	.05	.05	.05	.04	.04	.05	.05	.05
MGO	.13	.13	.28	1.65	1.35	1.13	1.24	1.35	.70	.59	.73
CAO	.40	.62	.53	3.09	2.79	2.41	3.17	3.10	2.78	1.89	2.40
NA2O	4.01	3.58	3.21	2.76	3.72	3.03	2.99	3.36	2.85	4.15	3.53
K2O	4.88	5.13	5.09	3.73	3.30	4.40	3.77	3.39	4.41	2.84	4.56
P2O5	.00	.02	.05	.13	.12	.10	.10	.12	.08	.07	.10
H2O-	.16	.10	.08	.03	.04	.04	.07	.11	.09	.04	.04
LOI	.20	.32	.80	1.61	1.85	1.16	1.58	1.34	1.40	2.05	.93
TOTAL	100.95	100.39	99.75	100.01	100.00	99.16	99.30	100.37	99.93	99.90	99.52
BA	445.00	84.50	659.00	1025.00	646.00	1010.00	956.00	1120.00	1040.00	2340.00	946.00
RB	184.00	314.71	279.00	134.00	155.00	210.00	181.00	98.86	123.00	81.00	190.00
ZR	186.00	87.26	121.00	161.00	141.06	146.00	142.00	91.33	130.00	271.00	174.00
NB	29.17	16.58	12.90	9.10	2.55	9.40	9.21	6.25	6.38	6.00	12.68
TH	29.33	37.74	18.70	11.40	13.51	18.76	12.37	9.94	25.41	9.63	18.10
PB	35.86	42.87	35.40	19.20	13.54	25.09	19.22	23.91	35.77	26.30	14.20
Y	48.13	16.16	13.90	17.10	5.20	12.09	11.52	6.86	11.16	15.20	25.00
ZN	12.31	8.46	21.30	34.00	43.00	52.00	30.00	24.00	22.00	86.00	48.00
SR	71.40	44.66	180.00	384.00	410.00	354.00	389.75	462.00	478.00	296.00	379.00
CU	13.19	2.11	5.65	88.00	799.00	1040.00	282.00	245.00	202.00	25.00	4.20
CO	.00	.00	2.43	9.00	4.56	3.82	6.43	1.32	5.56	6.05	8.10
NI	.02	.25	.00	9.50	11.20	6.93	9.82	6.01	7.25	25.00	6.10
CR	1.54	2.34	3.07	10.70	16.10	14.99	12.72	5.22	7.85	4.76	8.00
V	5.43	7.17	16.00	78.00	87.26	87.64	84.99	60.20	61.16	24.97	32.00
U	5.80	6.50	4.90	2.70	3.20	2.60	2.40	2.20	3.40	1.80	3.90

Appendix 4

RECALCULATED ANALYSES

The bulk major element analyses listed in Appendix 3 have been recalculated to 100 percent on a volatile free basis. Prior to recalculation Fe_2O_3 and FeO were estimated using the method of Le Maitre (1976b) which is as follows:

$$Ox = 0.93 - 0.0042SiO_2 - 0.022(Na_2O + K_2O) \quad \text{for volcanic rocks}$$

and

$$Ox = 0.88 - 0.0016SiO_2 - 0.027(Na_2O + K_2O) \quad \text{for plutonic rocks}$$

SiO_2, Na_2O and K_2O abundance data used are those in the bulk analyses

$Ox = FeO/(FeO + Fe_2O_3)$ weight percent

CIPW norms were determined from the recalculated analyses. All the samples listed in the following tables are in the same order as in Appendix 3.

	BA									
	DRL-49	DRL-50	DRL-65	DRL-74	DRL-42	DRL-57	DRL-43	DRL-45	DRL-48	DRL-67
SIO2	53.58	54.19	55.60	55.44	55.96	56.41	56.31	57.87	57.70	58.06
TIO2	.72	.73	.77	.74	.70	.71	.72	.74	.82	.83
AL2O3	14.97	14.94	15.00	15.13	14.60	15.35	14.81	15.30	15.96	15.87
FE2O3	3.31	3.33	3.30	3.31	3.39	3.11	3.40	3.24	3.40	3.00
FEO	6.03	5.76	5.63	5.16	5.19	5.05	5.32	5.00	4.90	4.46
MNO	.17	.16	.16	.15	.15	.14	.13	.14	.14	.12
MGO	8.41	8.54	8.00	7.43	8.07	7.15	8.28	6.25	5.68	5.67
CAO	9.58	8.71	7.92	8.03	7.21	8.04	6.56	7.22	6.68	7.20
NA2O	1.97	2.03	1.29	2.15	1.93	2.42	2.60	2.31	2.05	2.25
K2O	1.02	1.39	2.12	2.18	2.60	1.38	1.67	1.73	2.49	2.25
P2O5	.22	.22	.20	.29	.21	.24	.19	.20	.19	.28
H2O+	.00	.00	.00	.00	.00	.00	.00	.00	.00	.00
LOI	.00	.00	.00	.00	.00	.00	.00	.00	.00	.00
TOTAL	99.98	100.00	99.99	100.01	100.01	100.00	99.99	100.00	100.01	99.99
QZ	6.07	6.21	10.60	7.24	7.59	9.66	7.81	12.85	12.74	12.78
C	.00	.00	.00	.00	.00	.00	.00	.00	.00	.00
OR	6.03	8.21	12.53	12.08	15.36	8.15	9.87	10.22	14.71	13.30
AB	16.67	17.18	10.92	18.19	16.33	20.48	22.00	19.55	17.35	19.24
AN	28.99	27.55	28.88	25.19	23.50	26.95	23.81	26.27	26.99	26.56
DI-MO	7.14	5.94	3.80	5.32	4.55	4.75	3.13	3.44	2.05	3.06
DI-EN	4.85	4.11	2.62	3.71	3.22	3.29	2.21	2.34	1.39	2.12
DI-FS	1.73	1.34	.87	1.16	.94	1.07	.65	.83	.50	.69
DI	13.72	11.39	7.30	10.20	8.71	9.11	5.99	6.62	3.94	5.87
HY-EN	18.09	17.15	17.30	14.79	16.88	14.52	18.41	13.23	12.76	12.00
HY-FS	5.74	5.58	5.76	4.63	4.92	4.72	5.37	4.71	4.59	3.88
HY	21.83	22.73	23.07	19.42	21.79	19.24	23.78	17.94	17.35	15.88
OL-FO	.00	.00	.00	.00	.00	.00	.00	.00	.00	.00
OL-FA	.00	.00	.00	.00	.00	.00	.00	.00	.00	.00
OL	.00	.00	.00	.00	.00	.00	.00	.00	.00	.00
MT	4.80	4.83	4.78	4.80	4.92	4.51	4.93	4.70	4.93	4.35
IL	1.37	1.39	1.46	1.41	1.33	1.35	1.37	1.41	1.56	1.58
AP	.52	.52	.47	.69	.50	.57	.45	.47	.45	.66
D.I.	28.76	31.60	34.04	38.32	39.28	38.29	39.68	42.62	44.80	45.11

	BA					A				
	DRL-41	DRL-123	DRL-125	DRL-126	DRL-127	DRL-62	DRP-04	DRL-73	DRL-56	DRL-89
SIO2	59.29	57.12	57.57	56.72	59.35	59.61	61.35	59.09	60.04	61.38
TIO2	.84	.82	.83	.84	.78	.67	.67	.74	.66	.72
AL2O3	15.83	15.69	15.67	15.84	15.61	16.44	16.24	17.06	16.01	18.43
FE2O3	2.86	3.45	3.46	3.40	3.22	2.77	3.04	3.08	2.78	2.21
FEO	4.12	5.07	5.07	5.14	4.32	3.43	3.91	3.85	3.28	2.36
MNO	.10	.14	.14	.13	.15	.10	.16	.11	.10	.08
MGO	5.09	5.92	5.63	6.10	4.55	4.93	4.05	3.44	3.86	1.55
CAO	7.20	6.88	6.81	7.11	6.67	5.64	4.97	6.28	6.22	5.64
NA2O	1.92	2.34	2.27	2.39	1.60	2.61	1.87	3.08	4.84	3.54
K2O	2.76	2.35	2.34	2.14	3.60	3.57	3.57	2.99	1.92	3.77
P2O5	.20	.20	.20	.20	.15	.23	.17	.29	.27	.31
H2O+	.00	.00	.00	.00	.00	.00	.00	.00	.00	.00
LOI	.00	.00	.00	.00	.00	.00	.00	.00	.00	.00
TOTAL	100.01	99.98	99.99	100.01	99.98	100.00	100.00	100.01	99.98	100.00
QZ	14.86	10.68	12.03	10.05	15.27	11.41	18.85	11.53	7.70	12.76
C	.00	.00	.00	.00	.00	.00	.67	.00	.00	.00
OR	16.31	13.89	13.83	12.65	21.27	21.10	21.10	17.67	11.35	22.28
AB	16.25	19.80	19.21	20.22	13.54	22.09	15.82	26.06	40.95	29.05
AN	26.42	25.37	25.66	26.17	24.78	22.60	23.55	23.89	16.29	23.26
DI-MO	3.34	3.11	2.85	3.25	3.06	1.62	.00	2.24	3.35	1.12
DI-EN	2.29	2.11	1.91	2.21	2.06	1.17	.00	1.48	3.78	.75
DI-FS	.78	.77	.73	.80	.77	.30	.00	.60	1.11	.29
DI	6.41	5.99	5.48	6.26	5.89	3.09	.00	4.32	10.23	2.16
HY-EN	10.39	12.64	12.11	12.99	9.27	11.10	10.09	7.09	5.84	3.11
HY-FS	3.55	4.60	4.61	4.69	3.46	2.79	3.86	2.90	1.71	1.18
HY	13.94	17.24	16.73	17.67	12.73	13.90	13.95	9.99	7.55	4.30
OL-FO	.00	.00	.00	.00	.00	.00	.00	.00	.00	.00
OL-FA	.00	.00	.00	.00	.00	.00	.00	.00	.00	.00
OL	.00	.00	.00	.00	.00	.00	.00	.00	.00	.00
MT	4.15	5.00	5.02	4.93	4.67	4.02	4.41	4.47	4.03	3.20
IL	1.22	1.59	1.58	1.60	1.48	1.27	1.27	1.41	1.25	1.37
AP	.47	.47	.47	.47	.36	.54	.40	.69	.64	.73
D.I.	47.42	44.37	45.07	42.92	50.09	54.59	55.77	55.26	60.00	65.00

HAIH VOLCANICS	FRAGMENTALS	VOLATILE FREE							
	DRL-21	DRL-70	DRL-72	DR-08	DRL-81	DR-05-1	DRL-40B	DRL-22	DRL-77	DRL-15
SIO2	63.66	54.92	54.13	54.11	55.94	51.24	60.46	57.19	60.29	60.94
TIO2	.64	.67	.64	.74	.69	.97	.66	.79	.59	.80
AL2O3	16.32	13.83	13.27	13.92	14.81	19.48	13.75	17.67	18.83	17.58
FE2O3	2.29	3.31	3.18	3.38	3.27	3.77	3.52	3.01	1.80	2.55
FEO	2.61	5.96	5.45	5.10	5.18	4.76	5.88	3.98	2.28	2.90
MNO	.07	.16	.17	.17	.16	.20	.15	.13	.07	.11
MGO	3.44	10.24	12.45	11.36	7.00	7.61	5.97	3.90	3.80	4.24
CAO	4.24	7.68	6.79	6.10	8.63	3.92	6.68	6.83	6.57	3.74
NA2O	2.79	1.84	1.83	1.41	3.40	2.19	1.15	1.56	3.41	5.26
K2O	3.70	1.19	1.91	3.51	.68	5.61	1.54	4.64	2.15	1.69
P2O5	.24	.21	.19	.20	.25	.25	.24	.31	.21	.19
H2O-	.00	.00	.00	.00	.00	.00	.00	.00	.00	.00
LOI	.00	.00	.00	.00	.00	.00	.00	.00	.00	.00
TOTAL	100.00	100.01	100.01	100.00	100.01	100.00	100.00	100.01	100.00	100.00
QZ	18.84	7.49	2.76	2.11	6.52	.00	22.93	10.01	12.56	9.12
C	.59	.00	.00	.00	.00	3.28	.00	.00	.00	.75
OR	21.86	7.03	11.29	20.74	4.02	33.15	9.10	27.42	12.70	9.99
AB	23.61	15.57	15.48	11.93	28.77	18.53	9.73	13.20	28.85	44.51
AN	19.47	25.96	22.35	21.29	23.14	17.81	27.81	27.51	29.72	17.31
DI	.00	8.60	8.02	6.08	14.46	.00	3.04	3.50	1.19	.00
HY	10.54	28.80	33.85	31.08	16.47	9.33	20.48	11.79	10.76	12.66
OL	.00	.00	.00	.00	.00	10.01	.00	.00	.00	.00
MT	3.32	4.80	4.61	4.90	4.74	5.47	5.10	4.36	2.61	3.70
HM	.00	.00	.00	.00	.00	.00	.00	.00	.00	.00
IL	1.22	1.27	1.22	1.41	1.31	1.84	1.25	1.50	1.12	1.52
AP	.57	.50	.45	.47	.59	.59	.57	.73	.50	.45
D.I.	64.31	30.09	29.53	34.78	39.31	51.68	41.76	50.63	54.12	63.62
	DRL-23	DR-05-5	DR-02	DR-03	DRL-17	DR-07	DRL-19	DRL-20	DRL-40A	DRH-01
SIO2	61.81	58.62	62.60	62.05	67.29	66.15	66.00	63.53	64.33	65.59
TIO2	.75	.86	.59	.83	.47	.78	.70	.60	.79	.77
AL2O3	16.67	17.12	14.33	15.35	13.54	14.63	15.84	15.01	16.42	15.69
FE2O3	2.70	2.93	2.83	2.77	2.41	2.39	2.30	2.09	3.86	2.53
FEO	2.79	3.56	3.73	3.02	2.91	2.60	2.51	2.35	4.16	2.41
MNO	.10	.14	.11	.09	.07	.09	.10	.12	.03	.08
MGO	2.23	5.19	6.47	6.05	3.40	3.27	2.67	3.68	1.06	1.82
CAO	5.18	4.87	4.27	2.44	4.88	3.60	3.33	6.46	2.28	3.06
NA2O	3.92	2.48	1.93	2.81	4.24	3.44	2.86	1.47	5.12	3.61
K2O	3.59	4.02	2.99	4.39	.67	2.85	3.52	4.39	1.67	4.19
P2O5	.27	.20	.15	.19	.11	.20	.17	.30	.29	.24
H2O-	.00	.00	.00	.00	.00	.00	.00	.00	.00	.00
LOI	.00	.00	.00	.00	.00	.00	.00	.00	.00	.00
TOTAL	100.01	99.99	100.00	99.99	99.99	100.00	100.00	100.00	100.01	99.99
QZ	12.21	9.86	19.86	14.26	25.25	22.55	24.47	20.75	21.05	19.41
C	.00	.31	.51	1.99	.00	.00	1.68	.00	2.74	.23
OR	21.21	23.76	17.67	25.94	3.96	16.84	20.80	25.84	6.87	24.76
AB	33.17	20.99	16.33	23.78	35.88	29.11	24.20	12.44	43.32	30.55
AN	17.29	22.85	20.20	10.86	15.93	16.06	15.41	21.39	9.42	13.61
DI	5.33	.00	.00	.00	6.05	.39	.00	6.90	.00	.00
HY	4.84	15.88	19.86	17.12	8.28	9.64	8.39	7.72	5.84	5.75
OL	.00	.00	.00	.00	.00	.00	.00	.00	.00	.00
MT	3.91	4.25	4.10	4.02	3.49	3.47	3.33	3.03	5.60	3.67
HM	.00	.00	.00	.00	.00	.00	.00	.00	.00	.00
IL	1.42	1.63	1.12	1.58	.89	1.48	1.33	1.14	1.50	1.46
AP	.64	.47	.36	.45	.26	.47	.40	.71	.69	.57
D.I.	66.59	54.60	53.86	63.98	65.09	68.50	69.47	59.13	74.25	74.72

	HAIH VOLCANICS	FRAGMENTALS	VOLATILE FREE						
	DRL-11	DRA-01	DR-05-2	DR-05-6	DR-06	DR-04	DRL-14	DR-05-3	DR-05-4
SIO2	67.88	63.05	66.36	64.51	69.57	71.11	71.10	70.21	69.81
TIO2	.68	.95	.77	.63	.63	.72	.59	.76	.77
AL203	14.42	17.22	14.75	14.16	14.32	13.14	13.60	12.81	13.29
FE203	2.22	2.48	2.22	2.65	1.95	1.85	1.92	1.94	1.93
FEO	2.24	2.14	2.38	3.02	1.99	1.93	1.77	2.16	2.10
MNO	.08	.08	.10	.13	.07	.08	.07	.09	.09
MGO	2.27	1.54	3.61	6.08	1.35	2.06	1.39	2.42	2.33
CAO	3.40	2.73	3.15	2.44	3.84	3.22	2.32	4.11	4.04
NA20	5.58	2.25	3.55	2.41	4.47	4.30	6.43	3.21	3.05
K20	1.06	7.25	2.92	3.83	1.64	1.45	.63	2.11	2.40
P205	.17	.29	.17	.14	.17	.15	.17	.17	.18
H20-	.00	.00	.00	.00	.00	.00	.00	.00	.00
LOI	.00	.00	.00	.00	.00	.00	.00	.00	.00
TOTAL	100.00	99.98	99.98	100.00	100.00	100.01	99.99	99.99	99.99
QZ	21.57	14.68	22.22	20.77	27.83	31.15	25.22	32.02	31.47
C	.00	1.40	.43	1.95	.00	.00	.00	.00	.00
OR	6.26	42.84	17.26	22.63	9.69	8.57	3.72	12.47	14.18
AB	47.22	19.04	30.04	20.39	37.82	36.39	54.41	27.16	25.81
AN	11.17	11.65	14.52	11.19	14.17	12.27	6.39	14.31	15.48
DI	3.65	.00	.00	.00	3.03	2.16	3.19	3.94	2.68
HY	5.23	4.30	10.44	17.70	3.05	5.08	2.76	5.43	5.69
OL	.00	.00	.00	.00	.00	.00	.00	.00	.00
MT	3.22	3.60	3.22	3.84	2.83	2.68	2.78	2.81	2.80
HM	.00	.00	.00	.00	.00	.00	.00	.00	.00
IL	1.29	1.80	1.46	1.20	1.20	1.37	1.12	1.44	1.46
AP	.40	.69	.40	.33	.40	.36	.40	.40	.43
D.I.	75.05	76.56	69.52	63.80	75.35	76.10	83.35	71.65	71.46

	T					G				
	DRV-73	DRV-75	DRV-49	DRV-C	DRV-55	DRV-15	DRV-15A	DRV-15C	DRV-15D	DRV-15E
SIO2	60.34	63.45	60.85	60.77	62.95	66.41	66.03	66.49	65.97	62.00
TIO2	1.03	.73	.68	.53	.70	.55	.53	.56	.58	.75
AL2O3	16.49	17.02	18.49	17.07	16.82	15.27	15.37	15.44	15.29	16.36
FE2O3	2.73	1.93	1.82	2.20	2.08	1.84	1.72	1.75	1.83	2.33
FEO	4.37	3.26	2.88	4.32	2.96	2.52	2.38	2.51	2.57	3.41
MNO	.13	.08	.09	.12	.08	.08	.07	.07	.07	.10
MGO	2.81	2.20	1.81	3.59	2.17	1.83	2.53	1.89	2.28	3.06
CAO	5.40	5.38	6.56	6.61	4.83	3.88	3.86	4.08	3.95	5.19
NA2O	3.39	3.15	2.83	2.93	3.49	3.03	3.22	3.14	3.09	3.65
K2O	3.01	2.59	3.78	1.72	3.65	4.39	4.11	3.89	4.16	3.69
P2O5	.32	.22	.21	.13	.26	.18	.18	.18	.20	.26
H2O-	.00	.00	.00	.00	.00	.00	.00	.00	.00	.00
LOI	.00	.00	.00	.00	.00	.00	.00	.00	.00	.00
TOTAL	100.02	100.01	100.00	99.99	99.99	99.98	100.00	100.00	99.99	100.01
QZ	13.11	19.64	13.46	16.29	15.20	21.02	19.60	21.75	20.28	14.81
C	.00	.00	.00	.00	.00	.00	.00	.00	.00	.00
OR	17.79	15.31	22.34	10.16	21.57	25.94	24.29	22.99	24.58	21.37
AB	28.69	26.65	23.95	24.79	29.53	25.64	27.25	26.57	26.15	25.81
AN	20.89	24.65	26.58	28.35	19.45	15.10	15.35	16.55	15.56	20.32
DIWO	1.59	.25	1.92	1.50	1.17	1.24	1.10	1.05	1.14	1.56
DIEN	.94	.15	1.12	.89	.73	.77	.75	.66	.75	1.01
DIFS	.58	.09	.70	.54	.37	.40	.26	.33	.31	.45
DI	3.10	.49	3.74	2.93	2.28	2.41	2.11	2.04	2.20	3.01
HYEN	6.06	5.33	3.39	8.05	4.67	3.79	5.55	4.05	4.93	6.61
HYFS	3.73	3.25	2.13	4.92	2.34	1.95	1.94	2.04	2.07	2.62
HY	9.80	8.58	5.51	12.98	7.01	5.74	7.49	6.09	7.00	9.55
OLFO	.00	.00	.00	.00	.00	.00	.00	.00	.00	.00
OLFA	.00	.00	.00	.00	.00	.00	.00	.00	.00	.00
OL	.00	.00	.00	.00	.00	.00	.00	.00	.00	.00
MT	3.96	2.80	2.64	3.19	3.02	2.67	2.49	2.54	2.65	3.23
IL	1.96	1.39	1.29	1.01	1.33	1.04	1.01	1.06	1.10	1.42
AP	.76	.52	.50	.31	.62	.43	.43	.43	.47	.62
D.I.	59.58	61.60	59.75	51.24	66.30	72.60	71.13	71.31	71.01	61.89

	G							AD		
	DRV-15F	DRV-09	DRV-32	DRV-33	DRV-38	DRV-57	DRV-39	DRV-01	DRV-02	DRV-03
SIO2	66.15	65.88	67.11	64.65	65.65	64.94	67.78	70.07	69.36	66.10
TIO2	.53	.44	.47	.65	.58	.80	.44	.50	.51	.75
AL2O3	15.78	15.21	15.07	16.72	15.43	16.07	15.40	14.30	15.05	15.42
FE2O3	1.80	1.85	1.73	1.69	2.02	2.01	1.67	1.34	1.39	2.05
FEO	2.31	2.61	2.78	2.17	3.07	2.87	2.24	1.70	1.83	2.81
MNO	.07	.08	.09	.07	.10	.10	.06	.07	.07	.08
MGO	2.14	2.41	2.60	1.73	2.59	2.09	1.09	1.36	1.07	1.40
CAO	3.52	4.05	4.07	4.07	4.07	3.72	3.50	2.69	2.98	3.70
NA2O	3.31	2.73	2.46	3.13	2.88	2.98	3.22	3.11	2.93	3.00
K2O	4.20	4.61	3.52	4.86	3.48	4.17	4.49	4.72	4.68	4.64
P2O5	.17	.12	.11	.25	.14	.25	.10	.14	.13	.22
H2O-	.00	.00	.00	.00	.00	.00	.00	.00	.00	.00
LOI	.00	.00	.00	.00	.00	.00	.00	.00	.00	.00
TOTAL	99.98	99.99	100.01	99.99	100.01	100.00	99.99	100.00	100.00	100.00
QZ	19.78	20.00	25.65	16.79	22.02	20.14	22.58	26.20	26.11	21.55
C	.00	.00	.08	.00	.00	.49	.00	.00	.06	.00
OR	24.82	27.24	20.80	28.72	20.56	24.64	26.53	27.89	27.66	26.83
AB	28.01	23.10	20.82	26.49	24.37	25.22	27.25	26.32	24.79	24.71
AN	15.80	15.63	19.47	17.22	18.90	16.82	14.31	11.12	13.93	15.56
DIWO	.23	1.53	.00	.56	.16	.00	1.00	.55	.00	.57
DIEN	.16	.99	.00	.37	.10	.00	.54	.37	.00	.32
DIFS	.06	.44	.00	.14	.05	.00	.42	.14	.00	.22
DI	.45	2.97	.00	1.08	.31	.00	1.97	1.05	.00	1.11
HYEN	5.17	5.01	6.48	3.93	6.35	5.21	2.17	3.02	2.66	3.16
HYFS	1.95	2.24	3.07	1.50	3.15	2.47	1.69	1.18	1.50	2.17
HY	7.12	7.26	9.54	5.44	9.50	7.68	3.86	4.20	4.16	5.34
OLFO	.00	.00	.00	.00	.00	.00	.00	.00	.00	.00
OLFA	.00	.00	.00	.00	.00	.00	.00	.00	.00	.00
OL	.00	.00	.00	.00	.00	.00	.00	.00	.00	.00
MT	2.61	2.68	2.51	2.45	2.93	2.91	2.42	1.94	2.02	2.97
IL	1.01	.84	.89	1.23	1.10	1.52	.84	.95	.97	1.42
AP	.40	.28	.26	.59	.33	.59	.24	.33	.31	.52
D.I.	72.60	70.34	67.26	71.99	66.95	70.00	76.36	80.41	78.56	73.09

	L DRV-12A	DRV-12B	DRV-12C	DRV-12D	DRV-12E	DRV-16	DRV-34	DRV-35	DRV-58	DRV-59
SIO2	77.03	74.02	73.97	73.86	73.77	77.81	76.27	76.89	77.69	76.74
TIO2	.12	.29	.29	.28	.25	.09	.12	.13	.13	.15
AL203	12.30	13.58	13.36	13.30	13.65	12.12	12.70	12.15	12.18	12.46
FE203	.36	.82	.90	.82	.76	.17	.40	.49	.39	.40
FEO	.38	.92	1.03	.88	.82	.18	.40	.50	.42	.43
MNO	.03	.04	.03	.02	.04	.01	.03	.01	.04	.03
MGO	.00	.18	.60	.58	.41	.00	.24	.09	.00	.27
CAO	.71	1.41	1.27	1.18	1.31	.69	.44	.51	.53	.44
NA2O	3.65	3.63	3.20	3.42	3.39	3.56	3.96	3.70	3.69	3.59
K2O	5.41	5.05	5.30	5.57	5.56	5.36	5.43	5.53	4.94	5.47
P2O5	.01	.06	.04	.08	.04	.01	.02	.00	.00	.02
H2O-	.00	.00	.00	.00	.00	.00	.00	.00	.00	.00
LOI	.00	.00	.00	.00	.00	.00	.00	.00	.00	.00
TOTAL	100.00	100.00	99.99	99.99	100.00	100.00	100.01	100.00	100.01	100.00
QZ	33.97	30.35	31.24	29.43	29.36	35.57	31.35	33.33	36.16	33.58
C	.00	.00	.15	.00	.00	.00	.00	.00	.00	.00
OR	31.97	29.84	31.32	32.91	32.86	31.67	32.09	32.68	29.19	32.32
AB	30.89	30.72	27.08	28.94	28.69	30.12	33.51	31.31	31.22	30.58
AN	1.20	5.65	6.04	4.49	5.61	1.26	.84	.21	2.08	1.73
DIWO	.23	.32	.00	.35	.26	.05	.51	.54	.23	.13
DIEN	.00	.13	.00	.24	.16	.00	.33	.22	.00	.00
DIFS	.26	.18	.00	.09	.09	.06	.14	.32	.26	.04
DI	.49	.63	.00	.68	.51	.11	.98	1.08	.49	.26
HYEN	.00	.31	1.49	1.21	.86	.00	.27	.00	.00	.58
HYFS	.00	.43	.72	.43	.65	.00	.12	.00	.05	.23
HY	.00	.74	2.22	1.63	1.31	.00	.39	.00	.05	.81
OLFO	.00	.00	.00	.00	.00	.00	.00	.00	.00	.00
OLFA	.00	.00	.00	.00	.00	.00	.00	.00	.00	.00
OL	.00	.00	.00	.00	.00	.00	.00	.00	.00	.00
MT	.52	1.19	1.30	1.19	1.10	.25	.58	.71	.57	.58
IL	.23	.55	.55	.53	.47	.17	.23	.25	.25	.28
AP	.02	.14	.09	.19	.09	.02	.05	.00	.00	.05
D.I.	96.83	90.90	89.64	91.29	90.90	97.36	96.95	97.32	96.58	96.29

	L DRV-60	DRV-71	DRH-06	HP DRP-01	RT-01	RT-02	RT-03	DRP-01A	DRP-09	DRP-05	DRP-02
SIO2	76.39	77.45	74.65	68.75	68.75	68.62	68.72	69.90	70.26	73.69	69.21
TIO2	.23	.13	.19	.45	.49	.45	.45	.36	.38	.42	.42
AL203	12.80	12.15	14.26	15.46	16.04	15.35	15.55	15.31	15.24	14.24	16.22
FE203	.57	.36	.73	1.50	1.32	1.80	1.50	1.20	1.31	1.05	1.15
FEO	.61	.39	.85	2.22	1.84	2.40	2.17	1.71	1.76	1.43	1.42
MNO	.05	.03	.04	.05	.05	.05	.04	.04	.05	.05	.08
MGO	.13	.13	.28	1.68	1.38	1.16	1.27	1.37	.71	.55	.74
CAO	.40	.62	.54	3.15	2.85	2.47	3.25	3.14	2.83	1.32	2.44
NA2O	3.99	3.58	3.25	2.81	3.80	3.10	3.07	3.40	2.90	4.25	3.59
K2O	4.85	5.13	5.15	3.80	3.37	4.50	3.87	3.43	4.49	2.91	4.63
P2O5	.00	.02	.05	.13	.12	.10	.10	.12	.08	.07	.10
H2O-	.00	.00	.00	.00	.00	.00	.00	.00	.00	.00	.00
LOI	.00	.00	.00	.00	.00	.00	.00	.00	.00	.00	.00
TOTAL	100.02	99.99	99.99	100.00	100.01	100.00	99.99	99.98	100.01	99.98	100.00
QZ	33.41	35.63	34.28	27.98	25.21	25.59	26.53	27.82	28.58	33.95	24.05
C	.26	.00	2.48	1.31	1.25	1.13	.64	.58	.66	1.47	1.11
OR	28.66	30.31	30.43	22.46	19.91	26.59	22.87	20.27	26.53	17.20	27.36
AB	33.76	30.29	27.50	23.78	32.15	26.23	25.98	28.77	24.54	35.96	30.38
AN	1.98	1.93	2.35	14.78	13.35	11.60	15.47	14.79	13.52	6.09	11.45
DIWO	.00	.42	.00	.00	.00	.00	.00	.00	.00	.00	.00
DIEN	.00	.23	.00	.00	.00	.00	.00	.00	.00	.00	.00
DIFS	.00	.16	.00	.00	.00	.00	.00	.00	.00	.00	.00
DI	.00	.85	.00	.00	.00	.00	.00	.00	.00	.00	.00
HYEN	.32	.10	.70	4.18	3.44	2.89	3.16	3.41	1.77	1.37	1.84
HYFS	.36	.06	.72	2.19	1.57	2.27	2.08	1.63	1.62	1.16	1.11
HY	.69	.17	1.42	6.37	5.01	5.16	5.24	5.04	3.38	2.53	2.96
OLFO	.00	.00	.00	.00	.00	.00	.00	.00	.00	.00	.00
OLFA	.00	.00	.00	.00	.00	.00	.00	.00	.00	.00	.00
OL	.00	.00	.00	.00	.00	.00	.00	.00	.00	.00	.00
MT	.83	.52	1.06	2.17	1.91	2.61	2.17	1.74	1.90	1.52	1.67
IL	.44	.25	.36	.85	.93	.85	.85	.68	.72	.80	.84
AP	.00	.05	.12	.31	.28	.24	.24	.28	.19	.17	.24
D.I.	95.83	96.24	92.21	74.21	77.28	78.42	75.38	76.86	79.65	87.01	81.79

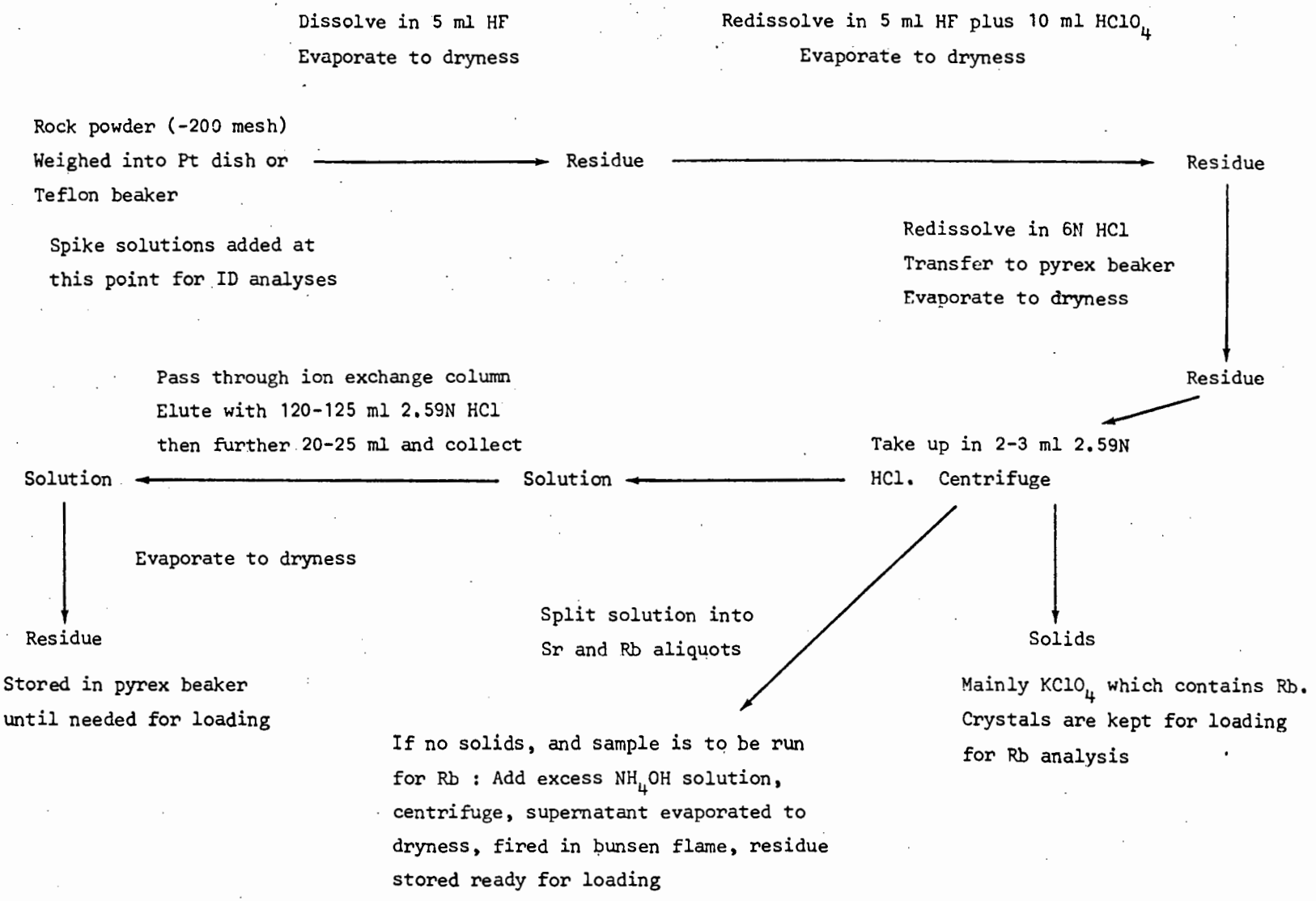

Fig. A5.1. Sample preparation for Sr and Rb analysis by mass spectrometry

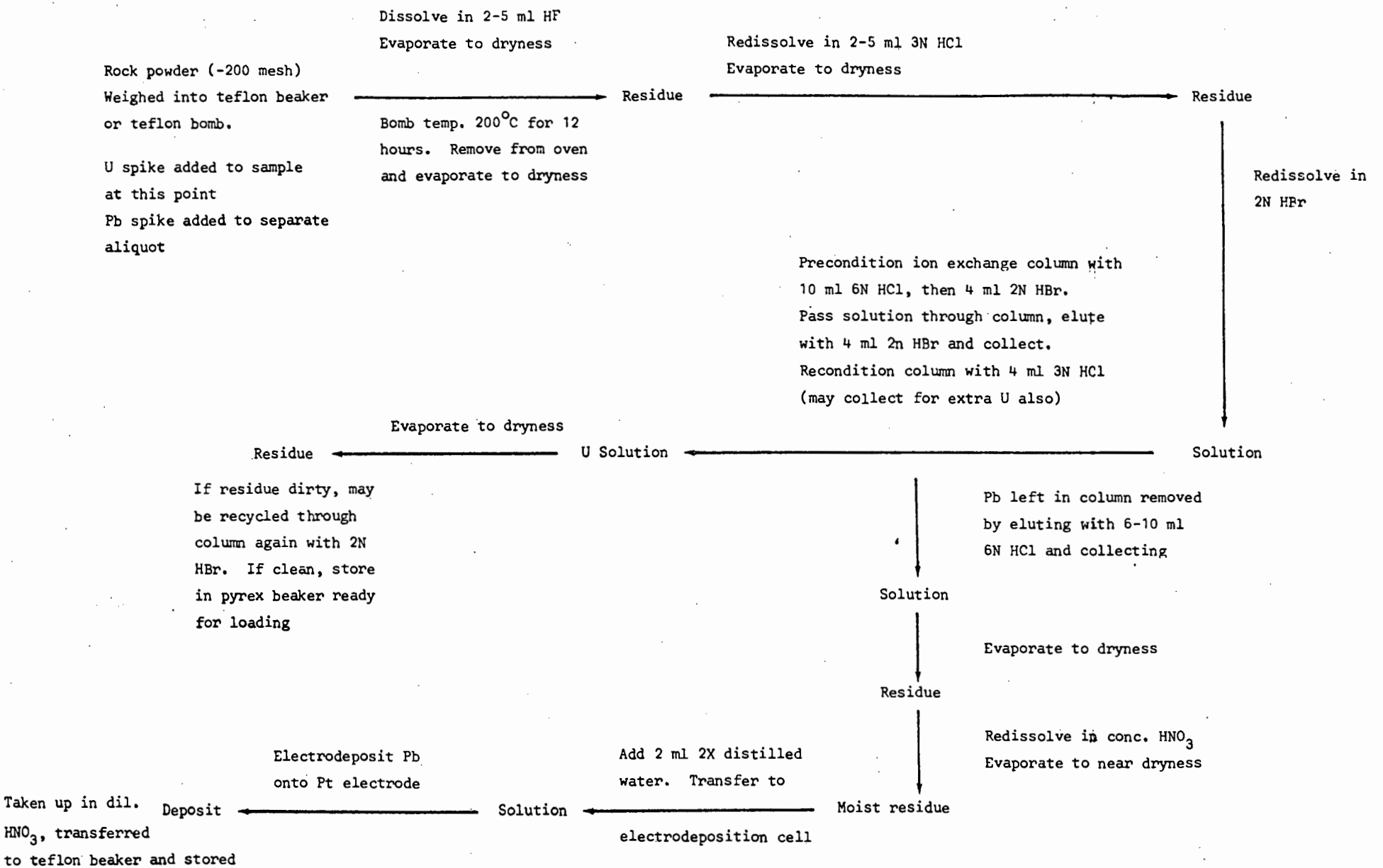

Fig. A5.2. Sample preparation for U and Pb analysis by mass spectrometry

Th/U ratio of 4, since the data by XRF was available. As it worked out, most of the samples were overspiked, but not to the extent that the U^{238}/U^{235} ratio of the mixture approached that of the pure spike. Six samples were analysed for Pb in order to provide checks for the XRF data.

A5.3. Instrument specifications

Details of the 3 mass spectrometers used during the present study are given in Table A5.1. Only the MAT CH4 was used during 1974, all the data being read from chart recordings. In 1975 the computer-controlled Micromass 30 and "DTM-BPI" instruments were available and the resulting data is more precise than that obtained from the MAT CH4. The increased precision is simply due to the ease of collecting multiple blocks of peak and background data with computer control. Operating conditions used during the analytical work are summarised in Tables A5.2. and A5.3. The final residue was taken up with acid or triple-distilled water using a micropipette that was discarded after each load. The solution was transferred to the filament by gently blowing through the opposite end of the pipette. Separate micropipettes were used for precoating the filament where necessary.

A5.3. Isotope Dilution - Data reduction

Spike equation for Rb

The spike equation was used for (1) estimating the amount of sample necessary to attain a Rb^{85}/Rb^{87} ratio of about 1, when 1,0 g of spike solution was added, and (2) calculating the concentration when the isotopic ratio was actually measured with a mass spectrometer. The following equation was used:

$$C_r = \frac{W_s \times C_s}{W_r} \times \frac{(85/87)_m - (85/87)_s}{(85/87)_r - (85/87)_m}$$

Table A5.1. Details of mass spectrometers used during the study

INSTRUMENT	RADIUS OF CURVATURE	FIELD SECTOR	SOURCE	ACCELERATING POTENTIAL
VG Micromass 30	30 cm	90°	Surface ionisation from Re or Ta filament. Equipped for 1, 2 or 3 filament runs	8000 V
Atlas-Varian MAT CH4	20 cm	60°	Same as above	3000 V
"DTM - BPI"	9 in	60°	Same as above	3600 V for Sr, Rb 3800 V for U

MAGNET	COLLECTION, AMPLIFICATION	DATA RECORDING	DATA REDUCTION
Hard wired field control Automatic peak switching	Faraday Cup, Cary VRE	Digital voltmeter to:- visual display, printer, computer memory	On line mini-computer (NOVA 2) utilising BASIC software and NOVA ASSEMBLER drivers
Current control Manual peak switching	Same as above	Chart recorder with X10 expanded scale	Net peaks read off charts and input to minicomputer (NOVA 1200) utilising BASIC software
Computer driven field control and peak switching	Same as above	Digital voltmeter to:- visual display, chart recorder, computer memory	On line minicomputer (NOVA 1200) utilising BASIC software and NOVA ASSEMBLER drivers

Table A5.3. Details of isotopic data collection

INSTRUMENT	RUN	BLOCK SEQUENCE	AVERAGE BLOCKS	INTERGRATION TIME	DELAY
VG Micromass 30	Nat. Sr	B-85-86-87-88-B-B	80	5 sec	0.3 sec
	Nat. Pb	208-207-206-B-204-B	80	5 sec	0.3 sec
	Spiked Pb	208-207-206-B-204-B	40	5 sec	0.3 sec
MAT CH4	Nat. Sr	B at start and at end 85 at start and end 88-87-86-87-88	20	Manual control About 5-6 sec	-
	Spiked Sr	B at start and end 88-86-84-86-88	20	As above	-
	Spiked Rb	B at start and end 85-87-85	20	As above	-
"DTM - BPI"	Spiked Sr	B at start and end 86-87-88	40	15 sec	4 sec
	Spiked Rb	B at start and end 85-87	40	15 sec	4 sec
	Spiked U	B at start and end 235-238	40	15 sec	4 sec

Table A5.4. Data obtained for the Sr and Pb standards during the present study

EIMER & AMEND $SrCO_3$ STANDARD

Instrument: MAT CH4 with chart recorder (1974)

October (1)	0.70808 ± 0.00008
October (2)	0.7079 ± 0.0001
November	0.7080 ± 0.0001

Instrument: MICROMASS 30 with computer control (1975)

October	0.70806 ± 0.00003
November	0.70808 ± 0.00004
December	0.70805 ± 0.00002

NBS 981 Pb STANDARD

Instrument: MICROMASS 30 with computer control (1975)

	(Pb^{208}/Pb^{204})	(Pb^{207}/Pb^{204})	(Pb^{206}/Pb^{204})
Adopted Values	36.721	15.491	16.938
November (1)	36.469 ± 0.005	15.413 ± 0.002	16.870 ± 0.002
% MF	0.17	0.17	0.20
November (2)	36.512 ± 0.005	15.428 ± 0.002	16.883 ± 0.002
% MF	0.14	0.14	0.16
December	36.388 ± 0.008	15.383 ± 0.004	16.838 ± 0.003
% MF	0.23	0.23	0.30
January	36.540 ± 0.010	15.433 ± 0.005	16.897 ± 0.006
% MF	0.12	0.13	0.12

$$\therefore \quad Sr^{total}/Sr^{86}(ppm) = (84/86)_{atomic} \times 84/86 + (87/86)_{atomic} \times 87/86 + (88/86)_{atomic} \times 88/86 + 1$$

Substituting natural values for ratios, and reducing,

$$Sr^{total}/Sr^{86}(ppm) = 0,0557 + (87/86)_{atomic} \times 1,0116 + 8,5698$$

$$= 9,6255 + (87/86)_{atomic} \times 1,0116$$

$$Rb^{total}(ppm) = Rb^{85} + Rb^{87}$$

$$\therefore \quad Rb^{total}/Rb^{87}(ppm) = Rb^{85}/Rb^{87} + 1$$

$$\text{if} \quad (Rb^{85}/Rb^{87})_{atomic} = 2,600$$

$$\text{then} \quad Rb^{total}/Rb^{87}(ppm) = 2,600 \times 85/87 + 1$$

$$= 3,5402$$

combining the two expression,

$$(Rb^{total}/Rb^{87})/(Sr^{total}/Sr^{86})_{ppm} = \frac{3,5402}{9,6255 + (87/86)_{atomic} \times 1,0116}$$

rearranging,

$$(Rb^{87}/Sr^{86})_{ppm} = Rb^{total}/Sr^{total} \times \frac{9,6255 + (87/86)_{atomic} \times 1,0116}{3,5402}$$

$$= (Rb/Sr)_{ppm} \times (2,7189 + 0,2857 \times (87/86)_{atomic}$$

converting to atomic ratio,

$$(Rb^{87}/Sr^{86})_{atomic} = (Rb/Sr)_{ppm} \times (2,688 + 0,2824 \times (87/86)_{atomic}$$

The formula above was used to calculate the atomic ratio by substituting the Rb/Sr ratio determined by XRF and the (Sr^{87}/Sr^{86}) atomic ratio as determined in the natural Sr run.

A5.7. Comparison between XRF and ID analyses

All samples used for geochronology were first analysed for Rb and Sr

Table A5.5. Comparison between Sr and Rb abundance data obtained by X-Ray Fluorescence (XRF) and Isotope Dilution (ID). Differences (Δ) are expressed as a percentage of the ID data.

STANDARD	ELEMENT	UCT	ID	Δ (%)
PG-11	Sr	129	130	0.8
	Rb	241	242	0.4
	Rb/Sr	1.853	1.858	0.3
KL-11	Sr	201	203	1.0
	Rb	14.0	14.7	5.0
	Rb/Sr	0.070	0.073	4.3
M-38	Sr	76.0	76.2	0.3
	Rb	205	210	2.4
	Rb/Sr	2.697	2.722	0.9
OK-272	Sr	108	108	0.0
	Rb	86.0	86.0	0.0
	Rb/Sr	0.796	0.797	0.0
SAMPLE				
DRV-15E	Sr	584	593	1.5
	Rb	125	126	0.8
	Rb/Sr	0.214	0.213	0.5
DRV-16	Sr	42.2	42.7	1.2
	Rb	337	344	1.9
	Rb/Sr	7.986	8.045	0.7
DRL-45	Sr	483	465	3.7
	Rb	57.2	56.8	0.7
	Rb/Sr	0.123	0.118	4.2
DRL-78B	Sr	466	466	0.0
	Rb	119	117	1.7
	Rb/Sr	0.255	0.251	1.6
DRL-127	Sr	423	431	1.9
	Rb	179	179	0.0
	Rb/Sr	0.423	0.415	1.9

by XRF. In order to check that the Rb/Sr ratios obtained by XRF were accurate, a few samples were analysed for Rb and Sr by ID. The absolute Rb and Sr concentrations and the Rb/Sr ratio of the selected samples are listed in Table A5.5. All nine samples listed in the table were analysed by XRF using USGS standards for calibration. Sr and Rb values adopted for these standards are listed in Table A5.6., together with values obtained in other laboratories.

In view of the close agreement between the adopted Sr and Rb abundances in the USGS standard with those obtained by other laboratories, the XRF data listed in Table A5.5. can be considered satisfactory. The information summarised in Tables A5.5. and A5.6. can be used as evidence to justify the use of XRF data in all the isochron diagrams presented in Chapter 3. Six samples were analysed for Pb by ID in order to provide checks for the XRF data. ID and XRF analyses are given in Table A5.7. and their close agreement suggests that the XRF technique has probably produced reasonably accurate data.

Table A5.7. Comparison between ID and XRF Pb analyses. Differences expressed as a percentage of ID data.

Sample	ID	XRF	Δ(%)
DRL-41	27.5	27.3	.7
DRL-45	14.9	14.3	4.0
DRL-48	16.9	17.1	1.2
DRL-49	15.0	15.4	2.7
DRL-50	15.1	16.6	9.9
DRL-65	20.3	22.9	12.8

A5.8. Quality of Th and U data

All Th data used for geochronology were obtained by XRF, using four USGS standards; G-1, G-2, GSP-1 and AGV-1. Adopted Th values for these standards are listed in Table A5.8., together with recommended values from

Table A5.8. Th abundance data for standards and comparison between XRF and data obtained by Delayed Neutron Activation (DNA).

STANDARD CALIBRATION

STANDARD	UCT	RECOMMENDED	SOURCE
G-1	50.0	52	Fleischer (1969)
G-2	24.0	24	Doe (USGS Private Newsletter)[2]
GSP-1	104	102-111 (inhomogeneous)	Doe (USGS Private Newsletter)
AGV-1	6.32	6.32	Doe (USGS Private Newsletter)

DATA FOR OTHER KNOWN STANDARDS

STANDARD	UCT	ADOPTED VALUE	SOURCE
BCR-1	6.3±0.8[1]	5.95±0.12	Doe (USGS Private Newsletter)
W-1	2.8±0.8	2.4	Fleischer (1969)
PG-11	60.8±0.9	63.0	XRF by Cherry et al (1970)
		63.1	Gamma Spectroscopy by Cherry et al (1970)

COMPARISON BETWEEN XRF AND DELAYED NEUTRON ACTIVATION

SAMPLE	UCT	HARWELL[3]	PELINDABA[4]
VT-38	68.9±0.7	67.4	67.5
VT-40	44.3±0.7	43.3	43.9
VT-41	30.6±0.6	22.9	28.1
VT-505	7.6±0.5	7.8	8.8
VT-524	8.9±0.7	9.3	
KK-9	6.4±0.7	8.4	
KK-11	12.0±0.6	11.1	
VT-121	3.0±0.6	3.8	

1 = Errors cited for UCT analyses are 2 sigma standard counting error

2 = Newsletter dated December 1975.

3 = Data supplied by R.J.Hart (Ph.D. thesis in preparation). Technique after Gale (1967).

4 = Data supplied by M.C.B.Smit, using techniques described by him in an AEB internal report.

various sources. Data obtained for BCR-1 and W-1 are also included. Other checks for accuracy include the comparison between XRF and Delayed Neutron Activation (DNA) and between XRF and Gamma Spectroscopy (all included in Table A5.8.).

U was analysed by ID for U-Pb total rock dating, since the low levels involved precluded any attempt by XRF. In view of the considerable amount of work necessary for producing U data by ID, the 18 samples involved were analysed by a more rapid method - Delayed Neutron Activation (Gale, 1967). The technique used has not been published formally but is contained in an unpublished internal AEB report by M.C.B. Smit. The data are listed in Table A5.9. and show reasonable agreement, considering the DNA data is rather imprecise (estimated precision is between 10-15%, Smit, pers. comm., 1975). Although the DNA method is very rapid and reasonably accurate, the 10-15% precision imposes severe limitations to its applicability for geochronology. In this respect, ID is the best suited technique for U analyses of rocks.

A5.9. Estimates of Uncertainty

The uncertainities included in the tables of Sr and Pb isotopic ratios, are two standard deviations, determined from data collected during the analytical run. The figures cited depend entirely on the stability during the analytical run and the more stable the run, the lower the uncertainty. The overall precision as determined by replicate analyses is probably a more constant figure, although insufficient replicate data exist to accurately estimate this (for the Micromass at least). To be conservative, the precision is taken as something of the order of the worst runs, which results in a precision of 0.014% relative for Sr^{87}/Sr^{86}, 0.03% relative for Pb^{208}/Pb^{204} and 0.1% relative for Pb^{207}/Pb^{204} and Pb^{206}/Pb^{204}. The data correspond to absolute precisions of $\pm$ 0.0001 for Sr^{87}/Sr^{86} and $\pm$ 0.02 for all three Pb isotopic ratios.

Table A5.9. Comparison between isotope dilution (ID) and delayed neutron activation (DNA) techniques for the analysis of U in total rock samples

SAMPLE	B.P.I.(ID)	PELINDABA (DNA)	Δ(%)
DRL-41	0.96	1.2	25.0
DRL-45	1.06	1.1	3.8
DRL-48	1.09	1.0	8.3
DRL-49	0.67	0.4	40.3
DRL-50	0.65	0.6	7.7
DRL-65	0.95	0.9	5.3
DRL-92	3.93	4.3	9.4
DRL-93	3.88	3.9	0.5
DRL-107	7.48	8.0	7.0
DRL-113	1.92	1.8	6.3
DRL-121	5.00	5.6	12.0
DRL-122	5.29	5.3	0.2
DRV-12A	5.85	6.4	9.4
DRV-12B	6.42	7.1	14.1
DRV-12E	4.89	5.2	19.2
DRV-16	6.17	7.6	13.2
DRV-59	2.44	2.5	2.5

B.P.I. = Bernard Price Institute for Geophysical Research
PELINDABA = Chemistry Division, Atomic Energy Board, Pelindaba
Δ = difference expressed as a percentage of the ID data

In the case of the Sr^{87}/Sr^{86} ratio, most of the measured values fall in a narrow range between 0,7 and 1,0, so a constant uncertainty may be taken (cf. Brooks et al., 1972). The accuracy of the Sr^{87}/Sr^{86} ratios can be estimated by inspecting the data for the Eimer and Amend Sr standard (Table A5.4.). The adopted value for the Eimer and Amend standard is 0,70800 (cf. O'Nions and Pankhurst, 1974), so the data obtained during the present

study indicate that no normalisation is necessary and that the accuracy is satisfactory. The error in the Sr^{87}/Sr^{86} ratio may be considered to be equivalent to the overall precision of .014% relative.

With regards Pb isotopes, the accuracy of the data is difficult to estimate, because (1) the three ratios (206/204, 207/204, 208/204) are subject to radiogenic modification and (2) their measurement is subject to mass fractionation. Since the difference between the adopted values for the NBS 981 Pb standard and the measured values are ascribed to mass fractionation, no estimation of accuracy can be made. At present, none of the samples have been analysed in another laboratory, so the only guideline is that of the values obtained for the USGS rock standard BCR-1. Data obtained (Welke pers. comm., 1975) for BCR-1 are as follows:

206/204	207/204	208/204
18,82	15,61	38,63

Values cited by Doe (USGS Private Newsletter, December 1975) are:

18,785±0,100	15,620±0,020	38,675±0,101

The main uncertainty in the Rb^{87}/Sr^{86} ratio is that for the Rb/Sr ratio as determined by XRF. The only other measurement involved is the Sr^{87}/Sr^{86} ratio which is by far more precisely known. The uncertainty in the Rb/Sr ratio is a function of the analytical precision and the quality of the standard calibration. Replicate XRF analyses of some of the samples yield a precision of better than 1,0% relative, for values of the Rb/Sr ratios from 0,1 to 8,0. The main factor influencing the precision is detecting low amounts of Rb (<5ppm), since no analysed sample had Sr contents less than 20 ppm. Some of the low Rb samples (1-2 ppm) (peridotite, troctolite) yielded very imprecise Rb/Sr ratios by XRF, and so were analysed for Rb by ID.

Standard data were with 1-2% of the adopted values, which was comparable

with the estimated precision. Since the range observed for the majority of measured Rb/Sr ratios was not extreme (0,1-8,0) a "blanket" error of 2,0% was applied (cf. Brooks et al., 1972).

A5.10. Regression technique

The regression technique used in the present study is that of York (1966), which has been subsequently referred to as YORK MODEL I (Brooks et al., 1972). However, the treatment in this study is more or less equivalent to MCINTYRE MODEL I since "blanket" errors have been used (cf. Brooks et al., 1972). Weighting factors used are the reciprocal of the squares of the absolute uncertainties, York (1967, Fig. 2):

$$w(X_i) = \frac{1}{(\sigma_x)^2}, \quad w(Y_i) = \frac{1}{(\sigma_y)^2}$$

σ = absolute error in X and Y

$X = Rb^{87}/Sr^{86}$

$Y = Sr^{87}/Sr^{86}$

$w(X_i)$, $w(Y_i)$ = weighting factors for the ith data point

The degree of scatter about the line of best fit has been estimated by calculating MSUM (Brooks et al., 1972). MSUM values for each individual Rb-Sr plot are given and evaluated in the appropriate sections in Chapter 3.